

The high pressure phase behaviour of detergent range alcohols and alkanes

by

Frederick Christiaan van Niekerk Fourie

Dissertation presented for the Degree



DOCTOR OF PHILOSOPHY

(Chemical Engineering)

UNIVERSITEIT
STELLENBOSCH
UNIVERSITY

in the Faculty of Engineering

at Stellenbosch University

100
1918 · 2018

The financial assistance of the National Research Foundation (NRF) towards this research is hereby acknowledged. Opinions expressed and conclusions arrived at are those of the author and are not necessarily attributed to the NRF.

Supervisor

Prof J.H. Knoetze

Co-Supervisor

Prof C.E. Schwarz

March 2018

DECLARATION

By submitting this dissertation electronically, I declare that the entirety of the work contained therein is my own, original work, that I am the sole author thereof (save to the extent explicitly otherwise stated), that reproduction and publication thereof by Stellenbosch University will not infringe any third party rights and that I have not previously in its entirety or in part submitted it for obtaining any qualification.

This dissertation includes three original papers published in peer-reviewed journals or books and two unpublished publications. The development and writing of the papers (published and unpublished) were the principal responsibility of myself and, for each of the cases where this is not the case, a declaration is included in the dissertation indicating the nature and extent of the contributions of co-authors.

ABSTRACT

Supercritical fluids fulfil specialised roles in the food and beverage, petroleum, natural gas, polymers, pharmaceuticals and novel materials development industries. Supercritical fluid extraction (SFE) represents a separations niche and utilises the tuneable properties of a high pressure solvent to execute challenging extractions. One such example is the purification of detergent alcohol product streams. These streams often exhibit a range of carbon backbone lengths and contain significant residual alkanes, linear and branched alcohol isomers. The boiling and crystallisation points of these species are often narrowly distributed or overlap and SFE is considered as an alternative means of product purification.

Robust thermodynamic models are key to designing SFE processes but model development is partially reliant on access to accurate and comprehensive high pressure phase equilibria data. Vapour-liquid equilibria (VLE) data of ternary solvent + solute A + solute B systems are particularly useful because the solute A-solute B interaction, a determining factor in mixture phase behaviour, is inherently incorporated. Unfortunately these data remain scarce because the requisite analytical equipment is complex and costly.

A high pressure multi-component static analytic phase equilibria setup capable of operation at 150 °C and 300 bar was developed. It features a visual, variable volume equilibrium cell incorporating two ROLSI™ samplers. Simultaneous sampling from two phases coupled with concurrent parallel online analysis via gas chromatography (GC) is possible. Additional features include vertical adjustment of both samplers whilst maintaining system pressure, reduced cell dead volume and a high definition camera enabling the observation of internal phenomena not visible with the naked eye. Heating is achieved using jacketed fluid circulation coupled with a forced convection oven. The GC contains two inlets, four columns, two switch valves and three detectors arranged in parallel pathways and is equipped to handle mixture constituents from volatile gases to mid-length hydrocarbons. Adapted manual injection techniques enabled quantitative GC calibration methods that are decoupled from the equilibrium cell. The setup was validated by sampling from a one-phase ternary of known composition and comparison with binary and ternary literature data.

Observation of the cell contents has proven essential for accurate vapor phase sampling. Visuals were used to indicate that sampling can disrupt a high-pressure equilibrium system even if pressure and temperature remain constant to within 0.1 bar and 0.01 °C. Such disruptions may manifest in one of three phenomena: global mist formation, localized mist formation, or no-warning droplet formation. In a similar fashion, the impact of temperature gradients and particularly the small scale of the resultant disruptions, are conveyed.

The new apparatus was used to study nine ternary mixtures comprising the solvent CO₂ and different combinations of the solutes *n*-dodecane (*n*C₁₂), 3,7-dimethyl-1-octanol (37DM1O) and 1-decanol (C₁₀OH). Three ternary mixtures – [CO₂ + *n*C₁₂ + 37DM1O], [CO₂ + 37DM1O + C₁₀OH] and [CO₂ + *n*C₁₂ + C₁₀OH] – were each investigated at bulk CO₂-free solute A:solute B mass ratios of 75:25, 50:50 and 25:75. Phase compositions were measured at 35, 55 and 75 °C and pressures between 68 and 237 bar. The experimental outline and target reduced pressures in particular enable a comparative study using ethane as solvent.

Phase behaviour in the two alkane-containing mixtures – *n*C₁₂ + 37DM1O and *n*C₁₂ + C₁₀OH – displayed similarities and deviated from behaviour in the alcohol + alcohol mixture, 37DM1O + C₁₀OH. The presence of *n*C₁₂ led to enhanced solubility in the ternary mixture and, in the high-*n*C₁₂ region, co-solvency. On Gibbs diagrams this presents as s-shaped convex-to-concave liquid curvature, concave vapour curvature and, at intermediate pressures, a pinched two-phase band. In the CO₂ + 37DM1O + C₁₀OH system enhanced solubility or pinched two-phase bands were not detected and liquid curves remained convex throughout.

Relative solubility (α_{ij}) and separation potential (SP_{ij}) were used to evaluate solvent efficacy. The former is an indicator of attainable fractionation sharpness whilst the latter incorporates α_{ij} coupled with vapour phase loading of the more soluble solute. The suitability for fractionation using high pressure CO₂ decreased in the order [*n*C₁₂ + C₁₀OH] > [*n*C₁₂ + 37DM1O] > [37DM1O + C₁₀OH]. In both *n*C₁₂-containing systems, α_{ij} 's and to a large extent also SP_{ij} 's were positively correlated with bulk fraction of the *less* soluble solute species. In CO₂ + 37DM1O + C₁₀OH, α_{ij} 's were insensitive to solute ratio and, as a result, SP_{ij} 's were positively correlated with bulk fraction of the *more* soluble species. The alkane + alcohol α_{ij} compositional dependency may enable optimisation of a SFE process with a variable or manipulable feed composition.

Four thermodynamic models were evaluated for their ability to correlate the experimental vapour and liquid phase equilibrium pressures and compositions. The models, presented in order of decreasing performance, were RK-ASPEN, SR-POLAR, PR-BM and PC-SAFT. In the two C₁₀OH-containing systems at 35 °C, all four models essentially failed. Regardless the mixture, RK-ASPEN and PC-SAFT respectively produced the best and worst pressure correlations with percentage average absolute deviations of 3.1, 4.0 and 3.1 % (RK-ASPEN) and 8.5, 18.3 and 12.9 % (PC-SAFT). RK-ASPEN and SR-POLAR were superior at capturing the s-shaped liquid phase complexity and co-solvency pinch in the high-*n*C₁₂ regions. In general, however, RK-ASPEN produced the best composition estimates, particularly for the vapour phase.

Model-predicted relative solubilities and separation potentials were also evaluated. RK-ASPEN and PC-SAFT correctly ranked the systems in terms of suitability for SFE with CO₂ and, on average, produced the smallest absolute deviations in α_{ij} . Regardless the mixture, SP_{ij} estimates via PC-SAFT, surprisingly, were superior.

Density inversions or barotropy was detected in the high-C₁₀OH region of both C₁₀OH-containing systems at 35 °C and pressures in the approximate range 180 to 190 bar. Interesting images illustrating surface tension effects at the inverted conditions and a pressure reduction sequence passing through the inversion point are presented.

A number of valuable academic contributions have emanated from this work.

- i. Content from the equipment design review was published as a chapter in an edited volume and serves as a valuable point of departure for those who intend to construct similar equipment.
In: M.R. Belinsky (Ed.), *Supercritical Fluids*, Nova Publishers, New York, 2010, Ch.6.
- ii. The apparatus, design considerations and unique aspects of the equilibrium cell were discussed in a journal publication. This expands the body of knowledge related to high-pressure research.
Chemical Engineering & Technology 38 (2015) 1165-1172.
- iii. A second methodology paper covered GC design criteria and quantitative calibration methods, and presented novel visuals illustrating the challenges associated with high-pressure sampling.
Chemical Engineering & Technology 39 (2016) 1475-1482.
- iv. New phase composition data and modelling results for CO₂ + nC₁₂ + 37DM10 were presented in a journal publication. Given the scarcity of and challenges associated with producing high-pressure ternary VLE data, this represents a valuable contribution.
The Journal of Supercritical Fluids 130 (2017) 105-117.
- v. New phase composition data and modelling results for CO₂ + 37DM10 + C₁₀OH, and visuals illustrating density inversion behaviour, were in September 2017 submitted for publication.
- vi. New phase composition data were measured for CO₂ + nC₁₂ + C₁₀OH and the data were used to evaluate four thermodynamic models. A manuscript presenting these results and a comparative discussion on phase behaviour of the three ternaries is currently in preparation.

OPSOMMING

Superkritiese vloeiers word benut binne gespesialiseerde toepassings in die voedsel-en-drink, petroleum, aardgas, polimere, farmaseutiese en gevorderde materiale industrieë. Superkritiese vloeier ekstraksie (SVE) verteenwoordig 'n skeidingsnis en maak gebruik van die manipuleerbare eienskappe van 'n hoë-druk oplosmiddel om sodoende uitdagende ekstraksies te bewerkstellig. Een voorbeeld hiervan behels die suiwing van alkohol produktstrome in die sogenaamde 'wasmiddel' industrie. Dié strome vertoon dikwels 'n reeks van koolstofkettinglengtes en bevat noemenswaardige hoeveelhede alkaanreste tesame met lineêre en vertakte alkoholomere. Die kook en vriespunte van dié komponente is dikwels nou-verspreid of oorvleuel en SVE word oorweeg as 'n alternatiewe tegnologie vir produksuiwing.

Robuuste termodinamiese modelle staan sentraal tot SVE prosesontwerp, maar modelontwikkeling berus deels op akkurate en omvattende hoë-druk fase-ewewigsdata. Damp-vloeistofewewigsdata van ternêre oplosmiddel + opgeloste stof A + opgeloste stof B sisteme is veral nuttig, want die wisselwerking tussen opgeloste stof A en opgeloste stof B – 'n faktor wat mengselgedrag bepaal – word inherent inaggeneem. Ongelukkig bly data van dié aard skaars, want die nodige analitiese toerusting is ingewikkeld en duur.

'n Hoë-druk, multi-komponent fase-ewewigsopstelling is ontwerp, met dié ontwerp gebaseer op die statiese-analitiese beginsel. Die opstelling kan bedryf word by maksimum temperatuur en drukke van 150 °C en 300 bar. Die ewewigsel maak voorsiening vir veranderbare volume en besigtiging van die totale binneruim, en is toegerus met twee ROLSI™ monstertoestelle. Dié konfigurasie ondersteun gelyktydige monsterneming uit twee fases gevolg deur gelyktydige parallelle aanlyn analyses via gaschromatografie (GC). Bykomende eienskappe van die opstelling sluit in die vertikale verstelling van beide monstertoestelle terwyl die sisteem onder druk verkeer en verminderde dooie-volume. 'n Hoë-definisie kamera stel die operateur in staat om fisiese verskynsels, maar ook fynere detail wat die akkuraatheid van monsterneming en analyses beïnvloed, waar te neem. Vloeistofsirkulasie deur 'n mantel tesame met 'n konveksieoond word gebruik om die ewewigsel te verhit. Die aanlyn gaschromatograaf is toegerus met twee split-splitlose inlate, vier kolomme, twee skakelkleppe en drie detektors. Dié hardeware is rangskik in twee parallelle paaie en onderskraag die gelyktydige analyse van twee monsters met beide vlugtige gasse en medium-lengte koolwaterstowwe. Aangepaste handspuittegnieke het die daarstelling van kwantitatiewe GC kalibrasiemetodes, wat ontkoppel is van die ewewigsel, moontlik gemaak. Die opstelling is geverifieer deur monsterneming vanuit 'n homogene ternêre mengsel van bekende samestelling en vegelyking met binêre en ternêre verwysingsdata vanuit literatuur.

Visuele waarneming van die selinhoud het gebyk noodsaaklik te wees vir akkurate monsterneming van die dampfase. Beeldmateriaal toon dat monsterneming 'n hoë-druk ewewigsisteem kan versteur selfs al bly die druk en temperatuur stabiel tot binne 0.1 bar en 0.01 °C. Versteurings van dié aard manifesteer in een van drie fenomene: globale misvorming, lokale misvorming, of geen-waarskuwing druppelvorming. Op 'n soortgelyke wyse word die impak van temperatuurgradiënte, en veral die klein skaal van die versteurings wat volg, oorgedra.

Die nuwe apparaat is gebruik vir eksperimentele metings van nege mengsels bestaande uit die oplosmiddel CO₂ en verskillende kombinasies van die opgeloste stowwe *n*-dodekaan (*n*C₁₂), 3,7-dimetiel-1-oktanol (37DM10) en 1-dekanol (C₁₀OH). Drie ternêre mengsels – [CO₂ + *n*C₁₂ + 37DM10], [CO₂ + 37DM10 + C₁₀OH] en [CO₂ + *n*C₁₂ + C₁₀OH] – is elk bestudeer by CO₂-vrye algehele opgeloste stof A:opgeloste stof B massaverhoudings van 75:25, 50:50 en 25:75. Fasesamestellings is gemeet by 35, 55 en 75 °C en drukke tussen 68 en 237 bar. Die eksperimentele raamwerk en veral teiken-gereduseerde drukke ondersteun 'n vergelykende studie met etaan as oplosmiddel.

Fasegedrag in die twee alkaan-bevattende mengsels – *n*C₁₂ + 37DM10 en *n*C₁₂ + C₁₀OH – het ooreenkomste getoon en afgewyk van gedrag in die alkohol + alkohol mengsel, 37DM10 + C₁₀OH. Die teenwoordigheid van *n*C₁₂ het gelei tot verhoogde oplosbaarheid in die ternêre mengsel en in die hoë-*n*C₁₂ gebied is ko-solvensie waargeneem. Op Gibbs fasesdiagramme vertoon dié as s-vormige konvekse-na-konkawe vloeistoffase krommings, konkawe dampfase krommings en, by intermediêre drukke, 'n geknypte tweefaseband. In die CO₂ + 37DM10 + C₁₀OH sisteem is geen verhoogde oplosbaarheid of geknypte tweefasebande waargeneem nie en vloeistoffase kurwes was deurgaans konveks van aard.

Relatiewe oplosbaarheid (α_{ij}) en skeidingspotensiaal (SP_{ij}) is gebruik as parameters om die doeltreffendheid van die oplosmiddel te evalueer. Eersgenoemde omskryf die bereikbare skeidingskerpte terwyl laasgenoedme 'n funksie is van beide α_{ij} en die dampfasefraksie van die meer oplosbare koolwaterstof. Die geskiktheid vir skeiding deur middel van hoë-druk CO₂ het afgeneem in die volgorde [*n*C₁₂ + C₁₀OH] > [*n*C₁₂ + 37DM10] > [37DM10 + C₁₀OH]. In beide die *n*C₁₂-bevattende sisteme was α_{ij} 's, en tot 'n groot mate ook SP_{ij} 's, positief gekorreleerd met die algehele fraksie van die *minder* oplosbare koolwaterstof. In die CO₂ + 37DM10 + C₁₀OH sisteem was daar geen verwantskap tussen α_{ij} 's en die verhouding van opgeloste stowwe nie en gevolglik was SP_{ij} 's positief gekorreleerd met algehele fraksie van die *meer* oplosbare koolwaterstof. Die samestelling-afhanklikheid van α_{ij} 's in die alkaan + alkohol mengsels kan benut word om 'n SVE proses met variërende of manipuleerbare voersamestelling te optimeer.

Vier termodinamiese modelle is getoets vir hul vermoë om die eksperimentele ewewigsdrukke en samestellings van die damp en vloeistoffases te korreleer. Die modelle, gerangskik volgens afnemende prestasievermoë, was RK-ASPEN, SR-POLAR, PR-BM en PC-SAFT. In die twee C₁₀OH-bevattende mengsels by 35 °C het al vier modelle gefaal om sisteemgedrag te beskryf. Ongeag die mengsel, RK-ASPEN en PC-SAFT het onderskeidelik die beste en slegste drukkorrelasies, met persentasie gemiddelde absolute afwykings van 3.1, 4.0 and 3.1 % (RK-ASPEN) en 8.5, 18.3 and 12.9 % (PC-SAFT), gelewer. Wat betref die beskrywing van die s-vormige vloeistoffase-kompleksiteit asook die ko-solvensie vernouing het RK-ASPEN en SR-POLAR die ander modelle oortroef. RK-ASPEN het egter, in die algemeen, die mees akkurate samestellingskattings gelewer en veral só vir die dampfase.

’n Evaluasie van die modelle se vermoë om relatiewe oplosbaarheid en skeidingspotensiaal te voorspel, is ook uitgevoer. RK-ASPEN en PC-SAFT het die drie sisteme korrek rangskik in terme van geskiktheid vir SVE met CO₂ en het, in die reël, die kleinste absolute afwykings in α_{ij} gelewer. Ongeag die mengsel, PC-SAFT het, verrassend, die mees akkurate SP_{ij} skattings gelewer.

Digtheidsinversies of barotropie het voorgekom in die hoë-C₁₀OH gebied van beide C₁₀OH-bevattende sisteme by 35 °C en drukke van ongeveer 180 tot 190 bar. Interessante beeldmateriaal wat oppervlakspanningseffekte by die omgekeerde toestande en ’n druverlagingsreeks wat deur die inversiepunt beweeg uitbeeld, word getoon.

’n Aantal waardevolle akademiese bydrae het vanuit dié studie voortgevloei:

- i. Die hersiening van toerustingontwerpe is gepubliseer as boekhoostuk in ’n saamgestelde volume en dien as handige vertrekpunt vir andere wat beoog om soortgelyke toerusting te bou.
In: M.R. Belinsky (Red.), *Supercritical Fluids*, Nova Publishers, New York, 2010, Hfst.6.
- ii. Die apparaat, ontwerpsoorwegings en unieke aspekte van die ewewigsel is bespreek in ’n joernaalpublikasie wat die kennisbasis rakende hoë-druk navorsing verbreed.
Chemical Engineering & Technology 38 (2015) 1165-1172.
- iii. ’n Tweede metodologie-publikasie het GC ontwerpskriteria en kwantitatiewe kalibrasiemetodes gedek, en beeldmateriaal wat die uitdagings van hoë-druk monsterneming uitbeeld, getoon.
Chemical Engineering & Technology 39 (2016) 1475-1482.

- iv. Nuwe fasesamestellingsdata en modelleringsresultate vir $\text{CO}_2 + n\text{C}_{12} + 37\text{DM1O}$ is gepubliseer. Gegewe die skaarsheid en uitdagings gepaardgaande die produksie van hoë-druk ternêre damp-vloeistofewewigsdata is dié publikasie 'n noemenswaardige bydrae.

The Journal of Supercritical Fluids 130 (2017) 105-117.

- v. Nuwe fasesamestellingsdata en modelleringsresultate vir $\text{CO}_2 + 37\text{DM1O} + \text{C}_{10}\text{OH}$, en beeldmateriaal wat die digtheidsinversies uitbeeld, is in September 2017 ingedien vir publikasie.
- vi. Nuwe fasesamestellingsdata is gemeet vir $\text{CO}_2 + n\text{C}_{12} + \text{C}_{10}\text{OH}$ en dié data is gebruik in 'n evaluasie van vier termodinamiese modelle. 'n Manuskrip wat dié resultate kommunikeer en 'n vergelykende bespreking van fasegedrag in die drie ternêre mengsels aanbied, word tans voorberei.

ACADEMIC CONTRIBUTIONS

Journal publications and book chapter

- i. F.C.v.N. Fourie, C.E. Schwarz, J.H. Knoetze, CO₂ + *n*-dodecane + 3,7-dimethyl-1-octanol: High pressure experimental phase equilibria data and thermodynamic modelling, *J. Supercrit. Fluids* 130 (2017) 105-117.
- ii. F.C.v.N. Fourie, C.E. Schwarz, J.H. Knoetze, Analytic High-Pressure Phase Equilibria Part II: Gas Chromatography and Sampling Method Development, *Chem. Eng. Technol.* 39 (2016) 1475-1482.
- iii. F.C.v.N. Fourie, C.E. Schwarz, J.H. Knoetze, Analytic Setup for Multicomponent High-Pressure Phase Equilibria via Dual Online Gas Chromatography, *Chem. Eng. Technol.* 38 (2015) 1165-1172.
- iv. F.C.v.N. Fourie, C.E. Schwarz, J.H. Knoetze, Considerations for the Design of High-Pressure Phase Equilibrium and Solubility Measurements Equipment, in: M.R. Belinsky (Ed.), *Supercritical Fluids*, Nova Publishers, New York, 2010, Ch.6.

Peer-reviewed conference proceedings

- v. F.C.v.N. Fourie, C.E. Schwarz, J.H. Knoetze, New Experimental Phase Equilibria Data For Ternary Supercritical Solvent – Alkane – Alcohol Systems, Poster communication, 6th International Symposium on High Pressure Processes Technology, Belgrade, Serbia, 2013.
- vi. F.C.v.N. Fourie, C.E. Schwarz, J.H. Knoetze, Experimental Supercritical Phase Equilibria Measurements of Multi-component Systems, Oral presentation, 10th International Symposium on Supercritical Fluids, San Francisco, USA, 2012.
- vii. F.C.v.N. Fourie, C.E. Schwarz, J.H. Knoetze, Equipment Design, Construction and Evaluation for High-Pressure and High-Temperature Phase Equilibrium Measurements, Oral presentation, South African Chemical Engineering Congress, Somerset West, South Africa, 2009, ISBN: 978-1-920355-21-0.

Non-refereed conference contributions

- viii. F.C.v.N. Fourie, C.E. Schwarz, J.H. Knoetze, Experimental Measurement of Supercritical CO₂ + Alkane + Alcohol Ternary Systems, Poster communication, 24th IUPAC International Conference on Chemical Thermodynamics, Guilin, China, 2016.
- ix. F.C.v.N. Fourie, C.E. Schwarz, J.H. Knoetze, Experimental phase behaviour of supercritical CO₂ + alkane + alcohol systems, Poster communication, 28th European Symposium on Applied Thermodynamics, Athens, Greece, 2015.
- x. J.H. Knoetze, C.E. Schwarz, M. Zamudio-Du Preez, J.E. Lombard, S.A.M. Smith, F.C.v.N. Fourie, Phase equilibria of hydrocarbons in supercritical solvents: the way forward, Oral presentation, 28th European Symposium on Applied Thermodynamics, Athens, Greece, 2015.
- xi. F.C.v.N. Fourie, C.E. Schwarz, J.H. Knoetze, Ternary detergent range alcohol-alkane-CO₂ mixtures: experimental high pressure phase behaviour observations and analytical phase composition data, Oral presentation, 21st International Congress of Chemical and Process Engineering, Prague, Czech Republic, 2014.
- xii. F.C.v.N. Fourie, C.E. Schwarz, J.H. Knoetze, Experimental Analytical Phase Equilibria of Ternary Supercritical Solvent + Alkane + Alcohol systems, Poster communication, South African Chemical Engineering Congress, Durban, South Africa, 2014.
- xiii. F.C.v.N. Fourie, C.E. Schwarz, J.H. Knoetze, A High-Pressure Multi-Component Phase Equilibria Setup Utilising Online Gas Chromatography, Poster communication, 13th European Meeting on Supercritical Fluids, The Hague, Netherlands, 2011.
- xiv. F.C.v.N. Fourie, C.E. Schwarz, J.H. Knoetze, Design considerations for multi-component high-pressure phase equilibria measurements, Oral presentation, 8th World Congress of Chemical Engineering, Montreal, Canada, 2009.

ACKNOWLEDGEMENTS

This work is based on the research supported in part by the National Research Foundation of South Africa (Grant specific unique reference number (UID) 83966), Department of Trade and Industry (DTI) of South Africa through the Technology and Human Resources for Industry Programme (THRIP), and Sasol Technology (Pty) Ltd. The financial assistance of the National Research Foundation (DAAD-NRF) and the Skye Foundation Trust is also acknowledged. The authors acknowledge that opinions, findings, and conclusions or recommendations expressed in any publication generated by the supported research are those of the authors, and that the sponsors accept no liability whatsoever in this regard. Aspen Plus® is a registered trademark of Aspen Technology Inc.

In addition, I am particularly grateful to:

- My supervisor, Prof Hansie Knoetze, and co-supervisor, Prof Cara Schwarz. You provided continuous guidance and yet sufficient freedom to allow me to grow. I appreciate the innumerable ways in which you supported my undertakings.
- The staff at Stellenbosch University Department of Process Engineering and, in particular, Juliana Steyl, Francis Layman, Jannie Barnard, Anton Cordier, Jos Weerdenburg and Hanlie Botha.
- The Separations Technology research group, for being a friendly, dedicated and inspirational bunch.
- The National Research Foundation, Sasol Technology (Pty) Ltd, the DAAD-NRF and the Skye Foundation Trust for personal financial support.
- Finally, my father Chris, mother Mariana, sister Elize and brother Philip. Without your unconditional love and never ending support this journey would not have been possible.

*To my parents, Chris and Mariana,
who never stopped believing.*

TABLE OF CONTENTS

ABSTRACT	I
OPSOMMING	IV
ACADEMIC CONTRIBUTIONS	VIII
ACKNOWLEDGEMENTS	X
LIST OF FIGURES	XXI
LIST OF TABLES	XXIII
CHAPTER 1 : INTRODUCTION	1
CHAPTER 2 : EQUIPMENT REVIEW AND CONCEPTUAL DESIGN	12
CHAPTER 3 : PUBLICATION 1	59
CHAPTER 4 : PUBLICATION 2	79

CHAPTER 5 : PUBLICATION 3	98
<hr/>	
CHAPTER 6 : MANUSCRIPT 4	139
<hr/>	
CHAPTER 7 : MANUSCRIPT 5	175
<hr/>	
CHAPTER 8 : CONSOLIDATING TERNARY PHASE BEHAVIOUR	215
<hr/>	
CHAPTER 9 : CONCLUSIONS	224
<hr/>	
CHAPTER 10 : RECOMMENDATIONS AND FUTURE WORK	232
<hr/>	
APPENDIX A. PUBLICATION 1 SUPPORTING INFORMATION	235
<hr/>	
APPENDIX B. TECHNICAL DRAWINGS	239
<hr/>	
APPENDIX C. FINITE ELEMENT METHOD ANALYSIS REPORT	263
<hr/>	
APPENDIX D. T, P AND MASS CALIBRATIONS	277
<hr/>	
APPENDIX E. GAS CHROMATOGRAPH CALIBRATION CURVES	349
<hr/>	

CHAPTER 1 : INTRODUCTION 1

1.1 Supercritical fluid extraction 1

1.2 Detergent alcohols 2

1.3 Study context..... 2

1.4 Study objectives and document outline..... 3

1.5 Nomenclature..... 6

1.6 References..... 6

CHAPTER 2 : EQUIPMENT REVIEW AND CONCEPTUAL DESIGN 12

2.1 Classification of experimental equipment..... 12

2.1.1 Synthetic equipment 14

2.1.2 Static analytical equipment 15

2.1.3 Dynamic analytical equipment 16

2.1.3.1 Flow equipment..... 16

2.1.3.1 a) Continuous-flow equipment 17

2.1.3.1 b) Semi-flow equipment 17

2.1.3.2 Circulation equipment..... 17

2.1.3.2 a) Single-phase circulation equipment..... 18

2.1.3.2 b) Multi-phase circulation equipment..... 19

2.2 Detailed design considerations 19

2.2.1 Mixing 19

2.2.1.1 Mixing in static systems..... 19

2.2.1.2 Mixing in circulation systems 20

2.2.1.3 Mixing in flow systems 20

2.2.2 Equilibrium identification 21

2.2.3 Sampling 21

2.2.3.1 Sampling capillaries 22

2.2.3.2 Multi-port sampling valves 23

2.2.3.3	ROLSI™ and microsamplers.....	25
2.2.3.3 a)	The Rapid Online Sample Injector (ROLSI™)	25
2.2.3.3 b)	Microsamplers.....	26
2.2.3.4	Sampling from continuous and semi-flow systems.....	27
2.2.3.5	Additional sampling considerations	27
2.2.3.5 a)	Sampling from three-phase equilibria.....	27
2.2.3.5 b)	Sample extraction sequence	28
2.2.4	Sample homogenisation and preparation.....	28
2.2.4.1	Sample homogeneity during the sampling procedure.....	29
2.2.4.2	Sample homogeneity after the sampling procedure.....	30
2.2.5	Analysis method	31
2.2.5.1	Direct chromatographic analysis	31
2.2.5.2	Phase separation of samples prior to further analyses.....	31
2.2.5.3	In situ spectroscopic analyses	32
2.2.6	Injection, compression, pressure control and measurement	33
2.2.6.1	Circulation and static systems	34
2.2.6.2	Continuous and semi-flow systems.....	36
2.2.6.3	Pressure measurement	36
2.2.7	Temperature control	37
2.2.8	Observation windows and transparent equilibrium cells	38
2.2.9	Degassing of liquids and solids	39
2.2.10	Mechanical design and construction.....	40
2.3	Additional thermodynamic and physical properties	41
2.3.1	Excess molar enthalpy	41
2.3.2	Speed of sound	41
2.3.3	Interfacial tension.....	42
2.3.4	Density.....	42
2.4	Equipment evaluation and conceptual design	43
2.5	References.....	47

CHAPTER 3 : PUBLICATION 1**59**

Abstract	61
1. Introduction.....	62
2. Experimental.....	63
2.1 Setup.....	63
2.2 Equilibrium Cell.....	65
2.3 Sample Extraction.....	66
2.4 Gas Chromatography Analysis.....	67
2.5 Temperature and Pressure: Control, Accuracy and Calibrations	68
2.6 Equipment Design and Operation: Observations of Benefit to Related Studies.....	70
2.7 Experimental Procedure.....	71
2.7.1 Loading, Equilibrium Attainment and Sampling.....	71
2.7.2 Materials used	72
3. Validation of the Experimental Setup	72
4. Conclusions.....	75
Acknowledgement.....	76
References.....	76

CHAPTER 4 : PUBLICATION 2**79**

Abstract	81
1. Introduction.....	82
2. Materials and Methods	83
2.1 Experimental Setup	83
2.2 Sampling	83
2.3 Optimum Sample Size.....	84
3. GC Analysis	85
3.1 GC Calibration Method Development	87
3.2 GC Calibration Procedures.....	88

4. Experimental Difficulties: System Sensitivity and Visual Observations.....	89
4.1 Temperature gradients.....	89
4.2 Excessive sampling	92
4.2.1 Global Mist Formation.....	92
4.2.2 Localized Mist Formation	93
4.2.3 No-warning Droplet Formation	93
4.3 Vapor Capillary Cone	94
5. Conclusions.....	95
Acknowledgements	95
Abbreviations.....	96
References.....	96

CHAPTER 5 : PUBLICATION 3 98

Abstract	100
Nomenclature.....	100
1. Introduction.....	103
2. Materials and methods	104
2.1 Project outline	104
2.2 Experimental method.....	106
2.3 Modelling theory	108
2.3.1 RK-ASPEN.....	108
2.3.2 SR-POLAR.....	108
2.3.3 PR-BM	109
2.3.4 PC-SAFT.....	109
3. Results and discussion.....	110
3.1 Experimental reproducibility.....	110
3.2 Experimental data	112
3.3 Modelling.....	113
3.3.1 RK-ASPEN.....	114

3.3.2	SR-POLAR	115
3.3.3	PR-BM	115
3.3.4	PC-SAFT	116
3.4	Comparison of model-predicted ternary mixture vapour and liquid phase pressures.....	118
3.5	Experimental and model-predicted ternary mixture phase behaviour	119
3.6	Evaluating CO ₂ as solvent to fractionate nC ₁₂ + 37DM1O	129
3.6.1	Experimental ternary mixture relative solubilities and separation potentials.....	129
3.6.2	Model-predicted ternary mixture relative solubilities and separation potentials.....	131
4.	Conclusions.....	133
	Acknowledgements	134
	References.....	135

CHAPTER 6 : MANUSCRIPT 4

139

Abstract	141
Nomenclature.....	141
1. Introduction.....	143
2. Materials and methods	144
2.1 Experimental method.....	144
2.2 Modelling.....	145
3. Results and discussion	146
3.1 Experimental data	146
3.2 Modelling.....	148
3.2.1 RK-ASPEN.....	149
3.2.2 SR-POLAR.....	149
3.2.3 PR-BM	150
3.2.4 PC-SAFT.....	150
3.3 Comparison of model-predicted ternary mixture vapour and liquid phase pressures.....	152
3.4 Experimental and model predicted ternary mixture phase behaviour.....	153
3.5 Evaluating CO ₂ as solvent to fractionate 37DM1O + C ₁₀ OH	165

3.5.1	Experimental ternary mixture relative solubilities and separation potentials.....	165
3.5.2	Model-predicted ternary mixture relative solubilities and separation potentials.....	167
3.6	Density inversion	167
4.	Conclusions.....	169
	Acknowledgements	170
	References.....	171

CHAPTER 7 : MANUSCRIPT 5 175

	Abstract	177
	Nomenclature.....	177
1.	Introduction.....	180
2.	Materials and methods	181
2.1	Experimental method.....	181
2.2	Modelling.....	182
3.	Results and discussion.....	183
3.1	Experimental data	183
3.2	Modelling.....	185
3.2.1	RK-ASPEN.....	185
3.2.2	SR-POLAR.....	186
3.2.3	PR-BM	186
3.2.4	PC-SAFT.....	186
3.3	Comparison of model-predicted ternary mixture vapour and liquid phase pressures.....	188
3.4	Experimental and model predicted ternary mixture phase behaviour.....	189
3.5	Evaluating CO ₂ as solvent to fractionate $nC_{12} + C_{10}OH$	202
3.5.1	Experimental ternary mixture relative solubilities and separation potentials.....	202
3.5.2	Model-predicted ternary mixture relative solubilities and separation potentials.....	206
4.	Conclusions.....	209
	Acknowledgements	210
	References.....	211

CHAPTER 8 : CONSOLIDATING TERNARY PHASE BEHAVIOUR 215

8.1 Experimental..... 215

 8.1.1 Ternary mixture phase behaviour 215

 8.1.2 Ternary mixture relative solubility and separation potential..... 217

8.2 Modelling..... 221

 8.2.1 Model-predicted ternary mixture vapour and liquid pressures..... 221

 8.2.2 Model-predicted ternary mixture phase behaviour..... 221

8.3 References..... 222

CHAPTER 9 : CONCLUSIONS 224

9.1 Chapter 2: Equipment review and conceptual design 224

9.2 Chapter 3: Publication 1 (p. 75)..... 225

9.3 Chapter 4: Publication 2 (p. 95)..... 225

9.4 Chapter 5: Publication 3 (p. 134)..... 226

9.5 Chapter 6: Manuscript 4 (p. 172) 227

9.6 Chapter 7: Manuscript 5 (p. 212) 228

9.7 Chapter 8: Consolidating ternary phase behaviour..... 229

9.8 Summary remarks..... 230

CHAPTER 10 : RECOMMENDATIONS AND FUTURE WORK 232

References..... 234

LIST OF FIGURES

Figure 1-1. Document layout illustrating the relation between different chapters.....	5
Figure 2-1. Classification of phase equilibria equipment	13
Figure 2-2. Classification of experimental phase equilibria equipment.....	14
Figure 2-3. A manually operated 2-way expansion valve.....	22
Figure 2-4. Multiport sampling valves	23
Figure 2-5. The operation of a 6-port sampling valve	23
Figure 2-6. The (a) pneumatic and (b) electromagnetic ROLSI™	25
Figure 2-7. Micrometering valves.....	27
Figure 2-8. An example of a hand pump	34
Figure 2-9. Schematic diagram of conceptual design 1.....	44
Figure 2-10. Routing of the vapour and liquid phase flows in conceptual design 1	45
Figure 2-11. Sample valve configuration for the liquid density co-current circulation scenario	46
Figure 3-1. Cross-sectional schematic of the high-pressure analytic phase equilibria setup	64
Figure 3-2. Overview of the high-pressure analytic phase equilibria setup.....	64
Figure 3-3. (a) Side view of the equilibrium cell; (b) sectioned assembly of the equilibrium cell	66
Figure 3-4. Schematic of the GC configuration	67
Figure 3-5. (a) The temperature control approach	70
Figure 3-6. The CO ₂ + 1-octanol system at 65.0 °C: comparing data from this work with literature.....	73
Figure 3-7. The CO ₂ + 1-dodecanol + n-hexadecane system at 60.0 °C.....	74
Figure 3-8. The CO ₂ + 1-dodecanol + n-hexadecane system at 80.0 °C.....	74
Figure 4-1. A slow purge run from CO ₂ + nC ₁₂ + C ₁₀ OH	84
Figure 4-2. GC configuration.....	86
Figure 4-3. Schematic of a split-splitless GC inlet.....	87
Figure 4-4. (a) Linear detector responses with ROLSI™ sample time from ethane, 79 bar, 80 °C	87
Figure 4-5. Temperature gradient effects	90
Figure 4-6. The equilibrium cell temperature profiles at 35, 55 and 75 °C.....	91
Figure 4-7. Global mist formation	92
Figure 4-8. Localized mist formation of high intensity in CO ₂ + 37DM10 + C ₁₀ OH	93
Figure 4-9. No-warning droplet formation in CO ₂ + 37DM10 + C ₁₀ OH	94
Figure 4-10. Turbulent mixing when stirring at 130 rpm in CO ₂ + 37DM10 + C ₁₀ OH.....	94

Figure 5-1. Binary total solubility pressures (TSP) and experimental outline	105
Figure 5-2. Average absolute deviations for vapour phase equilibrium pressure predictions	119
Figure 5-3. CO ₂ + nC ₁₂ + 37DM10 at 35.0 °C	120
Figure 5-4. CO ₂ + nC ₁₂ + 37DM10 at 55.0 °C	122
Figure 5-5. Vapour phase detail for CO ₂ + nC ₁₂ + 37DM10 at 55.0 °C	124
Figure 5-6. CO ₂ + nC ₁₂ + 37DM10 at 75.0 °C	124
Figure 5-7. Vapour phase detail for CO ₂ + nC ₁₂ + 37DM10 at 75.0 °C	127
Figure 5-8. Experimental (a) relative solubility; and (b) separation potential	130
Figure 5-9. Vapour phase detail for CO ₂ + nC ₁₂ + 37DM10 at 55 °C and 106.5 bar	131
Figure 5-10. Model-predicted (a) relative solubility; and (b) separation potential	132
Figure 6-1. CO ₂ + 37DM10 + C ₁₀ OH at 35.0 °C	154
Figure 6-2. Vapour phase detail for CO ₂ + 37DM10 + C ₁₀ OH at 35.0 °C	155
Figure 6-3. CO ₂ + 37DM10 + C ₁₀ OH at 35.0 °C and 104, 123, 140, 157, 182, 200, 217 and 237 bar	155
Figure 6-4. CO ₂ + 37DM10 + C ₁₀ OH at 55.0 °C	156
Figure 6-5. Vapour phase detail for CO ₂ + 37DM10 + C ₁₀ OH at 55.0 °C	159
Figure 6-6. CO ₂ + 37DM10 + C ₁₀ OH at 75.0 °C	160
Figure 6-7. Vapour phase detail for CO ₂ + 37DM10 + C ₁₀ OH at 75.0 °C	163
Figure 6-8. Experimental (a) relative solubility; and (b) separation potential	166
Figure 6-9. The 25:75 37DM10:C ₁₀ OH mixture of CO ₂ + 37DM10 + C ₁₀ OH at 35.0 °C and 187.7 bar	168
Figure 6-10. The 25:75 37DM10:C ₁₀ OH mixture of CO ₂ + 37DM10 + C ₁₀ OH at 35.0 °C	168
Figure 6-11. A pressure reduction sequence at 35.0 °C illustrating the density inversion	169
Figure 7-1. CO ₂ + nC ₁₂ + C ₁₀ OH at 35.0 °C	191
Figure 7-2. Vapour phase detail for CO ₂ + nC ₁₂ + C ₁₀ OH at 35.0 °C	192
Figure 7-3. CO ₂ + nC ₁₂ + C ₁₀ OH at 35.0 °C and 68, 83, 104, 123, 140, 157, 182 and 200 bar	192
Figure 7-4. CO ₂ + nC ₁₂ + C ₁₀ OH at 55.0 °C	193
Figure 7-5. Vapour phase detail for CO ₂ + nC ₁₂ + C ₁₀ OH at 55.0 °C	196
Figure 7-6. CO ₂ + nC ₁₂ + C ₁₀ OH at 75 °C	197
Figure 7-7. Vapour phase detail for CO ₂ + nC ₁₂ + C ₁₀ OH at 75.0 °C	200
Figure 7-8. Experimental (a) relative solubility; and (b) separation potential	205
Figure 7-9. Vapour phase detail for CO ₂ + nC ₁₂ + C ₁₀ OH at 75.0 °C and 140 bar	206
Figure 7-10. (a) Model-predicted and experimental relative solubility	207
Figure 8-1. Comparative experimental and model-predicted ternary mixture phase behaviour.....	216
Figure 8-2. Comparing experimental relative solubility, α_{ij}	218
Figure 8-3. Comparing experimental separation potential, SP _{ij}	219

LIST OF TABLES

Table 2-1. Reported vapour and liquid-phase sample loop volumes.....	24
Table 2-2. Equilibrium cell materials of construction used in phase behaviour studies.....	40
Table 2-3. Characteristics of two conceptual designs considered	43
Table 3-1. GC method parameters for online analysis and calibration runs.....	68
Table 3-2. Materials used in this study.....	72
Table 3-3. Mass fraction averages and root mean square errors (RMSE), on parallel analysis pathways.....	72
Table 3-4. Phase composition data for the CO ₂ + 1-dodecanol (C ₁₂ OH) + n-hexadecane (nC ₁₆) system.	75
Table 4-1. Materials.....	83
Table 5-1. Binary mixture total solubility pressures [bar]	105
Table 5-2. Estimated maximum absolute uncertainty in phase composition, expressed as mass %	107
Table 5-3. Materials used	107
Table 5-4. Long term reproducibility of the experimental data.....	111
Table 5-5. Experimental data for CO ₂ + nC ₁₂ + 37DM10 at 35.0, 55.0 and 75.0 °C.....	112
Table 5-6. RK-ASPEN pure component polar parameters regressed in this work	114
Table 5-7. SR-POLAR pure component polar parameters regressed in this work.....	115
Table 5-8. PC-SAFT pure component parameters	117
Table 5-9. Binary interaction parameters regressed in this work	117
Table 5-10. %AAD in P, T, and solute mass fraction in the liquid (X) and vapour (Y) phases.....	117
Table 5-11. %AAD _p values for the model-predicted liquid and vapour phase equilibrium pressures	118
Table 5-12. Relative solubility (α_{ij}) and separation potential (SP _{ij})	133
Table 6-1: Estimated maximum absolute uncertainty in phase composition, expressed as mass %	145
Table 6-2: Materials used	145
Table 6-3: Experimental data for CO ₂ + 37DM10 + C ₁₀ OH at 35.0, 55.0 and 75.0 °C	146
Table 6-4: RK-ASPEN pure component polar parameters used in this work	149
Table 6-5: SR-POLAR pure component parameters used in this study	149
Table 6-6: PC-SAFT pure component parameters used in this work.....	151
Table 6-7: Binary interaction parameters used in this work	151
Table 6-8: %AAD in pressure, temperature and solute mass fractions for the regression of BIP's	151
Table 6-9: %AAD _p values for the model-predicted liquid and vapour phase equilibrium pressures	152
Table 6-10: Experimental and model predicted α_{ij} and SP _{ij} values, and their qualitative sensitivity	167

Table 7-1: Estimated maximum absolute uncertainty in phase composition, expressed as mass %	182
Table 7-2: Materials used	182
Table 7-3: Experimental data for CO ₂ + nC ₁₂ + C ₁₀ OH at 35.0, 55.0 and 75.0 °C	183
Table 7-4: RK-ASPEN pure component polar parameters used in this work	185
Table 7-5: SR-POLAR pure component parameters used in this work.....	186
Table 7-6: PC-SAFT pure component parameters used in this work.....	187
Table 7-7: Binary interaction parameters used in this work	187
Table 7-8: %AAD in pressure, temperature and solute mass fractions for the regression of BIP's	187
Table 7-9: %AAD _p values for the model-predicted liquid and vapour phase equilibrium pressures	188
Table 7-10. Average experimental and model-predicted α_{ij} and SP_{ij} values.....	208
Table 7-11. Relative solubilities, calculated using VLE data of the constituent CO ₂ + solute binaries.....	209
Table 8-1. Actual and binary-predicted relative solubilities.....	220
Table 8-2. Overall-Combined %AAD _p values	221

Chapter 1: INTRODUCTION

1.1 SUPERCRITICAL FLUID EXTRACTION

Supercritical fluid extraction (SFE) uses the tuneable properties of a high pressure solvent to manipulate selectivity and solvating ability and, in doing so, enables the isolation of a targeted compound or mixture of compounds. Initial industrial applications focused mainly on the extraction of high value organic products from natural matrices but nowadays high pressure extraction and solvation technologies are applied in the natural gas [1,2], enhanced oil recovery [3-5], food [6,7], pharmaceutical [8,9] and polymer [10,11] industries. Recent review articles on the application of supercritical fluids in the drug delivery [12], food [13] and polymer [14,15] industries are available.

The sizing of and control logic development for extractive or equilibrium-driven processes require a sound understanding of the mixture phase behaviour [16-18] and in this regard both predictive models and experimental data have important roles to fulfil [19]. The development of robust predictive thermodynamic models is partially reliant on access to accurate and comprehensive experimental phase equilibria data. This is particularly true for asymmetric mixtures containing a supercritical solvent and one or more polar, low-volatility solutes [18,20-22] where steep density and concentration gradients often cause mathematical correlations to fail [23].

The literature collection of high pressure binary solvent + solute phase behaviour data is significant though never complete. The associated experimental methods are typically well-established and new data are generated with reasonable efficiency via these existing techniques. However, ternary solvent + solute A + solute B mixtures are more representative of the system considered for fractionation and incorporate the solute A-solute B interactions. Studying ternary and higher mixture phase behaviour using synthetic equipment, a concept expanded upon in Chapter 2, usually involves the measurement of bubble and dew-point and critical endpoint data. However, synthetic methods are not well-suited to determine the compositions of co-existing vapour and liquid phases in ternary and higher mixtures. Analytical methods enable these measurements but at the expense of increased hardware complexity and cost.

1.2 DETERGENT ALCOHOLS

Fatty alcohols with carbon numbers ranging between 6 and 22 enjoy widespread application in the production of household detergents, cosmetics, textile processors, agrochemicals, plasticisers and lubricants [24,25]. Mid-cuts from this range, known as detergent alcohols, represent the largest fraction of this US\$ 4.7 billion global market [26] and are often used as precursors in the production of alcohol ethoxylate surfactants [27]. Two popular catalytic detergent alcohol production pathways involve the hydroformylation of an alkene and subsequent hydrogenation of the aldehyde [27,28] or direct oxidation of an alkane [29,30]. The hydroformylation/hydrogenation approach is often applied to a distillation cut containing both alkenes and inert alkanes, whilst the alkane oxygenation approach is often incomplete. To drive economies of scale the feed stream may also contain a variety of carbon backbone lengths [28]. As a result, detergent alcohol product streams may exhibit a range of carbon backbone lengths and contain significant residual alkanes, linear and branched alcohol isomers. The boiling and crystallisation points of these species are often narrowly distributed or overlap and SFE is considered as an alternative means of product purification.

1.3 STUDY CONTEXT

This study complements former and ongoing research by Stellenbosch University on the use of SFE to separate a post-production mixture of detergent alcohols and alkanes (Section 1.2). Within the larger project the solvents CO₂, ethane and propane together with solutes in the range C₈ to C₆₀, but especially C₈ to C₂₂, have been studied [31-34]. Different solute functional groups, isomerism and solute-solute interactions have been investigated as factors affecting system behaviour [35-41]. To date the research has involved high pressure bubble and dew point measurements [31-41], piloting [42-45], viscosity measurements [46], column hydrodynamic studies [47], low pressure VLE and VLLE measurements and theoretical modelling [48-51].

The hydrocarbon species *n*-dodecane (*n*C₁₂), 3,7-dimethyl-1-octanol (37DM1O) and 1-decanol (C₁₀OH) were previously identified as model components representing a detergent alcohol product stream [42,50]. High pressure phase composition measurements and thermodynamic modelling of ternary mixtures comprising CO₂ and different combinations of these hydrocarbon solutes was identified as a worthwhile course of study that would benefit local research and academia at large.

The study context, which considers SFE as an alternative for purifying post-production mixtures of detergent alcohols and alkanes, guided the thermodynamic modelling approach. In this sense, holistic process modelling of industrial relevance, and not only modelling of the VLE behaviour, is the ultimate aim. As such, the author restricted himself to thermodynamic models available within a well-known and commercially-available process simulator, Aspen Plus®.

1.4 STUDY OBJECTIVES AND DOCUMENT OUTLINE

The main objectives of this study are to:

- i. Design, construct and commission an analytic experimental setup for high pressure multi-component phase composition measurements. The apparatus should be able to handle asymmetric mixtures comprising the solvent CO₂ or ethane and, as solutes, alkanes and alcohols in the range C₈ - C₁₆. Furthermore, the setup should enable operation up to 150 °C and 300 bar.
- ii. Define an experimental outline and measure ternary mixture phase composition data for three systems. These are a) CO₂ + nC₁₂ + 37DM10; b) CO₂ + 37DM10 + C₁₀OH; and c) CO₂ + nC₁₂ + C₁₀OH. The experimental outline should also enable a comparative study using ethane as solvent.
- iii. Evaluate CO₂ as solvent to fractionate the three hydrocarbon mixtures mentioned in [ii].
- iv. Evaluate four thermodynamic models, available in commercial process simulators, for their ability to correlate the experimental vapour and liquid phase pressures and compositions measured in [ii].

Fig. 1-1 illustrates the outline of this document. The greater part of Chapter 2 was published as a book chapter in an edited volume. Chapters 3 - 5 represent three published journal papers whilst Chapters 6 and 7 respectively represent a manuscript submitted for publication and a manuscript in preparation. These chapters reflect the style of the specific book or journal where they were published or are intended to be published. Figure, table and equation captions are the exception and were adapted to reflect the chapter in which they appear (i.e., Fig. 1 became Fig. 3-1).

Fig. 1-1 also illustrates the relation between publications 1 and 2 with an equipment and methodology focus, and publication 3 and manuscripts 4 and 5 with a focus on experimental phase behaviour and thermodynamic modelling. Chapter 8 consolidates the results of and findings from this study. The focus thereof is ternary mixture phase behaviour (Chapters 5 - 7) and not equipment design, construction and commissioning (Chapters 3 and 4).

Conventions with regard to notation and terminology used in Chapters 5 - 10 include:

- References to solute A:solute B ratios imply solute A is the more soluble solute.
- References to solvent + solute A + solute B ternaries imply solute A is the more soluble solute.
- Gibbs diagrams of CO₂ + solute A + solute B ternaries present CO₂ fractions on the bottom, solute A fractions on the right-hand and solute B fractions on the left-hand axes.
- With the exception of validation data and troubleshooting results presented in Chapters 3 and 4, no binary data were measured in this study. In Chapters 5 - 10, references to solute A + solute B hydrocarbon mixtures imply the presence of CO₂.
- Throughout, the thermodynamic models were implemented in a fully predictive sense, without binary interaction parameters (BIP), to establish base case scenarios. However, these results are not reported in this document. All reported modelling results are correlative (i.e., BIP's were incorporated) but the terms *correlated* and *predicted* are used interchangeably.
- Footnotes used in Chapters 3 - 7 do not form part of the publications or manuscripts but are intended to assist the reader in navigating this document.

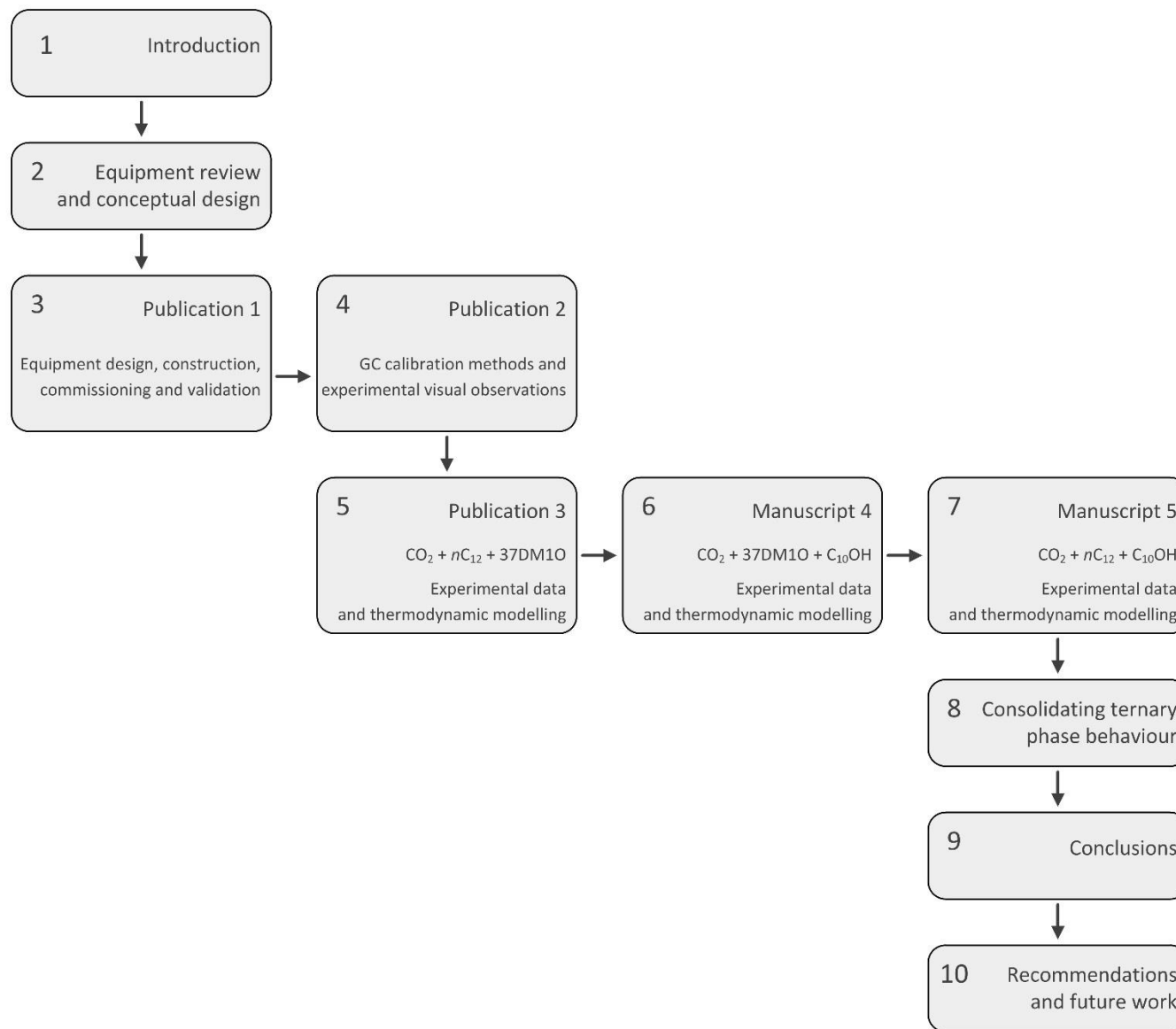


Figure 1-1. Document layout illustrating the relation between different chapters and, where applicable, a summary of the chapter content.

1.5 NOMENCLATURE

37DM1O	:	3,7-Dimethyl-1-octanol
BIP	:	Binary interaction parameter
C ₁₀ OH	:	1-Decanol
VLE	:	Vapour-liquid equilibrium
VLLE	:	Vapour-liquid-liquid equilibrium
<i>n</i> C ₁₂	:	<i>n</i> -Dodecane
37DM1O	:	3,7-Dimethyl-1-octanol
SFE	:	Supercritical fluid extraction
Solute	:	<i>n</i> C ₁₂ , 37DM1O or C ₁₀ OH
Solvent	:	CO ₂ , ethane or propane

1.6 REFERENCES

1. G.K. Folas, O.J. Berg, E. Solbraa, A.O. Fredheim, G.M. Kontogeorgis, M.L. Michelsen, E.H. Stenby, High-pressure vapor–liquid equilibria of systems containing ethylene glycol, water and methane: Experimental measurements and modelling, *Fluid Phase Equilib.* 251 (2007) 52-58.
2. D. Guerrero-Zárate, A. Estrada-Baltazar, G.A. Iglesias-Silva, Calculation of critical points for natural gas mixtures with the GERG-2008 equation of state, *Fluid Phase Equilib.* 437 (2017) 69-82.
3. M. Cao, Y. Gu, Temperature effects on the phase behaviour, mutual interactions and oil recovery of a light crude oil-CO₂ system, *Fluid Phase Equilib.* 356 (2013) 78-89.
4. M. Lashkarbolooki, A., Vaezian, A. Zeinolabedini Hezave, S. Ayatollahi, M. Riazi, Experimental investigation of the influence of supercritical carbon dioxide and supercritical nitrogen injection on tertiary live-oil recovery, *J. Supercrit. Fluids* 117 (2016) 260-269.
5. S.M. Seyyedsar, S.A. Farzaneh, M. Sohrabi, Experimental investigation of tertiary CO₂ injection for enhanced heavy oil recovery, *J. Nat. Gas. Sci. Eng.* 34 (2016) 1205-1214.
6. J.J. Schuster, L.A. Bahr, L.Fehr, M. Tippelt, J. Schulmeyr, A. Wuzik, A.S. Braeuer, Online monitoring of the supercritical CO₂ extraction of hop, *J. Supercrit. Fluids* 133 (2018) 139-145.
7. A. Bejarano, J.M. del Valle, Countercurrent fractionation of aqueous apple aroma constituents using supercritical carbon dioxide, *J. Supercrit. Fluids* 120 (2017) 266-274.
8. V. Prosapio, E. Reverchon, I. De Marco, Coprecipitation of Polyvinylpyrrolidone/ β -Carotene by Supercritical Antisolvent Processing, *Ind. Eng. Chem. Res.* 54 (2015) 11568-11575.

9. G. Liu, J. Pang, Y. Huang, Q. Xie, G. Guan, Y. Jiang, Self-Assembled Nanospheres of Folate-Decorated Zein for the Targeted Delivery of 10-Hydroxycamptothecin, *Ind. Eng. Chem. Res.* 56 (2017) 8517-8527.
10. B.-S. Lee, W.-H. Yeo, H.-S. Byun, Phase Behavior for the Poly(phenyl methacrylate) and Phenyl Methacrylate in Supercritical Carbon Dioxide and Dimethyl Ether, *J. Chem. Eng. Data* 62 (2017) 1876-1883.
11. H.M.N.T. Avelino, J.M.N.A. Fareleira, D. Gourgouillon, J.M. Igreja, M. Nunes da Ponte, Viscosity of poly(ethyleneglycol) 200 [PEG 200] saturated with supercritical carbon dioxide, *J. Supercrit. Fluids* 128 (2017) 300-307.
12. P. Gurikov, I. Smirnova, Amorphization of drugs by adsorptive precipitation from supercritical solutions: A review, *J. Supercrit. Fluids* (2017), <http://dx.doi.org/10.1016/j.supflu.2017.03.005>.
13. F. Sahena, I.S.M. Zaidul, S. Jinap, A.A. Karim, K.A. Abbas, N.A.N. Norulaini, A.K.M. Omar, Application of supercritical CO₂ in lipid extraction - A review, *J. Food Eng.* 95 (2009) 240-253.
14. M.S. Kondratenko, I.V. Elmanovich, M.O. Gallyamov, Polymer materials for electrochemical applications: Processing in supercritical fluids, *J. Supercrit. Fluids* 127 (2017) 229-246.
15. E. Kiran, Supercritical fluids and polymers – The year in review – 2014, *J. Supercrit. Fluids* 110 (2016) 126-153.
16. J. Gross, G. Sadowski, Modeling Polymer Systems Using the Perturbed-Chain Statistical Associating Fluid Theory Equation of State, *Ind. Eng. Chem. Res.* 41 (2002) 1084-1093.
17. R. Fingerhut, W.-L. Chen, A. Schedemann, W. Cordes, J. Rarey, C.-M. Hsieh, J. Vrabec, S.-T. Lin, Comprehensive Assessment of COSMO-SAC Models for Predictions of Fluid-Phase Equilibria, *Ind. Eng. Chem. Res.* 56 (2017) 9868-9884.
18. G. Sieder, G. Maurer, An extension of the Peng–Robinson equation of state for the correlation and prediction of high-pressure phase equilibrium in systems containing supercritical carbon dioxide and a salt, *Fluid Phase Equilib.* 225 (2004) 85-99.
19. E. Hendriks, G.M. Kontogeorgis, R. Dohrn, J.-C. De Hemptinne, I.G. Economou, L. Fele-Žilnik, V. Vesovic, Industrial Requirements for Thermodynamics and Transport Properties, *Ind. Eng. Chem. Res.* 49 (2010) 11131-11141.
20. K. Gauter, C.J. Peters, A.L. Scheidgen, G.M. Schneider, Cosolvency effects, miscibility windows and two-phase lg holes in three-phase llg surfaces in ternary systems: a status report, *Fluid Phase Equilib.* 171 (2000) 127-149.
21. M. Grigante, P. Stringari, G. Scalabrin, E.C. Ihmels, K. Fischer, J. Gmehling, (Vapour + liquid + liquid) equilibria and excess molar enthalpies of binary and ternary mixtures of isopropanol, water, and propylene, *J. Chem. Thermodyn.* 40 (2008) 537-548.

22. W. Gao, R.L. Robinson Jr., K.A.M. Gasem, Solubilities of Hydrogen in Hexane and of Carbon Monoxide in Cyclohexane at Temperatures from 344.3 to 410.9 K and Pressures to 15 MPa, *J. Chem. Eng. Data* 46,3 (2001) 609-612.
23. J. Cai, J.M. Prausnitz, Thermodynamics for fluid mixtures near to and far from the vapor–liquid critical point, *Fluid Phase Equilib.* 219 (2004) 205–217.
24. K. Noweck, W. Grafahrend, Fatty Alcohols, *Ullmann’s Encyclopedia of Industrial Chemistry*, 2006.
25. Sasol North America Inc., 2011. SAFOL® 23 Alcohol Technical Data Sheet. [online] Available at: <<http://www.sasoltechdata.com/tds/SAFOL%2023%20Alcohol%20TDS.pdf>> [Accessed 20 February 2012].
26. Markets Insider, 19 September 2017. Fatty Alcohols Market Worth 6.01 Billion USD by 2022. [online] Available at: < <http://markets.businessinsider.com/news/stocks/Fatty-Alcohols-Market-Worth-6-01-Billion-USD-by-2022-1002382273>> [Accessed 4 October 2017].
27. M. Grant-Huysen, S. Maharaj, L. Matheson, L. Rowe, E. Sones, Ethoxylation of Detergent-Range Oxo Alcohols Derived from Fischer-Tropsch α -Olefins, *J. Surfactants Deterg.* 7 (2004) 397-407.
28. J.C. Crause, Production of detergent range alcohols (2009), US Patent 2009/0054696 A1.
29. R.M. Deshpande, V.H. Rane, R.V. Chaudhari, Process for preparation of a mixture of alcohols and ketones by liquid phase oxidation of higher alkanes (2006), US Patent 2006/0094905 A1.
30. K.W. Lee, M.J. Choi, S.B. Kim, C.S. Choi, Liquid-phase oxidation of *n*-dodecane in the presence of boric acid, *Ind. Eng. Chem. Res.* 26 (1987) 1951-1955.
31. C.E. Schwarz, I. Nieuwoudt, J.H. Knoetze, Phase equilibria of long chain *n*-alkanes in supercritical ethane: Review, measurements and prediction, *J Supercrit. Fluids* 46 (2008) 226-232.
32. C.E. Schwarz, I. Nieuwoudt, J.H. Knoetze, Phase equilibrium of propane and alkanes Part III: Beyond hexacontane, *J. Supercrit. Fluids* 41 (2007) 327-334.
33. I. Nieuwoudt, M. du Rand, Measurement of phase equilibria of supercritical carbon dioxide and paraffins, *J. Supercrit. Fluids* 22 (2002) 185-199.
34. M. du Rand, I. Nieuwoudt, Measurement of phase equilibria of supercritical ethane and paraffins, *J. Supercrit. Fluids* 21 (2001) 181-193.
35. M. Ferreira, C.E. Schwarz, Super- and near-critical fluid phase behavior and phenomena of the ternary system CO₂ + 1-decanol + *n*-tetradecane, *J. Chem. Thermodyn.* 111 (2017) 88-99.
36. C.E. Schwarz, Q.H. Paulse, J.H. Knoetze, Phase equilibria of methyl esters in supercritical propane, *J. Supercrit. Fluids* 99 (2015) 61-67.
37. C.E. Schwarz, K.G. Chobanov, Phase equilibria of linear saturated high molecular mass acids in supercritical ethane, *J. Supercrit. Fluids* 87 (2014) 40-49.
38. C.E. Schwarz, J.H. Knoetze, Phase equilibrium measurements of long chain acids in supercritical carbon dioxide, *J. Supercrit. Fluids* 66 (2012) 36-48.

39. M. Zamudio, C.E. Schwarz, J.H. Knoetze, Phase equilibria of branched isomers of C₁₀-alcohols and C₁₀-alkanes in supercritical carbon dioxide, *J. Supercrit. Fluids* 59 (2011) 14-26.
40. C.E. Schwarz, F.C.v.N. Fourie, J.H. Knoetze, Phase equilibria of alcohols in supercritical fluids Part II. The effect of side branching on C₈ alcohols in supercritical carbon dioxide, *J. Supercrit. Fluids* 51 (2009) 128-135.
41. F.C.v.N. Fourie, C.E. Schwarz, J.H. Knoetze, Phase equilibria of alcohols in supercritical fluids Part I. The effect of the position of the hydroxyl group for linear C₈ alcohols in supercritical carbon dioxide, *J. Supercrit. Fluids* 47 (2008) 161-167.
42. M. Zamudio, The Separation of Detergent Range Alkanes and Alcohol Isomers with Supercritical Carbon Dioxide, PhD Dissertation, Stellenbosch University, South Africa, 2014.
43. M. Zamudio, C.E. Schwarz, J.H. Knoetze, The effect of branched alcohol isomers on the separation of alkanes and alcohols with supercritical CO₂, Poster communication, 13th European Meeting on Supercritical Fluids, The Hague, Netherlands, 2011.
44. C.E. Schwarz, G.J.K. Bonthuys, R.F. van Schalkwyk, D.L. Laubscher, A.J. Burger, J.H. Knoetze, Separation of alkanes and alcohols with supercritical fluids. Part II. Influence of process parameters and size of operating range, *J. Supercrit. Fluids* 58 (2011) 352-359.
45. C.E. Schwarz, I. Nieuwoudt, J.H. Knoetze, Additional Pilot Plant Measurements with Incorporation of Reflux for the Fractionation of Wax Derivatives with Supercritical Propane, *Ind. Eng. Chem. Res.* 49 (2010) 4462-4467.
46. H.H. Franken, J.H. Knoetze, C.E. Schwarz, Equipment for the Simultaneous Measurement of Supercritical Binary Phase Equilibrium, Density and Viscosity, in: 15th European Meeting on Supercritical Fluids, Essen, Germany, 2016.
47. H.H. Franken, Establishment of a supercritical pilot plant and the hydrodynamics of supercritical countercurrent columns, MSc Thesis, Stellenbosch University, South Africa, 2014.
48. J.E. Lombard, Thermodynamic modelling of hydrocarbon-chains and light-weight supercritical solvents, MSc Thesis, Stellenbosch University, South Africa, 2015.
49. A.J. de Villiers, C.E. Schwarz, A.J. Burger, G.M. Kontogeorgis, Evaluation of the PC-SAFT, SAFT and CPA equations of state in predicting derivative properties of selected non-polar and hydrogen-bonding compounds, *Fluid Phase Equilib.* 338 (2013) 1-15.
50. M. Zamudio, C.E. Schwarz, J.H. Knoetze, Experimental measurement and modelling with Aspen Plus[®] of the phase behaviour of supercritical CO₂ + (*n*-dodecane + 1-decanol + 3,7-dimethyl-1-octanol), *J. Supercrit. Fluids* 84 (2013) 132-145.
51. C.E. Schwarz, A.J. de Villiers, C.B. McClune, G.J.K. Bonthuys, A.J. Burger, J.H. Knoetze, High pressure phase equilibrium measurements of long chain alcohols in supercritical ethane, *J. Supercrit. Fluids* 55 (2010) 554-565.

52. M. Zamudio, The Separation of Detergent Range Alkanes and Alcohol Isomers with Supercritical Carbon Dioxide, PhD Dissertation, Stellenbosch University, South Africa, 2014.

Chapter 2: EQUIPMENT REVIEW AND CONCEPTUAL DESIGN

This chapter presents a review of published equipment designs for high-pressure phase equilibria studies. It starts with an overview of the classification system and a summary of the methods reported in literature. Thereafter, key aspects, among which sampling, sample homogenisation, analysis methods and temperature and pressure control, are discussed in more detail. Throughout, the advantages and disadvantages of the experimental method as a whole, but also detailed design considerations, are reported. Excess molar enthalpy, speed of sound, interfacial tension and density are regarded as additional thermodynamic and physical properties and their measurement is touched upon because the incorporation thereof into one single experimental method should be considered early in the equipment design stage. The content of this review served as point of departure for, and the chapter concludes with a section on, method evaluation and conceptual equipment design.

It would be inappropriate to discuss phase equilibria equipment without referring to the review articles in the High-pressure fluid-phase equilibria series. The articles by Fornari et al. [1], Dohrn and Brunner [2], Christov and Dohrn [3], Dohrn et al. [4] and Fonseca et al. [5] discuss phase equilibria equipment but the predominant focus thereof are to summarise all studies which produced high-pressure phase equilibria data within the applicable period [3]. In contrast, this chapter does not focus on experimental data but rather on equipment design considerations. Publications from the abovementioned series offer valuable reference material and the inclusion thereof in future equipment design reviews is recommended.

Content from this literature review was published as a chapter titled *Considerations for the design of high-pressure phase equilibrium and solubility measurements equipment in Supercritical Fluids* [6].

2.1 CLASSIFICATION OF EXPERIMENTAL EQUIPMENT

Literature attempts to categorise the experimental methods used in phase equilibria studies.¹ Given the quantity and diversity of methods used to date, an all-encompassing categorical system is beyond reach and variations within a specific category further increase the complexity of such a classification system. As a start, experimental methods are grouped according to:

- Whether or not composition analysis of co-existing phases are performed.
- If and how species move through the experimental setup.

¹ The isothermal category as used by Dohrn and Brunner [2] and Christov and Dohrn [3] corresponds to the static and circulation categories of this chapter whilst their isobaric-isothermal category corresponds to the flow category of this chapter. Low-pressure applications, which correspond to their isobaric category, are not covered in this chapter.

Regarding the analysis of phase compositions, one distinguishes between synthetic and analytical methods. Synthetic equipment is predominantly used to identify a phase transition point and, as such, no analysis of phase compositions are required. In contrast, analytical equipment allows phase separation to progress to equilibrium, and attempts to quantify the compositions of these co-existing equilibrium phases. Regarding the movement of species through the experimental setup, static and dynamic methods exist. In static systems, all chemical species remain within the equilibrium cell throughout the entire experiment while in dynamic equipment, all or some of the chemical species move through the equilibrium cell on a continuous or intermittent basis. Since species movement and composition analysis are independent, two classification pathways can be used (Fig. 2-1).

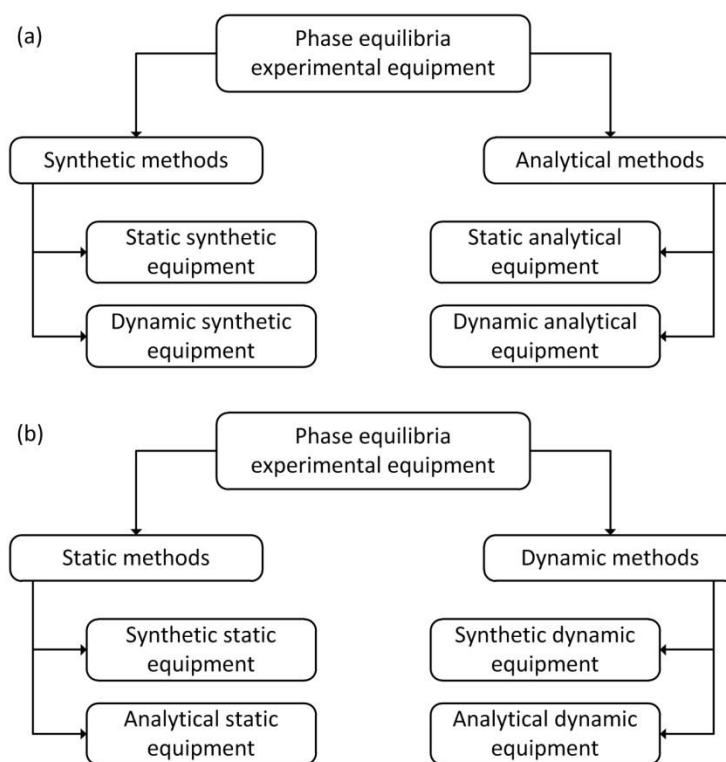


Figure 2-1. Classification of phase equilibria equipment according to (a) composition analysis; and (b) species movement through the apparatus.

The dynamic category comprises both circulation and flow equipment. Within the former, liquid-phase, vapour-phase and multi-phase circulation methods, with each of these being either counter or co-current, exist. Within the latter, both continuous and semi-flow methods exist. Shown in Fig. 2-2 is Fig. 2-1 a expanded to include the different dynamic methods.

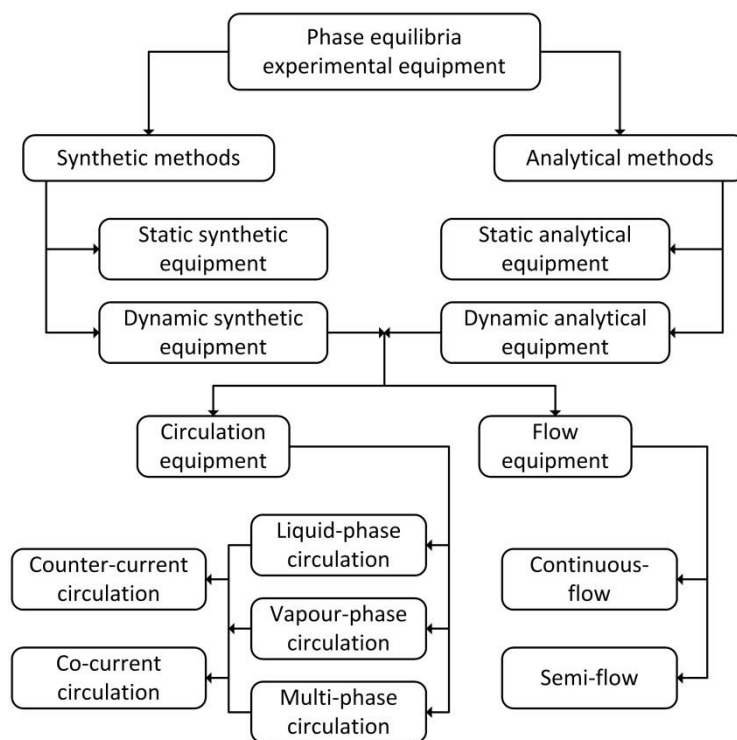


Figure 2-2. Classification of experimental phase equilibria equipment.

2.1.1 Synthetic equipment

This section discusses the static and dynamic synthetic methods. Synthetic methods are, by and large, of the static type and therefore dynamic synthetic equipment is discussed only as an extension of this section. Synthetic equipment is not designed with the analysis of phase compositions in mind but, instead, these systems are mostly used to identify the transition between single-phase (homogeneous) and multi-phase (heterogeneous) regions, enabling one to generate bubble, dew and critical-point data. Visual observation is often, though not exclusively, relied upon to identify the phase transition point.

The Cailletet apparatus is an example of a well-established and well-documented synthetic apparatus capable of operation at moderate pressures [7-8]. In this apparatus, a sample of known composition is contained within a thick-walled Pyrex glass tube. Mercury is used for pressure transmission and sealing the open end of the Pyrex tube, and the tube itself is located within a glass jacket to achieve temperature control. A magnetic stirring device is placed in the sample mixture to enable stirring thereof and phase transitions are observed visually. The underlying principles of the Cailletet apparatus has stood the test of time and many synthetic setups designed today are still based on the same fundamentals.

Although visual observation is the norm, certain studies have used more infrequent and specialised methods to identify the phase transition point. In studies by Bouchot and Richon [9] and Kayukawa et al. [10], bulk density was monitored by means of a vibrating tube densimeter. Sudden and significant changes

in density would signify the phase transition point. A difference in ultrasonic velocity in gas and liquid phases enabled Takagi et al. [11] to identify the phase transition. Goodwin et al. [12] developed an automated radio frequency cavity resonator capable of detecting phase boundaries within fluid mixtures. May et al. [13] built upon this work and developed a microwave apparatus sensitive to small amounts of liquid-phase within a predominantly gaseous-phase to generate dew point data. Abedi et al. [14] developed an X-ray apparatus which relied upon transmitted X-rays as opposed to visible light for the detection of phase transitions.

Dynamic synthetic equipment is seldom used. However, studies by Rosenthal and Teja [15], Hortstmann et al. [16] and Du Rand [17] used dynamic synthetic equipment to identify the critical, bubble and dew points of pure species and binary mixtures.

The use of synthetic phase equilibria equipment presents the following advantages:

- The absence of sampling and analysis systems enables relatively simple and inexpensive designs.
- The absence of sampling reduces running costs and enables the investigation of high-value species.
- In static equipment, temperature equilibrium is simplified as no species exit the equilibrium cell.

The use of synthetic phase equilibria equipment presents the following disadvantages:

- Limited use for the study of ternary and higher mixtures [3].
- Long residence times in static equipment prohibit the study of thermally unstable species.
- Synthetic methods are mostly of the static type which implies co-existing phases are not continuously removed from the cell. This complicates the measurement of the equilibrium densities of the co-existing vapour and liquid phases.

2.1.2 Static analytical equipment

The static analytic method refers to an experimental setup in which all chemical species remain within the equilibrium cell and composition analysis of co-existing phases is performed.² This method also falls within the stoichiometric grouping because bulk mixture composition is dependent only on the amount of species introduced initially. In simplified terms, static analytic equipment is operated as follows: a mixture of species is loaded in the cell, equilibrium is obtained at predefined pressure and temperature conditions, and composition analysis is performed either in situ or subsequent to sampling. The static analytic method has been used by numerous researchers [18-37], and the use thereof provides the following advantages:

² A distinction is made between species removal during equilibration and species removal during sampling. The former is necessarily classified as dynamic whilst the latter could be either static analytic or dynamic analytic.

- Unlike for flow systems, small quantities of materials are sufficient [23].
- Thermal equilibrium is simplified since no species exit the equilibrium cell.
- Simple physical construction compared to flow and circulation systems [23].
- The internal environment is more controllable than in circulation and especially flow systems.
- Relative to dynamic analytical equipment, operation in the mixture critical region is simplified.
- The method is suited for generating phase composition data for three and multi-phase systems.

Disadvantages of using static analytic equipment include the following:

- Circulating streams cannot be used to enhance the approach to equilibrium.
- Long residence times often prohibit the analysis of thermally unstable species.
- Unlike flow and circulation systems, co-existing equilibrium phases are not removed from the cell on a continuous basis and, as a result, sampling and the effect thereof is complicated.
- Compared to circulation analytical equipment, the measurement of equilibrium density is complicated since co-existing equilibrium phases are not continuously removed from the cell.

2.1.3 Dynamic analytical equipment

Dynamic analytical equipment involves the movement of species through the experimental system coupled with the ability to analyse phase compositions. The dynamic grouping comprises both circulation and flow methods which differ according to the manner in which mobile phases are transported.

2.1.3.1 Flow equipment

Flow equipment includes any system in which at least one species is continuously fed to the equilibrium cell and at least one phase is continuously removed from the equilibrium cell. Two types, continuous and semi-flow equipment exist and these are discussed in Sections 2.1.3.1 a) and 2.1.3.1 b) respectively. Advantages of using flow equipment include the following:

- Large amounts of data can be collected quickly [38].
- The apparatus is adaptable to a wide variety of feedstock [39].
- Equilibrium, stripping or fractionation data can be obtained [39].
- Within limits, phase compositions are independent of species flow rates [39,40].
- Short residence times enable the analysis of thermally unstable products [39-42].
- The sampling procedure is simplified and less likely to cause pressure disturbances [41-43].

Disadvantages of using flow equipment include the following:

- Large quantities of materials are required [23].
- Analyses of three and multi-phase equilibria are difficult.
- Insufficient phase separation in the mixture critical region may occur [17].
- Heavy solids or liquids can clog the metering valves in effluent outlet tubing [39].
- Undetected phase changes can occur in the pre-saturator or equilibrium cell [39].
- The time in which to reach equilibrium is limited, precluding the analysis of certain systems.

2.1.3.1 a) Continuous-flow equipment

In continuous-flow systems, all species are continuously fed to and removed from the system. The species are usually pre-heated, joined in a static mixer to attain equilibrium and fed to the equilibrium cell which acts only as a phase separator. Co-existing phases are continuously withdrawn through effluent lines to be analysed once equilibrium is reached. Continuous-flow systems are very popular and have been used by numerous researchers [40-46].

2.1.3.1 b) Semi-flow equipment

In semi-flow systems, at least one component (normally a liquid) is loaded in the cell beforehand and at least one component (normally a gas) is preheated and fed to the cell continuously. This implies that equilibrium is only reached in the equilibrium cell and not beforehand, as is the case with continuous-flow systems. The vapour-like phase is withdrawn continuously via an effluent line to be analysed once equilibrium is reached. If at all, the liquid-like phase is withdrawn only for analysis once equilibrium has been reached. In comparison to continuous-flow systems, these systems consume smaller quantities of liquid component and are therefore better suited for studies which involve expensive liquid species. Semi-flow systems, though frequently used, appear to be somewhat less popular than their continuous equivalent [39,47-53].

2.1.3.2 Circulation equipment

Circulation devices are similar to static systems in that overall composition is known from the amount of species initially loaded in the cell. However, these are classified as dynamic systems due to the constant circulation of one or more co-existing phases. It is possible to circulate either the liquid, vapour or multiple phases in a counter or co-current fashion. In this context, counter-current implies the vapour and liquid phases re-enter the cell via the liquid and vapour phases respectively, and co-current implies each

circulated phase is returned to the phase from which it was formerly withdrawn. Note the following with regard to counter and co-current circulation:

- Counter-current circulation maximises the rate of equilibrium attainment.
- In the mixture critical region where phase densities differ minimally, counter current circulation may result in the clouding of phases.
- To prevent sample contamination in a counter-current circulation system the inlet to and outlet from a specific phase should be located as far apart from one another as possible.
- Switching from counter-current to co-current circulation prior to sampling may eliminate problems related to phase clouding and sample contamination.

Advantages of using circulation equipment include the following:

- These systems enable the analysis of three- and multi-phase equilibria.
- Smaller quantities of materials are required than is the case for flow systems.
- Circulation enhances mixing due to increased contact between co-existing phases.
- Sampling is simplified due to the continuous removal of matter from equilibrated phases.
- Continuous circulation of phases simplifies the measurement of additional equilibrium data.

Disadvantages of using circulation equipment include the following:

- Circulation equipment increases capital expenditure.
- Thermal equilibrium requires temperature control in the circulation lines.
- Larger quantities of materials are required than is the case for static systems.
- Demister pads may be required to prevent the entrainment of liquids in the gaseous phase.
- Pulsation disturbances may require a form of dampening and, even then, could preclude measurements in the mixture critical region.

2.1.3.2 a) Single-phase circulation equipment

In single-phase circulation systems, only the vapour or liquid phase is circulated. Due to reduced contact area between co-existing phases, mixing is less efficient than is the case for multi-phase circulation systems. In addition, sampling and density measurements of the non-circulated phase are performed with less ease. Although single-phase circulation systems have been used [54-58], they are less popular than their multi-phase counterparts.

2.1.3.2 b) *Multi-phase circulation equipment*

Multi-phase circulation systems involve the continuous circulation of two or more phases through the apparatus. Mixing is optimised due to increased contact area whilst sampling and online density measurements of all phases are simplified. Even though dual-phase circulation is the norm [59-71], a few studies have utilised three-phase circulation equipment [72-74]. The majority of these studies were operated in a counter-current fashion with only Wendland et al. [64], Freitag et al. [70], Wendland [71] and Tanaka and Kato [73] using co-current circulation.

2.2 DETAILED DESIGN CONSIDERATIONS

This section discusses in greater detail a number of considerations related to equipment design and operation. Some of these are specific to static, dynamic, synthetic or analytical methods only. The aspects addressed in the remainder of this section are:

- Mixing
- Equilibrium identification
- Sampling
- Sample homogenisation and preparation
- Analysis methods
- Injection, compression and pressure control
- Temperature control and measurement
- Observation windows
- Degassing of liquids and solids
- Mechanical design and construction

2.2.1 *Mixing*

Analytical phase equilibria studies require two or more co-existing phases to equilibrate whilst synthetic studies require the bulk system to reach mechanical and thermal equilibrium. Depending on the species and operating conditions, equilibrium attainment can be time consuming and often results in a bottle neck in data generation. As such, a form of mixing is normally employed. The mixing method is partially limited by the method of study and is therefore discussed accordingly.

2.2.1.1 *Mixing in static systems*

Most static systems rely on either magnetic or mechanical stirring to achieve equilibrium. Magnetic stirring is advantageous since no direct contact is required between the stirring device located outside the equilibrium cell and the stirrer located inside the cell. In contrast, mechanical stirring requires direct contact between the drive shaft and motor which necessitates sealing between the driven rod and

equilibrium cell. Even though mechanical stirring has been used [35,60,73], magnetic stirring is the more popular choice and has been employed by a great number of researchers [18,24,28,31-34,36-38,75].

An alternative approach to mixing in static systems is the use of a pivoting or rocking equilibrium cell [76-81]. In these systems, the entire cell assembly is rocked to ensure adequate mixing of the content. In selected cases, mixing balls were placed within the cell to further improve mixing efficiency.

2.2.1.2 *Mixing in circulation systems*

In counter-current circulation systems, mixing induced by phase circulation is usually adequate to achieve equilibrium within an acceptable time. This is not the case, however, in co-current circulation systems which almost always utilise either magnetic or mechanical stirring in addition to circulation [64,70,71,73]. To achieve maximum mixing efficiency, the simultaneous use of counter-current circulation and magnetic or mechanical stirring is suggested [60,69,72]. In counter-current circulation systems, a porous filter may be placed inside the liquid phase to ensure homogenous vapour distribution [54,61] because, according to Chen et al. [61], improved vapour distribution in the liquid speeds up the approach to equilibrium. The type of pump used for phase circulation is often mentioned and examples are listed below but, unfortunately, information on their respective advantages and disadvantages for this application is lacking:

- Air-driven piston pumps [54]
- Metering pumps [55,59,69]
- Magnetic pumps [60,62,63,66,68]
- HPLC pumps [64,70]
- Gear pumps [58]

In studies utilising single-phase counter-current circulation, the time to equilibrium varied between 1 and 12 h [54-56,58,66] whilst 5 min to 4 h were encountered for studies utilising multi-phase counter-current circulation [59,60,63,68]. The use of multi-phase circulation together with either mechanical or magnetic stirring produced time to equilibrium values between 1 and 3 h [60,69,70,73]. Unfortunately the differences in cell geometry, component characteristics and operating conditions between these studies do not allow for useful comparisons.

2.2.1.3 *Mixing in flow systems*

Continuous-flow systems tend to use a static inline mixer to achieve phase equilibrium. The species are joined before the mixer and attain equilibrium before entering the phase separation cell [40-43,45]. In semi-flow systems, the use of a static mixer is not sufficient since at least one of the liquid species is loaded

in the cell beforehand. Uribe-Vargas and Trejo [50] used a perforated coil allowing the mobile gas phase to bubble through the liquid mixture. The use of glass wool, glass beads and other packing material in the equilibrium cell reduces the time to equilibrium by increasing surface area between the mobile gaseous and stationary liquid phases, and prevents entrainment of the latter [47-49,51-53]. It is not uncommon to pass the gaseous phase through a pre-saturator prior to entering the equilibrium cell [39,49,52] or to plug the equilibrium cell exit to reduce liquid entrainment [48,52,53].

2.2.2 *Equilibrium identification*

In analytical phase equilibria studies it is important that equilibrium be fully established before phase composition analysis is performed. The system geometry, method of stirring, component characteristics and operating conditions all impact the time required to attain equilibrium. The majority of authors define equilibrium as the point at which all measured properties remain constant or fluctuate within predefined limits. Summarised below are equilibrium definitions as reported in literature:

- Temperature and pressure remain constant [29,37,50,68]
- Pressure remains constant [36,74]
- Pressure remains steady within 1 kPa [82]
- Pressure fluctuates within ± 1.0 kPa during a period of 10 min under efficient stirring [83]
- Temperature remains within ± 0.005 K for 30 min and pressure remains within ± 0.01 % [57]
- Pressure remains within ± 0.001 MPa and density remains within ± 0.1 kg/m³ [60]
- Pressure and density remain stable [66]
- Pressure and interfacial levels remain constant [72]
- Interface of both phases remains stable [41,42]
- Pressure and infrared spectra remain constant for 1 h [84]

Static and circulation systems frequently allow for a rest period after equilibrium is reached to enable co-existing phases to separate and settle. During this rest period no magnetic or mechanical mixing is performed whilst the use of circulation varies between studies. For the studies considered, rest periods varied between 5 min and 6 h with an average of approximately 2 h [21,25,30,32,55,69,73,79,85].

2.2.3 *Sampling*

Sampling of co-existing equilibrium phases is, by definition, not applicable to synthetic or non-intrusive analytical studies. However, the large number of studies that utilise sampling justifies a dedicated discussion thereof and Section 2.2.3 focuses on reported sampling procedures, their advantages and

disadvantages. An effective sampling procedure should produce representative samples, not affect overall composition and not disturb equilibrium pressure and temperature [60,86]. However, sample extraction from a high-pressure equilibrium state is a complex exercise and, in theory, the aforementioned requisites are beyond reach [23]. This is particularly true for static and circulation methods where the experimental system represents a closed boundary. The goal, then, is to ensure that errors fall within the accuracy limits of the experiment [24]. Challenges experienced with high pressure sampling procedures include:

- Changes in phase compositions during the sampling procedure [17].
- The compromise between representative sampling and pressure disturbance.
- Insufficient phase separation in, especially, the mixture critical region [17,22].
- The disturbance of equilibrium pressure and temperature [17,19,22,24,30,31,36].

2.2.3.1 Sampling capillaries

High-pressure studies of the static type often make use of thin capillaries for sample extraction [19,23,24,28,32,35,36]. The capillary protrudes into the phase of interest and samples are withdrawn via small controlled pressure reductions. As defined in this context, sampling capillaries are frequently used in conjunction with manually operated 2-way expansion valves, an example of which is shown in Fig. 2-3.



Figure 2-3. A manually operated 2-way expansion valve. [Photo Courtesy of Snap-tite Technologies, Inc., Copyright, Snap-tite Technologies, Inc., Erie, Pa, U.S.A., 2009, All Rights Reserved]

The valve is opened momentarily and the pressure differential enables sample extraction. This approach provides the benefit of high operating temperatures and pressures but inefficient mixing in the sample capillary could lead to dead volume and, crucially, the manual nature of operation does not enable the extraction of sufficiently small samples. As a result, buffer autoclaves [19,35] and variable volume cells [32,36] have been used in conjunction with sampling capillaries to ensure constant pressure during sampling. Where similar preventative measures were not used, small pressure disturbances were experienced during sampling [23,24]. Samples withdrawn via capillaries and manual expansion valves are

often analysed via phase separation in sample traps (see Section 2.2.5.2) because a) the pressure reduction promotes phase separation, and b) 2-way valves do not support continuous carrier gas flow which precludes online chromatography.

2.2.3.2 Multi-port sampling valves

The use of 4, 6, 8 and 10-port sampling valves is popular in high-pressure phase equilibria studies of the circulation type [55,58-64,66,68-70,74]. An equilibrated phase is circulated through the valve sample loop which could be either internal or external to the valve itself (Fig. 2-4). Upon sampling the valve is switched, GC carrier gas is routed through the sample loop, and the sample is swept into the GC column. An illustration thereof is shown in Fig. 2-5.

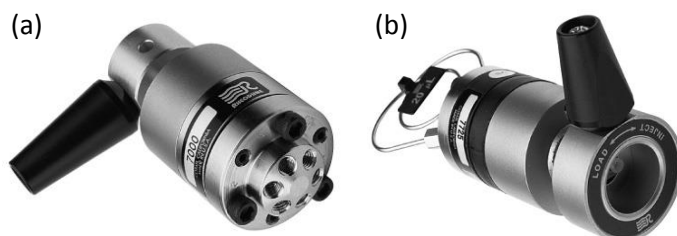


Figure 2-4. Multiport sampling valves containing an (a) internal; and (b) external sampling loop. [Rheodyne® valve product shots reprinted with permission from IDEX Health & Science LLC]

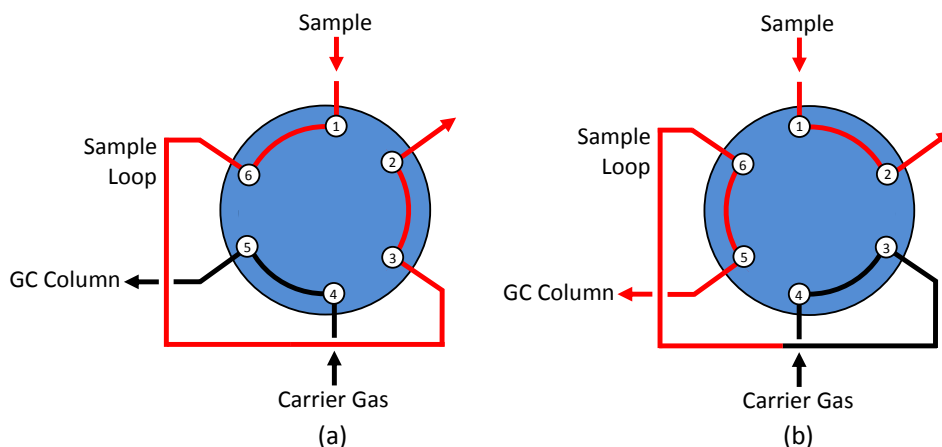


Figure 2-5. The operation of a 6-port sampling valve: (a) the sample loop is located in the circulation line; and (b) after switching the sample loop is located in the GC carrier gas line. [Image reproduced with permission from VICI Valco Instruments Co. Inc.]

Multi-port sampling valves manufactured by Rheodyne and VICI Valco are regularly used in phase equilibria research. In general, smaller-sized sample loops are used for liquid phase sampling whilst larger sample loops are used for the vapour phase (Table 2-1). This choice is governed, in part, by molecular density of the phase in question, and GC column and detector requirements and limitations.

Table 2-1. Reported vapour and liquid-phase sample loop volumes used for high pressure phase equilibria research.

Sample loop volume			Sample loop volume		
Liquid	Vapour	Reference	Liquid	Vapour	Reference
0.5 μl	10 μl	[87]	1 μl	10 μl	[89]
0.5 μl	31 μl	[68]	1 μl	20 μl	[69]
0.5 μl	500 μl	[85]	1 μl	100 μl	[74]
1 μl	1 μl	[61]	5 μl	20 μl	[55]
1 μl	1 μl	[66]	10 μl	100 μl	[60]
1 μl	1 μl	[64]	18 μl	455 μl	[63]
1 μl	5 μl	[88]	100 μl	100 μl	[58]

Multi-port sampling valves provide the following benefits:

- Sampling is conducted online and close to operating conditions.
- They are multifunctional and can be used for applications other than sampling.
- No dead volume exists because the sample loops forms part of the circulation line.
- Continuous circulation is compatible with online density and surface tension measurements.
- Low-volume sample loops enable sampling without any significant impact on system pressure.

Negative aspects of multi-port sampling valves include the following:

- A small-diameter sample loop may cause pressure drop across the circulation line [60].
- Depending on the loop configuration, carrier gas is added to the cell with each actuation.
- Operation is often limited to either high pressure or high temperature, but seldom both [37].

The impact of small quantities of inert carrier gas on phase behaviour is in all probability overshadowed by inherent experimental inaccuracies [90]. However, this may not be the case after multiple sample extractions at different pressure and temperature conditions within a single experimental run. A potential solution involves the use of 8 or 10-port valves with vacuum applied to the sample loop after GC injection, but the effect of this small-volume vacuum on equilibrium pressure would have to be evaluated.

Multi-port sampling valves are placed either directly within [58,59,61,62,64,66,68-70,74,85,87] or outside the circulation line [55,60,63]. The latter requires an additional valve configuration to reroute species through the sample valves once equilibrium is reached. This rerouting procedure is undesirable because a) the bypassed circulation line creates dead volume, and b) any volume difference between the bypassed circulation line and sample loop may disrupt system pressure upon valve switching. In addition to valve-placement, options exist with regard to the timing of sample withdrawal. Sampling via multi-port valves is

normally performed while circulation is in motion as this ensures uniformity between samples and the equilibrated phases. However, some researchers believe that pressure gradients inherent to circulation may affect equilibrium phase compositions and therefore sample in the absence of circulation [69,73,90].

2.2.3.3 ROLSI™ and microsamplers

This section discusses the Rapid Online Sampler Injector (ROLSI™) and microsamplers as high-pressure sampling tools. In all but one of the case studies, capillaries were used to transport the sample from the cell interior. However, these devices differ from those in Section 2.2.3.1 in terms of the method used to initiate sample movement and post-withdrawal sample treatment.

2.2.3.3 a) The Rapid Online Sample Injector (ROLSI™)

The ROLSI™ enables the withdrawal of small samples via a capillary connection. The first version, developed by Laugier and Richon [37], gave rise to the pneumatic ROLSI™ as described by Guilbot et al. [91] and subsequent improvements led to the development of an electromagnetic model (Fig. 2-6). Both versions have been used to good effect by a number of research groups [18,31,33,34,83].

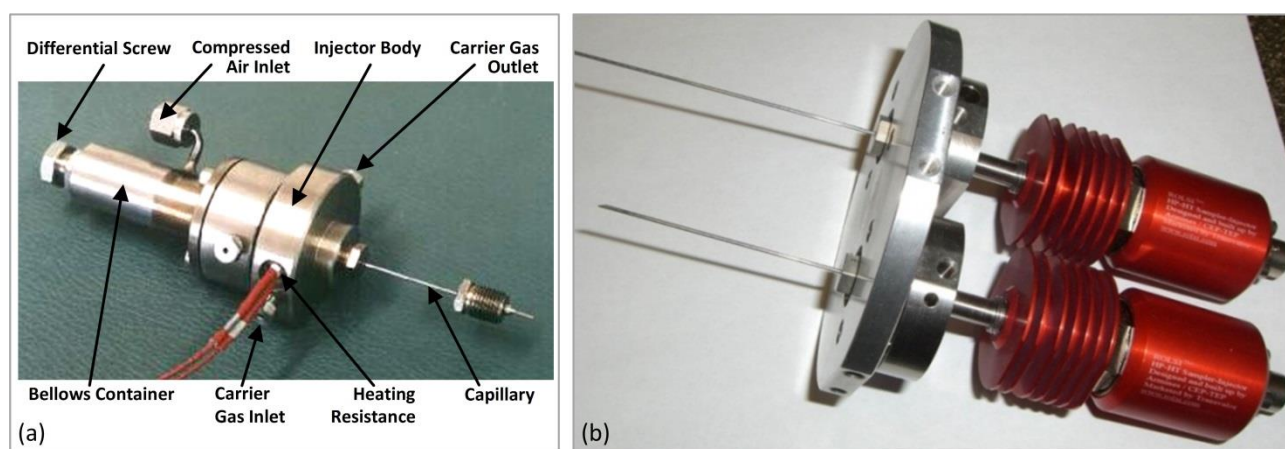


Figure 2-6. The (a) pneumatic and (b) electromagnetic ROLSI™. [Figures reproduced with agreement of ARMINES/Transvalor, proprietary of the ROLSI Trade Mark]

Benefits of using the ROLSI™ for sampling include the following: [18,31,33,34,91]:

- Simultaneous operation at high temperatures and pressures (1000 bar and 600 °C, and 800 bar and 250 °C for the pneumatic and electromagnetic models respectively).
- Multiple sample extractions without any disturbance to equilibrium conditions.
- Independent heating of the ROLSI™ ensures sample homogeneity.
- Fast and complete sample transfer to the GC.

- Continuously adjustable sample volume.
- The ROLSI™ is commercially available.
- Good volume repeatability.
- Corrosion resistance.

Disadvantages of using the ROLSI™ include the following:

- The ROLSI™ is relatively expensive.
- The absence of local distributors may complicate after-sales service.
- To ensure representative sampling, the capillary internal volume (generally less than 1 µl) must be purged prior to sampling a new phase or composition.
- Compared to manual valves (Section 2.2.3.1), multi-port sampling valves and micrometering valves (Section 2.2.3.4), the ROLSI™ is less-suited for applications other than sampling.

2.2.3.3 b) *Microsamplers*

Most microsamplers are capillary-type samplers with a sophisticated sample extraction system that enables the withdrawal of small samples from the equilibrium cell. Although similarities exist, the author differentiates between the commercially-available ROLSI™ and other lesser-known capillary-type microsamplers.

Galicía-Luna et al. [29] used an electronically-monitored pneumatic sampler injector to extract and inject samples, via a capillary, into the GC carrier gas circuit. A differential screw was used to vary pressure drop at the capillary exit and, in turn, sample size. Laugier and Richon [37] used spring-loaded microsamplers connected to the cell interior via capillaries. Light shocks applied to the springs withdrew small samples into an expansion chamber to be swept away by GC carrier gas. Chou et al. [56] made use of 30 µl microcells located within the circulation line. After simultaneous trapping of both vapour and liquid samples, the microcells were placed in a secondary circulation line from which GC injection occurred. Although good results have been obtained by using various microsamplers, the use thereof presents the following disadvantages:

- Capillary-type microsamplers may create dead volume due to inefficient mixing in the capillary.
- Microsamplers are normally developed by a research group and are not commercially available, which presents an obstacle to developing research groups who lack experience in this regard.
- Unlike manual valves (Section 2.2.3.1), multi-port sampling valves and micrometering valves (Section 2.2.3.4), microsamplers are not multifunctional, i.e., they can be used for sampling only.

2.2.3.4 Sampling from continuous and semi-flow systems

Sampling from continuous and semi-flow systems does not present as many difficulties as sampling from circulation and static systems. By definition, one or both of the co-existing phases are continuously removed from the cell via effluent lines and therefore the requirements for an effective sampling system are more easily satisfied. Sampling from continuous-flow systems often utilises micrometering (Fig. 2-7) and expansion valves within both the light and heavy effluent lines [40-46]. Sample depressurisation across these valves and, in some cases, cooling thereafter result in separation of the heavy condensable species from the light gaseous species allowing further analyses thereof. The sampling procedure for semi-flow systems is by and large similar to continuous-flow systems. However, in most semi-flow systems only the lighter mobile phase is sampled [39,47-49,51-53]. Uribe-Vargas and Trejo [50] sampled the vapour and liquid phases in their semi-flow system but withdrawal of the latter was intermittent.

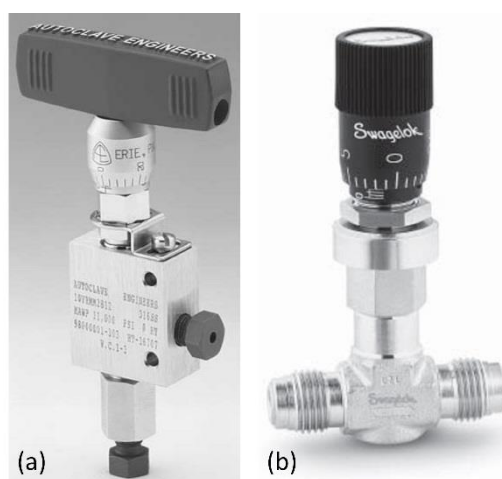


Figure 2-7. Micrometering valves by (a) Autoclave Engineers [Photo Courtesy of Snap-tite Technologies, Inc., Copyright, Snap-tite Technologies, Inc., Erie, Pa, U.S.A., 2009, All Rights Reserved]; and (b) Swagelok. [©2009 Swagelok Company]

2.2.3.5 Additional sampling considerations

2.2.3.5 a) Sampling from three-phase equilibria

The measurement of three- and multi-phase equilibria places a number of constraints on the experimental setup. The ability to extract samples from three or more locations which differ sufficiently in height is essential. The relative amount and therefore height of each phase will differ between experimental runs and ideally one should be able to monitor and adjust the sampling location of especially the middle phase or phases. It has been mentioned that three-phase equilibrium measurement is generally incompatible with continuous and semi-flow systems while three circulation pumps may be required in circulation systems. Notwithstanding all of the above, a number of groups have measured three phase equilibria using

static and circulation systems [18,25,26,28,29,32,33,52,61,67,69,73]. All these apparatuses used external windows enabling observation of the entire cell interior or, as a minimum, the central section containing the middle phase.

Vertically movable capillaries, allowing sampling from any height within the cell, were used by Galicia-Luna et al. [29], Silva-Oliver et al. [31] and Laursen et al. [85]. This approach, although very versatile, may result in problems with sealing. Studies by Grigante et al. [18], Winkler and Stephan [28], Wendland et al. [64] and Freitag et al. [70] used rotatable cells which allowed sampling from multiple points within the cell. The remainder of the studies listed above sampled from fixed locations and variations in initial species-quantities were required to ensure sampling from the correct phase [32,36,55,72-74].

2.2.3.5 b) Sample extraction sequence

In static analytic and circulation analytic studies the sample extraction sequence requires consideration. Wäterling et al. [23] and Wagner and Wichterle [25] reported that sampling of the liquid phase should occur first as this has the smallest effect on pressure within the cell.³ Ideally, the liquid and vapour phases should be sampled simultaneously as this ensures that potential disturbances to equilibrium caused by sampling do not affect a single measurement. However, simultaneous sampling of all phases creates a problem for the analysis section of the apparatus. Unless analyses can also be performed simultaneously, some means of preserving the sample is required. Sample preservation and simultaneous analyses are given further consideration in Sections 2.2.4 and 2.2.5 respectively.

2.2.4 Sample homogenisation and preparation

Section 2.2.3 focused on the withdrawal of representative samples from co-existing equilibrium phases. This section, in turn, discusses preparation of these samples for composition analysis. Firstly, a well-prepared sample is homogeneous, at the correct temperature and pressure, in the correct phase and sufficiently diluted. Requirements regarding the correct temperature, pressure, phase and dilution ratio differ according to the analysis method and sample composition. Sample homogeneity, however, is of critical importance to ensure accurate composition analysis. The greater part of this section focuses on homogeneity and the manner in which it is affected by species characteristics, pressure and temperature.

³ In the author's experience, if both phases cannot be sampled simultaneously it is preferred to sample the vapour phase first and not the liquid phase. Disruptions to equilibrium conditions are more likely to impact the vapour phase sampling procedures whilst liquid phase sampling is, in this sense, more robust (see Section 4.2 in Chapter 4).

According to Mühlbauer and Raal [22], sample homogeneity is difficult to achieve in systems containing species of greatly differing volatility, and the possibility of phase separation among condensed species at room temperature and atmospheric pressure is highlighted by Shimoyama et al. [41] and Haruki et al. [42].

The injection of a high-pressure sample into a carrier gas stream is usually accompanied by a reduction in pressure which creates the possibility of fractional separation and, in turn, erroneous composition analysis [60]. Pressure drop along the capillaries used by Lhoták and Wichterle [24] changed the sample aggregation state which resulted in the formation of large vapour bubbles or liquid droplets in the liquid and vapour samples respectively [25]. According to Wäterling et al. [23], samples withdrawn from vapour or liquid phases invariably fractionate into two phases due to changes in pressure.

A reduction in sample temperature may cause selective condensation from a vapour sample [21], and the evaporation of liquid samples via increased temperature is often required prior to analysis. Sample temperature control is an important aspect of virtually every analytical method discussed in this chapter.

2.2.4.1 Sample homogeneity during the sampling procedure

Precautionary measures taken during the sampling procedure may contribute toward ensuring sample homogeneity. Ideally, all sampling equipment such as circulation pumps, valves, capillaries and circulation lines should be located within the same thermo-regulated environment as the equilibrium cell. In circulation systems especially, this would benefit not only sample homogeneity but also temperature stability within the cell itself. However, it is often necessary to remove sampling equipment from the equilibrium cell environment which necessitates a different approach to sample temperature control.

Electrical heating jackets and independent air baths were used by Freitag et al. [70] and Takishima et al. [72] respectively to heat circulation pumps located outside the central thermo-regulated environment. To prevent partial condensation, sampling capillaries and circulation lines located outside the central thermo-regulated environment were superheated by respectively Pfohl et al. [35] and Elbaccouch et al. [68]. Independent thermostatic baths, heat boxes and heating jackets have been used to ensure sample homogeneity where sample valves, injectors and ampoules are located outside the central thermo-regulated environment [28,35,43,60,67,68,72]. In this regard, microsamplers with heated expansion chambers [29,37] and the ROLSI™, which enables independent heating [18,31,33], are advantageous.

2.2.4.2 *Sample homogeneity after the sampling procedure*

This discussion relates to systems that utilise direct GC analysis, phase separation via sample traps, secondary sample loops or mixing vessels. Online GC analysis requires the transportation of a sample from within the thermo-regulated environment to the GC by means of a carrier gas. Electrical heating tape is often used to superheat transfer lines which prevents the condensation and adsorption of high boilers, and ensures vaporisation of liquid samples [18,28,29,31,33,50,55,60,64,65,67,68,70]. This ensures that entire and/or representative samples are injected into the GC. In addition to heating transfer lines, the carrier gas itself can also be superheated [60].

In static and dynamic systems that utilise phase separation via cold traps either exclusively or prior to GC analysis (refer to Section 2.2.5.2 on page 31), sample homogeneity is as essential. Sample valves and lines may require solvent washing to ensure homogeneity among condensed species within a sample trap [41,42,58]. Expansion valves, micrometering valves and tubing through which samples pass before reaching cold traps are often heated to prevent premature condensation [43], counteract Joule-Thompson cooling effects [46,92], and ensure the complete transfer of vapour and liquid samples [23].

Secondary sample loops, typically located in independently heated air baths, have been used to ensure sample homogeneity after extraction from the equilibrium cell [56,62,63,72,73]. These loops attempt to dilute, vaporise, homogenise and in some cases pressurise samples before GC injection. To accomplish this, secondary loops normally contain a circulation pump, flash tank or expansion vessel, method of introducing pressurised carrier gas, and GC injection valve. If secondary sample loops are used, only a fraction of the original sample is injected into the GC. This is both an advantage and disadvantage because multiple injections enable validation of GC accuracy but incomplete homogenisation could result in erroneous analysis. According to Chou et al. [56] and Adams et al. [63], the acquisition of time-invariant reproducible peaks for all components signifies complete sample preparation. Secondary sample loops present an additional advantage in that simultaneous sampling is supported irrespective of whether simultaneous analyses are possible.

Small mixing vessels have also been used to ensure sample homogeneity. Mühlbauer and Raal [22] developed a conical static jet mixer which produced high-speed circulatory flow, and Wagner and Wichterle [25] placed a 0.8 ml intensely stirred superheated glass vessel within the sampling line. In analogy to microsamplers (Section 2.2.3.3), mixing vessels as defined in this context are not commercially available which limits the use thereof by developing research groups.

2.2.5 Analysis method

Three categories of analysis are discussed. These are direct chromatographic analysis, the intentional phase separation of samples prior to analysis, and in situ spectroscopic analysis.

2.2.5.1 Direct chromatographic analysis

Direct GC analysis of an entire sample is often used in analytical phase equilibria studies [18,31,33,34,50,56,60,62,63,66,67,69,72,73,83,85,87-89]. This approach is beneficial because it enables one to:

- Process very small samples.
- Investigate costly species that can only be obtained in small quantities.
- Verify analysis reproducibility by analysing a single, diluted sample several times.
- Verify sampling accuracy by analysing multiple samples without disrupting equilibrium.

Disadvantages of analysis via GC include the following:

- A GC and the associated equipment are expensive.
- GC analysis necessitates sampling which presents problems in itself (Section 2.2.3).
- Phase equilibria studies often involve a mixture of species with large variation in molecular weight, necessitating very different GC approaches. This can be overcome by using columns in series [50] and other intricate GC methods which, inevitably, further raises capital cost.

If, in addition to simultaneous sampling, simultaneous analyses are possible, the experimental time could be reduced. Oh et al. [67] used two sets, each comprising a detector and column, in their GC. A similar setup would be valuable in a study where different sample constituents ideally require different detectors.

2.2.5.2 Phase separation of samples prior to further analyses

Intentional sample fractionation is often used to simplify analysis of the different sample components [19,21,23,30,32,35,36,39-41,43,44,46,54,59]. This is achieved by means of pressure reduction and/or cooling which cause the heavy condensables and light non-condensables to separate. A cold trap and liquid collection vessel are typically used to capture the condensable species. Cooling mediums referenced in literature include water, ice, dry ice + acetone, dry ice + 2-propanol, and dry ice + water + CaCl₂ mixtures [19,36,46,54]. Multiple traps in series have been used where cooling and separation in a single trap was deemed insufficient [35,54].

After phase separation is finished the vapour and especially liquid components may require further analysis. To what extent this is required depends on the nature and number of species involved in the study. In binary systems, each sample may separate into a vapour and liquid fraction containing a single species each, but in ternary and higher systems, the condensed fraction obtained from each sample will often contain two species. If one component is present in the condensed fraction, weighing the collection vessel to determine the condensed mass is sufficient [21,46]. However, if the condensed fraction contains two or more species, further analysis is required. Additional analysis via gas chromatography [30,32,40,41,43], Karl Fischer titration [19,35,54] and ultraviolet-visible (UV-Vis) spectrometry [48,49] have been used. It is common to assume the vapour fraction removed from a sample contains a single species only [32]. As such, compositional analysis is not required and the vapour mass can be calculated via:

- The measurement of water displacement [35,36].
- The use of wet and dry test gas meters [32,39,40,43,44,46].
- The measurement of pressure increase in a calibrated vessel [21,23,30,40,54,59].

Advantages of using phase separation via a sample trap include:

- In binary systems particularly, the use of expensive chromatographic equipment is avoided.
- The analysis of samples containing species of greatly differing molecular size is simplified because small and large molecules do not pass through the same analysis pathway.
- In binary systems particularly, analysis could be performed faster since potentially lengthy chromatographic column retention times are avoided.

Disadvantages of using phase separation via a sample trap include:

- Sampling, and the problems associated therewith, is unavoidable (refer to Section 2.2.3).
- Compared to direct GC analysis, larger sample volumes are required and if high-value species are studied, experimental cost may become a limiting factor.
- The assumptions that no heavy species remain in the vapour phase and no light species remain dissolved in the condensed phase may lead to erroneous results.

2.2.5.3 *In situ spectroscopic analyses*

Direct chromatographic analysis (Section 2.2.5.1) and phase separation in a sample trap (Section 2.2.5.2) require sampling and are therefore classified as intrusive analysis methods. Non-intrusive or in-situ analysis methods, which do not require sampling, have been developed and are gaining in popularity but the use thereof remains the exception. Near-infrared (NIR), mid-infrared (MIR) and UV-Vis spectroscopy have been used as in-situ analysis methods in phase equilibria and solubility studies related to the chemical, natural

gas and, especially, polymer industries. In the latter case, studies often investigate sorption rates and according to Yurekli and Altinkaya [93], experimental methods based on IR spectroscopy are now favoured above the conventional methods based on gravimetric and volumetric sorption. In-situ spectroscopic phase composition analysis has been used in conjunction with static and circulation methods⁴ at various combinations of high and moderate temperatures and pressures [84,93,95-110]. Some of the different techniques utilised include Raman, Fourier Transform infrared (FTIR), Nuclear Magnetic Resonance (NMR) and Attenuated Total Reflectance infrared (ATR IR) spectroscopy. Advantages of using in situ spectroscopic analysis include:

- The ability to gain molecular level insight [97].
- The ability to investigate highly viscous systems [95].
- Non-destructive analysis results in lower material costs.
- No adsorption to un-equilibrated surfaces during sampling [98].
- Analysis is performed without disturbance of equilibrium conditions [98].
- Sampling, and the problems associated therewith, are avoided (refer to Section 2.2.3).

Disadvantages of using in situ spectroscopic analysis include:

- Calibrations are sophisticated and lengthy [95,111].
- Analysis accuracy is often temperature dependent [100].
- Calibrations are temperature-specific which further increases the complexity thereof [95,111].
- Molecular interactions at high temperatures or high pressures may affect the IR spectra and preventative measures are required to ensure accuracy of analysis [99].
- Spectroscopy is a specialised field and a difference in background between phase equilibria and spectroscopic specialists may complicate the equipment design and commissioning processes.

2.2.6 Injection, compression, pressure control and measurement

Injection, compression and pressure control, as defined in this context, refer to processes occurring at different times in the experimental procedure. Injection (delivering species to the cell chamber) and compression (obtaining the initial pressures required) occur at the beginning of an experimental run whilst pressure control (increasing and fine tuning pressure between experimental conditions) occurs throughout an experimental run. In most cases these processes are inextricable and, as such, they are discussed simultaneously. The requirements for static and circulation (closed) systems differ from those for continuous and semi-flow (open) systems and are discussed separately. Pressure measurement is an important aspect of pressure control and is covered toward the end of this section.

⁴ Spectroscopic analysis applied in flow systems [49,94] are not classified as in-situ because the setup possesses open boundaries.

2.2.6.1 Circulation and static systems

Most synthetic and analytic equipment of the static and circulation type operates pseudo-isothermally with temperature adjusted in an incremental manner. In synthetic equipment, pressure is varied to identify bubble, dew or critical-points at each temperature set point. In analytical equipment, pressure is adjusted incrementally to enable equilibration, phase separation and sampling at a number of pressures for every temperature set point. This approach favours metallic high-pressure equilibrium cells where large wall thicknesses equate to large thermal masses. For these methods, which both comprise an enclosed environment, system pressure is a function of volume, temperature and the amount of species.

In phase equilibria studies that involve components of which at least one is a gas and one is a liquid at normal temperature and pressure, the following procedure is common: liquids are inserted in the cell at atmospheric pressure, the cell is closed and gaseous species are injected until the desired pressure is reached [24,28,31,32,36,56,66]. Measurements would often start at a low pressure and move on to subsequently higher pressures by injecting additional gaseous species. Thus, the injection of species is used to achieve both compression and pressure control.

The liquefaction of gaseous species, a form of temperature control in itself, has been used to obtain high pressures within an equilibrium cell. Upon an increase in temperature these liquefied species vaporise resulting in increased pressure. Vaporisation directly within the equilibrium cell is normally used during initial compression only [35,59,68,69] whilst expansion within an additional high-pressure container, referred to as a thermal compressor, enables greater control and is used for both initial compression and pressure control [23,33,37].

Hand pumps are relatively inexpensive piston-cylinder devices used for initial compression and pressure control via the injection of liquids or gases at high pressure [30,33,46,56,63-66,68-70]. These pumps, of which an example is shown in Fig. 2-8, enable small pressures adjustments and, in turn, accurate pressure control [56,69].



Figure 2-8. An example of a hand pump. [Image reprinted with permission from SITEC-Sieber Engineering AG]

In addition to thermal compressors and hand pumps, a variety of equipment has been used to achieve initial compression and pressure control via the injection of species. Examples are listed below but unfortunately literature contains little information on the benefits and limitations of these units:

- HPLC pumps to feed liquids [28].
- Pneumatic pumps to feed gases [62].
- Diaphragm pumps to feed liquids [65].
- Double cylinder proportioning pumps to feed liquids [60].
- Metering syringe pumps to feed liquids and gases [19,20,36].
- Positive displacement pumps to feed liquids and gases [18,24,26].
- Manual, reciprocating and membrane compressors to feed gases [19,23,28,32,56,70].

Changes to bulk composition and feed lines that could create dead volume and therefore solute losses are two negative aspects associated with the injection of additional species to achieve pressure control. To mitigate the latter, Lhoták and Wichterle [24] and Chylinski et al. [60] have suggested the use of check valves located within feed lines, or inlet valves protruding into the cell cavity. These problems notwithstanding, the ability to inject any species and remove any phase during an experimental run greatly enhances equipment versatility and operational efficiency [37].

Variable volume equilibrium cells are useful for manipulating pressure during an experimental run and are frequently used [17,21,32,36,38,46,75,112]. This usually involves a piston-cylinder construction and in some cases a form of pressure intensification is incorporated. Gases are the more popular pressurising media but the use of liquid water and mercury, which are less susceptible to temperature expansion and contraction, has been reported [32,46]. Kühne et al. [7] and Raeissi and Peters [8] used mercury as an intermediate pressure transmitter between the hydraulic oil and the sample itself. Advantages of using a variable volume equilibrium cell include:

- The ability to adjust system pressure without altering bulk composition.
- The piston forms part of the cell chamber and, as such, pressure increases do not expose the cell to dead volume, and solute losses into feed lines cannot occur.

However, variable volume cells present the following disadvantages:

- Increased complexity of design.
- Leakages may occur around the piston device.
- Piston seal replacement or maintenance may hamper experimental efficiency.
- Piston seal friction may lead to erratic pressure propagation between the pressure control and equilibrium chambers. This, in turn, may disrupt equilibrium conditions.

2.2.6.2 *Continuous and semi-flow systems*

In contrast to their static and circulation counterparts, continuous and semi-flow systems have open boundaries. In continuous-flow systems, all species are fed to the cell on a continuous basis whilst in semi-flow systems, liquid species are normally loaded in the cell at atmospheric pressure before feeding of the pressurised gas commences. A variety of pumps and compressors have been used to inject high-pressure liquids and gases in continuous and semi-flow systems. Examples are listed below but literature on the benefits and limitations of these units, as applied in this context, is lacking:

- Piston pumps to feed liquids [44].
- Non-pulsating pumps to feed liquids [40,41,52,53].
- Syringe pumps to feed liquids and gases [16,48].
- Diaphragm pumps to feed liquefied gases [44].
- Positive displacement metering pumps to feed liquids [45].
- Electrical and thermal compressors to feed gases and liquefied gases [39,40,50].

Pressure control during operation is primarily achieved by one of the following methods:

- The use of back-pressure regulators [40-42,44,46,51-53].
- Adjusting the temperature of a thermal compressor located in the feed line [39,50].
- Adjusting the outlet pressure of an electrical compressor located in the feed line [39,50].
- Adjustment of micrometering valves (see Fig. 2-7) in effluent outlet lines [16,43-45,48].

2.2.6.3 *Pressure measurement*

It is important to control the temperature at which pressure measurement equipment operates. If pressure is measured directly in the equilibrium cell, the transducer membrane is at the equilibrium temperature and condensation cannot occur [58]. If this is not the case cooling and condensation can occur before the transducer membrane resulting in faulty measurements. The pressure transducers used by Silva-Oliver et al. [31] and Jennings and Shucker [46] were connected to the equilibrium cell with heated capillary tubing. Pressure transducers are often placed in a dedicated temperature-regulated environment with the latter maintained at a constant temperature which is higher than the highest experimental temperature [24,29,34,57]. According to Lhoták and Wichterle [24], the transducer inlet should be positioned as close as possible to the cell outlet so as to minimise dead volume. A transducer with the front membrane thereof flush with the cell inner wall negates this problem [38,58,75].

2.2.7 Temperature control

The quality of temperature control has a significant impact on the quality of the experimental data. Whereas Section 2.2.4 focuses on sample temperature control during and after the sampling procedure, this section discusses temperature control in the equilibrium cell during equilibration. In this sense, temperature control is typically achieved through the use of constant temperature baths, inline preheating and cooling coils, heating and cooling jackets and electrical heating tape. Phase equilibria studies have been conducted at sub-ambient temperatures but the majority of research is focused on phase behaviour at elevated temperatures and, as such, require heating.

Static and dynamic methods often utilise a constant temperature bath for temperature control. Gases and liquids are used as heat transfer media, with air, N₂, oil, water, refrigerants, glycol, ethanol and ethanol aqueous mixtures being popular choices [22,24-26,29-33,35,36,40,43-46,54-56,60-63,65,66,68-70,113-117]. Gaseous heat transfer media are low in weight and enable ease of operation. Air is freely available while N₂ has the added advantage of creating a non-explosive environment [46,60]. Given their weight, liquid baths are often cumbersome to handle but if designed appropriately they can serve as a moderate shock buffer. The thermostatic bath heat transfer medium may impact visual observation of the cell interior and, in this sense, gases are less likely than liquids to create distortion. The heat capacity of the heat transfer medium requires consideration. Compared to low-heat capacity media, high-heat capacity media require extended equilibration periods but usually offer superior temperature stability. If suitably designed, thermostatic baths enable simultaneous and uniform temperature control of all auxiliary equipment and not only the equilibrium cell. Valve operation from outside the thermostatic bath, either via valve extensions or automation, is necessary to prevent temperature disturbances.

All thermostatic baths, irrespective of the medium used, require a circulation device and some form of insulation. Circulation or stirring of the heat transfer medium reduces thermal gradients inside the bath [22]. Fans or blowers are typically used to circulate gaseous media in a forced convection bath [30,63,65,66,69]. Radiation effects from an electrical element can be eliminated by positioning a thermal block between the element and equilibrium cell [22,30,56]. Liquid baths usually contain a stirrer or circulation pump, with the former being more popular. To improve temperature uniformity, Chylinski et al. [60] bubbled N₂ through a diffuser box located on the bottom of their oil bath.

Insulating a thermostatic bath improves the stability of temperature control and, in this regard, cork, rock wool or fibreglass and double-paned windows are often used [22-24,31,70]. Mühlbauer and Raal [22] also applied a copper lining to the interior of their bath walls to further promote a uniform temperature environment. Visual observation of the cell chamber (Section 2.2.8) requires the use of partially-

transparent bath wall and insulation, an aperture in the bath wall or a camera. Visibility baths, fitted with double-glazed windowed panels, are used extensively in phase equilibria studies.

The majority of continuous and semi-flow systems make use of inline heating or cooling coils either exclusively or in addition to thermostatic baths [39-43,45,46,48,49,51-53]. These coils increase residence time in the thermo-regulated environment enabling species to reach thermal equilibrium.

Heating and cooling jackets, which ensure continuous contact between the equilibrium cell and a circulated temperature controlled fluid, are popular choices [18,21,38,64,70,75,118,119]. The use of electrical heating tape is usually restricted to sampling capillaries, circulation lines and GC connecting lines but a few studies have used heating tape to heat the equilibrium cell itself [41,42].

2.2.8 Observation windows and transparent equilibrium cells

Exterior observation windows and transparent equilibrium cells of borosilicate, sapphire or Pyrex are used frequently in phase equilibria studies of the static, circulation and flow type [21,25,29,31,33,38,41-43,45,55,57-59,64,67,68,70,72,74,75]. Chylinski et al. [60] developed an unusual setup which involved a borescope and video camera inserted in a glass tube protruding into the cell interior. Unfortunately, video images were of poor quality and required digital processing. Regardless the experimental method, the ability to see the cell interior during operation contributes to equipment versatility [43].⁵ In addition, visual observation of the cell chamber is important to [29,31,33,68,74]:

- Observe the formation and behaviour of unexpected additional phases.
- Ensure circulation of and sampling from the correct phase in a multi-phase system.
- Identity the onset of a two-phase region, or determine if the mixture critical point is reached.
- Monitor mass transfer during the approach to equilibrium, and the progression of phase settling.

However, a windowed equilibrium cell design presents a number of challenges [60,56,102]:

- Ensuring sealing integrity could be challenging and costly.
- The window and the windowed area may increase the risk of mechanical failure.
- Slow heating of the cell is necessary to prevent thermal stresses on glass windows.
- Compatibility with a thermostatic bath requires a transparent bath medium and window.
- The use of observation windows increases both construction cost and complexity of design.

⁵ Many of the learnings from this study, and particularly those communicated in Chapter 4, would not have been possible without the ability to see the cell interior.

Cameras, endoscopes and borescopes are often used together with observation windows [38,41,42,46,75]. This frees up the operator, enables video recording and nullifies the risk of having to look directly at the window. The use of two or more windows not only enlarges the visible zone but is reported to eliminate the need for an additional light source and, as such, this approach is popular [21,25,29,31,33,55,57-59,64,65,67,68,70,72]. Using a transparent borosilicate, sapphire or Pyrex tube within the equilibrium cell offers similar advantages but often restricts the cell geometry.

2.2.9 Degassing of liquids and solids

Van Ness and Abbott [120] define degassing as the removal of highly volatile components from a relatively non-volatile liquid. Degassing is an important step in phase equilibria studies and may occur either before or after feeding the liquid species to the equilibrium cell.

Degassing before liquid injection is popular [16,18,34,55] with the methods developed by Van Ness and Abbott [120] and Battino et al. [121] particularly so [26,29,31,33,37,74,122]. The former achieved degassing with minimal liquid losses by exposing the slow-boiling liquid to vacuum via a condenser and fine capillary. The latter degassed by employing magnetic stirring and periodic exposure, via a condenser to minimise liquid losses, to vacuum. Another method suited for degassing of liquids and solids repeatedly exposes the species to a freezing, vacuum extraction and melting cycle [123-126]. Degassing prior to species injection or loading generally requires a sizable quantity of solids or liquids and is therefore not well-suited for studies involving high-cost components.

Where high-value chemicals are studied, degassing after injection or loading is beneficial and frequently used [38,46,56,57,60,75,127,128]. This normally involves a series of vacuum extractions coupled with pressure monitoring, visual observation or weighing of the equilibrium cell to ensure negligible solute losses. In this sense, analytical methods enables flexibility since stoichiometric loading is less critical, albeit helpful, and volatile impurities, if present, can be detected during subsequent phase composition analysis.

2.2.10 Mechanical design and construction

This section briefly covers materials of construction, cell geometry and volume, and dead volume. Table 2-2 lists different equilibrium cell materials of construction that have been used in phase behaviour studies.

Table 2-2. Equilibrium cell materials of construction used in phase behaviour studies

Materials of construction	Reference
Stainless Steel	[26,35,43,50,54,55,58,59,69]
316 Stainless Steel	[40,57,68]
321 Stainless Steel	[60]
Non-magnetic Stainless Steel	[37,70]
Hastelloy	[18,34,41,42]
Titanium	[31]
Sapphire	[30]
Pyrex	[7,8]
Tempered kovar glass	[24]

Cell geometry could affect the accuracy of experimental data in the mixture critical region where the densities of coexisting phases differ only marginally and phase separation via gravity is ineffective. This is particularly applicable to the zone surrounding the phase interface where cross-contamination may occur. A vertically orientated equilibrium cell will aid phase separation and may improve the accuracy of experimental data by enabling larger vertical separation between the liquid and vapour sample points.

Cell geometry also affects liquid species recovery and cell cleaning. The cell design should enable maximum recovery of liquid compounds after completion of a run, whilst efficient and effective cell cleaning will reduce experimental time and the risk of residual contaminants.

Equilibrium cell volume is an important consideration. Larger cell volumes generally improve experimental accuracy [38] but also increase operational costs. Furthermore, enlarging the cell volume will contribute toward mitigating the impact of sampling on equilibrium pressure.

Given the importance of mixing (see Section 2.2.1), dead volume in the cell chamber should be minimised. Dead volume could arise due to holes drilled through the cell wall to accommodate thermocouples, pressure sensors and inlet valves. Compared to small equilibrium cells, larger cell volumes require more aggressive mixing over a prolonged period of time to achieve mass transfer equilibrium.

2.3 ADDITIONAL THERMODYNAMIC AND PHYSICAL PROPERTIES

Phase equilibria studies typically focus on the measurement of bubble, dew and critical-point data or equilibrium phase compositions. However, an increasing number of studies are more holistic in approach and also focus on generating additional thermodynamic and physical properties to support the development of more accurate and robust predictive models. These properties, among which excess molar enthalpy, speed of sound, interfacial tension and density, have an important function to fulfil in the continued drive toward improved high pressure process design and control. Equipment for the measurement of these properties is not the focus of this review. However, opportunities may exist to incorporate the measurement of two or more data types within one experimental apparatus. To exploit such opportunities it is important that they be identified and considered early in the equipment design process.

2.3.1 *Excess molar enthalpy*

Excess molar enthalpies are determined via heat of mixing measurements and, if used in conjunction with VLE data, present a powerful platform for thermodynamic model development [129,130]. According to Pérez et al. [131], excess molar enthalpy plays a vital role in the design and scale-up of extraction processes. As such, heats of mixing were measured to complement existing VLE data. According to Gragante et al. [18], limited thermodynamic knowledge of a process prohibits the optimisation of overall efficiency and energy consumption, and to address this shortfall they measured heats of mixing and excess molar enthalpies. Zhang et al.'s [132] justification for measuring excess molar enthalpy is the fundamental role thereof in designing and developing industrial processes. In all of these cases an isothermal flow calorimeter was used in an experimental setup independent of, and unrelated to, the phase equilibria setup.

2.3.2 *Speed of sound*

Speed of sound or sound velocity is a thermodynamic property often measured by research groups in the petrochemical and polymer-related industries, and the full value thereof is realised through derived properties, notably isentropic compressibility and excess isentropic compressibility [133]. Sound velocity measurements are performed because the data and accompanying derived properties:

- Aid in the design and operation of equipment in the petroleum industry [134]
- Provide information on thermo-physical properties of chemical substances and their mixtures, enabling the development of accurate theoretical models [135,136].

- Enable identification of the structure and nature of molecular interactions within a polymer solution, and the differences between polymer solution and ideal solution behaviour [137,138].

The pulse-echo-overlap technique [133,136,139,140] and units by Anton Paar [130] are popular for sound velocity measurements. These methods are generally not compatible with the phase equilibria equipment discussed thus far and, as such, an independent experimental setup is required. Although the exception at present, sound velocity data have been measured at pressures up to as high as 100 MPa [136,139-141].

2.3.3 *Interfacial tension*

Interfacial tension is an important parameter in chemical and petroleum reservoir applications [142-144]. It impacts the efficiency of petroleum recovery processes [145,146] and product quality in the coatings and agrochemical industries [142]. In addition, interfacial tension assists in understanding and controlling polymer-gas systems [147] and developing new equations of state [66]. Interfacial tension is measured experimentally or determined via numerical estimates with the well-documented gradient theory of fluid interfaces, with the latter being a very cost-effective approach [142,144]. The photographic pendant drop technique is often used for interfacial tension measurements. This method is well-established, convenient, well-documented and versatile [143,148]. It is suitable for high pressure applications and has been used to quantify interfacial tensions at pressures as high as 280, 160 and 130 bar [66,143,148].

2.3.4 *Density*

Phase-specific density measurements are the most common of the four properties discussed in Section 2.3, and a number of research groups have measured the densities of co-existing equilibrium phases during an analytical phase equilibria experiment [9,60,64,66,70,73,149]. All of these studies used vibrating tube densimeters located within vapour and liquid circulation lines. According to Chylinski et al. [60], incorporating densimeters into circulation lines is essential to avoid cold points and saturated vapour phases inside the vibrating tube. The vibrating tube densimeter is well-suited for rapid and accurate density measurements over wide temperature and pressure ranges but it requires calibrations with a fluid of known density [150]. To prevent pulsation disturbances, density measurements are typically conducted with circulation pumps switched off [64,66,70,73]. However, Chylinski et al. [60] found disturbances to be negligible and conducted measurements in the presence of circulation. In addition to being equilibrium indicators, high pressure densities of co-existing phases are required to [60,66,137,138,150,151]:

- Enable hydrodynamic characterisation of the system.
- Evaluate existing and develop new equations of state.

- Determine excess molar volumes, Gibbs potential, isentropic compressibility and thermal expansion coefficients in order to better understand molecular interaction effects.

2.4 EQUIPMENT EVALUATION AND CONCEPTUAL DESIGN

Based on the review presented in this chapter, two conceptual equipment designs were considered. Concept 1 was a dynamic analytical system with dual-phase circulation whilst concept 2 was a static analytical system. Characteristics of these alternatives are listed in Table 2-3.

Table 2-3. Characteristics of two conceptual designs considered

Parameter	Concept 1	Concept 2
• Classification: Level 1	Analytic	Analytic
• Classification: Level 2	Dynamic	Static
	Dual phase circulation	
• Sampling	2 × GC / HPLC switch valves	2 × ROLSI™
• Analysis	Online GC	Online GC
• Temperature control	Air bath, heating element & fan	Heating jacket & fluid circulator
• Additional data measured	1 × Vibrating U-tube densimeter	None
• Mixing / phase movement	2 × Circulation pumps	Magnetic stirring
	Magnetic stirring	
• Variable cell volume	Yes	Yes
• Variation of sampling height	No	Yes
• Equilibrium cell orientation	Vertical	Horizontal
• Sight glass quantity	2	1

A schematic diagram of concept 1 is shown in Fig. 2-9. This design enables both counter and co-current circulation coupled with density measurements of both liquid and vapour phases utilising a single densimeter. The densimeter considered for this application was an Anton Paar DMA HPM, a modular unit consisting of a density measurement module and a separate evaluation unit. The density module enables operation at a maximum pressure and temperature of 1400 bar and 200 °C, but is not submersible.

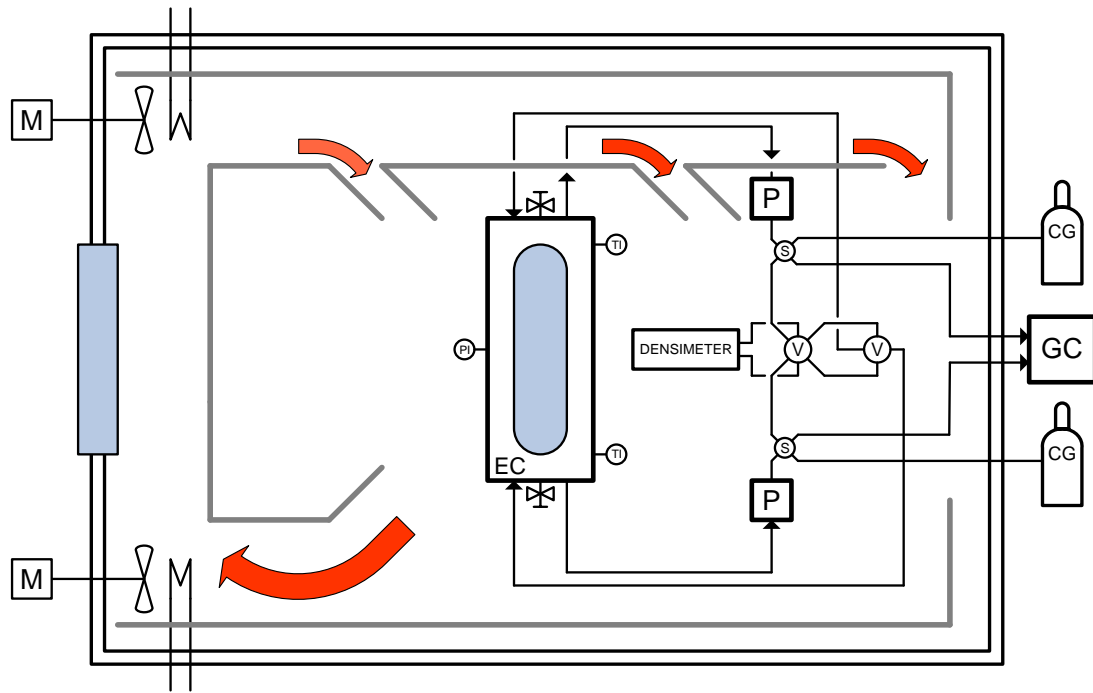


Figure 2-9. Schematic diagram of conceptual design 1

Routing of vapour and liquid phases is achieved by using two 6-port sampling valves with sample loops, one 6-port switch valve and one 4-port switch valve. This configuration is shown in Fig. 2-10 for the four possible circulation scenarios.

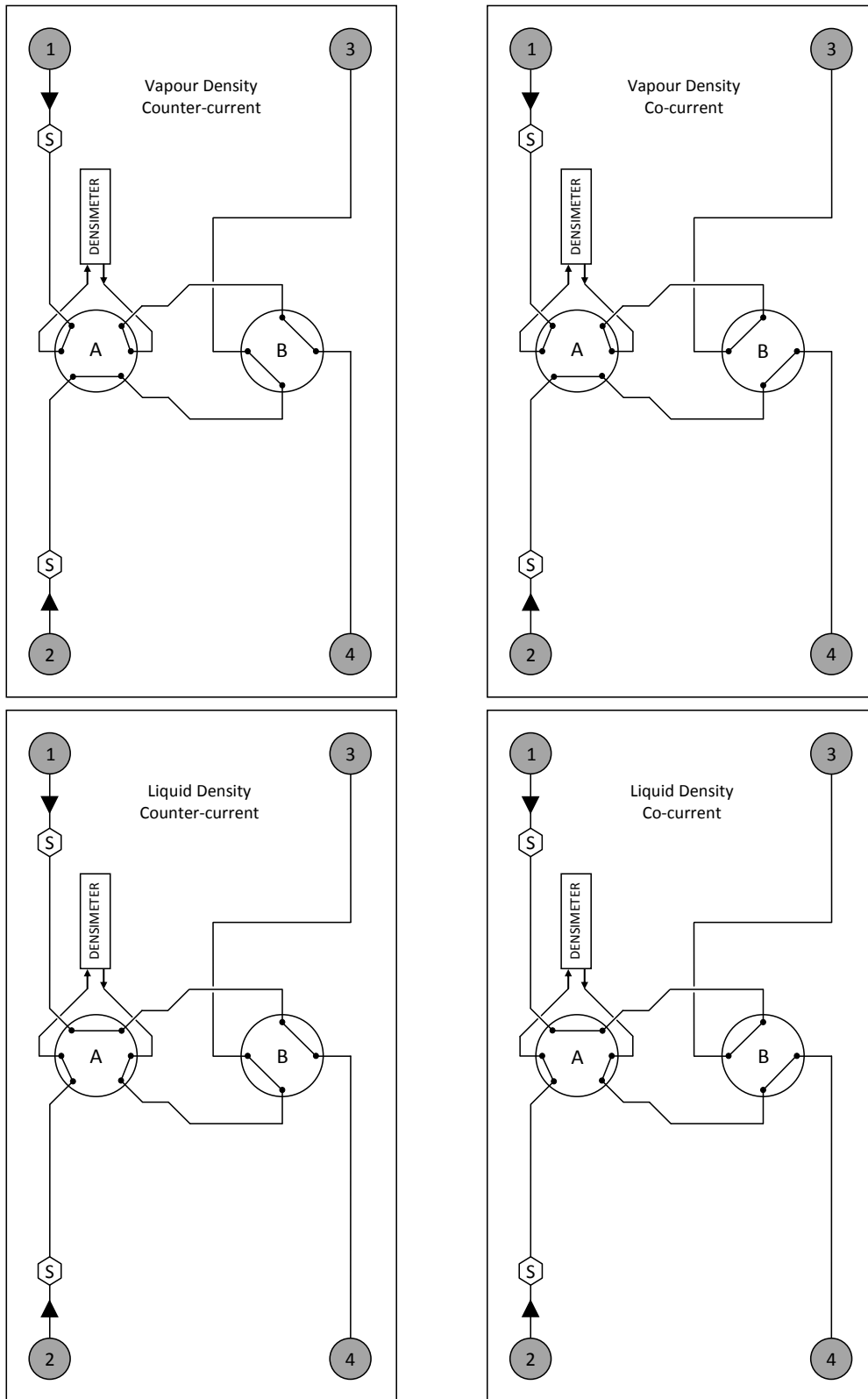


Figure 2-10. Routing of the vapour and liquid phase flows in conceptual design 1. Points 1 and 3 represent vapour phase exit and entry points whilst points 2 and 4 represent liquid phase exit and entry points. The hexagons labelled "S" indicate 6-port sampling valves.

For the “liquid density co-current” flow scenario from above, Fig. 2-11 illustrates the sample valve configuration during the final approach to equilibrium and sampling.

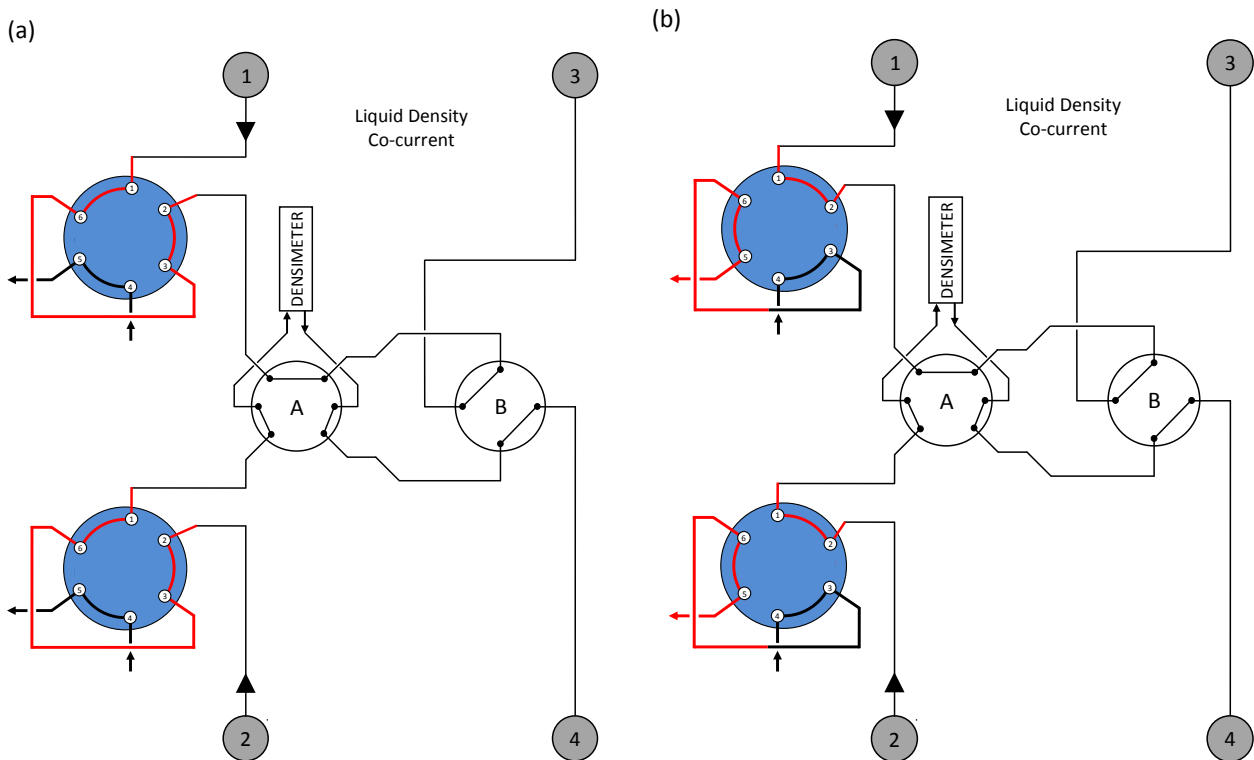


Figure 2-11. Sample valve configuration for the liquid density co-current circulation scenario during (a) the approach to equilibrium; and (b) sampling. The 6-port sample valves are shown in blue, points 1 and 3 refer to vapour phase exit and entry points, and points 2 and 4 refer to liquid phase exit and entry points.

Conceptual design 1 as outlined above represents a versatile setup with the benefit of being able to measure phase compositions and densities. However, two stumbling blocks were encountered:

- Two circulation pumps are needed to circulate the vapour and liquid phases. Uncertainty existed around the potential for and magnitude of pulsation disturbances and the impact this may have on measurements close to the mixture total solubility pressure. Suppliers were unfamiliar with the effect of a supercritical fluid on pump performance which further compounded the problem.
- Sampling and switch valves capable of withstanding the required pressure and temperature could be obtained but without any guarantee on performance or lifetime.

In light of the above, conceptual design 1 was abandoned in favour of conceptual design 2, which gave rise to the phase equilibria apparatus as communicated in Chapters 3 and 4.

2.5 REFERENCES

1. R.E. Fornari, P. Alessi, I. Kikic, High-Pressure Fluid-Phase Equilibria: Experimental Methods and Systems Investigated (1978-1987), *Fluid Phase Equilib.* 57 (1990) 1-33.
2. R. Dohrn, G. Brunner, High-Pressure Fluid-Phase Equilibria: Experimental Methods and Systems Investigated (1988-1993), *Fluid Phase Equilib.* 106 (1995) 213-282.
3. M. Christov, R. Dohrn, High-pressure fluid phase equilibria: Experimental methods and systems investigated (1994-1999), *Fluid Phase Equilib.* 202 (2002) 153-218.
4. R. Dohrn, S. Peper, J.M.S. Fonseca, High-pressure fluid-phase equilibria: Experimental methods and systems investigated (2000-2004), *Fluid Phase Equilib.* 288 (2010) 1-54.
5. J.M.S. Fonseca, R. Dohrn, S. Peper, High-pressure fluid-phase equilibria: Experimental methods and systems investigated (2005-2008), *Fluid Phase Equilib.* 300 (2011) 1-69.
6. F.C.v.N Fourie, C.E. Schwarz, J.H. Knoetze, Considerations for the Design of High-Pressure Phase Equilibrium and Solubility Measurements Equipment, in: M.R. Belinsky (Ed.), *Supercritical Fluids*, Nova Publishers, New York, 2010, Ch.6.
7. E. Kühne, E. Saez Calvo, G.J. Witkamp, C.J. Peters, Fluid phase behaviour of the ternary system bmim[BF₄] + 1-(4-isobutylphenyl)-ethanol + carbon dioxide, *J. Supercrit. Fluids* 45 (2008) 293-297.
8. S. Raeissi, C.J. Peters, Experimental determination of high-pressure phase equilibria of the ternary system carbon dioxide + limonene + linalool, *J. Supercrit. Fluids* 35 (2005) 10-17.
9. C. Bouchot, D. Richon, Direct Pressure-Volume-Temperature and Vapor-Liquid Equilibrium Measurements with a Single Equipment Using a Vibrating Tube Densimeter up to 393 K and 40 MPa: Description of the Original Apparatus and New Data, *Ind. Eng. Chem. Res.* 37 (1998) 3295-3304.
10. Y. Kayukawa, M. Hasumoto, Y. Kano, K. Watanabe, Liquid-Phase Thermodynamic Properties for the Binary and Ternary Systems of Propane (1), *n*-Butane (2), and Isobutane (3), *J. Chem. Eng. Data* 50 (2005) 565-578.
11. T. Takagi, T. Sakura, T. Tsuji, M. Hongo, Bubble point pressure for binary mixtures of difluoromethane with pentafluoroethane and 1,1,1,2-tetrafluoroethane, *Fluid Phase Equilib.* 162 (1999) 171-179.
12. A.R.H. Goodwin, J.B. Mehl, M.R. Moldover, Reentrant radio-frequency resonator for automated phase-equilibria and dielectric measurements in fluids, *Rev. Sci. Instrum.* 67,12 (1996) 4294-4303.
13. E.F. May, T.J. Edwards, A.G. Mann, C. Edwards, An improved microwave apparatus for phase behaviour measurements in lean gas condensate fluids, *Fluid Phase Equilib.* 215 (2004) 245-252.
14. S.J. Abedi, H.-Y. Cai, S. Seyfaie, J.M. Shaw, Simultaneous phase behaviour, elemental composition and density measurement using X-ray imaging, *Fluid Phase Equilib.* 158-160 (1999) 775-781.
15. D.J. Rosenthal, A.S. Teja, The critical properties of *n*-alkanes using a low-residence time flow apparatus, *AIChE J.* 35 (1989) 1829-1834.

16. S. Horstmann, K. Fischer, J. Gmehling, Experimental determination of critical data of mixtures and their relevance for the development of thermodynamic models, *Chem. Eng. Science* 56 (2001) 6905-6913.
17. M. Du Rand, High pressure fluid phase equilibria, Masters Thesis in Chemical Engineering, Stellenbosch University, South Africa, 2000.
18. M. Grigante, P. Stringari, G. Scalabrin, E.C. Ihmels, K. Fischer, J. Gmehling, (Vapour + liquid + liquid) equilibria and excess molar enthalpies of binary and ternary mixtures of isopropanol, water, and propylene, *J. Chem. Thermodyn.* 40 (2008) 537-548.
19. G. Brunner, A. Steffen, R. Dohrn, High-pressure liquid-liquid equilibria in ternary systems containing water, benzene, toluene, *n*-hexane and *n*-hexadecane, *Fluid Phase Equilib.* 82 (1993) 165-172.
20. D. Fu, X. Sun, Y. Qiu, X. Jiang, S. Zhao, High-pressure phase behavior of the ternary system CO₂ + ionic liquid [bmim][PF₆] + naphthalene, *Fluid Phase Equilib.* 251 (2007) 114-120.
21. C. Secuianu, V. Feroiu, D. Geana, High-Pressure Vapor-Liquid Equilibria in the System Carbon Dioxide and 2-Propanol at Temperatures from 293.25 K to 323.15 K, *J. Chem. Eng. Data* 48 (2003) 1384-1386.
22. A.L. Mühlbauer, J.D. Raal, High-Pressure Vapor-Liquid Equilibria in the Propane-1-Propanol System, *AIChE J.* 39,4 (1993) 677-688.
23. U. Wäterling, D. Zheng, H. Knapp, Vapour-Liquid Equilibria at High Temperatures and Pressures in Binary Mixtures Containing H₂, CH₄ and CO₂ with High Boiling Hydrocarbons: Experimental Equipment and Results, *Chem. Eng. Process.* 29 (1991) 155-164.
24. V. Lhoták, I. Wichterle, Vapour-liquid equilibria in the ethane-*n*-butane system at high pressures, *Fluid Phase Equilib.* 6 (1981) 229-235.
25. Z. Wagner, I. Wichterle, High-pressure vapour-liquid equilibrium in systems containing carbon dioxide, 1-hexene, and *n*-hexane, *Fluid Phase Equilib.* 33 (1987) 109-123.
26. L.M. Lozano, E.A. Montero, M.C. Martin, M.A. Villamanan, Vapor-liquid equilibria of binary mixtures containing methyl tert-butyl ether (MTBE) and/or substitution hydrocarbons at 298.15 K and 313.15 K, *Fluid Phase Equilib.* 110 (1995) 219-230.
27. P. Marteau, J. Obriot, A. Barreau, V. Ruffier-Meray, E. Behar, Experimental determination of the phase behavior of the binary mixtures: methane-hexane and methane-benzene, *Fluid Phase Equilib.* 129 (1997) 285-305.
28. S. Winkler, K. Stephan, Fluid multiphase behavior in ternary mixtures of CO₂, H₂O and 1-butanol, *Fluid Phase Equilib.* 137 (1997) 247-263.
29. L.A. Galicia-Luna, A. Ortega-Rodriguez, D. Richon, New Apparatus for the Fast Determination of High-Pressure Vapor-Liquid Equilibria of Mixtures and of Accurate Critical Pressures, *J. Chem. Eng. Data* 45 (2000) 265-271.

30. M. Vázquez da Silva, D. Barbosa, High pressure vapor–liquid equilibrium data for the systems carbon dioxide/2-methyl-1-propanol and carbon dioxide/3-methyl-1-butanol at 288.2, 303.2 and 313.2 K, *Fluid Phase Equilib.* 198 (2002) 229-237.
31. G. Silva-Oliver, G. Elosa-Jiménez, F. García-Sánchez, J.R. Avendaño-Gómez, High-pressure vapor–liquid equilibria in the nitrogen–*n*-pentane system, *Fluid Phase Equilib.* 250 (2006) 37-48.
32. A. Paiva, K. Gerasimov, G. Brunner, Phase equilibria of the ternary system vinyl acetate/(R,S)-1-phenylethanol/carbon dioxide at high pressure conditions, *Fluid Phase Equilib.* 267 (2008) 98-106.
33. H. Gardeler, K. Fischer, J. Gmehling, Experimental Determination of Vapor-Liquid Equilibrium Data for Asymmetric Systems, *Ind. Eng. Chem. Res.* 41 (2002) 1051-1056.
34. A. Chapoy, C. Coquelet, D. Richon, Measurement of the Water Solubility in the Gas Phase of the Ethane + Water Binary System near Hydrate Forming Conditions, *J. Chem. Eng. Data* 48 (2003) 957-966.
35. O. Pfohl, J. Petersen, R. Dohrn, G. Brunner, Partitioning of carbohydrates in the vapor-liquid-liquid region of the 2-propanol + water + carbon dioxide system, *J. Supercrit. Fluids* 10 (1997) 95-103.
36. Z. Zhang, W. Wu, Z. Liu, B. Han, H. Gao, T. Jiang, A study of tri-phasic behavior of ionic liquid–methanol–CO₂ systems at elevated pressures, *Phys. Chem. Chem. Phys.* 6 (2004) 2352-2357.
37. S. Laugier, D. Richon, New apparatus to perform fast determinations of mixture vapor-liquid equilibria up to 10 MPa and 423 K, *Rev. Sci. Instrum.* 57,3 (1986) 469-472.
38. C.E. Schwarz, The phase equilibria of alkanes and supercritical fluids, Masters Thesis in Chemical Engineering, Stellenbosch University, South Africa, 2001.
39. R. Eustaquio-Rincón, A. Trejo, Solubility of *n*-octadecane in supercritical carbon dioxide at 310, 313, 333, and 353 K, in the range 10–20 MPa, *Fluid Phase Equilib.* 185 (2001) 231-239.
40. H. Inomata, K. Arat, S. Saito, Measurement of vapour-liquid equilibria at elevated temperatures and pressures using a flow type apparatus, *Fluid Phase Equilib.* 29 (1986) 225-232.
41. Y. Shimoyama, M. Haruki, Y. Iwai, Y. Arai, Measurement and Prediction of Liquid-Liquid Equilibria for Water + Hexane + Hexadecane, Water + Toluene + Decane, and Water + Toluene + Ethylbenzene Ternary Systems at High Temperatures and Pressures, *J. Chem. Eng. Data* 47 (2002) 1232-1236.
42. M. Haruki, Y. Iwai, S. Nagao, Y. Yahiro, Y. Arai, Measurement and Correlation of Phase Equilibria for Water + Hydrocarbon Systems near the Critical Temperature and Pressure of Water, *Ind. Eng. Chem. Res.* 39 (2000) 4516-4520.
43. J.A. Briones, J.C. Mullins, M.C. Thies, B.U. Kim, Ternary phase equilibria for acetic acid–water mixtures with supercritical carbon dioxide, *Fluid Phase Equilib.* 36 (1987) 235-246.
44. N.E. Durling, O.J. Catchpole, S.J. Tallon, J.B. Grey, Measurement and modelling of the ternary phase equilibria for high pressure carbon dioxide–ethanol–water mixtures, *Fluid Phase Equilib.* 252 (2007) 103-113.

45. A.M. Beard, J.C. Mullins, C.H. Barron, G.A. Daniels, Vapor-Liquid Phase Equilibrium at High Pressures for the Ethane-Trinormalbutylaluminum and Ethane-Trinormalhexylaluminum Systems, *Fluid Phase Equilib.* 116 (1996) 429-436.
46. D.W. Jennings, R.C. Schucker, Comparison of High-Pressure Vapor-Liquid Equilibria of Mixtures of CO₂ or Propane with Nonane and C₉ Alkylbenzenes, *J. Chem. Eng. Data* 41 (1996) 831-838.
47. D. Dimitrelis, J.M. Prausnitz, Solubilities of *n*-Octadecane, Phenanthrene, and *n*-Octadecane/Phenanthrene Mixtures in Supercritical Propane at 390 and 420 K and Pressures to 60 bar, *J. Chem. Eng. Data* 34,3 (1989) 286-291.
48. K. Khimeche, P. Alessi, I. Kikic, A. Dahmani, Solubility of diamines in supercritical carbon dioxide Experimental determination and correlation, *J. Supercrit. Fluids* 41 (2007) 10-19.
49. Y.P. Chen, Y.M. Chen, M. Tang, Solubilities of cinnamic acid, phenoxyacetic acid and 4-methoxyphenylacetic acid in supercritical carbon dioxide, *Fluid Phase Equilib.* 275 (2009) 33-38.
50. V. Uribe-Vargas, A. Trejo, Vapor-liquid equilibrium of nitrogen in an equimolar hexane + decane mixture at temperatures of 258, 273, and 298 K and pressures to 20 MPa, *Fluid Phase Equilib.* 220 (2004) 137-145.
51. H.S. Ghaziaskar, M. Nikraves, Solubility of hexanoic acid and butyl acetate in supercritical carbon dioxide, *Fluid Phase Equilib.* 206 (2003) 215-221.
52. Z. Huang, S. Kawi, Y.C. Chiew, Solubility of cholesterol and its esters in supercritical carbon dioxide with and without cosolvents, *J. Supercrit. Fluids* 30 (2004) 25-39.
53. Z. Huang, M. Feng, Y. Guo, J. Su, L. Teng, T. Liu, Y.C. Chiew, Ternary solubility of mixed cholesteryl esters in supercritical carbon dioxide, *Fluid Phase Equilib.* 272 (2008) 8-17.
54. R. Dohrn, A.P. Bunz, F. Devlieghere, D. Thelen, Experimental measurement of phase equilibria for ternary and quaternary systems of glucose, water, CO₂ and ethanol with a novel apparatus, *Fluid Phase Equilib.* 83 (1993) 149-158.
55. C.H. Cheng, Y.P. Chen, Vapor-liquid equilibria of carbon dioxide with isopropyl acetate, diethyl carbonate and ethyl butyrate at elevated pressures, *Fluid Phase Equilib.* 234 (2005) 77-83.
56. G.F. Chou, R.R. Forbert, J.M. Prausnitz, High-pressure Vapor-Liquid Equilibria for CO₂/*n*-Decane, CO₂/Tetralin, and CO₂/*n*-Decane/Tetralin at 71 .1 and 104.4 °C, *J. Chem. Eng. Data* 35,1 (1990) 26-29.
57. S.L. Outcalt, B.-C. Lee, A Small-Volume Apparatus for the Measurement of Phase Equilibria, *J. Res. Nat. Inst. Stand. Technol.* 109 (2004) 525-531.
58. K. Brudi, N. Dahmen, H. Schmieder, Partition Coefficients of Organic Substances in Two-Phase Mixtures of Water and Carbon Dioxide at Pressures of 8 to 30 MPa and Temperatures of 313 to 333 K, *J. Supercrit. Fluids* 9 (1996) 146-151.
59. R. D'souza, J.R. Patrick, A.S. Teja, High Pressure Phase Equilibria in the Carbon Dioxide – *n*-Hexadecane and Carbon Dioxide – Water Systems, *Can. J. Chem. Eng.* 66 (1988) 319-323.

60. K. Chylinski, M.J. Cebola, A. Meredith, G. Saville, W.A. Wakeham, Apparatus for phase equilibrium measurements at high temperatures and pressures, *J. Chem. Thermodyn.* 34 (2002) 1703-1728.
61. H. Chen, H. Chang, E.T.S. Huang, T. Huang, A New Phase Behavior Apparatus for Supercritical Fluid Extraction Study, *Ind. Eng. Chem. Res.* 39 (2000) 4849-4852.
62. Y. Kayukawa, F. Kenichi, Y. Higashi, Vapor-Liquid Equilibrium Properties for the Binary Systems Propane (1) + *n*-Butane (2) and Propane (1) + Isobutane (3), *J. Chem. Eng. Data* 50 (2005) 579-582.
63. W.R. Adams, J.A. Zollweg, W.B. Streett, S.S.H. Rizvi, New Apparatus for Measurement of Supercritical Fluid-Liquid Phase Equilibria, *AIChE J.* 34,8 (1988) 1387-1391.
64. M. Wendland, H. Hasse, G. Maurer, Multiphase High-Pressure Equilibria of Carbon Dioxide-Water-Isopropanol, *J. Supercrit. Fluids* 6 (1993) 211-222.
65. J. Seo, J. Lee, H. Kim, Isothermal vapor-liquid equilibria for ethanol and *n*-pentane system at the near critical region, *Fluid Phase Equilib.* 172 (2000) 211-219.
66. R.D. Shaver, R.L. Robinson Jr., K.A.M. Gasem, An automated apparatus for equilibrium phase compositions, densities, and interfacial tensions: data for carbon dioxide + decane, *Fluid Phase Equilib.* 179 (2001) 43-66.
67. B.C. Oh, Y. Kim, H.Y. Shin, H. Kim, Vapor-liquid equilibria for the system 1-propanol + *n*-hexane near the critical region, *Fluid Phase Equilib.* 220 (2004) 41-46.
68. M.M. Elbaccouch, M.B. Raymond, J.R. Elliott, High-Pressure Vapor-Liquid Equilibrium for R-22 + Ethanol and R-22 + Ethanol + Water, *J. Chem. Eng. Data* 45 (2000) 280-287.
69. C.H. Kwon, M.D. Seo, W.K. Kim, C.S. Lee, J.W. Kang, Vapor-Liquid Equilibrium for Carbon Dioxide + Isopropyl, Isobutyl, and Isoamyl Acetates, *J. Chem. Eng. Data* 52 (2007) 727-730.
70. J. Freitag, M.T. Sanz Diez, D. Tuma, T.V. Ulanova, G. Maurer, High-pressure multiphase behavior of the ternary systems (ethene + water + 1-propanol) and (ethene + water + 2-propanol) Part I: Experimental investigation, *J. Supercrit. Fluids* 32 (2004) 1-13.
71. Wendland, M. Hochdruckmehrphasengleichgewichte in ternären Gemischen aus Kohlendioxid, Wasser und einem organischen Lösungsmittel, Doctoral Dissertation, Universität Kaiserslautern, Germany, 1994.
72. S. Takishima, K. Saiki, K. Arai, S. Saito, Phase equilibria for CO₂-C₂H₅OH-H₂O system, *J. Chem. Eng. Jpn.* 19,1 (1986) 48-56.
73. H. Tanaka, M. Kato, Vapour-liquid equilibrium properties of carbon dioxide + ethanol mixture at high pressures, *J. Chem. Eng. Jpn.* 28,3 (1995) 263-266.
74. M.-J. Lee, L.-H. Tsai, G.-B. Hong, H.-m. Lin, Multiphase Coexistence for Aqueous Systems with Amyl Alcohol and Amyl Acetate, *Ind. Eng. Chem. Res.* 41 (2002) 3247-3252.
75. F.C.v.N. Fourie, C.E. Schwarz, J.H. Knoetze, Phase equilibria of alcohols in supercritical fluids Part I. The effect of the position of the hydroxyl group for linear C₈ alcohols in supercritical carbon dioxide, *J. Supercrit. Fluids* 47 (2008) 161-167.

76. W. Gao, R.L. Robinson Jr., K.A.M. Gasem, Solubilities of Hydrogen in Hexane and of Carbon Monoxide in Cyclohexane at Temperatures from 344.3 to 410.9 K and Pressures to 15 MPa, *J. Chem. Eng. Data* 46,3 (2001) 609-612.
77. J. Park, R.L. Robinson Jr., K.A.M. Gasem, Solubilities of Hydrogen in Aromatic Hydrocarbons from 323 to 433 K and Pressures to 21.7 MPa, *J. Chem. Eng. Data* 41 (1996) 70-73.
78. H. Najibi, A. Chapoy, H. Haghghi, B. Tohidi, Experimental determination and prediction of methane hydrate stability in alcohols and electrolyte solutions, *Fluid Phase Equilib.* 275 (2008) 127-131.
79. M. Drescher, O. Seidel, D. Geana, High pressure vapor-liquid equilibria in the ternary system orange peel oil (limonene) + ethanol + carbon dioxide, *J. Supercrit. Fluids* 23 (2002) 103-111.
80. B.A. Stradi, M.A. Stadtherr, J.F. Brennecke, Multicomponent phase equilibrium measurements and modeling for the allylic epoxidation of *trans*-2-hexen-1-ol to (2R,3R)-(+)-3-propyloxiranemethanol in high-pressure carbon dioxide, *J. Supercrit. Fluids* 20 (2001) 1-13.
81. A.-D. Leu, D.B. Robinson, Vapor-Liquid Equilibrium for Four Binary Systems, *J. Chem. Eng. Data* 44,3 (1999) 398-400.
82. P. Naidoo, D. Ramjugernath, J.D. Raal, A new high-pressure vapour-liquid equilibrium apparatus, *Fluid Phase Equilib.* 269 (2008) 104-112.
83. H. Madani, A. Valtz, C. Coquelet, A. Hassen Meniai, D. Richon, (Vapor + liquid) equilibrium data for (carbon dioxide + 1,1-difluoroethane) system at temperatures from (258 to 343) K and pressures up to about 8 MPa, *J. Chem. Thermodyn.* 40 (2008) 1490-1494.
84. A. Archane, L. Gicquel, E. Provost, W. Fürst, *Chem. Eng. Res. Des.* 86 (2008) 592-599.
85. T. Laursen, P. Rasmussen, S.I. Andersen, VLE and VLE Measurements of Dimethyl Ether Containing Systems, *J. Chem. Eng. Data* 47 (2002) 198-202.
86. S. Peper, R. Dohrn, Sampling from fluid mixtures under high pressure: Review, case study and evaluation, *J. Supercrit. Fluids* 66 (2012) 2-15.
87. J. Im, W. Bae, J. Lee, H. Kim, Vapor-Liquid Equilibria of the Binary Carbon Dioxide-Tetrahydrofuran Mixture System, *J. Chem. Eng. Data* 49 (2004) 35-37.
88. J.S. Lim, J.M. Jin, K.-P. Yoo, VLE measurement for binary systems of CO₂ + 1,1,1,2-tetrafluoroethane (HFC-134a) at high pressures, *J. Supercrit. Fluids* 44 (2008) 279-283.
89. Y. Yun, J. Im, M.S. Shin, Y.-W. Lee, H. Kim, Vapor-liquid equilibria of the 1,1-difluoroethane (HFC-152a) + isobutene system, *Fluid Phase Equilib.* 271 (2008) 34-37.
90. J.W. Kang, 2008, Discussion on high-pressure VLE [e-mail] (Personal communication, 21 August 2008).
91. P. Guilbot, A. Valtz, H. Legendre, D. Richon, Rapid on-line sampler-injector: a reliable tool for HT-HP sampling and on-line GC analysis, *Analisis* 28 (2000) 426-431.
92. D. Jerinić, J. Schmidt, K. Fischer, L. Friedel, Measurement of the triethylene glycol solubility in supercritical methane at pressures up to 9MPa, *Fluid Phase Equilib.* 264 (2008) 253-258.

93. Y. Yurekli, S.A. Altinkaya, Measurement of ternary polymer/solvent equilibrium data by vapor-phase infrared spectroscopy, *Fluid Phase Equilib.* 277 (2009) 35-41
94. A. Sane, S. Taylor, Y.-P. Sun, M.C. Thies, A semicontinuous flow apparatus for measuring the solubility of opaque solids in supercritical solutions, *J. Supercrit. Fluids* 28 (2004) 277-285.
95. M. Görnert, G. Sadowski, Phase-equilibrium measurement and modeling of the PMMA/MMA/carbon dioxide ternary system, *J. Supercrit. Fluids* 46 (2008) 218-225
96. M. Görnert, G. Sadowski, Phase-Equilibrium Measurements of the Polystyrene/Styrene/Carbon Dioxide Ternary System at Elevated Pressures Using ATR-FTIR Spectroscopy, *Macromol. Symp.* 259,1 (2007) 236-242.
97. N.H. Brantley, S.G. Kazarian, C.A. Eckert, In Situ FTIR Measurement of Carbon Dioxide Sorption into Poly(ethylene terephthalate) at Elevated Pressures, *J. Appl. Polym. Sci.* 77 (2000) 764-775.
98. W.J. Rogers, J.A. Bullin, R.R. Davison, R.E. Frazier, K.N. Marsh, FTIR Method for VLE Measurements of Acid-Gas-Alkanolamine Systems, *AIChE J.* 43,12 (1997) 3223-3231.
99. A. Stratmann, G. Schweiger, Fluid Phase Equilibria of Ethanol and Carbon Dioxide Mixtures with Concentration Measurements by Raman Spectroscopy, *Appl. Spectrosc.* 56,6 (2002) 783-788.
100. W. Böttinger, M. Maiwald, H. Hasse, Online NMR Spectroscopic Study of Species Distribution in MDEA-H₂O-CO₂ and MDEA-PIP-H₂O-CO₂, *Ind. Eng. Chem. Res.* 47 (2008) 7917-7926.
101. I. Swaid, D. Nickel, G.M. Schneider, NIR-spectroscopic investigations on phase behaviour of low-volatile organic substances in supercritical carbon dioxide, *Fluid Phase Equilib.* 21 (1985) 95-112.
102. S. Brunsgaard Hansen, R.W. Berg, E.H. Stenby, High-Pressure Measuring Cell for Raman Spectroscopic Studies of Natural Gas, *Appl. Spectrosc.* 55,1 (2001) 55-60.
103. S.G. Kazarian, M.F. Vincent, C.A. Eckert, Infrared cell for supercritical fluid-polymer interactions, *Rev. Sci. Instrum.* 67,4 (1996) 1586-1589.
104. Z. Xiao, Y. Jia, L. Haoran, H. Shijun, Prediction of Vapor-Liquid Equilibrium Data from C-H Band Shift of IR Spectra in Some Binary Systems, *Chin. J. Chem. Eng.* 15,1 (2007) 97-101.
105. A. Braeuer, *In situ Spectroscopic Techniques at High Pressure*, Volume 7, first ed., Elsevier, Amsterdam, 2015.
106. S.K. Luther, J.J. Schuster, A. Leipertz, A. Braeuer, Non-invasive quantification of phase equilibria of ternary mixtures composed of carbon dioxide, organic solvent and water, *J. Supercrit. Fluids* 84 (2013) 146-154.
107. R. Adami, J. Schuster, S. Liparoti, E. Reverchon, A. Leipertz, A. Braeuer, A Raman spectroscopic method for the determination of high pressure vapour liquid equilibria, *Fluid Phase Equilib.* 360 (2013) 265-273.
108. L. Geng, K. Qu, W. Lu, L. Jiang, I.M. Chou, In situ Raman spectroscopic study of the pressure effect on the concentration of CO₂ in water at hydrate-liquid water equilibrium up to 900 bar, *Fluid Phase Equilib.* 438 (2017) 37-43.

109. W. Ou, L. Geng, W. Lu, H. Guo, K. Qu, P. Mao, Quantitative Raman spectroscopic investigation of geofluids high-pressure phase equilibria: Part II. Accurate determination of CH₄ solubility in water from 273 to 603 K and from 5 to 140 MPa and refining the parameters of the thermodynamic model, *Fluid Phase Equilib.* 391 (2015) 18-30.
110. B. Liebergesell, C. Flake, T. Brands, H.J. Koß, A. Bardow, A milliliter-scale setup for the efficient characterization of isothermal vapor-liquid equilibria using Raman spectroscopy, *Fluid Phase Equilib.* 446 (2017) 36-45.
111. F. Alsmeyer, W. Marquardt, G. Olf, A new method for phase equilibrium measurements in reacting mixtures, *Fluid Phase Equilib.* 203 (2002) 31-51.
112. E Vyhmeister, A.J. Muscat, D. Suleiman, L.A. Estévez, High-pressure phase equilibria for chlorosilane + carbon dioxide mixtures, *Fluid Phase Equilib.* 270 (2008) 121-128.
113. C.-Y. Sun, C.-F. Ma, G.-J. Chen, S.-X. Zhang, Experimental and simulation of single equilibrium stage separation of (methane + hydrogen) mixtures via forming hydrate, *Fluid Phase Equilib.* 261 (2007) 85-91.
114. L. Fedele, F. Pernechele, S. Bobbo, M. Scattolini, R. Stryjek, Solubility of carbon dioxide in pentaerythritol tetraoctanoate, *Fluid Phase Equilib.* 277 (2009) 55-60.
115. S.-P. Kang, J.-W. Lee, H.-J. Ryu, Phase behavior of methane and carbon dioxide hydrates in meso- and macro-sized porous media, *Fluid Phase Equilib.* 274 (2008) 68-72.
116. C. Zhu, X. Wu, D. Zheng, W. He, S. Jing, Measurement and correlation of vapour-liquid equilibria for the system carbon dioxide-diisopropyl ether, *Fluid Phase Equilib.* 264 (2008) 259-263.
117. S.K. Chaudhari, D. Salavera, X. Esteve, A. Coronas, Vapour-liquid equilibria of the system 1,1,1,2-tetrafluoroethane + monoethylene-glycol dimethylether from 283.15 to 353.15 K: New modified UNIFAC parameters, *Fluid Phase Equilib.* 271 (2008) 28-33.
118. M.M. Mooijer-van den Heuvel, C.J. Peters, J. de Swaan Arons, Influence of water-insoluble organic components on the gas hydrate equilibrium conditions of methane, *Fluid Phase Equilib.* 172 (2000) 73-91.
119. K. Thamanavat, T. Sun, A.S. Teja, High-pressure phase equilibria in the carbon dioxide + pyrrole system, *Fluid Phase Equilib.* 275 (2009) 60-63.
120. H.C. Van Ness, M.M. Abbott, A Procedure for Rapid Degassing of Liquids, *Ind. Eng. Chem. Fundam.* 17,1 (1978) 66-67.
121. R. Battino, M. Banzhof, M. Bogan, E. Wilhelm, Apparatus for Rapid Degassing of Liquids. Part III, *Anal. Chem.* 43,6 (1971) 806-807.
122. B. Ramsauer, R. Neueder, W. Kunz, Isobaric vapour-liquid equilibria of binary 1-propoxy-2-propanol mixtures with water and alcohols at reduced pressure, *Fluid Phase Equilib.* 272 (2008) 84-92.
123. S.K. Chaudhari, K.R. Patil, J. Allepús, A. Coronas, Measurement of the vapor pressure of 2,2,2-trifluoroethanol and tetraethylene glycol dimethyl ether by static method, *Fluid Phase Equilib.* 108 (1995) 159-165.

124. J.J.B. Machado, Th.W. de Loos, High pressure solid–fluid and vapour–liquid equilibria in model hyperbaric fluids: the system methane + tetracosane + triacontane, *Fluid Phase Equilib.* 228-229 (2005) 261-268.
125. R.P. Bonifácio, M.F. Costa Gomes, E.J.M. Filipe, Solubility of xenon in *n*-hexane between 257 and 333 K, *Fluid Phase Equilib.* 193 (2002) 41-51.
126. K.N. Habchi Tounsi, A. Barreau, E. Le Corre, P. Mougin, E. Neau, Measurement of Carbon Dioxide Solubility in a Solution of Diethanolamine Mixed with Methanol, *Ind. Eng. Chem. Res.* 44 (2005) 9239-9243.
127. I. Dalmolin, E. Skovroinski, A. Biasi, M.L. Corazza, C. Dariva, J. Vladimir Oliveira, Solubility of carbon dioxide in binary and ternary mixtures with ethanol and water, *Fluid Phase Equilib.* 245 (2006) 193-200.
128. D. Le Tourneux, I. Iliuta, M.C. Iliuta, S. Fradette, F. Larachi, Solubility of carbon dioxide in aqueous solutions of 2-amino-2-hydroxymethyl-1,3-propanediol, *Fluid Phase Equilib.* 268 (2008) 121-129.
129. G. García-Miaja, J. Troncoso, L. Romaní, Excess properties for binary systems ionic liquid + ethanol: Experimental results and theoretical description using the ERAS model, *Fluid Phase Equilib.* 274 (2008) 59-67.
130. R. Gonzalez-Olmos, M. Iglesias, Influence of temperature on thermodynamics of ethers + xylenes, *Fluid Phase Equilib.* 267 (2008) 133-139.
131. E. Pérez, Y. Sánchez-Vicente, A. Cabañas, C. Pando, J.A.R. Renuncio, Excess molar enthalpies for mixtures of supercritical carbon dioxide and water + ethanol solutions, *J. Supercrit. Fluids* 36 (2005) 23-30.
132. R. Zhang, W. Yan, X. Wang, R. Lin, Molar excess enthalpies of ethyl acetate + alkanols at $T = 298.15$ K, $p = 10.0$ MPa, *Thermochim. Acta* 429 (2005) 155-161.
133. E. Zorębski, B. Lubowiecka-Kostka, Thermodynamic and transport properties of (1,2-ethanediol + 1-nonanol) at temperatures from (298.15 to 313.15) K, *J. Chem. Thermodyn.* 41 (2009) 197-204.
134. C. Lundstrøm, M.L. Michelsen, G.M. Kontogeorgis, K.S. Pedersen, H. Sørensen, Comparison of the SRK and CPA equations of state for physical properties of water and methanol, *Fluid Phase Equilib.* 247 (2006) 149-157.
135. R. Gomes de Azevedo, J. Szydłowski, P.F. Pires, J.M.S.S. Esperança, H.J.R. Guedes, L.P.N. Rebelo, A novel non-intrusive microcell for sound-speed measurements in liquids. Speed of sound and thermodynamic properties of 2-propanone at pressures up to 160 MPa, *J. Chem. Thermodyn.* 36 (2004) 211-222.
136. M.M. Piñeiro, F. Plantier, D. Bessières, J.L. Legido, J.L. Daridon, High-pressure speed of sound measurements in methyl nonafluorobutyl ether and ethyl nonafluorobutyl ether, *Fluid Phase Equilib.* 222-223 (2004) 297-302.

137. M.T. Zafarani-Moattar, R. Majdan-Cegincara, Density, Speed of Sound, and Viscosity of Binary Mixtures of Poly(propyleneglycol) 400 + Ethanol and + 2-Propanol at Different Temperatures, *J. Chem. Eng. Data* 53 (2008) 2211-2216.
138. M.T. Zafarani-Moattar, N. Tohidifar, Vapor–Liquid Equilibria, Density, Speed of Sound, and Viscosity for the System Poly(ethylene glycol) 400 + Ethanol at Different Temperatures, *J. Chem. Eng. Data* 53 (2008) 785-793.
139. T.S. Khasanshin, O.G. Poddubskij, A.P. Shchamialiou, V.S. Samuilov, The thermodynamic properties of 1-alkenes in the liquid state: 1-Hexadecene, *Fluid Phase Equilib.* 245 (2006) 26-31.
140. T.S. Khasanshin, O.G. Poddubskii, A.P. Shchemelev, Sound Velocity in Liquid 1-Alkenes, *High Temp.* 43,4 (2005) 530-537.
141. N.G. Polikhronidi, I.M. Abdulagatov, G.V. Stepanov, R.G. Batyrova, Isochoric heat capacity measurements for pure ethanol in the near-critical and supercritical regions, *J. Supercrit. Fluids* 43 (2007) 1-24.
142. M.B. Oliveira, I.M. Marrucho, J.A.P. Coutinho, A.J. Queimada, Surface tension of chain molecules through a combination of the gradient theory with the CPA EoS, *Fluid Phase Equilib.* 267 (2008) 83-91.
143. A. Bahramian, A. Danesh, F. Gozalpour, B. Tohidi, A.C. Todd, Vapour–liquid interfacial tension of water and hydrocarbon mixture at high pressure and high temperature conditions, *Fluid Phase Equilib.* 252 (2007) 66-73.
144. C. Miqueu, B. Mendiboure, C. Graciaa, J. Lachaise, Modelling of the surface tension of binary and ternary mixtures with the gradient theory of fluid interfaces, *Fluid Phase Equilib.* 218 (2004) 189-203.
145. J.J.-C. Hsu, N. Nagarajan, R.L. Robinson Jr., Equilibrium Phase Compositions, Phase Densities, and Interfacial Tensions for CO₂ + Hydrocarbon Systems. 1. CO₂ + *n*-Butane, *J. Chem. Eng. Data* 30,4 (1985) 485-491.
146. N. Nagarajan, R.L. Robinson Jr., Equilibrium Phase Compositions, Phase Densities, and Interfacial Tensions for CO₂ + Hydrocarbon Systems. 2. CO₂ + *n*-Decane, *J. Chem. Eng. Data* 31 (1986) 168-171.
147. Y.G. Li, C.B. Park, H.B. Li, J. Wang, Measurement of the PVT property of PP/CO₂ solution, *Fluid Phase Equilib.* 270 (2008) 15-22.
148. T. Akutsu, Y. Yamaji, H. Yamaguchi, M. Watanabe, R.L. Smith Jr., H. Inomata, Interfacial tension between water and high pressure CO₂ in the presence of hydrocarbon surfactants, *Fluid Phase Equilib.* 257 (2007) 163-168.
149. M. Stievano, N. Elvassore, High-pressure density and vapour-liquid equilibrium for the binary systems carbon dioxide-ethanol, carbon dioxide-acetone and carbon dioxide-dichloromethane, *J. Supercrit. Fluids* 33 (2005) 7-14.
150. I.M. Abdulagatov, J.T. Safarov, F.Sh. Aliyev, M.A. Talibov, A.N. Shahverdiyev, E.P. Hassel, Experimental densities and derived thermodynamic properties of liquid propan-1-ol at temperatures from 298 to 423 K and at pressures up to 40MPa, *Fluid Phase Equilib.* 268 (2008) 21-33.

151. B. Orge, M. Iglesias, G. Marino, M. Domínguez, M.M. Piñeiro, J. Tojo, Mixing properties of benzene + 2-methyl-2-butanol + 1-pentanol at 298.15 K. Experimental results and comparison between ERAS model and cubic EOS estimations for excess molar volumes, *Fluid Phase Equilib.* 170 (2000) 151-163.

Chapter 3: PUBLICATION 1

Analytic Setup for Multicomponent High-Pressure Phase Equilibria via Dual Online Gas Chromatography

Frederick C. v. N. Fourie, Cara E. Schwarz, Johannes H. Knoetze*

Stellenbosch University, Department of Process Engineering, Private Bag X1, Matieland, 7602, South Africa,

Tel: +27 21 808 4204, Fax: +27 21 808 2059, E-mail: jhk@sun.ac.za

Chemical Engineering & Technology 38,7 (2015) 1165-1172.

Received 31 October 2014; Revised 22 December 2014; Accepted 2 February 2015

DOI: 10.1002/ceat.201400643

Declaration by the candidate

With regard to Chapter 3, the nature and scope of my contribution were as follows:

<u>Nature of contribution</u>	<u>Extent of contribution (%)</u>
I was responsible for equipment design, procurement, construction, commissioning and validation. I was the primary publication author responsible for compiling the text and publication submission.	90 %

The following co-authors contributed to Chapter 3:

<u>Name</u>	<u>E-mail address</u>	<u>Nature of contribution</u>	<u>Extent of Contribution (%)</u>
Johannes H. Knoetze	jhk@sun.ac.za	Supervisor to the student, F.C.v.N Fourie.	5 %
Cara E. Schwarz	cschwarz@sun.ac.za	Co-supervisor to the student, F.C.v.N. Fourie.	5 %

Signature of candidate : Declaration with signature in possession of candidate and supervisor

Date : 10 November 2017

Declaration by co-authors

The undersigned hereby confirm that:

1. The declaration above accurately reflects the nature and extent of the contributions of the candidate and the co-authors to Chapter 3.
2. No other authors contributed to Chapter 3 besides those specified above.
3. Potential conflicts of interest have been revealed to all interested parties and that the necessary arrangements have been made to use the material in Chapter 3 of this dissertation.

<u>Signature</u>	<u>Institutional affiliation</u>	<u>Date</u>
Declaration with signature in possession of candidate and supervisor	Supervisor to the student, F.C.v.N Fourie.	10 November 2017
Declaration with signature in possession of candidate and supervisor	Co-supervisor to the student, F.C.v.N. Fourie.	10 November 2017

ABSTRACT

A high-pressure analytic phase equilibria setup, capable of operation at 150 °C and 30 MPa, was developed. The variable-volume view cell contains two height-adjustable samplers enabling simultaneous sampling from two phases. Concurrent analysis of both samples was performed with dual online gas chromatography (GC). The GC comprises two inlets, four columns, two switch valves, and three detectors, arranged in parallel pathways. Quantitative detector calibrations were used. The setup was validated by sampling from a one-phase ternary of known composition, and comparison with binary and ternary literature data. The setup produces accurate phase composition data for supercritical systems and is well-suited to handle mixture constituents ranging from volatile gases to mid-length hydrocarbons.

Keywords: High-pressure phase equilibria, Online gas chromatography, Phase composition, Supercritical systems, Ternary

1. INTRODUCTION

Supercritical fluids are applied in the natural gas [1], petroleum [1-2], food [3-4], polymer [5-6] and pharmaceutical [3,7] industries. These solvents may provide improved selectivity or solvating ability, enabling the execution of difficult extractions. Phase equilibria data are required to design, operate and optimize supercritical fluid extraction (SFE) processes [2,8-10]. This is done, in part, via the development of predictive models which enable the correlation of thermodynamic properties and the prediction of phase behavior in the high-pressure region [1]. Developing accurate and robust models require accurate and comprehensive experimental data. This is true for asymmetric mixtures containing a supercritical solvent and one, or more, low-volatility hydrocarbon solutes [11-12].

Ternary and multi-component high-pressure equilibrium phase composition data are scarce. Literature does contain large amounts of binary data, the associated experimental methods are established, and expanding the collection of binary data is achieved efficiently via the application of these existing techniques. However, binary solvent-solute systems are not representative of the actual mixture considered for treatment with SFE. The addition of more solutes, to form ternary and higher systems, introduces solute-solute interactions. As a result, many predictive models perform poorly.

Analytic high-pressure phase equilibria equipment is expensive to construct and complex to operate. Synthetic methods, which focus mostly on the identification of phase transitions, are used to study bubble-points, dew-points and critical endpoints in ternary and higher systems. However, synthetic equipment is not well suited to determine the compositions of co-existing equilibrium phases in ternary or higher mixtures. This is best achieved with analytic methods which quantify the compositions of two or more co-existing phases. Unfortunately, few high-pressure analytic setups exist. Valuable reviews on equipment and methods are available [13-16], but the aspects of design, construction and commissioning are often not communicated in sufficient detail. A paradigm shift is required to address this deficiency. Only in recognizing the importance of quality equipment in producing accurate experimental data will the needs of industry be met.

The work presented here complements ongoing high-pressure research at Stellenbosch University. One focus area thereof considers SFE to separate post-production mixtures of close-boiling detergent range alcohols and alkanes. Synthetic and pilot plant studies on binary, ternary and multi-component systems have indicated the existence of a) significant solute-solute interactions [17]; and b) discrepancies between binary phase behavior data and observed piloting trends [18-19]. Equilibrium phase composition data for the relevant solvent + solute A + solute B systems are required to explain these phenomena.

The objective of this work is to report on the development and verification of a high-pressure analytic phase equilibria setup. Ternary and multi-component mixtures comprising CO₂ together with the solutes *n*-dodecane, 1-decanol and 3,7-dimethyl-1-octanol will be the immediate focus. Similar systems were thus used for validation purposes, and are reported on here. Unique characteristics of the analysis approach and equilibrium cell are presented. Small variations in temperature may affect phase behavior which hampers the extraction of representative samples, and therefore details on temperature control and monitoring are included. Supporting Information is available online.⁶

2. EXPERIMENTAL

2.1 Setup

The static-analytic experimental setup comprises a sample preparation vessel, or equilibrium cell, a sample transfer section and a sample analysis section. A static setup was favored because of the a) high materials cost associated with continuous-flow systems; b) difficulty of sampling the stationary phase in semi-flow systems; and c) uncertainty surrounding pulsation disturbances in circulation systems. The variable volume (75 - 125 ml) equilibrium cell was manufactured from stainless steel 316L, and the content is magnetically stirred.

Dual simultaneous sample extraction and concurrent parallel online analysis via gas chromatography (GC) are possible. A sapphire window, together with a high definition medical camera and endoscope (Stryker Endoscopy, 1088 HD), enables observation of internal phenomena not visible with the naked eye. The upper operating limits of the setup are 30 MPa at 150 °C. Heating of the equilibrium cell is performed using a Julabo circulating liquid bath and a forced convection oven. Cell pressure is measured using an ONEhalf20 melt pressure transmitter. A cross-sectional schematic and overview of the setup are provided in Figs. 3-1 and 3-2 respectively.

⁶ The supporting information specific to Publication 1 is available in Appendix A.

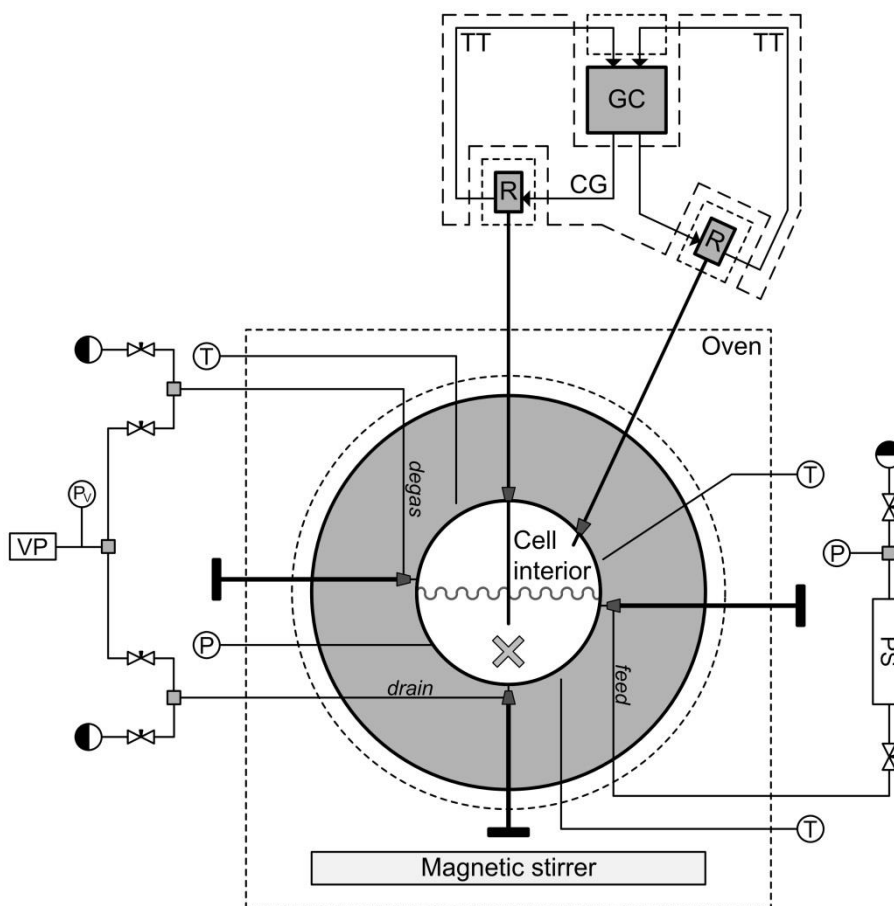


Figure 3-1. Cross-sectional schematic of the high-pressure analytic phase equilibria setup: (GC) gas chromatograph; (P) pressure transmitter; (PS) pressurized solvent; (Pv) vacuum gauge; (R) ROLSI™ sampler; (T) Pt100; (TT) carrier gas and sample transfer tubing; (VP) vacuum pump; broken lines indicate temperature controlled regions.

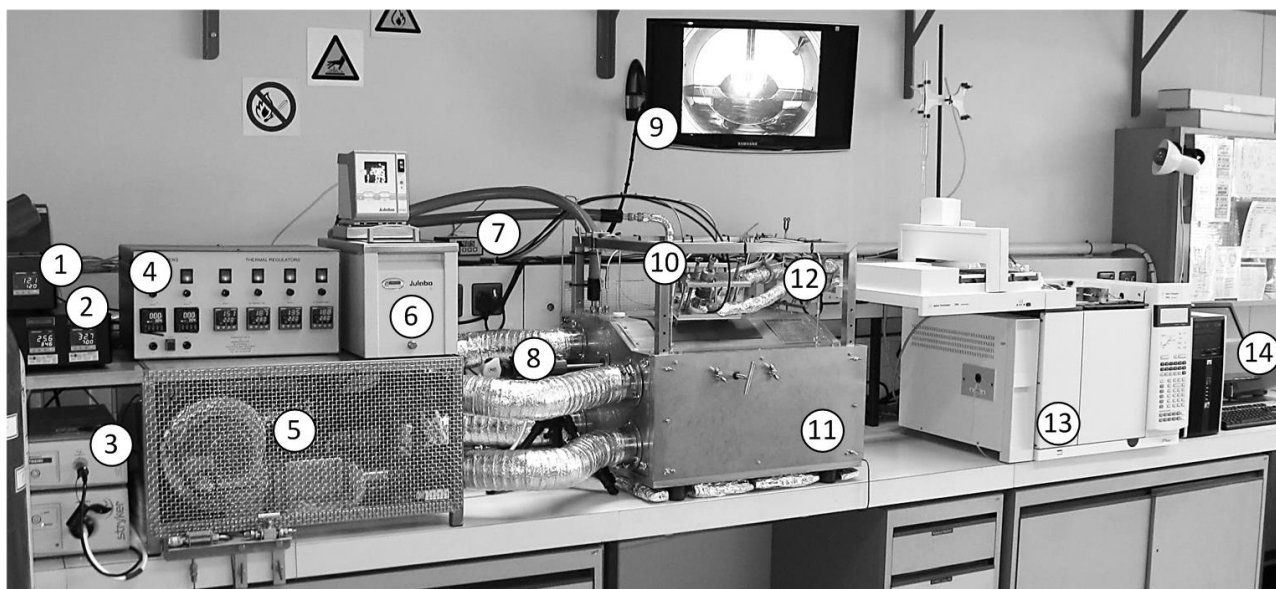


Figure 3-2. Overview of the high-pressure analytic phase equilibria setup: (1) GC transfer tubing temperature control; (2) oven temperature control; (3) camera and light source; (4) ROLSI™ sampler controls; (5) oven elements and fan; (6) circulating liquid heating bath; (7) pressure display; (8) endoscope; (9) monitor; (10) 2 × ROLSI™ sampler and displacement device; (11) oven with equilibrium cell, pressure intensifier and stirrer; (12) heated sample transfer tubing; (13) gas chromatograph; (14) data acquisition unit.

2.2 Equilibrium Cell

A side view of the equilibrium cell is shown in Fig. 3-3 a. A 28 mm diameter sapphire window (SITEC-Sieber Engineering, 50 MPa at 200 °C) is located in area A. Increased vertical variation between top and bottom sampling points reduces the possibility of cross-contamination across the phase interface. This is achieved by having the cell interior taper outward at a 35 °C angle (refer to the areas labelled B). The piston cylinder (C in Fig. 3-3 a) enables cell volume variations. Cylinder diameter is a balance between maximum required cell volume, pressure variation with minimum incremental piston adjustments, required range of volume variation, and achievement of sufficient mixing inside the cylinder. The cylinder is located off-center relative to the equilibrium cell to provide a continuous bottom interior. This enables movement of the stirring magnet into the cylinder, and shear forces from magnet rotation to create stirring inside the cylinder. The piston and pressure intensifier connect to the area labelled D, and are shown in a sectioned assembly in Fig. 3-3 b. N₂ gas, with a pressure step-up factor of 38, is used as pressurizing medium.

A 22 mm wide ribbon (E in Fig. 3-3 a) spanning the cell circumference contains the pressure measurement port, feed, degas and drain lines, two sample ports and three temperature measurement ports. The plane XX in Fig. 3-3 a contains two additional temperature measurement ports (also see Fig. 3-5 b). If valves are located on the outer perimeter of the equilibrium cell, a distinct dead volume is unavoidable. In high-pressure research, where large wall thicknesses are typically encountered, this is particularly pertinent. To minimize the dead volume, needle valves were machined into the equilibrium cell wall, enabling needle block-off 2 mm from the equilibrium cell interior. Female profiles of the valves were machined via spark erosion. The feed and degas lines, and the drain line, of 1 and 2 mm diameter respectively, were machined via electron discharge machining (Fig. 3-1).

A linear static finite element method analysis indicated maximum Von Mises stresses of 97.5 MPa at an internal pressure of 30 MPa, equating to a safety factor of 2.7. The vessel was hydrostatically tested to 30.5 MPa and certified, by TÜV Rheinland, to 35.6 MPa.

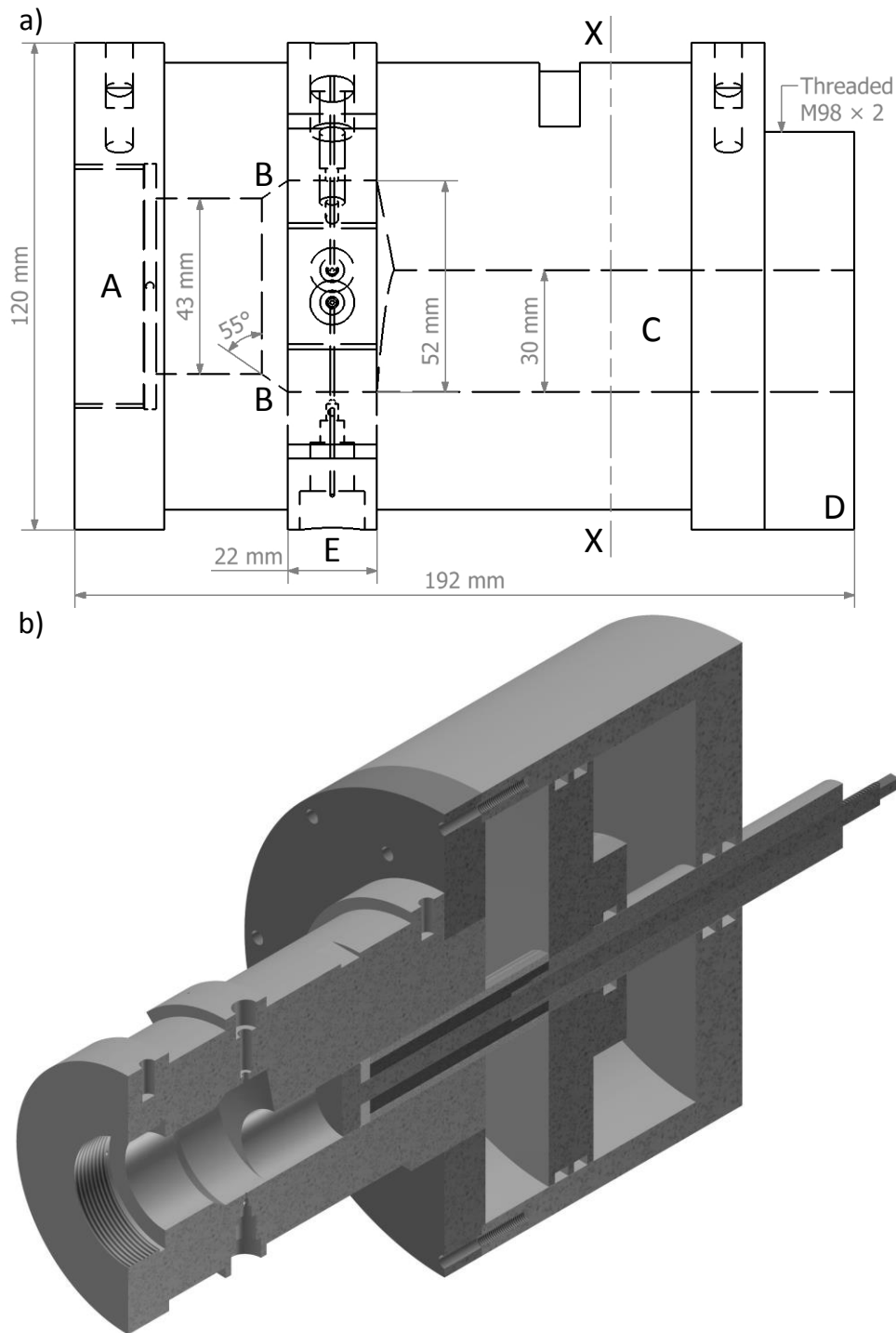


Figure 3-3. (a) Side view of the equilibrium cell; (b) sectioned assembly of the equilibrium cell, piston and pressure intensifier.

2.3 Sample Extraction

The equilibrium cell is fitted with two electromagnetic ROLSI™ samplers (Armines, France). The ROLSI™ capillary protrudes into the equilibrium cell and the top end thereof is sealed with a movable piston. The capillary length and internal diameter are 15 cm and 0.15 mm respectively. Each ROLSI™ is fixed to a

manual displacement device which enables ROLSI™ height adjustments whilst maintaining system pressure at 30 MPa (refer to Fig. S1 in Section S1 of the Supporting Information).⁷ The mass per individual vapor sample varied between 0.04 and 0.77 mg. Liquid sample mass varied between 0.07 and 1.1 mg, equating to a maximum of 0.002 % of total cell contents.

2.4 Gas Chromatography Analysis

Phase composition analysis was performed by online GC. A schematic of the GC configuration is shown in Fig. 3-4 and the method parameters are listed in Table 3-1. The hardware is arranged in two parallel pathways enabling simultaneous analysis of two samples with constituents ranging from volatile gases to mid-length hydrocarbons. A sample chromatogram is shown in Fig. S2 in Section S2 of the Supporting Information.

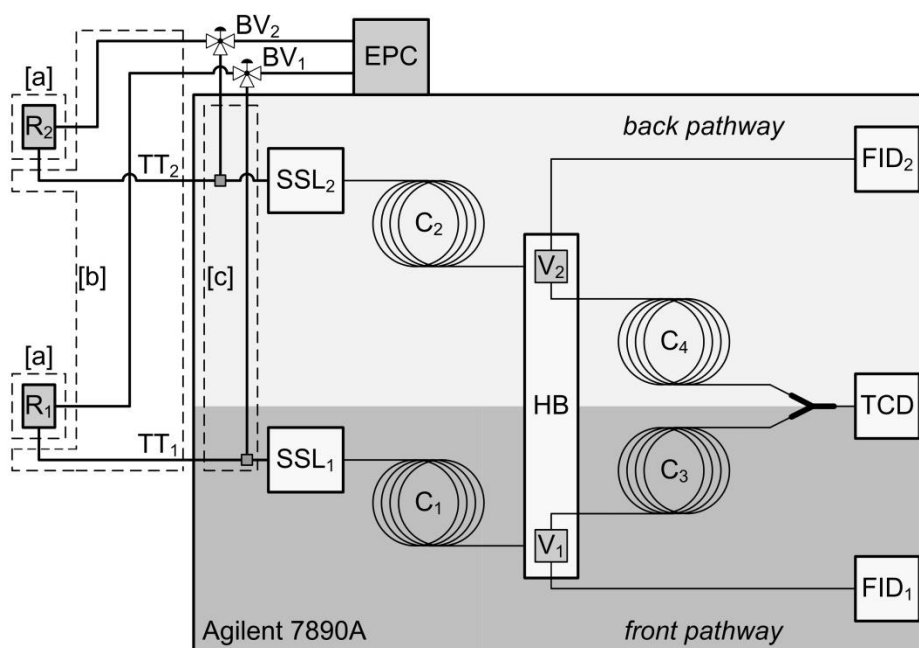


Figure 3-4. Schematic of the GC configuration: (BV) ball valve; (C₁ & C₂) DB-1, $l = 30\text{ m}$, $\phi = 0.53\text{ mm}$, film = $1.5\ \mu\text{m}$; (C₃) HP-PLOT/Q, $l = 15\text{ m}$, $\phi = 0.53\text{ mm}$, film = $40\ \mu\text{m}$; (C₄) HP-PLOT/Q, $l = 30\text{ m}$, $\phi = 0.53\text{ mm}$, film = $40\ \mu\text{m}$; (EPC) carrier gas control; (FID) flame ionization detector; (HB) heated valve box; (R) ROLSI™; (SSL) split-splitless inlet; (TCD) thermal conductivity detector; (TT) transfer tubing; (V) 4-port switch valve; broken lines indicate temperature controlled regions [a], [b] and [c].

⁷ The supporting information specific to Publication 1 is available in Appendix A.

Table 3-1. GC method parameters for online analysis and calibration runs.

GC Unit	Operating parameters
Oven	T ₁ = 100 °C [2 min] Ramp = 30 °C/min [5 min] T ₂ = 250 °C [3 min]
Flame ionization detectors	T = 300 °C
Thermal conductivity detector	T = 250 °C
Inlets	T = 300 °C Split ratio = 5:1, 20:1 or 80:1
Carrier gas	Helium
Columns	Flow = 3 ml/min
Valves	Switching at 4.5 min
Valve box	T = 195 °C

Quantitative GC detector calibration procedures, which involve the manual injection of a known mass of liquid or gas, were developed. The mass injected is related to detector peak area response in a quantitative calibration curve. This approach is independent of the equilibrium cell sample extraction, transfer and injection pathway. As such, it serves as a rigorous test for systemic errors, or repeatable inaccuracies. Three to eight calibration points were used for each species, with three replicate injections per mass. Linear calibration curves, with R² values no smaller than 0.9995, were obtained throughout.⁸

2.5 Temperature and Pressure: Control, Accuracy and Calibrations

Temperature control of the equilibrium cell utilizes two units – a Julabo ME-6 circulation bath (stability: ± 0.01 °C, resolution: 0.01 °C) and a forced convection oven (see Fig. 3-5 a). The Julabo unit circulates liquid through a 5 mm jacket surrounding the equilibrium cell, is used in external control mode, and enables control of the equilibrium cell temperature. The oven uses 3 × 850 Watt heater elements and a 550 m³/h centrifugal fan (ebm-papst, G2E 140-AG 02-05) to regulate the temperature of a 95 liter space surrounding the equilibrium cell and pressure intensifier. The double-paneled oven walls are filled with ceramic blanket of 25 mm thickness. Twelve Pt100's are used for monitoring purposes – four probes in the equilibrium cell block, four probes in the heating fluid inlets and outlet, and four probes inside the oven environment.

⁸ The GC calibration curves used throughout this study are presented in Appendix E. FS and BS, or Front Spot and Back Spot, refer to spot check calibration injections on the front and back pathways respectively. Spot check injections were performed during an experimental run to test the validity of the prevailing calibration curves.

The Pt100's labelled 1 to 4 in Fig. 3-5 a contain 4-wire simplex 1/10th DIN Class B resistors ($\alpha = 0.00385 \Omega \cdot \Omega^{-1} \cdot ^\circ\text{C}^{-1}$) with tolerance in temperature measurement specified as $\pm (0.03 + 0.0005 |T|) ^\circ\text{C}$. The twelve monitoring probes labelled 2 to 4 connect to an Agilent 34972A data acquisition unit (one year RTD accuracy: 0.06 $^\circ\text{C}$, resolution: 0.00001 $^\circ\text{C}$). The Pt100's labelled 5 and 6 serve as oven control and element protection probes. These air probes contain 3-wire Class A resistors exposed inside a perforated tube. Each air probe connects to a Gefran 600 controller. Prior to calibration, each of the fifteen Pt100's was paired with a dedicated controller or recording channel, and used as such throughout. The Pt100-controller/logger pair was calibrated in unison, which compensates for probe-, controller- and logger-inaccuracies. Calibrations were performed by InterCal, a South African National Accreditation System (SANAS) accredited institute. SANAS is a member of the International Laboratory Accreditation Cooperation. The total uncertainty of calibration was $\pm 0.1 ^\circ\text{C}$. The Pt100's labelled 1 and 2 in Fig. 3-5 a were calibrated at five points between 30 and 150 $^\circ\text{C}$, whilst probes 3 to 6 were calibrated at three points across the same range. Calibration data were used to establish correction curves for each Pt100. The five equilibrium cell Pt100's were positioned to identify potential temperature gradients inside the cell block. Thermowells were machined on two axial planes and different radial locations, as shown in Fig. 3-5 b.

Equilibrium cell pressure is measured with an ONEhalf20 melt transmitter (CTDLX6MA-3.5CB, range: 0 to 35 MPa, repeatability: 0.10 % of full scale output (FSO)). The transmitter diaphragm is located flush with the vessel inner surface to eliminate dead volume. Pressure values are displayed (DPM 4001) and logged (Agilent 34972A). A Barnet Instruments dead weight tester was used to calibrate the transmitter at 1.5 MPa increments between 0 and 30 MPa. The pressure transmitter and display were calibrated in unison to compensate for inaccuracies arising from both units. Calibrations were performed at each operating temperature, thereby incorporating temperature dependency of the pressure transmitting fluid and electronics. These data were used to establish temperature-specific pressure correction curves. The uncertainty in pressure measurement is 0.035 MPa or smaller.

Atmospheric pressure measurements, which form part of the GC calibration procedure, were conducted using a transmitter by Wika (UniTrans UT-10, pressure range: 0 – 1 600 mbar, accuracy: 0.1 % of FSO) or Afriso (31148S, pressure range: 0 – 1 000 mbar, accuracy: 0.35 % of FSO). The former was calibrated by Wika Calibration Laboratory DKD-K-03701 between 0 and 1 600 mbar, and calibrated values never deviated by more than 0.03 % of the pressure value. The latter was calibrated by SA Metrology (SANAS accredited) according to ISO 17025:2005. In the calibrated range between 800 and 1 000 mbar, all deviations were smaller than 0.3 mbar, and the measurement uncertainty for the procedure was $\pm 0.1 \%$.

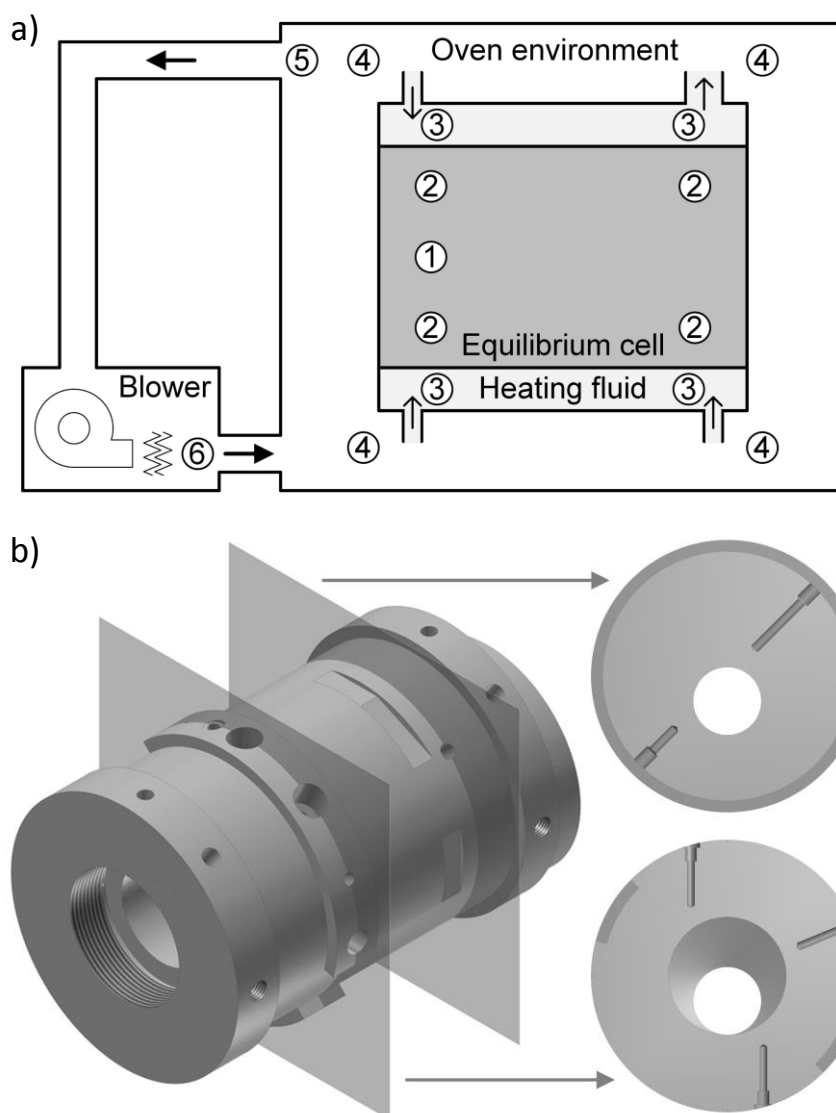


Figure 3-5. (a) The temperature control approach: (1) Julabo control of cell temperature; (2) monitoring cell temperature; (3) monitoring heating fluid inlet and outlet temperatures; (4) monitoring oven temperature; (5) control of oven temperature; (6) safety on oven elements; (b) axial and radial positions of the equilibrium cell Pt100's.

2.6 Equipment Design and Operation: Observations of Benefit to Related Studies

- Variable cell volume is not required for analytic phase equilibria studies but it provides versatility by enabling one to a) increase pressure and sample from the one-phase region; b) identify bubble- and dew point pressures; c) generate data at predetermined pressures without changing the bulk mixture composition; and d) vent from the one-phase region and operate at lower pressures but constant bulk mixture composition.

- An adjustable sampling height simplifies the study of three-phase equilibria, and is a troubleshooting tool. Two samplers can be used to extract separate samples from the same phase. Comparing results from parallel online analyses assists in the identification of systemic errors.
- Commissioning is simplified if all species appear on one GC detector. Uncalibrated peak area fractions may provide a quick, albeit imprecise, estimate of sample composition. This is a rapid method to identify changes in system behavior.
- Do not sample in the presence of stirring since potential particulates, which may block sample capillaries, are more likely to occur in suspension.

2.7 Experimental Procedure

2.7.1 Loading, Equilibrium Attainment and Sampling

A known mass (Precisa XT4200C) of liquid solute(s) is loaded in the equilibrium cell at 27 °C and atmospheric pressure. The liquid is exposed to vacuum (Oerlikon Leybold Trivac D 2.5 E) in the presence of magnetic stirring. A known mass of pressurized solvent is transferred from a 300 ml sample cylinder (Swagelok, 316L-50DF4-300).

After loading, the oven paneling is installed, set point temperature is approached, pressure is adjusted via piston movements, and the content is stirred (Thermo VARIOMAG® Maxi 20). Changes in pressure and temperature usually cause one of two visual disturbances: a rising phase of intermediate density which eventually 'consumes' the existing vapor phase, or liquid deposition from the vapor phase. When temperature and pressure are close to set point values, the dense-phase ROLSI™ is adjusted to ensure the capillary tip thereof is located in the bottom phase. This should be done in advance since capillary movements may affect the equilibrium cell pressure. Once set point pressure and temperature are reached and the system is visually stable, the content is stirred for an additional 60 min. Stirring is stopped, and a 60-min waiting period allows for phase separation.

The two-part sampling process starts with a slow purge run which lasts between 45 and 90 minutes and entails consecutive extractions from both phases until stable peak heights are obtained. The second part involves alternating fast purge and analysis runs, with the former lasting 1.8 minutes. For each combination of pressure and temperature, a minimum of five consecutive samples of satisfactory composition-repeatability are withdrawn. Satisfactory implies target and maximum allowable species-specific standard deviations in mass fraction of 0.003 and 0.009 respectively. The sampling procedure typically requires 2 to 4 hours to complete, during which temperature and pressure fluctuate by no more than ± 0.01 °C and ± 0.01 MPa.

2.7.2 Materials used

The materials used in this study are listed in Table 3-2. All species were used without further purification.

Table 3-2. Materials used in this study.

Component	CAS number	Purity	Supplier	Catalogue number
<i>n</i> -Hexadecane (<i>n</i> C ₁₆)	544-76-3	> 99 %	Sigma-Aldrich	H-0255
1-Dodecanol (C ₁₂ OH)	112-53-8	98 %	Sigma-Aldrich	12,679-9
2-Ethyl-1-hexanol	104-76-7	≥ 99.6 %	Sigma-Aldrich	538051-4L
1-Octanol (C ₈ OH)	111-87-5	≥ 99 %	Sigma-Aldrich	360562-1L
Ethane	78-84-0	≥ 99.5%	Afrox	545201-SE-C
CO ₂	124-38-9	99.0%	Afrox	40-RC-W

3. VALIDATION OF THE EXPERIMENTAL SETUP

A three-step process was used to validate the setup. Firstly, the accuracy of the extraction, injection and analysis pathways was tested by sampling from a one-phase ethane + 1-dodecanol + *n*-hexadecane ternary of known composition at 12.1 MPa and 63.0 °C. The species-specific mass fraction averages and root mean square errors are listed in Table 3-3. Mass fraction results for ethane and 1-dodecanol are shown in Fig. S3 in Section S3 of the Supporting Information.⁹ Accurate and repeatable data were obtained via both pathways.

Table 3-3. Mass fraction averages and root mean square errors (RMSE), on parallel analysis pathways, for a one-phase ethane + 1-dodecanol (C₁₂OH) + *n*-hexadecane (*n*C₁₆) system of known composition.

Species	Mass fraction (known)	Front pathway (15 samples)		Back pathway (24 samples)	
		Mass fraction (average)	RMSE (mass fraction)	Mass fraction (average)	RMSE (mass fraction)
Ethane	0.611	0.613	0.007	0.608	0.004
C ₁₂ OH	0.193	0.191	0.004	0.195	0.002
<i>n</i> C ₁₆	0.196	0.195	0.003	0.197	0.002

⁹ The supporting information specific to Publication 1 is available in Appendix A.

Secondly, the CO₂ + 1-octanol system was studied at 65.0 °C for comparison with existing binary data [9,20] and results are presented in Fig. 3-6. Interpolation on trend lines was used to generate averaged reference data at pressures corresponding to the experimental pressures from this work. Absolute deviations in mass fraction 1-octanol are shown in brackets adjacent to each data point. The deviations of 3.5 and 6.9 mass % at 16.6 MPa may be a result of the difficulty of data generation when operating at 98 % of the mixture phase transition pressure, where the small difference in phase densities, and subsequent system sensitivity, further complicates the sampling process. The bubble-point composition at 16.9 MPa, which deviates by 0.5 mass %, was measured by sampling from the one phase region and not via stoichiometric loading. Different experimental methods may possess different inherent inaccuracies [21]. It is worth mentioning that both Byun and Kwak [9] and Fourie et al. [20] used synthetic equipment coupled with visual observation of phase transitions.

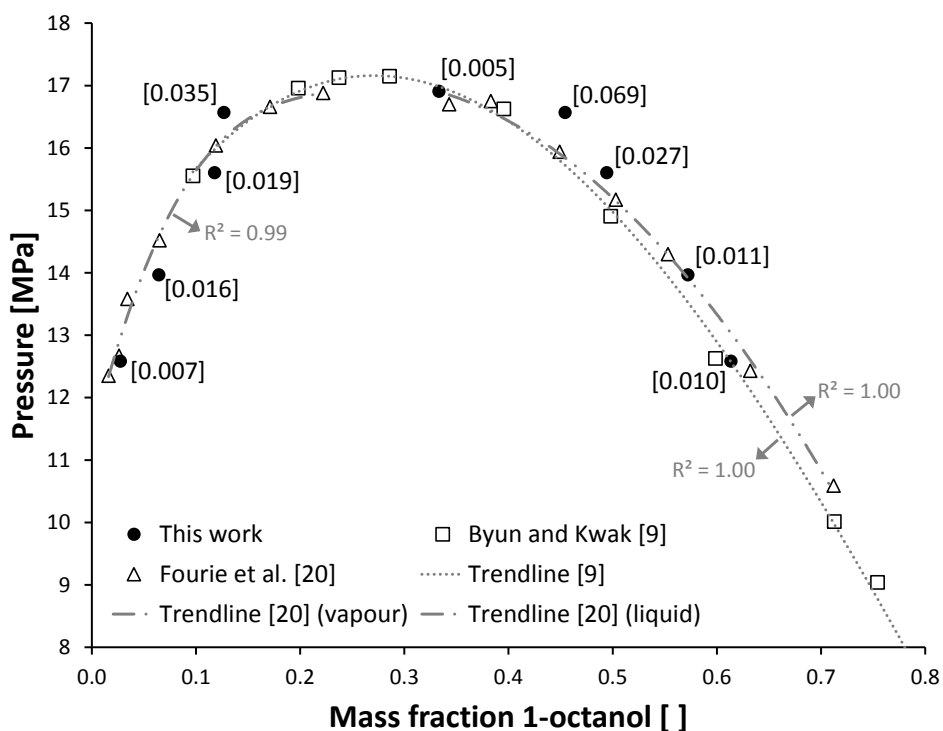


Figure 3-6. The CO₂ + 1-octanol system at 65.0 °C: comparing data from this work with literature data [9,20].

Lastly, the CO₂ + 1-dodecanol + *n*-hexadecane system was studied to enable comparison with existing ternary data [22-23]. Both Hölscher [22] and Kordikowski [23] made use of a sampling approach which deliberately splits the sample into a gaseous fraction containing most of the CO₂ and a liquid fraction containing the hydrocarbons. The CO₂ mass was determined via an equation of state whilst the hydrocarbons were rinsed from the sampling system and analyzed after the addition of an internal standard. Results at 60.0 °C and 80.0 °C are shown in Figs. 3-7 and 3-8. The corresponding data, standard deviations and deviations from reference data are provided in Table 3-4. The 8 comparative phase compositions represent 24 species-specific mass fractions, of which 22 deviate from reference

data by 0.03 or less (i.e. 3 percentage points, or less). Via extension of tie lines from this work, the liquid phase CO₂ mass fraction in Fig. 3-7 a and the vapor phase CO₂ mass fraction in Fig. 3-8 b deviate from reference data by 5 and 4 percentage points respectively. The known bulk compositions, labelled as “Loading” in Figs. 3-7 and 3-8, were determined gravimetrically and are independent of the sampling and analysis procedure. As is required by a mass balance, all tie lines from this work pass through the bulk mixture composition. Based on results from this three-step approach, the new setup was deemed successfully validated.

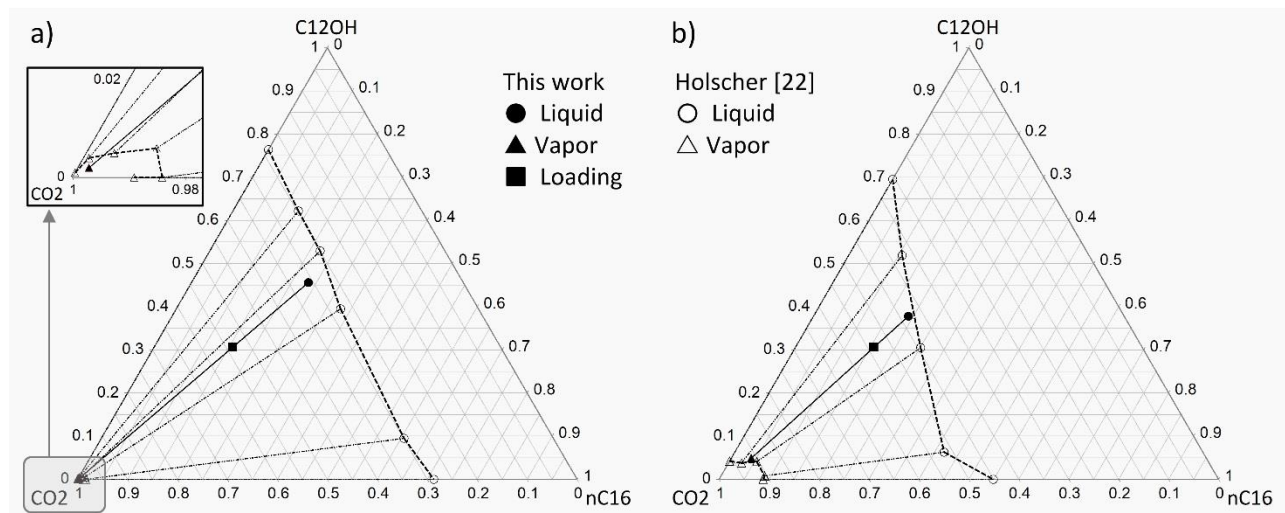


Figure 3-7. The CO₂ + 1-dodecanol + n-hexadecane system at 60.0 °C: comparing data from this work with literature data [22] at (a) 10.0 MPa and (b) 15.0 MPa.

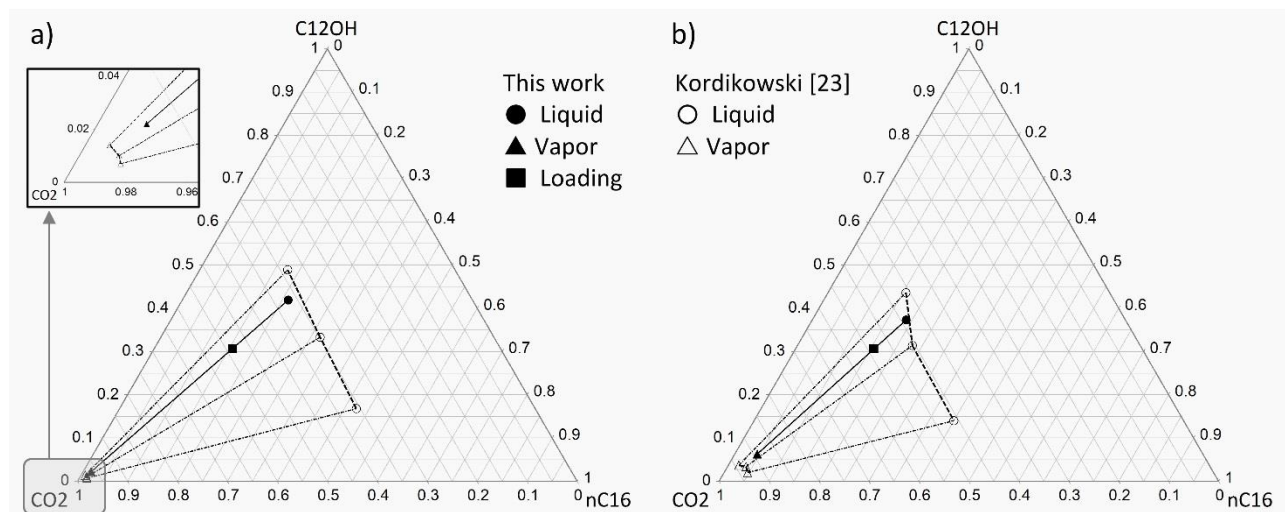


Figure 3-8. The CO₂ + 1-dodecanol + n-hexadecane system at 80.0 °C: comparing data from this work with literature data [23] at (a) 15.0 MPa and (b) 17.5 MPa.

Table 3-4. Phase composition data for the CO₂ + 1-dodecanol (C₁₂OH) + *n*-hexadecane (nC₁₆) system.

T [°C]	P [MPa]	Phase	Mass fraction (average of 5 samples)			Standard deviation (mass fraction)			Deviation from reference data mass fraction			
			CO ₂	C ₁₂ OH	nC ₁₆	CO ₂	C ₁₂ OH	nC ₁₆	CO ₂	C ₁₂ OH	nC ₁₆	
60.0	10.0	Liquid	0.311	0.456	0.234	0.002	0.002	0.001	0.05	0.03	0.02	[22]
		Vapor	0.996	0.002	0.002	0.000	0.000	0.000	0.00	0.00	0.00	
	15.0	Liquid	0.432	0.378	0.190	0.002	0.001	0.001	0.01	0.01	0.01	
		Vapor	0.911	0.049	0.040	0.003	0.002	0.001	0.01	0.01	0.00	
80.0	15.0	Liquid	0.369	0.419	0.212	0.006	0.004	0.002	0.03	0.02	0.01	[23]
		Vapor	0.962	0.022	0.016	0.000	0.000	0.000	0.02	0.01	0.01	
	17.5	Liquid	0.440	0.373	0.188	0.005	0.003	0.002	0.01	0.01	0.00	
		Vapor	0.892	0.063	0.045	0.002	0.001	0.001	0.04	0.03	0.01	

4. CONCLUSIONS

Equilibrium phase composition data for high-pressure ternary and multi-component systems are important, but design and construction of the associated equipment is often neglected in literature. This work reports on the development of a new high-pressure analytic phase equilibria setup. The equipment is well-suited to study ternary and higher mixtures with constituents ranging from volatile gases to mid-length hydrocarbons. Simultaneous sampling from two co-existing phases coupled with a unique GC configuration and quantitative calibration methods enable concurrent parallel online analysis.

The setup was successfully validated in a three-step process. Analyzing a one-phase ethane + 1-dodecanol + *n*-hexadecane system of known composition, root mean square errors in species-specific mass fraction ranged from 0.002 to 0.007. The CO₂ + 1-octanol binary was studied at 65.0 °C and pressures up to 16.9 MPa to enable comparison with literature data. Likewise, the CO₂ + 1-dodecanol + *n*-hexadecane ternary was investigated at 60.0 and 80.0 °C and pressures up to 17.5 MPa. Satisfactory agreement with reference data was obtained.

ACKNOWLEDGEMENT

This work is based on the research supported in part by the National Research Foundation of South Africa (Grant specific unique reference number (UID) 83966), Department of Trade and Industry (DTI) of South Africa through the Technology and Human Resources for Industry Programme (THRIP), and Sasol Technology (Pty) Ltd. The financial assistance of the National Research Foundation (DAAD-NRF) and the Skye Foundation Trust is also acknowledged. The authors acknowledge that opinions, findings and conclusions or recommendations expressed in any publication generated by the supported research are those of the authors, and that the sponsors accept no liability whatsoever in this regard.

REFERENCES

1. L. Gil, S.F. Otín, J. Muñoz Embid, M. Asunción Gallardo, S. Blanco, M. Artal, I. Velasco, *J. Supercrit. Fluids* **2008**, *44* (2), 123-138. DOI: 10.1016/j.supflu.2007.11.003
2. C.J. Chang, K.-L. Chiu, C.-Y. Day, *J. Supercrit. Fluids* **1998**, *12* (3), 223-237. DOI: 10.1016/S0896-8446(98)00076-X
3. H.S. Ghaziaskar, H. Eskandari, A. Daneshfar, *J. Chem. Eng. Data* **2003**, *48* (2), 236-240. DOI: 10.1021/je020074I
4. K. Khimeche, P. Alessi, I. Kikic, A. Dahmani, *J. Supercrit. Fluids* **2007**, *41* (1), 10-19. DOI: 10.1016/j.supflu.2006.09.004
5. Y. Yurekli, S.A. Altinkaya, *Fluid Phase Equilib.* **2009**, *277* (1), 35-41. DOI: 10.1016/j.fluid.2008.11.002
6. M. Görnert, G. Sadowski, *J. Supercrit. Fluids* **2008**, *46* (3), 218-225. DOI: 10.1016/j.supflu.2008.02.009
7. W. Dai, K. Kojima, K. Ochi, *J. Chem. Eng. Data* **1999**, *44* (1), 161-164. DOI: 10.1021/je980191+
8. G. Silva-Oliver, L.A. Galicia-Luna, S.I. Sandler, *Fluid Phase Equilib.* **2002**, *200* (1), 161-172. DOI: 10.1016/S0378-3812(02)00024-9
9. H. Byun, C. Kwak, *Kor. J. Chem. Eng.* **2002**, *19* (6), 1007-1013. DOI: 10.1007/BF02707225
10. G. Sieder, G. Maurer, *Fluid Phase Equilib.* **2004**, *225*, 85-99. DOI: 10.1016/j.fluid.2004.08.005
11. W. Gao, R.L. Robinson Jr., K.A.M. Gasem, *J. Chem. Eng. Data* **2001**, *46* (3), 609-612. DOI: 10.1021/je0003546
12. J. Ke, K.E. Reid, M. Poliakoff, *J. Supercrit. Fluids* **2007**, *40* (1), 27-39. DOI: 10.1016/j.supflu.2006.05.003
13. J.M.S. Fonseca, R. Dohrn, S. Peper, *Fluid Phase Equilib.* **2011**, *300* (1-2), 1-69. DOI: 10.1016/j.fluid.2010.09.017
14. S. Peper, R. Dohrn, *J. Supercrit. Fluids* **2012**, *66*, 2-15. DOI: 10.1016/j.supflu.2011.09.021

15. R. Dohrn, J.M.S. Fonseca, S. Peper, *Annu. Rev. Chem. Biomol. Eng.* **2012**, *3*, 343-367. DOI: 10.1146/annurev-chembioeng-062011-081008
16. F.C.v.N. Fourie, C.E. Schwarz, J.H. Knoetze, in *Supercritical Fluids*, 1st ed. (Ed: M.R. Belinsky), Nova Science Publishers, New York **2010**, Ch. 6.
17. M. Zamudio, C.E. Schwarz, J.H. Knoetze, *J. Supercrit. Fluids* **2013**, *84*, 132-145. DOI: 10.1016/j.supflu.2013.09.015
18. G.J.K. Bonthuys, C.E. Schwarz, A.J. Burger, J.H. Knoetze, *J. Supercrit. Fluids* **2011**, *57 (2)*, 101-111. DOI: 10.1016/j.supflu.2011.02.012
19. C.E. Schwarz, G.J.K. Bonthuys, R.F. van Schalkwyk, D.L. Laubscher, A.J. Burger, J.H. Knoetze, *J. Supercrit. Fluids* **2011**, *58 (3)*, 352-359. DOI: 10.1016/j.supflu.2011.07.005
20. F.C.v.N. Fourie, C.E. Schwarz, J.H. Knoetze, *J. Supercrit. Fluids* **2008**, *47 (2)*, 161-167. DOI: 10.1016/j.supflu.2008.07.001
21. S. Peper, V. Haverkamp, R. Dohrn, *J. Supercrit. Fluids* **2010**, *55 (2)*, 537-544. DOI: 10.1016/j.supflu.2010.09.014
22. I.F. Hölscher, *Ph.D. Thesis*, Ruhr-Universität Bochum **1988**.
23. A. Kordikowski, *Ph.D. Thesis*, Ruhr-Universität Bochum **1992**.

Chapter 4: PUBLICATION 2

**Analytic High-Pressure Phase Equilibria Part II:
Gas Chromatography and Sampling Method Development**

Frederick C. v. N. Fourie, Cara E. Schwarz*, Johannes H. Knoetze

Stellenbosch University, Department of Process Engineering, Private Bag X1, Matieland, 7602, South Africa,

Tel: +27 21 808 4487, Fax: +27 21 808 2059, E-mail: cschwarz@sun.ac.za

Chemical Engineering & Technology 39,8 (2016) 1475-1482.

Received 26 October 2015; Revised 9 February 2016; Accepted 31 March 2016

DOI: 10.1002/ceat.201500633

Declaration by the candidate

With regard to Chapter 4, the nature and scope of my contribution were as follows:

<u>Nature of contribution</u>	<u>Extent of contribution (%)</u>
I developed the sampling and calibration methods, identified and captured the disturbance types and conducted troubleshooting. I was the primary author, compiled the text and submitted the publication.	90 %

The following co-authors contributed to Chapter 4:

<u>Name</u>	<u>E-mail address</u>	<u>Nature of contribution</u>	<u>Extent of Contribution (%)</u>
Johannes H. Knoetze	jhk@sun.ac.za	Supervisor to the student, F.C.v.N Fourie	5 %
Cara E. Schwarz	cschwarz@sun.ac.za	Co-supervisor to the student, F.C.v.N. Fourie	5 %

Signature of candidate : Declaration with signature in possession of candidate and supervisor

Date : 10 November 2017

Declaration by co-authors

The undersigned hereby confirm that:

1. The declaration above accurately reflects the nature and extent of the contributions of the candidate and the co-authors to Chapter 4.
2. No other authors contributed to Chapter 4 besides those specified above.
3. Potential conflicts of interest have been revealed to all interested parties and that the necessary arrangements have been made to use the material in Chapter 4 of this dissertation.

<u>Signature</u>	<u>Institutional affiliation</u>	<u>Date</u>
Declaration with signature in possession of candidate and supervisor	Supervisor to the student, F.C.v.N Fourie	10 November 2017
Declaration with signature in possession of candidate and supervisor	Co-supervisor to the student, F.C.v.N. Fourie	10 November 2017

ABSTRACT

The phase equilibria of supercritical CO₂-alkane-alcohol mixtures were studied using online gas chromatography. Gas chromatograph design criteria and quantitative detector calibration methods are presented. An adapted manual calibration injection technique eliminated liner overload and pressure wave effects. Observation of the cell contents has proven essential for accurate vapor phase sampling. Visuals, often not visible to the naked eye, show that sampling can disrupt an equilibrated high-pressure system even though pressure and temperature remain constant to within 0.1 bar and 0.01 °C. Such disruptions may manifest in one of three phenomena: global mist formation, localized mist formation, or no-warning droplet formation.

Keywords: Detergents, High-pressure sampling, Online gas chromatography, Phase equilibria, Split injection

1. INTRODUCTION

High-pressure phase behavior is important for supercritical extraction process development. Phase behavior may refer to bubble - and dew point transitions [1], critical end point identification [2,3] or classifying phase behavior type [4]. In the context of this work, the focus is on quantifying two co-existing equilibrium phases in a ternary solvent-solute A-solute B mixture at temperatures above the solvent critical temperature.

This work was conducted as part of a project which considers supercritical extraction to separate detergent range alcohols and alkanes. The solvents CO₂, ethane and propane together with solutes in the range C₈ to C₆₀, but especially C₈ to C₂₂, have been studied [5,6]. Different functional groups, isomerism, and solute-solute interactions have been investigated as factors affecting system behavior [7,8]. Within this project, an analytic apparatus to measure multicomponent high-pressure phase equilibria via online gas chromatography (GC) was developed [9]. This apparatus is currently used to study ternary mixtures comprising CO₂ and the solutes *n*-dodecane (*n*C₁₂), 3,7-dimethyl-1-octanol (37DM1O) and 1-decanol (C₁₀OH).

The objective of this paper is threefold. Firstly, the experimental procedure from Fourie et al. [9] is expanded with an emphasis on the sampling procedure and optimum sample size. Secondly, online GC analysis is covered in detail. GC design criteria and requisite operator practices are presented. Development of and procedures for the quantitative solvent and solute calibration methods are discussed. Thirdly, experimental visuals and difficulties that stem from the sensitivity of a high-pressure equilibrium system are presented. Communicating these experiences may enable others to avoid similar pitfalls. Visual observations of the equilibrium cell contents depicting the effects of temperature non-uniformities and three different cases of sampling disturbances are presented. These effects are often not visible to the naked eye and, to the authors' knowledge, similar visuals are not available in literature. The sampling disturbances occurred even though pressure and temperature remained constant to within 0.1 bar and 0.01 °C, which highlights the challenges associated with high-pressure sampling.

Experimental procedures, and problems in particular, are too seldom communicated with the necessary clarity to benefit others. The authors hope to address this shortcoming and, in doing so, contribute toward the development of improved equipment and high-pressure sampling systems. Supporting information is available online.¹⁰

¹⁰ The supporting information specific to Publication 2 comprised two videos illustrating phenomena related to excessive sampling. Screen shots thereof are presented in Sections 4.2.1 and 4.2.2 of the main article.

2. MATERIALS AND METHODS

2.1 Experimental Setup

A static analytic apparatus with upper operating limits of 300 bar and 150 °C was used. The variable volume (75 - 125 ml) equilibrium cell enables visual observation of the interior and uses magnetic stirring. Two ROLSI™ samplers (Armines) feed to two parallel online GC pathways. The cell is heated with circulated liquid and a forced convection oven. Pressure is measured with an ONEhalf20 melt transmitter. Refer to Fourie et al. [9] for more detail on the apparatus. The materials listed in Table 4-1 were used without further purification.

Table 4-1. Materials.

Component	CAS	Purity	Supplier	Cat. No.
C ₁₂ OH	112-53-8	98 %	Sigma	12,679-9
nC ₁₂	112-40-3	99+ %	Sigma	29,787-9
C ₁₀ OH	112-30-1	≥ 98 %	Sigma	W23,650-0-K
		99 %		150584-3KG
37DM10	106-21-8	≥ 98 %	Sigma	W23,910-0-K
		≥ 98 %		W239100-1KG-K
2E1H	104-76-7	≥ 99.6 %	Sigma	538051-4L
		≥ 99.0 %	Fluka	04050
Ethane	78-84-0	≥ 99.5 %	Afrox	545201-SE-C
CO ₂	124-38-9	99.995 %	Air Products	K243C

2.2 Sampling

The sampling procedure uses three types of extraction and GC runs: slow purge, fast purge and analysis. Sampling starts with a slow purge run which involves successive vapor- and liquid-phase extractions until peak heights stabilize (Fig. 4-1). The time lapse between extractions varies from 20 s to 5 min and is governed by the sampled phase, sample size and system sensitivity. The latter increases as the total solubility pressure is approached, i.e., the pressure at which the mixture enters a one-phase region. Slow purge runs are conducted with an isothermal GC oven (250 °C), all flow routed toward the flame ionization detectors (FIDs), and last between 45 and 90 min in total. Multiple smaller purge extractions are used to clear the vapor phase capillary. This has proven more effective and less disruptive to system equilibrium than fewer large extractions. Conversely, a small number of larger extractions are suitable for liquid-phase purges. Interestingly, in proximity to the total solubility pressure where the vapor becomes more liquid-like, a typical liquid-purge approach works better for the vapor purges.

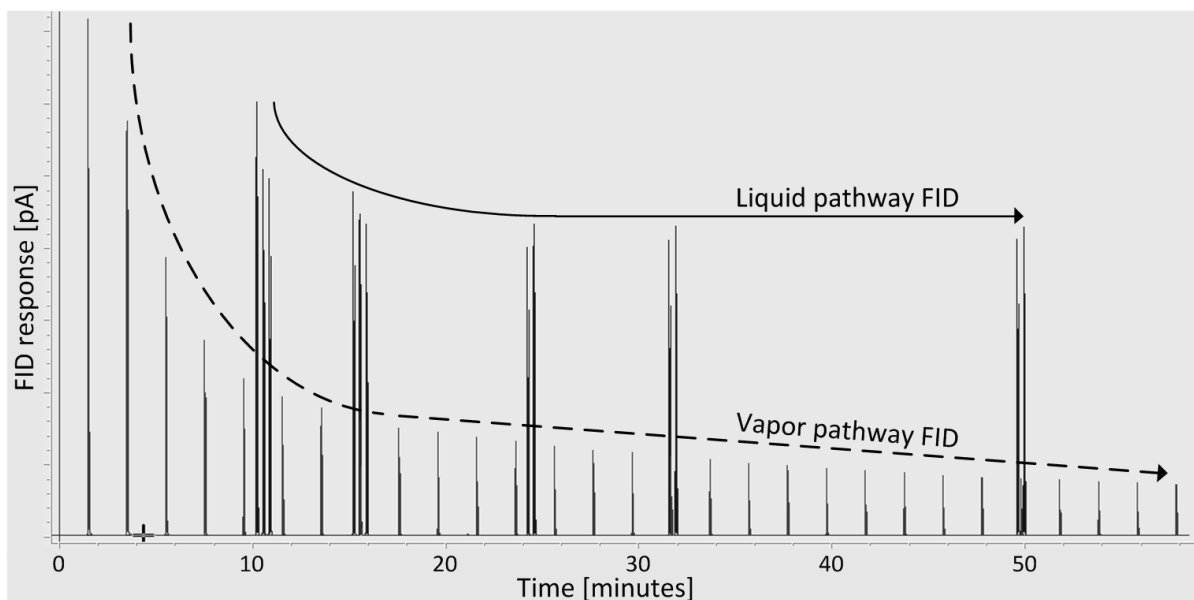


Figure 4-1. A slow purge run from $\text{CO}_2 + n\text{C}_{12} + \text{C}_{10}\text{OH}$ showing consecutive vapor purges and batches of liquid purges, 68.1 bar, 35.0 °C.

After slow purging, fast purge and analysis runs are alternated. Each 10-min analysis run is preceded by a fast purge run which entails three to five consecutive extractions, spaced 4 s apart, from both phases. Fast purge runs are conducted with an isothermal GC oven (250 °C), all flow routed to the FIDs, last 1.8 min and utilize an upward ramp in column flow. The latter enables one to start the run with a high split ratio and small column flow and after activating the gas saver, accelerate the species through the columns. Refer to Section 3 for details on analysis runs.

2.3 Optimum Sample Size

Two ROLSI™ are used for sampling. The optimum sample size is governed by:

- equilibrium pressure and temperature, phase composition, and physical properties of the sample constituents, all of which affect sample mobility.
- the ability to sample representatively. Small samples are often not representative, i.e., wrong, and unrepeatable. However, somewhat larger samples were found to be repeatable, but still not representative. This error is difficult to identify.
- chromatogram peak shape and accurate area integration. For lengthy sample times, solutes are easily refocused in the column inlet but volatile solvents may display skewed peaks for sample times in excess of 4 s.
- not disturbing equilibrium conditions even after repeated extractions.

- GC pneumatic control and the maximum split ratio.
- GC column and detector capacities for each species and the concentration thereof in the sample.
- attainable GC detector calibrations. Inlet dynamics (Section 3.1) and chromatogram peak shape impose respective upper and lower limits on the sample introduction rate. Gaseous species may present maximum calibrated quantities that are too small.

3. GC ANALYSIS

Design criteria affecting the online GC configuration (Fig. 4-2) include:

- Simultaneous analysis of both phases is preferred. If sampling disrupts the system the two samples in question are from the same equilibrium.
- Each sample contains two or more high boiling solutes and one volatile solvent. These groups often require diverse chromatography.
- CO₂ is an important supercritical solvent but is not detectable on an FID. Given its superior detection limits, an FID is preferred for hydrocarbon analysis. This is pertinent to analysis of the vapor phase which often contains small solute fractions.
- Methanizers enable FID analysis of CO₂ but are not well-suited for the solvent-rich vapor phases often encountered.
- Binary systems where solvent and solute differ greatly, may allow for aggressive GC methods. Solute similarity in ternary systems requires a more delicate approach.
- Optimum sample size varies (Section 2.3) and the ability to split samples offers valuable flexibility.

The analysis procedure is explained as follows: helium carrier gas is routed via heated tubing to and from the ROLSI™. Two samples, simultaneously extracted from the vapor and liquid phases, are vaporized, enter the inlets and pass through columns C₁ and C₂. These columns retain higher-boiling solutes and allow the solvent to pass unaffected. If the solvent is not suited for FID detection (CO₂), valves V₁ and V₂ direct the light fractions toward columns C₃ and C₄, the outlets of which are joined in a Y-piece before entering one thermal conductivity detector (TCD). C₃ and C₄ ensure some retention of the light fractions and, importantly, differ in length by a factor of two. This enables staggered analysis of two solvent peaks on one TCD. After all solvent has passed V₁ and V₂, the valves are switched and the higher boiling solutes are routed to the FIDs. Columns C₁ and C₂ separate the solutes contained in each sample. If the solvent is suited for FID detection (ethane), flow is directed to the FIDs throughout the run. This approach enables concurrent liquid- and vapor-phase analysis for mixture species ranging from light gases to mid-length hydrocarbons. Method parameters are tabulated in Fourie et al. [9].

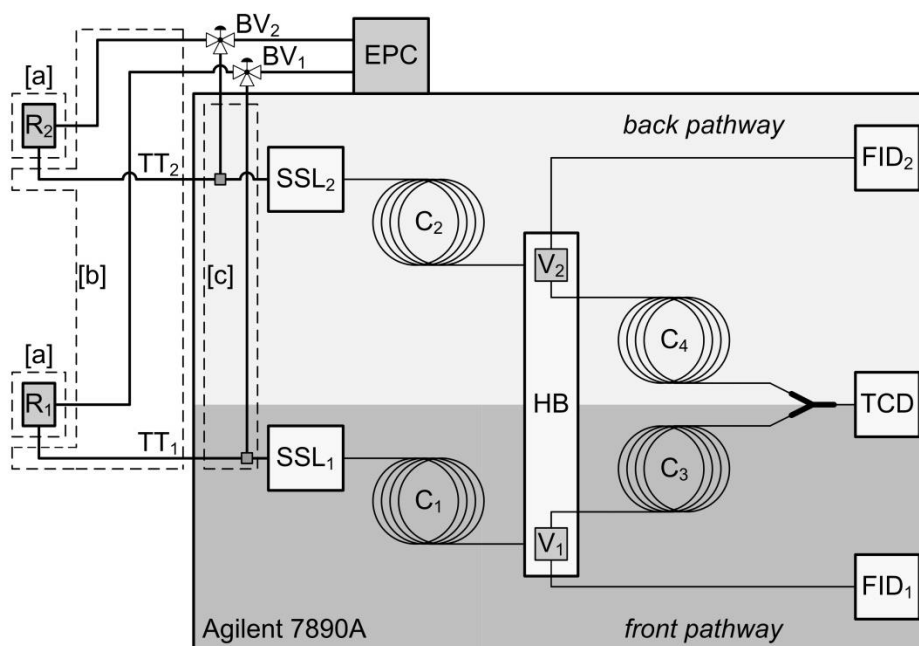


Figure 4-2. GC configuration: (BV) ball valve; (C₁, C₂) DB-1, $l = 30\text{ m}$, $\phi = 0.53\text{ mm}$, film = $1.5\ \mu\text{m}$; (C₃) HP-PLOT/Q, $l = 15\text{ m}$, $\phi = 0.53\text{ mm}$, film = $40\ \mu\text{m}$; (C₄) HP-PLOT/Q, $l = 30\text{ m}$, $\phi = 0.53\text{ mm}$, film = $40\ \mu\text{m}$; (EPC) carrier gas control; (HB) heated valve box; (R) ROLSI™; (SSL) split-splitless inlet; (TT) transfer tubing; (V) 4-port valve; broken lines indicate temperature controlled regions [a], [b] and [c]; reproduced from [9].

Split and septum purge flow affect the success of this GC method:

- The effective split ratio is dependent on split vent flow (Fig. 4-3). Split flow should be monitored for drift which could render calibration curves incorrect. Using a bubble flow meter, three flow rates are measured on each split vent for each sample or calibration injection.
- Septum purge flow should be deactivated during the sample transfer window (Fig. 4-3).
- If a gas saver function is used, it should be deactivated prior to the start of a run. This ensures stable split vent flow during the sample transfer window. For similar reasons, premature reactivation thereof should also be avoided. The minimum gas saver time depends on sample time, carrier gas linear velocity in the transfer tubing, transfer tubing length, inlet liner volume and total inlet flow rate.

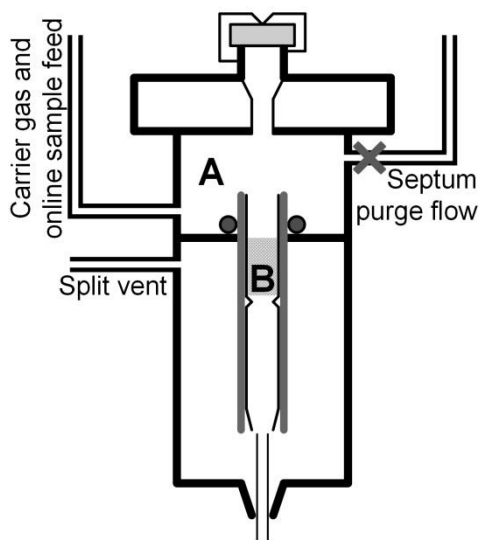


Figure 4-3. Schematic of a split-splitless GC inlet showing the different areas of sample introduction (A) and (B), and the requirement that septum purge flow be closed.

3.1 GC Calibration Method Development

Quantitative detector calibrations, based on the manual injection of a known mass, are used for all species. This decoupled technique is not affected by the equilibrium cell, sampling devices or sample transfer pathway. Calibration method development highlighted interesting inlet behavior. Samples withdrawn from the equilibrium cell travel 1.5 m prior to reaching the GC inlets. In contrast, manual calibration injections are introduced directly into the GC inlets. Sampling from ethane provided linear relationships between ROLSI™ opening time and detector response (Fig. 4-4 a). Initially, linear responses were not observed for manual ethane injections, which is a problematic discrepancy (dashed line in Fig. 4-4 b).

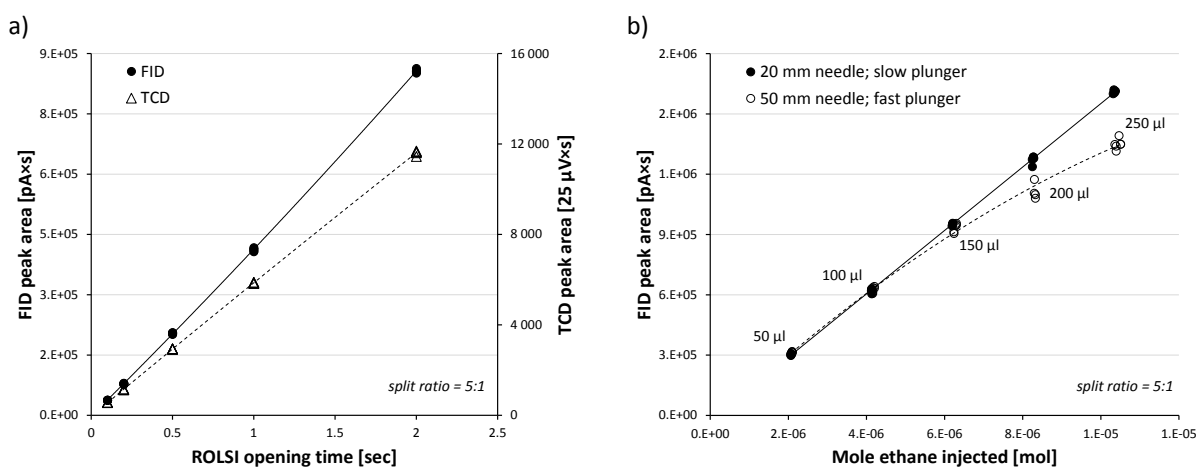


Figure 4-4. (a) Linear detector responses with ROLSI™ sample time from ethane, 79 bar, 80 °C; (b) needle length and plunger depression rate effects on manual ethane injections.

Grob [10] discusses liner overload and pressure wave effects. Gas is heated when injected into a hot inlet causing an increase in gas volume and inlet pressure. Liner overload occurs if the increased gas volume exceeds the liner internal volume, causing vapor to escape upward into the injection port. In addition, the inlet pressure spike may create a pressure wave which moves down the liner and disrupts the actual split ratio at the crucial time of sample splitting. A longer syringe needle reduces the pressure wave travel length and effective liner volume, both of which increase the pressure wave intensity upon reaching the column inlet. Compared to a manually injected sample, a sample transported from the ROLSI™ undergoes modifications which reduce the potential for pressure wave effects and liner overload: (i) the sample is broadened in space, (ii) the sample is vaporized prior to reaching the GC inlet, and (iii) transfer tubing plumbing delivers online samples to region A in Fig. 4-3 whilst manual injections with a 50-mm needle delivers samples to region B.

One can replicate these conditions for manual syringe injections by reducing the rapidity of sample introduction and lifting the sample introduction point. For an Agilent G3440A 112 inlet, an effective needle length of 20 mm ensures an injection height matching the online sample feed point. Custom syringe spacers and a slow plunger depression duration of roughly 4 s was incorporated in an adapted injection technique which produced linear relationships between injected mass and detector response (solid line in Fig. 4-4 b). Agreement at smaller and deviation at larger injected quantities support the pressure wave and liner overload theories.

3.2 GC Calibration Procedures

The guidelines in this section enable three-replicate injections with relative standard deviation values smaller than 1 % and four-point linear calibration curves with $R^2 \geq 0.9995$. Solvent calibrations involve the injection of a known gaseous volume at known temperature and pressure, which equates to a known mass. Characteristics of this procedure are:

- Samples are withdrawn from a glass cylinder filled from a gas bomb at high pressure. Expansion cooling causes a drop in gas temperature. The glass cylinder and solvent must equilibrate with ambient temperature before performing calibrations.
- Gas injections are performed with a cold needle, i.e., after insertion in the inlet there is no waiting period to heat the needle, and a slow plunger depression duration of ~ 4 s.
- A low thermal conductivity syringe handle prevents body heat transfer.
- To prevent parallax errors, only volumes of which the graduation is continued on the back of the syringe are used; this also applies to solute calibrations.
- Four samples washes and two sample pumps are standard.

Solute calibrations involve the injection of a known liquid volume. With density known, this equates to a known mass. Characteristics of this procedure are:

- Only plunger-in-needle syringes are used.
- Dilutions enable a range of solute calibrations. Liquid evaporation inside the needle during injection may cause species discrimination [10]. This risk is reduced by using a liquid solvent with comparable boiling point, a cold needle injection technique and a fast plunger depression rate. The solvent 2-ethyl-1-hexanol (2E1H) has a high boiling point which ensures gradual evaporation. As such, pressure wave effects and liner overload (Section 3.1) do not occur.
- Liners with glass wool packing (Agilent, 5183 4647) are used. The low thermal mass glass wool is cooled to the liquid boiling point enabling gradual liquid evaporation [10].
- 15 pre-injection solvent washes (2E1H), ten sample washes, two sample pumps, and 15 post-injection solvent washes (acetone) are standard.

4. EXPERIMENTAL DIFFICULTIES: SYSTEM SENSITIVITY AND VISUAL OBSERVATIONS

Experimental difficulties resulting from system sensitivity to temperature gradients or sampling disturbances are presented. In doing so, the authors attempt to convey how easily an equilibrated high-pressure system is disrupted and, consequently, the challenges associated with sampling such systems. Visual observation of the cell contents has proven essential for successful sampling from a high-pressure equilibrium system. This pertains to vapor phase sampling especially. A sapphire window and high-definition medical endoscope enable the operator to observe detail not visible to the naked eye.

4.1 *Temperature gradients*

Temperature gradients always exist in an equilibrium cell but should be small enough not to affect the experiment. Initially, heating of the cell relied only on liquid circulation through a jacket. This approach has proven sufficient for bubble and dew point studies where the dynamic nature of the experiment is compatible with larger temperature non-uniformities. However, in an equilibrated system, after phase settling and prior to any sampling, the authors observed tiny champagne-like bubbles, not visible to the naked eye, rising upward inside the liquid phase (Fig. 4-5 a). In addition, periodic droplet formation on, and separation from, the tip of the vapor-phase sample capillary was observed (Fig. 4-5 b).

A droplet would form without any visual disturbance of the surrounding vapor phase. After parting from the capillary tip, a thin liquid film remained which covered the capillary opening and hampered vapor phase sampling. Droplet regeneration rates varied from 6 sec to more than 20 min. Heat conduction along and seepage from the capillary were investigated and excluded as droplet formation causes.

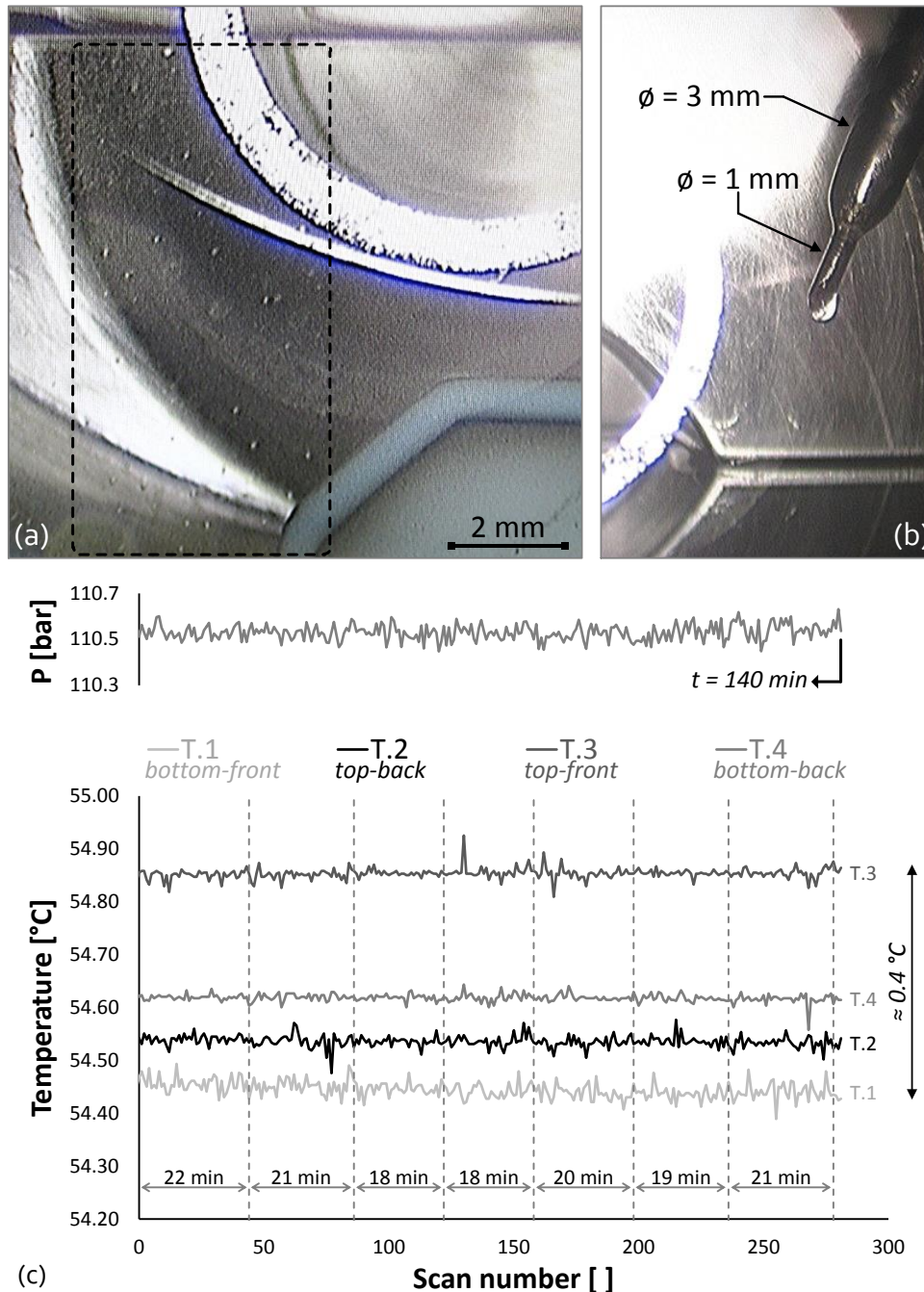


Figure 4-5. Temperature gradient effects: (a) liquid phase bubble formation in ethane + $C_{12}OH$, 140 bar, 63 °C; (b) vapor capillary droplet formation in ethane + $C_{12}OH$, 126 bar, 80 °C; and (c) recreation of droplet formation in $CO_2 + nC_{12} + C_{10}OH$. Pressure and temperature (T.1 to T.4) profiles after completion of stirring and phase settling. No sampling was conducted. Broken lines indicate droplet separation.

A forced convection oven, together with improved temperature monitoring capabilities [9], was constructed to address potential temperature gradients. This eliminated bubble formation in the liquid phase and pre-sampling droplet formation on the vapor capillary. The authors believe small temperature gradients may cause non-visible liquid particles to settle from the vapor phase. These non-visible particles then contact, coagulate on, and trickle down the vapor capillary culminating in a visible droplet.

Four Pt100's, T.1 to T.4, monitor the temperature in different areas of the equilibrium cell [9]. The Pt100 locations and cell temperature profiles are shown in Fig. 4-6. At all operating temperatures, T.1 to T.4 fall within a 0.05 °C band. For illustrative purposes, vapor capillary droplet formation as a result of temperature gradients was recreated by imposing a 0.4 °C temperature spread in the cell, i.e., $T.3 - T.1 \approx 0.4$ °C. After stirring and phase settling, in the absence of any sampling, a droplet separated every 18 to 22 min despite stable pressure and temperature behavior (Fig. 4-5 c). It is difficult to define a maximum allowable temperature spread that will not result in droplet formation because it depends on the species involved, phase compositions, temperature and pressure.

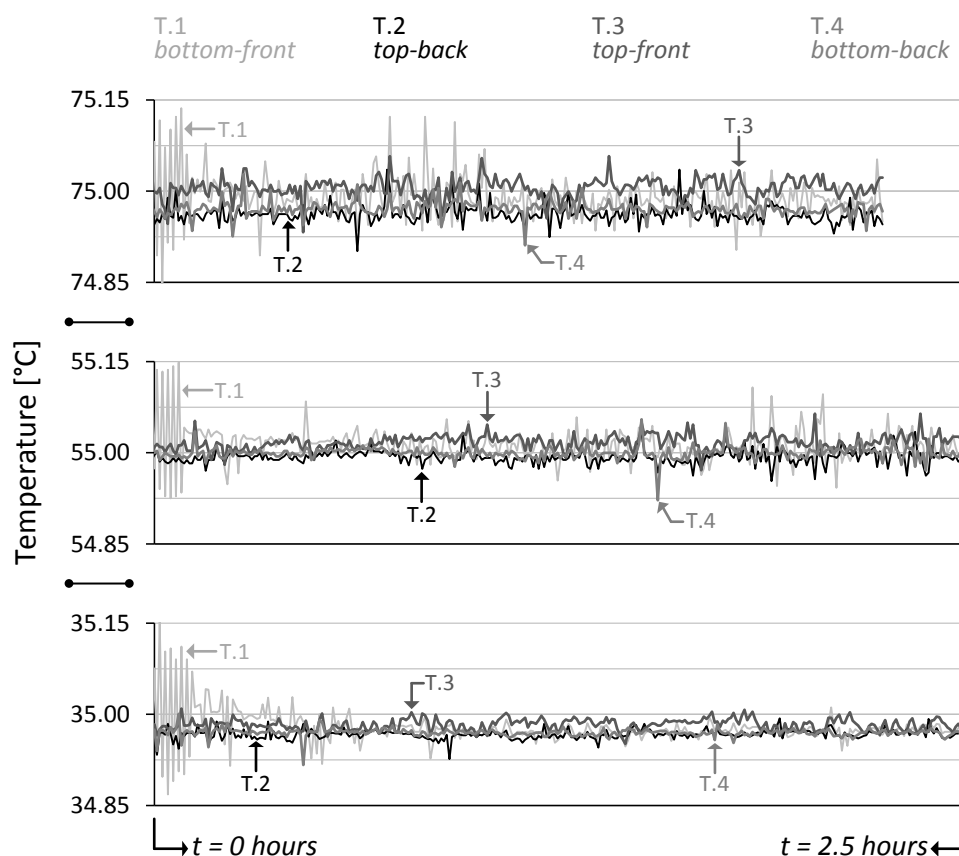


Figure 4-6. The equilibrium cell temperature profiles at 35, 55 and 75 °C. T.1 to T.4 are located in the cell. T.1 is destabilized during magnetic stirring but normalizes thereafter.

4.2 Excessive sampling

Optimum sample size varies, is difficult to predict, and requires adjustment as one moves between different temperatures and pressures (Section 2.3). Consequently, the operator may encounter occasional sampling-related disturbances. Vapor phase sampling has proven more likely to disrupt an equilibrium system than liquid phase sampling. Three sampling disturbances are discussed: global mist formation, localized mist formation, and no-warning droplet formation. The authors concede this terminology is not universal or fully descriptive. All phenomena depicted in Section 4.2 were observed (i) in an equilibrated system after phase separation, (ii) in the absence of stirring, (iii) whilst pressure and temperature remained constant to within 0.1 bar and 0.01 °C, and (iv) during the sampling procedure as described in Section 2.2.

4.2.1 Global Mist Formation

Global mist formation occurs when sampling causes small mist-like liquid particles to gently settle from the vapor phase (Fig. 4-7). Global implies the mist particles are distributed more or less throughout the entire vapor phase. The mist particle size and intensity may vary, but it is often not visible to the naked eye. Low-intensity mist could not be captured for printing purposes. Also refer to Video S1 in the Supporting Information. The occurrence of global mist formation is dependent on the equilibrium conditions, species involved, disturbance size, and proximity to total solubility pressure. These factors also govern the time required for mist particles to clear; anything from 30 s to 60 min was observed. Apart from being an obvious disturbance that should be avoided, mist particles may coagulate on the vapor sample capillary culminating in a liquid film covering the capillary opening. This further hampers the vapor sampling procedure.

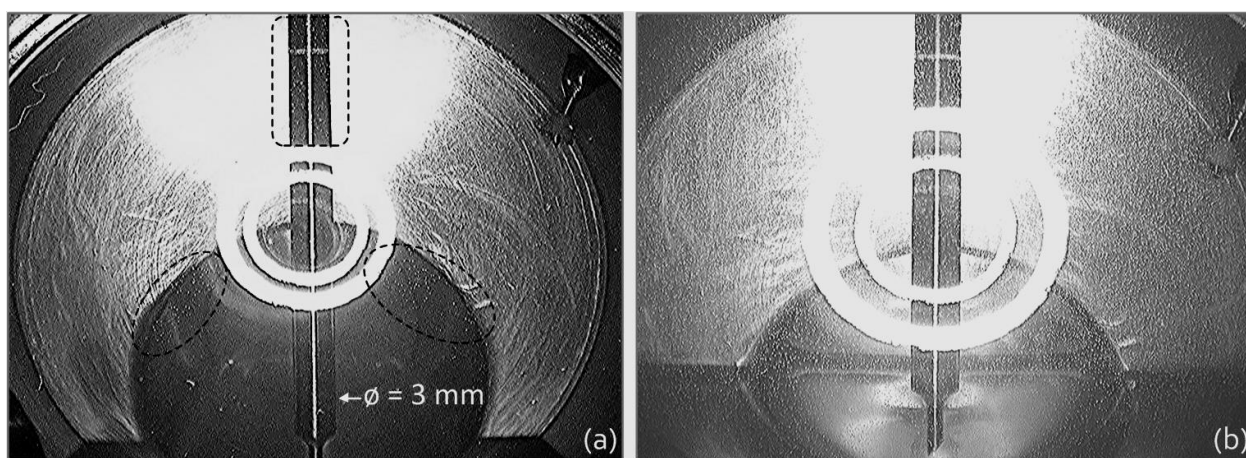


Figure 4-7. Global mist formation of (a) medium intensity in $\text{CO}_2 + n\text{C}_{12} + \text{C}_{10}\text{OH}$, 123.0 bar, 55.0 °C;
(b) high intensity in $\text{CO}_2 + 37\text{DM}10 + \text{C}_{10}\text{OH}$, 182.1 bar, 35.0 °C.

4.2.2 Localized Mist Formation

Localized mist formation occurs when extracting a large vapor sample over a short time period at high pressure. The visual effect is more intense, confined to a smaller, localized area and of shorter duration compared to global mist formation. Mist particles rapidly form at and spread from the vapor capillary opening in a nebulized cloud or whip-like fashion (Fig. 4-8). Video S2 better illustrates the rapidity thereof. In the authors' experience, accurate vapor phase quantification is possible despite localized mist formation and, although best avoided, it is less detrimental to the experimental procedure than global mist formation.

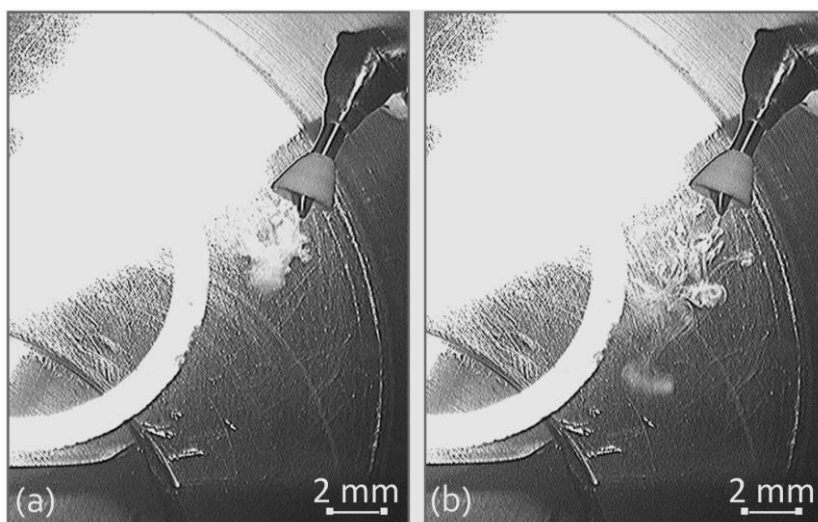


Figure 4-8. Localized mist formation of high intensity in $\text{CO}_2 + 37\text{DM10} + \text{C}_{10}\text{OH}$, 182.2 bar, 35.0 °C: vapor-phase capillary (a) at the time of sampling; (b) 0.2 s after sampling. Sample time: 0.01 s.

4.2.3 No-warning Droplet Formation

In proximity to the total solubility pressure, equilibrium systems are prone to disturbances. When sampling such a system, even a gentle approach may lead to liquid, which seems to appear from nowhere, forming on the vapor phase capillary tip. This happens without any visual warning, i.e., there is no visible mist formation preceding droplet formation, and might be the result of a phenomenon similar to global mist formation, but occurring on a nonvisible scale. The extent of liquid formation can range from a thin film to a complete droplet eventually separating from the capillary tip (Fig. 4-9), all of which jeopardize sampling via liquid contamination of the vapor sample.

A time lag exists in the cause-effect relationship; no-warning droplet formation has been observed up to 50 min after sampling was stopped. There appears to be a parallel between small temperature gradients (Section 4.1) and small sampling disturbances, both of which may create nonvisible liquid particles coagulating on the vapor capillary culminating in a visible droplet.

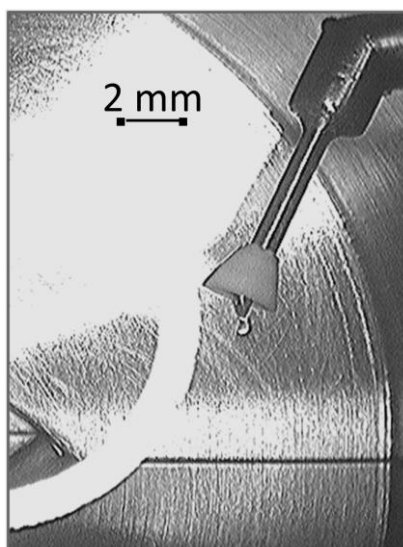


Figure 4-9. No-warning droplet formation in $\text{CO}_2 + 37\text{DM10} + \text{C}_{10}\text{OH}$, 157.2 bar, 55.0 °C.

4.3 Vapor Capillary Cone

In Figs. 4-7 to 4-9, a hollow polyether ether ketone (PEEK) cone, with chamfered interior to provide a sharp outer edge, is visible on the vapor sample capillary. This cone serves to decrease the long-term impact of global mist formation by reducing liquid deposit on the capillary opening. Global mist formation is not condoned; if it does occur, the operator must adjust the sampling approach. However, minimizing liquid deposition reduces subsequent down time since fewer purge extractions are required to clear the liquid contaminant. The cone may prove counter-productive: when vapor and liquid densities are similar, even slow stirring creates turbulent mixing (Fig. 4-10) and suspended liquid particles may clog the cone, which hampers vapor phase sampling. One can circumvent this problem by stirring in a stop-start fashion but this reduces stirring efficiency to a point where in excess of 8 hours may be required for the transitional phase [9] to develop fully.

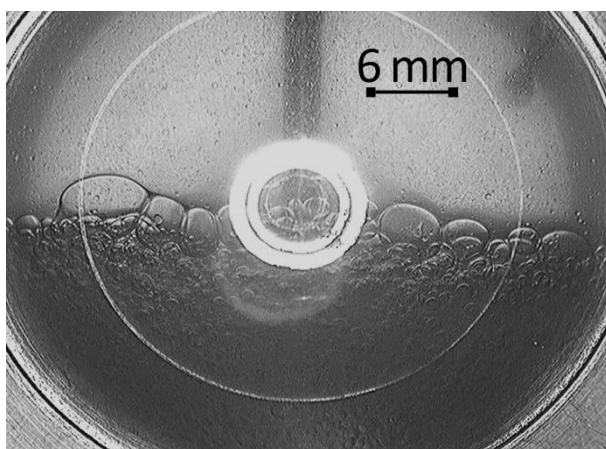


Figure 4-10. Turbulent mixing when stirring at 130 rpm in $\text{CO}_2 + 37\text{DM10} + \text{C}_{10}\text{OH}$, 182.1 bar, 35 °C.

5. CONCLUSIONS

The preferred approach to sampling an equilibrated high-pressure two-phase system is phase-specific and the vapor-approach in particular requires adaptation as one approaches the total solubility pressure. Optimum sample size is governed by many factors, is difficult to predict, and requires adjustment for different operating conditions. Development of the quantitative GC calibration methods highlighted interesting inlet behavior. An adapted manual injection technique with reduced effective needle length and rate of sample introduction was necessary to avoid liner overload and pressure wave effects. Repeatable injections (relative standard deviation < 1 %) and linear calibration curves ($R^2 \geq 0.9995$) were obtained.

Equilibrium cell temperature non-uniformities may cause droplet formation on a vapor phase capillary, but the maximum allowable temperature spread is difficult to define. Visual observation of the cell contents has proven essential for accurate vapor phase sampling. Even if pressure remains unaffected to within 0.1 bar, sampling disturbances may manifest in one of three visible phenomena: global mist formation, localized mist formation, or no-warning droplet formation. Depending on the disturbance intensity, the aforementioned three phenomena may not be visible to the naked eye, being a consideration to keep in mind during equipment design.

ACKNOWLEDGEMENTS

This work is based on research supported in part by the National Research Foundation of South Africa (Grant specific unique reference number (UID) 83966), the Department of Trade and Industry (DTI) of South Africa through the Technology and Human Resources for Industry Programme (THRIP), and Sasol Technology (Pty) Ltd. The financial assistance of the DAAD-NRF and the Skye Foundation Trust is also acknowledged. The authors acknowledge that opinions, findings, and conclusions or recommendations expressed in any publication generated by the supported research are those of the authors, and that the sponsors accept no liability whatsoever in this regard.

ABBREVIATIONS

2E1H	:	2-ethyl-1-hexanol
37DM10	:	3,7-dimethyl-1-octanol
C ₁₀ OH	:	1-decanol
C ₁₂ OH	:	1-dodecanol
FID	:	flame ionization detector
nC ₁₂	:	n-dodecane
PEEK	:	polyether ether ketone
TCD	:	thermal conductivity detector

REFERENCES

1. S. Raeissi, C.J. Peters, *J. Supercrit. Fluids* **2002**, *23* (1), 1-9. DOI: 10.1016/S0896-8446(01)00137-1
2. L.E. Gutiérrez M, K.D. Luks, *Fluid Phase Equilib.* **2002**, *198* (1), 29-36. DOI: 10.1016/S0378-3812(01)00735-X
3. G.M. Schneider, A.L. Scheidgen, D. Klante, *Ind. Eng. Chem. Res.* **2000**, *39* (12), 4476-4480. DOI: 10.1021/ie0001669
4. K. Gauter, L.J. Florusse, C.J. Peters, J. de Swaan Arons, *Fluid Phase Equilib.* **1996**, *116* (1-2), 445-453. DOI: 10.1016/0378-3812(95)02917-6
5. C.E. Schwarz, I. Nieuwoudt, J.H. Knoetze, *Fluid Phase Equilib.* **2006**, *247* (1-2), 169-174. DOI: 10.1016/j.fluid.2006.06.023
6. C.E. Schwarz, I. Nieuwoudt, J.H. Knoetze, *J. Supercrit. Fluids* **2008**, *46* (3), 226-232. DOI: 10.1016/j.supflu.2008.05.007
7. F.C.v.N. Fourie, C.E. Schwarz, J.H. Knoetze, *J. Supercrit. Fluids* **2008**, *47* (2), 161-167. DOI: 10.1016/j.supflu.2008.07.001
8. M. Zamudio, C.E. Schwarz, J.H. Knoetze, *J. Supercrit. Fluids* **2013**, *84*, 132-145. DOI: doi:10.1016/j.supflu.2013.09.015
9. F.C.v.N. Fourie, C.E. Schwarz, J.H. Knoetze, *Chem. Eng. Technol.* **2015**, *38* (7), 1165-1172. DOI: 10.1002/ceat.201400643
10. K. Grob, *Split and Splitless Injection for Quantitative Gas Chromatography*, 4th ed., Wiley-VCH, Weinheim **2001**.

Chapter 5: PUBLICATION 3

**CO₂ + *n*-dodecane + 3,7-dimethyl-1-octanol: High pressure experimental
phase equilibria data and thermodynamic modelling**

Frederick C. v. N. Fourie^{a,1}, Cara E. Schwarz^a, Johannes H. Knoetze^{a,*}

^aStellenbosch University, Department of Process Engineering, Private Bag X1, Matieland, 7602, South Africa,

Tel: +27 21 808 4204, Fax: +27 21 808 2059, E-mail: jhk@sun.ac.za

¹Present address: Sasol, 1 Klasie Havenga, Sasolburg, 1947, South Africa, Tel: +27 16 960 2611

The Journal of Supercritical Fluids 130 (2017) 105-117.

Received 27 May 2017; Revised 20 July 2017; Accepted 21 July 2017

DOI: 10.1016/j.supflu.2017.07.027

Declaration by the candidate

With regard to Chapter 5, the nature and scope of my contribution were as follows:

<u>Nature of contribution</u>	<u>Extent of contribution (%)</u>
I was responsible for experimental work, thermodynamic modelling, processing of results and interpretation of system behaviour. I was the primary author, compiled the text and submitted the publication.	90 %

The following co-authors contributed to Chapter 5:

<u>Name</u>	<u>E-mail address</u>	<u>Nature of contribution</u>	<u>Extent of Contribution (%)</u>
Johannes H. Knoetze	jhk@sun.ac.za	Supervisor to the student, F.C.v.N Fourie	5 %
Cara E. Schwarz	cschwarz@sun.ac.za	Co-supervisor to the student, F.C.v.N. Fourie	5 %

Signature of candidate : Declaration with signature in possession of candidate and supervisor

Date : 10 November 2017

Declaration by co-authors

The undersigned hereby confirm that:

1. The declaration above accurately reflects the nature and extent of the contributions of the candidate and the co-authors to Chapter 5.
2. No other authors contributed to Chapter 5 besides those specified above.
3. Potential conflicts of interest have been revealed to all interested parties and that the necessary arrangements have been made to use the material in Chapter 5 of this dissertation.

<u>Signature</u>	<u>Institutional affiliation</u>	<u>Date</u>
Declaration with signature in possession of candidate and supervisor	Supervisor to the student, F.C.v.N Fourie	10 November 2017
Declaration with signature in possession of candidate and supervisor	Co-supervisor to the student, F.C.v.N. Fourie	10 November 2017

ABSTRACT

New high pressure VLE data for the ternary mixture CO₂ + *n*-dodecane (*n*C₁₂) + 3,7-dimethyl-1-octanol (37DM1O) are presented. A static apparatus with online analysis was used to measure phase compositions at 35, 55 and 75 °C, and pressures between 68 and 157 bar. In the high-*n*C₁₂ region the mixture displayed enhanced solubility, presenting as a pinched two-phase band and s-shaped liquid phase curves. Relative solubility, an indicator of fractionation sharpness, increased with 37DM1O content and the 75:25 *n*C₁₂:37DM1O mixture cannot be separated using CO₂. RK-ASPEN, SR-POLAR, PR-BM and PC-SAFT models were evaluated for their ability to correlate these data. RK-ASPEN and PC-SAFT models provided the best and worst correlation of equilibrium pressures with respective percentage average absolute deviations of 3.1 % and 8.5 %. RK-ASPEN model was impressive in its ability to capture the co-solubility pinch seen for the 75:25 *n*C₁₂:37DM1O mixture and the resultant s-shaped liquid phase complexity.

Keywords: Detergents, Supercritical, Analytical VLE, Fractionation, Cubic EOS, PC-SAFT

Highlights

- New ternary high pressure VLE data for CO₂ + *n*-dodecane + 3,7-dimethyl-1-octanol
- Enhanced solubility in the high-*n*C₁₂ region presents as a pinched two-phase band
- Relative solubility increases with bulk solvent-free 3,7-dimethyl-1-octanol content
- RK-ASPEN enabled a %AAD_p of 3.1 % coupled with good qualitative correlations

NOMENCLATURE

2E1H	:	2-Ethyl-1-hexanol
37DM1O	:	3,7-Dimethyl-1-octanol
AAD	:	Average absolute deviation
BIP	:	Binary interaction parameter
C ₁₀ OH	:	1-Decanol
CSSRL	:	Constant solute-solute ratio lines
<i>k</i> _{ij}	:	Binary interaction parameter
<i>l</i> _{ij}	:	Binary interaction parameter
<i>m</i>	:	Segment number in PC-SAFT

M	:	Number of data points
nC_{12}	:	<i>n</i> -Dodecane
$\rho_{1/2/3}$:	SR-POLAR polar parameter
P	:	Pressure
P_c	:	Critical pressure
P_r	:	Reduced pressure (P/P_c)
p^{sat}	:	Saturated vapour pressure
ROLSI™	:	Rapid On-Line Sampler Injector
SFE	:	Supercritical fluid extraction
SP_{ij}	:	Separation potential between species <i>i</i> and <i>j</i>
Solute	:	nC_{12} or 37DM10 or $C_{10}OH$
Solvent	:	CO_2 or ethane
T	:	Temperature
T_c	:	Critical temperature
T_r	:	Reduced temperature (T/T_c)
TSP	:	Total solubility pressure
u	:	Absolute uncertainty
x_i	:	Mole fraction of species <i>i</i>
X_i	:	Liquid phase mass fraction of species <i>i</i>
Y_i	:	Vapour phase mass fraction of species <i>i</i>
Z_i	:	Bulk solvent-free mass fraction of species <i>i</i>

Greek letters

α_{ij}	:	Relative solubility between species <i>i</i> and <i>j</i>
η_i	:	RK-ASPEN polar parameter
ε/k	:	Dispersion energy parameter in PC-SAFT

ε^{AB}/k	:	Association energy parameter in PC-SAFT
κ^{AB}	:	Effective association volume parameter in PC-SAFT
σ	:	Segment diameter in PC-SAFT
ρ^{sat}	:	Saturated liquid density
ω	:	Acentric factor

Superscripts and subscripts

<i>exp</i>	:	Experimental
<i>i,j</i>	:	Component identifications
<i>sat</i>	:	Saturated
<i>TSP</i>	:	Total solubility pressure
\S	:	Extrapolation to 35 °C
*	:	VLE data via simultaneous sampling with two samplers

1. INTRODUCTION

Continued research on the use of supercritical solvents has enabled the development of a separations technology niche. Initial industrial applications focused mainly on the extraction of high value organic products from natural matrices but nowadays the tuneable properties of supercritical solvents are utilised in, amongst other, pharmaceuticals and novel materials development [1], enhanced oil recovery [2] and liquefied natural gas transport [3].

Detergent alcohols in the range $C_8 - C_{20}$ are often used as precursors in the production of alcohol ethoxylate surfactants [4]. Two popular catalytic detergent alcohol production pathways involve the hydroformylation of an alkene and subsequent hydrogenation of the aldehyde [4,5] or direct oxidation of an alkane [6,7]. The hydroformylation/hydrogenation approach is often applied to a distillation cut containing both alkenes and inert alkanes, whilst the alkane oxygenation approach is often incomplete. To drive economies of scale the feed stream may also contain a variety of carbon backbone lengths [5]. As a result, detergent alcohol product streams may exhibit a range of carbon backbone lengths, and contain significant residual alkanes, linear and branched alcohol isomers. These species' boiling points are often narrowly distributed or overlap, and supercritical fluid extraction (SFE) is considered as an alternative means of product fractionation.

Sizing of and control logic development for a SFE process requires a sound understanding of the mixture phase behaviour [8] and, in this regard, accurate and robust predictive models are valuable [9]. However, predictive models often fail for such systems because complex phase behaviour exists in high pressure mixtures containing one supercritical species [10]. In addition, systems containing both polar and non-polar species often exhibit strong deviations from ideality [11,12]. Experimental phase equilibria data remains a key contributor toward bridging this gap. Binary solvent-solute data, though useful, do not capture the solute-solute interactions that exist in ternary and higher mixtures. Ternary VLE data is better suited toward quantifying such solute-solute interactions but, unfortunately, remain scarce because the experiments are costly, time-consuming, and often reliant on successive, representative yet non-disruptive sampling from a small volume, high pressure equilibrium state [13].

This background has, to some extent, driven high pressure phase equilibria research at Stellenbosch University and the work presented forms part of a larger project which investigates the phase behaviour of the solutes nC_{12} , 37DM1O and $C_{10}OH$ in two different solvents, CO_2 and ethane. These solute species are representative of the aforementioned detergent alcohol product stream, and the solvents CO_2 and ethane have shown promise in their ability to fractionate similar mixtures [14].

The three key objectives of this study are to i) generate high pressure phase equilibria data for the ternary mixture $\text{CO}_2 + n\text{C}_{12} + 37\text{DM1O}$ at 35, 55 and 75 °C; ii) assess the ability of CO_2 to separate the solute species $n\text{C}_{12}$ and 37DM1O; and iii) use the new VLE data to evaluate the ability of four thermodynamic models, available within in a commercial process simulator, to correlate the measured equilibrium pressures and compositions.

2. MATERIALS AND METHODS

2.1 Project outline

Experimental data for $\text{CO}_2 + n\text{C}_{12} + 37\text{DM1O}$ were measured at 35, 55 and 75 °C and pressures between 68 and 157 bar. The larger project, which is also concerned with C_{10}OH and ethane, governed the target pressures, and three factors were considered when defining these: i) overlapping reduced pressures; ii) overlapping absolute pressures; and iii) binary total solubility pressures (TSP):

- i. The solvents CO_2 and ethane possess different critical pressures: $P_{c,\text{CO}_2} = 73.82$ bar and $P_{c,\text{ethane}} = 48.84$ bar. Thus, experimental pressures for CO_2 -containing systems will necessarily be higher than for ethane-containing systems. Comparisons between these studies will be more informative if reduced pressures are similar.
- ii. For comparative purposes, overlapping absolute pressures, both inter- and intra-solvent, are beneficial.
- iii. The temperature-specific total solubility pressure (TSP), defined as the highest binary mixture bubble or dew point pressure, was identified for each of the six binaries and is listed in Table 5-1. For each ternary mixture, the TSP of the more soluble species (i.e., the lower TSP) was used as guideline. Preliminary experiments [15] and former pilot plant studies [14,16] have shown, at least qualitatively, that interesting phase behaviour might exist in the ternary system at pressures marginally higher than the lower of the two binary TSP's. As such, one target pressure was selected close to yet above the lower TSP.

An overall reduced pressure minimum of 0.9, which equates to 68 and 45 bar for CO_2 and ethane respectively, was chosen. The resulting target experimental pressures and system-specific TSP's are listed in Fig. 5-1. The temperature-specific minimum experimental pressure was stepped up by one pressure-increment for each temperature-increment (i.e., 68 bar at 35 °C, 83 bar at 55 °C and 104 bar at 75 °C, with CO_2 as solvent).

Table 5-1. Binary mixture total solubility pressures [bar]

Solvent	Solute	Temperature [°C]			Reference
		35	55	75	
CO ₂	<i>n</i> C ₁₂	75	114	152	[17]
	37DM10	125	152	180	[18]
	C ₁₀ OH	328 [§]	211	211	[18]
Ethane	<i>n</i> C ₁₂	51 [§]	68	87	[19]
	37DM10	69	102	128	[20]
	C ₁₀ OH	95	126	148	[20]

CO ₂				Ethane		
TSP (<i>n</i> C ₁₂)	Pressure [bar]	TSP (37DM10)	P _r []	TSP (<i>n</i> C ₁₂)	Pressure [bar]	TSP (37DM10)
	68		0.9		45	
75 bar, 35 °C ←				51 bar, 35 °C ←		
	83		1.1		55	
	104		1.4	68 bar, 55 °C ←	68	→ 69 bar, 35 °C
114 bar, 55 °C ←					83	
	123	→ 125 bar, 35 °C	1.7	87 bar, 75 °C ←		
	140		1.9		93	
152 bar, 75 °C ←		→ 152 bar, 55 °C	2.1		104	→ 102 bar, 55 °C
	157	→ 180 bar, 75 °C	2.5		123	
	182		2.7		133	→ 128 bar, 75 °C
	200		2.9		140	
	217		3.2		157	
[17]	237	[18]		[19]		[20]

Figure 5-1. Binary total solubility pressures (TSP) and experimental outline for the ternary mixtures CO₂ + *n*C₁₂ + 37DM10 and ethane + *n*C₁₂ + 37DM10.

Three CO₂ + *n*C₁₂ + 37DM10 mixtures, which differ in solute-to-solute ratio, were studied experimentally. The three bulk *n*C₁₂:37DM10 mass fraction ratios, calculated on a solvent free basis, were 75:25, 50:50 and 25:75. In all subsequent references to solute ratios the first value applies to *n*C₁₂ and the second to 37DM10. The mixture-specific maximum experimental pressure was governed by the phase transition pressure thereof. No binary data were measured in this study. Binary data used for regressions or phase diagrams were obtained from literature and are referenced accordingly.

2.2 Experimental method

Experiments were conducted on a variable-volume (75 - 125 ml) static analytic apparatus. The setup enables visual observation of the cell contents with a medical endoscope, and operation at upper limits of 150 °C and 300 bar. Jacketed liquid circulation in combination with a forced convection oven is used to heat the cell, and the content is magnetically stirred. ROLSI™ samplers (Armines, France) coupled with online gas chromatography were used for sample extraction and analysis respectively. Refer to Fourie et al. [21] for a comprehensive discussion on the experimental setup, equilibrium cell design, temperature control and monitoring approach, and system validation. Refer to Fourie et al. [13] for information on the GC hardware configuration, analysis and detector calibration procedures, and optimum sample size. Furthermore, photo and video material illustrating the ease with which sampling can disrupt a high pressure equilibrium system, and the small scale of such disruptions, is available [13].

The procedure described by Fourie et al. [21] utilises two ROLSI™ samplers and dual simultaneous GC analysis on parallel pathways. During the course of this study one sampling and analysis pathway was temporarily defective and the majority of data presented here was produced using a single sampler. For these data, the initial part of the experimental procedure, which includes attaining temperature and pressure equilibrium, stirring, attaining visual stability, and phase settling, remained unchanged. The remainder of the experimental method was adapted as follows:

- A sample series was started with the functional sampler in the vapour phase and the defective sampler in the liquid phase. The vapour phase was sampled first. This involved a slow purge of the capillary, followed by alternating fast purge and analysis runs. Four samples of satisfactory composition repeatability [21] were withdrawn.
- The functional sampler was lowered into the liquid phase whilst simultaneously lifting the defective sampler to prevent variations in pressure. This procedure took 45 - 75 min to complete during which pressure remained constant to a resolution of 0.1 bar. The vapour phase was intentionally sampled first because potential system disturbances arising from pressure fluctuations are more likely to impact vapour phase sampling than liquid phase sampling [13]. That being said, the authors were able to swap the samplers without inducing any of the visual disturbances described by Fourie et al. [13].¹¹
- Brief, low-rpm stirring of the liquid phase was performed (3 min at 175 rpm was typical).
- Liquid phase sampling, which also entails a slow purge and alternating fast purge and analysis runs, was conducted. Again, four samples of satisfactory repeatability [21] were withdrawn.

¹¹ See also Section 4.2 on p. 90.

For the data reported in this work, the total uncertainties in pressure and temperature measurement were 0.35 bar and ± 0.1 °C [21]. The estimated absolute uncertainties in phase composition, $u(X_i)$ and $u(Y_i)$, depend on the phase, species and composition, and are reported in Table 5-2. The directional deviations of both solute species tend to be similar which should dampen the impact thereof on relative solute distributions (see Section 3.6.1).

Table 5-2. Estimated maximum absolute uncertainty in phase composition, expressed as mass %, for data reported in this work.

Liquid phase		Vapour phase			
Solutes	Solvent	Solutes		Solvent	
$u(X_i)$	$u(X_i)$	Mass % range	$u(Y_i)$	Mass % range	$u(Y_i)$
0.90 %	1.30 %	0 - 4 %	0.15 %	100 - 95 %	0.20 %
		4 - 8 %	0.30 %	95 - 90 %	0.35 %
		8 - 11 %	0.55 %	90 - 84 %	0.65 %

The materials listed in Table 5-3 were used without further purification.

Table 5-3. Materials used

Component	CAS	Purity	Supplier	Cat. No.
nC_{12}	112-40-3	99+ %	Sigma	29,787-9
		≥ 99 %	Sigma	D221104-2.5L
37DM1O	106-21-8	≥ 98 %	Sigma	W239100-1KG-K
		≥ 98 %	Sigma	W239100-4KG-K
		≥ 98 %	Sigma	W23,910-O-K
$C_{10}OH$	112-30-1	99 %	Sigma	150584-3KG
		≥ 98 %	Sigma	W23,650-O-K
2E1H	104-76-7	≥ 99.0 %	Fluka	04050-250ML
CO_2	124-38-9	99.995 %	Air Products	K243C

2.3 Modelling theory

The context of this study, which considers SFE as a means of detergent range alcohol product fractionation, guided the thermodynamic modelling approach. In this sense, holistic process modelling of industrial relevance, and not only modelling of the VLE behaviour, is the ultimate aim. As such, the authors restricted themselves to thermodynamic models available within a widely used commercial process simulator, Aspen Plus®. Four different approaches to modelling the new experimental data were used: three cubic equations of state (EOS) and PC-SAFT. The cubic EOS evaluated were RK-ASPEN, PR-BM and SR-POLAR. Zamudio et al. [17] have shown that these cubic models, and RK-ASPEN in particular, show promise in their ability to model systems similar to that investigated here. PC-SAFT, from within the SAFT family of EOS, was chosen as one example of what is currently regarded an advanced or state of the art thermodynamic model [22-24]. Concise background information on these models follows and modelling results are discussed in Section 3.3.

2.3.1 RK-ASPEN

The Redlich-Kwong-Aspen EOS is an extension of the Redlich-Kwong-Soave EOS [25]. Quadratic mixing rules are used for both the energy parameter a and the co-volume parameter b , and the binary interaction parameters (BIP) may incorporate linear temperature dependency [26]. Following the work by Soave [25], the species-specific energy parameter a_i is a function of temperature via the non-dimensional α_i whilst the co-volume parameter b_i remains temperature independent. If $T_{r,i} < 1$ the Mathias alpha function is applicable [26] whilst the Boston-Mathias extrapolation with modified d_i parameter is used for supercritical temperatures [27]. The polar parameter η_i is regressed off pure component saturated vapour pressure data.

2.3.2 SR-POLAR

The Redlich-Kwong-UNIFAC model [28] used the Redlich-Kwong-Soave EOS [25,26] as point of departure and forms the basis of the SR-POLAR property method. SR-POLAR is similar in structure to RK-ASPEN but the energy parameter a incorporates a second BIP, l_{ij} , and linear temperature dependency in T or $1/T$ may be incorporated for all BIP's [28]. Furthermore, up to three pure component polar parameters, $p_1 - p_{3,i}$, may be regressed off pure component saturated vapour pressure data. The Extended Mathias Alpha Function [26] is used for subcritical temperatures whilst the Boston-Mathias Extrapolation with modified d_i parameter is used if $T_{r,i} > 1$ [27].

2.3.3 PR-BM

The original form of the Peng-Robinson EOS [29], coupled with two adaptations, forms the basis for the PR-BM model. Firstly, asymmetric mixing rules were incorporated into the energy parameter a via a second BIP, l_{ij} , whilst the weighted-average co-volume parameter b remained unchanged [30]. Within PR-BM, BIP temperature dependency is structured similarly to that of SR-POLAR and the pure component parameters a_i and b_i are temperature dependent and independent respectively. The second change relates to the alpha function, α_i . Whilst the Soave-modified alpha function [25] is retained for subcritical temperatures, the Boston-Mathias Extrapolation thereof [27] is applicable if $T_{r,i} > 1$. T_c , P_c and ω are used as input quantities and, unlike the other three models evaluated in this work, no additional pure component parameter regression is required.

2.3.4 PC-SAFT

Gross and Sadowski [31,32] expanded upon earlier work by Chapmen et al. [33] and Huang and Radosz [34] to develop PC-SAFT. Within PC-SAFT, molecules are approximated as hard chains composed of spherical segments with dispersive forces assigned to the hard chains and not, as was the case for the earlier SAFT versions, to the hard spheres. This enables PC-SAFT to better capture the chain-length dependence of the attractive interactions [31]. Three pure component parameters are required for non-associating species – the segment number m , segment diameter σ , and segment energy parameter ε/k . Associating species require two additional pure component parameters – the association energy ε^{AB}/k , and effective association volume, κ^{AB} . In this work, 37DM1O was approximated as an associating non-polar species using the 2B association scheme. In similar fashion to Gross and Sadowski's original formulation [31], the cross dispersion energy term was corrected using a k_{ij} interaction parameter with optional linear temperature dependence in T (Eq. 5-1).

$$k_{ij} = k_{ij}^{(0)} + k_{ij}^{(1)} \times \frac{T [K]}{298.15}$$

Equation 5-1

For further detail on PC-SAFT refer to the original works of Gross and Sadowski [31,32] and, in addition, the publications by Mejbri et al. [24] and Diamantonis and Economou [35] which provide good breakdowns of the model equations.

3. RESULTS AND DISCUSSION

3.1 *Experimental reproducibility*

Table 5-4 indicates the long term reproducibility of the experimental method. Data are shown not only for $\text{CO}_2 + n\text{C}_{12} + 37\text{DM10}$ but also for the other two ternaries that form part of the larger study. Unlike repeatability, where the equilibrium conditions are preserved (Section 2.2), reproducibility implies the equilibrium conditions are willingly disrupted or a new loading is performed. A new loading involves an unload, equipment clean and reload of the experimental system. Each row in Table 5-4 reflects the mass % difference in composition between two different sample series at the same temperature, pressure and solute-solute ratio. The proximity to total solubility pressure (TSP), time interval between the two series, and whether or not a new loading was performed are also shown. The maximum absolute and average absolute for mass % deviations listed in Table 5-4 are 1.2 % and 0.3 % respectively.

Table 5-4. Long term reproducibility of the experimental data

T [°C]	P [bar]	Solute ratio []	$P_{TSP} - P_{exp}$ [bar]	Days between sample series	New loading?	Δ Vapour			Δ Liquid		
						CO ₂	Solute A	Solute B	CO ₂	Solute A	Solute B
$\text{CO}_2 + n\text{-dodecane} + 3,7\text{-dimethyl-1-octanol}$											
35	83.0	25:75	4.4	2	✘	0.1%	-0.1%	0.0%	-0.1%	-0.1%	0.1%
55	104.0	75:25	2.8	12	✘	0.1%	-0.1%	0.0%	-0.1%	0.1%	0.0%
	104.0	50:50	-	45	✓	0.3%	0.0%	-0.3%	-0.9%	0.3%	0.6%
			-	282	✓	0.6%	-0.2%	-0.5%	0.9%	0.0%	-0.9%
	106.5	50:50	5.4	6	✘	0.4%	-0.3%	-0.2%	-0.8%	0.3%	0.4%
75	123.0	50:50	-	530	✓	0.1%	0.0%	0.0%	-	-	-
	140.0	50:50	8.3	525	✓	-0.4%	0.3%	0.1%	-	-	-
$\text{CO}_2 + n\text{-dodecane} + 1\text{-decanol}$											
35	83.0	50:50	12.5	15	✘	0.7%	-0.2%	-0.5%	-0.5%	-0.1%	0.6%
55	123.0	25:75	39.9	49	✘	-0.2%	0.2%	0.1%	-0.1%	0.4%	-0.3%
75	140.0	75:25	9.0	12	✘	0.3%	-0.2%	0.0%	-0.1%	-0.1%	0.2%
$\text{CO}_2 + 3,7\text{-dimethyl-1-octanol} + 1\text{-decanol}$											
55	123.0	50:50	51.8	518	✓	-1.0%	0.5%	0.5%	1.2%	-0.6%	-0.6%
55	140.0	50:50	34.8	518	✓	0.4%	-0.3%	-0.2%	0.8%	-0.4%	-0.4%

3.2 Experimental data

Table 5-5 contains new experimental VLE data for the system $\text{CO}_2 + n\text{C}_{12} + 37\text{DM1O}$ at 35, 55 and 75 °C. All data not marked with an * were produced using only one sampler (see Section 2.2). Estimates of the absolute uncertainty in phase composition are provided in Table 5-2. The experimental data, along with modelling results, are also presented in Figs. 5-3 - 5-7.

Table 5-5. Experimental data for $\text{CO}_2 + n\text{C}_{12} + 37\text{DM1O}$ at 35.0, 55.0 and 75.0 °C, and pressures between 68.0 and 157.0 bar. An average of 4.2 and a minimum of 4 samples were analysed for each of the vapour and liquid phase data points. The average standard deviation in composition, obtained under repeatability conditions, was 0.0014 in mass fraction, or 0.14 mass %.

Temperature [°C]	Pressure [bar]	Liquid			Vapour		
		CO_2	$n\text{C}_{12}$	37DM1O	CO_2	$n\text{C}_{12}$	37DM1O
35.0	68.0	0.494	0.383	0.123	0.991	0.006	0.003
	68.0*	0.458	0.274	0.268	0.994	0.004	0.003
	68.0	0.380	0.162	0.458	0.996	0.002	0.002
	72.0	0.692	0.232	0.076	0.995	0.003	0.002
	72.0	0.571	0.215	0.213	0.995	0.003	0.002
	72.0	0.425	0.148	0.428	0.995	0.003	0.002
	83.0	0.605	0.085	0.309	0.875	0.040	0.085
55.0	83.0	0.373	0.476	0.152	0.991	0.006	0.002
	83.0*	0.359	0.325	0.316	0.996	0.003	0.001
	83.0	0.313	0.177	0.510	0.994	0.003	0.003
	104.0	0.631	0.279	0.090	0.969	0.023	0.008
	104.0*	0.546	0.229	0.225	0.974	0.016	0.010
	104.0	0.453	0.139	0.408	0.981	0.009	0.010
	106.5	0.696	0.230	0.075	0.959	0.031	0.010
	106.5	0.599	0.199	0.201	0.967	0.020	0.012
	106.5	0.483	0.131	0.386	0.979	0.010	0.011
	123.0	0.651	0.081	0.268	0.845	0.048	0.106
75.0	104.0	0.362	0.483	0.155	0.988	0.009	0.003
	104.0*	0.351	0.326	0.323	0.991	0.006	0.003
	104.0	0.325	0.176	0.499	0.988	0.005	0.007

Temperature [°C]	Pressure [bar]	Liquid			Vapour		
		CO ₂	nC ₁₂	37DM1O	CO ₂	nC ₁₂	37DM1O
75.0	123.0	0.484	0.391	0.125	0.969	0.023	0.008
	123.0	0.465	0.268	0.267	0.974	0.016	0.010
	123.0	0.396	0.152	0.452	0.980	0.009	0.011
	140.0	0.649	0.266	0.085	0.916	0.063	0.021
	140.0	0.601	0.197	0.202	0.934	0.038	0.028
	140.0	0.498	0.125	0.377	0.947	0.021	0.032
	143.5	0.722	0.210	0.068	0.877	0.092	0.031
	143.5	0.640	0.178	0.182	0.912	0.050	0.038
	143.5	0.524	0.118	0.358	0.945	0.022	0.034
	157.0	0.651	0.082	0.266	0.861	0.043	0.097

3.3 Modelling

Modelling was conducted using the Aspen Plus® simulation package. The performance of each model was evaluated via two means. Firstly, predicting the equilibrium pressures of the vapour and liquid phases using temperature and composition as input. These results are reported as %AAD_p defined as

$$\%AAD_p = \frac{1}{M} \sum_{n=1}^M \left| \frac{P_{predict} - P_{experimental}}{P_{experimental}} \right| \times 100 \%$$

Equation 5-2

where M refers to the number of data points. Secondly, predicting the equilibrium vapour and liquid compositions using temperature and pressure as input. These results are reported on ternary Gibbs phase diagrams and provide a valuable visual indication of the qualitative performance of a specific model (Section 3.5). For instance, a straight line correctly positioned through a concave curve could produce reasonable %AAD values even though it captures none of the system concavity. The input quantities used in approach 1, temperature and composition, and approach 2, temperature and pressure, were obtained from the ternary experimental data produced in this work. The low temperature experimental data at 35 °C, known to be challenging from a modelling point of view, was included in all theoretical work conducted in this study.

Saturated vapour pressure data were used to regress pure component parameters within the RK-ASPEN, SR-POLAR and PC-SAFT frameworks. The Extended Antoine vapour pressure equation was used to generate P^{sat} data for CO₂ and *n*C₁₂ whilst the NIST Wagner 25 liquid vapour pressure equation was used for 37DM1O [36].

Literature data for CO₂ + *n*C₁₂ [17,37-39] and CO₂ + 37DM1O [18,37] were used to regress solvent-solute binary interaction parameters (BIP). P - x_i envelopes and isobars at 2 bar increments were used to generate these data. The high pressure ternary experimental data produced in this work, at 35, 55 and 75 °C, were then used to regress solute-solute BIP's.

3.3.1 RK-ASPEN

RK-ASPEN pure component polar parameters (η_i), regressed off P^{sat} data [36], are listed in Table 5-6. A polar parameter was used for both the quadrupolar CO₂ and non-polar *n*C₁₂ because, according to Mathias [26], the polar parameter bears little relation to the pure component dipole moment. It should, instead, be viewed as an empirical parameter representing multiple lumped effects. The CO₂ + *n*C₁₂ and *n*C₁₂ + 37DM1O binary interactions were captured using temperature independent $k_{a,ij}^{(0)}$ and $k_{b,ij}^{(0)}$ parameters. Temperature dependency was incorporated for the CO₂ + 37DM1O interactions via the use of $k_{a,ij}^{(0)}$ and $k_{a,ij}^{(1)}$ parameters. These results are listed in Table 5-9 and the %AAD's in pressure, temperature, and vapour and liquid phase solute fractions are shown in Table 5-10. Despite efforts to optimise within each binary regression case, RK-ASPEN and the three models discussed hereafter all produced a larger error in vapour phase solute fraction for the CO₂ + alkane system than for the CO₂ + alcohol system (Table 5-10). This is counter-intuitive because the behaviour of an *n*-paraffin, with little functionality, should be easier to model than that of a branched alcohol.

Table 5-6. RK-ASPEN pure component polar parameters regressed in this work

Component	η_i []	%AAD P^{sat} [%]	T -range [°C]
CO ₂	0.0481	0.03	-23.15 - 27.85
<i>n</i> C ₁₂	0.0087	0.05	11.85 - 126.85
37DM1O	0.5008	0.12	11.85 - 131.85

3.3.2 SR-POLAR

Within SR-POLAR, P^{sat} data were used to regress two pure component polar parameters, p_1 and p_2 , for each of CO₂, nC₁₂ and 37DM1O (Table 5-7). The solvent-solute interactions were each characterised with one temperature independent $k_{\alpha,ij}^{(0)}$ parameter whilst the solute-solute interaction was best captured using two BIP's – a temperature independent $k_{\alpha,ij}^{(0)}$ together with a temperature dependent $k_{b,ij}$ (linear dependence in T). These parameters and the regression %AAD values are provided in Tables 5-9 and 5-10 respectively. The use of $I_{ij}^{(0)}$ and $I_{ji}^{(0)}$ parameters in conjunction with $k_{\alpha,ij}$'s, with the latter being either temperature dependent or independent, to describe the CO₂ + nC₁₂, CO₂ + 37DM1O and nC₁₂ + 37DM1O interactions was evaluated. This, however, led to degraded correlations of the new ternary VLE data and may allude to BIP inter-correlation, as observed by Lombard [40], resulting from the inclusion of a second BIP in the energy parameter a .

Table 5-7. SR-POLAR pure component polar parameters regressed in this work

Component	p_1 []	p_2 []	%AAD P^{sat} [%]	T -range [°C]
CO ₂	0.1221	-1.2224	0.01	-23.15 - 27.85
nC ₁₂	-0.0173	-2.1786	0.02	11.85 - 126.85
37DM1O	0.4004	-1.5001	0.03	11.85 - 131.85

3.3.3 PR-BM

The PR-BM method uses only three pure component parameters – P_c , T_c and ω – and does not require the regression of any additional pure component parameters. Linearly temperature dependent k_{ij} 's were regressed for all three interaction pairs (i.e., CO₂ + nC₁₂, CO₂ + 37DM1O, and nC₁₂ + 37DM1O) and are listed in Table 5-9. As was the case for SR-POLAR, incorporation of the I_{ij} and I_{ji} parameters within the energy parameter a led to degraded correlations of the new ternary VLE data, and therefore the I -parameters were excluded.

3.3.4 PC-SAFT

PC-SAFT pure component parameters for CO₂ and nC₁₂ were obtained from Gross and Sadowski [31]. In addition to P^{sat} data mentioned in Section 3.3, saturated liquid density (ρ^{sat}) and binary ethane + 37DM10 VLE data [20] were used to regress 37DM10 pure component dispersion (m , σ and ε/k) and association (ε^{AB}/k and κ^{AB}) parameters. The regression was augmented with binary VLE data because the inclusion of polar or association contributions along with dispersion effects may, according to Dominik et al. [41], result in multiple parameter sets which accurately correlate pure component data yet fail to predict mixture behaviour. The inclusion of one binary VLE data set in the regression helps to obtain a unique set of parameters. Ethane was chosen as binary solvent because pure component parameters thereof are well defined [31] and it contains no polar, association, or cyclic functionality. 37DM10 ρ^{sat} data were estimated using the VDNS-type NIST TDE Expansion equation [36]. The PC-SAFT pure component parameters used in this work are listed in Table 5-8. Temperature independent k_{ij}' s were used for the CO₂ + nC₁₂ and nC₁₂ + 37DM10 interactions whilst linear dependency in temperature was assigned to the CO₂ + 37DM10 interaction. These parameters and their associated regression errors are tabulated in Tables 5-9 and 5-10 respectively.

Table 5-8. PC-SAFT pure component parameters

Component	m	σ	ε/k	ε^{AB}/k	κ^{AB}	%AAD P^{sat}	%AAD ρ^{sat}	T-range	Reference
	[]	[Å]	[°C]	[°C]	[]	[%]	[%]	[°C]	
CO ₂	2.0729	2.7852	-103.94	-	-	2.78	2.73	-57.15 - 30.85	[31]
Ethane	1.6069	3.5206	-81.73	-	-	0.30	0.57	-183.15 - 31.85	[31,36]
nC ₁₂	5.3060	3.8959	-23.94	-	-	2.10	0.93	-10.15 - 384.85	[31,36]
37DM10	4.4587	3.8325	-2.75	2217.20	0.0029	0.71	6.63	11.85 - 131.85	This work

Table 5-9. Binary interaction parameters regressed in this work

Interaction pair	RK-ASPEN			SR-POLAR			PR-BM		PC-SAFT	
	$k_{a,ij}^{(0)}$	$k_{a,ij}^{(1)}$	$k_{b,ij}^{(0)}$	$k_{a,ij}^{(0)}$	$k_{b,ij}^{(0)}$	$k_{b,ij}^{(1)}$	$k_{ij}^{(0)}$	$k_{ij}^{(1)}$	$k_{ij}^{(0)}$	$k_{ij}^{(1)}$
CO ₂ + nC ₁₂	0.0883	-	0.0041	0.1059	-	-	0.3998	-0.0009	0.1223	-
CO ₂ + 37DM10	0.3127	-0.6997	-	0.0801	-	-	0.5499	-0.0015	0.2801	-0.1699
nC ₁₂ + 37DM10	0.1183	-	0.1491	0.0995	0.4718	-0.0013	0.5475	-0.0015	0.0240	-

Table 5-10. %AAD in P, T, and solute mass fraction in the liquid (X) and vapour (Y) phases for the BIP regressions from this work.

BIP's for CO₂ + nC₁₂ [17,37-39] and CO₂ + 37DM10 [17,37] were regressed off binary literature data. BIP's for nC₁₂ + 37DM10 were regressed of ternary experimental data from this work. Solute mass fraction deviations for the nC₁₂ + 37DM10 interaction are reported as an average of the nC₁₂ and 37DM10 deviations.

Interaction	RK-ASPEN				SR-POLAR				PR-BM				PC-SAFT			
	%AAD _P	%AAD _T	%AAD _X	%AAD _Y	%AAD _P	%AAD _T	%AAD _X	%AAD _Y	%AAD _P	%AAD _T	%AAD _X	%AAD _Y	%AAD _P	%AAD _T	%AAD _X	%AAD _Y
CO ₂ + nC ₁₂	1.54	3.25	0.53	23.04	3.07	6.10	1.40	69.94	3.00	3.39	1.04	52.17	4.59	11.96	1.77	56.23
CO ₂ + 37DM10	0.99	1.17	0.37	13.53	1.96	8.32	1.40	27.53	10.96	14.02	3.21	29.54	5.93	9.62	1.62	39.57
nC ₁₂ + 37DM10	1.26	0.87	0.32	27.52	0.37	3.61	0.40	26.53	3.35	3.47	0.63	33.46	4.34	9.12	0.75	36.33
TOTAL	73 %				151 %				158 %				182 %			

3.4 Comparison of model-predicted ternary mixture vapour and liquid phase pressures

The BIP's in Table 5-9 and the temperature and phase composition data in Table 5-5 were used to predict thirty equilibrium pressures for each of the vapour and liquid phases (Table 5-11). All three cubic EOS predicted a pressure in excess of 2 000 bar for the vapour phase simulation at 35 °C and 83 bar (refer to row 7 of Table 5-5), and these results were excluded from the %AAD_p calculations in Table 5-11. PC-SAFT was the exception with a more realistic albeit poor prediction of 55 bar. It is crude and yet interesting to note that totalising the twelve model-specific %AAD's from Table 5-10 matches the relative performance in terms of %AAD_p in predicted equilibrium pressure as observed in the combined-overall column of Table 5-11: RK-ASPEN < SR-POLAR < PR-BM < PC-SAFT.

Table 5-11. %AAD_p values for the model-predicted liquid and vapour phase equilibrium pressures in the system CO₂ + nC₁₂ + 37DM10. The experimental temperatures and vapour and liquid phase compositions from this work were used as inputs to the simulation cases. Deviations labelled as Overall were calculated across all 3 temperatures and deviations labelled as Combined were calculated for both the liquid and vapour phases.

Model	Liquid				Vapour				Combined			
	35 °C	55 °C	75 °C	Overall	35 °C	55 °C	75 °C	Overall	35 °C	55 °C	75 °C	Overall
RK-ASPEN	2.0	2.5	2.1	2.2	10.6	3.0	1.7	4.0	6.0	2.7	1.9	3.1
SR-POLAR	5.1	3.8	2.3	3.5	10.9	3.1	2.0	4.2	7.8	3.5	2.1	3.8
PR-BM	3.0	3.2	4.2	3.6	9.9	3.3	2.5	4.3	6.2	3.3	3.3	3.9
PC-SAFT	2.4	6.4	8.2	6.3	11.1	12.5	9.2	10.7	6.7	9.5	8.7	8.5

The %AAD_p's for vapour phase pressure predictions via all three cubic EOS are negatively correlated with temperature and decrease significantly from an average of 10.5 % at 35 °C to an average of 3.1 % at 55 °C. No temperature inversions were observed in this ternary system and therefore lower temperatures imply lower experimental pressures, which contribute to the large relative deviations witnessed at 35 °C. However, vapour phase average absolute pressure deviations, defined as

$$AAD_p = \frac{1}{M} \sum_{n=1}^M |P_{predict} - P_{experimental}|$$

Equation 5-3

where M is the number of data points and AAD_p is in units of pressure, also decrease markedly between 35 and 55 °C (Fig. 5-2). Behavioural complexity and therefore model deficiencies are known to occur at

temperatures marginally higher than the solvent T_c because of the steep solvent $d\rho/dP$ gradient encountered in this region [10]. This may explain the large improvement in cubic EOS performance between 35 and 55 °C. The temperature-dependency of deviations via PC-SAFT contrasts notably (Fig. 5-2). This discrepancy might be a result of the difference in underlying fundamentals between the cubic and SAFT-family EOS.

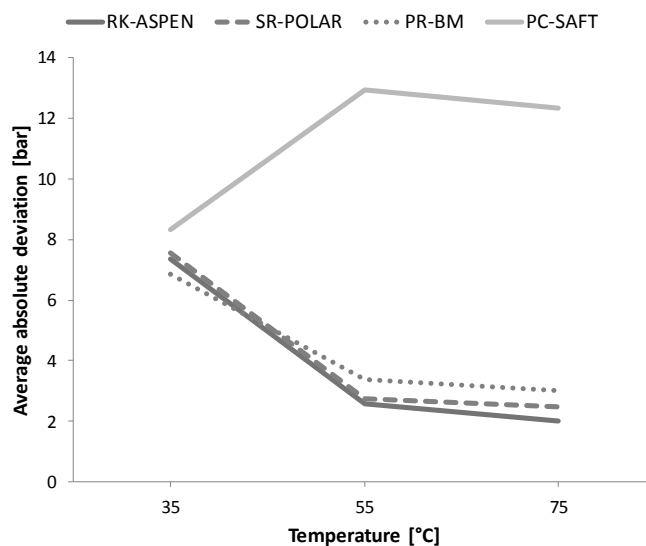


Figure 5-2. Average absolute deviations for vapour phase equilibrium pressure predictions, AAD_p , at 35, 55 and 75 °C.

The high vapour phase $\%AAD_p$ values obtained with PC-SAFT is eventually reflected in the inability of this model to predict vapour phase compositions with sufficient solute loading (Figs. 5-5, 5-6 e and 5-7). Liquid phase $\%AAD_p$ values via SR-POLAR decrease with increasing temperature whilst the opposite is true for PC-SAFT. Both these trends are visible in the Gibbs diagrams of Figs. 5-3, 5-4 and 5-6.

3.5 Experimental and model-predicted ternary mixture phase behaviour

The experimental data from this work and model predictions at 35, 55 and 75 °C are shown on truncated Gibbs diagrams in Figs. 5-3 - 5-7. References to low, medium and high pressures should be seen in the context of a 68 - 157 bar working pressure range. Vapour phase detail is shown only where the CO_2 mass fraction therein is smaller than 0.988. Ternary literature data shown in Figs. 5-3 - 5-7 were produced using a static-synthetic apparatus [17] and cannot provide information on ternary tie lines.

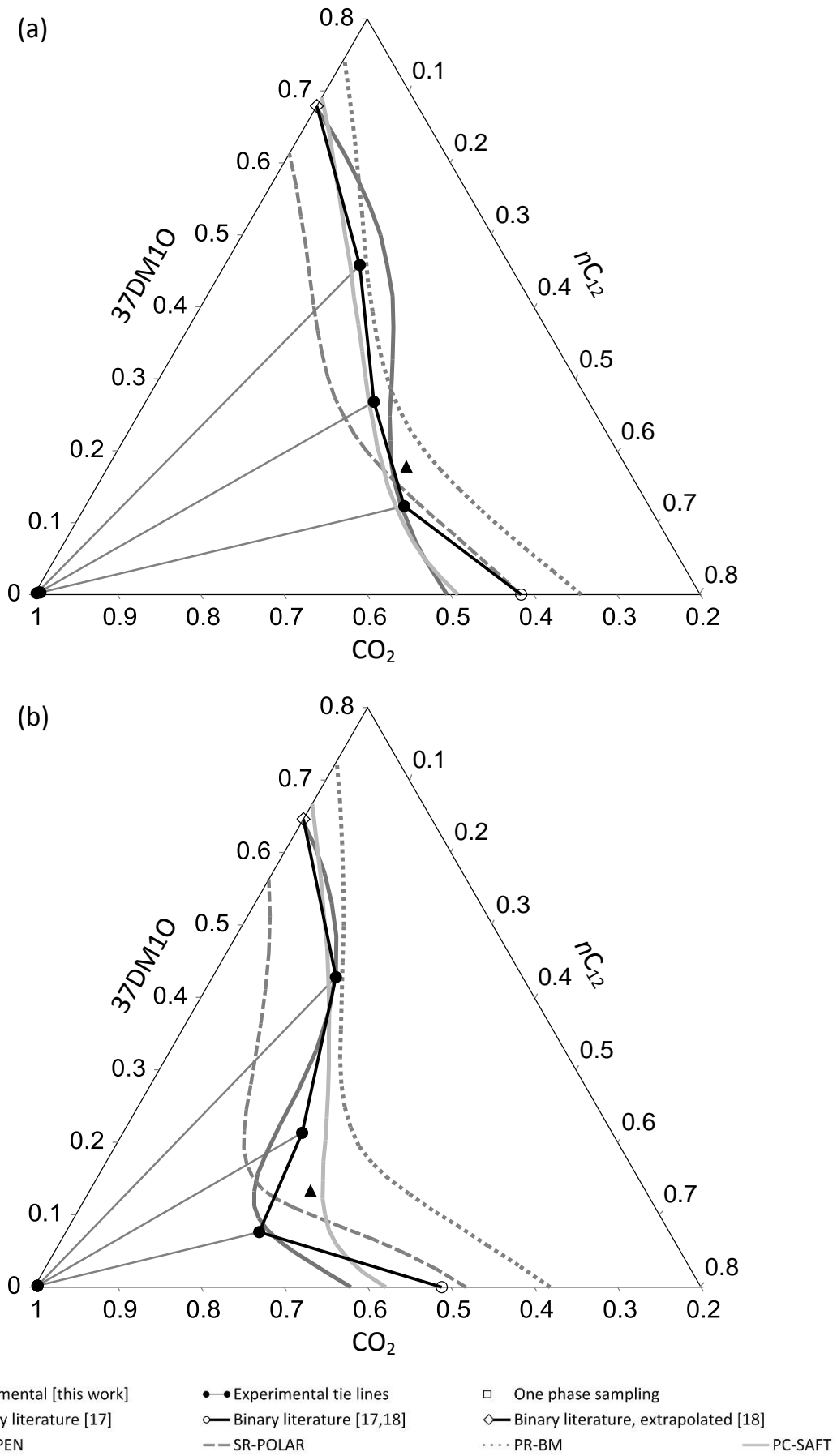


Figure 5-3. $\text{CO}_2 + n\text{C}_{12} + 37\text{DM}10$ at $35.0\text{ }^\circ\text{C}$ and (a) 68.0 bar ; (b) 72.0 bar ; and (c) 83.0 bar .

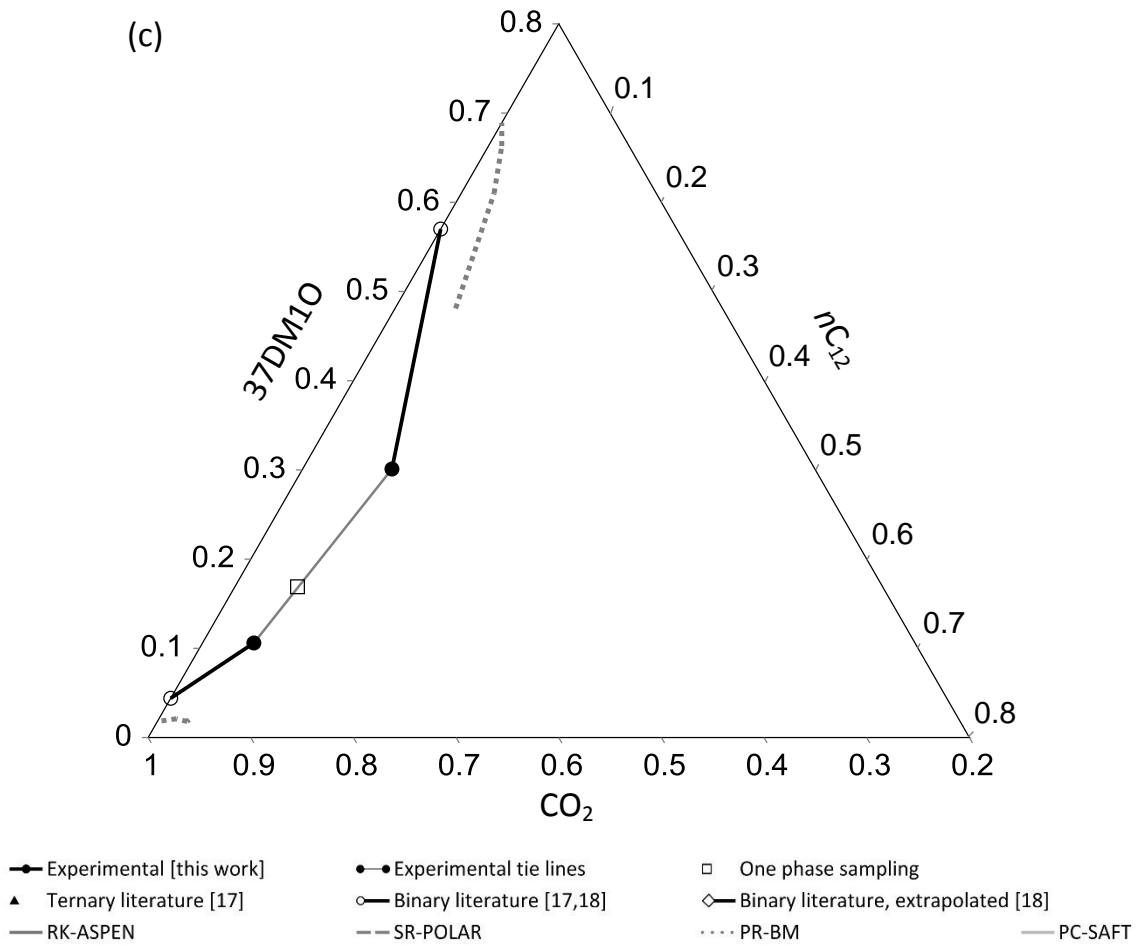
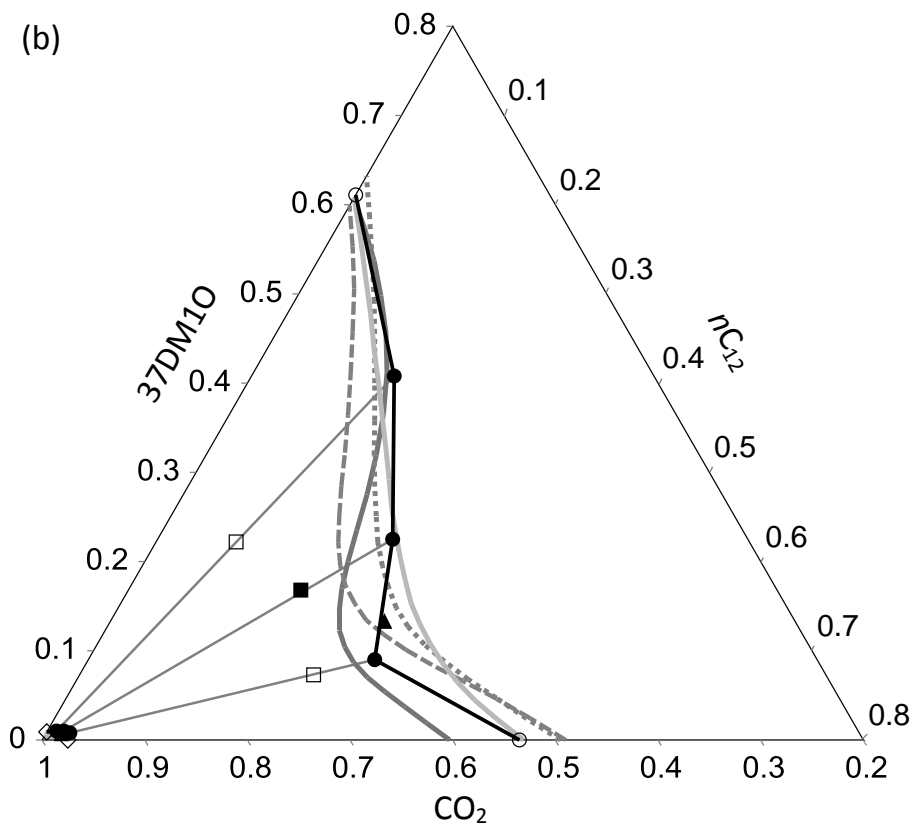
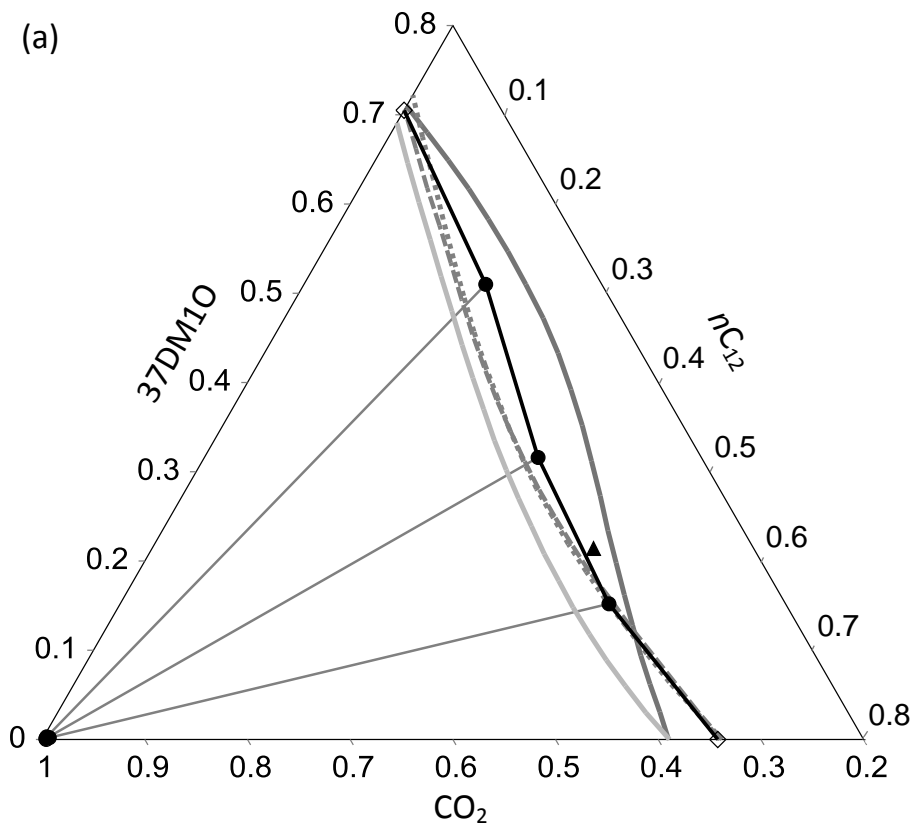
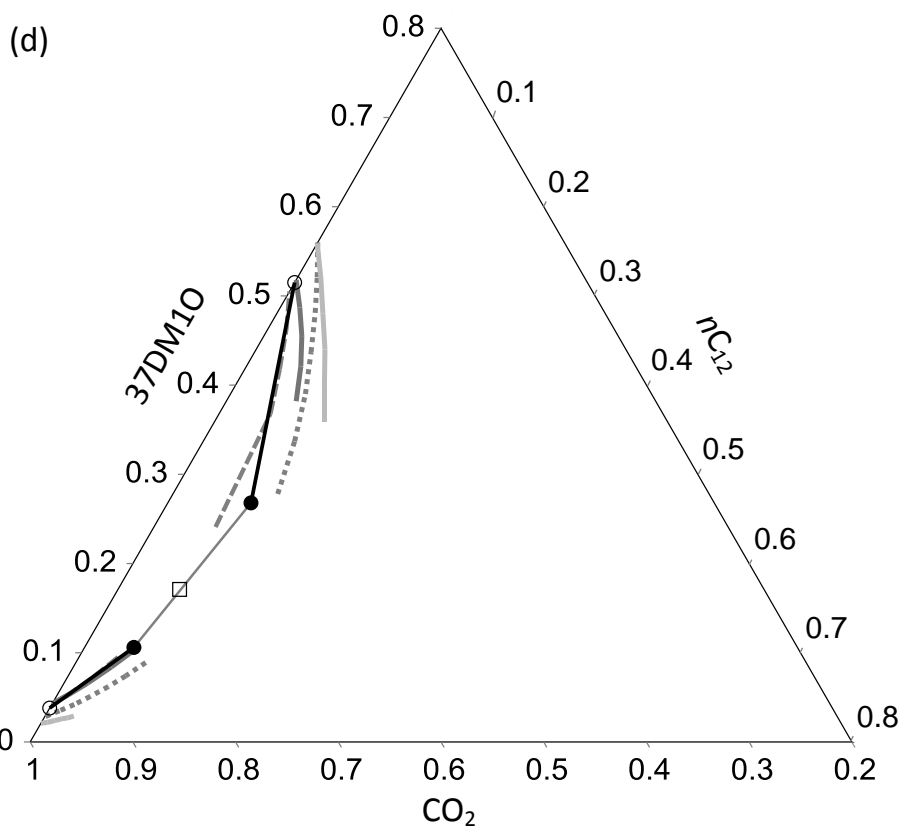
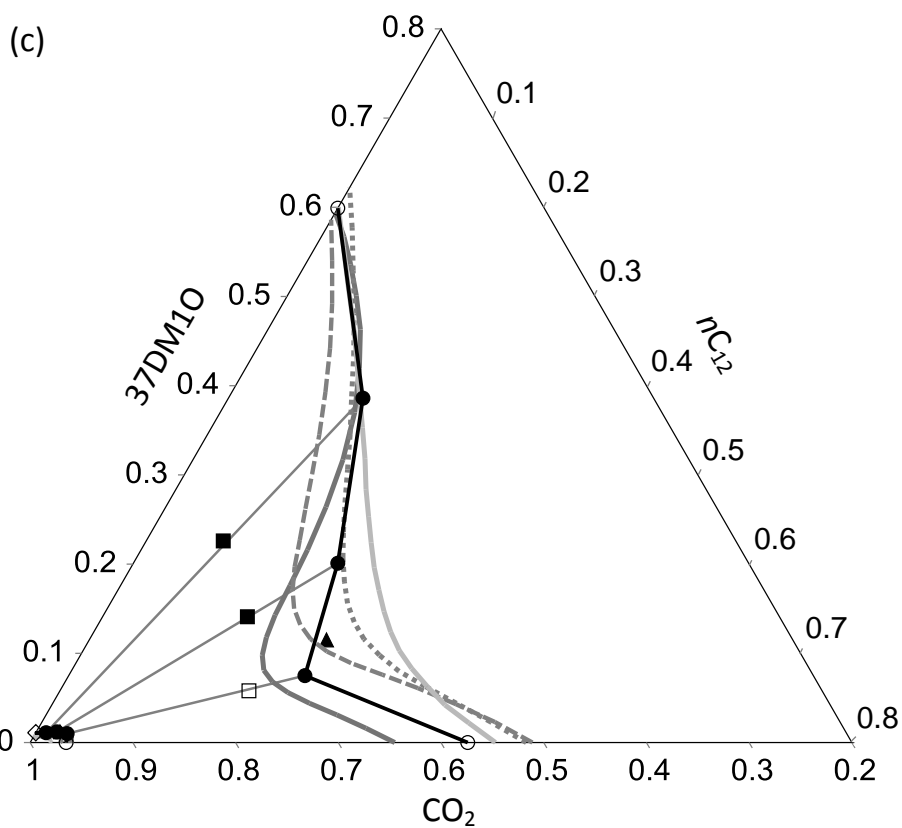


Figure 5-3. CO₂ + nC₁₂ + 37DM10 at 35.0 °C and (a) 68.0 bar; (b) 72.0 bar; and (c) 83.0 bar.



- Experimental [this work]
- ▲ Ternary literature [17]
- RK-ASPEN
- Experimental tie lines
- Binary literature [17,18,39,42]
- SR-POLAR
- Quantitative loading
- ◇— Binary literature, extrapolated [17,18,39]
- ⋯ PR-BM
- One phase sampling
- PC-SAFT

Figure 5-4. $\text{CO}_2 + n\text{C}_{12} + 37\text{DM}10$ at $55.0\text{ }^\circ\text{C}$ and (a) 83.0 bar ; (b) 104.0 bar ; (c) 106.5 bar ; and (d) 123.0 bar .



- Experimental [this work]
- Experimental tie lines
- Quantitative loading
- One phase sampling
- ▲ Ternary literature [17]
- Binary literature [17,18,39,42]
- ◇ Binary literature, extrapolated [17,18,39]
- RK-ASPEN
- SR-POLAR
- ⋯ PR-BM
- PC-SAFT

Figure 5-4. $\text{CO}_2 + n\text{C}_{12} + 37\text{DM}10$ at 55.0°C and (a) 83.0 bar ; (b) 104.0 bar ; (c) 106.5 bar ; and (d) 123.0 bar .

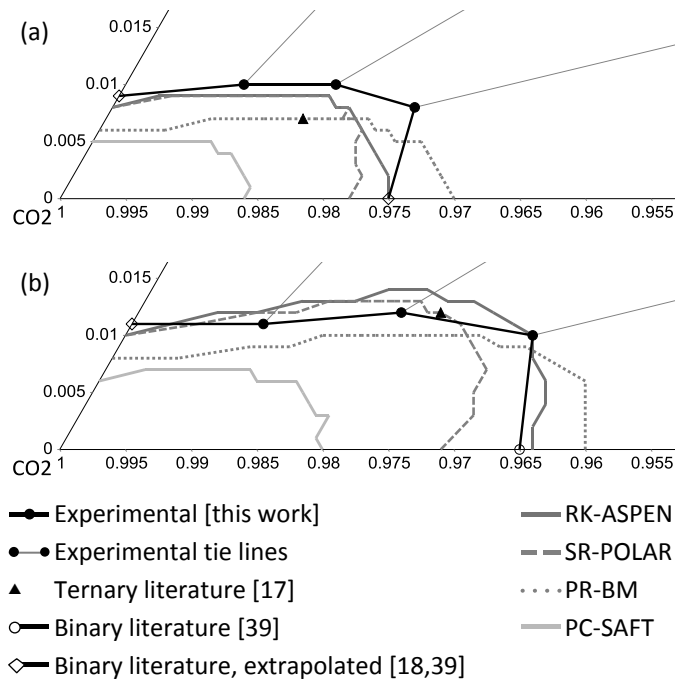


Figure 5-5. Vapour phase detail for $\text{CO}_2 + n\text{C}_{12} + 37\text{DM10}$ at 55.0°C and (a) 104.0 bar ; and (b) 106.5 bar .

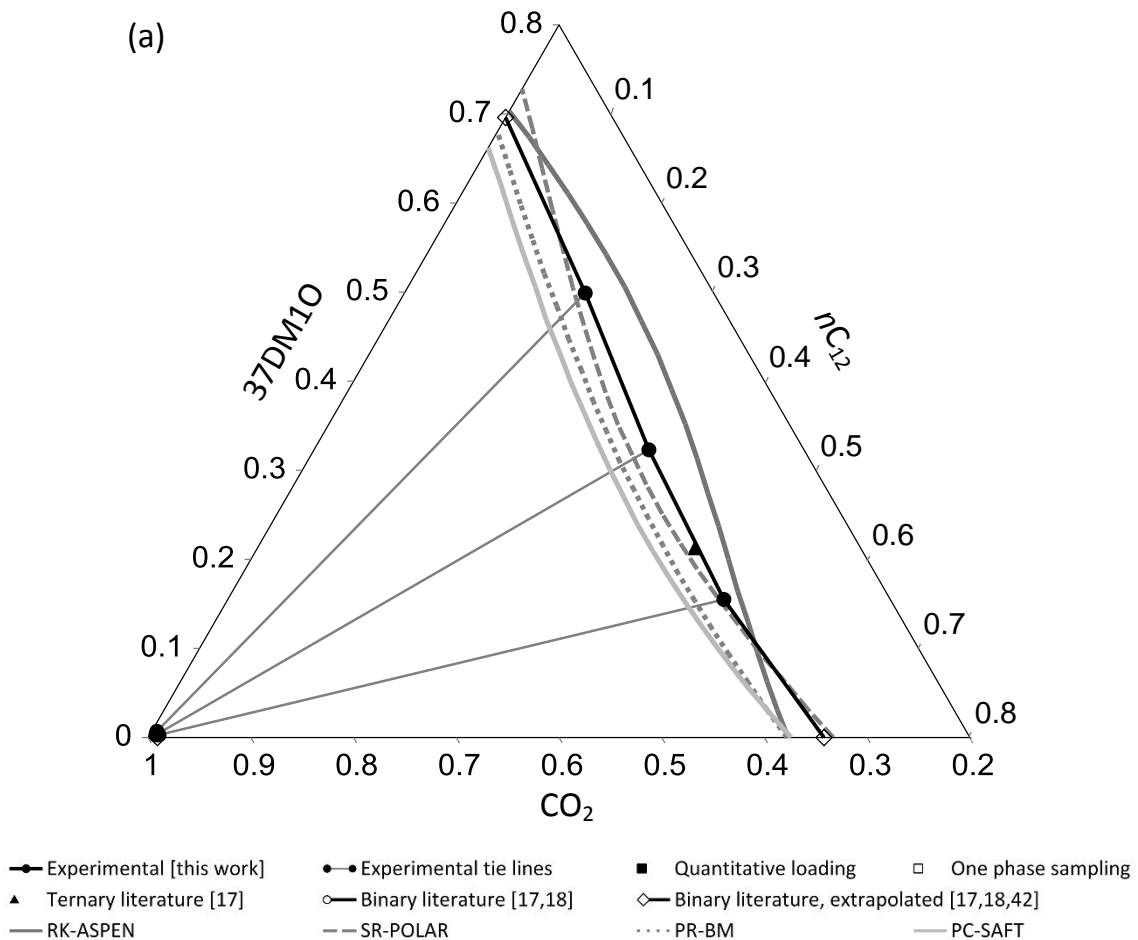
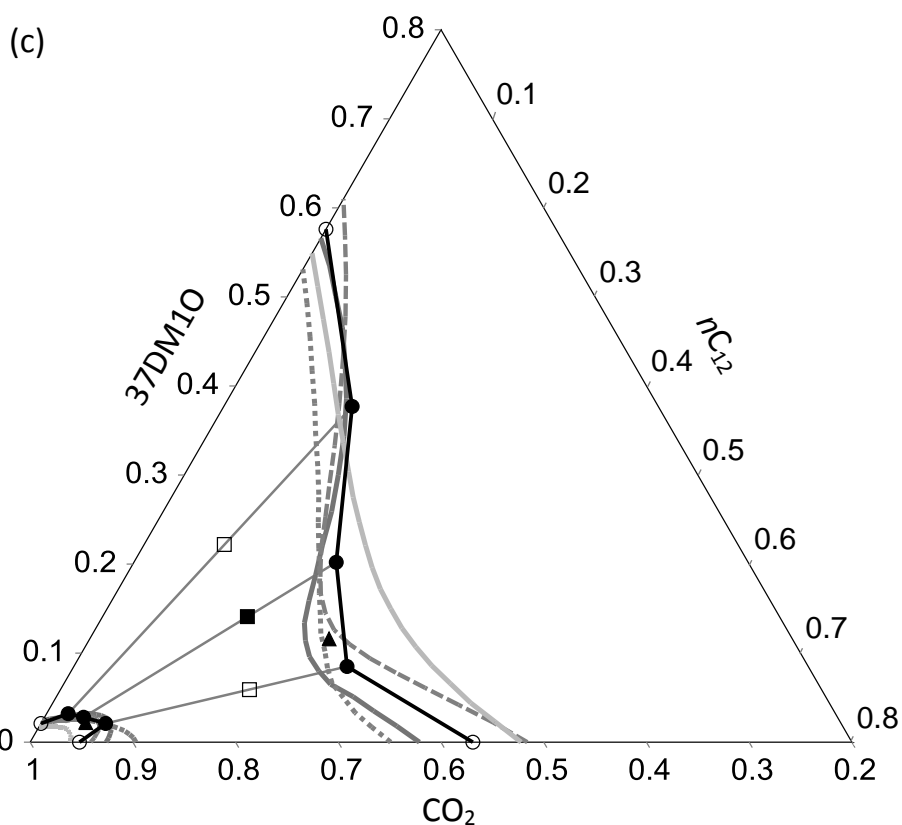
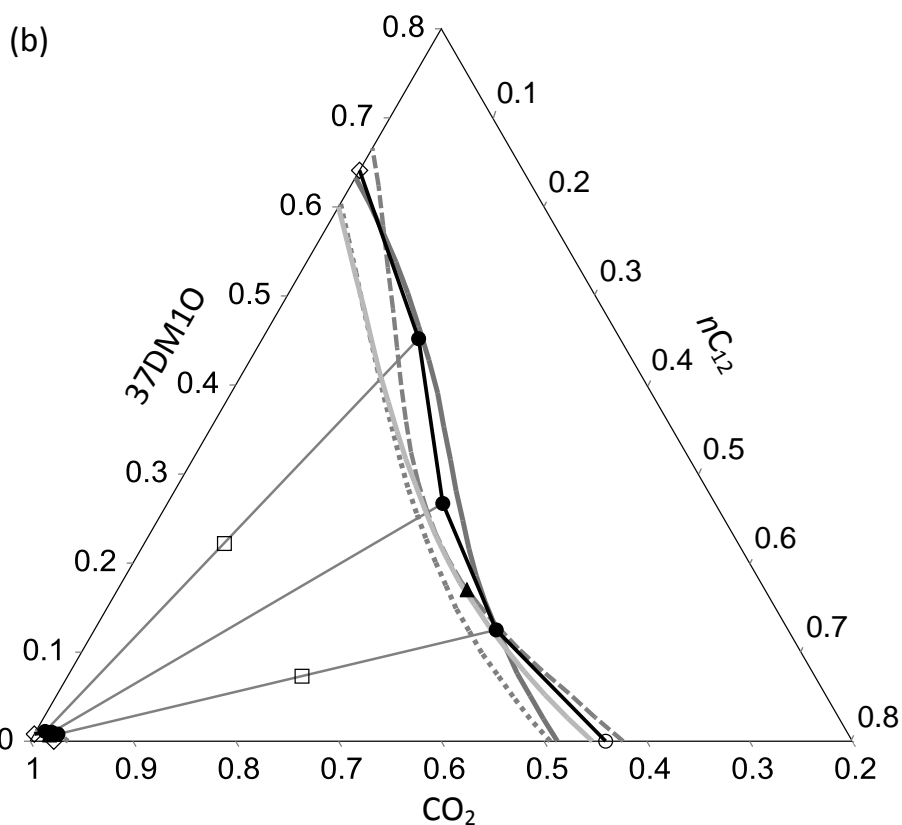
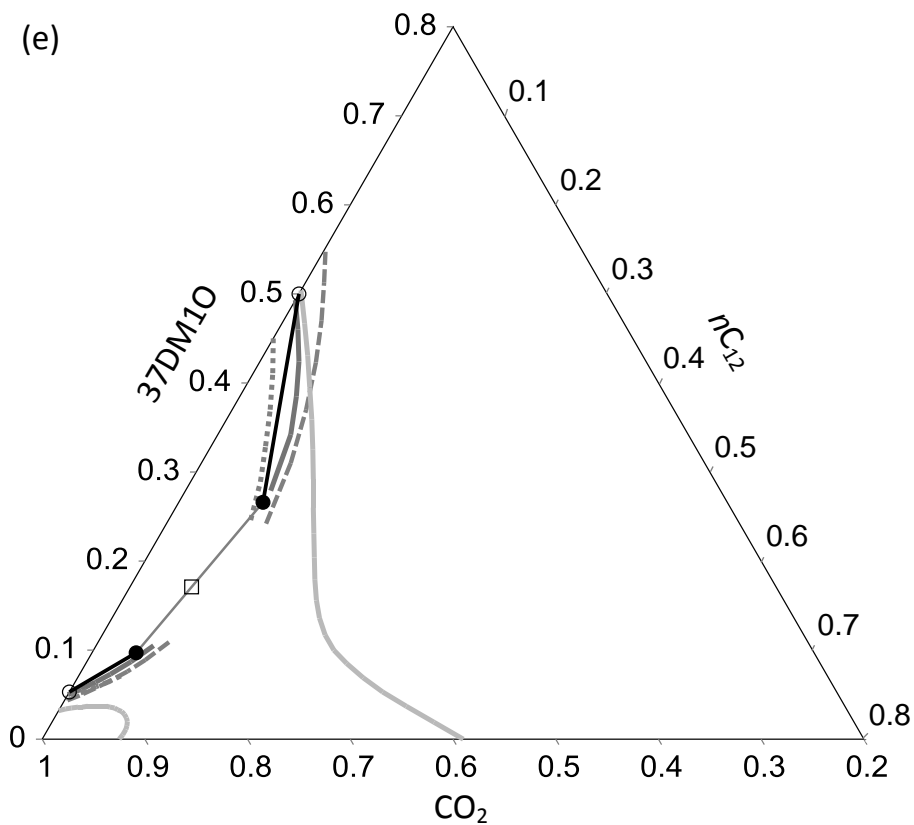
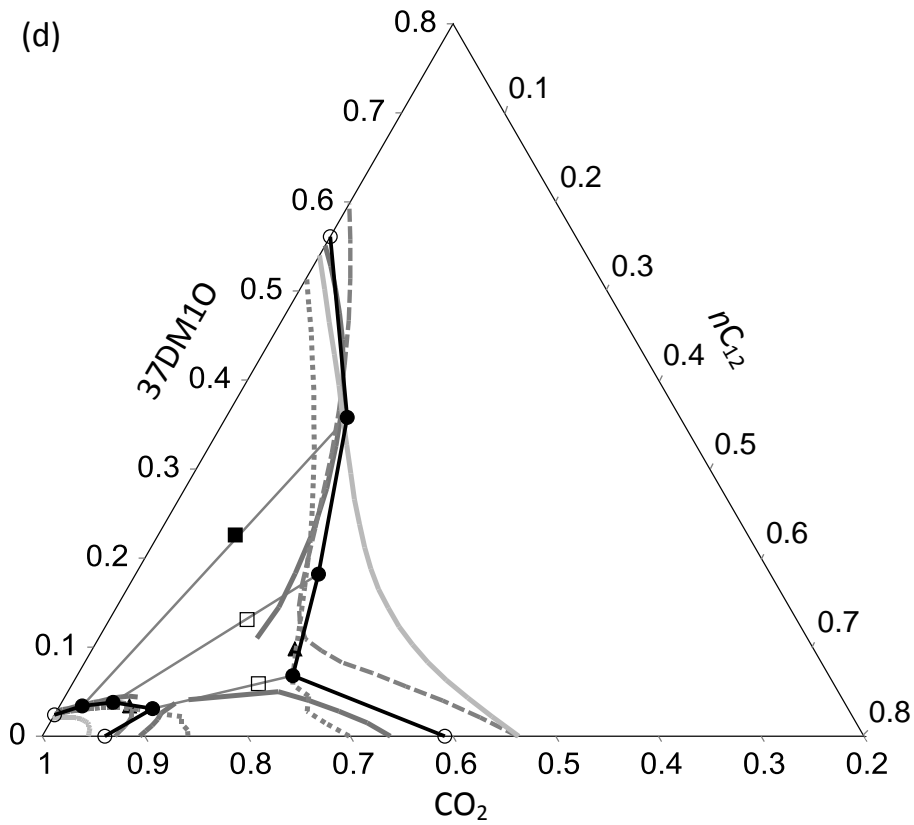


Figure 5-6. $\text{CO}_2 + n\text{C}_{12} + 37\text{DM10}$ at 75.0°C and (a) 104.0 bar ; (b) 123.0 bar ; (c) 140.0 bar ; (d) 143.5 bar ; and (e) 157.0 bar .



- Experimental [this work]
- ▲ Ternary literature [17]
- RK-ASPEN
- Experimental tie lines
- Binary literature [17,18]
- SR-POLAR
- Quantitative loading
- ◇ Binary literature, extrapolated [17,18,42]
- ⋯ PR-BM
- One phase sampling
- PC-SAFT

Figure 5-6. $\text{CO}_2 + n\text{C}_{12} + 37\text{DM}10$ at $75.0\text{ }^\circ\text{C}$ and (a) 104.0 bar ; (b) 123.0 bar ; (c) 140.0 bar ; (d) 143.5 bar ; and (e) 157.0 bar .



- Experimental [this work]
- ▲ Ternary literature [17]
- RK-ASPEN
- Experimental tie lines
- Binary literature [17,18]
- SR-POLAR
- Quantitative loading
- ◇ Binary literature, extrapolated [17,18,42]
- ⋯ PR-BM
- One phase sampling
- PC-SAFT

Figure 5-6. $\text{CO}_2 + n\text{C}_{12} + 37\text{DM}10$ at 75.0°C and (a) 104.0 bar; (b) 123.0 bar; (c) 140.0 bar; (d) 143.5 bar; and (e) 157.0 bar.

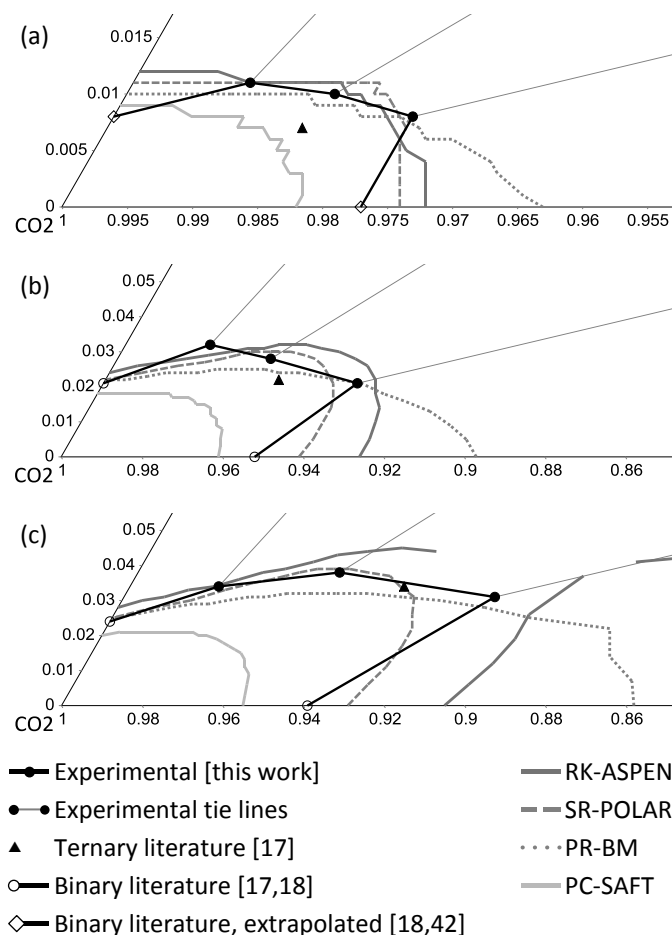


Figure 5-7. Vapour phase detail for $\text{CO}_2 + n\text{C}_{12} + 37\text{DM10}$ at $75.0\text{ }^\circ\text{C}$ and (a) 123.0 bar ; (b) 140.0 bar ; and (c) 143.5 bar .

RK-ASPEN is impressive in its ability to capture the high solubility pinch, or co-solubility, seen for the 75:25 $n\text{C}_{12}$:37DM10 mixture as well as the convex-to-concave, or s-shaped, liquid phase complexity of the higher-pressure systems (Figs. 5-3 b, 5-4 b, c and 5-6 c).¹² It outperforms the other three models in its ability to correlate liquid phase behaviour at $35\text{ }^\circ\text{C}$ and 72 bar . At 104 and 106.5 bar ($55\text{ }^\circ\text{C}$) and 140 and 143.5 bar ($75\text{ }^\circ\text{C}$), liquid phase correlations are qualitatively sound albeit somewhat CO_2 -rich. As a result of this CO_2 solubility over-estimation RK-ASPEN predicts two separate two-phase regions at 143.5 bar and $75\text{ }^\circ\text{C}$ (Fig. 5-6 d). At $75\text{ }^\circ\text{C}$ the phase transition pressure of the 75:25 solute ratio mixture was 144.4 bar – only 0.9 bar above the target experimental pressure of 143.5 bar . Thus, even a small solubility over-estimation is sufficient for the pinch to touch and break the continuous two-phase band. The successes described above come at the expense of poor qualitative behaviour at lower pressures. In Figs. 5-4 a and 5-6 a, RK-ASPEN predicts fully convex-shaped liquid curves which are CO_2 -deficient for the greater part thereof and do not match the concavity, or increased solubility, starting to develop in the high- $n\text{C}_{12}$ region of the mixture.

¹² The heterogeneous (two-phase) to homogenous (one-phase) transition in the 75:25 $n\text{C}_{12}$:37DM10 mixture occurred at 72.4 , 108.3 and 144.4 bar at 35 , 55 and $75\text{ }^\circ\text{C}$ respectively. A comparative $\text{CO}_2 + n\text{C}_{12}$ system – the more soluble of the two binary mixtures – with bulk CO_2 mass fraction of 0.758 transitions at higher pressures of 75.0 , 113.4 and 151.4 bar at 35 , 55 and $75\text{ }^\circ\text{C}$ [17].

RK-ASPEN produces accurate vapour phase correlations at 55 and 75 °C. The largest deviations, seen in the high- nC_{12} regions of Fig. 5-7 b and c where solute loading is overestimated, still fall within 3 mass % CO_2 of the experimental trends. Accurate correlations of the small two-phase regions at 123 bar (55 °C, Fig. 5-4 d) and 157 bar (75 °C, Fig. 5-6 e) are obtained with RK-ASPEN.

SR-POLAR liquid phase predictions improve visibly with an increase in temperature (also see Table 5-11). Low pressure liquid phase correlations are fully concave in shape and therefore, regardless the temperature, more accurate in the high- nC_{12} range of the ternary mixture (Fig. 5-3 a, 5-4 a and 5-6 a). As regards liquid phase predictions in the medium-to-high pressure range, different behaviour is observed. At 35 °C, predictions are more accurate in the high- nC_{12} range of the ternary system (Fig. 5-3 a and b). Moving to 55 °C, deviations in the high-37DM10 region decrease significantly (Fig. 5-4 c). At 75 °C, liquid phase correlation errors are relatively insensitive to solute-solute ratio and, if anything, predictions are more accurate in the high-37DM10 range of the mixture (Fig. 5-6 c and d). Thus, the extent to which medium-to-high pressure predicted liquid trends can capture the convex-to-concave transition is temperature dependent. SR-POLAR produces good vapour phase correlations at both 55 and 75 °C. The small two-phase region at 123 bar (55 °C, Fig. 5-4 d) is well-approximated whilst at 157 bar (75 °C, Fig. 5-6 e) the predicted solubility is too low (i.e., the surface area is too large) but still reasonable.

PR-BM liquid phase predictions at 35 °C are too rich in solutes (i.e., lower CO_2 solubility) and, as a result, it is the only model evaluated that still predicts a two-phase region at 35 °C and 83 bar, albeit with large errors (Fig. 5-3 c). At 35 °C and 83 bar the other three models have all transitioned to predicting total solubility. In all but the highest-pressure system at each temperature, PR-BM is not able to capture the curvature of either the liquid or vapour phase. Concave or L-shaped liquid curves, which do not match the s-shaped behaviour of the experimental curve, are predicted whilst vapour phase solute loading is overestimated in the high- nC_{12} area of the ternary system. Low-pressure liquid phase correlations at 83 bar (55 °C, Fig. 5-4 a) and 104 bar (75 °C, Fig. 5-6 a) appear reasonable because the convex-to-concave complexity in the experimental data is only starting to develop. At higher pressures a two-phase band that narrows considerably toward the nC_{12} -end of the mixture is predicted. This deviation from experimental mixture behaviour is particularly pertinent at 140.0 and 143.5 bar (75 °C, Fig. 5-6 c and d). At 143.5 bar the solvent mass % of the $CO_2 + nC_{12}$ binary vapour and liquid phases differ by 33.1 % for the experimental system but only by 15.7 % for the model-predicted system. The PR-BM correlation of the small two-phase region at 157 bar (75 °C, Fig. 5-6 e) appears to be more accurate than is the case at 123 bar (55 °C, Fig. 5-4 d), where a two-phase region too large in surface area is predicted.

PC-SAFT mostly predicts CO₂-deficient liquid phases and overly CO₂-rich vapour phases (i.e., solubilities erring on the low side), and is not successful at modelling the co-solubility pinch behaviour seen in the high-*n*C₁₂ region of the ternaries. Liquid phase curves that remain concave or, at best, L-shaped, and do not follow the s-shaped behaviour of the experimental data are predicted. Fig. 5-3 b, with marginal convex-to-concave liquid curvature, is the exception. The positive correlation between temperature and PC-SAFT-predicted liquid phase %AAD_p (Table 5-11) reflects in the Gibbs diagrams of Figs. 5-3, 5-4 and 5-6. Qualitatively, vapour phase trends are reasonable but the low solute loadings are evident in Figs. 5-5 and 5-7. As the two-phase region breaks away from the CO₂ + *n*C₁₂ axis, predicted solubilities remain low which presents as a two-phase envelope too large in surface area (Fig. 5-4 d) or, in the extreme, an erroneous continuous two-phase band (Fig. 5-6 e). Low pressure liquid phase correlations – 68, 83 and 104 bar at 35, 55 and 75 °C respectively – are reasonably positioned but do not follow the marginal s-shaped nature of the experimental curves.

3.6 Evaluating CO₂ as solvent to fractionate *n*C₁₂ + 37DM10

3.6.1 Experimental ternary mixture relative solubilities and separation potentials

The experimental relative solubility, α_{ij} , and separation potential, SP_{ij} , defined in Eqs. 5-4 and 5-5 respectively, are plotted in Fig. 5-8 a and b. These values were calculated using the experimental data in Table 5-5. For the purposes of this discussion, *i* and *j* represent *n*C₁₂ and 37DM10 respectively. SP_{ij} , which incorporates not only a selectivity contribution ($\alpha_{ij} - 1$) but also a vapour phase solute loading contribution (Y_i), provides a crude indication of the solvent flow, and therefore equipment sizing, necessary to achieve the desired lights extraction. However, the trade-off between fractionation sharpness versus capital and operational expenditure can only be evaluated on a case-for-case basis. The 1000 constant in Eq. 5-5 was arbitrarily chosen to make for easily manageable values.

$$\alpha_{ij} = \frac{Y_i/X_i}{Y_j/X_j}$$

Equation 5-4

$$SP_{ij} = (\alpha_{ij} - 1) \times Y_i \times 1000$$

Equation 5-5

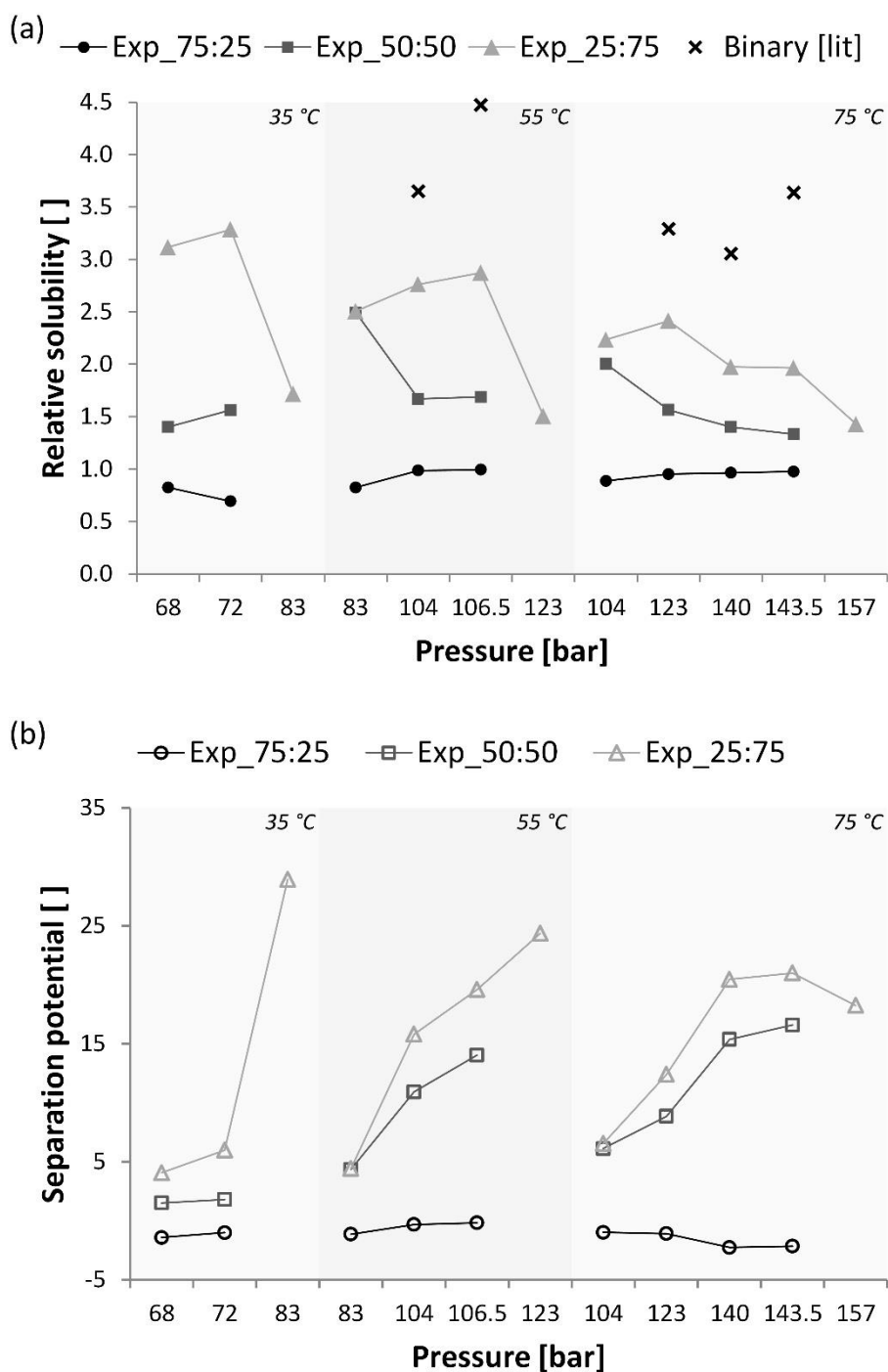


Figure 5-8. Experimental (a) relative solubility; and (b) separation potential for 75:25, 50:50 and 25:75 nC_{12} :37DM10 mass ratio mixtures of $CO_2 + nC_{12} + 37DM10$ at 35, 55 and 75 °C. Binary relative solubility values were calculated from data by [17,18,39,42].

Low pressure α_{ij} values are very sensitive to vapour phase solute fractions and should be interpreted with care. As an example: at 55 °C and 83 bar an α_{ij} value of 2.5 is obtained for the 50:50 mixture. Changing Y_{37DM10} from 0.001 to 0.002 (see Table 5-5), well within the accuracy of the experimental method, results in an α_{ij} value of 1.5.

In general, both α_{ij} and SP_{ij} increase with increasing bulk 37DM10 fraction and effective separation of the 75:25 nC_{12} :37DM10 mixture is not possible using high-pressure CO_2 . This is evident from the angular difference between experimental tie lines and constant solute-solute ratio lines (CSSRL), an example of which is shown in Fig. 5-9. At high nC_{12} fractions, tie lines and CSSRL run parallel to each other. As the bulk solvent-free 37DM10 fraction increases the angle between tie lines and CSSRL opens up, enabling separation. Using VLE data from the two constituent binaries [17,18,39,42] not only overestimates α_{ij} (Fig. 5-8 a) but its compositional dependence, an important concept for industrial SFE design [43], is not captured. At constant temperature and solute:solute ratio, the correlation between α_{ij} and pressure switches from positive in the low pressure region to negative in the higher pressure region. At lower pressures, a pressure increase will preferentially enhance the solubility of nC_{12} whilst at higher pressures a positive ΔP will favour the relative solubility of the less soluble species, 37DM10. SP_{ij} is, for the most part, positively correlated with pressure because the increase in $Y_{nC_{12}}$ exceeds the decrease in α_{ij} .

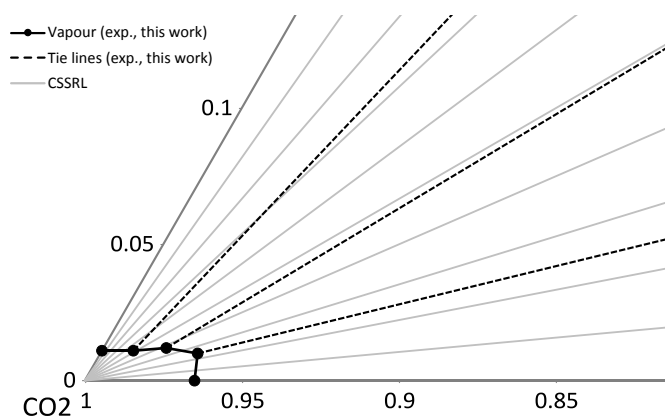


Figure 5-9. Vapour phase detail for $CO_2 + nC_{12} + 37DM10$ at $55\text{ }^\circ C$ and 106.5 bar . The angular difference between experimental tie lines and CSSRL opens up with increasing bulk solvent-free 37DM10 fraction.

3.6.2 Model-predicted ternary mixture relative solubilities and separation potentials

Relative solubilities and separation potentials calculated from model-predicted VLE data display qualitative behaviour similar to the experimental trends in Fig. 5-8. Via all four models and at all P and T conditions evaluated, the predicted α_{ij} is positively correlated with the bulk solvent-free 37DM10 mass fraction, Z_{37DM10} , across the entire range $0.05 < Z_{37DM10} < 0.95$. Furthermore, these smooth positive correlations, examples of which are shown in Fig. 5-10 a, are more pronounced for the model-predicted than for the experimental parameters. In Fig. 5-8 a, overlap occurs between experimental α_{ij} values for 50:50 and 25:75 mixtures but no such overlap is witnessed for the model-predicted α_{ij} trends.

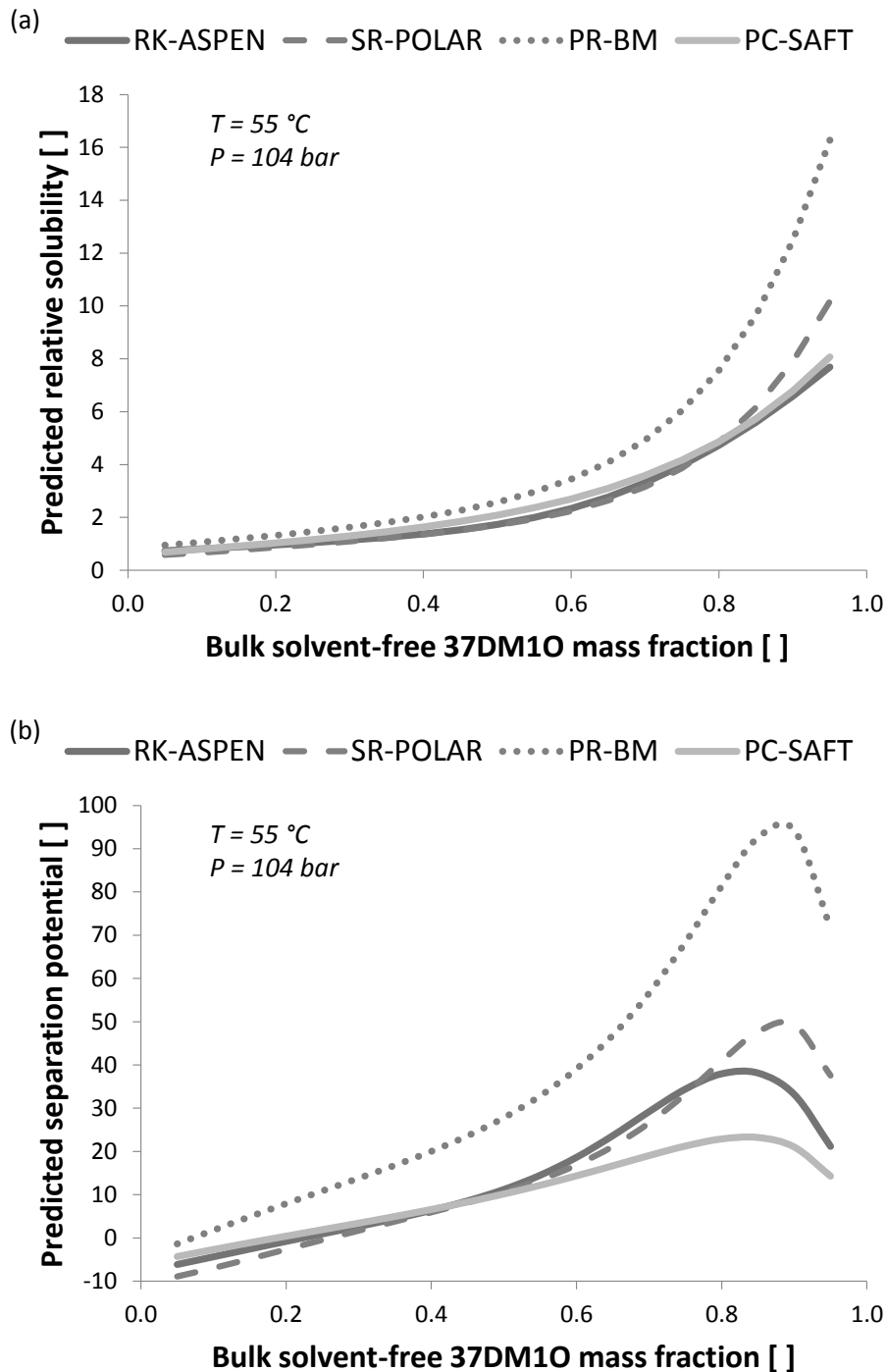


Figure 5-10. Model-predicted (a) relative solubility; and (b) separation potential as functions of bulk solvent-free 37DM10 mass fraction, Z_{37DM10} , for the system $\text{CO}_2 + n\text{C}_{12} + 37\text{DM10}$ at $55\text{ }^{\circ}\text{C}$ and 104 bar .

In 42 of the 45 scenarios evaluated the predicted separation potential increases with Z_{37DM10} but passes through an optimum in the vicinity of $Z_{37DM10} = 0.85$, examples of which are shown in Fig. 5-10 b. This decline in predicted $SP_{nC_{12},37DM10}$ occurs because the decrease in vapour phase $n\text{C}_{12}$ content outweighs the increase in $\alpha_{nC_{12},37DM10}$. The highest Z_{37DM10} measured experimentally was 0.75 and therefore the presence of a similar SP_{ij} -optimum in the experimental system could not be confirmed.

RK-ASPEN, SR-POLAR and PC-SAFT also indicate the 75:25 nC_{12} :37DM10 mixture cannot be separated using high-pressure CO_2 . PR-BM is the exception, predicting an average α -value of 1.49 for the 75:25 mixtures. Furthermore, as shown in Table 5-12, all four models predict larger averaged relative solubilities and separation potentials compared to the experimentally derived parameters. The low PC-SAFT derived average SP_{ij} of 10.6 is a result of the low vapour phase solute loadings discussed in Section 3.5 (see pp. 125 and 128).

Table 5-12. Relative solubility (α_{ij}) and separation potential (SP_{ij}) for the experimental and model-predicted systems. Data are averaged for the 75:25, 50:50 and 25:75 mixtures, and across all temperatures and pressures studied in this work (see Table 5).

Data source	α_{ij} []	SP_{ij} []
Experimental	1.7	8.4
RK-ASPEN	2.2	17.0
SR-POLAR	2.3	16.9
PR-BM	3.8	28.0
PC-SAFT	2.4	10.6

4. CONCLUSIONS

This study presented new high pressure VLE data for the $CO_2 + nC_{12} + 37DM10$ ternary mixture. Sampling and online analysis were used to quantify vapour and liquid equilibrium phase compositions at 35, 55 and 75 °C and pressures between 68 and 157 bar. To complement previous equipment verification, the authors have also shown the analytic experimental setup is capable of generating reproducible data over an extended period of time. Literature contains large collections of useful binary solvent-solute phase behaviour data. However, the solute-solute interactions encountered in this work has highlighted the importance of studying ternary mixtures and, furthermore, doing so at multiple solute A:solute B ratios. The new data were used to evaluate the ability of a) high-pressure CO_2 to fractionate a mixture of nC_{12} and 37DM10; and b) the RK-ASPEN, SR-POLAR, PR-BM and PC-SAFT thermodynamic models to correlate these data.

Experimental $\alpha_{nC_{12},37DM10}$ and $SP_{nC_{12},37DM10}$ increase with increasing bulk solvent-free 37DM10 fraction and effective separation of the 75:25 nC_{12} :37DM10 mixture is not possible using high pressure CO_2 . Using VLE data from the two respective binaries overestimates α_{ij} and, vitally, cannot capture this compositional dependence. At constant temperature and solute:solute ratio, the α_{ij} - P relationship switches from positive in the low pressure region to negative in the higher pressure region whilst SP_{ij} - P is, for the most part,

positively correlated. Relative solubility values calculated off model-predicted VLE data follow similar qualitative trends, increase exponentially with Z_{37DM10} in a series of smooth well-behaved curves, and are consistently larger than $\alpha_{ij,exp}$. Model-predicted separation potentials increase with increasing Z_{37DM10} but pass through an optimum in the vicinity of $Z_{37DM10} = 0.85$.

RK-ASPEN and PC-SAFT provided the best and worst correlation of equilibrium pressures with respective overall combined %AAD_p values of 3.1 % and 8.5 %. SR-POLAR and PR-BM performed similarly, but the latter outclassed the other three models in terms of ease of use and, it seems, robustness. The %AAD_p and AAD_p in vapour phase pressure predictions via all three cubic EOS are negatively correlated with temperature and decrease significantly when moving away from the solvent T_C . Interestingly, the opposite is observed for PC-SAFT.

The experimental 75:25 nC_{12} :37DM10 mixture displayed significant enhanced solubility which starts out as convex-to-concave liquid phase complexity and eventually presents as a pinched two-phase band. In addition, asymmetric vapour phase curves slanting toward the $CO_2 + nC_{12}$ axis were observed. RK-ASPEN was impressive in its ability to capture this behaviour. PC-SAFT mostly predicts vapour phases with insufficient solute loading, cannot model the aforementioned pinch, and the authors suggest that in future work CO_2 be modelled as a quadrupole using the Perturbed-Chain Polar Statistical Associating Fluid Theory variant.

ACKNOWLEDGEMENTS

This work is based on the research supported in part by the National Research Foundation of South Africa (Grant specific unique reference number (UID) 83966), Department of Trade and Industry (DTI) of South Africa through the Technology and Human Resources for Industry Programme (THRIP), Sasol Technology (Pty) Ltd., the National Research Foundation (DAAD-NRF) and the Skye Foundation Trust. The authors acknowledge that opinions, findings, and conclusions or recommendations expressed in any publication generated by the supported research are those of the authors, and that the sponsors accept no liability whatsoever in this regard. Aspen Plus® is a registered trademark of Aspen Technology Inc.

REFERENCES

1. E. Kiran, Supercritical fluids and polymers – The year in review – 2014, *J. Supercrit. Fluids* 110 (2016) 126-153.
2. G. Eliosa-Jiménez, G. Silva-Oliver, F. García-Sánchez, A. De la Torre, High-Pressure Vapor-Liquid Equilibria in the Nitrogen + *n*-Hexane System, *J. Chem. Eng. Data* 52 (2007) 395-404.
3. G.K. Folas, O.J. Berg, E. Solbraa, A.O. Fredheim, G.M. Kontogeorgis, M.L. Michelsen, E.H. Stenby, High-pressure vapor–liquid equilibria of systems containing ethylene glycol, water and methane: Experimental measurements and modelling, *Fluid Phase Equilib.* 251 (2007) 52-58.
4. M. Grant-Huysen, S. Maharaj, L. Matheson, L. Rowe, E. Sones, Ethoxylation of Detergent-Range Oxo Alcohols Derived from Fischer-Tropsch α -Olefins, *J. Surfactants Deterg.* 7 (2004) 397-407.
5. J.C. Crause, Production of detergent range alcohols (2009), US Patent 2009/0054696 A1.
6. R.M. Deshpande, V.H. Rane, R.V. Chaudhari, Process for preparation of a mixture of alcohols and ketones by liquid phase oxidation of higher alkanes (2006), US Patent 2006/0094905 A1.
7. K.W. Lee, M.J. Choi, S.B. Kim, C.S. Choi, Liquid-phase oxidation of *n*-dodecane in the presence of boric acid, *Ind. Eng. Chem. Res.* 26 (1987) 1951-1955.
8. J. Gross, G. Sadowski, Modeling Polymer Systems Using the Perturbed-Chain Statistical Associating Fluid Theory Equation of State, *Ind. Eng. Chem. Res.* 41 (2002) 1084-1093.
9. Traub, K. Stephan, High-pressure phase equilibria of the system CO₂-water-acetone measured with a new apparatus, *Chem. Eng. Sci.* 45 (1990) 751-758.
10. J. Cai, J.M. Prausnitz, Thermodynamics for fluid mixtures near to and far from the vapour-liquid critical point, *Fluid Phase Equilib.* 219 (2004) 205-217.
11. A. Dominik, W.G. Chapman, M. Kleiner, G. Sadowski, Modeling of Polar Systems with the Perturbed-Chain SAFT Equation of State. Investigation of the Performance of Two Polar Terms, *Ind. Eng. Chem. Res.* 44 (2005) 6928-6938.
12. M. Takeo, K. Nishii, T. Nitta, T. Katayama, Isothermal vapor-liquid equilibria for two binary mixtures of heptane with 2-butanone and 4-4-methyl-2-pentanone measured by a dynamic still with a pressure regulation, *Fluid Phase Equilib.* 3 (1979) 123-131.
13. F.C.v.N. Fourie, C.E. Schwarz, J.H. Knoetze, Analytic High-Pressure Phase Equilibria Part II: Gas Chromatography and Sampling Method Development, *Chem. Eng. Technol.* 39 (2016) 1475-1482.
14. G.J.K. Bonthuys; Separation of 1-dodecanol and *n*-tetradecane through supercritical extraction, MSc Thesis, Stellenbosch University, South Africa, 2008.
15. F.C.v.N. Fourie, C.E. Schwarz, J.H. Knoetze, New Experimental Phase Equilibria Data For Ternary Supercritical Solvent - Alkane - Alcohol Systems, in: 6th International Symposium on High Pressure Processes Technology, Belgrade, Serbia, 2013.

16. G.J.K. Bonthuys, C.E. Schwarz, A.J. Burger, J.H. Knoetze, Separation of alkanes and alcohols with supercritical fluids. Part I: Phase equilibria and viability study, *J. Supercrit. Fluids* 57 (2011) 101-111.
17. M. Zamudio, C.E. Schwarz, J.H. Knoetze, Experimental measurement and modelling with Aspen Plus® of the phase behaviour of supercritical CO₂ + (*n*-dodecane + 1-decanol + 3,7-dimethyl-1-octanol), *J. Supercrit. Fluids* 84 (2013) 132-145.
18. M. Zamudio, C.E. Schwarz, J.H. Knoetze, Phase equilibria of branched isomers of C₁₀-alcohols and C₁₀-alkanes in supercritical carbon dioxide, *J. Supercrit. Fluids* 59 (2011) 14-26.
19. C.E. Schwarz, I. Nieuwoudt, J.H. Knoetze, Phase equilibria of long chain *n*-alkanes in supercritical ethane: Review, measurements and prediction, *J. Supercrit. Fluids* 46 (2008) 226-232.
20. M. Zamudio, C.E. Schwarz, J.H. Knoetze, Phase equilibria of branched isomers of C₁₀-alcohols and C₁₀-alkanes in supercritical ethane, *J. Supercrit. Fluids* 58 (2011) 330-342.
21. F.C.v.N. Fourie, C.E. Schwarz, J.H. Knoetze, Analytic Setup for Multicomponent High-Pressure Phase Equilibria via Dual Online Gas Chromatography, *Chem. Eng. Technol.* 38 (2015) 1165-1172.
22. E.C. Voutsas, G.D. Pappa, K. Magoulas, D.P. Tassios, Vapor liquid equilibrium modeling of alkane systems with Equations of State: "Simplicity versus complexity", *Fluid Phase Equilib.* 240 (2006) 127-139.
23. C.E. Schwarz, A.J. de Villiers, C.B. McClune, G.J.K. Bonthuys, A.J. Burger, J.H. Knoetze, High pressure phase equilibrium measurements of long chain alcohols in supercritical ethane, *J. Supercrit. Fluids* 55 (2010) 554-565.
24. K. Mejri, A. Taieb, A. Bellagi, Phase equilibria calculation of binary and ternary mixtures of associating fluids applying PC-SAFT equation of state, *J. Supercrit. Fluids* 104 (2015) 132-144.
25. G. Soave, Equilibrium constants from a modified Redlich-Kwong equation of state, *Chem. Eng. Sci.* 27 (1972) 1197-1203.
26. P.M. Mathias, A Versatile Phase Equilibrium Equation of State, *Ind. Eng. Chem. Process Des. Dev.* 22 (1983) 385-391.
27. J.F. Boston, P.M. Mathias, Phase Equilibria in a Third-Generation Process Simulator, in: 2nd International Conference on Phase Equilibria and Fluid Properties in the Chemical Process Industries, West Berlin, 1980.
28. J. Schwartzentruber, H. Renon, Extension of UNIFAC to High Pressures and Temperatures by the Use of a Cubic Equation of State, *Ind. Eng. Chem. Res.* 28 (1989) 1049-1955.
29. D.Y. Peng, D.B. Robinson, A New Two-Constant Equation of State, *Ind. Eng. Chem. Fund.* 15 (1976) 59-64.
30. P.M. Mathias, H.C. Klotz, J.M. Prausnitz, Equation-of-State mixing rules for multicomponent mixtures: the problem of invariance, *Fluid Phase Equilib.* 67 (1991) 31-44.
31. J. Gross, G. Sadowski, Perturbed-Chain SAFT: An Equation of State Based on a Perturbation Theory for Chain Molecules, *Ind. Eng. Chem. Res.* 40 (2001) 1244-1260.

32. J. Gross, G. Sadowski, Application of the Perturbed-Chain SAFT Equation of State to Associating Systems, *Ind. Eng. Chem. Res.* 41 (2002) 5510-5515.
33. W.G. Chapman, K.E. Gubbins, G. Jackson, M. Radosz, New Reference Equation of State for Associating Liquids, *Ind. Eng. Chem. Res.* 29 (1990) 1709-1721.
34. S.H. Huang, M. Radosz, Equation of state for small, large, polydisperse, and associating molecules: extension to fluid mixtures, *Ind. Eng. Chem. Res.* 30 (1991) 1994-2005.
35. N.I. Diamantonis, I.G. Economou, Evaluation of Statistical Associating Fluid Theory (SAFT) and Perturbed Chain-SAFT Equations of State for the Calculation of Thermodynamic Derivative Properties of Fluids Related to Carbon Capture and Sequestration, *Energ. Fuel.* 25 (2011) 3334-3343.
36. Aspen Plus® V8.8 (34.0.0.110).
37. M. Zamudio, The Separation of Detergent Range Alkanes and Alcohol Isomers with Supercritical Carbon Dioxide, PhD Dissertation, Stellenbosch University, South Africa, 2014.
38. H. Gardeler, K. Fischer, J. Gmehling, Experimental Determination of Vapor-Liquid Equilibrium Data for Asymmetric Systems, *Ind. Eng. Chem. Res.* 41 (2002) 1051-1056.
39. I. Nieuwoudt, M. du Rand, Measurement of phase equilibria of supercritical carbon dioxide and paraffins, *J. Supercrit. Fluids* 22 (2002) 185-199.
40. J.E. Lombard, Thermodynamic modelling of hydrocarbon-chains and light-weight supercritical solvents, MSc Thesis, Stellenbosch University, South Africa, 2015.
41. A. Dominik, W.G. Chapman, M. Kleiner, G. Sadowski, Modeling of Polar Systems with the Perturbed-Chain SAFT Equation of State. Investigation of the Performance of Two Polar Terms, *Ind. Eng. Chem. Res.* 44 (2005) 6928-6938.
42. A.B. De Haan, Supercritical fluid extraction of liquid hydrocarbon mixtures, PhD Dissertation, Delft University of Technology, Netherlands, 1991.
43. G. Brunner, Industrial process development. Countercurrent multistage gas extraction (SFE) processes, *J. Supercrit. Fluids* 13 (1998) 283-301.

Chapter 6: MANUSCRIPT 4

**CO₂ + 3,7-dimethyl-1-octanol + 1-decanol: High pressure experimental
phase equilibria data and thermodynamic modelling**

Frederick C. v. N. Fourie^{a,1}, Cara E. Schwarz^a, Johannes H. Knoetze^{a,*}

^aStellenbosch University, Department of Process Engineering, Private Bag X1, Matieland, 7602, South Africa,

Tel: +27 21 808 4204, Fax: +27 21 808 2059, E-mail: jhk@sun.ac.za

¹Present address: Sasol, 1 Klasie Havenga, Sasolburg, 1947, South Africa, Tel: +27 16 960 2611

The Journal of Supercritical Fluids
Manuscript submitted for publication.

Declaration by the candidate

With regard to Chapter 6, the nature and scope of my contribution were as follows:

<u>Nature of contribution</u>	<u>Extent of contribution (%)</u>
I am the primary author of this publication. I am responsible for the experimental work, thermodynamic modelling, and interpreting and communicating the actual and model-predicted mixture behaviour.	90 %

The following co-authors contributed to Chapter 6:

<u>Name</u>	<u>E-mail address</u>	<u>Nature of contribution</u>	<u>Extent of Contribution (%)</u>
Johannes H. Knoetze	jhk@sun.ac.za	Supervisor to the student, F.C.v.N Fourie	5 %
Cara E. Schwarz	cschwarz@sun.ac.za	Co-supervisor to the student, F.C.v.N. Fourie	5 %

Signature of candidate : Declaration with signature in possession of candidate and supervisor

Date : 10 November 2017

Declaration by co-authors

The undersigned hereby confirm that:

1. The declaration above accurately reflects the nature and extent of the contributions of the candidate and the co-authors to Chapter 6.
2. No other authors contributed to Chapter 6 besides those specified above.
3. Potential conflicts of interest have been revealed to all interested parties and that the necessary arrangements have been made to use the material in Chapter 6 of this dissertation.

<u>Signature</u>	<u>Institutional affiliation</u>	<u>Date</u>
Declaration with signature in possession of candidate and supervisor	Supervisor to the student, F.C.v.N Fourie	10 November 2017
Declaration with signature in possession of candidate and supervisor	Co-supervisor to the student, F.C.v.N. Fourie	10 November 2017

ABSTRACT

New VLE data are presented for CO₂ + 3,7-dimethyl-1-octanol (37DM1O) + 1-decanol (C₁₀OH) at 35, 55 and 75 °C and pressures between 68 and 237 bar. Phase compositions were analysed using a static analytic apparatus with dual sampling and online chromatography. The mixture displays virtually no enhanced solubility, liquid curves remain convex throughout, and coexisting detached two-phase regions were not detected. CO₂ can fractionate all measured 37DM1O:C₁₀OH ratios though with limited efficacy, as highlighted by relative solubilities ranging from 1.1 to 1.5. RK-ASPEN, SR-POLAR, PR-BM and PC-SAFT correlations failed at 35 °C, the optimum fractionation temperature. At 55 and 75 °C, RK-ASPEN and SR-POLAR produced the smallest percentage average absolute deviations in equilibrium pressure of 4.0 %, and RK-ASPEN was marginally superior at correlating vapour and liquid phase curves. At 35 °C and 187.5 bar, the 25:75 37DM1O:C₁₀OH mixture passed through a density inversion and interesting images thereof are presented.

Keywords: Barotropy, Cubic EOS, Density inversion, Detergents, PC-SAFT, Supercritical

Highlights

- New ternary high pressure VLE data for CO₂ + 3,7-dimethyl-1-octanol + 1-decanol
- No enhanced ternary solubility or coexisting detached two-phase regions detected
- CO₂ can separate the two alcohols at all measured ratios though with limited efficacy
- RK-ASPEN enabled a %AAD_p of 4.0 % coupled with reasonable qualitative correlations
- A density inversion, or barotropic phenomenon, was observed at 35 °C and 187.5 bar

NOMENCLATURE

2E1H	:	2-Ethyl-1-hexanol
37DM1O	:	3,7-Dimethyl-1-octanol
AAD	:	Average absolute deviation
BIP	:	Binary interaction parameter
C ₁₀ OH	:	1-Decanol
<i>k</i>	:	Boltzmann constant
<i>k_{ij}</i>	:	Binary interaction parameter
<i>l_{ij}</i>	:	Binary interaction parameter
<i>m</i>	:	Segment number in PC-SAFT

M	:	Number of data points
nC_{12}	:	n -Dodecane
ρ_i	:	SR-POLAR polar parameter
P	:	Pressure
p^{sat}	:	Saturated vapour pressure
ROLSI™	:	Rapid On-Line Sampler Injector
SFE	:	Supercritical fluid extraction
SP_{ij}	:	Separation potential between species i and j
Solute	:	nC_{12} or 37DM10 or $C_{10}OH$
Solvent	:	CO_2
T	:	Temperature
u	:	Absolute uncertainty
X_i	:	Liquid phase mass fraction of species i
Y_i	:	Vapour phase mass fraction of species i
Z_i	:	Bulk solvent-free mass fraction of species i

Greek letters

α_{ij}	:	Relative solubility between species i and j
η_i	:	RK-ASPEN polar parameter
ε/k	:	Dispersion energy parameter in PC-SAFT
ε^{AB}/k	:	Association energy parameter in PC-SAFT
κ^{AB}	:	Effective association volume parameter in PC-SAFT
σ	:	Segment diameter in PC-SAFT
ρ^{sat}	:	Saturated liquid density

Superscripts and subscripts

i, j	:	Component identifications
sat	:	Saturated

1. INTRODUCTION

Supercritical fluid extraction (SFE) utilises the tuneable properties of a high-pressure solvent to manipulate selectivity and solvating ability and, in doing so, enables the isolation of a targeted compound or mixture of compounds. Despite widespread research on applications for, amongst other, the food [1,2], drug development [3-6] and speciality chemicals [7-9] industries, SFE and related high pressure processes remain niche technologies. Almost twenty years on, high capital expenditure, whether actual or assumed [10], and bespoke process design requirements [11] prevail as contributing factors.

Understanding mixture phase behaviour and thermodynamic properties are paramount to the successful design of any extractive or equilibrium-driven process [12]. In this regard, both accurate experimental data and reliable predictive models have important roles to fulfil [13]. Experimental VLE data for ternary solvent + solute A + solute B systems are particularly valuable because they shed light on the interactions between the solute A and solute B species.

This research is positioned within a larger project which investigates SFE as a means of separating post-production mixtures of detergent range alcohols and alkanes. Given the carbon number distribution of and isomerism in these mixtures, product purification is difficult to achieve using conventional approaches. The specific context of this contribution is best described using a three tier approach. Tier one, of which this paper is the second in a series [14], investigates the phase behaviour of the solutes nC_{12} , 37DM10 and $C_{10}OH$ in supercritical CO_2 , and the reader is advised to view these publications as a collective. The three hydrocarbon solutes were selected to represent an industrially significant detergent alcohol product stream. Tier two is also concerned with the aforementioned species but, in addition, ethane is considered as solvent. Tier one and two combined governed the experimental pressures measured in this work and the rationale behind the values chosen has been discussed previously [14]. Tier three represents the overarching project and in this regard solutes in the range C_8 to C_{60} , but especially C_8 to C_{22} , and CO_2 , ethane and propane as solvents have been studied [15-19]. Please refer to Fourie et al. [14], Bonthuys et al. [18], and Zamudio et al. [19] for additional background to tier three.

The objective of this study is threefold. Firstly, generate high pressure VLE data for $CO_2 + 37DM10 + C_{10}OH$. Equilibrium phase compositions were measured for three mixtures of $CO_2 + 37DM10 + C_{10}OH$. These differed in bulk 37DM10: $C_{10}OH$ mass fraction ratio calculated on a CO_2 -free basis – 75:25, 50:50 and 25:75. In all subsequent references to solute ratios the more soluble species, 37DM10, is mentioned first. The temperatures and pressure range investigated were 35, 55 and 75 °C, and 68 to 237 bar. All binary data used for regressions or phase diagrams were obtained from literature and are referenced accordingly.

Secondly, quantify the ability of CO₂ to separate the solutes 37DM1O and C₁₀OH. This is done by evaluating two parameters, relative solubility and separation potential.

Lastly, use the new VLE data to test four thermodynamic models for their ability to correlate the experimental equilibrium pressures and compositions. Within the overarching project, which aims to purify detergent alcohol product streams, holistic process modelling, and not only VLE modelling, will provide maximum benefit to industry and is the ultimate objective. In light thereof, the authors restricted themselves to models available within Aspen Plus®, a well-known commercial process simulator. Three cubic equations of state (EOS), RK-ASPEN [20-22], SR-POLAR [20-23] and PR-BM [20,22,24,25], along with PC-SAFT [26,27] were evaluated for their ability to model the CO₂ + 37DM1O + C₁₀OH system.

The contribution concludes with a discussion on and interesting photos of a density inversion.

2. MATERIALS AND METHODS

2.1 *Experimental method*

A static analytic variable-volume (75 - 125 ml) apparatus, which allows for visual observation of the cell interior, was used to produce the ternary data. Heating is achieved with a forced convection oven in combination with jacketed liquid circulation, and magnetic stirring is used to accelerate the attainment of equilibrium. Two ROLSI™ samplers (Armines, France) feed to two separate online gas chromatograph analysis pathways, and enable dual simultaneous sampling from the vapour and liquid phases. The upper operating limits of the apparatus are 150 °C at 300 bar. Fourie et al. [28] provide information on the experimental setup, cell design, temperature control and monitoring, and system validation. Refer to Fourie et al. [29] for details on the GC configuration and calibrations, and photo and video material illustrating interesting experimental visual observations.

The total uncertainties in pressure and temperature measurement for data from this study are 0.35 bar and ± 0.1 °C [28]. The estimated absolute uncertainties in phase composition, $u(X_i)$ and $u(Y_i)$, are phase, species and composition dependent, and are listed in Table 6-1. The ability to produce repeatable and reproducible data with the experimental setup has been discussed and demonstrated previously [14].

Table 6-1: Estimated maximum absolute uncertainty in phase composition, expressed as mass %, for data reported in this work.

Liquid phase		Vapour phase			
Solutes	Solvent	Solutes		Solvent	
$u(X_i)$	$u(X_i)$	Mass % range	$u(Y_i)$	Mass % range	$u(Y_i)$
0.80%	1.05%	0 - 2 %	0.10%	100 - 94.5 %	0.25%
		2 - 5 %	0.20%	94.5 - 90.5 %	0.30%
		5 - 11 %	0.35%	90.5 - 85 %	0.50%
		11 - 14 %	0.50%	85 - 82 %	0.70%

The materials are listed in Table 6-2 and were used without further purification.

Table 6-2: Materials used

Component	CAS	Purity	Supplier	Cat. No.
37DM10	106-21-8	≥ 98 %	Sigma	W239100-1KG-K
		≥ 98 %	Sigma	W23,910-O-K
C ₁₀ OH	112-30-1	99 %	Sigma	150584-3KG
		≥ 98 %	Sigma	W23,650-O-K
2E1H	104-76-7	≥ 99.0 %	Fluka	04050-250ML
CO ₂	124-38-9	99.995 %	Air Products	K243C

2.2 Modelling

Aspen Plus®, a commercial process simulator, was used to test RK-ASPEN, SR-POLAR, PR-BM and PC-SAFT for their ability to model the new CO₂ + 37DM10 + C₁₀OH data. Refer to Fourie et al. [14] for background on why these models were chosen, and a brief theoretical discussion on each. Model evaluation was conducted via two means. Firstly, the experimental temperatures and compositions were used as inputs to predict the equilibrium pressures of the vapour and liquid phases. These results are reported as %AAD_p defined as

$$\%AAD_p = \frac{1}{M} \sum_{n=1}^M \left| \frac{P_{predict} - P_{experimental}}{P_{experimental}} \right| \times 100 \%$$

Equation 6-1

where M refers to the number of data points. Secondly, the experimental temperatures and pressures were used as inputs to predict the equilibrium compositions of the vapour and liquid phases.

Composition predictions are presented on truncated Gibbs phase diagrams. The input values used in the modelling approaches, temperature and composition for approach 1, and temperature and pressure for approach 2, were obtained from the experimental results of this study (Table 6-3).

Within the RK-ASPEN and SR-POLAR frameworks, C₁₀OH pure component parameters were regressed off saturated vapour pressure data. These P^{sat} data were generated using the Extended Antoine vapour pressure equation [30]. All other pure component parameters were obtained from literature and are referenced accordingly.

The model-specific CO₂ + 37DM10 binary interaction parameters (BIP) from Fourie et al. [14] were used in this study. Isobars at 2 bar increments applied to CO₂ + C₁₀OH P - x_i envelopes, with the latter obtained from literature [31,32], were used to generate data for the regression of CO₂ + C₁₀OH BIP's.

Solute-solute BIP's were then regressed off the ternary experimental data produced in this work.

3. RESULTS AND DISCUSSION

3.1 Experimental data

New experimental VLE data for the mixture CO₂ + 37DM10 + C₁₀OH at 35, 55 and 75 °C are presented in Table 6-3. Estimates of the absolute uncertainty in phase composition are listed in Table 6-1.

Table 6-3: Experimental data for CO₂ + 37DM10 + C₁₀OH at 35.0, 55.0 and 75.0 °C, and pressures between 68.0 and 237.0 bar. An average of 5.1 and a minimum of 5 samples were analysed for each of the vapour and liquid phase data points. The average standard deviation in composition, obtained under repeatability conditions, was 0.0016 in mass fraction, or 0.16 mass %.

Temperature [°C]	Pressure [bar]	Liquid			Vapour		
		CO ₂	37DM10	C ₁₀ OH	CO ₂	37DM10	C ₁₀ OH
35.0	68.0	0.284	0.532	0.185	0.993	0.005	0.001
	68.2	0.275	0.361	0.364	0.997	0.002	0.001
	68.1	0.275	0.183	0.542	0.998	0.001	0.001
	83.0	0.373	0.463	0.164	0.960	0.031	0.008
	83.2	0.368	0.311	0.321	0.964	0.020	0.016
	83.2	0.346	0.160	0.494	0.973	0.008	0.019
	104.0	0.431	0.420	0.149	0.935	0.050	0.014

Temperature [°C]	Pressure [bar]	Liquid			Vapour		
		CO ₂	37DM10	C ₁₀ OH	CO ₂	37DM10	C ₁₀ OH
35.0	104.1	0.400	0.295	0.306	0.945	0.030	0.025
	104.1	0.373	0.152	0.474	0.948	0.015	0.037
	123.1	0.496	0.372	0.133	0.921	0.061	0.018
	123.1	0.426	0.280	0.295	0.927	0.039	0.034
	123.2	0.398	0.146	0.456	0.933	0.019	0.048
	139.9	0.561	0.322	0.117	0.840	0.121	0.039
	140.0	0.460	0.264	0.276	0.908	0.048	0.044
	140.1	0.416	0.138	0.447	0.923	0.021	0.056
	157.2	0.491	0.249	0.260	0.880	0.061	0.059
	157.1	0.433	0.134	0.434	0.900	0.027	0.073
	182.2	0.566	0.212	0.222	0.849	0.076	0.075
	182.0	0.464	0.126	0.410	0.883	0.031	0.086
	200.0	0.486	0.120	0.394	0.870	0.037	0.094
	217.1	0.508	0.115	0.376	0.847	0.038	0.114
	237.0	0.535	0.109	0.356	0.835	0.041	0.124
55.0	83.1	0.247	0.559	0.194	0.993	0.005	0.001
	83.2	0.236	0.380	0.384	0.999	0.001	0.000
	83.1	0.241	0.190	0.569	0.991	0.003	0.006
	104.0	0.341	0.489	0.169	0.987	0.010	0.003
	104.2	0.315	0.340	0.345	0.993	0.004	0.003
	104.2	0.318	0.170	0.511	0.990	0.003	0.007
	123.1	0.417	0.431	0.151	0.950	0.039	0.011
	123.2	0.377	0.307	0.316	0.964	0.020	0.016
	123.1	0.379	0.152	0.469	0.960	0.011	0.028
	140.1	0.507	0.364	0.129	0.922	0.061	0.018
	140.2	0.424	0.283	0.294	0.926	0.040	0.034
	140.1	0.426	0.139	0.434	0.943	0.017	0.041
	157.0	0.629	0.274	0.097	0.826	0.130	0.043
	157.2	0.478	0.255	0.267	0.874	0.065	0.061
	157.0	0.465	0.129	0.406	0.903	0.026	0.070
	182.1	0.541	0.111	0.348	0.848	0.039	0.113

Temperature [°C]	Pressure [bar]	Liquid			Vapour		
		CO ₂	37DM1O	C ₁₀ OH	CO ₂	37DM1O	C ₁₀ OH
75.0	104.1	0.263	0.549	0.189	0.991	0.007	0.002
	104.2	0.246	0.374	0.379	0.997	0.002	0.001
	104.1	0.250	0.187	0.563	0.995	0.002	0.003
	123.0	0.331	0.498	0.171	0.986	0.011	0.003
	123.1	0.303	0.346	0.351	0.991	0.005	0.004
	123.0	0.297	0.177	0.527	0.989	0.004	0.007
	140.1	0.400	0.446	0.154	0.971	0.023	0.006
	140.2	0.354	0.319	0.327	0.977	0.013	0.010
	140.1	0.357	0.158	0.485	0.964	0.010	0.026
	157.1	0.468	0.394	0.138	0.940	0.047	0.014
	157.1	0.420	0.285	0.294	0.946	0.029	0.025
	157.2	0.412	0.143	0.445	0.953	0.013	0.033
	182.0	0.641	0.265	0.093	0.832	0.127	0.042
	182.0	0.530	0.230	0.240	0.860	0.072	0.069
	182.0	0.496	0.122	0.382	0.899	0.027	0.074
	200.2	0.600	0.098	0.302	0.823	0.045	0.132

3.2 Modelling

Initial modelling was conducted using CO₂ + C₁₀OH and 37DM1O + C₁₀OH BIP's regressed off data in the range 35 - 75 °C. Despite the inclusion of 35 °C data in the respective regression cases, the 35 °C ternary data set proved challenging to model and, in essence, all four models failed. In this regard, the two lowest pressure data points at 35 °C, 68 and 83 bar, were the exception (Fig. 6-1). Between 104 and 237 bar, however, phase composition and vapour phase pressure predictions failed completely whilst liquid phase pressure predictions were poor yet interpretable. The inclusion of low temperature data in the BIP regression cases necessarily impacts model performance at higher temperatures. As such, the revised approach to both modelling and model evaluation, which forms the basis of the subsequent discussions, excluded data at temperatures below 55 °C.

3.2.1 RK-ASPEN

The RK-ASPEN pure component parameters used in this study are listed in Table 6-4. Both the CO₂ + C₁₀OH and 37DM10 + C₁₀OH binary interactions were characterised using $k_{a,ij}$ and $k_{b,ij}$ parameters, with linear temperature dependency incorporated in the CO₂ + C₁₀OH $k_{a,ij}$. Refer to Table 6-7 for the BIP values and Table 6-8 for the regression %AAD's in pressure, temperature, and vapour and liquid phase solute fractions.

Table 6-4: RK-ASPEN pure component polar parameters used in this work

Component	η_i []	%AAD P^{sat} [%]	T-range [°C]	Reference
CO ₂	0.0481	0.03	-23.15 to 27.85	[14]
37DM10	0.5008	0.12	11.85 - 131.85	[14]
C ₁₀ OH	-0.4165	0.05	11.85 - 144.85	This work

3.2.2 SR-POLAR

The SR-POLAR pure component parameters used in this study are listed in Table 6-5. A single temperature independent $k_{a,ij}^{(0)}$ parameter was used for the CO₂ + C₁₀OH interaction whilst the solute-solute interaction was captured using two BIP's – a linearly temperature dependent $k_{a,ij}$ and a temperature independent $k_{b,ij}^{(0)}$ (Tables 6-7 and 6-8). For both the CO₂ + C₁₀OH and 37DM10 + C₁₀OH pairs, the inclusion of $I_{ij}^{(0)}$ and $I_{ij}^{(1)}$ parameters, in various combinations with other BIP's, was evaluated. This led to degraded correlations of the new ternary phase equilibria data, as had been the case for the CO₂ + n C₁₂ + 37DM10 system [14].

Table 6-5: SR-POLAR pure component parameters used in this study

Component	p_1 []	p_2 []	%AAD P^{sat} [%]	T-range [°C]	Reference
CO ₂	0.1221	-1.2224	0.01	-23.15 to 27.85	[14]
37DM10	0.4004	-1.5001	0.03	11.85 - 131.85	[14]
C ₁₀ OH	-0.5052	-2.4053	0.02	11.85 - 144.85	This work

3.2.3 PR-BM

Within PR-BM, temperature independent $k_{ij}^{(0)}$ and $l_{ij}^{(0)}$ parameters were used for both the CO₂ + C₁₀OH and 37DM10 + C₁₀OH interactions (Table 6-7). In contrast to SR-POLAR (Section 3.2.2) and prior experience with PR-BM [14], l_{ij} parameters were necessary to produce the required vapour phase concavity (Figs. 6-4 e, 6-6 e and 6-7 c), and the use thereof reduced the %AAD_p for pressure predictions in the ternary mixture.

3.2.4 PC-SAFT

The PC-SAFT pure component parameters used in this study are listed in Table 6-6. Three literature sets of C₁₀OH pure component parameters [33-35] were evaluated. Using the C₁₀OH parameters from Liang et al. [33] led to the smallest %AAD_p for ternary mixture pressure predictions and these form the basis of results presented here (Tables 6-7 - 6-9). Furthermore, using a single temperature independent $k_{ij}^{(0)}$ to describe the CO₂ + C₁₀OH interaction and, strangely, no solute-solute BIP, produced the smallest error in equilibrium pressure predictions (Table 6-9). Refer to Table 6-7 for the BIP's and Table 6-8 for the regression %AAD values.

Table 6-6: PC-SAFT pure component parameters used in this work

Component	m	σ	ε/k	ε^{AB}/k	κ^{AB}	%AAD P^{sat}	%AAD ρ^{sat}	T-range	Reference
	[]	[Å]	[°C]	[°C]	[]	[%]	[%]	[°C]	
CO ₂	2.0729	2.7852	-103.94	-	-	2.78	2.73	-57.15 to 30.85	[26]
37DM1O	4.4587	3.8325	-2.75	2217.20	0.002853	0.71	6.63	11.85 - 131.85	[14]
C ₁₀ OH	6.4558	3.4215	-34.20	3187.02	0.000102	3.02	1.48	68 - 349	[33]

Table 6-7: Binary interaction parameters used in this work

Interaction pair	RK-ASPEN			SR-POLAR			PR-BM			PC-SAFT			Reference
	$k_{a,ij}^{(0)}$	$k_{a,ij}^{(1)}$	$k_{b,ij}^{(0)}$	$k_{a,ij}^{(0)}$	$k_{a,ij}^{(1)}$	$k_{b,ij}^{(0)}$	$k_{ij}^{(0)}$	$k_{ij}^{(1)}$	$l_{ij}^{(0)}$	$l_{ij}^{(1)}$	$k_{ij}^{(0)}$	$k_{ij}^{(1)}$	
CO ₂ + 37DM1O	0.3127	-0.6997	-	0.0801	-	-	0.5499	-0.0015	-	-	0.2801	-0.1699	[14]
CO ₂ + C ₁₀ OH	0.1821	-0.2866	-0.0288	0.1191	-	-	0.1478	-	-0.3467	0.0605	0.0759	-	This work
37DM1O + C ₁₀ OH	0.0377	-	0.0645	-0.3021	0.0010	0.0606	0.0184	-	-0.0012	-0.0749	-	-	This work

Table 6-8: %AAD in pressure, temperature and solute mass fractions for the regression of BIP's used in this work.

Solute fraction deviations for the 37DM1O + C₁₀OH pair are reported as an average of 37DM1O and C₁₀OH deviations.

Interaction	RK-ASPEN				SR-POLAR				PR-BM				PC-SAFT				Reference
	%AAD _p	%AAD _T	%AAD _x	%AAD _y	%AAD _p	%AAD _T	%AAD _x	%AAD _y	%AAD _p	%AAD _T	%AAD _x	%AAD _y	%AAD _p	%AAD _T	%AAD _x	%AAD _y	
CO ₂ + 37DM1O	0.99	1.17	0.37	13.53	1.96	8.32	1.40	27.53	10.96	14.02	3.21	29.54	5.93	9.62	1.62	39.57	[14]
CO ₂ + C ₁₀ OH	1.40	1.44	0.49	10.53	3.16	3.18	1.34	27.04	2.42	3.06	0.92	27.64	6.81	4.91	2.13	28.00	This work
37DM1O + C ₁₀ OH	2.10	2.59	1.33	20.93	2.05	2.38	0.82	34.90	2.47	2.25	1.14	36.90	-	-	-	-	This work
TOTAL	57 %				114 %				135 %				-				

3.3 Comparison of model-predicted ternary mixture vapour and liquid phase pressures

The temperature and phase composition data in Table 6-3 and the BIP's in Table 6-7 were used to predict 54 equilibrium pressures for each of the vapour and liquid phase. As mentioned in Section 3.2, all four models essentially failed at 35 °C and therefore model evaluation is based on ternary data at 55 and 75 °C only, which equates to 32 pressures per phase. In addition, all three cubic EOS failed at one 55 °C vapour phase data point and PC-SAFT failed at four 55 °C and two 75 °C vapour phase data points. These failed predictions, all in excess of 2 000 bar, were excluded from the %AAD_p calculations in Table 6-9.

Table 6-9: %AAD_p values for the model-predicted liquid and vapour phase equilibrium pressures at 55 and 75 °C in the system CO₂ + 37DM10 + C₁₀OH. The experimental temperatures and vapour and liquid phase compositions from this work were used as inputs to the simulation cases. Deviations labelled as Overall were calculated for both temperatures and deviations labelled as Combined were calculated for both the liquid and vapour phases. No 35 °C data were incorporated in the deviation calculations.

Model	Liquid			Vapour			Combined		
	55 °C	75 °C	Overall	55 °C	75 °C	Overall	55 °C	75 °C	Overall
RK-ASPEN	3.8	2.5	3.2	5.8 ^a	4.1	4.9	4.8	3.3	4.0
SR-POLAR	2.4	2.9	2.6	5.6 ^a	5.0	5.3	4.0	4.0	4.0
PR-BM	3.0	3.5	3.3	6.2 ^a	4.8	5.5	4.6	4.1	4.4
PC-SAFT	10.3	12.6	11.5	35.0 ^b	19.5 ^c	26.7	20.9	15.8	18.3

^a One pressure prediction in excess of 2 000 bar excluded; ^b Four pressure predictions in excess of 2 000 bar excluded; ^c Two pressure predictions in excess of 2 000 bar excluded.

RK-ASPEN and SR-POLAR outperformed the other two models with combined-overall %AAD_p's of 4.0 %, whilst errors via PR-BM were marginally greater. PC-SAFT fared significantly worse, especially taking into account six failed predictions are excluded from the 18.3 % figure. Based on the phase-specific variation in %AAD_p between 55 and 75 °C, SR-POLAR performance is least sensitive to temperature. The crude approach of totalising the 12 model-specific %AAD's from Table 6-8 as an indicator of relative ability to predict ternary equilibrium pressures worked well for CO₂ + nC₁₂ + 37DM10 [14] but is not as effective here. It correctly positions PR-BM as the worst performing cubic EOS but could not predict the similarity in RK-ASPEN and SR-POLAR %AAD_p's (Table 6-9).

The %AAD_p's for liquid phase pressure predictions at 35 °C, referred to as *poor yet interpretable* in the first paragraph of Section 3.2, were 26.6, 26.2, 25.6 and 33.6 % for the RK-ASPEN, SR-POLAR, PR-BM and PC-SAFT models respectively. These values are not listed in Table 6-9. Having included 35 and 45 °C data in the CO₂ + C₁₀OH BIP regression and 35 °C data in the 37DM10 + C₁₀OH BIP regression, these errors were 29.9, 37.2, 23.6 and 32.9 % respectively. Thus, BIP regressions that are weighted toward high temperature

data had no significant adverse impact on liquid phase equilibrium pressure predictions at 35 °C, and in some cases the predictions even improved.

In general, the models struggled more with pressure predictions in this ternary mixture than was the case for $\text{CO}_2 + n\text{C}_{12} + 37\text{DM10}$ where the combined-overall %AAD_p's via RK-ASPEN, SR-POLAR, PR-BM and PC-SAFT, inclusive of 35 °C data, were 3.1, 3.8, 3.9 and 8.5 % respectively [14].¹³

3.4 Experimental and model predicted ternary mixture phase behaviour

The experimental data from this study, along with model predicted phase compositions, are presented on truncated Gibbs diagrams in Figs. 6-1 - 6-7. At 35 °C and pressures between 104 and 237 bar, all model predictions failed (see Section 3.2) and the experimental data for these systems are shown on one phase diagram (Fig. 6-3). The ternary literature data presented in Figs. 6-1 - 6-7 were generated using a static synthetic view cell [19] and therefore do not enable the connection of tie lines. References to low, medium and high pressures should be interpreted within the context of the temperature-specific working pressure ranges: 68 - 237 bar, 83 - 182 bar, and 104 - 200 bar.

Phase behaviour in the ternary mixture $\text{CO}_2 + 37\text{DM10} + \text{C}_{10}\text{OH}$ differs significantly from that of $\text{CO}_2 + n\text{C}_{12} + 37\text{DM10}$ [14].¹⁴ Liquid phase curves remain convex throughout the entire solute-solute ratio range and, in contrast to the $n\text{C}_{12}$ -containing system, no s-shaped liquid curvature is observed. These convex curves indicate reduced CO_2 solubility in the mixture liquid phase compared to the weighted average (i.e., a straight line connecting the two liquid phase binary data points). Furthermore, the absence of any co-solubility pinch [14] is noteworthy and none of the phase diagrams indicate the presence of two distinct two-phase regions.

Vapour phase trends at 35 °C (83 - 182 bar) and 55 °C (140 - 157 bar) seem to hint at a transition between convex curvature, or reduced solubility, in the high-37DM10 region to concave curvature, or increased solubility, in the high- C_{10}OH region

Compared to $n\text{C}_{12} + 37\text{DM10}$ [14], the $37\text{DM10} + \text{C}_{10}\text{OH}$ solute mixture is less soluble and at all temperatures studied two-phase VLE persists up to higher pressures. This is not surprising considering the relatively high CO_2 -solubility of $n\text{C}_{12}$ and the relatively low CO_2 -solubility of C_{10}OH [19,31]. Low temperature P - x_i envelopes in the $\text{CO}_2 + \text{C}_{10}\text{OH}$ binary system are known to cross and extend above those at higher temperatures [31]. This temperature inversion impacts ternary phase behaviour of the 25:75 solute ratio mixture in particular, where two-phase VLE could be measured up to 237 bar.

¹³ See also Table 5-11 on p. 118.

¹⁴ See also Section 3.5 on p. 119.

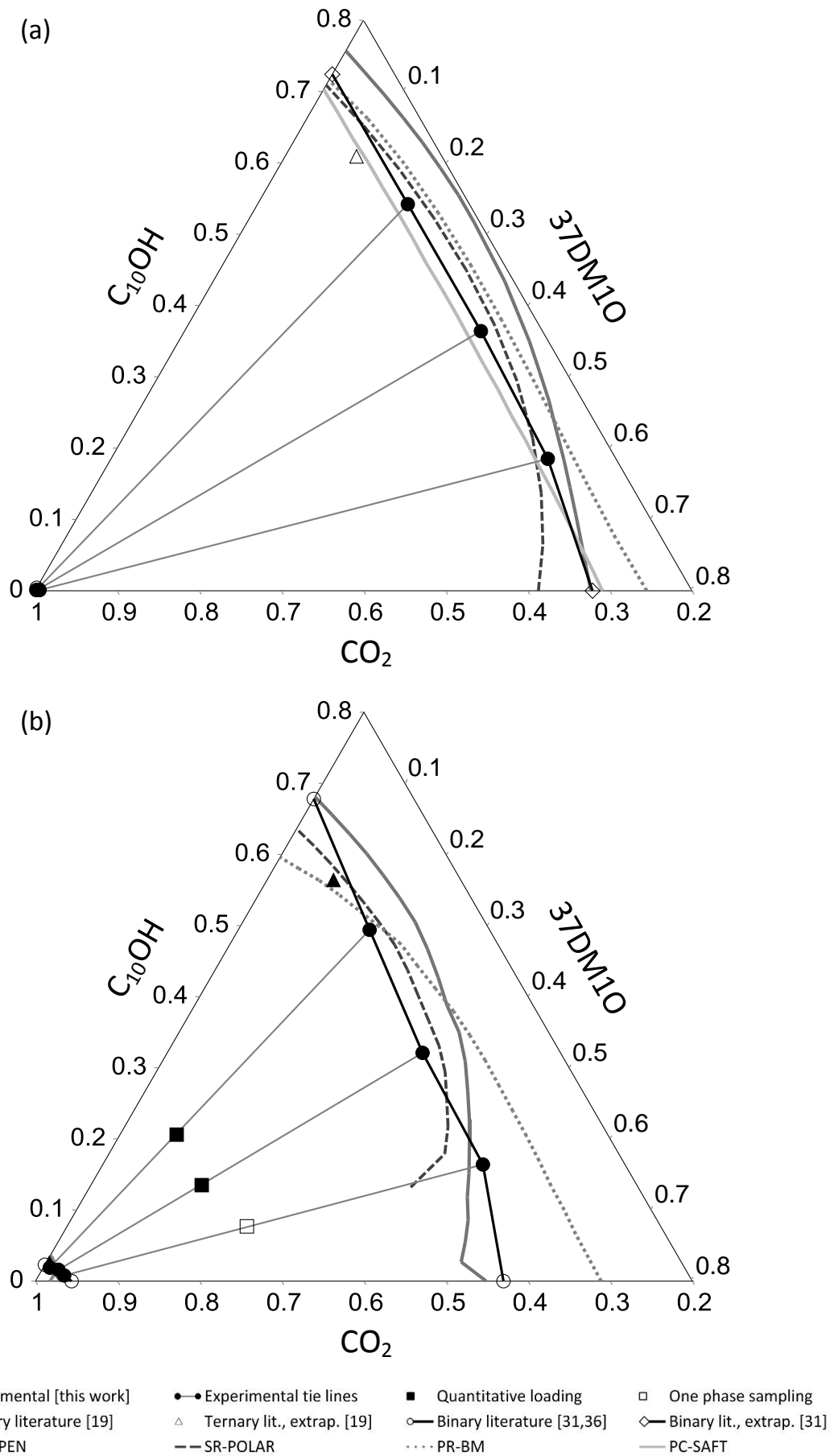


Figure 6-1. $\text{CO}_2 + 37\text{DM}10 + \text{C}_{10}\text{OH}$ at $35.0\text{ }^\circ\text{C}$ and (a) 68 bar; and (b) 83 bar.

PC-SAFT failed to predict two-phase VLE at 83 bar.

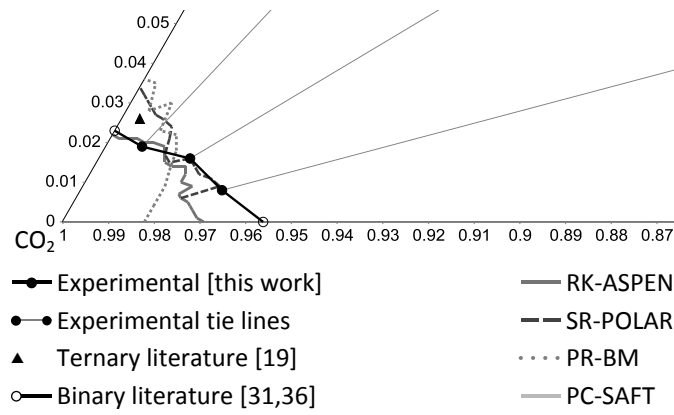


Figure 6-2. Vapour phase detail for $\text{CO}_2 + 37\text{DM}10 + \text{C}_{10}\text{OH}$ at $35.0\text{ }^\circ\text{C}$ and 83 bar .

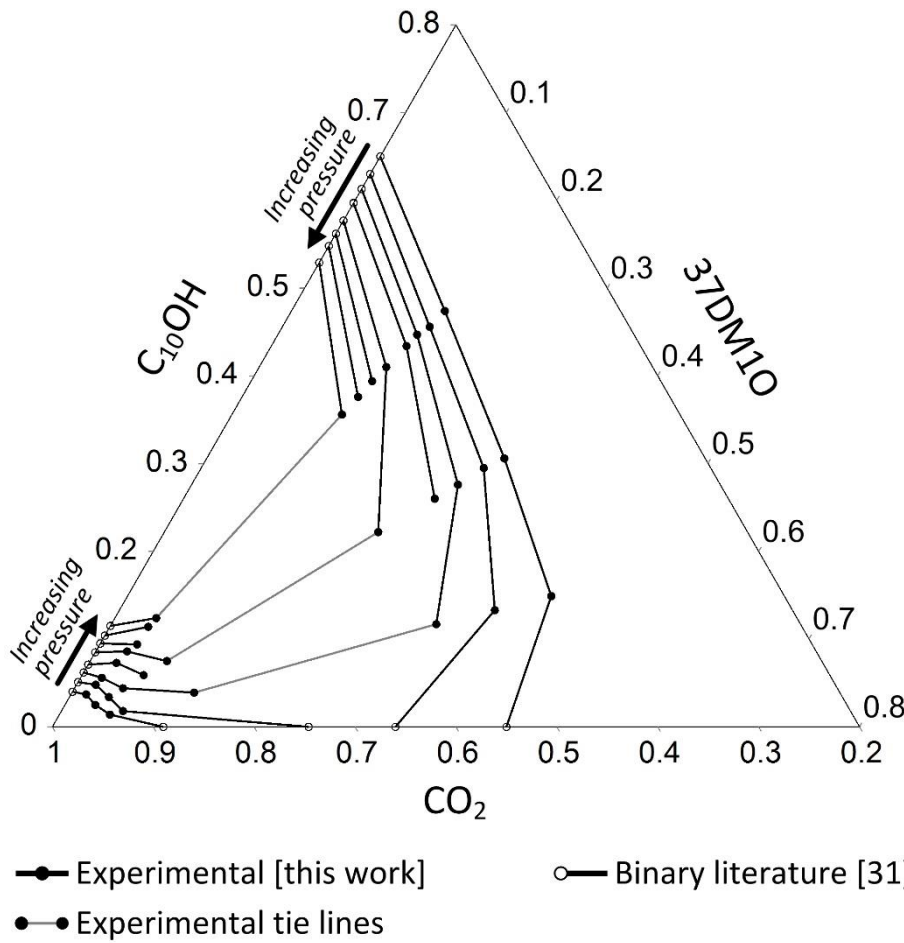
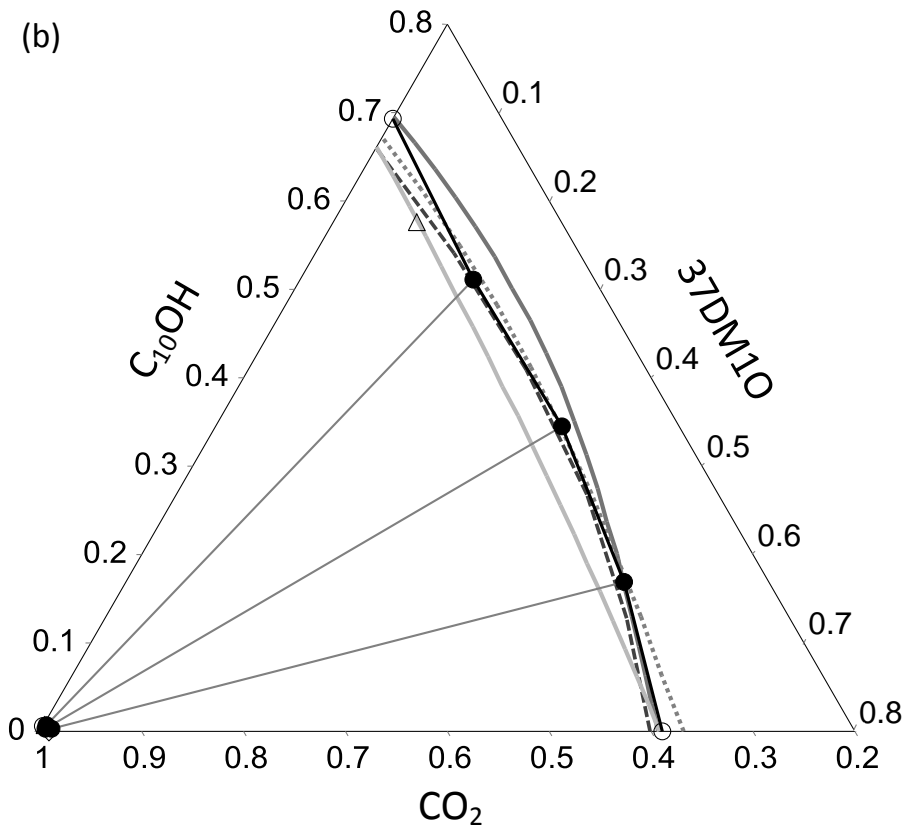
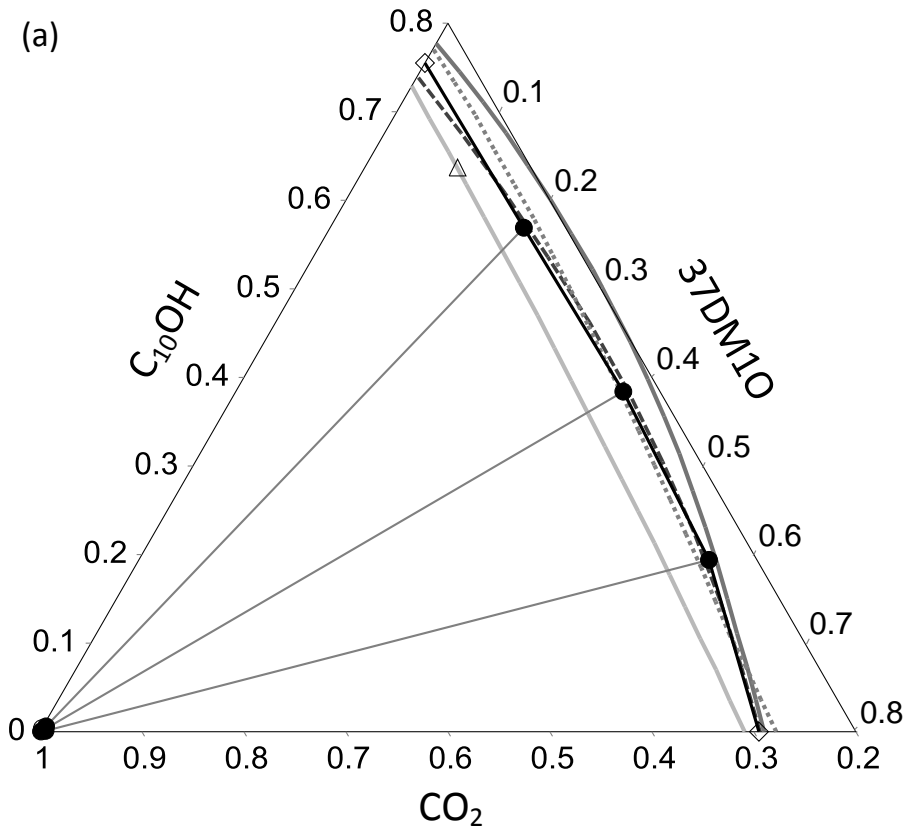


Figure 6-3. $\text{CO}_2 + 37\text{DM}10 + \text{C}_{10}\text{OH}$ at $35.0\text{ }^\circ\text{C}$ and $104, 123, 140, 157, 182, 200, 217$ and 237 bar . The arrows indicate the direction of increasing pressure. To eliminate clutter, only select tie lines were connected.



- | | | | |
|------------------------------|------------------------------|-----------------------------|-----------------------------|
| —●— Experimental [this work] | ●—● Experimental tie lines | ■ Quantitative loading | □ One phase sampling |
| ▲ Ternary literature [19] | △ Ternary lit., extrap. [19] | — Binary literature [31,36] | ◇ Binary lit., extrap. [31] |
| — RK-ASPEN | — SR-POLAR | ⋯ PR-BM | — PC-SAFT |

Figure 6-4. $\text{CO}_2 + 37\text{DM}10 + \text{C}_{10}\text{OH}$ at 55.0 °C and (a) 83 bar; (b) 104 bar; (c) 123 bar; (d) 140 bar; (e) 157 bar; and (f) 182 bar.

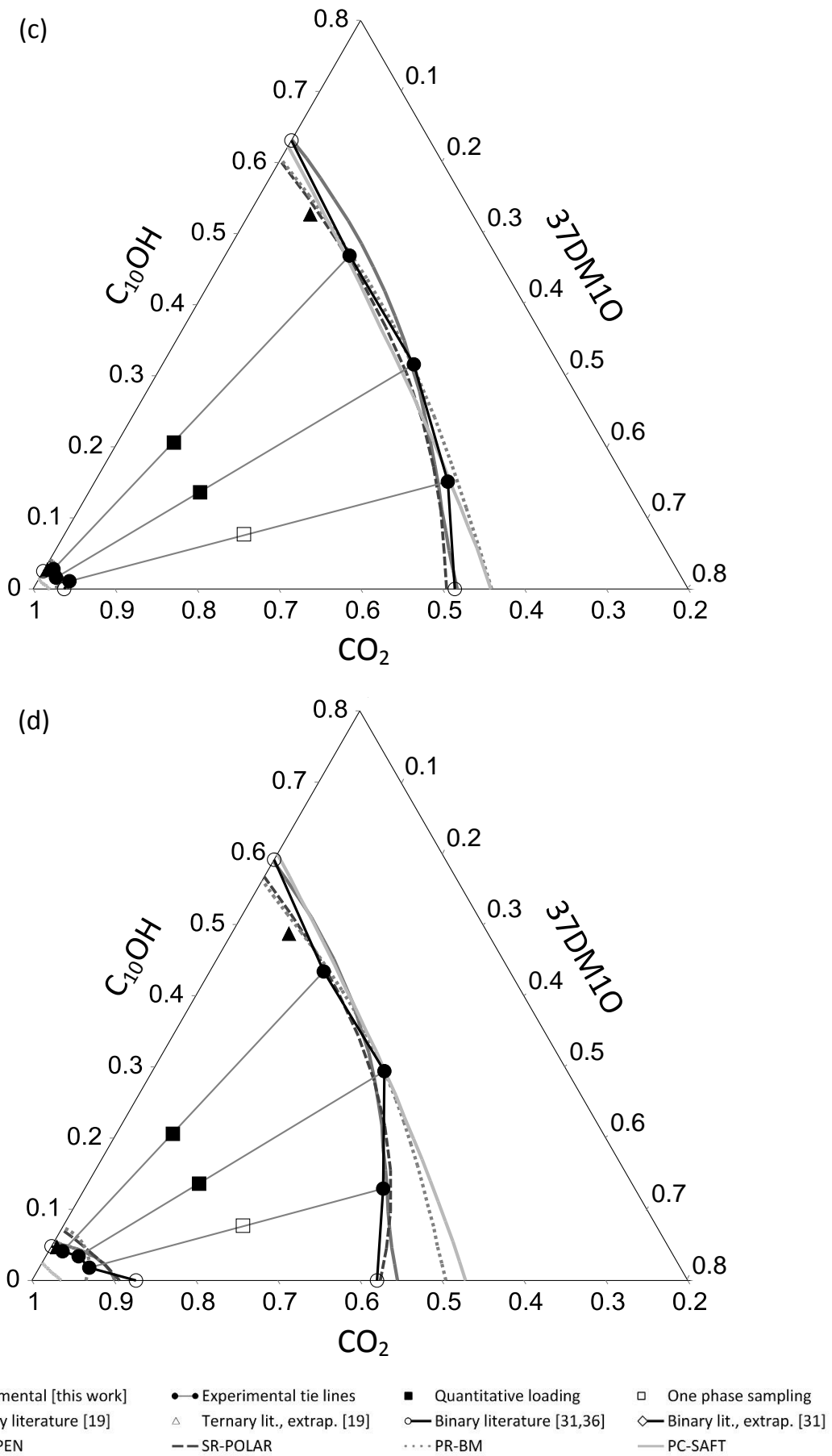


Figure 6-4. $\text{CO}_2 + 37\text{DM}10 + \text{C}_{10}\text{OH}$ at $55.0\text{ }^\circ\text{C}$ and (a) 83 bar; (b) 104 bar; (c) 123 bar; (d) 140 bar; (e) 157 bar; and (f) 182 bar.

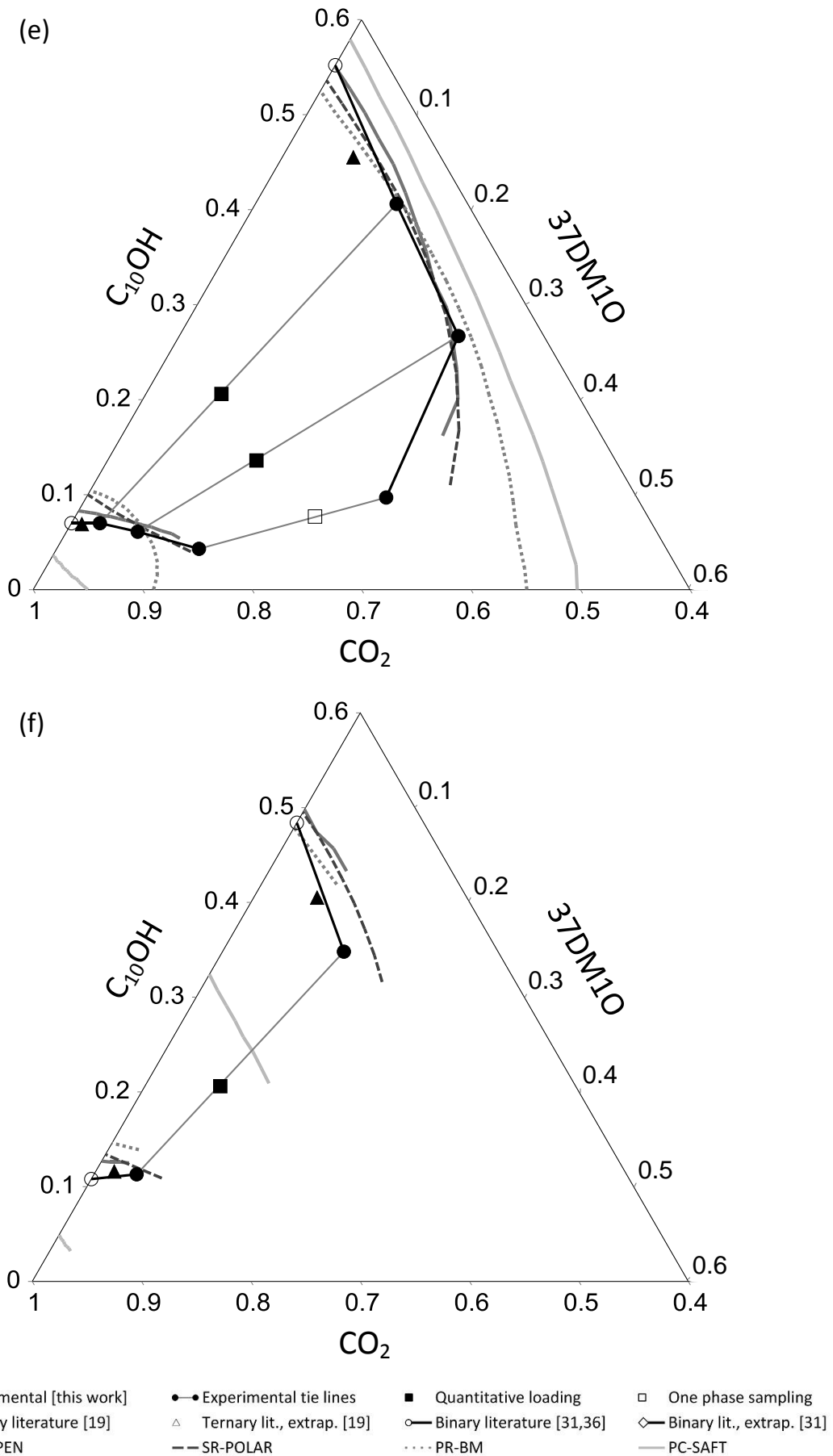


Figure 6-4. $\text{CO}_2 + 37\text{DM}10 + \text{C}_{10}\text{OH}$ at $55.0\text{ }^\circ\text{C}$ and (a) 83 bar; (b) 104 bar; (c) 123 bar; (d) 140 bar; (e) 157 bar; and (f) 182 bar.

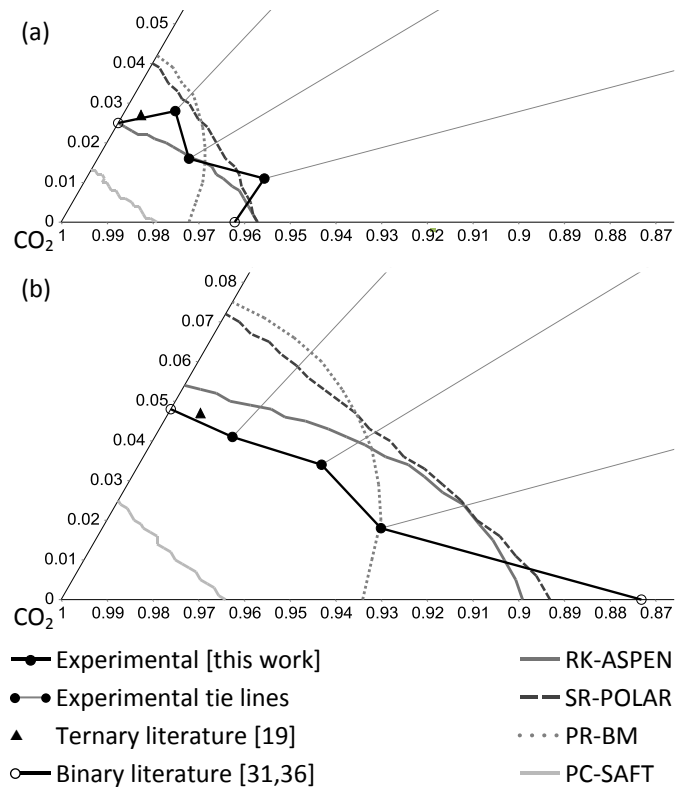


Figure 6-5. Vapour phase detail for CO₂ + 37DM10 + C₁₀OH at 55.0 °C and (a) 123 bar; and (b) 140 bar.

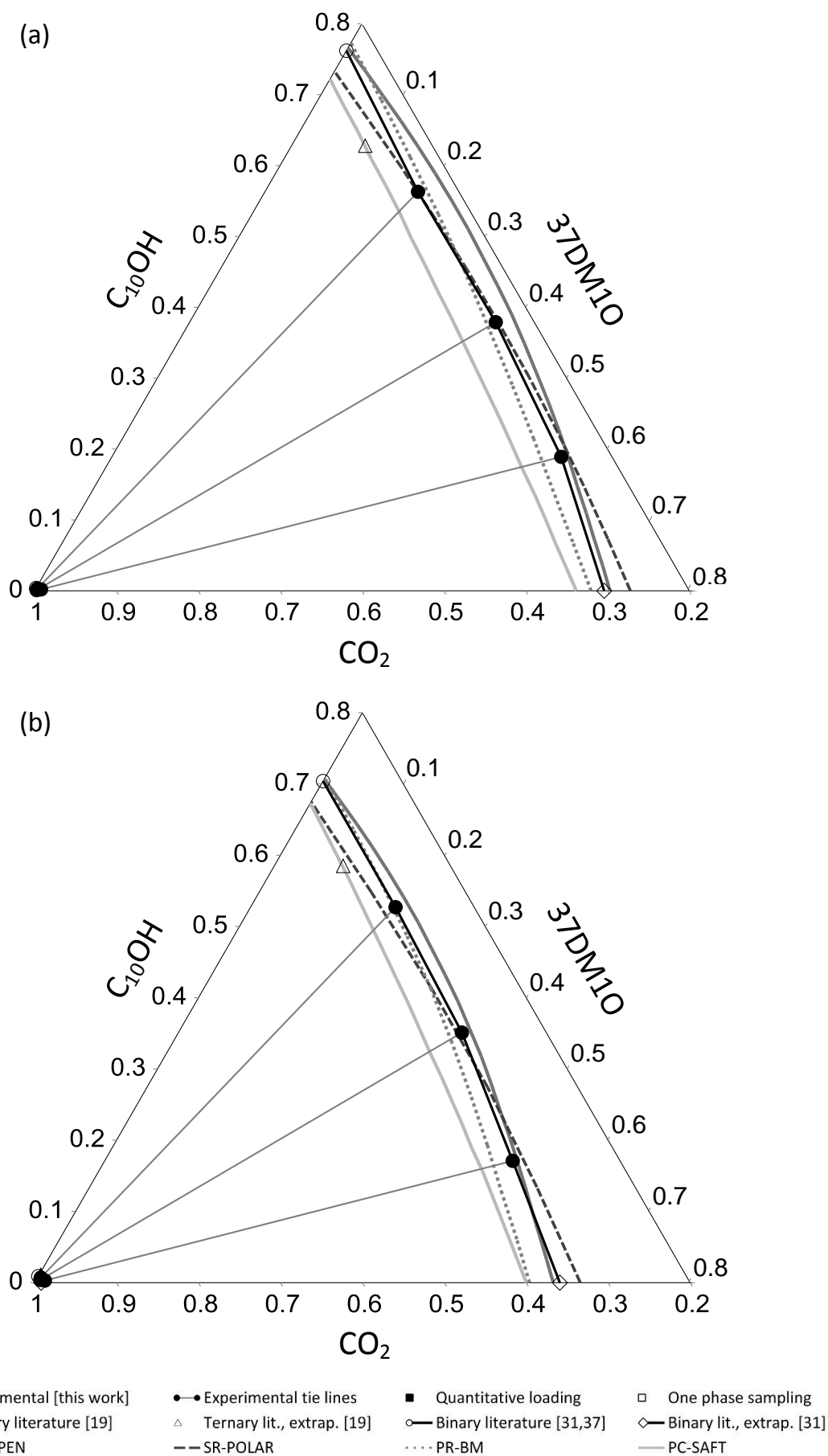


Figure 6-6. $\text{CO}_2 + 37\text{DM}10 + \text{C}_{10}\text{OH}$ at $75.0\text{ }^\circ\text{C}$ and (a) 104 bar; (b) 123 bar; (c) 140 bar; (d) 157 bar; (e) 182 bar; and (f) 200 bar.

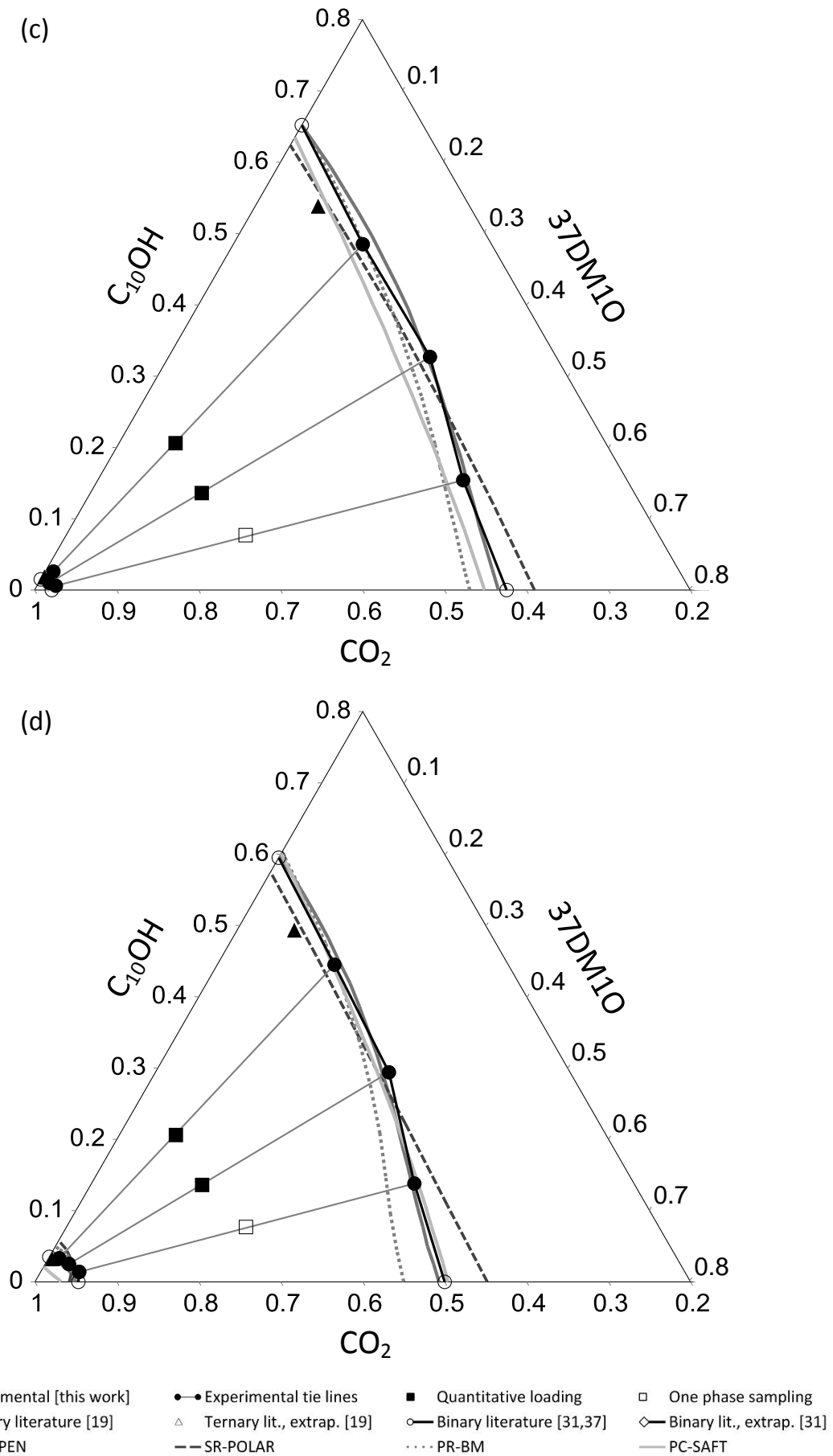
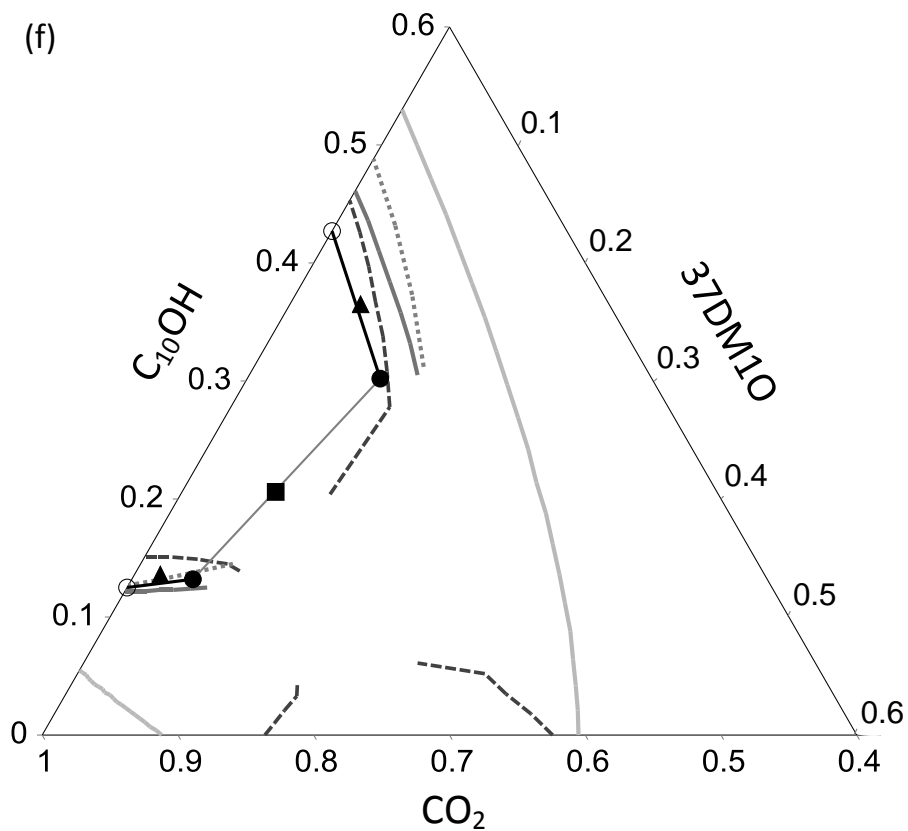
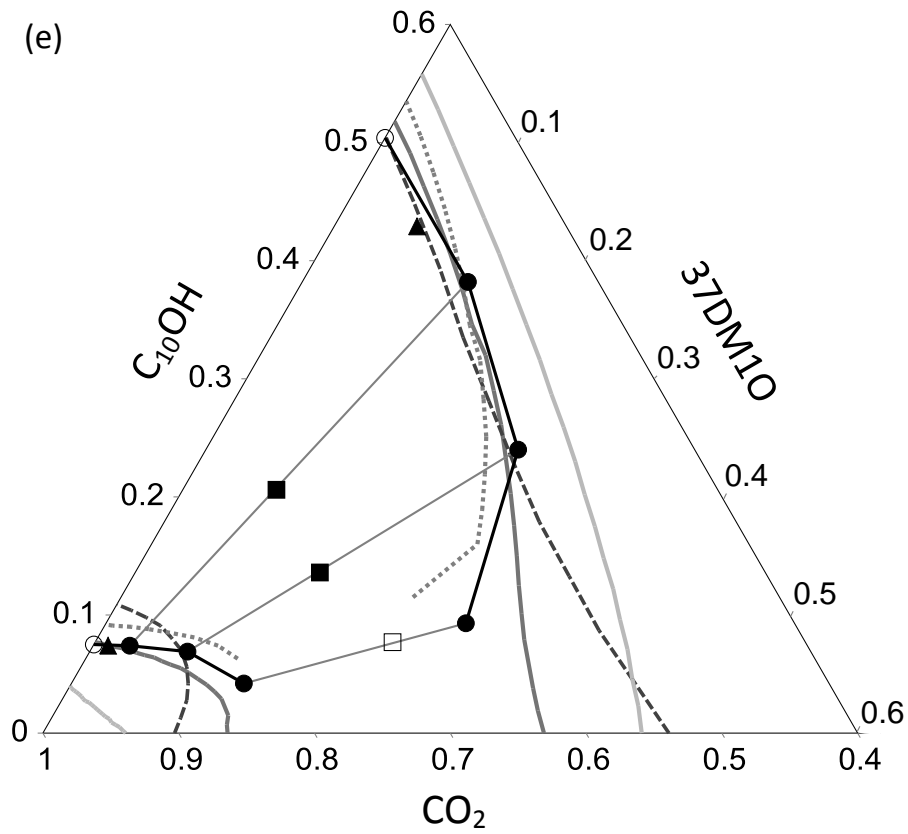


Figure 6-6. $\text{CO}_2 + 37\text{DM}10 + \text{C}_{10}\text{OH}$ at $75.0\text{ }^\circ\text{C}$ and (a) 104 bar; (b) 123 bar; (c) 140 bar; (d) 157 bar; (e) 182 bar; and (f) 200 bar.



- Experimental [this work]
- ▲ Ternary literature [19]
- RK-ASPEN
- Experimental tie lines
- △ Ternary lit., extrap. [19]
- SR-POLAR
- Quantitative loading
- Binary literature [31,37]
- ⋯ PR-BM
- One phase sampling
- ◇ Binary lit., extrap. [31]
- PC-SAFT

Figure 6-6. $\text{CO}_2 + 37\text{DM}10 + \text{C}_{10}\text{OH}$ at 75.0 °C and (a) 104 bar; (b) 123 bar; (c) 140 bar; (d) 157 bar; (e) 182 bar; and (f) 200 bar.

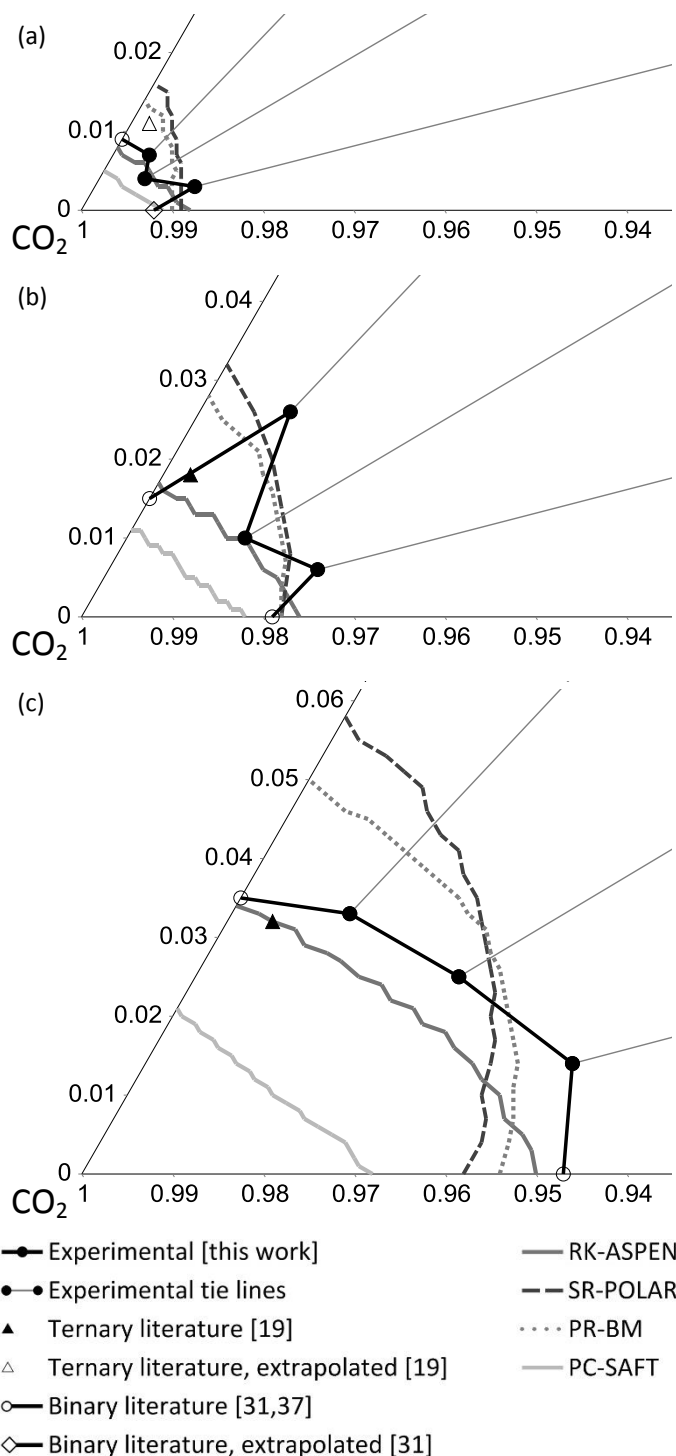


Figure 6-7. Vapour phase detail for CO₂ + 37DM10 + C₁₀OH at 75.0 °C and (a) 123 bar; (b) 140 bar; and (c) 157 bar.

RK-ASPEN low-pressure liquid phase correlations are overly solute-rich and convex. This applies to all three temperatures, but the error diminishes with increasing temperature (Figs. 6-1, 6-4 a, b and 6-6 a, b). At both 55 and 75 °C, medium pressure liquid curves are well-approximated (Figs. 6-4 c, d and 6-6 c, d). However, as pressure increases, RK-ASPEN is not successful at capturing the liquid curvature that develops in the high-37DM10 region (Figs. 6-4 e and 6-6 e), and predicts CO₂-deficient liquid trends (Figs. 6-4 f and 6-6 f). In general, very accurate vapour phase correlations are obtained via RK-ASPEN (Figs. 6-2, 6-4 e, f, 6-5, 6-6 e, f and 6-7). Solute solubility is marginally over-estimated in the high pressure region

at 55 °C (157 and 182 bar) whilst the opposite is true at 75 °C (182 and 200 bar), which leads to an erroneous continuous two-phase band in Fig. 6-6 e.

SR-POLAR liquid phase predictions at 35 °C are reasonably positioned but too convex in shape. Very accurate liquid correlations are obtained at 55 °C but, as the experimental two-phase region moves away from the CO₂ + 37DM10 axis, predicted compositions become somewhat CO₂-deficient. Low and medium pressure liquid trends at 75 °C are well positioned but too linear and incorrectly angled (i.e., CO₂-deficient in the high-37DM10 region and CO₂-rich in the high-C₁₀OH region). Solubility is severely under-predicted in the high pressure systems at 75 °C, resulting in a continuous two-phase band (Fig. 6-6 e) and two separate two-phase regions (Fig. 6-6 f). Vapour phase correlations at 55 and 75 °C are reasonably positioned but, by virtue of over-estimating solute content in the high-C₁₀OH region, do not follow the experimental curvature (Figs. 6-4 e, f, 6-5, 6-6 e, f and 6-7). At 75 °C this is aggravated by predicting solute-deficient trends in the high-37DM10 region, a phenomenon that becomes more pronounced as pressure increases and eventually contributes to the aforementioned continuous two-phase band and detached two-phase regions.

PR-BM liquid correlations tend to be more accurate in the high-C₁₀OH region than in the high-37DM10 region. Deviations at 35 and 55 °C are mostly solute-rich (Figs. 6-1 and 6-4 a - e) and differ from deviations at 75 °C which tend to be solute-deficient (Fig. 6-6 a - e). This 75 °C solute deficiency notwithstanding, PR-BM is impressive in its ability to capture the liquid phase curvature at 182 bar (Fig. 6-6 e). Strangely, the solute-deficiency transitions to CO₂-deficiency at 200 bar (Fig. 6-6 f). At 55 and 75 °C, vapour correlations in the high-C₁₀OH region are comparable to those obtained via SR-POLAR. However, a pressure-dependent shift toward solute-deficiency in the high-37DM10 region occurs at 55 °C and not at 75 °C, as was the case for SR-POLAR. This shift contributes toward the prediction of a faulty continuous two-phase band at 55 °C and 157 bar (Fig. 6-4 e). PR-BM vapour correlations at 75 °C improve with increasing pressure and it outperforms the other models at 182 and 200 bar (Fig. 6-6 e and f).

PC-SAFT produced an accurate liquid correlation at 35 °C and 68 bar but the model failed to predict VLE at 83 bar. At 55 and 75 °C, liquid trends shift from CO₂-rich to solute-rich as pressure increases, and cannot match the curvature that develops in the high-37DM10 region at higher pressures (Figs. 6-4 d, e and 6-6 e). The liquid phase prediction at 55 °C and 200 bar, where the model all but failed, presents dissimilar behaviour. Vapour phase predictions via PC-SAFT produced linear or marginally convex correlations which do not match the qualitative behaviour of the experimental data. Furthermore, in all scenarios evaluated the predicted vapour phase solute loading was too low. It is interesting to note the similarity in PC-SAFT performance at higher pressures in the ternary mixtures CO₂ + 37DM10 + C₁₀OH and CO₂ + *n*C₁₂ + 37DM10 [14]. In both cases, solubilities err on the low side which results in a two-phase envelope too large in surface area.

3.5 Evaluating CO₂ as solvent to fractionate 37DM10 + C₁₀OH

3.5.1 Experimental ternary mixture relative solubilities and separation potentials

The experimental data in Table 6-3 were used to calculate the experimental relative solubility α_{ij} , an indicator of fractionation sharpness, and separation potential SP_{ij} , which contains both a selectivity and a vapour phase solute loading contribution. These are defined as

$$\alpha_{ij} = \frac{Y_i/X_i}{Y_j/X_j}$$

Equation 6-2

$$SP_{ij} = (\alpha_{ij} - 1) \times Y_i \times 1000$$

Equation 6-3

where i and j represent 37DM10 and C₁₀OH respectively. These results, shown in Fig. 6-8 with y-axes scaled similarly to Fourie et al. [14], differ from those for the CO₂ + nC₁₂ + 37DM10 system [14] in four important aspects.¹⁵

- i. Relative solubility presents no clear dependence on solute-solute ratio. In contrast, α_{ij} values in the nC₁₂ + 37DM10 mixture were distinctly positively correlated with bulk fraction of the less soluble species, 37DM10.
- ii. Separation of 37DM10 + C₁₀OH using CO₂ is possible at all measured solute ratios. This was not the case for the 75:25 nC₁₂:37DM10 mixture.
- iii. Besides the 75:25 mixture mentioned in [ii], α_{ij} and SP_{ij} values from this work are considerably smaller. The average α_{ij} and SP_{ij} for all measured conditions are 1.3 and 5.2, compared to 1.7 and 8.4 for the CO₂ + nC₁₂ + 37DM10 ternary. Thus, CO₂ fractionation of the two alcohol species is possible across the entire solute ratio range but, in general, CO₂ is less effective as solvent for 37DM10 + C₁₀OH than for nC₁₂ + 37DM10.
- iv. Y_i dominates SP_{ij} behaviour and at constant temperature and pressure, SP_{ij} is positively correlated with bulk fraction of the *more* soluble species, 37DM10. In the CO₂ + nC₁₂ + 37DM10 system, α_{ij} dominated SP_{ij} behaviour and the latter was positively correlated with bulk fraction of the *less* soluble species, 37DM10.

¹⁵ See also Section 3.6.1 on p. 126.

The sensitivity of α_{ij} to small vapour phase solute fractions, as typically encountered at low pressures, has been discussed previously [14]. The values of 2.7 at 35 °C and 3.1 at 55 °C are based on vapour phase solute mass fractions smaller than 0.001, and may be misleading (Fig. 6-8 a). The α_{ij} and SP_{ij} values at 35 °C and 200 bar appear to be outliers (Fig. 6-8). This combination of T and P was the first to be measured after the density inversion and may justify re-sampling (also see Fig. 6-3). Fig. 6-8 b illustrates a noteworthy observation: the largest SP_{ij} value within each of the three solute-solute ratios occurs at 35 °C (this excludes the aforementioned outlier). Using binary data [31,36,37] to approximate α_{ij} results in significant α_{ij} -overestimation (Fig. 6-8 a) which qualitatively matches results for $\text{CO}_2 + n\text{C}_{12} + 37\text{DM10}$ [14].

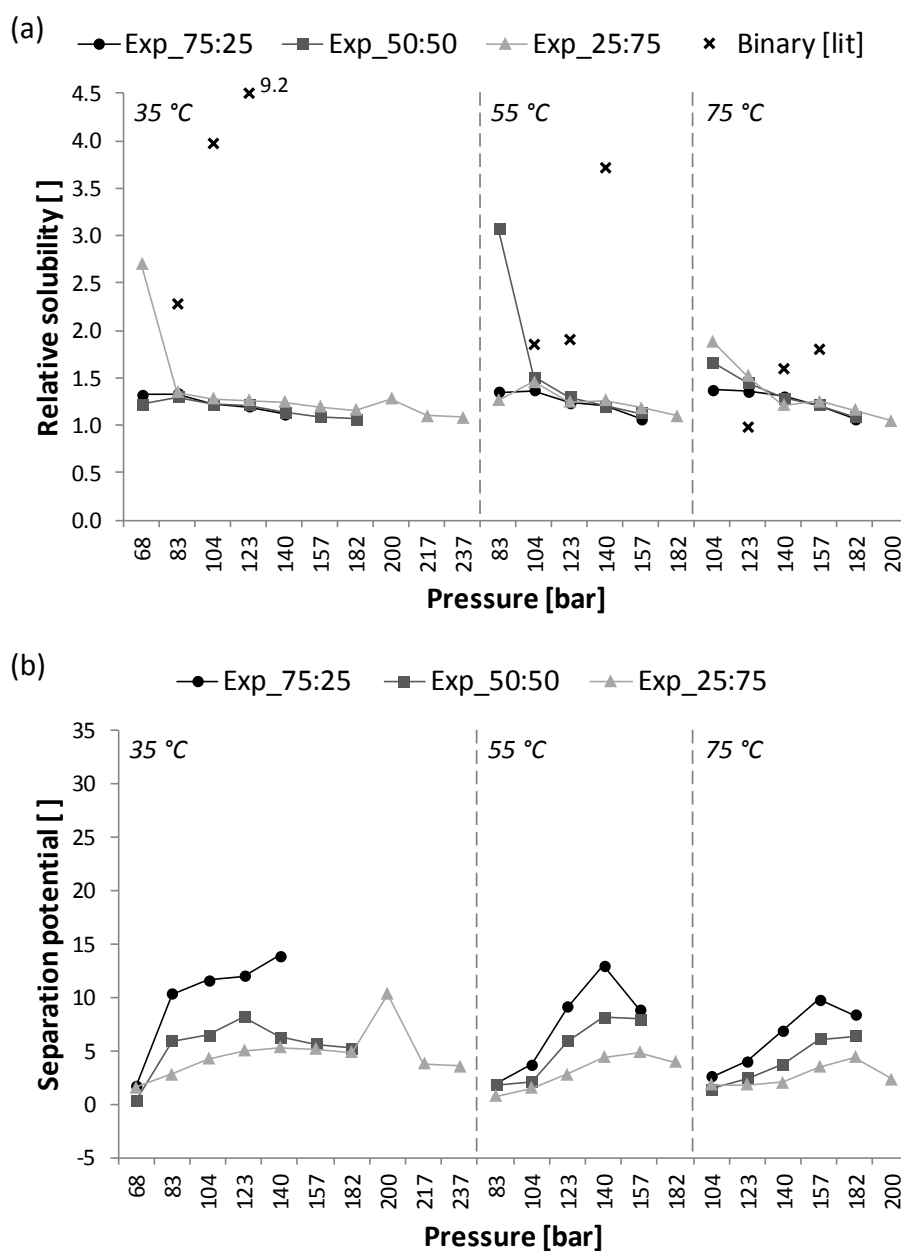


Figure 6-8. Experimental (a) relative solubility; and (b) separation potential for 75:25, 50:50 and 25:75 37DM10:C₁₀OH mass ratio mixtures of CO₂ + 37DM10 + C₁₀OH at 35, 55 and 75 °C. Binary relative solubility values were calculated from data by [31,36,37], tend to overestimate α_{ij} and the value of 9.2 should extend above the y-axis scale.

3.5.2 Model-predicted ternary mixture relative solubilities and separation potentials

The model-predicted VLE data were used to calculate predicted relative solubilities and separation potentials. In contrast to the $\text{CO}_2 + n\text{C}_{12} + 37\text{DM10}$ mixture [14], the qualitative dependence of α_{ij} and SP_{ij} on solute ratio, pressure and temperature varies amongst the four models, and no model matches the experimental trends in all three categories (Table 6-10).¹⁶ This is not surprising since the system in question is, in general, more difficult to model (Sections 3.3 and 3.4). Evaluating the averages, min-to-max ranges and qualitative sensitivities in Table 6-10, RK-ASPEN produced the best correlation of α_{ij} whilst RK-ASPEN and, surprisingly, PC-SAFT, performed similarly in correlating SP_{ij} . Crucially, SR-POLAR and PR-BM predict α_{ij} 's smaller than unity and, as a result, negative SP_{ij} 's.

Table 6-10: Experimental and model predicted α_{ij} and SP_{ij} values, and their qualitative sensitivity to $Z_{\text{C}_{10}\text{OH}}$, P and T , for $\text{CO}_2 + 37\text{DM10} + \text{C}_{10}\text{OH}$. To enable improved comparison, only 55 and 75 °C data were used to calculate min, avg. and max values, and model-predicted values were only considered in the range $0.25 < Z_{\text{C}_{10}\text{OH}} < 0.75$. For experimental α_{ij} values, the lowest-pressure data point at each temperature was ignored. Symbols: [+] positive correlation; [-] negative correlation; [0] no evident correlation; [<>] correlation too complex to warrant discussion here; [→] which then becomes; [/] different dependency at 55 °C, before dash, and 75 °C, after dash. Double symbols indicate a stronger correlation.

Property and source		Min	Avg.	Max	$Z_{\text{C}_{10}\text{OH}}$	P	T
α_{ij}	Experimental	1.1	1.2	1.5	0	-	0
	RK-ASPEN	1.0	1.4	2.1	++	--	-
	SR-POLAR	0.5	0.9	1.2	+ / ++	+	-
	PR-BM	0.5	0.8	1.2	++	++	+
	PC-SAFT	1.1	1.5	2.4	-	--	-
SP_{ij}	Experimental	0.7	4.6	13	--	++ → -	-
	RK-ASPEN	0.6	5.6	15	+ → -	++ → -	-
	SR-POLAR	-16	-0.4	9.2	++ → -	<>	--
	PR-BM	-15	-1.5	12	++ → -	<>	++
	PC-SAFT	0.3	3.8	12	--	++	+

3.6 Density inversion

An interesting density inversion, also referred to as a barotropic phenomenon, was observed at low temperature and high pressure in the 25:75 37DM10:C₁₀OH mass ratio mixture. Although not unheard of [38-41], density inversions are by no means common. At 35 °C and 200, 217 and 237 bar, the CO₂-rich

¹⁶ See also Figure 5-10 on p. 129.

phase was heavier and settled to the bottom of the equilibrium cell whilst the top, light phase was solute-rich. No density inversions were encountered for the other mass ratio mixtures or at 55 or 75 °C, nor were any observed for the $\text{CO}_2 + n\text{C}_{12} + 37\text{DM10}$ mixture [14]. The inversion zone was unstable and therefore difficult to pinpoint (Fig. 6-9) but occurred in the vicinity of 187.3 to 187.7 bar at 35 °C.

Despite the change in relative densities, surface tension effects appeared to be largely unaffected because, regardless the relative position of the hydrocarbon-rich phase, stirring caused lipid-like globules to detach from it and enter the CO_2 -rich phase (Fig. 6-10). Density inversions will have significant negative impact on SFE column hydrodynamics and are therefore important from an operating and control point of view.



Figure 6-9. The 25:75 37DM10: C_{10}OH mixture of $\text{CO}_2 + 37\text{DM10} + \text{C}_{10}\text{OH}$ at 35.0 °C and 187.7 bar. Even though phase settling, in the absence of any stirring, had been on-going for more than 60 min, the system remained dynamic with lipid-like globules in continuous motion.

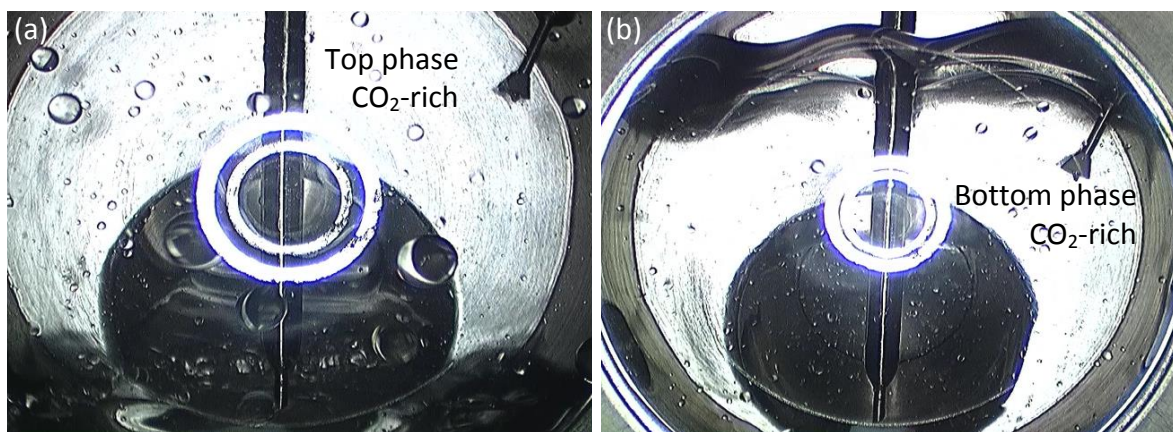


Figure 6-10. The 25:75 37DM10: C_{10}OH mixture of $\text{CO}_2 + 37\text{DM10} + \text{C}_{10}\text{OH}$ at 35.0 °C: (a) $P \approx 181$ bar, the solute-rich phase is located in the cell bottom and lipid-like globules are tossed upward as a result of stirring; and (b) $P \approx 191$ bar, the solute-rich phase is located in the top of the cell and similar globules are flung downward as a result of stirring.

In Fig. 6-11, nine screen shots indicate a pressure reduction sequence passing through the density inversion zone. These images cover a period of approximately eight minutes during which pressure was reduced from 191.6 to 187.2 bar in the presence of magnetic stirring. Initially, the hydrocarbon-rich phase is less-dense (Fig. 6-11 a and b) but, as pressure decreases, it migrates toward the bottom via the right-hand side of the equilibrium cell (Fig. 6-11 d - h).

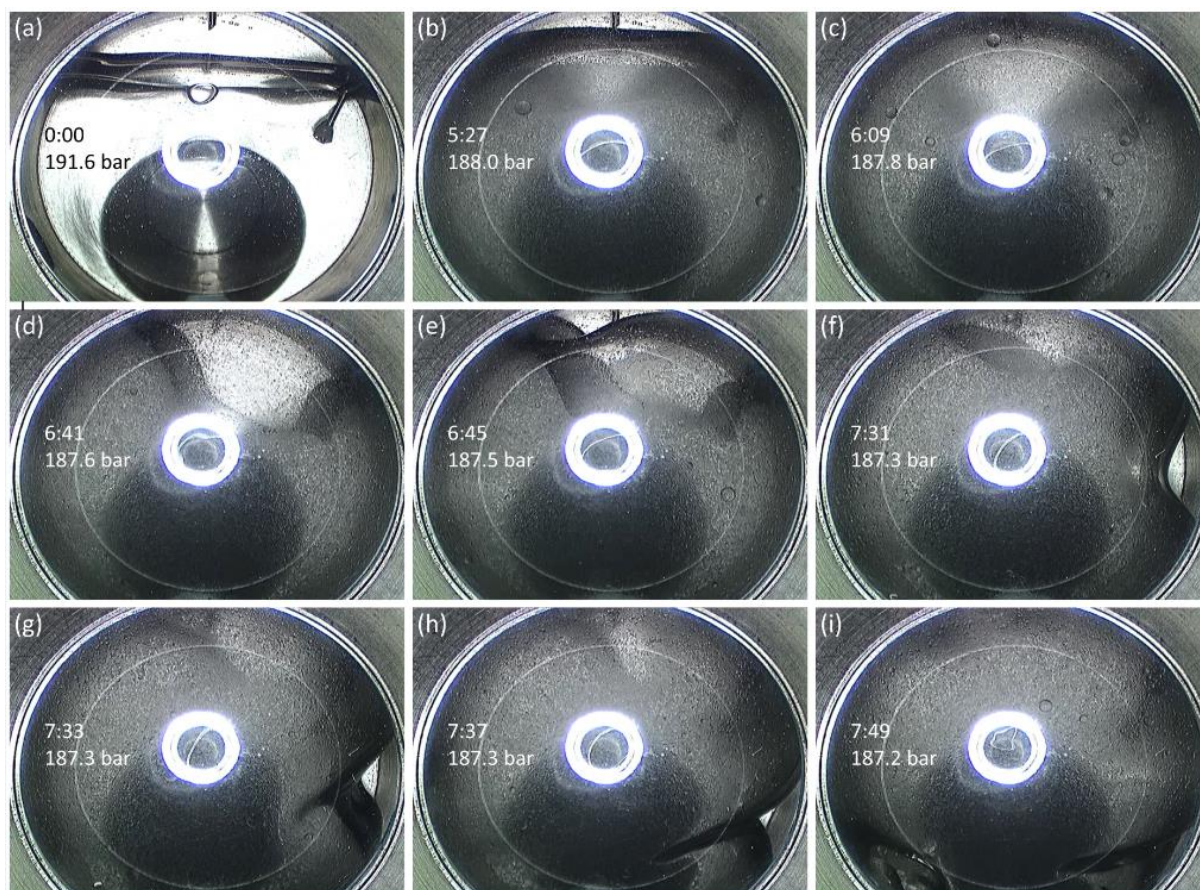


Figure 6-11. A pressure reduction sequence at 35.0 °C illustrating the density inversion in a 25:75 37DM10:C₁₀OH mixture of CO₂ + 37DM10 + C₁₀OH. Images are annotated with approximate time and pressure stamps. The solute-rich phase starts out at the top and, throughout the sequence, moves down the right-hand side to the cell bottom.

4. CONCLUSIONS

New high pressure equilibrium phase composition data were measured for CO₂ + 37DM10 + C₁₀OH at 35, 55 and 75 °C and pressures between 68 and 237 bar. Ternary mixtures were synthesised targeting three different solvent-free 37DM10:C₁₀OH mass ratio mixtures: 75:25, 50:50 and 25:75.

The phase behaviour of this ternary mixture differs significantly from CO₂ + *n*C₁₂ + 37DM10 in that no s-shaped liquid curvature or co-solubility pinch was observed, and none of the isobaric phase diagrams indicate the simultaneous presence of two distinct coexisting two-phase regions.

CO₂ can separate a mixture of 37DM10 + C₁₀OH across the entire solute ratio range, which is not the case for nC₁₂ + 37DM10 [14], and 35 °C appears to be the optimum fractionation temperature. In the mid and low-37DM10 range (50:50 and 25:75), however, CO₂ fractionation is less effective and α_{ij} 's and SP_{ij} 's from this work are considerably lower than was reported by Fourie et al. [14]. In contrast to CO₂ + nC₁₂ + 37DM10, experimental α_{ij} values are virtually independent of solute-solute ratio and SP_{ij} , being governed by Y_i , is positively correlated with bulk content of the more soluble species. A qualitative comparison of the model-predicted α_{ij} 's and SP_{ij} 's highlights inter-model variance, and no model was able to match the $Z_{C_{10OH}}$, P and T dependency of the actual system.

In general, the ternary mixture in question was more difficult to model than CO₂ + nC₁₂ + 37DM10 [14] and, essentially, all four models failed at 35 °C. RK-ASPEN and SR-POLAR provided the best correlation of equilibrium pressures with combined-overall %AAD's, exclusive of 35 °C data, of 4.0 %. Throughout, RK-ASPEN was superior at correlating experimental vapour curves. At 55 and 75 °C and low pressures, the cubic EOS achieved comparable liquid phase correlations. Medium and high pressure liquid phase predictions via RK-ASPEN were reasonable at 55 and 75 °C whilst SR-POLAR and PR-BM performed well at 55 and 75 °C respectively. PC-SAFT under-estimates the vapour phase solute loading which corresponds with former observations [14].

A density inversion was detected for the 25:75 37DM10:C₁₀OH mixture at 35 °C and roughly 187.5 bar. At all higher pressures, the CO-rich phase was denser than the solute-rich phase. Surface tension effects appeared unaffected and in this sense the CO₂-rich phase remained vapour-like whilst the solute-rich phase remained liquid-like.

ACKNOWLEDGEMENTS

This work is based on the research supported in part by the National Research Foundation of South Africa (Grant specific unique reference number (UID) 83966), Department of Trade and Industry (DTI) of South Africa through the Technology and Human Resources for Industry Programme (THRIP), and Sasol Technology (Pty) Ltd. The financial assistance of the National Research Foundation (DAAD-NRF) and the Skye Foundation Trust is also acknowledged. The authors acknowledge that opinions, findings, and conclusions or recommendations expressed in any publication generated by the supported research are those of the authors, and that the sponsors accept no liability whatsoever in this regard. Aspen Plus® is a registered trademark of Aspen Technology Inc.

REFERENCES

1. F. Sahena, I.S.M. Zaidul, S. Jinap, A.A. Karim, K.A. Abbas, N.A.N. Norulaini, A.K.M. Omar, Application of supercritical CO₂ in lipid extraction – A review, *J. Food Eng.* 95 (2009) 240-253.
2. K.M. Sharif, M.M. Rahman, J. Azmir, A. Mohamed, M.H.A. Jahurul, F. Sahena, I.S.M. Zaidul, Experimental design of supercritical fluid extraction – A review, *Journal of Food Engineering* 124 (2014) 105-116.
3. B.G. Silva, A.M.F. Fileti, M.A. Foglio, A.L.T.G. Ruiz, P.T.V. Rosa, Supercritical carbon dioxide extraction of compounds from *Schinus terebinthifolius* Raddi fruits: Effects of operating conditions on global yield, volatile compounds, and antiproliferative activity against human tumor cell lines, *J. Supercrit. Fluids* 130 (2017) 10-16.
4. P. Gurikov, I. Smirnova, Amorphization of drugs by adsorptive precipitation from supercritical solutions: A review, *J. Supercrit. Fluids* (2017), <http://dx.doi.org/10.1016/j.supflu.2017.03.005>.
5. O. Nuchuchua, M.R. Nejadnik, S.C. Goulooze, N.J. Lješević, H.A. Every, W. Jiskoot, Characterization of drug delivery particles produced by supercritical carbon dioxide technologies, *J. Supercritical Fluids* 128 (2017) 244-262.
6. R. Campardelli, L. Baldino, E. Reverchon, Supercritical fluids applications in nanomedicine, *J. Supercrit. Fluids* 101 (2015) 193-214.
7. S. Bektesevic, A.M. Kleman, A.E. Marteel-Parrish, M.A. Abraham, Hydroformylation in supercritical carbon dioxide: Catalysis and benign solvents, *J. Supercrit. Fluids* 38 (2006) 232-241.
8. K. Qin, K. Wang, R. Luo, Y. Li, T. Wang, Interfacial tension and wetting properties of 1-ethyl-3-methylimidazolium tetrafluoroborate in carbon dioxide, from atmospheric pressure to supercritical state, *J. Supercrit. Fluids* 116 (2016) 83-89.
9. E. Kiran, Supercritical fluids and polymers – The year in review – 2014, *J. Supercrit. Fluids* 110 (2016) 126-153.
10. M. Perrut, Supercritical Fluid Applications: Industrial Developments and Economic Issues, *Ind. Eng. Chem. Res.* 39 (2000) 4531-4535.
11. A.S. Teja, C.A. Eckert, Commentary on Supercritical Fluids: Research and Applications, *Ind. Eng. Chem. Res.* 39 (2000) 4442-4444.
12. R. Fingerhut, W.-L. Chen, A. Schedemann, W. Cordes, J. Rarey, C.-M. Hsieh, J. Vrabec, S.-T. Lin, Comprehensive Assessment of COSMO-SAC Models for Predictions of Fluid-Phase Equilibria, *Ind. Eng. Chem. Res.* (2017), <http://dx.doi.org/10.1021/acs.iecr.7b01360>.
13. E. Hendriks, G.M. Kontogeorgis, R. Dohrn, J.-C. De Hemptinne, I.G. Economou, L. Fele-Žilnik, V. Vesovic, Industrial Requirements for Thermodynamics and Transport Properties, *Ind. Eng. Chem. Res.* 49 (2010) 11131-11141.

14. F.C.v.N. Fourie, C.E. Schwarz, J.H. Knoetze, CO₂ + *n*-dodecane + 3,7-dimethyl-1-octanol: High pressure experimental phase equilibria data and thermodynamic modelling, *J. Supercrit. Fluids* 130 (2017) 105-117.
15. C.E. Schwarz, I. Nieuwoudt, J.H. Knoetze, Solubility measurements of high molecular mass *n*-alkanes, *n*-alcohols and alcohol ethoxylates in supercritical propane, *Fluid Phase Equilib.* 247 (2006) 169-174.
16. C.E. Schwarz, A.J. de Villiers, C.B. McClune, G.J.K. Bonthuys, A.J. Burger, J.H. Knoetze, High pressure phase equilibrium measurements of long chain alcohols in supercritical ethane, *J. of Supercrit. Fluids* 55 (2010) 554-565.
17. F.C.v.N. Fourie, C.E. Schwarz, J.H. Knoetze, Phase equilibria of alcohols in supercritical fluids Part I. The effect of the position of the hydroxyl group for linear C8 alcohols in supercritical carbon dioxide, *J. Supercrit. Fluids* 47 (2008) 161-167.
18. G.J.K. Bonthuys, C.E. Schwarz, A.J. Burger, J.H. Knoetze, Separation of alkanes and alcohols with supercritical fluids. Part I: Phase equilibria and viability study, *J. Supercrit. Fluids* 57 (2011) 101-111.
19. M. Zamudio, C.E. Schwarz, J.H. Knoetze, Experimental measurement and modelling with Aspen Plus® of the phase behaviour of supercritical CO₂ + (*n*-dodecane + 1-decanol + 3,7-dimethyl-1-octanol), *J. Supercrit. Fluids* 84 (2013) 132-145.
20. G. Soave, Equilibrium constants from a modified Redlich-Kwong equation of state, *Chem. Eng. Sci.* 27 (1972) 1197-1203.
21. P.M. Mathias, A Versatile Phase Equilibrium Equation of State, *Ind. Eng. Chem. Process Des. Dev.* 22 (1983) 385-391.
22. J.F. Boston, P.M. Mathias, Phase equilibria in a third-generation process simulator, 2nd International Conference on Phase Equilibria and Fluid Properties in the Chemical Process Industries, West Berlin, 1980.
23. J. Schwartzenuber, H. Renon, Extension of UNIFAC to High Pressures and Temperatures by the Use of a Cubic Equation of State, *Ind. Eng. Chem. Res.* 28 (1989) 1049-1955.
24. D.Y. Peng, D.B. Robinson, A New Two-Constant Equation of State, *Ind. Eng. Chem. Fund.* 15 (1976) 59-64.
25. P.M. Mathias, H.C. Klotz, J.M. Prausnitz, Equation-of-State mixing rules for multicomponent mixtures: the problem of invariance, *Fluid Phase Equilib.* 67 (1991) 31-44.
26. J. Gross, G. Sadowski, Perturbed-Chain SAFT: An Equation of State Based on a Perturbation Theory for Chain Molecules, *Ind. Eng. Chem. Res.* 40 (2001) 1244-1260.
27. J. Gross, G. Sadowski, Application of the Perturbed-Chain SAFT Equation of State to Associating Systems, *Ind. Eng. Chem. Res.* 41 (2002) 5510-5515.
28. F.C.v.N. Fourie, C.E. Schwarz, J.H. Knoetze, Analytic High-Pressure Phase Equilibria Part II: Gas Chromatography and Sampling Method Development, *Chem. Eng. Technol.* 39 (2016) 1475-1482.

29. F.C.v.N. Fourie, C.E. Schwarz, J.H. Knoetze, Analytic Setup for Multicomponent High-Pressure Phase Equilibria via Dual Online Gas Chromatography, *Chem. Eng. Technol.* 38 (2015) 1165-1172.
30. Aspen Plus® V8.8 (34.0.0.110)
31. M. Zamudio, C.E. Schwarz, J.H. Knoetze, Phase equilibria of branched isomers of C₁₀-alcohols and C₁₀-alkanes in supercritical carbon dioxide, *J. Supercrit. Fluids* 59 (2011) 14-26.
32. M. Zamudio, The Separation of Detergent Range Alkanes and Alcohol Isomers with Supercritical Carbon Dioxide, PhD Dissertation, Stellenbosch University, South Africa, 2014.
33. X. Liang, K. Thomsen, W. Yan, G.M. Kontogeorgis, Prediction of the vapor–liquid equilibria and speed of sound in binary systems of 1-alkanols and *n*-alkanes with the simplified PC-SAFT equation of state, *Fluid Phase Equilib.* 360 (2013) 222-232.
34. A. Grenner, G.M. Kontogeorgis, N. von Solms, M.L. Michelsen, Modeling phase equilibria of alkanols with the simplified PC-SAFT equation of state and generalized pure compound parameters, *Fluid Phase Equilib.* 258 (2007) 83-94.
35. M. Umer, K. Albers, G. Sadowski, K. Leonhard, PC-SAFT parameters from ab initio calculations, *Fluid Phase Equilib.* 362 (2014) 41-50.
36. C.J. Chang, K.-L. Chiu, C.-Y. Day, A new apparatus for the determination of P–x–y diagrams and Henry’s constants in high pressure alcohols with critical carbon dioxide, *J. Supercrit. Fluids* 12 (1998) 223-237.
37. W.-L. Weng, J.-T. Chen, M.-J. Lee, High-Pressure Vapor-Liquid Equilibria for Mixtures Containing a Supercritical Fluid, *Ind. Eng. Chem. Res.* 33 (1994) 1955-1961.
38. H. Quinteros-Lama, G. Pisoni, J.M. Garrido, A. Mejía, H. Segura, Barotropic phenomena in binary mixtures, *Fluid Phase Equilib.* 394 (2015) 175-185.
39. R. Smith, H. Inomata, C. Peters, Introduction to Supercritical Fluids: A Spreadsheet based Approach, Volume 4, first ed., Elsevier, Amsterdam, 2013.
40. G.M. Schneider, A.L. Scheidgen, D. Klante, Complex Phase Equilibrium Phenomena in Fluid Mixtures up to 2 GPa – Cosolvency, Holes, Windows, Closed Loops, High-Pressure Immiscibility, Barotropy, and Related Effects, *Ind. Eng. Chem. Res.* 39 (2000) 4476-4480.
41. M.A. McHugh, V.J. Krukoni, *Supercritical Fluid Extraction: Principles and Practice*, second ed., Butterworth-Heinemann, Waltham USA, 1994.

Chapter 7: MANUSCRIPT 5

**CO₂ + *n*-dodecane + 1-decanol: High pressure experimental
phase equilibria data and thermodynamic modelling**

Frederick C. v. N. Fourie^{a,1}, Cara E. Schwarz^a, Johannes H. Knoetze^{a,*}

^aStellenbosch University, Department of Process Engineering, Private Bag X1, Matieland, 7602, South Africa,

Tel: +27 21 808 4204, Fax: +27 21 808 2059, E-mail: jhk@sun.ac.za

¹Present address: Sasol, 1 Klasie Havenga, Sasolburg, 1947, South Africa, Tel: +27 16 960 2611

Manuscript in preparation.

Declaration by the candidate

With regard to Chapter 7, the nature and scope of my contribution were as follows:

<u>Nature of contribution</u>	<u>Extent of contribution (%)</u>
I am the primary author of this publication. I am responsible for the experimental work, thermodynamic modelling, and interpreting and communicating the actual and model-predicted mixture behaviour.	90 %

The following co-authors contributed to Chapter 7:

<u>Name</u>	<u>E-mail address</u>	<u>Nature of contribution</u>	<u>Extent of Contribution (%)</u>
Johannes H. Knoetze	jhk@sun.ac.za	Supervisor to the student, F.C.v.N Fourie	5 %
Cara E. Schwarz	cschwarz@sun.ac.za	Co-supervisor to the student, F.C.v.N. Fourie	5 %

Signature of candidate : Declaration with signature in possession of candidate and supervisor

Date : 10 November 2017

Declaration by co-authors

The undersigned hereby confirm that:

1. The declaration above accurately reflects the nature and extent of the contributions of the candidate and the co-authors to Chapter 7.
2. No other authors contributed to Chapter 7 besides those specified above.
3. Potential conflicts of interest have been revealed to all interested parties and that the necessary arrangements have been made to use the material in Chapter 7 of this dissertation.

<u>Signature</u>	<u>Institutional affiliation</u>	<u>Date</u>
Declaration with signature in possession of candidate and supervisor	Supervisor to the student, F.C.v.N Fourie	10 November 2017
Declaration with signature in possession of candidate and supervisor	Co-supervisor to the student, F.C.v.N. Fourie	10 November 2017

ABSTRACT

Ternary VLE data produced on a static analytic apparatus with dual sampling and online chromatography are presented for CO₂ + *n*-dodecane (*n*C₁₂) + 1-decanol (C₁₀OH) at 35, 55 and 75 °C and pressures between 68 and 200 bar. Gibbs diagrams indicate enhanced mixture solubility throughout the measured *n*C₁₂:C₁₀OH ratio range and a co-solvency pinch or s-shaped liquid curvature in the high-*n*C₁₂ region. Relative solubility, a selectivity indicator, increases with bulk C₁₀OH content and the average of 2.25 highlights solvent efficacy. Hydrocarbon separation is possible across the measured *n*C₁₂:C₁₀OH ratio range. RK-ASPEN, SR-POLAR, PR-BM and PC-SAFT correlations failed at 35 °C. At 55 and 75 °C, RK-ASPEN produced the best equilibrium pressure estimates with marginal superiority over SR-POLAR and PR-BM. SR-POLAR was best-able to correlate the acute co-solvency pinch, the three cubic EOS performed similarly in correlating high pressure liquid curvature and throughout RK-ASPEN vapour correlations were more accurate. Density inversions or barotropic phenomena were observed.

Keywords: Barotropy, Co-solvency, Cubic EOS, PC-SAFT, Supercritical, Ternary VLE

Highlights

- New high pressure VLE data for CO₂ + *n*-dodecane + 1-decanol
- Co-solvency in the high-*n*C₁₂ region presents as a pinched two-phase band
- CO₂ is effective at separating the alkane and alcohol at all measured ratios
- Fractionation sharpness increases with bulk solvent-free 1-decanol content
- RK-ASPEN produced a %AAD_p of 3.1 % and SR-POLAR could mimic the high-*n*C₁₂ pinch

NOMENCLATURE

2E1H	:	2-Ethyl-1-hexanol
37DM1O	:	3,7-Dimethyl-1-octanol
AAD	:	Average absolute deviation
BIP	:	Binary interaction parameter
C ₁₀ OH	:	1-Decanol
CSSRL	:	Constant solute-solute ration lines
<i>k</i> _{ij}	:	Binary interaction parameter
<i>l</i> _{ij}	:	Binary interaction parameter
<i>m</i>	:	Segment number in PC-SAFT

M	:	Number of data points
nC_{12}	:	n -Dodecane
$\rho_{1/2}$:	SR-POLAR polar parameter
P	:	Pressure
PCS	:	PC-SAFT
PRB	:	PR-BM
p^{sat}	:	Saturated vapour pressure
RKA	:	RK-ASPEN
ROLSI™	:	Rapid On-Line Sampler Injector
SFE	:	Supercritical fluid extraction
Solute	:	nC_{12} or 37DM10 or $C_{10}OH$
Solvent	:	CO_2
SP_{ij}	:	Separation potential between species i and j
SRP	:	SR-POLAR
STDEV	:	Species-specific standard deviation in mass fraction
T	:	Temperature
TAD	:	Totalised absolute deviation
TSP	:	Total solubility pressure
u	:	Absolute uncertainty
X_i	:	Liquid phase mass fraction of species i
Y_i	:	Vapour phase mass fraction of species i
Z_i	:	Bulk solvent-free mass fraction of solute species i

Greek letters

α_{ij}	:	Relative solubility between species i and j
η_i	:	RK-ASPEN polar parameter
ε/k	:	Dispersion energy parameter in PC-SAFT
ε^{AB}/k	:	Association energy parameter in PC-SAFT
κ^{AB}	:	Effective association volume parameter in PC-SAFT
σ	:	Segment diameter in PC-SAFT
ρ^{sat}	:	Saturated liquid density

Superscripts and subscripts

<i>exp</i>	:	Experimental
<i>i,j</i>	:	Component identifications
<i>sat</i>	:	Saturated

1. INTRODUCTION

This paper is the third in a series [1,2] which investigates the high pressure CO₂ + solute A + solute B phase behaviour of detergent range alcohols and alkanes, and ideally these publications should be seen as a collective. The series focuses on the solutes *n*C₁₂, 37DM1O and C₁₀OH, and supercritical CO₂ as solvent but is positioned within an overarching project that also considers supercritical ethane and propane as solvents. The larger project aims to evaluate supercritical fluid extraction (SFE) as a means of purifying detergent range alcohol product streams. To this end, bubble and dew point measurements, high and low pressure equilibrium phase compositions measurements, pilot plant runs and column hydrodynamic studies will all contribute toward enabling comprehensive process modelling.

This contribution has three key objectives. Firstly, measure new high pressure equilibrium phase composition data for CO₂ + *n*C₁₂ + C₁₀OH. Data were measured at 35, 55 and 75 °C and pressures ranging from 68 to 200 bar. Three different *n*C₁₂:C₁₀OH mass ratios were synthesised – 75:25, 50:50 and 25:75 calculated on a bulk solvent-free basis. In addition to the three standard [1] solute ratios, two non-standard *n*C₁₂:C₁₀OH mixtures were synthesised. These were 21.5:78.5 and 41.5:58.5, also calculated on a bulk solvent-free mass basis. The non-standard solute mixtures enabled measurements in regions where the mixture phase transition pressure was close to, but below, a target experimental pressure. In all subsequent references to solute ratios the more soluble species, *n*C₁₂, is mentioned first.

Secondly, quantify and discuss the technical viability of separating *n*C₁₂ and C₁₀OH using supercritical fluid extraction (SFE) with CO₂. This also involves a comparison between the three solute mixtures that constitute the larger project, i.e., *n*C₁₂ + 37DM1O [1], 37DM1O + C₁₀OH [2] and *n*C₁₂ + C₁₀OH.

Lastly, model the new phase behaviour data using three cubic equations of state [EOS], RK-ASPEN [3-5], SR-POLAR [3-6] and PR-BM [3,5,7,8], together with PC-SAFT [9,10], and quantify model performance. Model performance is also compared to results for the *n*C₁₂ + 37DM1O [1] and 37DM1O + C₁₀OH [2] mixtures. Comprehensive process modelling being the ultimate aim of the overarching project, the authors limited themselves to models available within Aspen Plus®, a popular and commercially available process simulation package. Fourie et al. [1] provided justification for the specific model choices.

2. MATERIALS AND METHODS

2.1 *Experimental method*

A static analytic variable-volume (75 - 125 ml) setup was used to measure ternary mixture equilibrium phase compositions. A forced convection oven and liquid jacket, with air and water as the respective heat transfer media, was used to heat the equilibrium cell. Pressure was measured with an ONEhalf20 melt pressure transmitter of which the diaphragm is flush with the cell inner wall, and temperature was monitored at five locations spread throughout the equilibrium cell block. The cell content was magnetically stirred during the approach to equilibrium, and observation of the cell interior is possible using a high definition medical endoscope (Stryker Endoscopy). The cell is equipped with two vertically-adjustable ROLSI™ samplers (Armines, France) that feed to two parallel online gas chromatograph analysis pathways (Agilent 7890A). The upper operating limits of the apparatus are 150 °C at 300 bar. The authors provide details on the experimental setup and system validation [11], and discuss the analysis method and present visuals illustrating the challenges associated with high pressure sampling [12] in previous publications.

One sampling and analysis pathway was not functional for a portion of this study. Four of the thirty-two reported vapour and liquid combinations were measured using a single sampler and the adapted experimental procedure as described by Fourie et al. [1].¹⁷ These data points are labelled in Section 3.1.

The total uncertainties in pressure and temperature measurement for data from this study are 0.35 bar and ± 0.1 °C [11]. The estimated maximum absolute uncertainties in phase composition, $u(X_i)$ and $u(Y_i)$, are phase, species and composition dependent, and are listed in Table 7-1. The solute species display similar qualitative sensitivity to the main uncertainty contributors which dampens the impact thereof on relative solute distributions (Section 3.5.1). The ability to produce repeatable and reproducible data with the experimental setup has been discussed previously [1].

The materials listed in Table 7-2 were used without further purification.

¹⁷ See also Section 2.2 on p. 106.

Table 7-1: Estimated maximum absolute uncertainty in phase composition, expressed as mass %, for data reported in this work.

Liquid phase				Vapour phase			
Solutes		Solvent		Solutes		Solvent	
Mass % range	$u(X_i)$	Mass % range	$u(X_i)$	Mass % range	$u(Y_i)$	Mass % range	$u(Y_i)$
0 - 15 %	0.25 %	0 - 30 %	1.05 %	0 - 2 %	0.10 %	100 - 96 %	0.15 %
15 - 25 %	0.55 %	30 - 62 %	1.20 %	2 - 4 %	0.20 %	96 - 92 %	0.35 %
25 - 56 %	0.90 %			4 - 7 %	0.25 %	92 - 87 %	0.45 %
				7 - 10.5 %	0.50 %	87 - 81 %	0.65 %
				10.5 - 19 %	0.75 %	81 - 75 %	1.10 %

Table 7-2: Materials used

Component	CAS	Purity	Supplier	Cat. No.
nC_{12}	112-40-3	99 + %	Sigma	29,787-9
$C_{10}OH$	112-30-1	99 %	Sigma	150584-3KG
		≥ 98 %	Sigma	W23,650-O-K
2E1H	104-76-7	≥ 99.0 %	Fluka	04050-250ML
CO_2	124-38-9	99.995 %	Air Products	K243C

2.2 Modelling

The RK-ASPEN, SR-POLAR, PR-BM and PC-SAFT thermodynamic models were evaluated for their ability to correlate the new $CO_2 + nC_{12} + C_{10}OH$ data. Fourie et al. [1] discussed the reasoning behind the model choices and provided concise model-specific theoretical background. Please consult the references in Section 1 for details on the development of these models. Holistic process modelling being the aim of the overarching project, the modelling work presented in this contribution was performed using a well-known commercial process simulator, Aspen Plus[®]. Model assessment was based on two measures: the ability to predict equilibrium i) pressures; and ii) compositions for the ternary mixture vapour and liquid phases. The first metric used, as input, ternary mixture temperature and composition data from this study (Table 7-3) to provide, as output, phase-specific pressures, and results are reported as %AAD_p where

$$\%AAD_p = \frac{1}{M} \sum_{n=1}^M \left| \frac{P_{predict} - P_{experimental}}{P_{experimental}} \right| \times 100 \%$$

Equation 7-1

and M represents the number of data points. The second metric used, as input, ternary mixture temperature and pressure data from this study (Table 7-3) to provide, as output, phase-specific compositions. Presenting these compositions on ternary Gibbs diagrams enables a fast qualitative assessment of the ability of a model to mimic actual mixture curvature.

PC-SAFT pure component parameters for CO_2 , $n\text{C}_{12}$ and C_{10}OH were obtained from literature. The authors have previously regressed corresponding pure component parameters for the RK-ASPEN and SR-POLAR models, as well as $\text{CO}_2 + n\text{C}_{12}$ and $\text{CO}_2 + \text{C}_{10}\text{OH}$ binary interaction parameters (BIP) specific to each of the four models. All pure component and binary interaction parameters are referenced appropriately in Section 3.2. New solute-solute BIP's were calculated using the ternary mixture experimental data produced in this work.

3. RESULTS AND DISCUSSION

3.1 Experimental data

New experimental VLE data for the mixture $\text{CO}_2 + n\text{C}_{12} + \text{C}_{10}\text{OH}$ at 35, 55 and 75 °C are presented in Table 7-3. Estimates of the maximum absolute uncertainty in phase composition are listed in Table 7-1. The standard deviation in species-specific mass fractions (STDEV) associated with two liquid phase compositions were larger than the maximum allowable of 0.009 previously defined by Fourie et al. [11]. These are labelled in Table 7-3 and shaded grey in Figs. 7-1 a, 7-3 and 7-6 a.

Table 7-3: Experimental data for $\text{CO}_2 + n\text{C}_{12} + \text{C}_{10}\text{OH}$ at 35.0, 55.0 and 75.0 °C, and pressures between 68.1 and 200.0 bar. An average of 5.0 and a minimum of 4 samples were analysed for each of the vapour and liquid phase data points. The average standard deviation in composition, obtained under repeatability conditions, was 0.0019 in mass fraction or 0.19 mass %.

Temperature [°C]	Pressure [bar]	Liquid			Vapour		
		CO_2	$n\text{C}_{12}$	C_{10}OH	CO_2	$n\text{C}_{12}$	C_{10}OH
35.0	68.1 ^a	0.451	0.409	0.140	0.988	0.009	0.003
	68.1	0.419	0.291	0.290	0.999	0.001	0.000
	68.1	0.323 ^b	0.173	0.503 ^c	0.998	0.001	0.001
83.1	53.3	0.533	0.189	0.278	0.810	0.109	0.081
	83.1	0.409	0.120	0.472	0.942	0.029	0.029
104.0	104.0	0.452	0.108	0.441	0.898	0.044	0.058
123.1	123.1	0.456	0.102	0.442	0.863	0.054	0.084

Temperature [°C]	Pressure [bar]	Liquid			Vapour		
		CO ₂	<i>n</i> C ₁₂	C ₁₀ OH	CO ₂	<i>n</i> C ₁₂	C ₁₀ OH
35.0	140.0	0.485	0.097	0.418	0.851	0.053	0.096
	157.1	0.518	0.092	0.390	0.816	0.059	0.125
	182.1	0.592	0.082	0.325	0.759	0.065	0.177
	200.0 ^d	0.598	0.070	0.331	0.759	0.055	0.185
55.0	83.0 ^a	0.355	0.482	0.164	0.993	0.006	0.002
	83.1	0.318	0.342	0.341	0.994	0.004	0.002
	83.1	0.263	0.185	0.552	0.997	0.002	0.002
	104.2	0.555	0.329	0.116	0.978	0.018	0.004
	104.0	0.489	0.253	0.257	0.980	0.015	0.005
	104.0	0.372	0.155	0.473	0.984	0.008	0.008
	123.0 ^e	0.565	0.162	0.273	0.858	0.074	0.068
	123.1	0.450	0.123	0.427	0.925	0.035	0.040
	140.1	0.510	0.106	0.383	0.862	0.054	0.085
	157.1	0.585	0.086	0.329	0.804	0.059	0.137
75.0	104.1 ^a	0.349	0.485	0.167	0.986	0.011	0.003
	104.1	0.319	0.344	0.337	0.986	0.009	0.005
	104.0	0.294 ^f	0.179	0.527 ^g	0.993	0.004	0.003
	123.1 ^a	0.466	0.400	0.135	0.979	0.017	0.004
	123.0	0.416	0.292	0.292	0.977	0.016	0.007
	123.1	0.361	0.162	0.477	0.984	0.008	0.008
	140.0	0.591	0.301	0.108	0.936	0.049	0.015
	140.0	0.526	0.230	0.244	0.943	0.036	0.021
	140.0	0.412	0.140	0.448	0.964	0.017	0.019
	157.0	0.487	0.118	0.396	0.920	0.033	0.047
	182.1 ^d	0.613	0.074	0.313	0.822	0.047	0.131

^a Liquid and vapour phase compositions measured with one sampler
Species-specific standard deviation in mass fraction for 5 samples: ^b 0.015; ^c 0.013; ^f 0.016; ^g 0.014
Bulk solvent-free *n*C₁₂:C₁₀OH mass ratio of: ^d 21.5:78.5; ^e 41.5:58.5

3.2 Modelling

Initial modelling used solvent + solute BIP's from Fourie et al. [1,2] and new ternary VLE data from this work, at 35, 55 and 75 °C, to regress $nC_{12} + C_{10}OH$ BIP's. As was the case for $CO_2 + 37DM10 + C_{10}OH$ [2], all four models essentially failed at 35 °C with the two lowest pressures, 68 and 83 bar, being the exceptions (Fig. 7-1).¹⁸ At 35 °C and pressures between 104 and 200 bar, liquid phase pressure predictions were poor whilst phase composition and vapour phase pressure predictions failed completely. The modified modelling approach, upon which the remainder of this contribution is based, excluded ternary VLE data at 35 °C from the solute-solute BIP regressions (Tables 7-7 and 7-8) and model assessments (Sections 3.3, 3.4 and 3.5.2).

3.2.1 RK-ASPEN

The RK-ASPEN pure component parameters used in this study are listed in Table 7-4. Similarly to $nC_{12} + 37DM10$ [1] and $37DM10 + C_{10}OH$ [2], the $nC_{12} + C_{10}OH$ binary interaction was characterised using temperature independent $k_{a,ij}^{(0)}$ and $k_{b,ij}^{(0)}$ parameters. The BIP values and the regression %AAD's in pressure, temperature, and vapour and liquid phase solute fractions are listed in Tables 7-7 and 7-8 respectively. Although the inclusion of temperature dependency in $k_{a,ij}$ led to a 0.2 % reduction in %AAD_p from 3.1 to 2.9 % (see Table 7-9), it had negligible impact on phase behaviour predictions (Section 3.4) and, as such, the added constraint of a $k_{a,ij}^{(1)}$ parameter cannot be justified.

Table 7-4: RK-ASPEN pure component polar parameters used in this work

Component	η_i []	%AAD P^{sat} [%]	T-range [°C]	Reference
CO ₂	0.0481	0.03	-23.15 to 27.85	[1]
nC_{12}	0.0087	0.05	11.85 - 126.85	[1]
C ₁₀ OH	-0.4165	0.05	11.85 - 144.85	[2]

¹⁸ See also Section 3.2 on p. 145.

3.2.2 SR-POLAR

The SR-POLAR pure component parameters used in this study are listed in Table 7-5. The solute-solute interaction was best captured using temperature independent $k_{\alpha,ij}^{(0)}$ and $l_{ij}^{(0)}$ parameters (Tables 7-7 and 7-8) which is interesting because in the $\text{CO}_2 + n\text{C}_{12} + 37\text{DM10}$ and $\text{CO}_2 + 37\text{DM10} + \text{C}_{10}\text{OH}$ systems the inclusion of l_{ij} parameters led to degraded correlations of the ternary VLE [1,2]. The inclusion of temperature dependency in the $n\text{C}_{12} + \text{C}_{10}\text{OH}$ BIP offered no additional benefit.

Table 7-5: SR-POLAR pure component parameters used in this work

Component	p_1	p_2	%AAD P^{sat}	T-range	Reference
	[]	[]	[%]	[°C]	
CO_2	0.1221	-1.2224	0.01	-23.15 to 27.85	[1]
$n\text{C}_{12}$	-0.0173	-2.1786	0.02	11.85 - 126.85	[1]
C_{10}OH	-0.5052	-2.4053	0.02	11.85 - 144.85	[2]

3.2.3 PR-BM

Within PR-BM, temperature independent $k_{ij}^{(0)}$ and $l_{ij}^{(0)}$ parameters were used for the $n\text{C}_{12} + \text{C}_{10}\text{OH}$ interaction (Tables 7-7 and 7-8). The authors used a similar configuration for the solute-solute interaction in the $\text{CO}_2 + 37\text{DM10} + \text{C}_{10}\text{OH}$ system [2]. The inclusion of temperature dependency in k_{ij} led to a 0.2 % reduction in %AAD_p from 3.4 to 3.2 % (see Table 7-9) and marginal improvement in the liquid correlation at 75 °C and 140 bar, but a less-specified system was deemed more valuable than these improvements.

3.2.4 PC-SAFT

The PC-SAFT pure component parameters used in this study are listed in Table 7-6. In a previous study [2] the authors evaluated the C_{10}OH pure component parameters of Liang et al. [14], Grenner et al. [15] and Umer et al. [16] in the system $\text{CO}_2 + 37\text{DM10} + \text{C}_{10}\text{OH}$, and found the first-mentioned to produce the best results. To enable a worthwhile comparison of model performance, the parameter set of Liang et al. [14] was also utilised in this work. A temperature independent solute-solute $k_{ij}^{(0)}$ was used (Tables 7-7 and 7-8) and, as was the case for SR-POLAR, the inclusion of temperature dependency offered no additional benefit.

Table 7-6: PC-SAFT pure component parameters used in this work

Component	m	σ	ε/k	ε^{AB}/k	κ^{AB}	%AAD P^{sat}	%AAD ρ^{sat}	T-range	Reference
	[]	[Å]	[°C]	[°C]	[]	[%]	[%]	[°C]	
CO ₂	2.0729	2.7852	-103.94	-	-	2.78	2.73	-57.15 to 30.85	[9]
<i>n</i> C ₁₂	5.3060	3.8959	-23.94	-	-	2.10	0.93	-10.15 to 384.85	[9,13]
C ₁₀ OH	6.4558	3.4215	-34.20	3187.02	0.000102	3.02	1.48	68 - 349	[14]

Table 7-7: Binary interaction parameters used in this work

Interaction pair	RK-ASPEN		SR-POLAR			PR-BM		PC-SAFT		Reference	
	$k_{a,ij}^{(0)}$	$k_{a,ij}^{(1)}$	$k_{b,ij}^{(0)}$	$k_{a,ij}^{(0)}$	$I_{ij}^{(0)}$	$k_{ij}^{(0)}$	$k_{ij}^{(1)}$	$I_{ij}^{(0)}$	$I_{ij}^{(0)}$		$k_{ij}^{(0)}$
CO ₂ + <i>n</i> C ₁₂	0.0883	-	0.0041	0.1059	-	0.3998	-0.0009	-	-	0.1223	[1]
CO ₂ + C ₁₀ OH	0.1821	-0.2866	-0.0288	0.1191	-	0.1478	-	-0.3467	0.0605	0.0759	[2]
<i>n</i> C ₁₂ + C ₁₀ OH	0.0612	-	0.0614	0.0541	0.0713	0.0588	-	0.1379	0.0046	0.0086	This work

Table 7-8: %AAD in pressure, temperature and solute mass fractions for the regression of BIP's used in this work.

Solute fraction deviations for the *n*C₁₂ + C₁₀OH pair are reported as an average of the *n*C₁₂ and C₁₀OH deviations.

Interaction	RK-ASPEN				SR-POLAR				PR-BM				PC-SAFT				Reference
	%AAD _P	%AAD _T	%AAD _X	%AAD _Y	%AAD _P	%AAD _T	%AAD _X	%AAD _Y	%AAD _P	%AAD _T	%AAD _X	%AAD _Y	%AAD _P	%AAD _T	%AAD _X	%AAD _Y	
CO ₂ + <i>n</i> C ₁₂	1.54	3.25	0.53	23.04	3.07	6.10	1.40	69.94	3.00	3.39	1.04	52.17	4.59	11.96	1.77	56.23	[1]
CO ₂ + C ₁₀ OH	1.40	1.44	0.49	10.53	3.16	3.18	1.34	27.04	2.42	3.06	0.92	27.64	6.81	4.91	2.13	28.00	[2]
<i>n</i> C ₁₂ + C ₁₀ OH	1.57	1.58	0.27	16.87	0.83	1.68	0.24	21.24	1.42	1.76	0.40	26.53	4.45	7.89	1.09	38.12	This work
TOTAL	63 %				139 %				124 %				168 %				

3.3 Comparison of model-predicted ternary mixture vapour and liquid phase pressures

The temperature and VLE data in Table 7-3 and the BIP's in Table 7-7 were used to predict vapour and liquid phase equilibrium pressures for the $\text{CO}_2 + n\text{C}_{12} + \text{C}_{10}\text{OH}$ system. At 35 °C and pressures higher than 83 bar, all four models essentially failed (Section 3.2) and, as such, the %AAD_p's presented in Table 7-9 are based only on pressure predictions at 55 and 75 °C. Furthermore, RK-ASPEN and PC-SAFT respectively predicted one and two vapour phase equilibrium pressures in excess of 2 000 bar. These failed predictions, which all occurred at the highest temperature-specific experimental pressure, skew model performance and were excluded from the calculated averages in Table 7-9.

Table 7-9: %AAD_p values for the model-predicted liquid and vapour phase equilibrium pressures at 55 and 75 °C in the system $\text{CO}_2 + n\text{C}_{12} + \text{C}_{10}\text{OH}$. The experimental temperatures and vapour and liquid phase compositions from this work were used as inputs to the simulation cases. Deviations labelled as Overall were calculated for both temperatures and deviations labelled as Combined were calculated for both the liquid and vapour phases. No 35 °C data were incorporated in the deviation calculations.

Model	Liquid			Vapour			Combined		
	55 °C	75 °C	Overall	55 °C	75 °C	Overall	55 °C	75 °C	Overall
RK-ASPEN	1.4	2.1	1.8	5.4 ^a	3.8	4.5	3.3	2.9	3.1
SR-POLAR	2.6	1.9	2.3	4.3	3.8	4.1	3.5	2.9	3.2
PR-BM	2.5	2.5	2.5	3.2	5.2	4.2	2.9	3.8	3.4
PC-SAFT	6.9	8.8	7.9	23.9 ^a	13.4 ^b	18.4	15.0	11.0	12.9

^a Pressure prediction at 55 °C and 157 bar was greater than 2 000 bar, and excluded; ^b Pressure prediction at 75 °C and 182 bar was greater than 2 000 bar, and excluded.

RK-ASPEN produced the most accurate equilibrium pressure estimates but its superiority over SR-POLAR and PR-BM is marginal, especially taking into account the latter two did not produce any failed predictions. Regardless the temperature or phase concerned, PC-SAFT produced the largest errors. The phase-specific errors indicate that all four models were more successful in the liquid phase. Relative model performance, which degrades in the order RK-ASPEN > SR-POLAR > PR-BM > PC-SAFT, corresponds to results reported by the authors for the $\text{CO}_2 + n\text{C}_{12} + 37\text{DM10}$ [1] and $\text{CO}_2 + 37\text{DM10} + \text{C}_{10}\text{OH}$ [2] mixtures.¹⁹

The initial modelling approach which incorporated ternary 35 °C data in the solute-solute BIP regression cases was characterised by poor yet interpretable liquid phase pressure predictions. Surprisingly, the

¹⁹ See also Table 5-11 on p. 118 and Table 6-9 on p. 149.

exclusion of 35 °C data improved model performance in the liquid phase at 35 °C and pressures between 68 and 200 bar. For these conditions the respective %AAD_p's via RK-ASPEN, SR-POLAR, PR-BM and PC-SAFT were 28, 27, 28 and 32 % before and 25, 24, 26 and 27 % after exclusion of the 35 °C data.

3.4 *Experimental and model predicted ternary mixture phase behaviour*

Experimental and model-predicted phase compositions from this study are presented on truncated Gibbs diagrams in Figs. 7-1 - 7-7. The four models were not able to predict VLE data at 35 °C and pressures between 104 and 200 bar (Section 3.2) and experimental phase behaviour at 35 °C is presented on one diagram (Fig. 7-3). Ternary literature data presented in Figs. 7-1, 7-2 and 7-4 - 7-7 were produced via synthetic methods [17,18] and cannot be used to construct tie lines. The working pressure ranges of 68 - 200 bar (35 °C), 83 - 157 bar (55 °C) and 104 - 182 bar (75 °C) provide context for references to low, medium and high pressures in the discussion that follows.

Phase behaviour in the CO₂ + *n*C₁₂ + C₁₀OH ternary exhibits similarities to that observed for the CO₂ + *n*C₁₂ + 37DM10 mixture [1].²⁰ In both cases the presence of *n*C₁₂ enhances solubility in the ternary mixture leading to s-shaped liquid phase curvature and, at higher pressures, a co-solvency pinch in the high-*n*C₁₂ region. The heterogeneous (two-phase) to homogenous (one-phase) transition in the 75:25 *n*C₁₂:C₁₀OH mixture occurred at 74.3, 112.2 and 148.9 bar at 35, 55 and 75 °C respectively. A comparative CO₂ + *n*C₁₂ binary with bulk CO₂ mass fraction of 0.733 transitions at higher pressures of 75.0, 113.2 and 151.2 bar at 35, 55 and 75 °C [17].²¹ Measuring the 75:25, 50:50 and 25:75 mixtures at 'non-standard' pressures of 73.5 bar (35 °C), 111.0 bar (55 °C) and 147.5 bar (75 °C) should make for interesting experimental work but fell outside the scope of the overarching project [1].

Zamudio et al. [17] and Smith and Schwarz [18] performed synthetic measurements of different CO₂ + *n*C₁₂ + 1-alcohol systems and identified enhanced solubility in the low-*n*C₁₂ region and co-solvency in the high-*n*C₁₂ region. For the CO₂ + *n*C₁₂ + C₁₀OH system, this behaviour led to the formation of detached two-phase regions [18]. Co-solvency was also observed by Scheidgen and Schneider [19,20] and Gauter et al. [21] when investigating a range of CO₂ + *n*-alkane + 1-alcohol mixtures and although they defined the mixture types [22,23], carbon chain lengths and pressure and temperature conditions likely to result in co-solvency, the aforementioned studies [17-21] were predominantly applied and not mechanistic in nature. Networked hydrogen bonds are stronger than the equivalent hydrogen bond occurring in

²⁰ See also Section 3.5 on p. 119.

²¹ See also Footnote 12 on p. 128.

isolation, a phenomenon referred to as hydrogen bond cooperativity [24]. Based on experimental CO₂ dissolution studies, Gui et al. [25] suggested that networked hydrogen bonding may lead to a more compact molecular structure and therefore reduced CO₂ solubility. Zamudio [26] used this as point of departure and hypothesised that non-polar *n*C₁₂ may disrupt the 1-alcohol networked structure thereby reducing the strength of the alcohol-alcohol interactions and increasing solubility in the CO₂ + *n*C₁₂ + 1-alcohol ternary mixture. This would explain enhanced solubility witnessed in the low-*n*C₁₂ region but not necessarily co-solvency witnessed in the high-*n*C₁₂ region. Dissolution studies have shown that CO₂ can participate in Lewis Acid-Lewis Base [27,28] and conventional hydrogen bonding interactions [29,30] which both serve to enhance solute solubility in CO₂, characteristics that are i) exploited to develop CO₂-philic materials [31-33]; and ii) not present in the CO₂ + *n*C₁₂ binary. Substantial *n*C₁₂-induced disruption of the self-association amongst 1-alcohol molecules could free up proton donors and acceptors, enable hydrogen bonding and Lewis Acid-Lewis Base interactions with the charge-separated CO₂ and ultimately lead to a ternary system more soluble than CO₂ + *n*C₁₂, i.e., co-solvency. However, this hypothesis would require further mechanistic research which falls outside the scope of this contribution.

Vapour phase curves of the continuous two-phase envelope are concave in shape (Figs. 7-5 a and 7-7) as a result of enhanced solubility but after detachment of the separate two-phase regions the vapour phase transitions to convex curvature (Figs. 7-1 b, 7-2, 7-4 c - e, 7-5 b and 7-6 d, e). This behaviour is yet another similarity between the *n*C₁₂ + C₁₀OH and *n*C₁₂ + 37DM10 [1] mixtures.

In Fig. 7-3, tie lines of the 50:50 mixture present a significant angular shift when moving from 68 bar, below the CO₂ + *n*C₁₂ total solubility pressure (TSP) to 83 bar, above the CO₂ + *n*C₁₂ TSP, where TSP is defined as the highest temperature-specific binary bubble or dew point pressure. The notion that interesting ternary mixture phase behaviour may exist at pressures marginally higher than the lower of the two binary TSP's was previously reported, and used as one governing factor when defining the outline of the overarching project [1].

At 35 °C, density inversions or barotropic phenomena were detected for the 25:75 and 21.5:78.5 *n*C₁₂:C₁₀OH mixtures at 182 and 200 bar respectively. At these conditions the hydrocarbon-rich phase was lighter and moved to the top of the equilibrium cell whilst the CO₂-rich was heavier and settled to the bottom. Fourie et al. [2] witnessed similar low temperature density inversions in the CO₂ + 37DM10 + C₁₀OH system and presented interesting photos that illustrate a pressure reduction sequence passing through the inversion point, and surface tension effects at the inverted conditions.

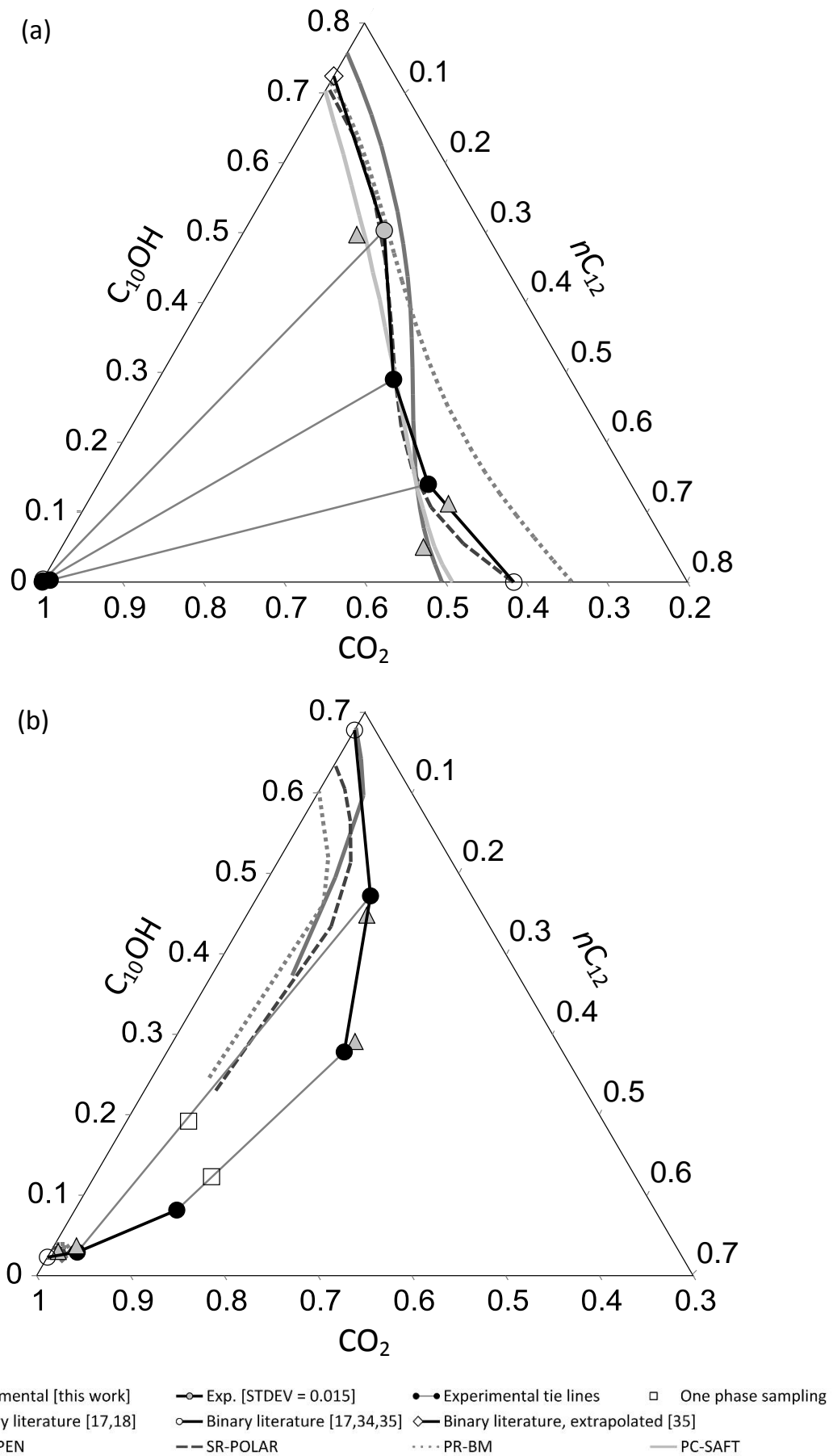


Figure 7-1. $\text{CO}_2 + n\text{C}_{12} + \text{C}_{10}\text{OH}$ at $35.0\text{ }^\circ\text{C}$ and (a) 68 bar; and (b) 83 bar.

PC-SAFT failed to predict two-phase VLE at 83 bar.

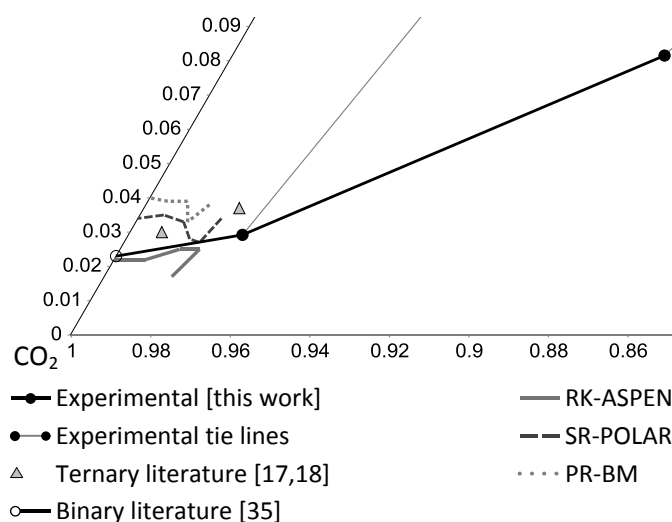


Figure 7-2. Vapour phase detail for $\text{CO}_2 + n\text{C}_{12} + \text{C}_{10}\text{OH}$ at $35.0\text{ }^\circ\text{C}$ and 83 bar .

PC-SAFT failed to predict two-phase VLE at 83 bar .

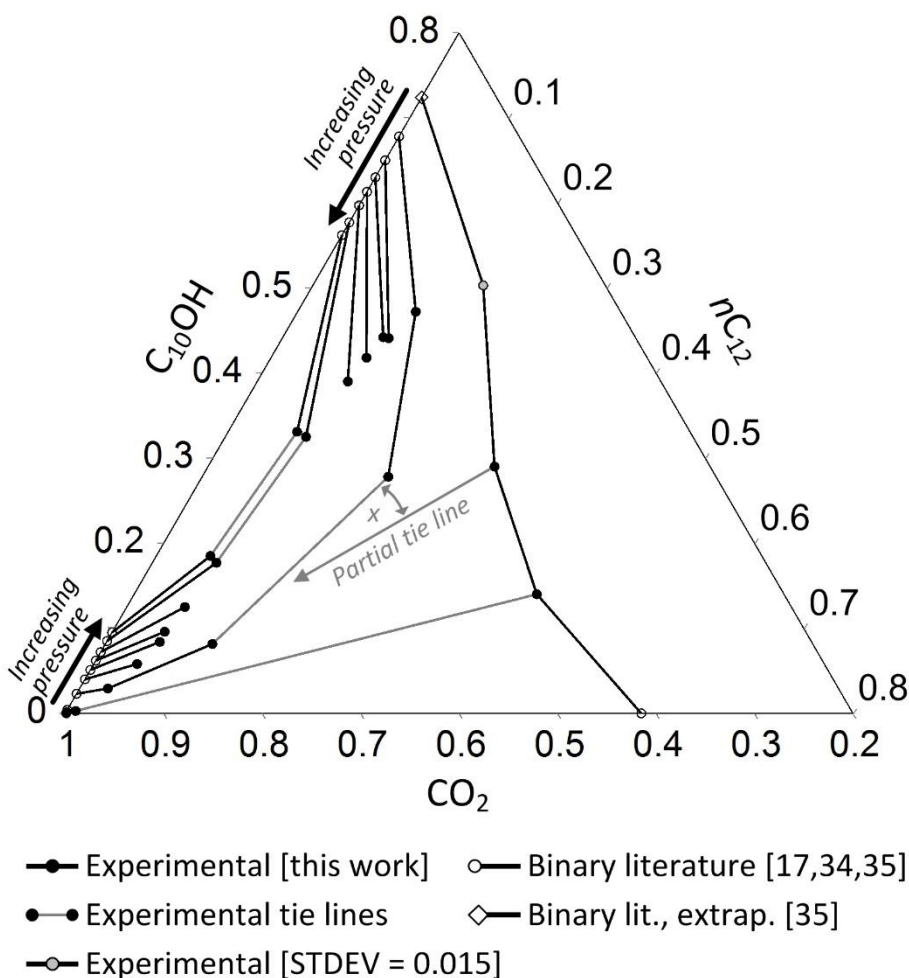


Figure 7-3. $\text{CO}_2 + n\text{C}_{12} + \text{C}_{10}\text{OH}$ at $35.0\text{ }^\circ\text{C}$ and $68, 83, 104, 123, 140, 157, 182$ and 200 bar . The arrows indicate the direction of increasing pressure. To eliminate clutter, only select tie lines were connected. The solvent-free $n\text{C}_{12}:\text{C}_{10}\text{OH}$ mass ratio for the innermost data point at 200 bar was $21.5:78.5$. The angle x between tie lines at 68 and 83 bar in the $50:50\text{ } n\text{C}_{12}:\text{C}_{10}\text{OH}$ mixture illustrates a significant liquid phase shift toward higher C_{10}OH content and a vapour phase shift toward lower C_{10}OH content when moving from 68 to 83 bar and, in the process, passing above the $\text{CO}_2 + n\text{C}_{12}$ total solubility pressure of 75 bar [17].

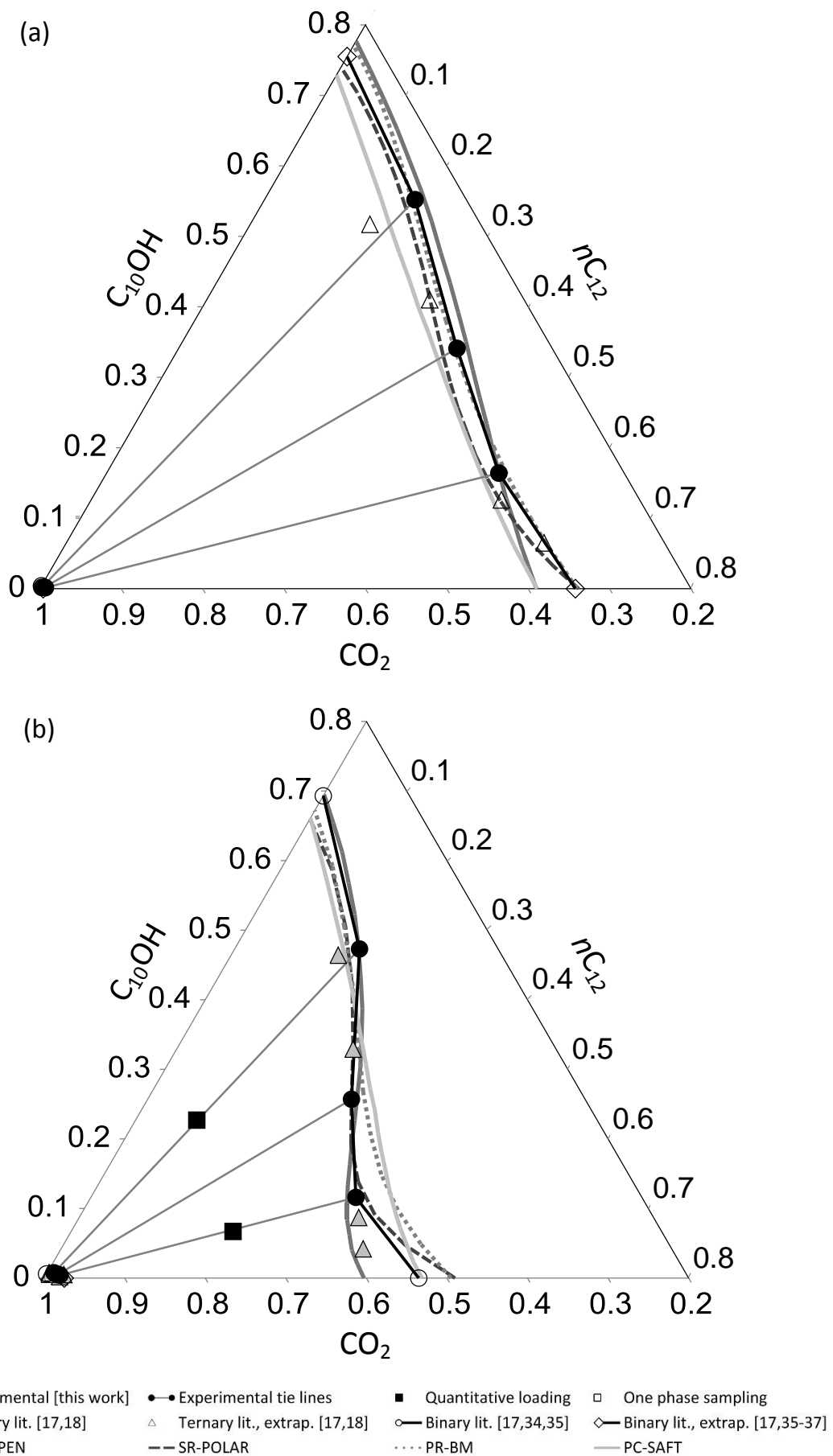
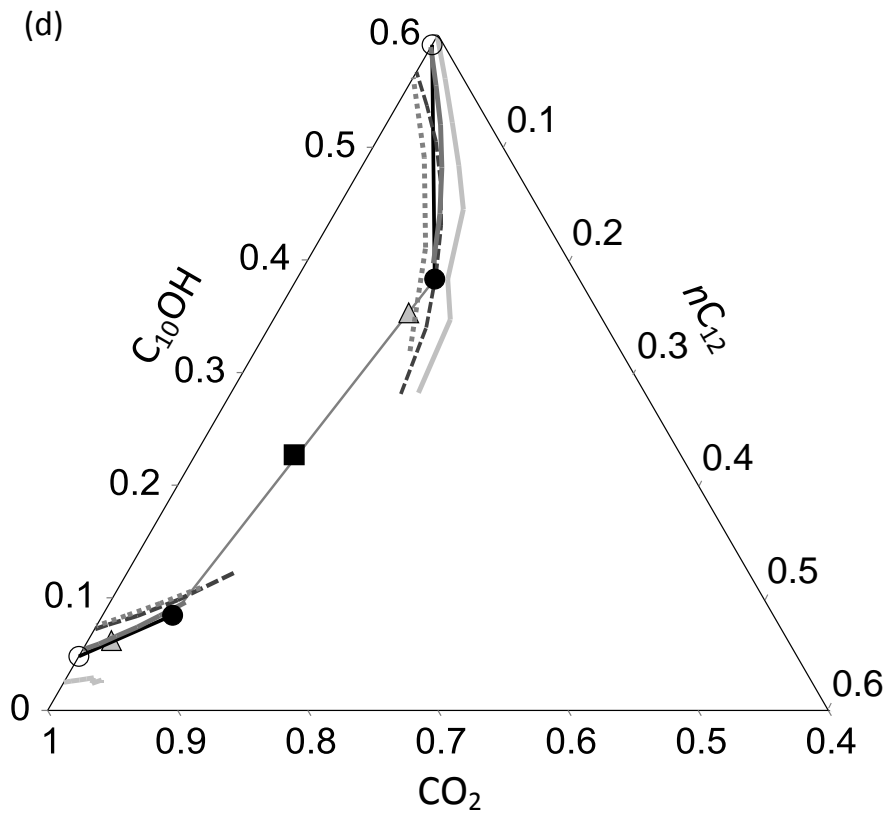
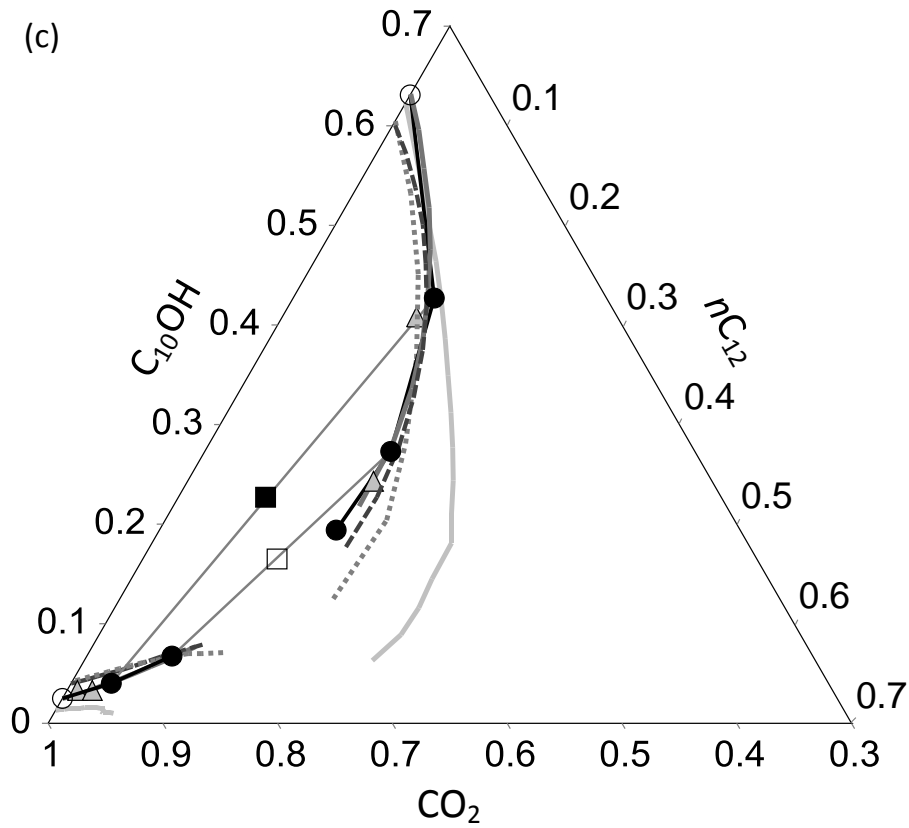


Figure 7-4. $\text{CO}_2 + n\text{C}_{12} + \text{C}_{10}\text{OH}$ at $55.0\text{ }^\circ\text{C}$ and (a) 83 bar; (b) 104 bar; (c) 123 bar; (d) 140 bar; and (e) 157 bar.



- | | | | |
|----------------------------|---------------------------------|--------------------------|-----------------------------------|
| ● Experimental [this work] | ● Experimental tie lines | ■ Quantitative loading | □ One phase sampling |
| △ Ternary lit. [17,18] | △ Ternary lit., extrap. [17,18] | ○ Binary lit. [17,34,35] | ◇ Binary lit., extrap. [17,35-37] |
| — RK-ASPEN | - - SR-POLAR | ⋯ PR-BM | — PC-SAFT |

Figure 7-4. $\text{CO}_2 + n\text{C}_{12} + \text{C}_{10}\text{OH}$ at 55.0 °C and (a) 83 bar; (b) 104 bar; (c) 123 bar; (d) 140 bar; and (e) 157 bar.

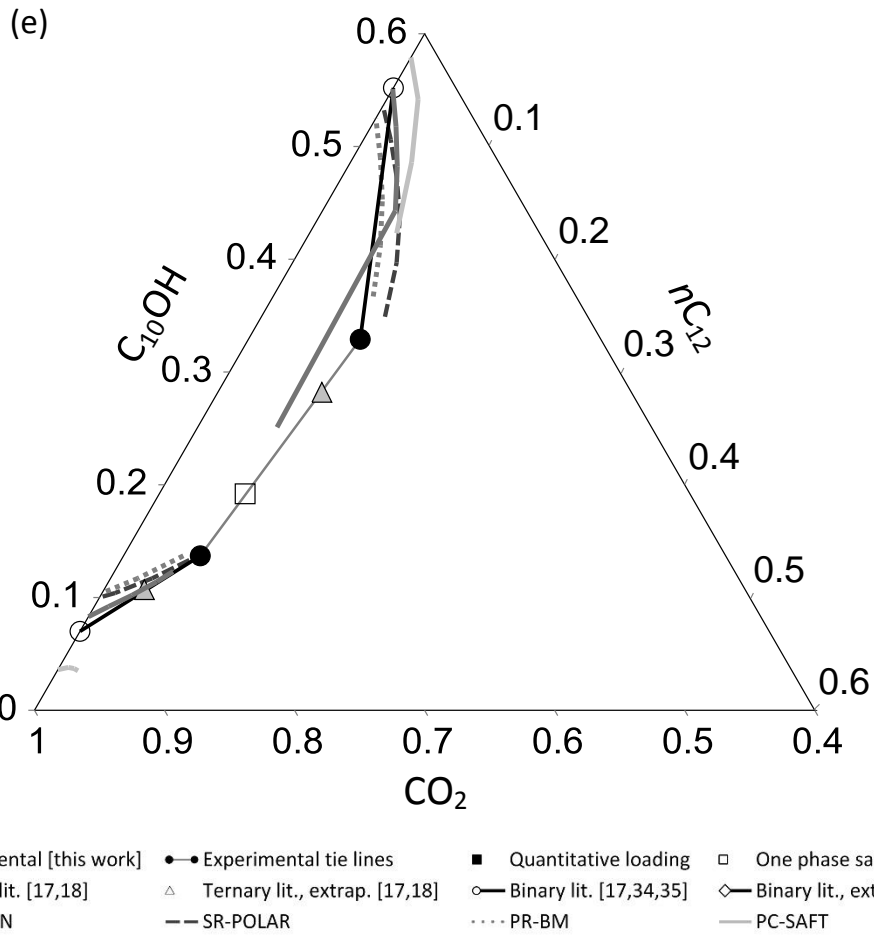


Figure 7-4. $\text{CO}_2 + n\text{C}_{12} + \text{C}_{10}\text{OH}$ at 55.0 °C and (a) 83 bar; (b) 104 bar; (c) 123 bar; (d) 140 bar; and (e) 157 bar.

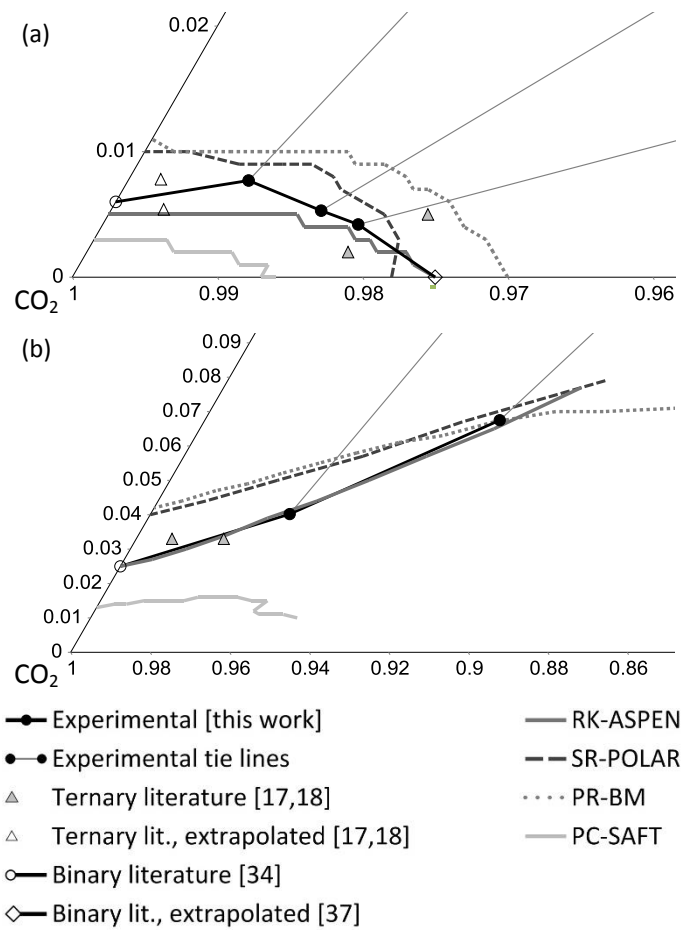


Figure 7-5. Vapour phase detail for CO₂ + nC₁₂ + C₁₀OH at 55.0 °C and (a) 104 bar; and (b) 123 bar.

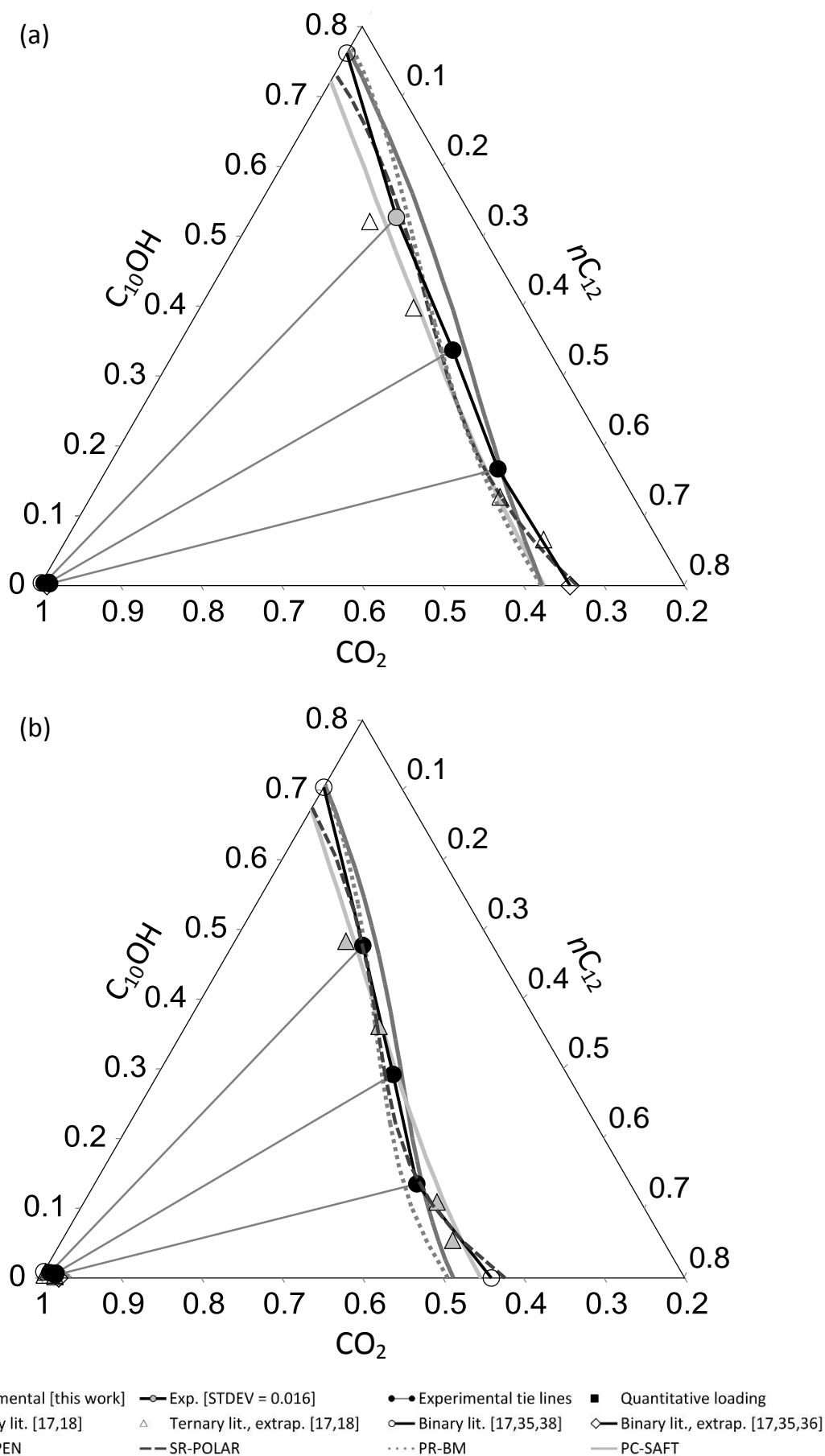


Figure 7-6. $\text{CO}_2 + n\text{C}_{12} + \text{C}_{10}\text{OH}$ at 75 °C and (a) 104 bar; (b) 123 bar; (c) 140 bar; (d) 157 bar; and (e) 182 bar.

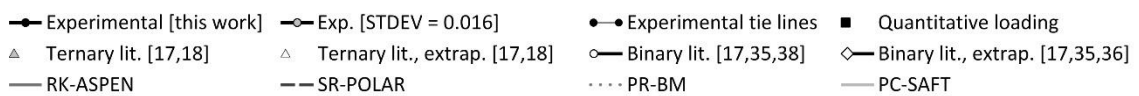
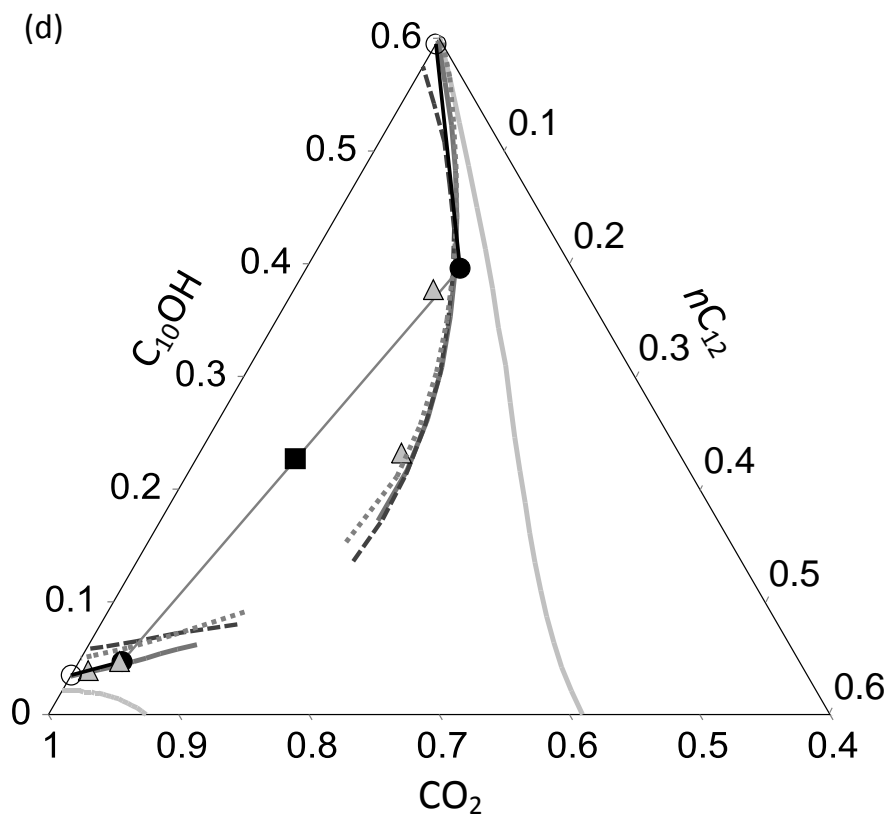
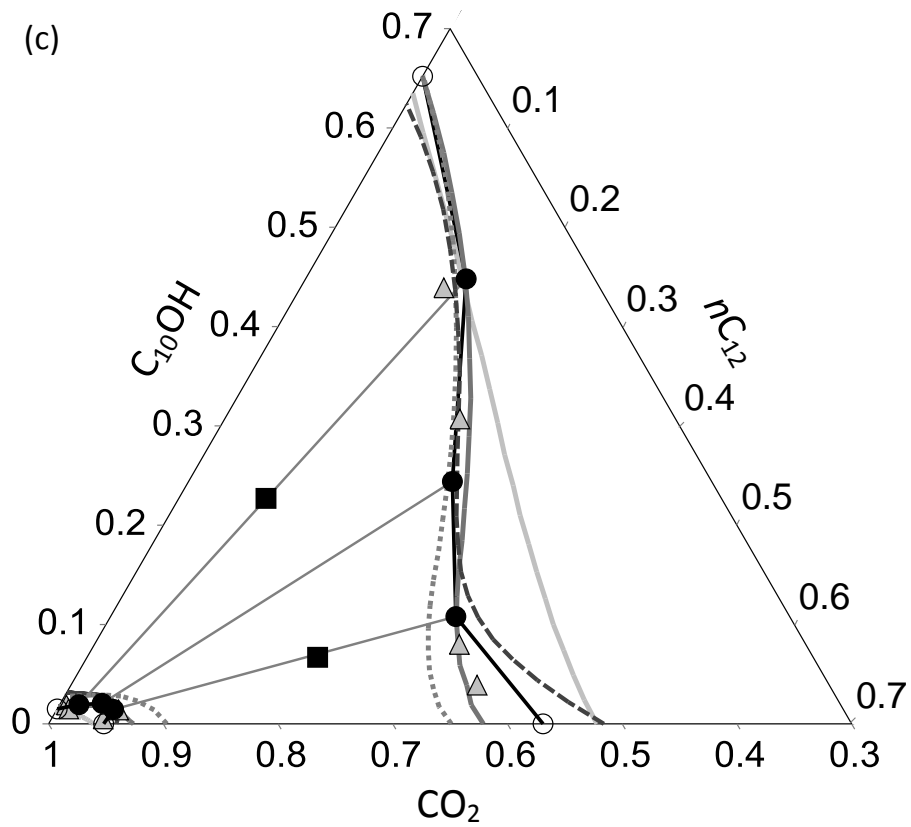


Figure 7-6. $\text{CO}_2 + n\text{C}_{12} + \text{C}_{10}\text{OH}$ at 75 °C and (a) 104 bar; (b) 123 bar; (c) 140 bar; (d) 157 bar; and (e) 182 bar.

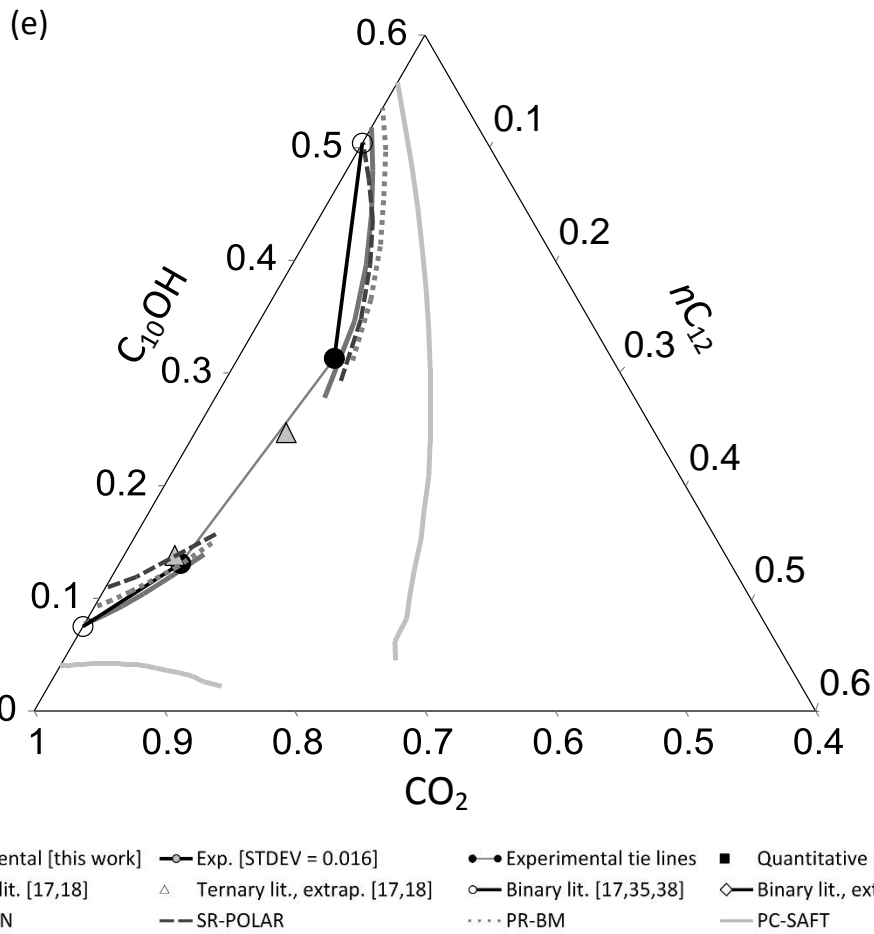


Figure 7-6. $\text{CO}_2 + n\text{C}_{12} + \text{C}_{10}\text{OH}$ at 75 °C and (a) 104 bar; (b) 123 bar; (c) 140 bar; (d) 157 bar; and (e) 182 bar.

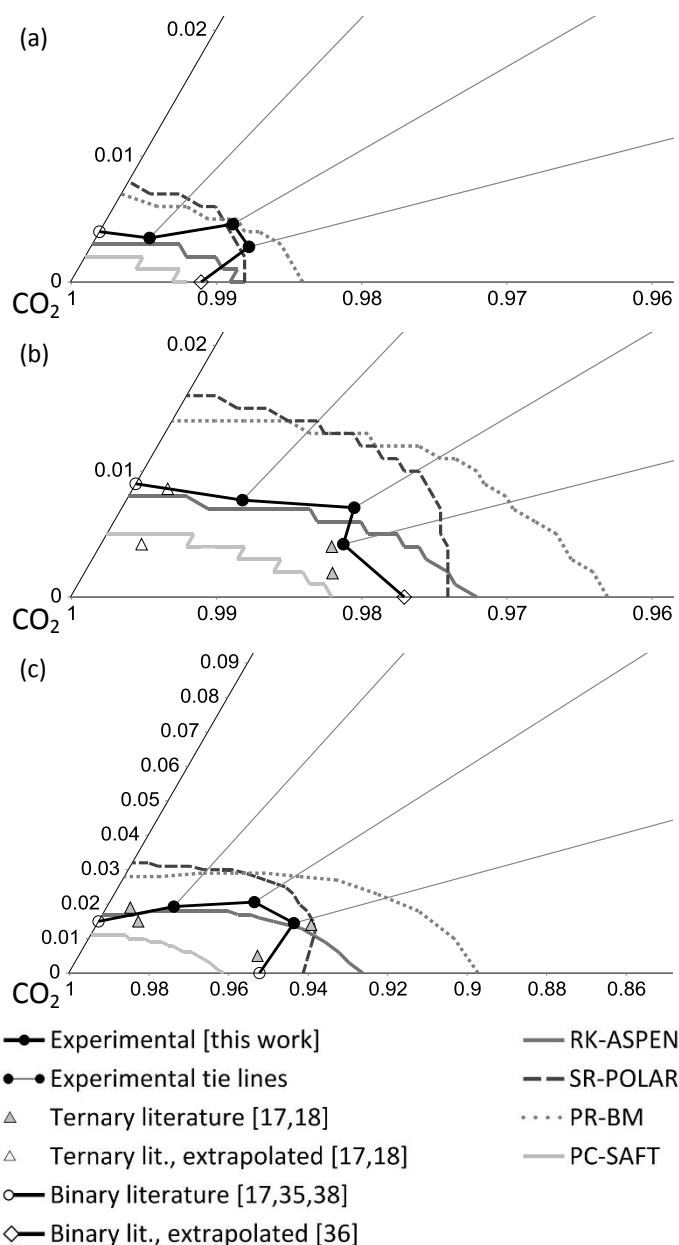


Figure 7-7. Vapour phase detail for $\text{CO}_2 + n\text{C}_{12} + \text{C}_{10}\text{OH}$ at $75.0\text{ }^\circ\text{C}$ and (a) 104 bar; (b) 123 bar; and (c) 140 bar.

RK-ASPEN low pressure liquid correlations are CO_2 -deficient in the high- C_{10}OH region and solute-deficient in the high- $n\text{C}_{12}$ region (Figs. 7-1 a, 7-4 a and 7-6 a, b). RK-ASPEN cannot capture the acute angle of the co-solvency pinch and the solute deficiency in the high- $n\text{C}_{12}$ region persists throughout the medium pressure range (Figs. 7-4 b and 7-6 c). At high pressures the model is very successful at correlating the convex liquid curvature in the high- C_{10}OH region (Figs. 7-4 c, d and 7-6 c - e). In this sense, $55\text{ }^\circ\text{C}$ and 157 bar (Fig. 7-4 e) is the exception, the model fails to complete the two-phase envelope and is outclassed by the other cubic EOS. At $35\text{ }^\circ\text{C}$ and 83 bar (Fig. 7-1 b), similar behaviour is witnessed but in this case it is the norm amongst the cubic EOS rather than RK-ASPEN being the exception. In the medium pressure range at $75\text{ }^\circ\text{C}$, and the high- $n\text{C}_{12}$ region in particular, RK-ASPEN is not able to fully capture the experimental vapour phase concavity (Fig. 7-7). In general, however, RK-ASPEN produced superb vapour phase correlations at 55 and $75\text{ }^\circ\text{C}$.

SR-POLAR proved superior at mimicking the acute angle of the co-solvency pinch in the high- nC_{12} region (Figs. 7-1 a, 7-4 b and 7-6 b, c). At 55 and 75 °C and low pressures it predicts a marginally CO_2 -rich liquid phase (Figs. 7-4 a, b and 7-6 a, b), an error that is more prominent at 55 than 75 °C and diminishes with increasing pressure. Dissimilar behaviour is witnessed at 35 °C and 68 bar where it produced an accurate liquid correlation (Fig. 7-1 a). At high pressures, SR-POLAR was successful at capturing the liquid phase convexity (Figs. 7-4 c - e and 7-6 c - e). SR-POLAR low pressure vapour phase predictions are reasonably shaped but overly solute-rich, particularly in the high- $C_{10}OH$ region (Figs. 7-5 a and 7-7). This CO_2 -deficiency continues after detachment of the two-phase regions and persists throughout the medium and high pressure range (Figs. 7-4 c - e and 7-6 d, e).

PR-BM liquid phase correlations are more accurate in the high- $C_{10}OH$ than high- nC_{12} region. Low pressure correlations exhibit inter-temperature variance: at 35 °C it fails in the high- nC_{12} region (Fig. 7-1 a), at 55 °C good results are obtained (Fig. 7-4 a) and at 75 °C the curve is well-positioned but the s-shaped nature thereof is excessive (Fig. 7-6 a). In the medium pressure range PR-BM liquid trends display convex-to-concave characteristics but in the high- nC_{12} region at 55 (Fig. 7-4 b) and 75 °C (Fig. 7-6 a - c) respectively, liquid compositions are CO_2 -deficient and CO_2 -rich. This behaviour continues up to the $CO_2 + nC_{12}$ binary axis. Medium pressure liquid correlations are accurate (Figs. 7-4 c and 7-6 d) but in the high pressure range, solubility is marginally over and underestimated at 55 and 75 °C respectively (Figs. 7-4 d, e and 7-6 e). PR-BM vapour correlations in the medium pressure range are qualitatively sound but solubility is overestimated and compositions are CO_2 -deficient (Figs. 7-5 a and 7-7). This behaviour persists throughout the high pressure range (Figs. 7-4 c - e, 7-5 b and 7-6 d, e).

PC-SAFT is not able to match the medium pressure convex-to-concave liquid phase complexity and trends are, at best, concave throughout the entire solute ratio range (Figs. 7-1 a, 7-4 a, b and 7-6 b, c). At 55 and 75 °C liquid correlations shift from solute-deficient to solute-rich with increasing pressure. Throughout, the vapour phase solute loading is under-predicted (Figs. 7-4 c - e, 7-5, 7-6 d, e and 7-7) which corresponds to model behaviour in the $CO_2 + nC_{12} + 37DM1O$ [1] and $CO_2 + 37DM1O + C_{10}OH$ [2] systems, and impacts separation potential predictions (Section 3.5.2). By virtue of underestimating the high pressure solubility, two-phase envelopes too large in surface area are obtained (Figs. 7-4 c - e and 7-6 c - e).

3.5 Evaluating CO₂ as solvent to fractionate nC₁₂ + C₁₀OH

3.5.1 Experimental ternary mixture relative solubilities and separation potentials

The VLE data in Table 7-3 were used to calculate the experimental relative solubility, α_{ij} , and separation potential, SP_{ij} , defined in Eqs. 7-2 and 7-3 where i and j represent nC₁₂ and C₁₀OH respectively. Relative solubility provides an indication of the attainable fractionation sharpness whilst separation potential, which also contains a vapour phase solute loading contribution, is an indicator of the requisite solvent flow in order to achieve the desired lights extraction.

$$\alpha_{ij} = \frac{Y_i/X_i}{Y_j/X_j}$$

Equation 7-2

$$SP_{ij} = (\alpha_{ij} - 1) \times Y_i \times 1000$$

Equation 7-3

Given the vapour phase solute fraction-sensitivity of low-pressure relative solubilities [1], coupled with the accuracy limitations of the experimental setup [1,2], the α_{ij} values at 35 °C and 68 bar, 55 °C and 83 bar, and 75 °C and 104 bar should be interpreted with caution. That being said, low-pressure α_{ij} 's at 55 and 75 °C appear well-behaved (Fig. 7-8 a) because the qualitative solute ratio-dependency is maintained when moving from 83 to 104 bar (55 °C) and 104 to 123 bar (75 °C). At 35 °C, however, the angular shift \times illustrated in Fig. 7-3 represents a liquid phase shift toward higher C₁₀OH content and a vapour phase shift toward lower C₁₀OH content when pressure in the 50:50 nC₁₂:C₁₀OH mixture is increased from 68 to 83 bar. This should translate to increased relative solubility but instead the opposite is observed and, as a result, the 50:50 and 25:75 curves in Fig. 7-8 a cross, and the qualitative solute ratio-dependency is not maintained. The α_{ij} of 2.0 at 35 °C and 83 bar represents a solute-rich vapour phase containing 10.9 mass % nC₁₂ and 8.1 mass % C₁₀OH, which lends stability to Eq. 7-2. In contrast, the α_{ij} of 3.5 at 35 °C and 68 bar represents a solute-lean vapour phase with only 0.09 mass % nC₁₂ and 0.02 mass % C₁₀OH and, most likely, errs on the high side.

Relative solubility and therefore separation potential are solute ratio-dependent and the α_{ij} 's and SP_{ij} 's associated with the non-standard nC_{12} : $C_{10}OH$ ratios of 41.5:58.5 and 21.5:78.5 appear as isolated points in Fig. 7-8. The α_{ij} trends were extrapolated using the temperature-specific relationship between α_{ij} and solute ratio at the nearest available pressure. Further details are provided in Fig. 7-8.

The remainder of this section focuses primarily on the system in question but also compares the behaviour thereof to $CO_2 + nC_{12} + 37DM1O$ and $CO_2 + 37DM1O + C_{10}OH$. Please refer to Fourie et al. [1,2] for the appropriate reference text. When referring to solute A + solute B mixtures the presence of CO_2 is implied.

In general, α_{ij} 's and SP_{ij} 's for $nC_{12} + C_{10}OH$ are larger than was observed for $nC_{12} + 37DM1O$ or $37DM1O + C_{10}OH$ (also see Table 7-10). Relative solubility is positively correlated with bulk fraction of the *less* soluble species, $C_{10}OH$ (Fig. 7-8 a). This corresponds with behaviour in the alkane + branched alcohol system but differs from that of the alcohol + alcohol system where α_{ij} was largely $Z_{C_{10}OH}$ -independent.²² Fig. 7-9, and the angle between experimental tie lines and constant solute-solute ratio lines (CSSRL) in particular, illustrates this dependency.²³ In the high- nC_{12} region, tie lines and CSSRL run virtually parallel to each other implying fractionation is either ineffective or impossible. As $Z_{C_{10}OH}$ increases the angles between tie lines and CSSRL, and therefore α_{ij} , also increase. The potential relationship between alkane-induced disruption of the self-association amongst 1-alcohols and both enhanced solubility and co-solvency – concepts not concerned with relative solute species distribution – was discussed on p. 192. Similar causality between this phenomenon and the Z_i -dependency of α_{ij} is conceivable. Relative solubility is a function of the difference in CO_2 -solubility between solutes i and j . Alkane-induced disruption of the 1-alcohol hydrogen bond cooperativity would enhance the 1-alcohol CO_2 -solubility and, in turn, lower α_{ij} . This theory corresponds with i) α_{ij} 's positively correlated with bulk 1-alcohol content in the nC_{12} -containing systems; and ii) α_{ij} 's virtually independent of solute-solute ratio in the $37DM1O + C_{10}OH$ mixture. Even though α_{ij} presents similar solute ratio-dependency in the two alkane-containing systems, the current mixture is suited for CO_2 fractionation across a wider solute ratio range which includes the 75:25 mixture. This was not the case for the 75:25 nC_{12} : $37DM1O$ mixture. Relative solubility estimates calculated via binary VLE data [17,34-38] tend to over-predict α_{ij} and its solute ratio dependence, a key aspect for industrial SFE [39], is not captured.

²² See also Section 3.6.1 on p. 126 and Section 3.5.1 on p. 158.

²³ See also Figure 5-9 on p. 128.

At constant temperature and solute-solute ratio, α_{ij} passes through a pressure-optimum. To paraphrase: at lower pressures a positive ΔP favours nC_{12} -solubility but at higher pressures an increase in pressure preferentially enhances $C_{10}OH$ -solubility. A similar P -dependent α_{ij} -optimum presented in the alkane + branched alcohol system but was absent from the alcohol + alcohol mixture.

At constant temperature and pressure, interesting SP_{ij} -behaviour is observed (Fig. 7-8 b). In the $nC_{12} + 37DM10$ system, SP_{ij} was governed by α_{ij} and, as a result, positively correlated with bulk fraction of the *less* soluble species. In the $37DM10 + C_{10}OH$ system the converse was true: SP_{ij} was dominated by Y_i and therefore positively correlated with bulk fraction of the *more* soluble species. In this study SP_{ij} passes through a $Z_{C_{10}OH}$ -optimum as highlighted by Fig. 7-8 b where the 50:50 SP_{ij} curves are positioned above the 75:25 and 25:75 curves. Fourie et al. [1] reported similar behaviour for the model-predicted separation potentials in $CO_2 + nC_{12} + 37DM10$.²⁴ However, these optima were positioned at $Z_{37DM10} \approx 0.85$ and since the highest Z_{37DM10} measured experimentally was 0.75 the occurrence of a similar Z_{37DM10} -dependent SP_{ij} -optimum could not be established. In this work, the aforementioned experimental SP_{ij} -optimum occurs at a significantly lower $Z_{C_{10}OH}$ and, as such, is visible within the range $0.25 < Z_{C_{10}OH} < 0.75$.

Conclusions regarding the SP_{ij} pressure-dependency are based on the behaviour of the 25:75 $nC_{12}:C_{10}OH$ mixture. SP_{ij} , being a function of α_{ij} , also passes through a pressure-optimum but the optimum itself is shifted toward higher pressures. This is to be expected because α_{ij} has to decrease significantly before the P -dependent increase in $Y_{nC_{12}}$ is eclipsed.

At constant pressure and $nC_{12}:C_{10}OH$ ratio, SP_{ij} is distinctly negatively correlated with temperature. This is a result of α_{ij} being largely T -independent (Fig. 7-8 a) and $Y_{nC_{12}}$ decreasing with increasing temperature. The latter corresponds to behaviour in the binary $CO_2 + nC_{12}$ system where solubility decreases or phase transition pressures increase in the order $35\text{ }^\circ\text{C} \rightarrow 55\text{ }^\circ\text{C} \rightarrow 75\text{ }^\circ\text{C}$ [17].

²⁴ See also Figure 5-10 on p. 129.

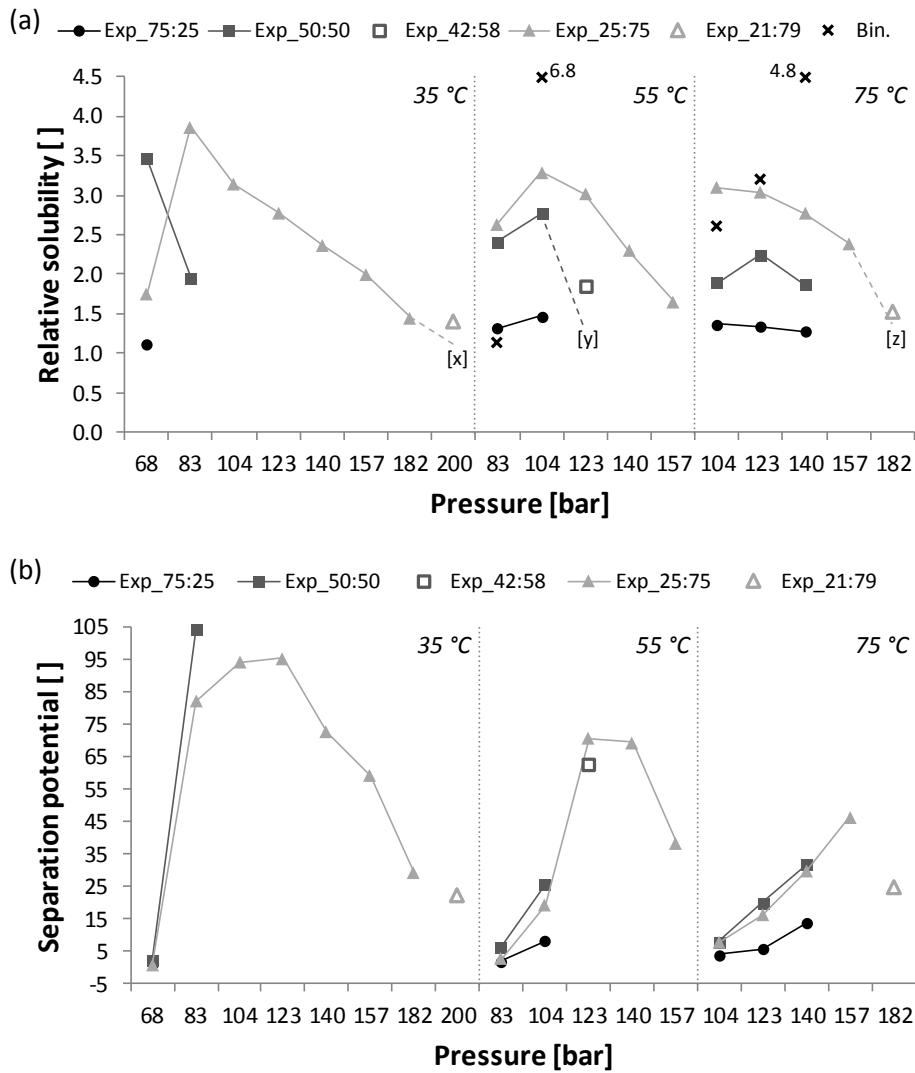


Figure 7-8. Experimental (a) relative solubility; and (b) separation potential for 75:25, 50:50, 41.5:58.5, 25:75 and 21.5:78.5 $nC_{12}:C_{10}OH$ mass ratio mixtures of $CO_2 + nC_{12} + C_{10}OH$ at 35.0, 55.0 and 75.0 °C. Dashed lines in (a) represent extrapolated curves using [x] the α_{ij} solute ratio-dependency at 35 °C and 83 bar, and the 21.5:78.5 data point; [y] the α_{ij} solute ratio-dependency at 55 °C and 123 bar, and the 41.5:58.5 data point; and [z] the α_{ij} solute ratio-dependency at 75 °C and 140 bar, and the 21.5:78.5 data point. Relative solubilities labelled Bin. were calculated off binary VLE data [17,34-38] and the values of 6.8 and 4.8 should extend above the y-axis scale.

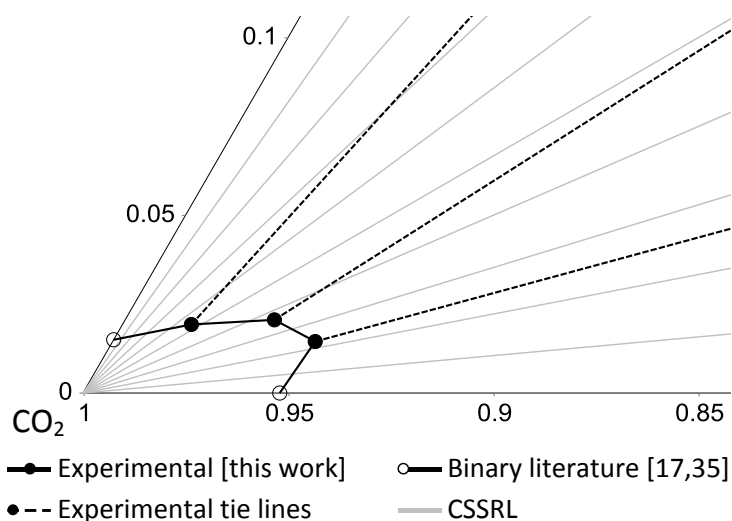


Figure 7-9. Vapour phase detail for CO₂ + nC₁₂ + C₁₀OH at 75.0 °C and 140 bar. In the high-nC₁₂ region, experimental tie lines and CSSRL run almost parallel to each other. As the bulk solvent-free C₁₀OH fraction increases the angle between tie lines and CSSRL opens up and the attainable fractionation sharpness increases.

3.5.2 Model-predicted ternary mixture relative solubilities and separation potentials

Model-predicted α_{ij} and SP_{ij} values were calculated using the model-predicted VLE data and selected results are presented in Fig. 7-10. Qualitatively, reasonable agreement exists between the four models and also between the models and the experimental trends. This matches observations for the CO₂ + nC₁₂ + 37DM10 mixture [1] but contradicts behaviour in the CO₂ + 37DM10 + C₁₀OH system where Fourie et al. [2] reported large variation amongst the models and no model being able to qualitatively replicate actual system behaviour.

Within the range $0.05 < Z_{C_{10OH}} < 0.95$, predicted relative solubilities also increase with $Z_{C_{10OH}}$, and RK-ASPEN and PC-SAFT predict larger α_{ij}' s than SR-POLAR and PR-BM (Fig. 7-10 a). SR-POLAR predicts α_{ij}' s that flatten out in the high- $Z_{C_{10OH}}$ region and, in this sense, is the exception. In contrast to the experimental system, none of the models predict a pressure-dependent α_{ij} -optimum. Instead, all four models predict α_{ij}' s that are negatively correlated with pressure within the temperature-specific pressure ranges evaluated. This is illustrated in Fig. 7-10 a where the RK-ASPEN curve at 55 °C and 104 bar is positioned beneath the 83 bar curve (see Fig. 7-8 a for actual system behaviour at these conditions). All four models correctly predict a $Z_{C_{10OH}}$ -dependent SP_{ij} -optimum (Fig. 7-10 b). In general, PC-SAFT positions this optimum at a lower $Z_{C_{10OH}}$ but only at 75 °C does it correctly predict smaller SP_{ij}' s for the 25:75 mixture than for the 50:50 mixture (see Fig. 7-8 b for actual system behaviour). In the low- $Z_{C_{10OH}}$ region, SR-POLAR predicts α_{ij}' s smaller than unity and, as a result, negative SP_{ij}' s.

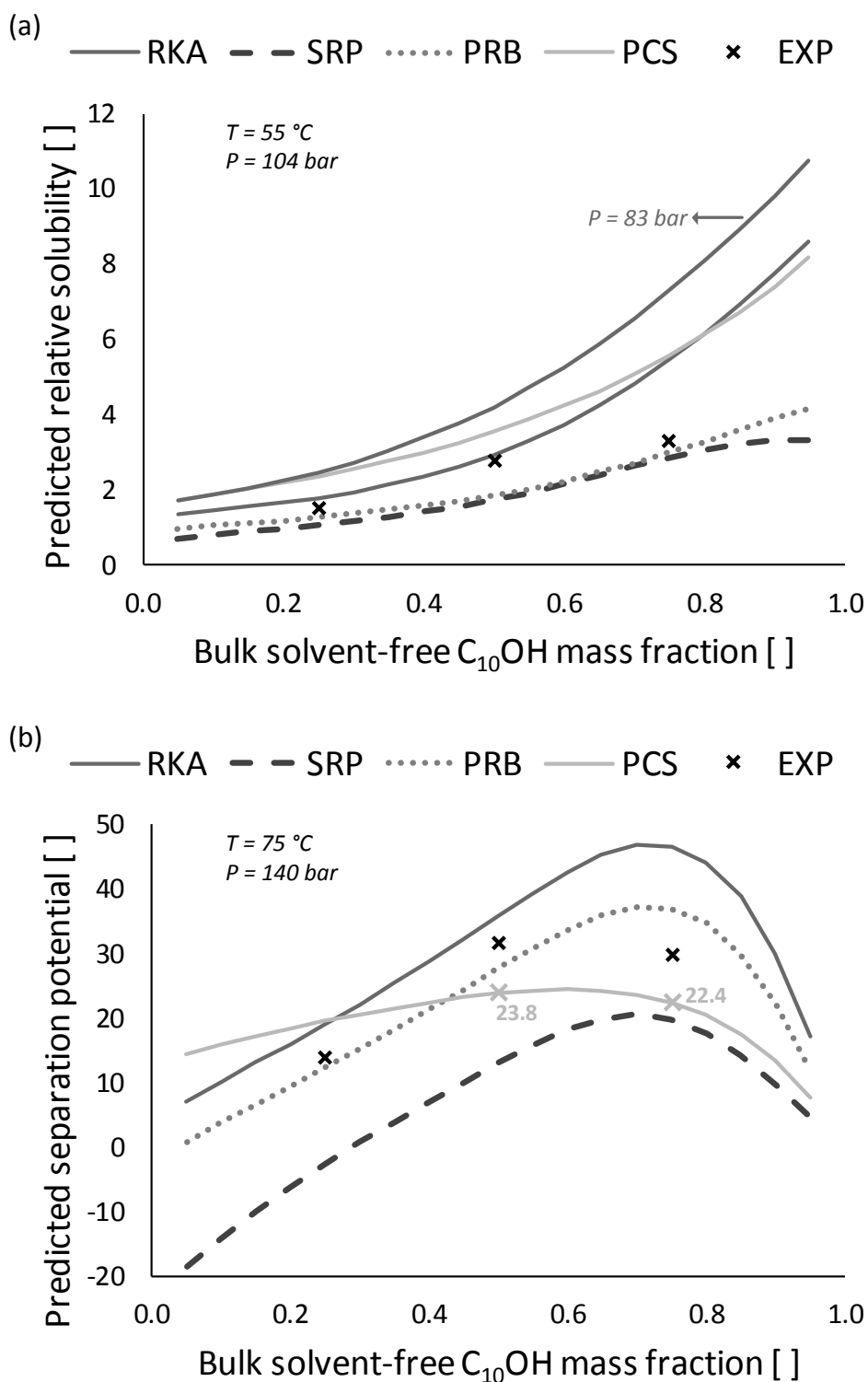


Figure 7-10. (a) Model-predicted and experimental relative solubility at 55 °C and 104 bar as a function of $Z_{\text{C}_{10}\text{OH}}$. Two RK-ASPEN curves are shown. The curve at the lower pressure of 83 bar is positioned above the curve at 104 bar illustrating the negative α_{ij} - P correlation that exists for all four models throughout the modelled pressure range. (b) Model-predicted and experimental separation potential at 75 °C and 140 bar as a function of $Z_{\text{C}_{10}\text{OH}}$. All four models predict an optimum in SP_{ij} but compared to the cubic EOS the PC-SAFT-optimum is positioned at a lower $Z_{\text{C}_{10}\text{OH}}$. As such, the PC-SAFT-predicted 50:50 SP_{ij} (23.8) is larger than the 25:75 SP_{ij} (22.4) which qualitatively matches experimental behaviour.

Table 7-10 summarises the experimental and predicted relative solubilities and separation potentials for the ternary mixture from this work, as well as the two ternaries studied by Fourie et al. [1,2]. Model correlations for the C₁₀OH-containing systems generally failed at 35 °C and, as such, experimental and model-predicted data at 35 °C were not incorporated in Table 7-10. The exclusion of 35 °C experimental data does not impact the relative order of the mixtures in terms of suitability for CO₂ fractionation. Given the erratic behaviour often witnessed for low-pressure α_{ij} 's, the lowest-pressure experimental α_{ij} values at each temperature were excluded from Table 7-10 (see Sections 3.4 and 3.5.1).

Table 7-10. Average experimental and model-predicted α_{ij} and SP_{ij} values for the CO₂ + 37DM10 + C₁₀OH, CO₂ + nC₁₂ + 37DM10 and CO₂ + nC₁₂ + C₁₀OH systems. Mixtures are ordered from least-suited (top) to best-suited (bottom) for fractionation with CO₂ using experimental values as criteria.^a

Solute mixture	Average relative solubility, α_{ij}					Average separation potential, SP_{ij}					Reference
	EXP	RKA	SRP	PRB	PCS	EXP	RKA	SRP	PRB	PCS	
37DM10 + C ₁₀ OH	1.2	1.4	0.9	0.8	1.5	4.6	5.6	-0.4	-1.5	3.8	[2]
nC ₁₂ + 37DM10	1.6	2.0	2.0	2.7	2.0	9.2	16.5	16.5	28.7	11.4	[1]
nC ₁₂ + C ₁₀ OH	2.2	2.9	1.6	1.8	2.9	24.4	29.0	12.8	18.3	21.8	This work
<i>TAD</i>	-	1.3	1.3	1.9	1.3	-	12.9	23.9	31.8	5.7	-

^a To enable improved comparison, only experimental and model-predicted data at 55 and 75 °C were used and model-predicted values were only considered in the range $0.25 < Z_i < 0.75$. At each temperature the lowest-pressure experimental α_{ij} 's were not incorporated but the SP_{ij} 's were. Extrapolated experimental values shown in Fig. 7-8 a were not incorporated when calculating averages. Totalised absolute deviation (*TAD*) sums the mixture-specific absolute deviations for each parameter and each model.

The nC₁₂ + C₁₀OH solute mixture is best-suited for SFE using CO₂ which matches an evaluation based solely on the difference in solubility pressures for the constituent CO₂ + solute binaries [17].²⁵ This approach, however, would erroneously position CO₂ + nC₁₂ + 37DM10 as the mixture least-suited for CO₂ fractionation because the total solubility pressures of the constituent binaries are in closest agreement [17,35]. Using binary VLE data to calculate ternary mixture relative solubilities tends to over-estimate α_{ij} values (Fig. 7-8 a and [1,2]) but, by and large, correctly orders the mixtures in terms of suitability for SFE using CO₂ (Table 7-11).

²⁵ See also Table 5-1 on p. 104 and particularly the difference between species-specific total solubility pressures at 55 and 75 °C.

Table 7-11. Relative solubilities, calculated using VLE data of the constituent CO_2 + solute binaries, for CO_2 + 37DM10 + C_{10}OH , CO_2 + $n\text{C}_{12}$ + 37DM10 and CO_2 + $n\text{C}_{12}$ + C_{10}OH . This procedure is helpful in a qualitative but not quantitative sense. In all but one scenario (75 °C, 123 bar) it correctly orders the solute mixtures in terms of suitability for CO_2 fractionation.

Solute mixture	55 °C	75 °C	75 °C	Reference
	104 bar	123 bar	140 bar	
37DM10 + C_{10}OH	1.9	1.0	1.6	[34,35,38]
$n\text{C}_{12}$ + 37DM10	3.6	3.3	3.1	[17,35-37]
$n\text{C}_{12}$ + C_{10}OH	6.8	3.2	4.8	[17,34-38]

The totalised absolute deviations (*TAD*) in the bottom row of Table 7-10 indicate that RK-ASPEN, SR-POLAR and PC-SAFT performed similarly at predicting α_{ij} values. However, RK-ASPEN and PC-SAFT correctly position the solute mixtures in terms of fractionation potential from least-suited in the top to most-suited in the bottom but in this regard SR-POLAR and PR-BM failed. PC-SAFT, strangely, produced the smallest *TAD* in SP_{ij} of 5.7 albeit because of a cancellation effect: it tends to over-predict α_{ij}' s and under-predict vapour phase solute loadings (Section 3.4 and [1,2]) which, in combination, produces reasonable SP_{ij} predictions. Nonetheless, it is interesting because throughout PC-SAFT produced the worst equilibrium pressure predictions (Section 3.3 and [1,2]).

4. CONCLUSIONS

This study presented new high pressure VLE data for the CO_2 + $n\text{C}_{12}$ + C_{10}OH ternary mixture. Dual sampling and online chromatography were used to measure phase compositions at 35, 55 and 75 °C and pressures between 68 and 200 bar.

The system exhibits phase behaviour similar to CO_2 + $n\text{C}_{12}$ + 37DM10 [1] but dissimilar to CO_2 + 37DM10 + C_{10}OH [2]. The presence of $n\text{C}_{12}$ enhances solubility in the ternary mixture leading to s-shaped liquid phase curvature and, at higher pressures, a co-solvency pinch in the high- $n\text{C}_{12}$ region. By virtue of this enhanced solubility, vapour phase curves of the continuous two-phase envelope are concave in shape and at higher pressures the existence of detached two-phase regions as witnessed by Smith and Schwarz [18] is conceivable.

Large experimental α_{ij} 's and SP_{ij} 's indicate greater CO₂ solvent efficacy than was observed for the nC_{12} + 37DM10 [1] and 37DM10 + C₁₀OH [2] mixtures. Relative solubility passes through a pressure-dependent optimum, is positively correlated with bulk fraction of the less soluble species, C₁₀OH, and separation of nC_{12} and C₁₀OH is possible across the entire measured solute ratio range. Separation potential passes through a $Z_{C_{10}OH}$ -dependent optimum between $0.50 < Z_{C_{10}OH} < 0.75$. A similar Z_{37DM10} -dependent optimum was not detected in the CO₂ + nC_{12} + 37DM10 system [1]. VLE data of the constituent binaries tend to overestimate α_{ij} which, coupled with the $Z_{C_{10}OH}$ -dependency of both α_{ij} and SP_{ij} , stresses the importance of studying ternary mixtures at multiple solute A:solute B ratios.

RK-ASPEN, SR-POLAR, PR-BM and PC-SAFT correlations failed at 35 °C and pressures between 104 and 200 bar. At 55 and 75 °C, equilibrium pressure correlations via these models produced combined-overall %AAD_p's of 3.1, 3.2, 3.4 and 12.9 %, the relative order of which is similar to results from analogous studies of nC_{12} + 37DM10 [1] and 37DM10 + C₁₀OH [2] mixtures. SR-POLAR was superior at capturing the acute co-solvency pinch, the cubic EOS performed similarly in correlating high pressure liquid curvature and throughout RK-ASPEN vapour trends were more accurate. PC-SAFT failed to match the aforementioned pinch and generally under-predicts solubility resulting in a two-phase envelope too large in surface area. All four models correctly predicted α_{ij} 's positively correlated with $Z_{C_{10}OH}$ and SP_{ij} 's passing through a $Z_{C_{10}OH}$ -dependent optimum. However, PC-SAFT positions these optima at lower $Z_{C_{10}OH}$ values and, in this sense, is more representative of actual system behaviour. Across this series of publications [1,2], predicted α_{ij} 's via RK-ASPEN and PC-SAFT were more accurate whilst PC-SAFT was superior at SP_{ij} estimates albeit because of a cancellation effect.

Density inversions or barotropy were witnessed in the high-C₁₀OH mixtures at 35 °C and high pressures.

ACKNOWLEDGEMENTS

This work is based on the research supported in part by the National Research Foundation of South Africa (Grant specific unique reference number (UID) 83966), Department of Trade and Industry (DTI) of South Africa through the Technology and Human Resources for Industry Programme (THRIP), and Sasol Technology (Pty) Ltd. The financial assistance of the National Research Foundation (DAAD-NRF) and the Skye Foundation Trust is also acknowledged. The authors acknowledge that opinions, findings, and conclusions or recommendations expressed in any publication generated by the supported research are those of the authors, and that the sponsors accept no liability whatsoever in this regard. Aspen Plus® is a registered trademark of Aspen Technology Inc.

REFERENCES

1. F.C.v.N. Fourie, C.E. Schwarz, J.H. Knoetze, CO₂ + *n*-dodecane + 3,7-dimethyl-1-octanol: High pressure experimental phase equilibria data and thermodynamic modelling, *J. Supercrit. Fluids* 130 (2017) 105-117.
2. F.C.v.N. Fourie, C.E. Schwarz, J.H. Knoetze, CO₂ + 3,7-dimethyl-1-octanol + 1-decanol: High pressure experimental phase equilibria data and thermodynamic modelling, *J. Supercrit. Fluids*
3. G. Soave, Equilibrium constants from a modified Redlich-Kwong equation of state, *Chem. Eng. Sci.* 27 (1972) 1197-1203.
4. P.M. Mathias, A Versatile Phase Equilibrium Equation of State, *Ind. Eng. Chem. Process Des. Dev.* 22 (1983) 385-391.
5. J.F. Boston, P.M. Mathias, Phase equilibria in a third-generation process simulator, 2nd International Conference on Phase Equilibria and Fluid Properties in the Chemical Process Industries, West Berlin, 1980.
6. J. Schwartzenuber, H. Renon, Extension of UNIFAC to High Pressures and Temperatures by the Use of a Cubic Equation of State, *Ind. Eng. Chem. Res.* 28 (1989) 1049-1955.
7. D.Y. Peng, D.B. Robinson, A New Two-Constant Equation of State, *Ind. Eng. Chem. Fund.* 15 (1976) 59-64.
8. P.M. Mathias, H.C. Klotz, J.M. Prausnitz, Equation-of-State mixing rules for multicomponent mixtures: the problem of invariance, *Fluid Phase Equilib.* 67 (1991) 31-44.
9. J. Gross, G. Sadowski, Perturbed-Chain SAFT: An Equation of State Based on a Perturbation Theory for Chain Molecules, *Ind. Eng. Chem. Res.* 40 (2001) 1244-1260.
10. J. Gross, G. Sadowski, Application of the Perturbed-Chain SAFT Equation of State to Associating Systems, *Ind. Eng. Chem. Res.* 41 (2002) 5510-5515.
11. F.C.v.N. Fourie, C.E. Schwarz, J.H. Knoetze, Analytic Setup for Multicomponent High-Pressure Phase Equilibria via Dual Online Gas Chromatography, *Chem. Eng. Technol.* 38 (2015) 1165-1172.
12. F.C.v.N. Fourie, C.E. Schwarz, J.H. Knoetze, Analytic High-Pressure Phase Equilibria Part II: Gas Chromatography and Sampling Method Development, *Chem. Eng. Technol.* 39 (2016) 1475-1482.
13. Aspen Plus® V8.8 (34.0.0.110)
14. X. Liang, K. Thomsen, W. Yan, G.M. Kontogeorgis, Prediction of the vapor–liquid equilibria and speed of sound in binary systems of 1-alkanols and *n*-alkanes with the simplified PC-SAFT equation of state, *Fluid Phase Equilib.* 360 (2013) 222-232.
15. A. Grenner, G.M. Kontogeorgis, N. von Solms, M.L. Michelsen, Modeling phase equilibria of alkanols with the simplified PC-SAFT equation of state and generalized pure compound parameters, *Fluid Phase Equilib.* 258 (2007) 83-94.

16. M. Umer, K. Albers, G. Sadowski, K. Leonhard, PC-SAFT parameters from ab initio calculations, *Fluid Phase Equilib.* 362 (2014) 41-50.
17. M. Zamudio, C.E. Schwarz, J.H. Knoetze, Experimental measurement and modelling with Aspen Plus® of the phase behaviour of supercritical CO₂ + (*n*-dodecane + 1-decanol + 3,7-dimethyl-1-octanol), *J. Supercrit. Fluids* 84 (2013) 132-145.
18. S.A.M. Smith, C.E. Schwarz, High pressure phase behaviour of the CO₂ + 1-decanol + *n*-dodecane system, *Fluid Phase Equilib.* 406 (2015) 1-9.
19. A.L. Scheidgen, G.M. Schneider, New phase phenomena in ternary systems at high pressures - Cosolvency and miscibility windows up to 100 MPa, *Phys. Chem. Chem. Phys.* 4,6 (2002) 963-967.
20. A. L. Scheidgen, G. M. Schneider, Fluid phase equilibria of (carbon dioxide + a 1-alkanol + an alkane) up to 100 MPa and T = 393 K: cosolvency effect, miscibility windows, and holes in the critical surface, *J. Chem. Thermodyn.* 32 (2000) 1183-201.
21. K. Gauter, C.J. Peters, A.L. Scheidgen, G.M. Schneider, Cosolvency effects, miscibility windows and two-phase lg holes in three-phase llg surfaces in ternary systems: a status report, *Fluid Phase Equilib.* 171 (2000) 127-149.
22. P.H. van Konynenburg, R.L. Scott, Critical lines and phase equilibria in binary van der Waals mixtures, *Phil. Trans. R. Soc. Lond. A* 298 (1980) 495-540.
23. R.L. Scott, P.H. van Konynenburg, Static properties of solutions. Van der Waals and related models for hydrocarbon mixtures, *Discuss. Faraday Soc.* 49 (1970) 87-97.
24. J. Nochebuena, C. Cautli, J. Ireta, Origin of cooperativity in hydrogen bonding, *Phys. Chem. Chem. Phys.* 19 (2017) 15256-15263.
25. X. Gui, Z. Tang, W. Fei, Solubility of CO₂ in Alcohols, Glycols, Ethers, and Ketones at High Pressures from (288.15 to 318.15) K, *J. Chem. Eng. Data* 56 (2011) 2420-2429.
26. M. Zamudio, The Separation of Detergent Range Alkanes and Alcohol Isomers with Supercritical Carbon Dioxide, Stellenbosch University, South Africa, 2014 PhD Dissertation.
27. Y. Wang, L. Hong, D. Tapriyal, I.C. Kim, I.-H. Paik, J.M. Crosthwaite, A.D. Hamilton, M.C. Thies, E.J. Beckman, R.M. Enick, J.K. Johnson, Design and Evaluation of Nonfluorous CO₂-Soluble Oligomers and Polymers, *J. Phys. Chem. B* 113 (2009) 14971-14980.
28. P.W. Bell, A.J. Thote, Y. Park, R.B. Gupta, C.B. Roberts, Strong Lewis Acid-Lewis Base Interactions between Supercritical Carbon Dioxide and Carboxylic Acids: Effects on Self-association, *Ind. Eng. Chem. Res.* 42 (2003) 6280-6289.
29. A. Fujii, T. Ebata, N. Mikami, Direct Observation of Weak Hydrogen Bonds in Microsolvated Phenol: Infrared Spectroscopy of OH Stretching Vibrations of Phenol-CO and -CO₂ in S0 and D0, *J. Phys. Chem. A* 106 (2002) 10124-10129.
30. P. Raveendran, Y. Ikushima, S.L. Wallen, Polar Attributes of Supercritical Carbon Dioxide, *Acc. Chem. Res.* 38 (2005) 478-485.

31. L. Bao, S. Fang, D. Hu, L. Zhao, W. Yuan, T. Liu, Enhancement of the CO₂-philicity of poly(vinyl ester)s by end-group modification with branched chains, *J. Supercrit. Fluids* 127 (2017) 129-136.
32. B. Gwinner, D. Roizard, F. Lapique, E. Favre, R. Cadours, P. Boucot, P.-L. Carrette, CO₂ Capture in Flue Gas: Semiempirical Approach to Select a Potential Physical Solvent, *Ind. Eng. Chem. Res.* 45 (2006) 5044-5049.
33. P. Raveendran, S.L. Wallen, Cooperative C–H...O Hydrogen Bonding in CO₂-Lewis Base Complexes: Implications for Solvation in Supercritical CO₂, *J. Am. Chem. Soc.* 124 (2002) 12590-12599.
34. C.J. Chang, K.-L. Chiu, C.-Y. Day, A new apparatus for the determination of P–x–y diagrams and Henry's constants in high pressure alcohols with critical carbon dioxide, *J. Supercrit. Fluids* 12 (1998) 223-237.
35. M. Zamudio, C.E. Schwarz, J.H. Knoetze, Phase equilibria of branched isomers of C₁₀-alcohols and C₁₀-alkanes in supercritical carbon dioxide, *J. Supercrit. Fluids* 59 (2011) 14-26.
36. A.B. De Haan, *Supercritical Fluid Extraction of Liquid Hydrocarbon Mixtures*, Delft University of Technology, Netherlands, 1991 PhD Dissertation.
37. I. Nieuwoudt, M. du Rand, Measurement of phase equilibria of supercritical carbon dioxide and paraffins, *J. Supercrit. Fluids* 22 (2002) 185-199.
38. W.-L. Weng, J.-T. Chen, M.-J. Lee, High-Pressure Vapor-Liquid Equilibria for Mixtures Containing a Supercritical Fluid, *Ind. Eng. Chem. Res.* 33 (1994) 1955-1961.
39. G. Brunner, Industrial process development. Countercurrent multistage gas extraction (SFE) processes, *J. Supercrit. Fluids* 13 (1998) 283-301.

Chapter 8: CONSOLIDATING TERNARY PHASE BEHAVIOUR

This chapter consolidates the results of the preceding three chapters with a focus on both experimental and model-predicted behaviour. A comparative discussion on model-predicted relative solubilities and separation potentials was provided in Chapter 7 (p. 211) and is not included in Chapter 8.

8.1 EXPERIMENTAL

8.1.1 Ternary mixture phase behaviour

The two nC_{12} -containing systems present enhanced solubility and a co-solvency pinch in the high- nC_{12} region (Sections 3.5 and 3.4 on pp. 120 and 192 respectively). By virtue of this enhanced solubility, concave vapour phase curvature occurs in the medium pressure range prior to detachment of the separate two-phase areas. Behaviour in the $CO_2 + 37DM10 + C_{10}OH$ system differs significantly and liquid phase curves remain convex regardless the solute ratio or pressure (Section 3.4 on p. 154). In general, the two nC_{12} -containing systems and $nC_{12} + 37DM10$ in particular are more soluble. In these systems pressure-dependent changes start to develop and complete miscibility is reached at lower pressures. Fig. 8-1 shows comparative phase behaviour at two temperatures and is effective at highlighting these differences. Each diagram in Fig. 8-1 represents the highest experimentally measured pressure, specific to that mixture and temperature, where a continuous two-phase envelope existed (i.e., the two-phase band has not yet detached from the more soluble binary axis). The exceptions are Fig. 8-1 a and d which could have illustrated phase behaviour at the non-standard pressures of 106.5 and 143.5 bar, but comparisons at the standard pressures of 104 bar (55 °C) and 140 bar (75 °C) are more informative.

The $C_{10}OH$ -containing systems display density inversions which could destabilize column hydrodynamics (Sections 3.6 and 3.4 on pp. 170 and 192 respectively). However, the low temperature and high pressure conditions where these were observed appear far removed from the preferred operating conditions of a SFE process (see Figs. 6-8 on p. 169 and 7-8 on p. 208).

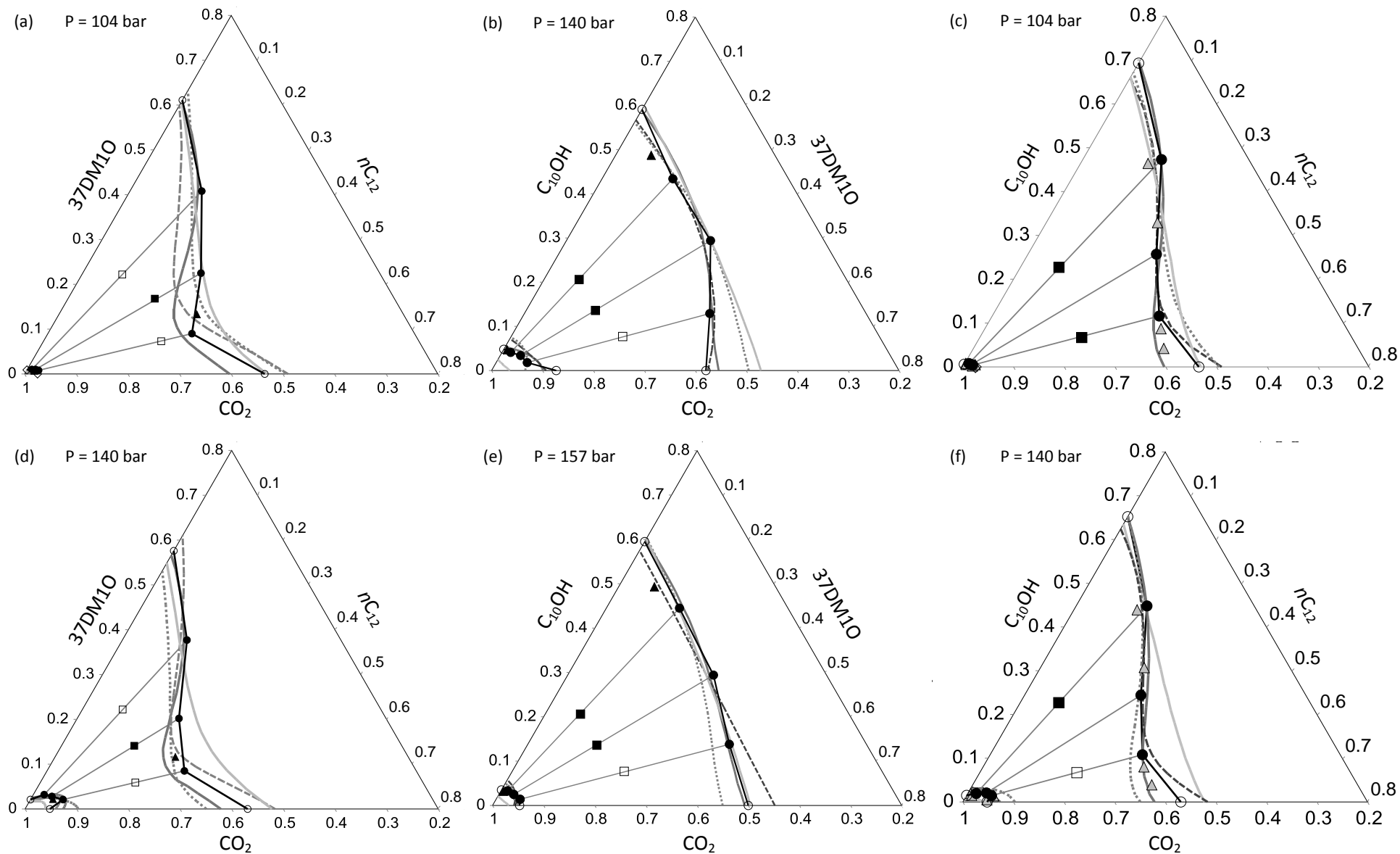


Figure 8-1. Comparative experimental and model-predicted ternary mixture phase behaviour at 55 °C for (a) CO₂ + nC₁₂ + 37DM10; (b) CO₂ + 37DM10 + C₁₀OH; (c) CO₂ + nC₁₂ + C₁₀OH; and at 75 °C for (d) CO₂ + nC₁₂ + 37DM10; (e) CO₂ + 37DM10 + C₁₀OH; and (f) CO₂ + nC₁₂ + C₁₀OH. Pressures are indicated on the diagrams.

8.1.2 Ternary mixture relative solubility and separation potential

In the two nC_{12} -containing systems, relative solubility (α_{ij}) is positively correlated with bulk content of the less soluble species (Sections 3.6.1 and 3.5.1 on pp. 130 and 205 respectively). In contrast, α_{ij} in the $CO_2 + 37DM10 + C_{10}OH$ systems presents no clear dependence on solute-solute ratio or Z_i (Section 3.5.1 on p. 167). This impacts separation potential (SP_{ij}) in the $CO_2 + \text{solute A} + \text{solute B}$ systems as follows:

- i. $nC_{12} + 37DM10$: α_{ij} governs SP_{ij} and the latter increases with bulk content of the less soluble species. A Z_{37DM10} -dependent SP_{ij} optimum may exist at $Z_{37DM10} > 0.75$ (Section 3.6.1 on p. 130).
- ii. $37DM10 + C_{10}OH$: α_{ij} is independent of $Z_{C_{10}OH}$ and therefore Y_i dominates SP_{ij} and the latter is positively correlated with bulk fraction of the less soluble species (Section 3.5.1 on p. 167).
- iii. $nC_{12} + C_{10}OH$: compared to [i] the α_{ij} and Y_i contributions to SP_{ij} are more balanced and SP_{ij} passes through a $Z_{C_{10}OH}$ -dependent optimum within the range $0.25 < Z_{C_{10}OH} < 0.75$ (Section 3.5.1 on p. 205).

These results could have interesting implications for a continuous SFE process with dynamic feed composition, or a SFE process where feed composition is intentionally manipulated to tune performance.

System-specific α_{ij} and SP_{ij} decrease in the order $[nC_{12} + C_{10}OH] > [nC_{12} + 37DM10] > [37DM10 + C_{10}OH]$. This trend is reflected in Table 7-10 on p. 211 but the comparative charts in Fig. 8-2 and particularly Fig. 8-3, each with similarly scaled y-axes, are revealing. The apparent inefficiency of separating 37DM10 and $C_{10}OH$ should be treated on a case for case basis. If the intent is to separate the two alcohols the small maximum α_{ij} 's presented in Fig. 8-2 are reason for concern. If, however, the intent is to remove nC_{12} from a mixed alcohol stream, the 37DM10 + $C_{10}OH$ interaction parameters from this work will aid the modelling of a four component system comprising $CO_2 + \text{alkane} + \text{branched alcohol} + \text{linear alcohol}$.

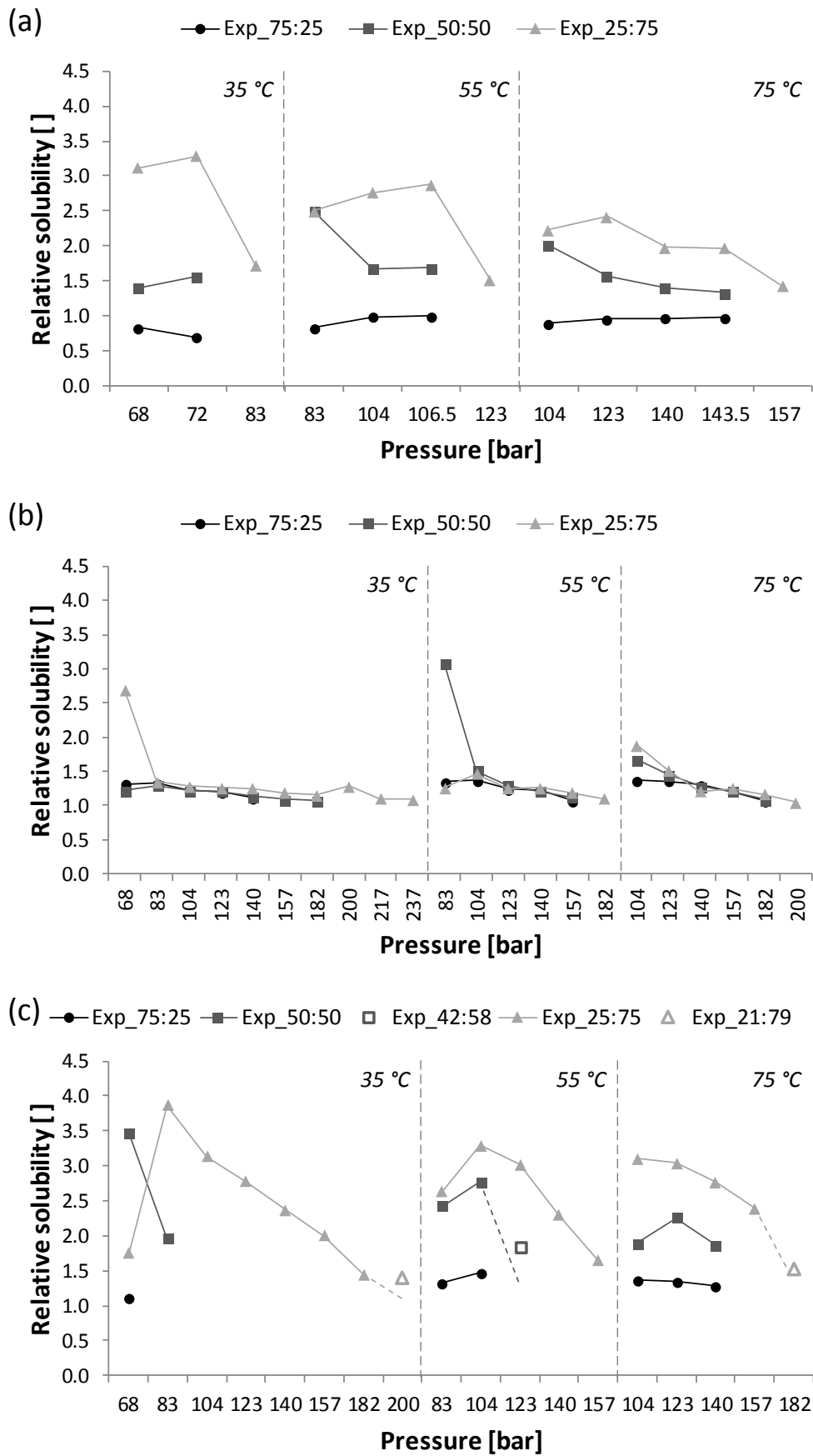


Figure 8-2. Comparing experimental relative solubility, α_{ij} , for the (a) CO₂ + nC₁₂ + 37DM10; (b) CO₂ + 37DM10 + C₁₀OH; and (c) CO₂ + nC₁₂ + C₁₀OH ternary mixtures.

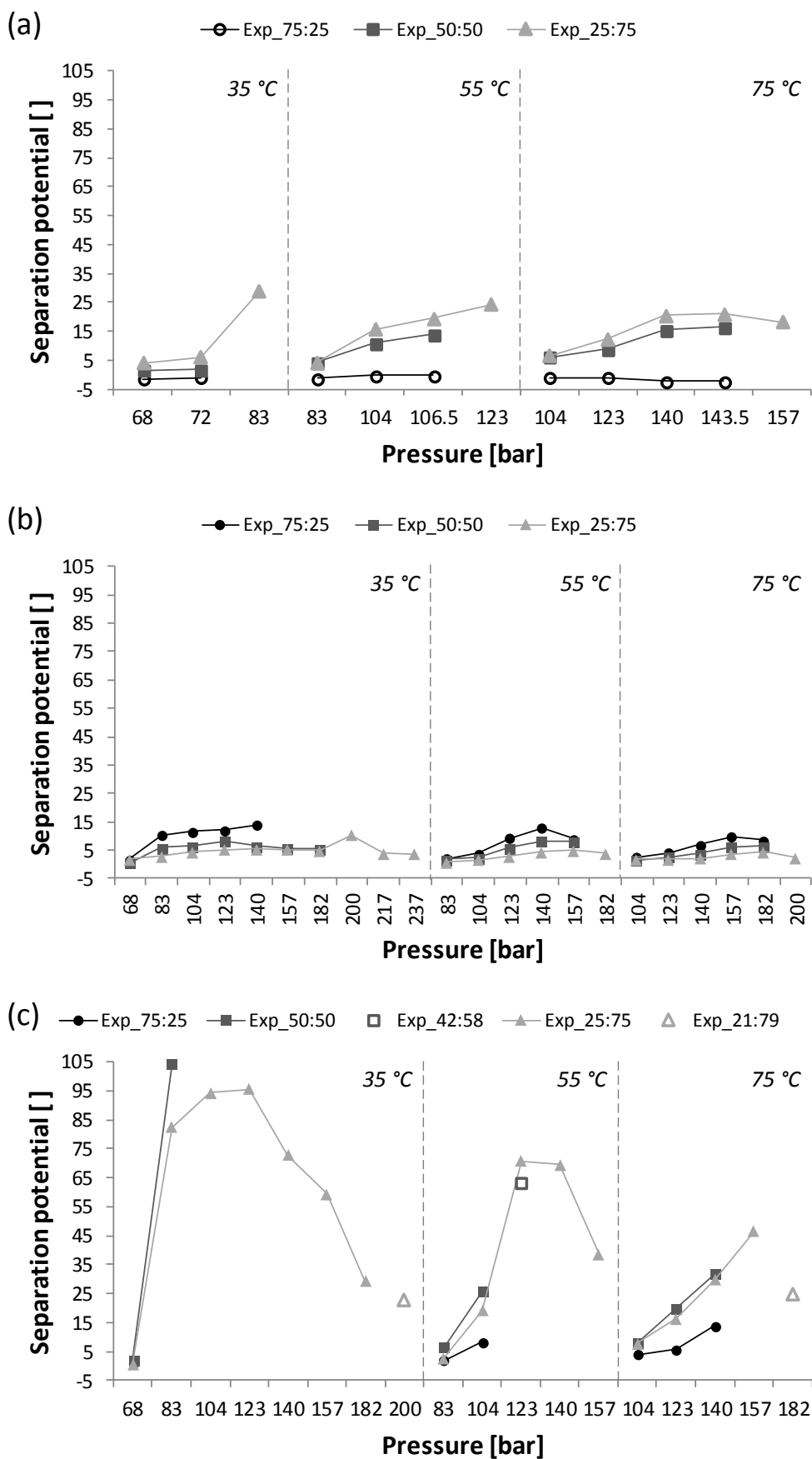


Figure 8-3. Comparing experimental separation potential, SP_{ij} , for the (a) $CO_2 + nC_{12} + 37DM10$; (b) $CO_2 + 37DM10 + C_{10}OH$; and (c) $CO_2 + nC_{12} + C_{10}OH$ ternary mixtures.

Relative solubility estimates using binary VLE data tend to overestimate α_{ij} and the errors are significant (Table 8-1, and Figs. 5-8 a, 6-8 a and 7-8 a on pp. 131, 169 and 208). Considering all three ternary mixtures, corresponding binary VLE data are available to estimate 19 α_{ij} values at temperature and pressure conditions matching those measured in this study. For this comparison, experimental α_{ij} 's were averaged for the 75:25, 50:50 and 25:75 mixtures. In 17 of the 19 cases, binary VLE data overestimate α_{ij} and the error expressed as %AAD_α for all 19 cases is 125 %. The extrapolation of binary P - x_i curves, though not ideal, does not detract from the key message: ignoring all entries based on at least one extrapolated binary composition, %AAD_α changes to 169 and 115 % with and without the outlier of 655 % included. These results reemphasise that ternary, and not only binary VLE data, are essential to accurate separation predictions.

Table 8-1. Actual and binary-predicted relative solubilities (α_{ij}) for the mixtures studied in this work. Estimating ternary mixture α_{ij} using VLE data of the constituent binary systems tends to over-predict α_{ij} and the error is significant.

T [°C]	P [bar]	CO ₂ + nC ₁₂ + 37DM10				CO ₂ + 37DM10 + C ₁₀ OH				CO ₂ + nC ₁₂ + C ₁₀ OH			
		$\alpha_{_3^\circ}$	$\alpha_{_2^\circ}$	%AD	Reference	$\alpha_{_3^\circ}$	$\alpha_{_2^\circ}$	%AD	Reference	$\alpha_{_3^\circ}$	$\alpha_{_2^\circ}$	%AD	Reference
35	83					1.3	2.3	72 %	[1,1,1,1]				
	104					1.2	4.0	219 %	[1,1,1,1]				
	123					1.2	9.2	655 %	[1,1,1,1]				
55	83									2.1	1.1*	46 %	[2,3,4,1]
	104	1.8	3.6	102 %	[5,3,1,1]	1.4	1.9	28 %	[1,1,4,1]	2.5	6.8	170 %	[5,3,4,1]
	106.5	1.9	4.5	142 %	[5,3,1,1]								
	123					1.3	1.9	51 %	[1,1,4,1]				
	140					1.2	3.7	203 %	[1,1,1,1]				
75	104									2.1	2.6	23 %	[2,3,6,6]
	123	1.6	3.3	100 %	[2,3,1,1]	1.4	1.0*	32 %	[1,1,6,6]	2.2	3.2	45 %	[2,3,6,6]
	140	1.4	3.1	111 %	[3,3,1,1]	1.3	1.6	25 %	[1,1,6,6]	2.0	4.8	145 %	[3,3,6,6]
	143.5	1.4	3.6	155 %	[3,3,1,1]								
	157					1.2	1.9	56 %	[1,1,6,6]				
%AAD between $\alpha_{_3^\circ}$ and $\alpha_{_2^\circ}$ (all entries)										19 values		125 %	
%AAD between $\alpha_{_3^\circ}$ and $\alpha_{_2^\circ}$ (entries with extrapolated binary data excluded)										10 values		169 %	
%AAD between $\alpha_{_3^\circ}$ and $\alpha_{_2^\circ}$ (entries with extrapolated binary data and 655 % excluded)										9 values		115 %	

($\alpha_{_3^\circ}$) Actual α_{ij} averaged for the 75:25, 50:50 and 25:75 mixtures using ternary VLE data; ($\alpha_{_2^\circ}$) Estimated α_{ij} using VLE data of the constituent binary systems; (%AD) Percentage absolute deviation; (*) $\alpha_{_3^\circ} > \alpha_{_2^\circ}$; (%AAD) Percentage average absolute deviation; The four references specific to each CO₂ + solute A + solute B mixture represent the binary solute A vapour, solute A liquid, solute B vapour and solute B liquid phases; Underlined references imply P - x_i envelopes were extrapolated to intersect the target isobars.

8.2 MODELLING

8.2.1 Model-predicted ternary mixture vapour and liquid pressures

In all three ternary mixtures the relative ability of the models to predict equilibrium pressures degrades in the order RK-ASPEN > SR-POLAR > PR-BM > PC-SAFT. All four models failed to predict 35 °C vapour phase pressures in the C₁₀OH-containing systems whilst liquid phase pressure predictions were poor. Throughout, the liquid-overall error in predicted pressure was smaller than the vapour-overall error (see Table 5-11 on p. 119, Table 6-9 on p. 153 and Table 7-9 on p. 191). For the three cubic EOS these differed by an average of 1.8 percentage points (9 values) whilst for PC-SAFT the average difference was 10 percentage points (3 values). The system-specific model performance is summarised in Table 8-2 where 35 °C data were excluded for CO₂ + nC₁₂ + 37DM10 to enable comparison with the C₁₀OH-containing systems.

Table 8-2. Overall-Combined %AAD_P values for the model-predicted liquid and vapour phase equilibrium pressures in the systems CO₂ + nC₁₂ + 37DM10, CO₂ + nC₁₂ + C₁₀OH and CO₂ + 37DM10 + C₁₀OH. Errors increase from left to right and from top to bottom.^a

Model	nC ₁₂ + 37DM10	nC ₁₂ + C ₁₀ OH	37DM10 + C ₁₀ OH
RK-ASPEN	2.3	3.1	4.0
SR-POLAR	2.7	3.2	4.0
PR-BM	3.3	3.4	4.4
PC-SAFT	9.0	12.9	18.3

^a To enable improved comparison only model-predicted data at 55 and 75 °C were considered. Overall implies deviations were calculated for both temperatures and Combined implies deviations were calculated for both the vapour and liquid phases.

8.2.2 Model-predicted ternary mixture phase behaviour

RK-ASPEN low pressure liquid correlations tend to be solute rich. It is able to capture the convex-to-concave transition in nC₁₂-containing systems but fared better in nC₁₂ + 37DM10 than in nC₁₂ + C₁₀OH. Throughout, RK-ASPEN produced the most accurate vapour correlations, an important aspect for SFE design. Excluding 35 °C in the C₁₀OH-containing systems, RK-ASPEN performance is largely temperature independent and, in general, RK-ASPEN outperformed SR-POLAR, PR-BM and PC-SAFT at correlating vapour and liquid phase compositions.

SR-POLAR can mimic the s-shaped liquid phase complexity that exists in the nC_{12} -containing systems but, in contrast to RK-ASPEN, it fared better in $nC_{12} + C_{10}OH$. Between 55 and 75 °C it exhibits more temperature dependence than RK-ASPEN, an observation applicable to both the vapour and liquid phases. SR-POLAR tends to over-predict vapour phase solubility in the high- $C_{10}OH$ regions.

PR-BM cannot match the acute angle of the co-solvency pinch in the high- nC_{12} regions. In agreement with SR-POLAR, vapour and liquid phase performance exhibits temperature dependence. In the nC_{12} -containing ternaries at 75 °C and medium-to-high pressures it predicts a two-phase band that narrows excessively toward the $CO_2 + nC_{12}$ binary axis. Where large vapour phase deviations occur, solubility is typically overestimated in the high- nC_{12} and $C_{10}OH$ regions and underestimated in the high-37DM1O regions.

PC-SAFT is unsuccessful at correlating any of the convex-to-concave liquid curvature that exists in the nC_{12} -containing systems. Throughout, liquid trends are solute-deficient at low pressures and, as pressure increases, trends progressively shift away from the CO_2 -corner to end up solute-rich. Vapour correlations start off being CO_2 -rich at low pressures, a deviation that worsens with increasing pressure.

Via all four models, phase composition predictions in the $C_{10}OH$ -containing systems failed at 35 °C and pressures higher than 83 bar (Section 3.2 on p. 187).

8.3 REFERENCES

1. M. Zamudio, C.E. Schwarz, J.H. Knoetze, Phase equilibria of branched isomers of C_{10} -alcohols and C_{10} -alkanes in supercritical carbon dioxide, *J. Supercrit. Fluids* 59 (2011) 14-26.
2. A.B. De Haan, *Supercritical Fluid Extraction of Liquid Hydrocarbon Mixtures*, Delft University of Technology, Netherlands, 1991 PhD Dissertation.
3. M. Zamudio, C.E. Schwarz, J.H. Knoetze, Experimental measurement and modelling with Aspen Plus® of the phase behaviour of supercritical $CO_2 + (n$ -dodecane + 1-decanol + 3,7-dimethyl-1-octanol), *J. Supercrit. Fluids* 84 (2013) 132-145.
4. C.J. Chang, K.-L. Chiu, C.-Y. Day, A new apparatus for the determination of P-x-y diagrams and Henry's constants in high pressure alcohols with critical carbon dioxide, *J. Supercrit. Fluids* 12 (1998) 223-237.
5. I. Nieuwoudt, M. du Rand, Measurement of phase equilibria of supercritical carbon dioxide and paraffins, *J. Supercrit. Fluids* 22 (2002) 185-199.
6. W.-L. Weng, J.-T. Chen, M.-J. Lee, High-Pressure Vapor-Liquid Equilibria for Mixtures Containing a Supercritical Fluid, *Ind. Eng. Chem. Res.* 33 (1994) 1955-1961.

Chapter 9: CONCLUSIONS

The main objectives of this study, as communicated in Section 1.4 of Chapter 1, were to:

- i. Design, construct and commission an analytic experimental setup for high pressure multi-component phase composition measurements. The apparatus should be able to handle alkanes and alcohols in the range $C_8 - C_{16}$ and enable operation up to 150 °C and 300 bar.
- ii. Define an experimental outline and measure ternary mixture phase composition data for three systems. These are a) $CO_2 + nC_{12} + 37DM10$; b) $CO_2 + 37DM10 + C_{10}OH$; and c) $CO_2 + nC_{12} + C_{10}OH$. The experimental outline should also enable a comparative study using ethane as solvent.
- iii. Evaluate CO_2 as solvent to fractionate the three hydrocarbon mixtures mentioned in [ii].
- iv. Evaluate four thermodynamic models for their ability to correlate the equilibrium vapour and liquid phase pressures and compositions measured in this study.

The remainder of this chapter summarises conclusions specific to Chapters 2 - 8. Conclusions central to achieving the abovementioned four objectives are labelled accordingly. Chapters 3 - 7 were written in manuscript style and contain separate conclusions sections, the page number locations of which are bracketed in the section headings that follow. Please revisit these and treat their content as supplemental to Chapter 9.

9.1 CHAPTER 2: EQUIPMENT REVIEW AND CONCEPTUAL DESIGN

A review of published equipment designs for high-pressure phase equilibria studies was conducted, and enabled the following conclusions:

- A paradigm shift is necessary to address the lack of detailed information on successes, and failures, related to high pressure phase equilibria equipment design, construction and operation. Visuals indicating to what extent, if at all, circulatory systems disrupt equilibrium is one such example.
- In situ analysis may dominate analytic phase equilibria studies in the long run but improved methods to extract, homogenise and transfer samples, and a larger variety of commercialised samplers, will benefit academia and industry in the medium term.
- Variable cell volume and sampling height and visual observation of the cell content are valuable.
- Cell internal geometry impacts mixing and phase separation efficiency and requires consideration.

- An analytical dual-phase circulation setup enabling counter and co-current circulation and online density measurement of both phases enables operational versatility and appears promising. Despite the stumbling blocks related to hardware, this method justifies consideration in future.
- A static analytical method was deemed optimal for this study.

9.2 CHAPTER 3: PUBLICATION 1 (P. 75)

Chapter 3 focussed on equipment design, construction, commissioning and validation. Conducting this work enabled the following learnings and conclusions:

- Variable cell volume enables dual one-phase region sampling, a troubleshooting tool, and venting from the one-phase region followed by operation at lower pressure but constant bulk composition.
- Adjustable sampling height is useful as a troubleshooting tool. The independent extraction and analysis of two samples from the same phase assists in the identification of systemic errors.
- The eccentric piston-cylinder assembly was effective at promoting mixing inside the cylinder.
- A high pressure analytic phase equilibria setup capable of operation at 150 °C and 300 bar was developed. The apparatus enables the study of ternary and higher mixtures with constituents ranging from volatile gases to mid-length hydrocarbons. Simultaneous sampling from two co-existing phases coupled with a unique GC configuration and quantitative calibration methods enable concurrent parallel online analysis. [objective i]

9.3 CHAPTER 4: PUBLICATION 2 (P. 95)

Chapter 4 covered additional details of the apparatus and experimental methodology. Visual observations of the cell interior, often not visible to the naked eye, were central to this work and a number of interesting learnings resulted. [objective i]

- An adapted manual calibration injection technique with syringe spacers and reduced rapidity of sample introduction limited liner overload and pressure wave effects. This enabled a decoupled calibration method that is independent of the equilibrium cell sample extraction, transfer and injection pathways, and serves as a rigorous test for systemic errors or repeatable inaccuracies.
- An upward ramp in GC column flow enables one to initially limit species transfer onto the column (i.e., high split ratio) followed by species acceleration through the column (i.e., low split ratio).

- At least eleven factors, some of which change throughout an experimental run, impact optimum sample size (Section 2.3 on p. 84). This highlights the complexity of the experimental work.
- A successful sampling methodology involving slow and fast purge and analysis runs was developed.
- As a means of temperature control, jacketed fluid circulation has proven sufficient for bubble and dew point studies where the dynamic nature of the experiment is compatible with larger temperature non-uniformities. However, the exclusive use of jacketed circulation was inadequate for the analysis of equilibrium phase compositions.
- Small temperature gradients may cause non-visible liquid particles to settle from the vapour phase and contact, coagulate on, and trickle down the vapour capillary culminating in a visible droplet. This was recreated for illustrative purposes by imposing a 0.4 °C temperature spread in the cell.
- Disruptions to equilibrium conditions proved more likely to impede vapour phase than liquid phase sampling. If sampling is conducted sequentially, start with the vapour phase.
- Three sampling-related disturbance types were identified and communicated to academia. Global mist formation, localized mist formation and no-warning droplet formation occurred even though pressure and temperature remained constant to within 0.1 bar and 0.01 °C.
- The vapour capillary PEEK cone reduced the negative impact of mist formation on sampling but could prove counter-productive if mixing created suspended liquid drops which clogged the cone.
- Considering the accuracy of temperature and pressure measurements typically encountered in related literature, the stability of these two parameters should be regarded as necessary but insufficient conditions for a stable equilibrated system. Visual observation of the cell contents, and the vapour phase in particular, was essential to gauge the extent of phase settling and ensure accurate vapour phase sampling.

9.4 CHAPTER 5: PUBLICATION 3 (P. 134)

Chapter 5 reported on the experimental and model-predicted phase behaviour of $\text{CO}_2 + n\text{C}_{12} + 37\text{DM10}$.

- An experimental outline was defined, it proved successful throughout the remainder of the study and shows promise for a comparative study using ethane as solvent. [objective ii]
- The apparatus enables the generation of reproducible data over an extended period of time.
- An adapted experimental method using one sampler was developed and temporarily implemented.

- New high pressure VLE data were measured for the ternary $\text{CO}_2 + n\text{C}_{12} + 37\text{DM10}$ mixture, and the RK-ASPEN, SR-POLAR, PR-BM and PC-SAFT models were evaluated for their ability to correlate these data. [objectives ii and iv]
- The ternary mixture displayed enhanced solubility presenting as s-shaped liquid curvature and, in the high- $n\text{C}_{12}$ region, a pinched two-phase band.
- Experimental α_{ij} and SP_{ij} values increased with bulk 37DM10 content, CO_2 cannot separate a 75:25 $n\text{C}_{12}$:37DM10 mixture, and low pressure α_{ij} 's should be interpreted with caution. [objective iii]
- RK-ASPEN and PC-SAFT provided the best and worst correlation of equilibrium pressures with respective %AAD_p's of 3.1 and 8.5 %. RK-ASPEN was impressive in its ability to capture the co-solvency pinch and s-shaped liquid phase complexity. The models did not fail at 35 °C. [objective iv]
- The four models correctly predicted α_{ij} 's increasing with $Z_{37\text{DM10}}$. The predicted $Z_{37\text{DM10}}$ -dependent SP_{ij} optima at $Z_{37\text{DM10}} > 0.75$ seem plausible but could not be validated for the experimental system.

9.5 CHAPTER 6: MANUSCRIPT 4 (P. 172)

Chapter 6 reported on the experimental and model-predicted phase behaviour of $\text{CO}_2 + 37\text{DM10} + \text{C}_{10}\text{OH}$.

- New high pressure VLE data were measured for the ternary $\text{CO}_2 + 37\text{DM10} + \text{C}_{10}\text{OH}$ mixture, and the RK-ASPEN, SR-POLAR, PR-BM and PC-SAFT models were evaluated for their ability to correlate these data. [objectives ii and iv]
- The absence of enhanced solubility coupled with convex liquid curves at all pressures were noteworthy and most likely indicate that coexisting detached two-phase regions do not occur.
- CO_2 can fractionate all measured 37DM10: C_{10}OH ratios but with limited efficacy. Experimental α_{ij} 's were virtually independent of solute-solute ratio and SP_{ij} , being governed by $Y_{37\text{DM10}}$, was positively correlated with bulk content of the more soluble species. The latter represents a significant behavioural difference between the $n\text{C}_{12} + 37\text{DM10}$ and $37\text{DM10} + \text{C}_{10}\text{OH}$ mixtures. [objective iii]
- In essence, all four models failed at 35 °C, the optimum fractionation temperature, and the system proved more challenging to model than $\text{CO}_2 + n\text{C}_{12} + 37\text{DM10}$. At 55 and 75 °C, RK-ASPEN and SR-POLAR produced the smallest %AAD_p's of 4.0 % and RK-ASPEN was marginally superior at correlating vapour and liquid phase compositions. [objective iv]
- A qualitative comparison of the model-predicted α_{ij} 's and SP_{ij} 's highlighted significant inter-model variance, and no model was able to match the $Z_{\text{C}_{10}\text{OH}}$, P and T dependency of the actual system.

- At 35 °C and 187.5 bar, the 25:75 37DM10:C₁₀OH mixture passed through a density inversion and interesting sequential images thereof were presented.

9.6 CHAPTER 7: MANUSCRIPT 5 (P. 212)

Chapter 7 reported on the experimental and model-predicted phase behaviour of CO₂ + *n*C₁₂ + C₁₀OH.

- New high pressure VLE data were measured for the ternary CO₂ + *n*C₁₂ + C₁₀OH mixture, and the RK-ASPEN, SR-POLAR, PR-BM and PC-SAFT models were evaluated for their ability to correlate these data. [objectives ii and iv]
- In agreement with *n*C₁₂ + 37DM10, *n*C₁₂ enhances ternary mixture solubility leading to s-shaped liquid phase curvature and, at higher pressures, a co-solvency pinch in the high-*n*C₁₂ region. The presence of two distinct coexisting two-phase regions, though not measured, is conceivable.
- Substantial *n*C₁₂-induced disruption of the cooperativity amongst 1-alcohols may i) weaken alcohol-alcohol interactions; and ii) free up proton donors and acceptors enabling hydrogen bonding and Lewis Acid-Lewis Base interactions with the charge-separated CO₂. In combination, these phenomena may present as co-solvency but this hypothesis requires further mechanistic research.
- CO₂ can separate all measured ratios of *n*C₁₂ and C₁₀OH, relative solubility increased with bulk C₁₀OH content and large α_{ij}' s and SP_{ij}' s indicated that within this study *n*C₁₂ + C₁₀OH is best-suited for fractionation with CO₂. Causality between *n*C₁₂-induced disruption of the 1-alcohol networked structure and solute ratio-dependent α_{ij}' s is conceivable. [objective iii]
- Balanced α_{ij} and Y_i contributions to SP_{ij} lead to a $Z_{C_{10}OH}$ -dependent SP_{ij} optimum between $0.50 < Z_{C_{10}OH} < 0.75$. A similar Z_{37DM10} -dependent SP_{ij} optimum was not present in *n*C₁₂ + 37DM10.
- The models mostly failed at 35 °C. At 55 and 75 °C, RK-ASPEN produced the lowest %AAD_P of 3.1 % with marginal superiority over SR-POLAR and PR-BM. SR-POLAR was best-able to correlate the acute co-solvency pinch and throughout RK-ASPEN vapour correlations were superior. [objective iv]
- The four models correctly predicted α_{ij}' s increasing with $Z_{C_{10}OH}$ and $Z_{C_{10}OH}$ -dependent SP_{ij} optima. PC-SAFT better approximated actual system behaviour by positioning the optima at lower $Z_{C_{10}OH}'$ s.
- Density inversions or barotropy occurred in the high-C₁₀OH mixtures at 35 °C and high pressures.

9.7 CHAPTER 8: CONSOLIDATING TERNARY PHASE BEHAVIOUR

Chapter 8 consolidated and compared experimental and model-predicted phase behaviour of the three measured systems. This enabled the following learnings and conclusions:

- The solute ratio-dependent α_{ij} 's and SP_{ij} 's of the nC_{12} -containing systems could have interesting implications for a SFE process with an unstable or manipulable feed composition. [objective iii]
- VLE data of the constituent binaries tended to significantly overestimate α_{ij} and the error, expressed as $\%AAD_{\alpha}$, was 125 %. In addition, this approach cannot capture the relationship between α_{ij} and bulk solute ratio as observed for the nC_{12} -containing systems. This emphasises the importance of ternary mixture VLE data in understanding and predicting separation performance.
- Regardless the model, $\%AAD_p$'s in predicted vapour and liquid phase pressures increased in the order $[nC_{12} + 37DM10] < [nC_{12} + C_{10}OH] < [37DM10 + C_{10}OH]$ and regardless the system, $\%AAD_p$'s increased in the order $RK-ASPEN < SR-POLAR < PR-BM < PC-SAFT$. Throughout, system and model-specific liquid phase $\%AAD_p$'s were smaller than those for the vapour phase. [objective iv]
- Equilibrium phase composition correlations also degraded in the order $RK-ASPEN \rightarrow SR-POLAR \rightarrow PR-BM \rightarrow PC-SAFT$. The accuracy of $RK-ASPEN$ vapour correlations is of importance for SFE design.
- At 35 °C in the $C_{10}OH$ -containing systems, model failure was prevalent and high pressure density inversions occurred in the high- $C_{10}OH$ region. A relation between these observations is not implied.
- $RK-ASPEN$ and $PC-SAFT$ correctly ordered the mixtures in terms of suitability for SFE using CO_2 and, on average, produced the best α_{ij} estimates. SP_{ij} estimates via $PC-SAFT$ were superior in all cases.

9.8 SUMMARY REMARKS

This study started with a review of published equipment designs for high-pressure phase equilibria research, which served as point of departure for method evaluation and conceptual equipment design. An apparatus suitable for the planned experimental work was successfully designed, constructed, commissioned, validated and, importantly, communicated to academia. Observation of the cell interior proved essential to gauge the extent of phase settling and ensure accurate vapour phase sampling, and images were used to convey the challenges associated with high-pressure sampling.

The new apparatus was used to study three asymmetric CO_2 + solute A + solute B mixtures in the temperature and pressure ranges 35 - 75 °C and 68 - 237 bar. The presence of $n\text{C}_{12}$ resulted in enhanced solubility and, in the high $n\text{C}_{12}$ -region, co-solvency. Relative solubility in the $n\text{C}_{12}$ + alcohol mixtures was dependent on bulk solute ratio which poses optimisation opportunities for related supercritical fluid extraction processes. The C_{10}OH -containing systems exhibited interesting density inversions and these were visually documented. Given the scarcity of high pressure ternary VLE data, each of the aforementioned three data sets represents a valuable academic contribution. The defined experimental outline not only proved successful but supports a comparative study using ethane as solvent.

Four thermodynamic models were evaluated for their ability to correlate the equilibrium pressures and phase compositions measured in this work. In general, model performance deteriorated in the order $\text{RK-ASPEN} \rightarrow \text{SR-POLAR} \rightarrow \text{PR-BM} \rightarrow \text{PC-SAFT}$. However, relative solubility and separation potential – important parameters for determining the viability of a supercritical fractionation process – were best approximated by PC-SAFT.

Chapter 10: RECOMMENDATIONS AND FUTURE WORK

Based on the results from this study, a number of areas for future investigation were identified. These recommendations are listed below.

- A dual-phase circulation method was rejected partly because of the potential for pulsation disturbances. It would be an interesting and valuable exercise to quantify the tendency of pulsation disturbances to disrupt equilibrium conditions far from, and near to, the mixture total solubility pressure. Using visuals to present these results, in a similar fashion to Chapter 4, would benefit academia. Chapter 4 has shown that equilibrium disruptions may occur even if pressure remains constant to a resolution of 0.1 bar which provides a point of departure for the requisite accuracy of pressure measurement to conduct this test.
- A dual-phase circulation method was rejected partly because performance and lifetime of the sampling valves could not be guaranteed. It would be worthwhile to revisit this proposal and research current product availability. Resources permitting and taking cognisance of the associated risk, one could utilise the valves considered originally and conduct an in-house performance test.
- Having quantified circulation pump and sampling valve performance, one may be better positioned to justify the expense associated with an online density measurement unit.
- GC inlet liner geometry, diameter and volume impact the reproducibility of calibration injections and online analysis. The Laminar Cup Splitter developed by Restek provides a convoluted flow path to promote linear splitting of high molecular weight species and may benefit future studies.
- An in-oven GC cooling trap will enhance flexibility of the sampling and calibration procedures. The JAS double chamber CryoTrap appears promising and warrants further product research.
- Using the new VLE data, thermodynamic model evaluation should be expanded with a specific focus on C₁₀OH-containing systems at 35 °C where RK-ASPEN, SR-POLAR, PR-BM and PC-SAFT failed.
- Treating CO₂ as a quadrupole within the appropriate Perturbed-Chain *Polar* SAFT variant may lead to improved PCP-SAFT performance and should be evaluated.
- Additional phase composition measurements for CO₂ + nC₁₂ + C₁₀OH at 73.5 bar (35 °C), 111.0 bar (55 °C) and 147.5 bar (75 °C) should make for challenging experimental work but interesting results. These 18 phase compositions will enable the construction of Gibbs diagrams that illustrate tie line angular behaviour close to the co-solvency pinch.

- Additional phase composition measurements for $\text{CO}_2 + n\text{C}_{12} + 37\text{DM10}$ at $0.85 < Z_{37\text{DM10}} < 0.90$ may enable one to pinpoint the SP_{ij} optimum indicated by the four evaluated models.
- Measuring VLE data for the quaternary $\text{CO}_2 + n\text{C}_{12} + 37\text{DM10} + \text{C}_{10}\text{OH}$ mixture is a logical next step. Using the BIP's developed in this work, model performance in the quaternary should be evaluated.
- Mechanistic research on the co-solvency phenomenon should make for an interesting study.
- To what extent the solute-solute BIP's from this work can be generalised or applied to similar systems should be evaluated. To rephrase, perhaps the linear C_{12} alkane + primary C_{10} alcohol BIP can be used to represent a linear C_{10} alkane + primary C_8 alcohol interaction.
- Zamudio [1] piloted the fractionation of n -decane + 1-decanol + 3,7-dimethyl-1-octanol + 2,6-dimethyl-2-octanol using supercritical CO_2 . An Aspen Plus® simulation [1,2] comprising i) a liquid-liquid extraction column representing the fractionation column; ii) a two-outlet flash drum representing the separation vessel; and iii) RK-ASPEN as thermodynamic model was evaluated for its ability to correlate the pilot plant data. Strangely, the exclusion of solute-solute BIP's led to improved simulation results. However, Zamudio [1,2] did not have access to ternary VLE data and used ternary mixture phase transition pressures to identify generalised BIP's by evaluating a range of user-defined BIP values. Incorporating the RK-ASPEN BIP's from this work in the Aspen Plus® simulation and re-evaluating the performance thereof would be an interesting exercise. In addition, the governing thermodynamic model could be adapted to SR-POLAR, PR-BM or PC-SAFT with relative ease. However, this would require BIP extrapolation or generalisation by assuming that [n -dodecane $\approx n$ -decane] and [3,7-dimethyl-1-octanol \approx 2,6-dimethyl-2-octanol].
- Bonthuys [3], Bonthuys et al. [4] and Schwarz et al. [5] piloted the fractionation of n -tetradecane + 1-dodecanol using supercritical CO_2 . The correlative ability of the simulation developed by Zamudio [1] coupled with the four model-specific sets of BIP's from this work could be evaluated using these pilot plant data. Once again, this would require BIP extrapolation or generalisation by assuming that [n -dodecane $\approx n$ -tetradecane] and [1-decanol \approx 1-dodecanol]. Roughly 30 % of the CO_2 -piloting conducted by Bonthuys [3] incorporated reflux. In this regard the simulation developed by Zamudio [1], which does not cater for reflux, would require adaptation.
- This study should be duplicated using ethane as solvent and the experimental outline in Fig. 5-1.

REFERENCES

1. M. Zamudio, The Separation of Detergent Range Alkanes and Alcohol Isomers with Supercritical Carbon Dioxide, Stellenbosch University, South Africa, 2014 PhD Dissertation.
2. M. Zamudio, C.E. Schwarz, J.H. Knoetze, Methodology for process modelling of supercritical fluid fractionation processes illustrated for the separation of alkane/alcohol isomer mixtures using CO₂, J. Supercrit. Fluids 104 (2015) 272-280.
3. G.J.K. Bonthuys; Separation of 1-dodecanol and *n*-tetradecane through supercritical extraction, MSc Thesis, Stellenbosch University, South Africa, 2008.
4. G.J.K. Bonthuys, C.E. Schwarz, A.J. Burger, J.H. Knoetze, Separation of alkanes and alcohols with supercritical fluids. Part I: Phase equilibria and viability study, J. Supercrit. Fluids 57 (2011) 101-111.
5. C.E. Schwarz, G.J.K. Bonthuys, R.F. van Schalkwyk, D.L. Laubscher, A.J. Burger, J.H. Knoetze, Separation of alkanes and alcohols with supercritical fluids. Part II. Influence of process parameters and size of operating range, J. Supercrit. Fluids 58 (2011) 352-359.

Appendix A. PUBLICATION 1 SUPPORTING INFORMATION

Supporting Information

Analytic Setup for Multicomponent High-Pressure Phase Equilibria via Dual Online Gas Chromatography

Frederick C. v. N. Fourie, Cara E. Schwarz, Johannes H. Knoetze*

Stellenbosch University, Department of Process Engineering, Private Bag X1, Matieland, 7602, South Africa,

Tel: +27 21 808 4204, Fax: +27 21 808 2059, E-mail: jhk@sun.ac.za

Chemical Engineering & Technology 38,7 (2015) 1165-1172.

Received 31 October 2014; Revised 22 December 2014; Accepted 2 February 2015

DOI: 10.1002/ceat.201400643

Table of contents

- S1. Sample extraction
- S2. Gas chromatography analysis
- S3. Validation of the experimental setup

S1. Sample extraction

Fig. S1 shows the two ROLSI™ samplers (Armines, France) fixed upon the manual displacement devices. More information on sample extraction and the sampling procedure is available in Sections 2.3 and 3.1 of the main article.



Figure S1. The ROLSI™ samplers and displacement devices.

S2. Gas chromatography analysis

A sample chromatogram for the ternary system CO_2 + 1-dodecanol + *n*-hexadecane is shown in Fig. S2. Refer to Section 2.4 of the main article for more information on the GC hardware, calibrations and method parameters.

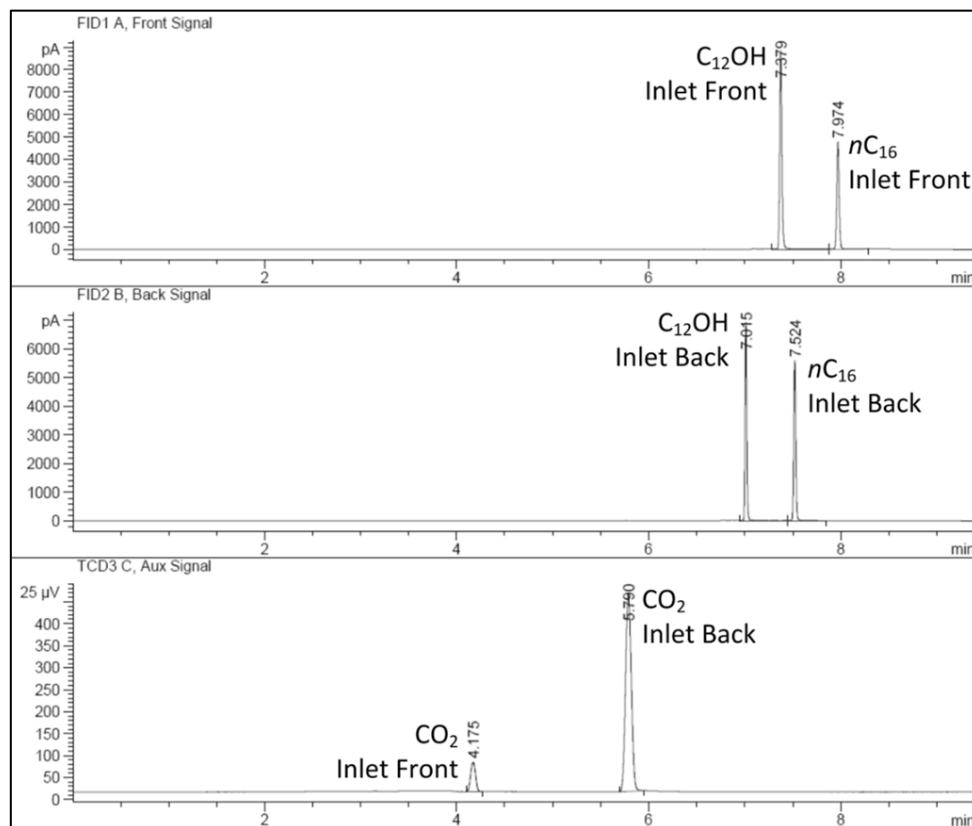


Figure S2. A sample chromatogram for the CO_2 + 1-dodecanol (C_{12}OH) + *n*-hexadecane ($n\text{C}_{16}$) system.

S3. Validation of the experimental setup

The accuracy of the extraction, injection and analysis pathways was confirmed by sampling from a one-phase ethane + 1-dodecanol + *n*-hexadecane ternary of known composition. The species-specific mass fraction averages and root mean square errors are listed in Tab. 3 of the main article. Mass fraction results for ethane and 1-dodecanol are shown in Fig. S3. Accurate and repeatable data were obtained via both pathways.

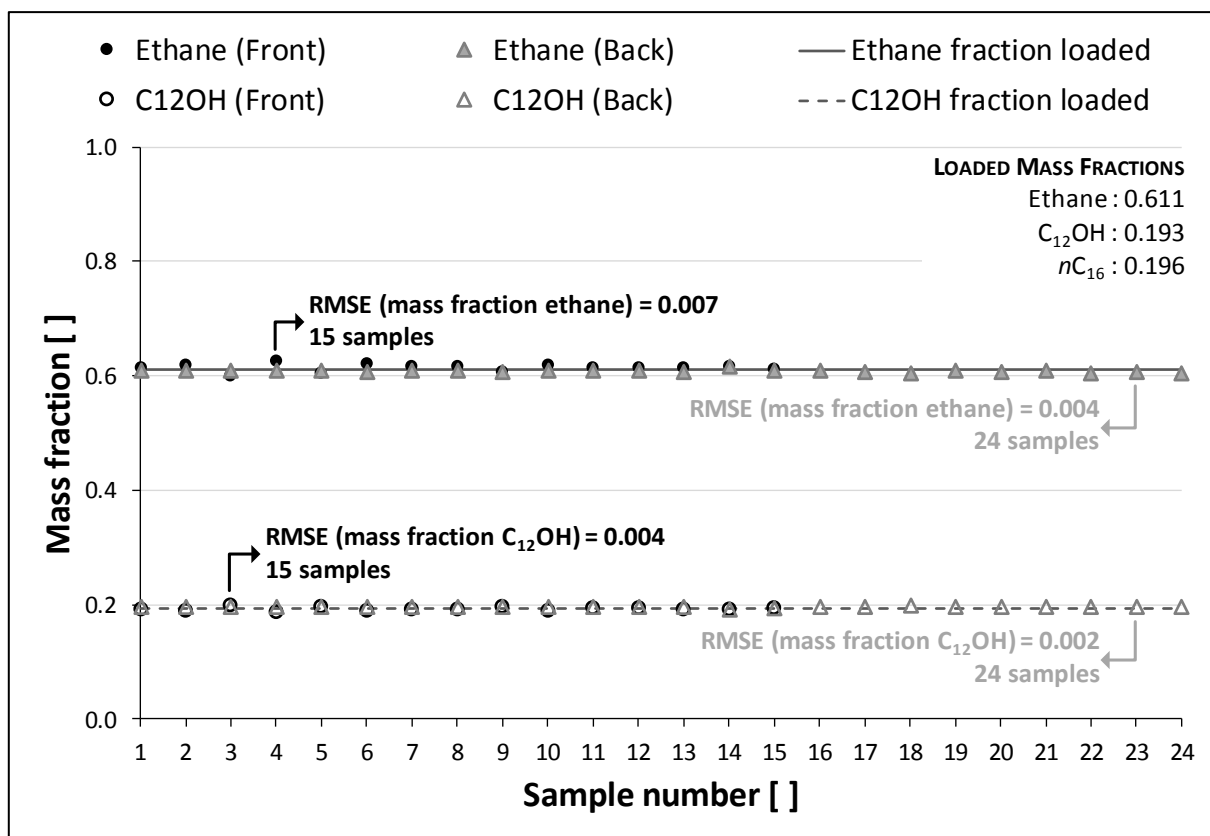
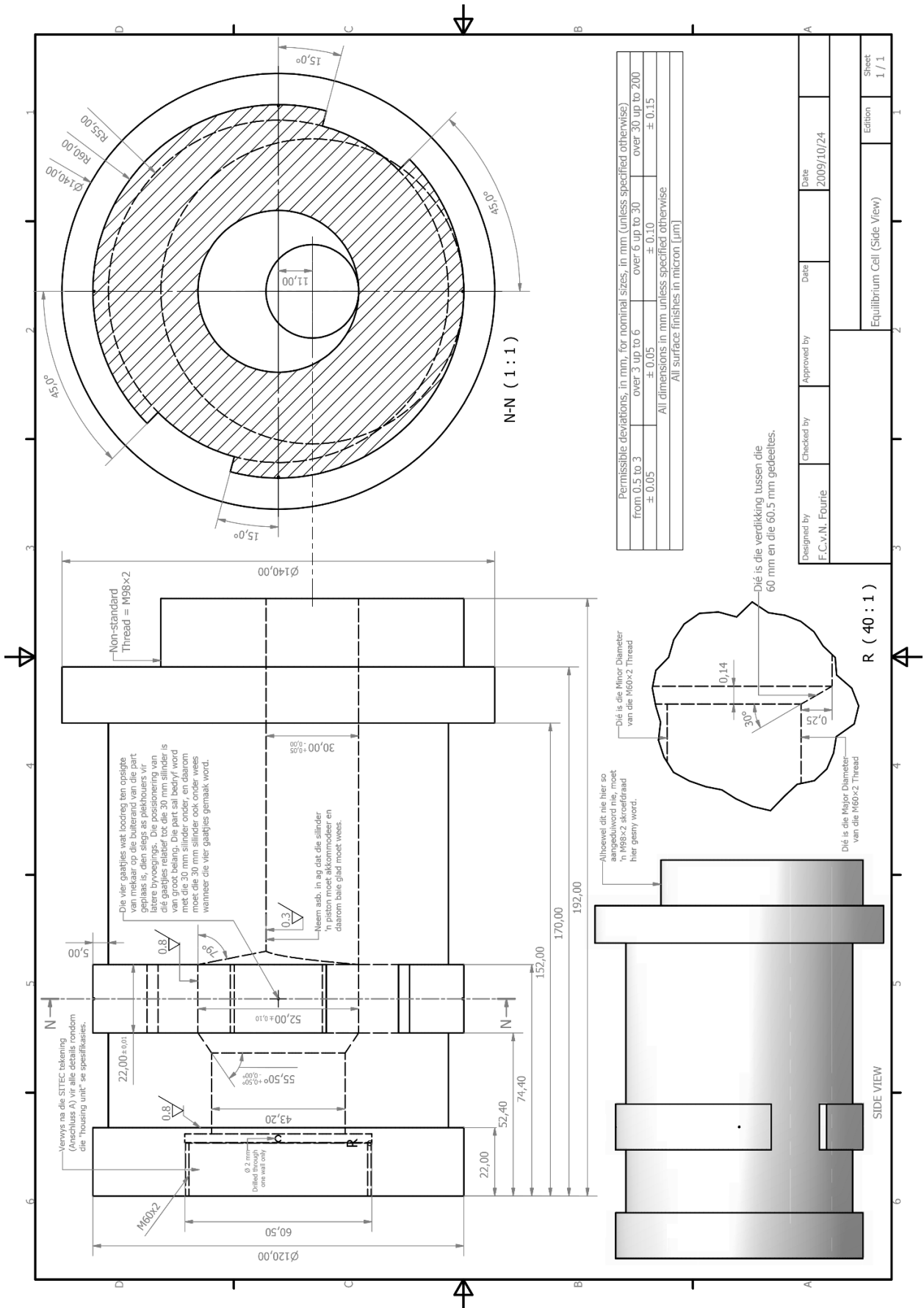
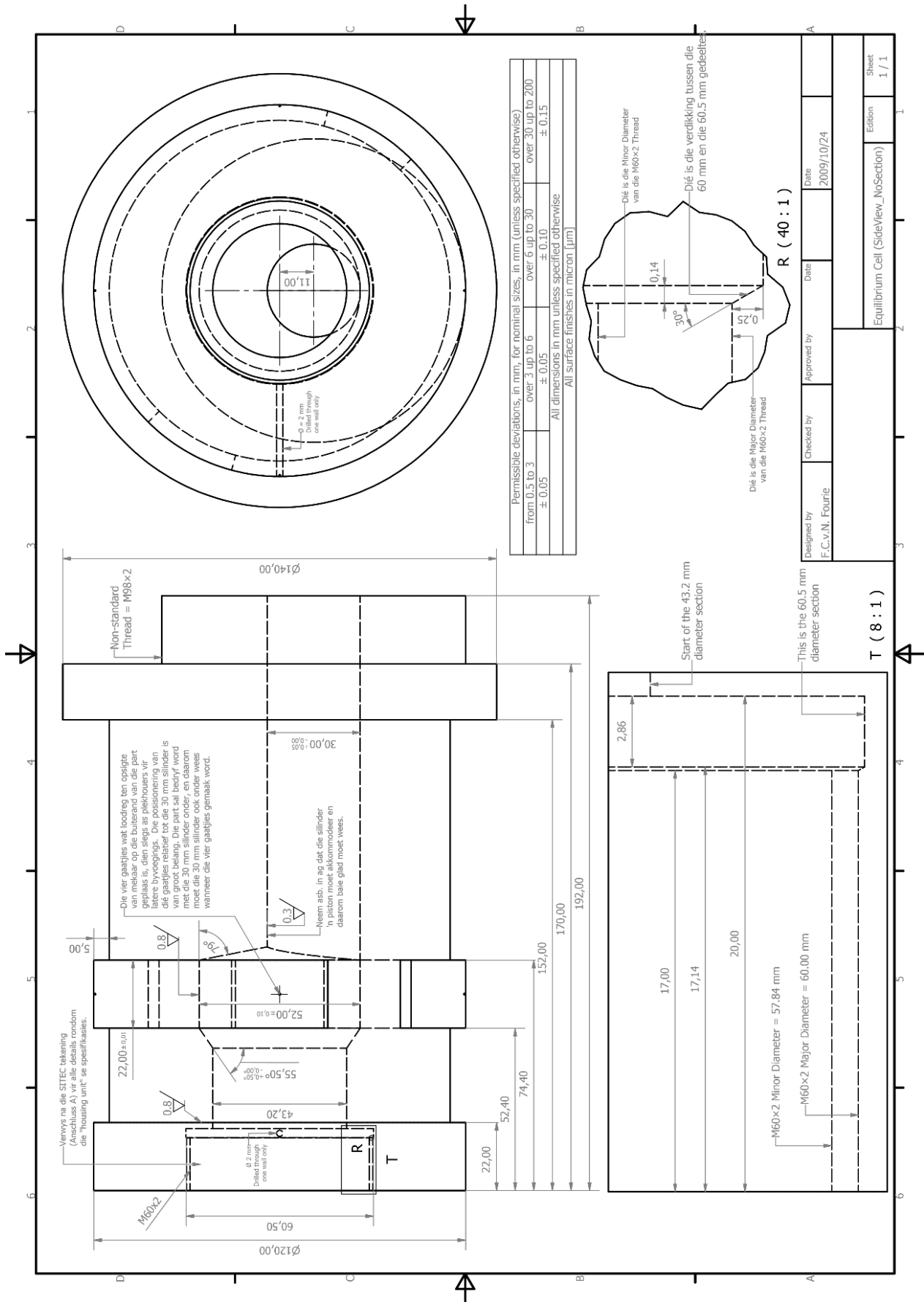


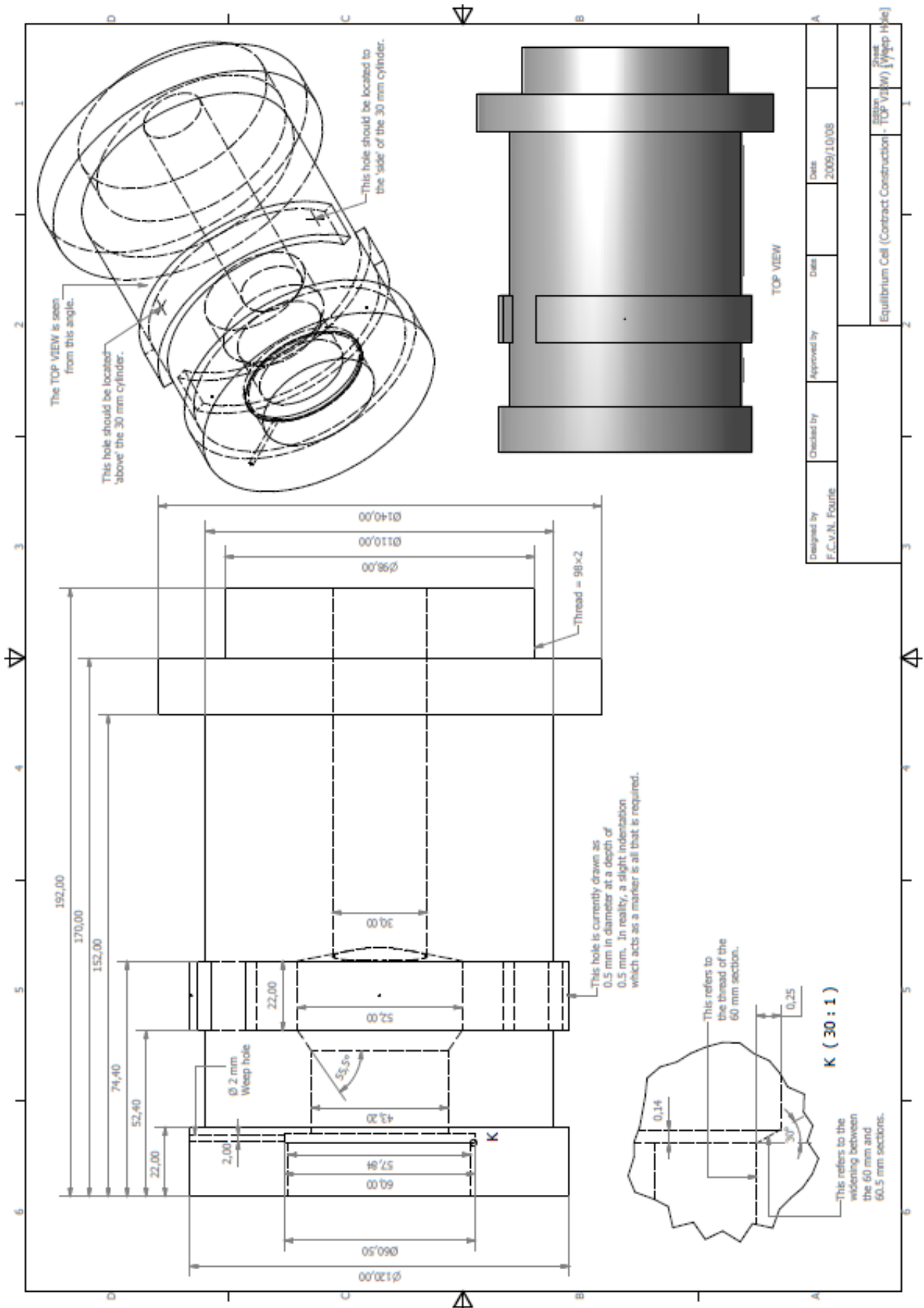
Figure S3. Corresponding and accurate quantification via both analysis pathways: ethane and 1-dodecanol (C₁₂OH) mass fractions as analyzed from a one-phase ethane + 1-dodecanol + *n*-hexadecane (nC₁₆) ternary system of known composition. Equilibrium cell pressure and temperature were 121 bar and 63.0 °C, and the split ratio 80:1. ROLSI™ opening times of 3.50 and 1.00 seconds were used on the front and back pathways respectively.

Appendix B. TECHNICAL DRAWINGS

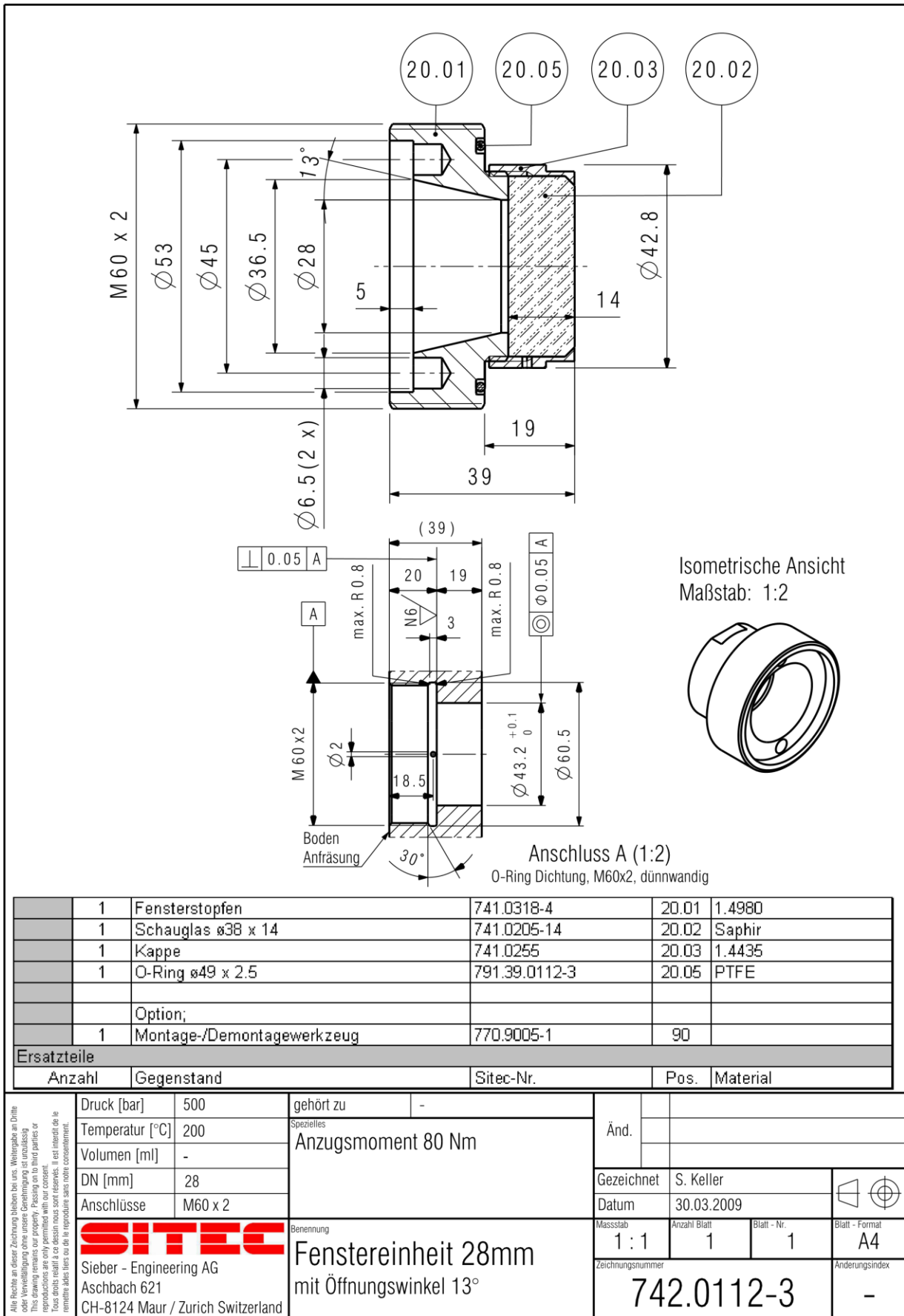
Appendix B-1	Equilibrium cell side view 1	240
Appendix B-2	Equilibrium cell side view 2	241
Appendix B-3	Equilibrium cell top view	242
Appendix B-4	SITEC-Sieber Engineering observation window	243
Appendix B-5	Rapid Product Development observation window measurements	244
Appendix B-6	Heating jacket	245
Appendix B-7	Spark erosion view 1	246
Appendix B-8	Spark erosion view 2	247
Appendix B-9	Spark erosion procedure	248
Appendix B-10	Valve components: Long	249
Appendix B-11	Valve components: Short	250
Appendix B-12	Equilibrium cell machining step 3	251
Appendix B-13	Equilibrium cell machining step 4 (1)	252
Appendix B-14	Equilibrium cell machining step 4 (2)	253
Appendix B-15	ROLSI™ displacement device	254
Appendix B-16	ROLSI™ compression seal assembly	255
Appendix B-17	Pressure intensifier: Pressure chamber	256
Appendix B-18	Pressure intensifier: Piston shaft	257
Appendix B-19	Pressure intensifier: Outer piston rod	258
Appendix B-20	Pressure intensifier: Inner piston rod	259
Appendix B-21	Pressure intensifier: Piston disc'	260
Appendix B-22	Pressure intensifier: Lower disc	261
Appendix B-23	Pressure intensifier: Leaded gunmetal 2 sheath	262

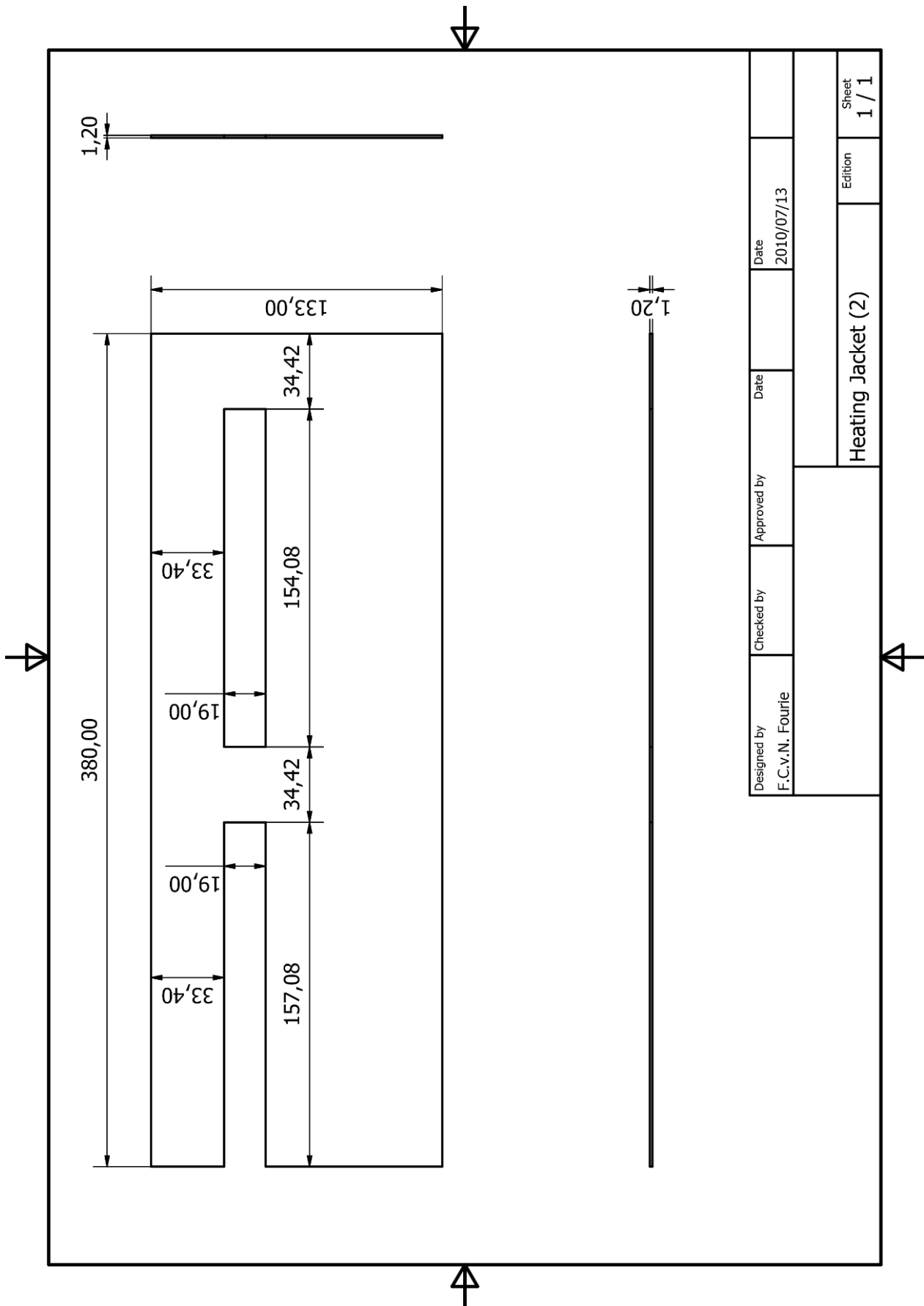


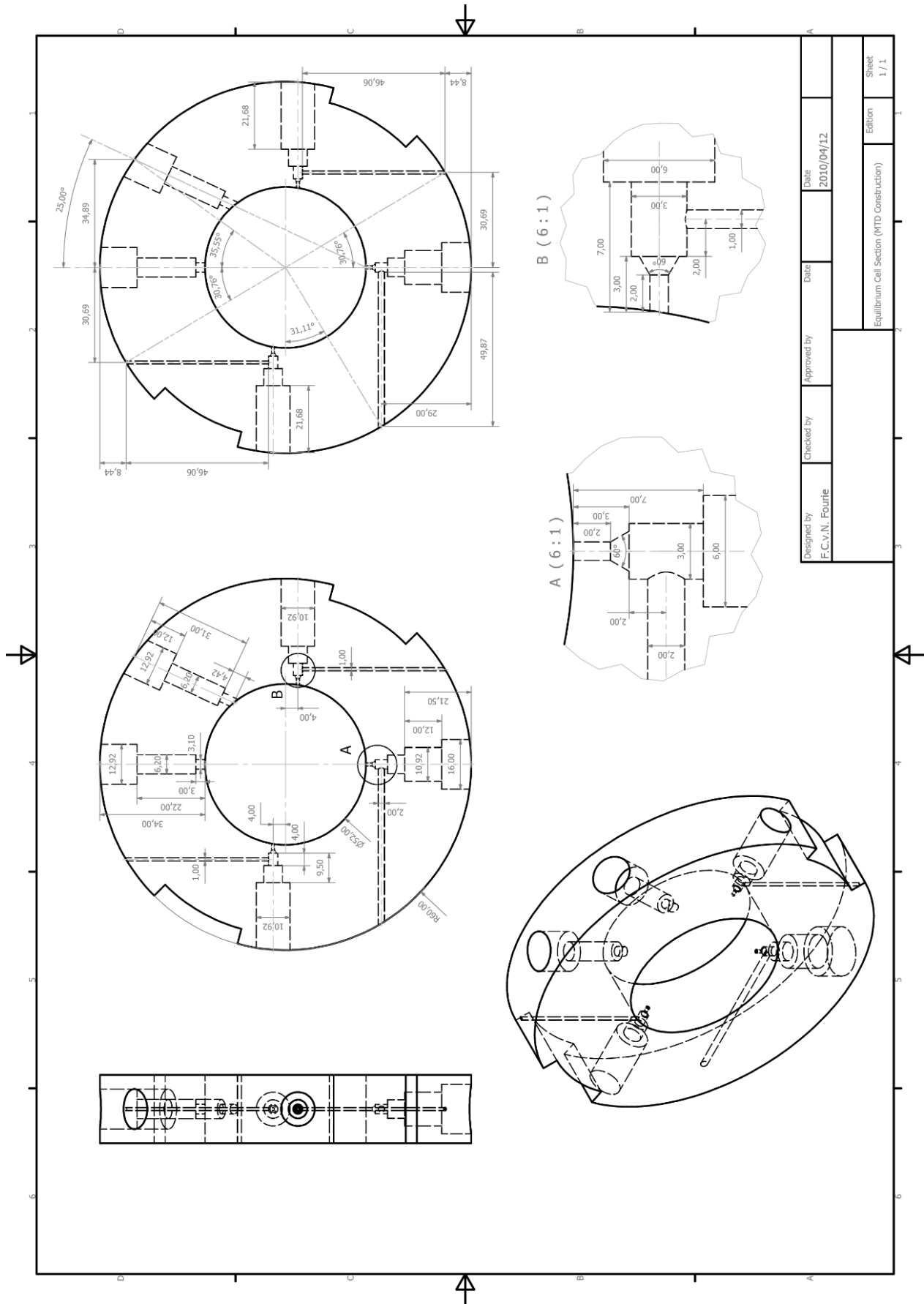




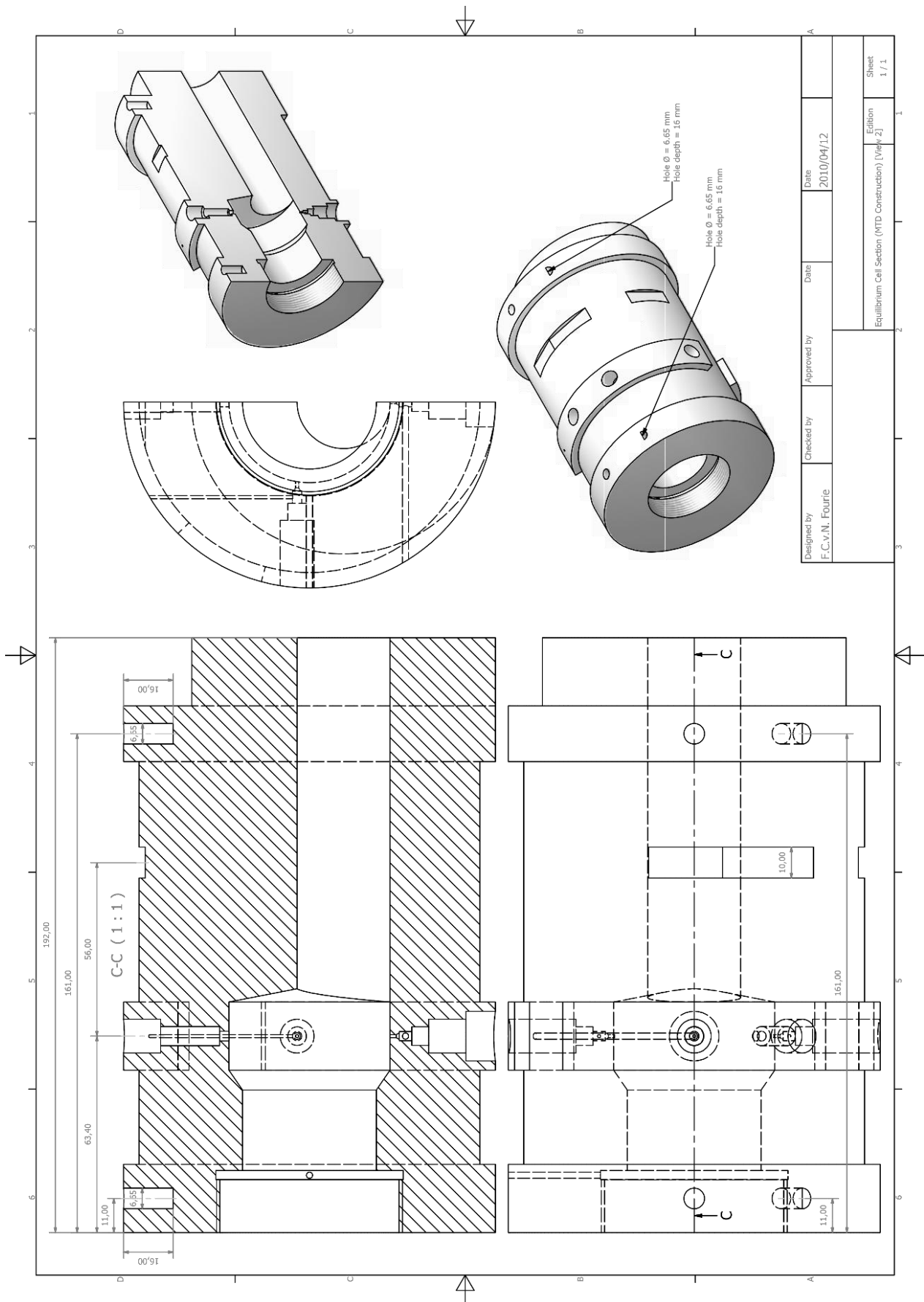
Designed by F.C.v.N. Fourie	Checked by	Approved by	Date 2009/10/08
Equilibrium Cell (Contract Construction - TOP VIEW) [Weep Hole]			Sheet EQUIL







Designed by F.C.v.N. Fourie	Checked by	Approved by	Date 2010/04/12
Equilibrium Cell Section (MTD Construction)			Sheet 1 / 1

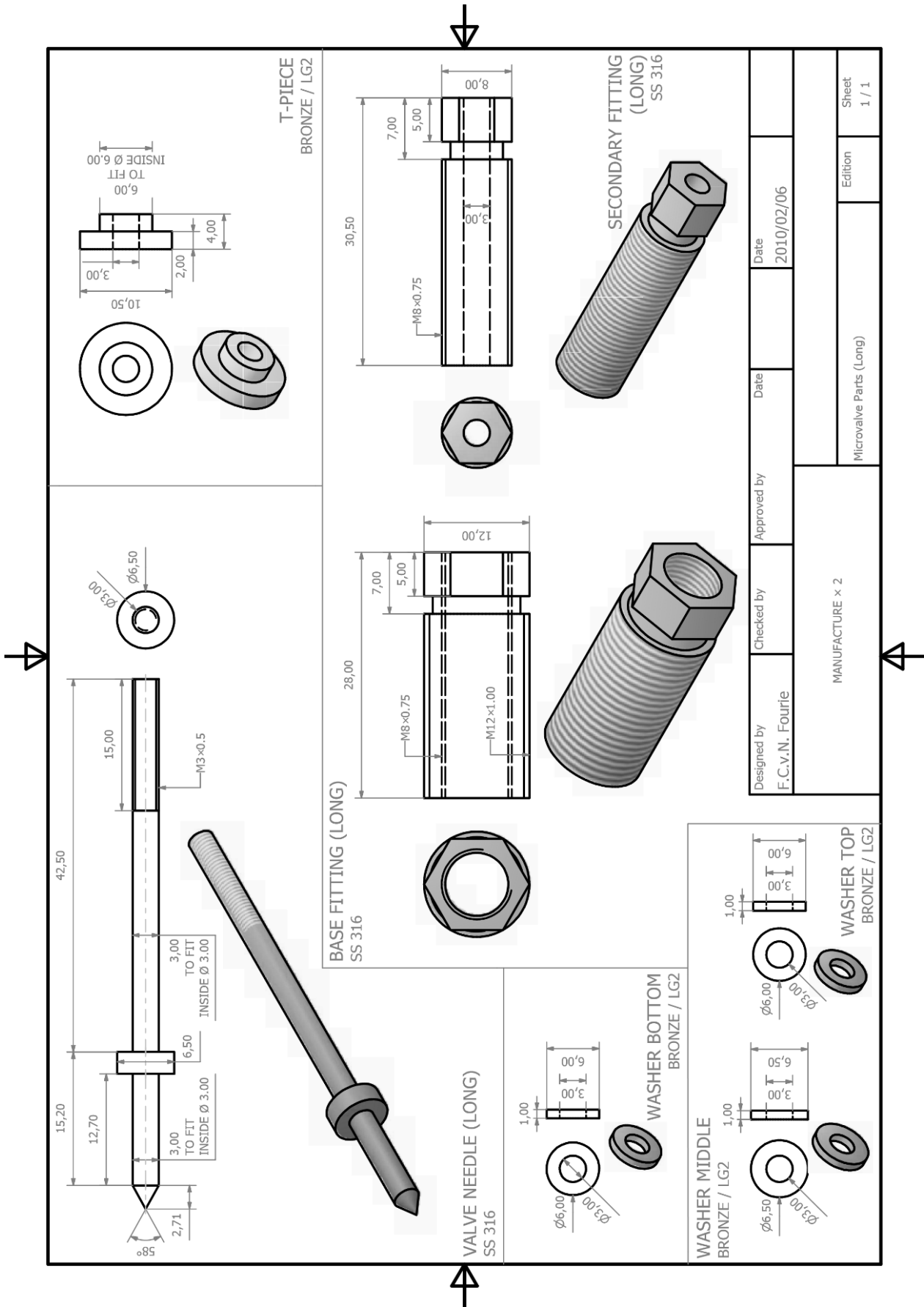


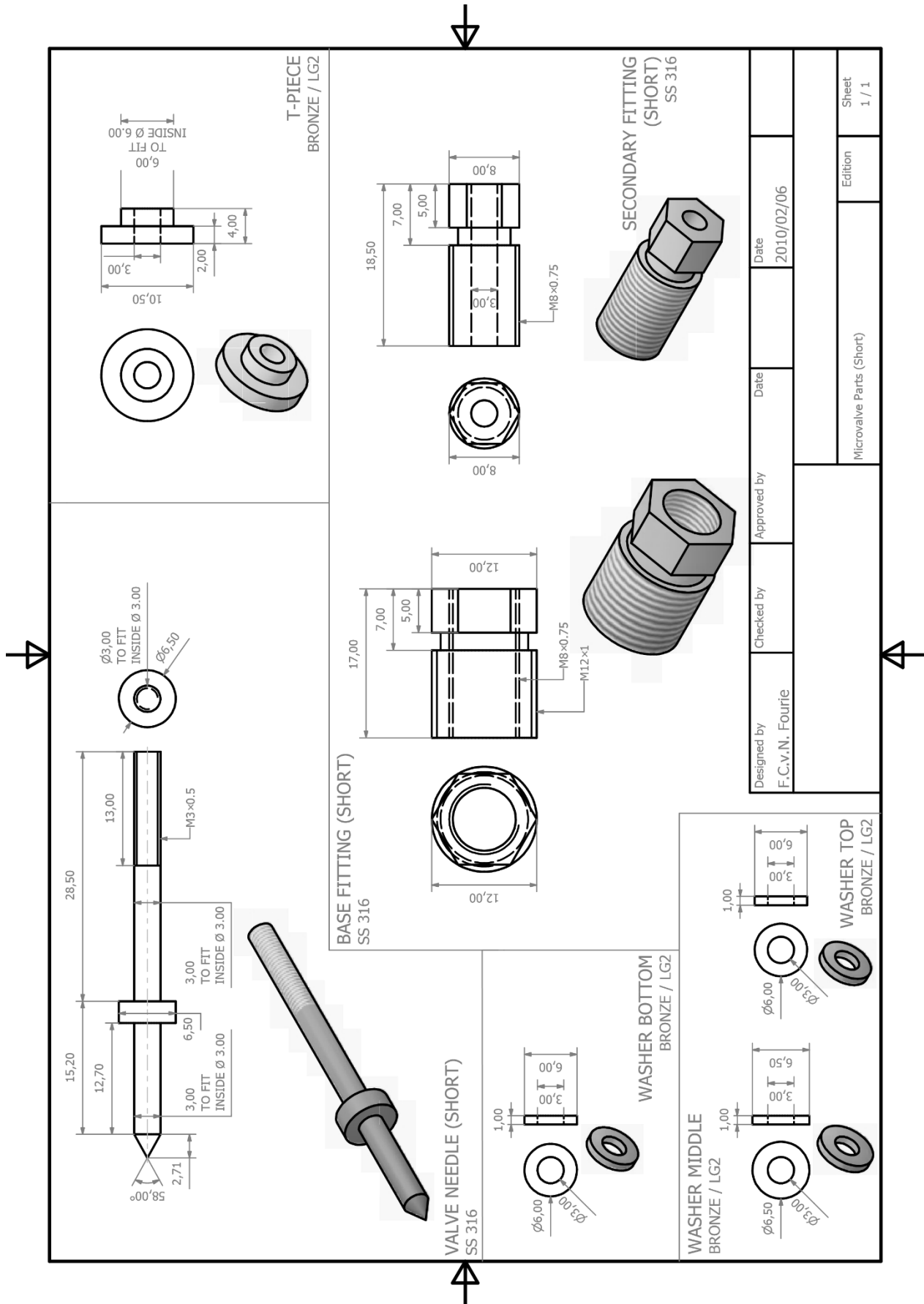
Extra requirements:

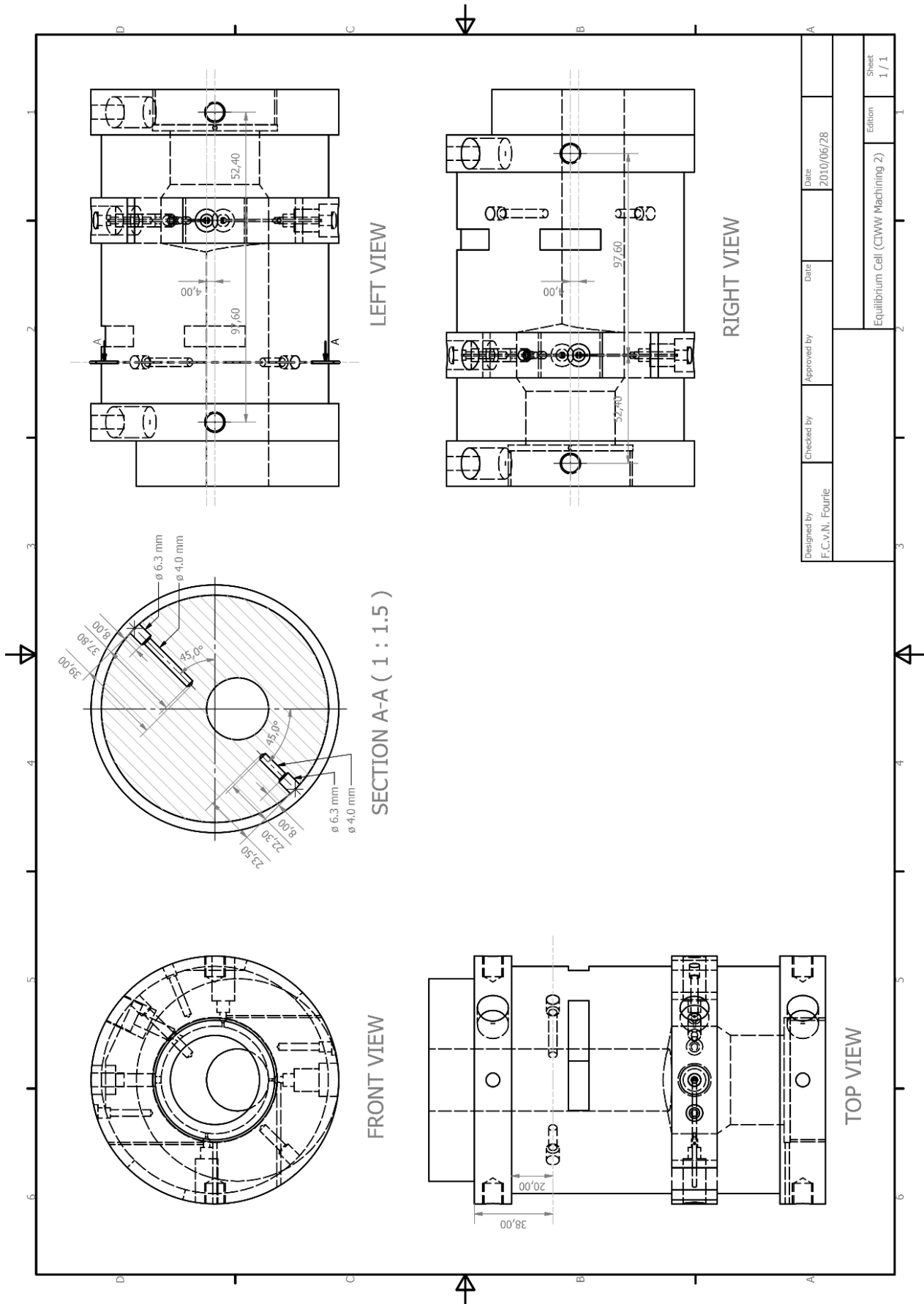
- 1 Off TURN Back OD from diameter 140 mm to diameter 120 mm
- 1 Off TURN Shaft for EDM drilling of feed line
- 1 Off MILL Reference flats for 32.55° / 25°, 0° and 90° (3 x flats in total)
- 1 Off MANUFACTURE Electrode A; 1 × Reface required
- 3 Off MANUFACTURE Electrode B (B1, B2 & B3); 2 × Reface required
- 1 Off MODIFY Jig A [Index on centre point (as per test piece but with modification)]
- 1 Off MANUFACTURE Jig B [Index on 32.55/25 degrees]

Kindly note the Test Piece Jig we manufactured will not suit the equilibrium cell and will need modifications.

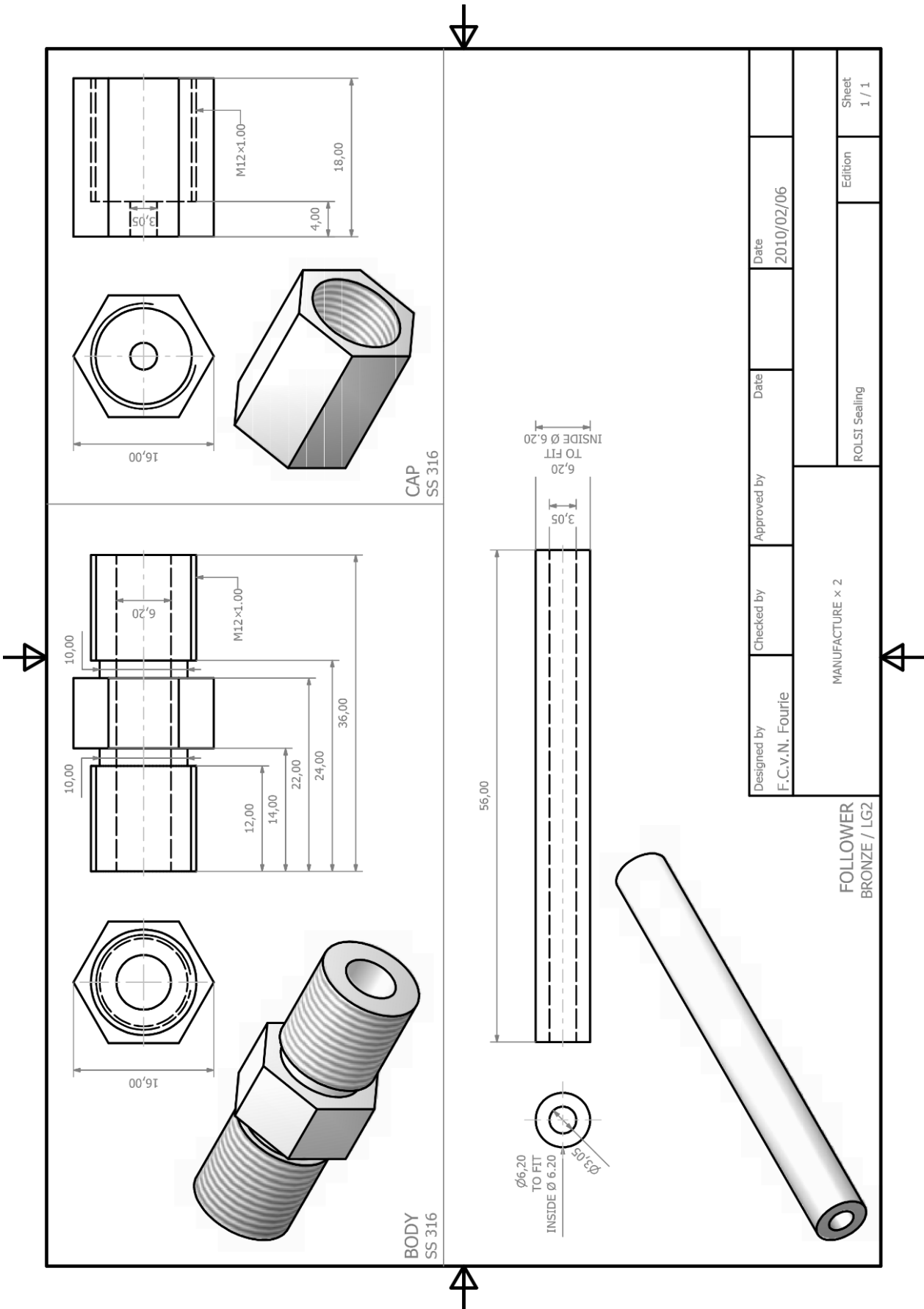
MILLING Operations				
Step Number	Angle from Centreline	Angle Actual	Operation	Comments
1	0	0	Drill & Tap displacement device Location Holes	Machine reference flat Drill ϕ 6.65 mm; 16 mm deep Tap M8 \times 1.25; 2 Off
2	0	0	Drill ROLSI housing Location Hole	Allow for Sparking
3	35.55	25	Drill & Tap displacement device Location Holes	Machine reference flat Drill ϕ 6.65 mm; 16 mm deep Tap M8 \times 1.25; 2 Off
4	35.55	25	Drill ROLSI housing Location Hole	Allow for Sparking
5	90	90 (off 4.00 mm)	Drill Microvalve Location hole	Machine reference flat Allow for Sparking
6	180	180	Drill Microvalve Location hole	Allow for Sparking
7	270	270 (off 4.00 mm)	Drill Microvalve Location hole	Allow for Sparking
SPARKING Operations				
9	0	0	Spark	Electrode A
10	35.55	25	Spark	Electrode A; Reface 1
11	90	90 (off 4.00 mm)	Spark	Electrodes B1, B2 & B3
12	180	180	Spark	Electrodes B1, B2 & B3; Reface 1
13	270	270 (off 4.00 mm)	Spark	Electrodes B1, B2 & B3; Reface 2
EDM DRILLING Operations				
15	0	0 (off -30.69 mm)	EDM	1 mm Feed line
16	90	90 (off 4.00 mm)	EDM	1 mm Hole
17	180	180 (off -30.69 mm)	EDM	1 mm Feed line
18	180	180	EDM	1 mm Hole
19	270	270 (off -31.00 mm)	EDM	2 mm Feed line
20	270	270 (off 4.00 mm)	EDM	1 mm Hole

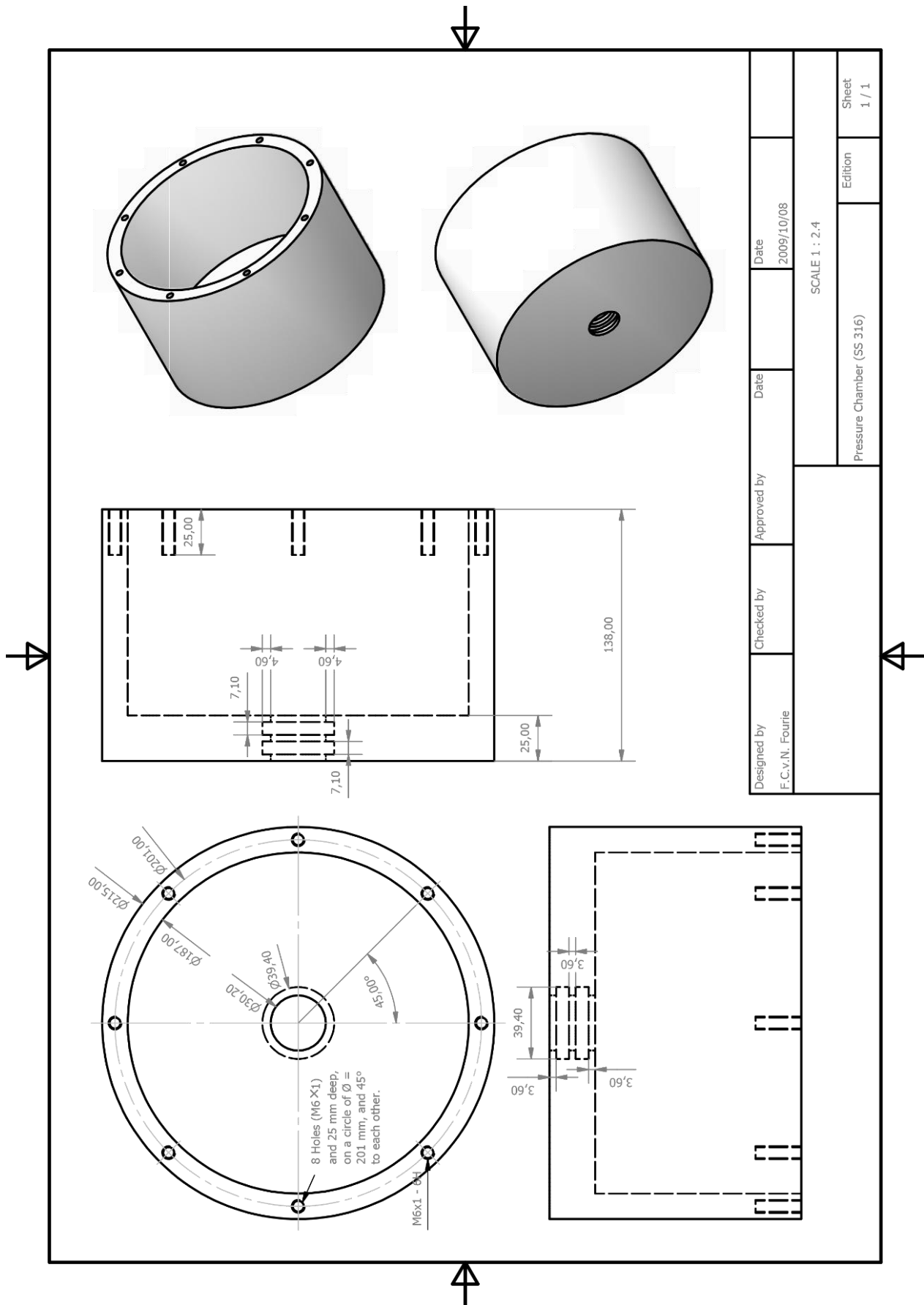




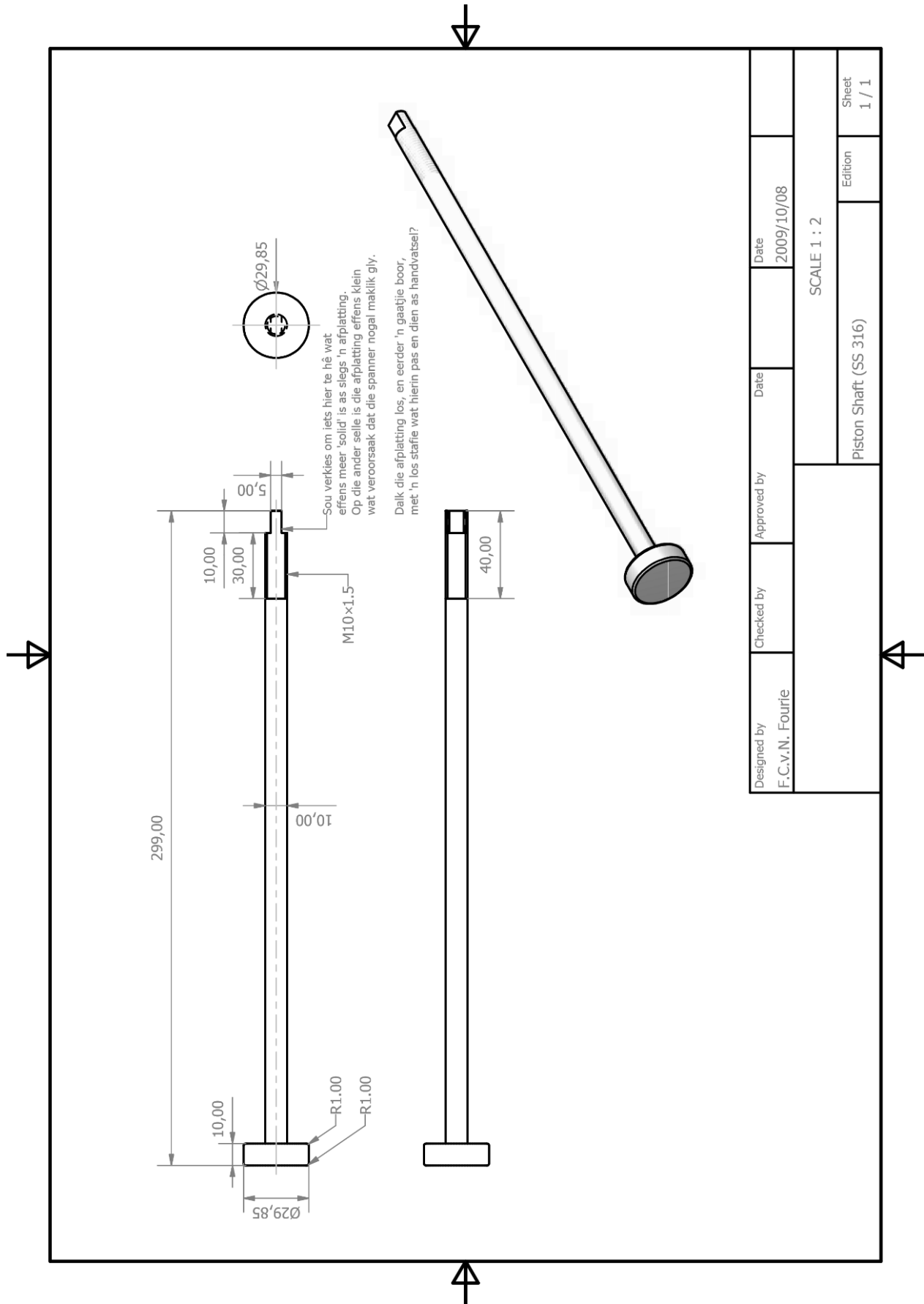


Designed by F.C.V.N. Fourie	Checked by	Approved by	Date 2010/06/28
Equilibrium Cell (CIWW Machining 2)			Sheet 1 / 1

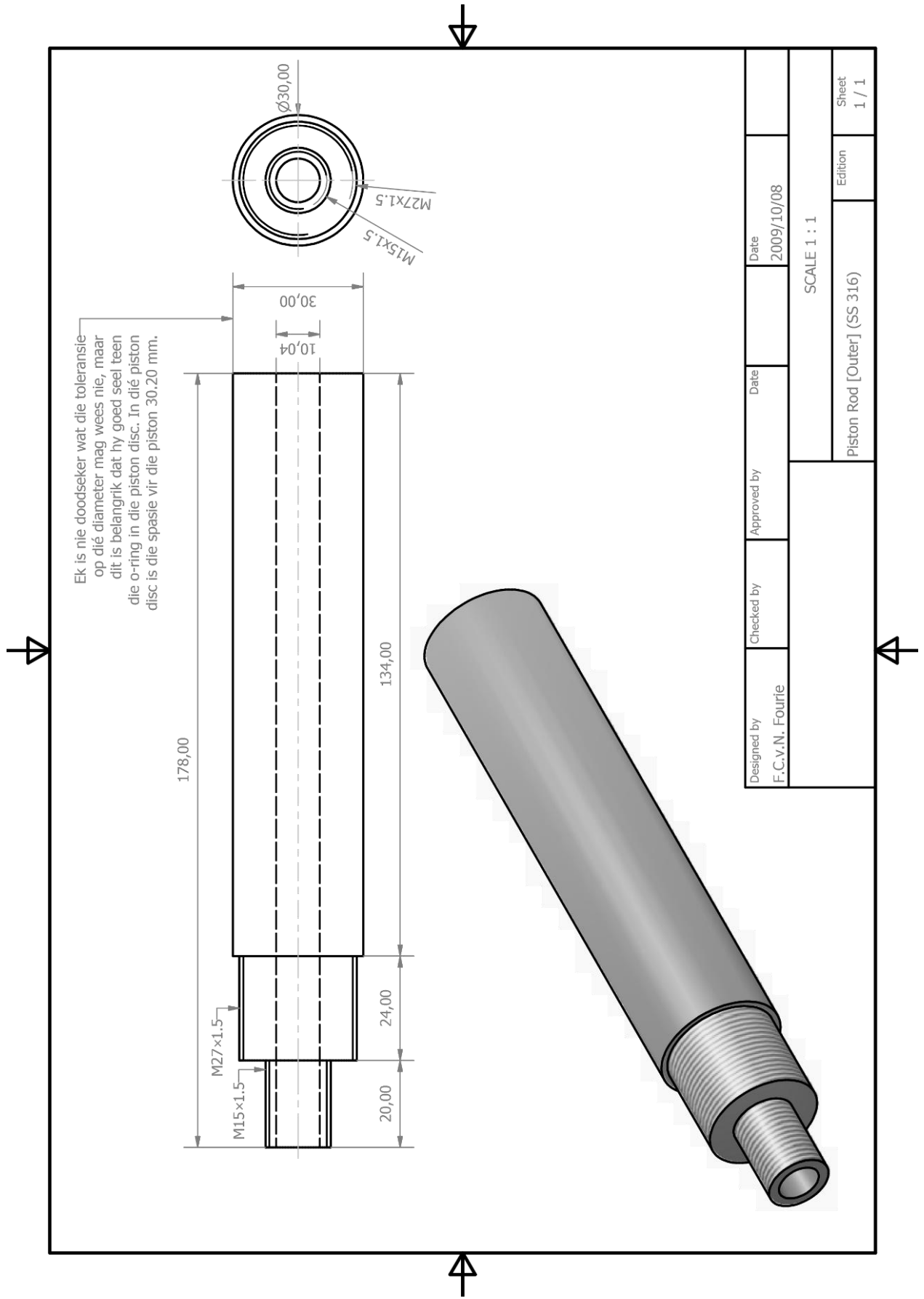




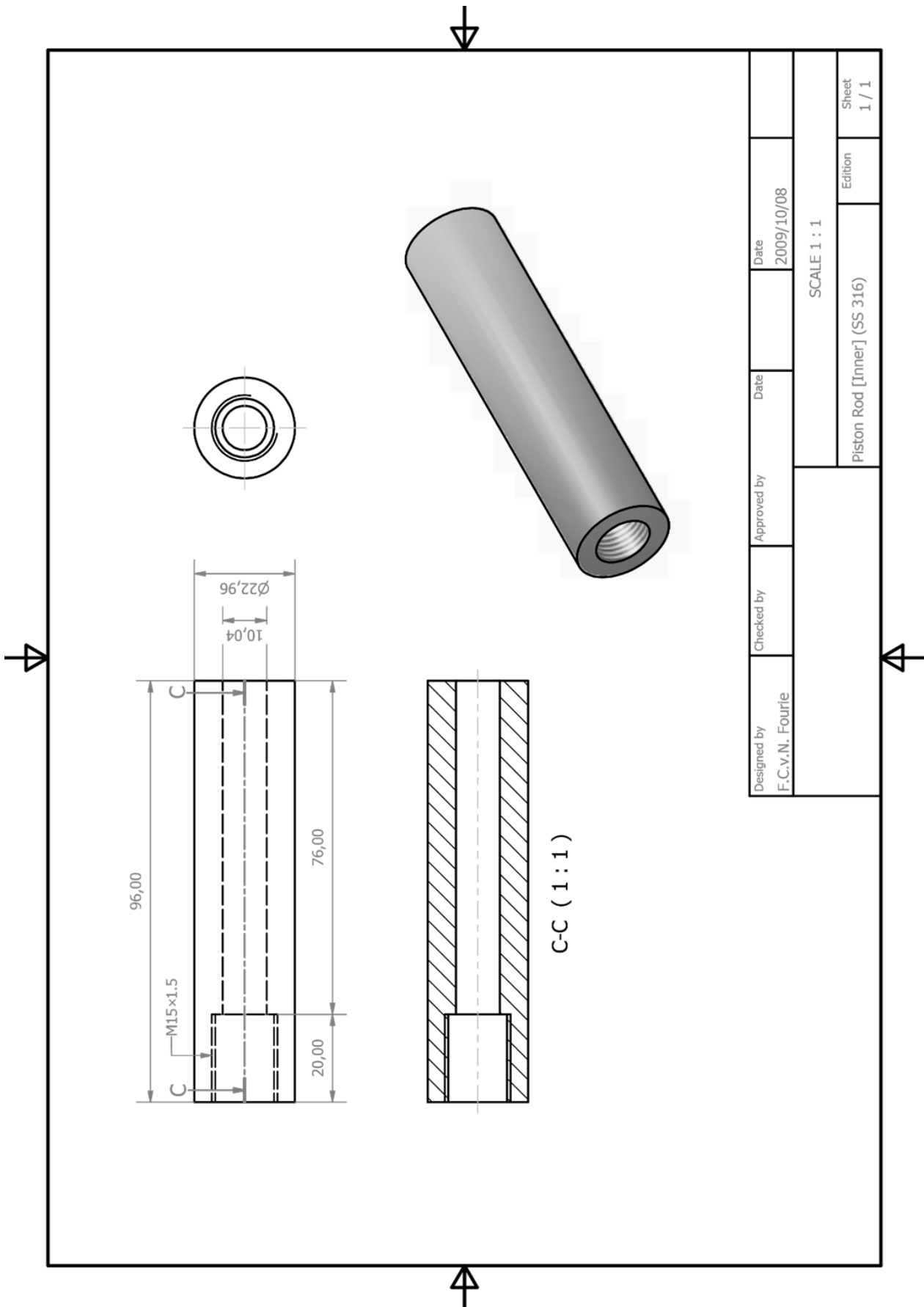
Designed by	Checked by	Approved by	Date	Date
F.C.v.N. Fourie			2009/10/08	
Pressure Chamber (SS 316)			SCALE 1 : 2,4	
Edition			Sheet	
			1 / 1	



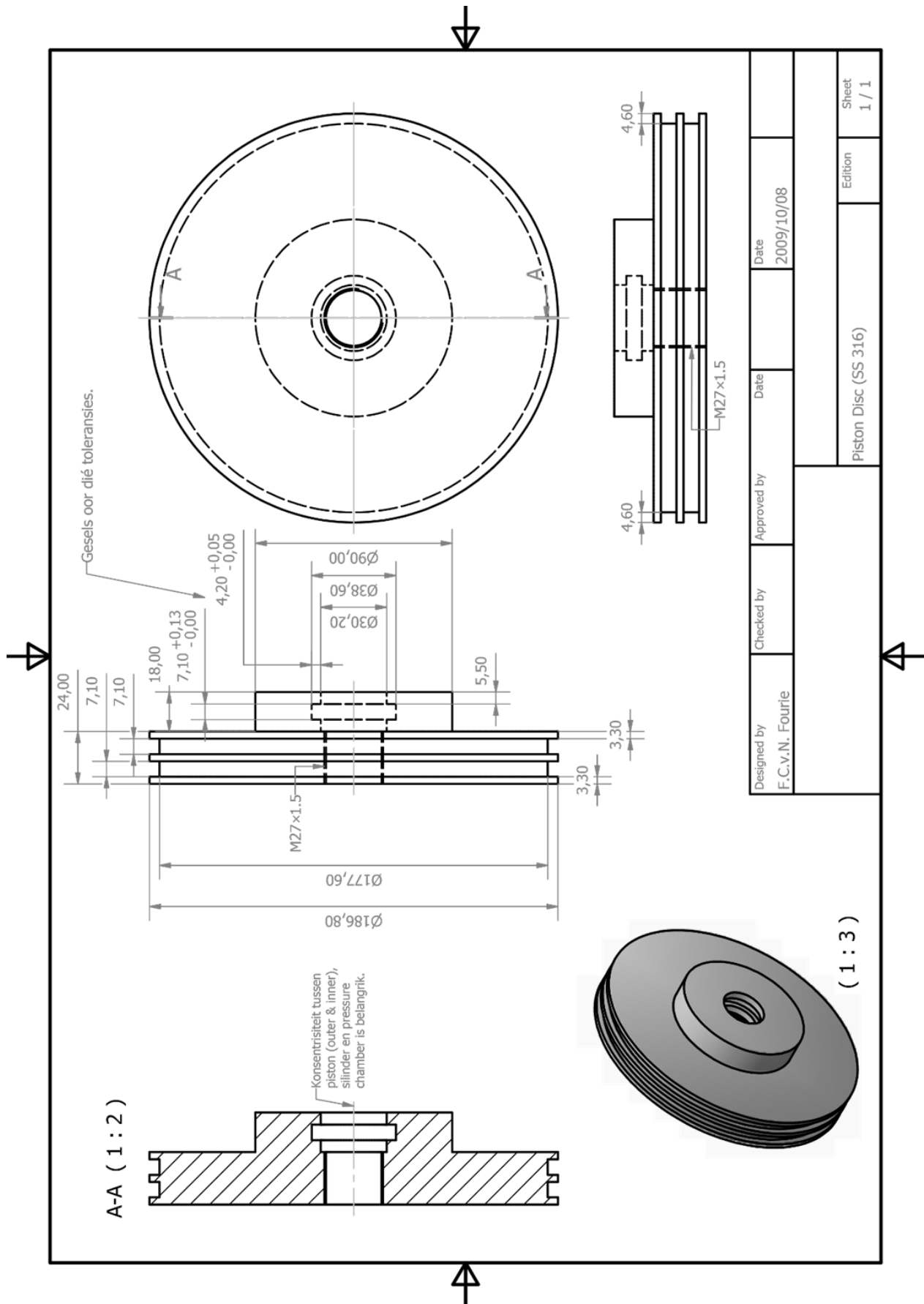
Designed by F.C.v.N. Fourie	Checked by	Approved by	Date 2009/10/08
Piston Shaft (SS 316)			SCALE 1 : 2
Edition			Sheet 1 / 1

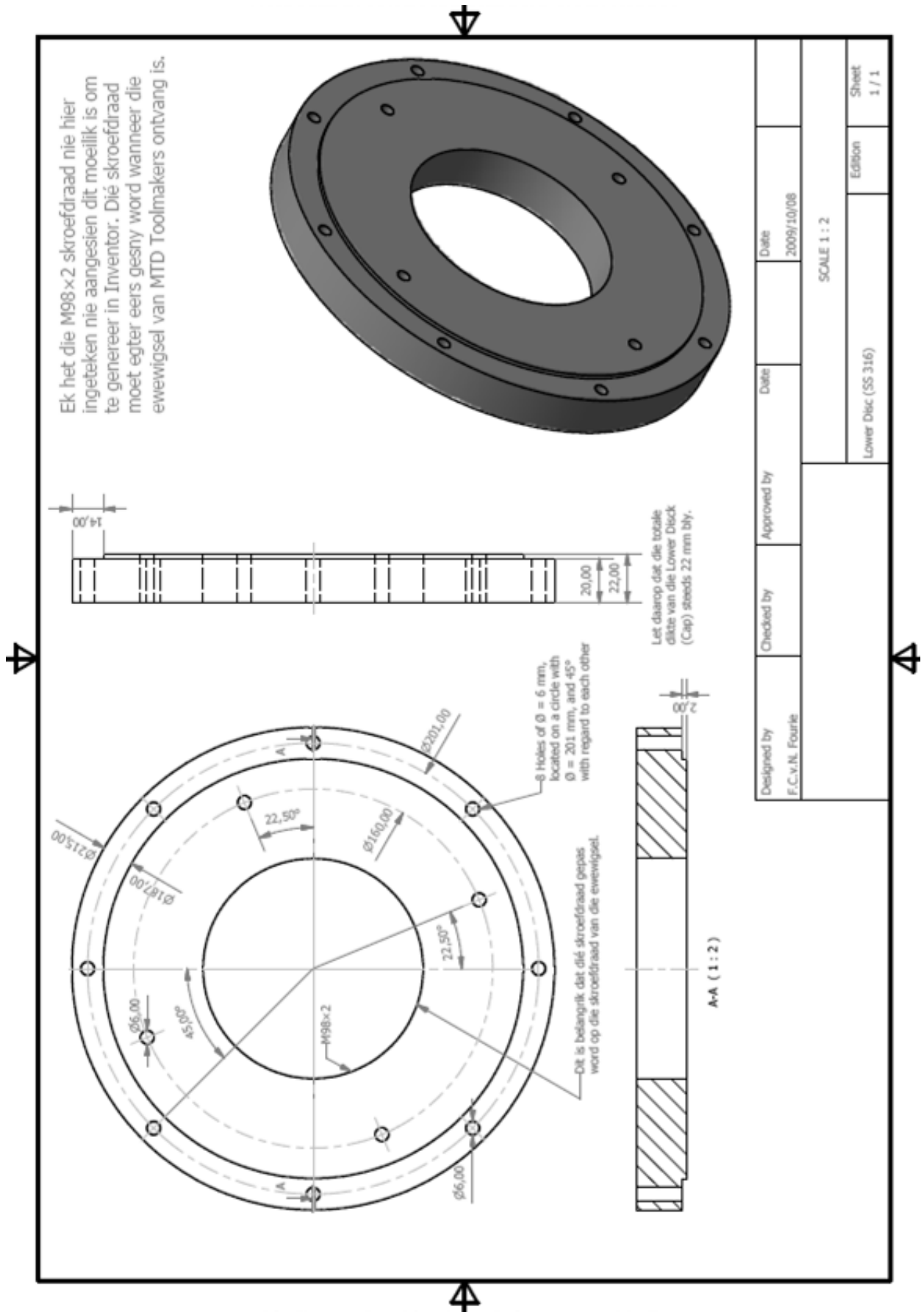


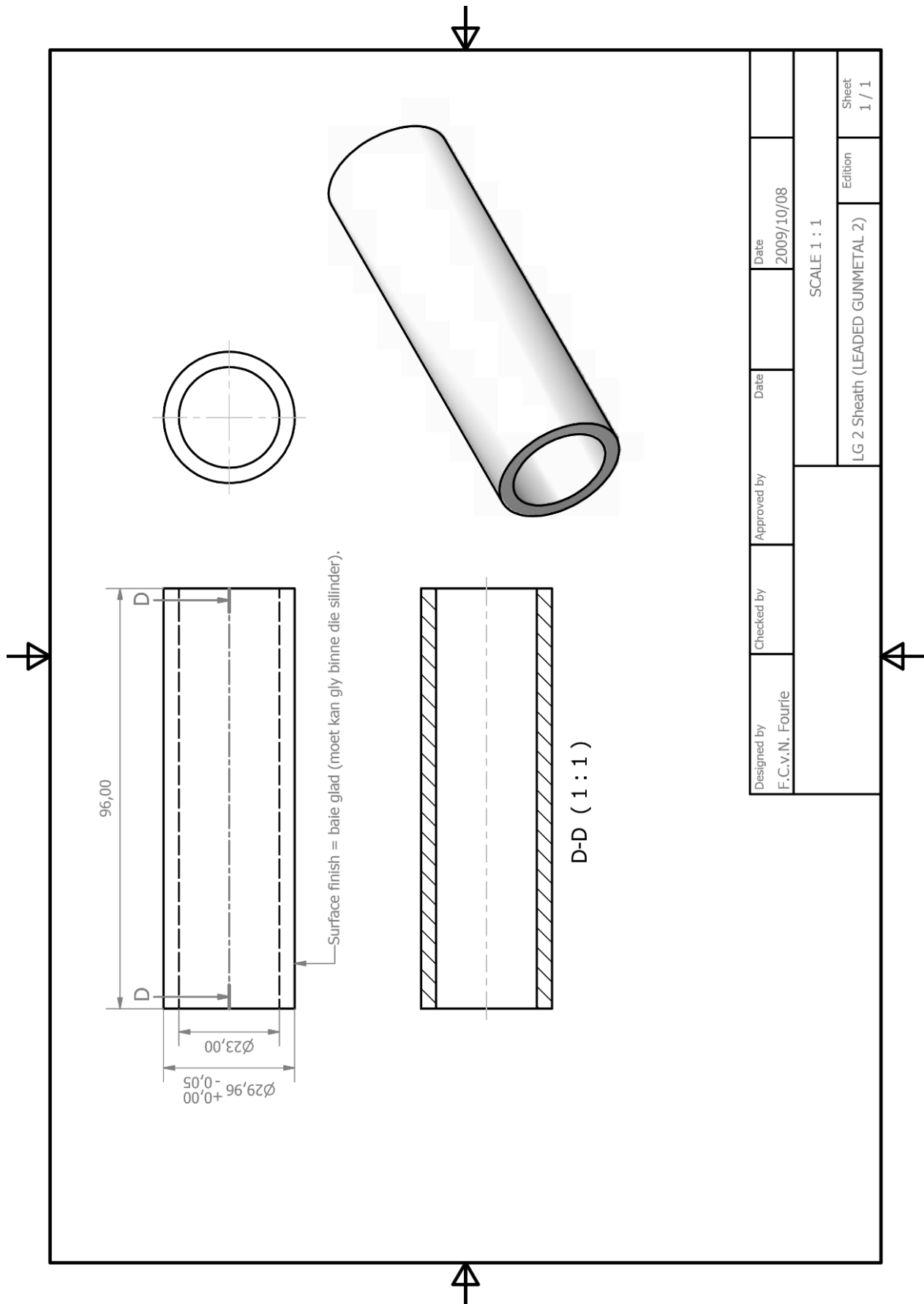
Designed by F.C.v.N. Fourie	Checked by	Approved by	Date 2009/10/08	Date 2009/10/08	Sheet 1 / 1
Piston Rod [Outer] (SS 316)			SCALE 1 : 1		Edition



Designed by F.C.v.N. Fourie	Checked by	Approved by	Date 2009/10/08	Date 2009/10/08	Sheet 1 / 1
			SCALE 1 : 1		Edition
			Piston Rod [Inner] (SS 316)		1 / 1







Appendix C. FINITE ELEMENT METHOD ANALYSIS REPORT

Appendix C-1	FEM analysis report	264
Appendix C-2	SS316L material batch test certificate	276



UNIVERSITEIT•STELLENBOSCH•UNIVERSITY
jou kennisvenoot • your knowledge partner

FEM Analysis of an Equilibrium Cell

Final Report



Gerhard Venter

Faculty of Engineering,
University of Stellenbosch

2009-07-28

PROCESS ENGINEERING: EQUILIBRIUM CELL

Contents

1	Background	2
2	Finite Element Model	3
2.1	Geometry and elements	3
2.2	Material	3
2.3	Loading	4
2.4	Boundary conditions	5
2.5	Analysis	5
3	Results	8
3.1	Case 1: 100 mm diameter cell	8
3.2	Case 2: 120 mm diameter cell	10
4	Concluding Remarks	12

1 Background

Mr Frederick Fourie of the Process Engineering Department at Stellenbosch University, requested a 3D linear finite element analysis of an equilibrium cell that he designed. The cell will be manufactured from 316 stainless steel and the goal of the study was to determine the Von Mises stress distribution in the structure at an operating condition of 300 bar internal pressure and a temperature of 150°C. A 3D image of the unit (cut in half along its axis of symmetry) is shown in Fig. 1 below.

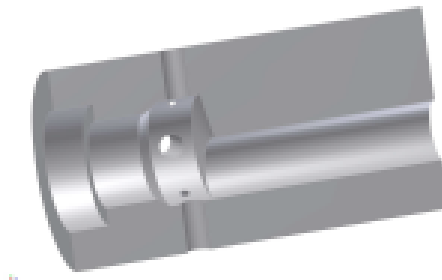


Figure 1: CAD image of equilibrium cell

2 Finite Element Model

2.1 Geometry and elements

Due to symmetry, only half the cell needs to be considered in the finite element model, as shown in Fig. 1. The finite element model was created from the 3D CAD data provided by the client, using 10 node (quadratic) tetrahedral elements and is shown in Fig. 2 below. Note that two finite element models were created. The first for a cell with an outer diameter of 100 mm (Fig. 2(a)) and the second for a cell with an outer diameter of 120 mm (Fig. 2(b)). The first model has a total of 174 972 elements and 247 523 nodes, while the second has a total of 35 753 elements and 22 843 nodes. The course mesh used for the second model was validated with a mesh refinement study of the first model.

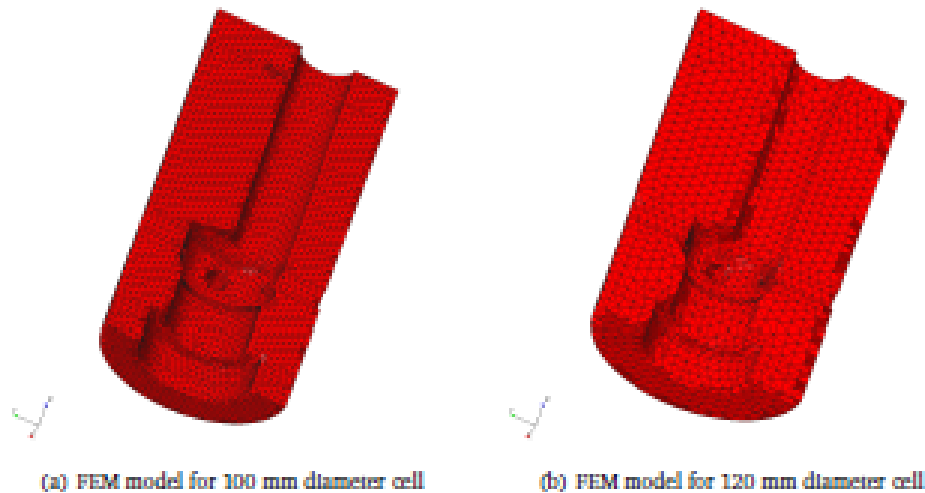


Figure 2: Finite element models for the equilibrium cell

2.2 Material

The unit will be manufactured from 316 stainless steel. The properties summarized in Table 1 were used in the finite element model. This data were obtained from the internet using the following sources:

1. http://www.azom.com/details.asp?Articleid=863#_Mechanical_Properties
2. <http://www.sandmeyersteel.com/316-316L.html>
3. <http://www.lenntech.com/Stainless-steel-316L.htm>

PROCESS ENGINEERING: EQUILIBRIUM CELL

4. <http://www.upmet.com/316-mechanical.shtml>
5. http://www.aksteel.com/pdf/markets_products/stainless/austenitic/316_316L_Data_Bulletin.pdf
6. http://www.efunda.com/materials/alloys/stainless_steels/show_stainless.cfm?ID=AISI_Type_316&prop=all&Page_Title=AISI_Type_316

Note that the yield strength of the material, which should be compared to the calculated maximum Von Mises stress to obtain the safety factor for the design, varies significantly. Values found on the internet ranged from 205 MPa to 310 MPa. In order to obtain a reliable safety factor, the client contacted the supplier of the material, which provided test data that specifies the yield strength at 263 MPa. The test data is within the range found on the internet and will be used from here onwards to obtain the safety factor.

Table 1: Stainless Steel 316 Material Properties

Property	Value
Modulus of Elasticity (E)	193 GPa
Young's Modulus (ν)	0.3
Coefficient of Thermal expansion (α)	$19.9 \times 10^{-6} \text{ } ^\circ\text{C}^{-1}$
Density (ρ)	8 000 kg/m ³
Yield Strength (from Internet) (σ_y)	205 - 310 MPa
Yield Strength (from supplier) (σ_y)	263 MPa

2.3 Loading

The operating conditions for the cell is an internal pressure of 300 bar (30 MPa) and a temperature of 150°C. The temperature load was applied as a constant temperature for the entire model. The pressure load was applied as three load components, as follows:

1. **Internal pressure:** The internal pressure of 30 MPa was applied on the internal surface of the cell, including the radial access holes that penetrate the cell, as shown in Fig. 3(a). Note that the pressure load does not extend all the way to the top of the piston shaft (top of Fig. 3(a)) and is only applied to the point where a looking glass will be installed (bottom of Fig. 3(a)).
2. **Pressure on the looking glass:** The looking glass itself was not modelled since this is purchased as a separate unit that is already certified for the operating conditions. The effect of the 30 MPa pressure on the looking glass was modelled by calculating the total force acting on the looking glass (a radius of 60.5 mm was used) and applying that to the surface containing the threads for installing the

PROCESS ENGINEERING: EQUILIBRIUM CELL

looking glass. This total load was calculated to be 86 242.61 N. Only half this load should be used in the symmetric model. However, to account for the effect of possible torquing of the looking glass unit, the full 86.2 kN force was applied. The looking glass has a thread pitch of 2 mm. From www.gizmology.net/nutsbolts.htm the load distribution on the threads was assumed to be 70% on the first 3 threads (6 mm) and 30% on the remainder of the threads (11 mm) as shown in Fig. 3(b) and Fig. 3(c) respectively. The thread load was thus applied on the first 17 mm of the access hole, as measured from the bottom edge of Fig. 3(a).

3. **Pressure on the radial access holes:** The outward effect of the pressure on the radial access holes was modelled by calculating the radial force acting on each hole (internal pressure times the area of the hole) and applying the resulting force as nodal forces around the outside perimeter of each hole. However, these forces were found to have no influence on the maximum Von Mises stresses calculated and are thus neglected in all the results presented here.

2.4 Boundary conditions

The boundary conditions applied were to account for symmetry and to prevent rigid body modes of the structure. These can be summarized as:

1. The symmetric boundary condition, which requires fixing all X displacements on the plane of symmetry (see Fig. 4(a))
2. Fixing the Y direction displacement at a single node (see Fig. 4(b))
3. Fixing all Z direction displacements at the one end point of the model (see Fig. 4(c))

2.5 Analysis

A linear static analysis was performed using the above described model.

PROCESS ENGINEERING: EQUILIBRIUM CELL

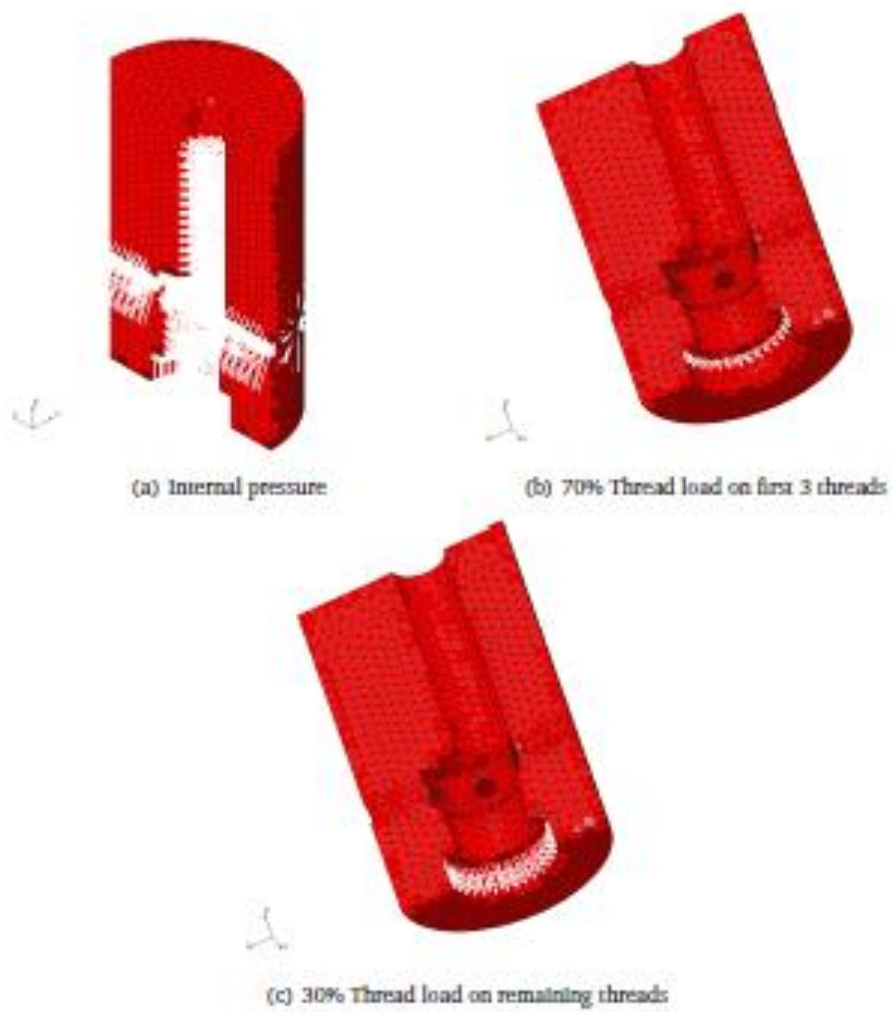


Figure 3: Finite element pressure load cases for the equilibrium cell

PROCESS ENGINEERING: EQUILIBRIUM CELL

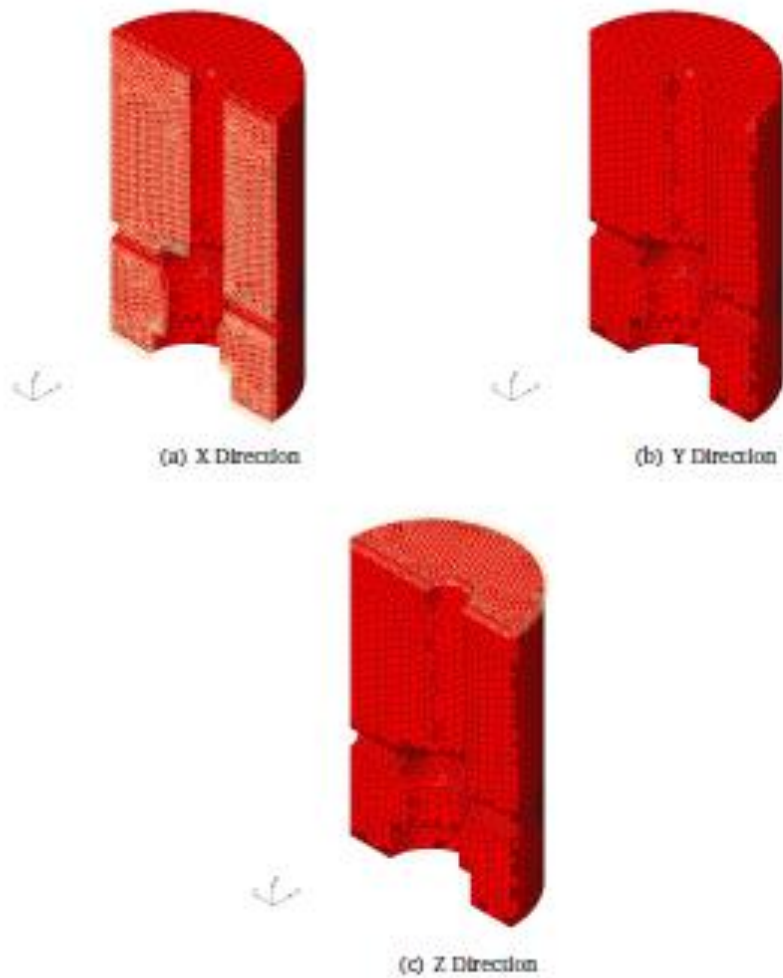


Figure 4: Finite element boundary conditions for the equilibrium cell

3 Results

3.1 Case 1: 100 mm diameter cell

The Von Mises stress distribution is shown in Fig. 5 below. Note that the highest stress values occur on the inside of the pressure vessel at the edge of the larger radial access holes. The stresses on the outside of the equilibrium cell are very small. There are stress concentrations where the radial access holes enter the pressure chamber, with a maximum Von Mises stress of 132 MPa. The safety factor for this design at the working pressure of 300 bar is thus 1.99.

PROCESS ENGINEERING: EQUILIBRIUM CELL

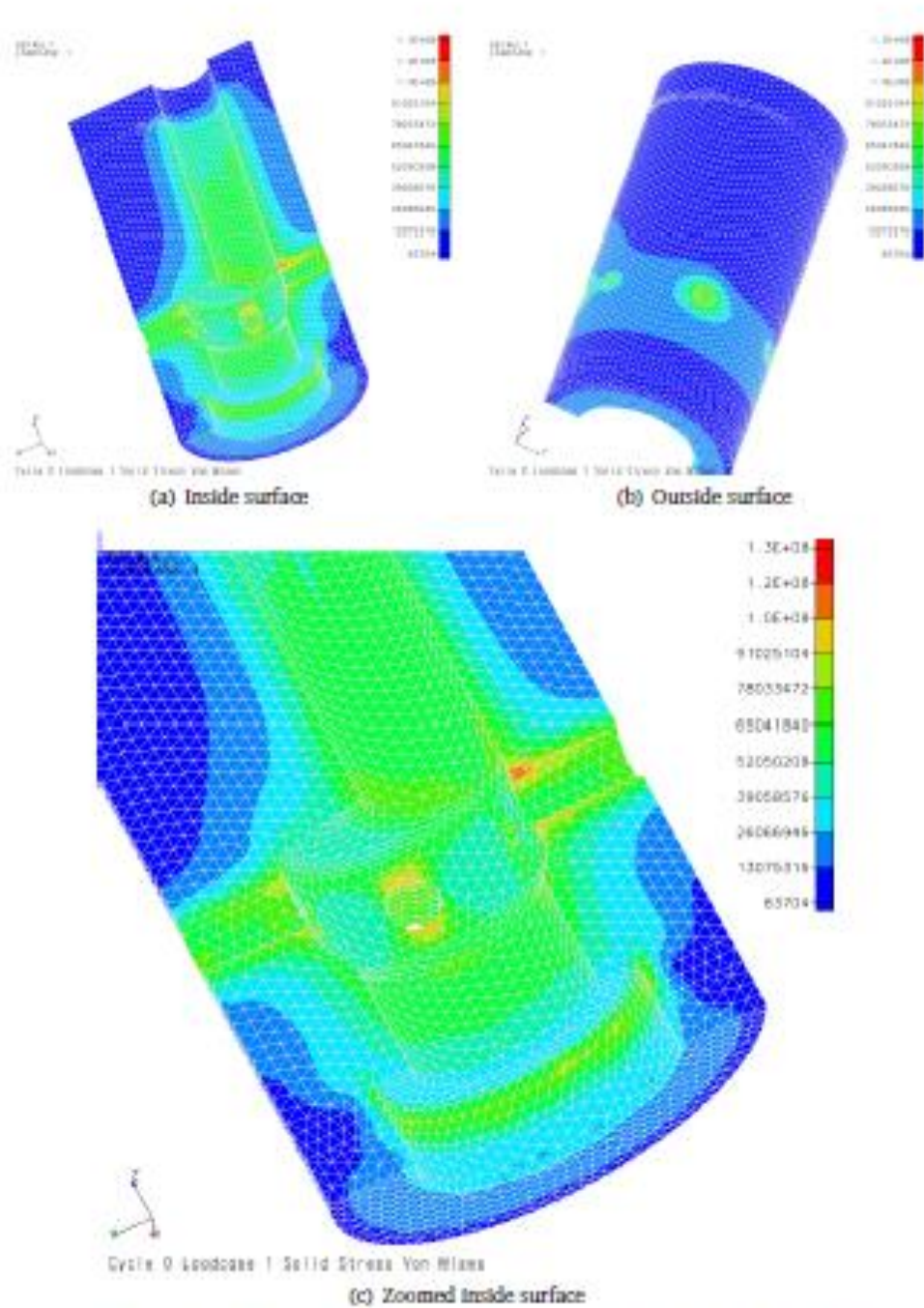


Figure 5: Von Mises stress distribution for the 100 mm diameter cell

PROCESS ENGINEERING: EQUILIBRIUM CELL

3.2 Case 2: 120 mm diameter cell

The Von Mises stress distribution for the 120 mm diameter equilibrium cell is shown in Fig. 6 below. Again the highest stress values occur on the inside of the pressure vessel at the edge of the larger radial access holes. However, increasing the diameter from 100 mm to 120 mm reduced the effect of this stress concentrations and the maximum Von Mises stress is reduced from 132 MPa to 97.5 MPa. The safety factor for this design at the working pressure of 300 bar is thus 2.70.

PROCESS ENGINEERING: EQUILIBRIUM CELL

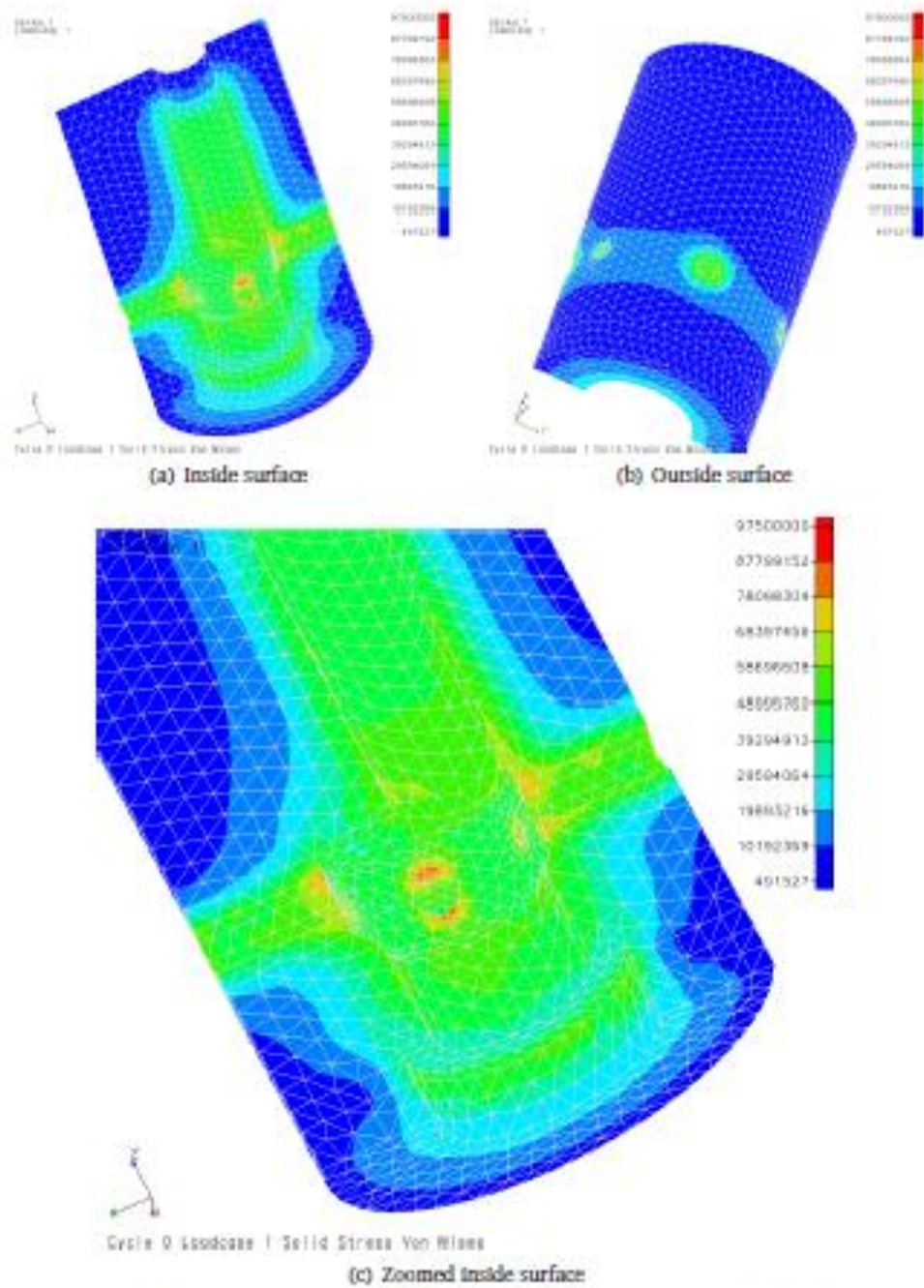


Figure 6: Von Mises stress distribution for the 120 mm diameter cell

4 Concluding Remarks

A detailed finite element analysis of an equilibrium cell was performed, using 3D CAD data provided by the client, material properties published on the web and a linear static finite element analysis. The yield strength of the material was obtained from test data provided by the supplier and was validated with values obtained from the web.

Two designs were considered, the first for a cell with an outer diameter of 100 mm, and the second for a cell with an outer diameter of 120 mm. The analysis identified stress concentrations where the radial access holes enter the cell. Where possible, the sharp edges of this interface should be avoided during manufacturing. With the stress concentrations present, the FEM analysis provided a maximum Von Mises stress of 132 MPa (safety factor of 1.99) for the 100 mm diameter cell and a maximum Von Mises stress of 97.5 MPa (safety factor of 2.70) for the 120 mm diameter cell.

Even though both designs have acceptable safety factors from a finite element perspective, it is still strongly recommended to perform a hydrostatic pressure test of the final design before making it available for general use. A good guideline for the hydrostatic test pressure is to use at least 1.4 times (according to the BS 5500 code) or 1.5 times (according to the ASME VIII Div. 1 code) the working pressure. If the more conservative ASME code is used, this would require a hydrostatic test pressure of 450 MPa. Both codes mentioned above are for pressure vessels. Note that according to the Occupational Health and Safety Act, 1993 (<http://www.labourwise.co.za/laws/Safety.PressureVessels.htm>) the equilibrium cell analyzed here is not considered a pressure vessel, since the volume in cubic meters (0.00015 m^3) times the pressure in Pascal (30 MPa) is less than 15 000. However, the pressure vessel hydrostatic test pressures should still provide a useful guideline for testing the unit.

VIRAJ PROFILES LIMITED

10 IMPERIAL CHAMBERS, 1ST FLOOR,
WILSON ROAD, BALLARD ESTATE
MUMBAI, 400 038, INDIA.

TEST CERTIFICATE

CUSTOMER :

DIVERSIFIED ALLOYS (PTY) LTD.
46 Milkyway Ave. Linbro Business Park,
Sandton, Gauteng, South Africa
(Tel) +2711 579 6100
(Fax) +2711 608 2292

ORDER NO .

PO#5192

PACKING LIST NO.

IMP/100800

INSPECTION NO

IMP/100800/13

DATE

07/09/2008

BUNDLE NO .

2715488,2715838,2715848

GRADE

AISI 316L

DESCRIPTION :

STAINLESS STEEL BRIGHT BARS

ROUGH TURNED

SIZE (MM)	SHAPE	TOLERANCE	LENGTH (MTR)	PIECES	WEIGHT (MTS)
140.000	ROUND	EN10060	5.00-6.00	3	1.942

CHEMICAL ANALYSIS

HEAT NO.											
C	Mn	Si	S	P	Ni	Cr	Mo	Cu	N	Co	
16052											
0.016	1.45	0.42	0.026	0.035	10.05	16.20	2.03	0.46	0.065	0.18	

TEST RESULT

.2% YIELD STRENGTH MPA	TENSILE STRENGTH MPA	ELONGATION %	REDUCTION OF AREA %	HARDNESS BHN
263	581	59	73	166

Specification :

MATERIAL CONFORMS TO EN 10088-3, ASTM A 276-06, COND A, ASTM A 320-05a, B8M CLASS 1, ASME SA 479-98, COND A, IGC TEST SATISFACTORY AS PER ASTM, 262-02a, PRAC. E, CERTIFIED AS PER EN 10204-3.1

Remarks :

MATERIAL IS FREE FROM MERCURY CONTAMINATION, FREE FROM WELD OR WELD REPAIRS, MANUFACTURED AND PROCESSED IN INDIA.

We hereby certified that the material described above has been tested and complies with the terms of order/contract.

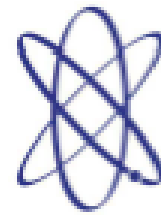

WORKS INSPECTOR

15347
15348
15349

Appendix D. *T, P* AND MASS CALIBRATIONS

Appendix D-1	Temperature calibrations (1).....	278
Appendix D-2	Temperature calibrations (2).....	282
Appendix D-3	Temperature calibrations (3).....	290
Appendix D-4	Temperature calibrations (4).....	308
Appendix D-5	Pressure calibrations (1).....	326
Appendix D-6	Pressure calibrations (2).....	329
Appendix D-7	Pressure calibrations (3).....	332
Appendix D-8	Pressure calibrations (4).....	333
Appendix D-9	Pressure calibrations (5).....	334
Appendix D-10	Pressure calibrations (6).....	335
Appendix D-11	Dead weight tester calibration	336
Appendix D-12	Low-pressure calibration (1).....	341
Appendix D-13	Low pressure calibration (2).....	344
Appendix D-14	Mass calibration (1).....	345
Appendix D-15	Mass calibration (2).....	346
Appendix D-16	Mass calibration (3).....	347
Appendix D-17	Mass calibration (4).....	348

SA Metrology
23 Platinum Business Park
Taurus Street
Brackenfell
Tel 0834502615 / Fax (086) 540 2384



SA METROLOGY

Certificate of Calibration

This certificate is issued in accordance with the ISO 17025:2005 International Standard and is traceable through the National Metrology Laboratory (NML) in Pretoria, SANAS recognised National or International Laboratories

Manufacturer : Julabo
Description : Water Bath with Controller unit & External Probe
Model No : ME6 / PT100
Serial No : Not Supplied
Asset No : WB1
Calibrated for : Department of Process Engineering : Stellenbosch University
: Stellenbosch
Temperature : 23 °C ± 3 °C
Relative humidity : 51 % RH ± 5 %RH
Date of calibration : 03 June 2011
Issue Date : 08 June 2011
Calibrated by : ZW de Witt

This Report is issued without alteration, Copyright of this Report is owned by SAMETand may not be reproduced other than in full, except with the prior written approval of SAMET. The values given in this Report were correct at the time of Test. Subsequently the accuracy will depend on factors such as care exercised in handling the instrument and frequency of use. Retest should be performed after a period, which has been chosen to ensure that, under normal circumstances, the instruments accuracy remains within the desired limits. The uncertainties of measurement were estimated for a coverage factor of $k=2$ which approximates a 95% confidence level.

A handwritten signature in black ink, appearing to be 'ZW de Witt', is written over a faint, larger version of the same signature.

Technical Signatory
ZW de Witt
Report no 3M32089

Page 1 of 4

Calibration Certificate

1. Standards and equipment

Ref	Make	Model	Description	Serial no
50	Fluke	5500A	Calibrator	7270009
18	Fluke	7103	Stirred Liquid Bath	A5B833
57	Hart Scientific	5699	SPRT Probe	0085
311	Fluke	712	RTD Calibrator	20091127

2. Procedure

- 2.1 The UUT (Unit under test) was calibrated in terms of the typical manufacturers' accuracy specification, referenced to the manufacturers recommended procedure
- 2.2 The Water Bath External Temperature Probe was calibrated against a known reference probe, inserted approximately 10 mm into calibration bath filled with silicon oil, the measured temperature was compared with the Process Variable (PV) displayed temperature on the UUT control unit
- 2.3 Typical accuracy tolerances values are used in the results

3. Results

3.1.1 Temperature controller probe accuracy test @ 0.0 °C

Set Point (°C)	Approximate (Min:Sec)	Applied Actual Temperature (°C)	Tolerance (°C)	PV Reading (°C)	Difference (°C)	Measurement uncertainty (°C)
0.0	0:00	0.00	± 1	-0.36	0.4	± 0.1
0.0	10:00	0.00	± 1	-0.34	0.3	± 0.1
0.0	15:00	0.00	± 1	-0.36	0.4	± 0.1
0.0	20:00	0.00	± 1	-0.35	0.4	± 0.1
0.0	25:00	0.00	± 1	-0.34	0.3	± 0.1
0.0	30:00	0.00	± 1	-0.35	0.4	± 0.1


 Technical Signatory
 ZW de Witt
 Report no SM32089

Page 2 of 4

Calibration Certificate

3.1.2 Temperature controller probe accuracy test @ 30.0 °C

Set Point (°C)	Approximate (Min:Sec)	Applied Actual Temperature (°C)	Tolerance (°C)	PV Reading (°C)	Difference (°C)	Measurement uncertainty (°C)
30.0	0:00	30.0	± 1	29.72	0.3	± 0.1
30.0	10:00	30.0	± 1	29.74	0.3	± 0.1
30.0	15:00	30.0	± 1	29.73	0.3	± 0.1
30.0	20:00	30.0	± 1	29.72	0.3	± 0.1
30.0	25:00	30.0	± 1	29.71	0.3	± 0.1
30.0	30:00	30.0	± 1	29.73	0.3	± 0.1

3.1.3 Temperature controller probe accuracy test @ 60.0 °C

Set Point (°C)	Approximate (Min:Sec)	Applied Actual Temperature (°C)	Tolerance (°C)	PV Reading (°C)	Difference (°C)	Measurement uncertainty (°C)
60.0	0:00	60.0	± 1	59.71	0.3	± 0.1
60.0	10:00	60.0	± 1	59.70	0.3	± 0.1
60.0	15:00	60.0	± 1	59.72	0.3	± 0.1
60.0	20:00	60.0	± 1	59.71	0.3	± 0.1
60.0	25:00	60.0	± 1	59.70	0.3	± 0.1
60.0	30:00	60.0	± 1	59.71	0.3	± 0.1

3.1.4 Temperature controller probe accuracy test @ 90.0 °C

Set Point (°C)	Approximate (Min:Sec)	Applied Actual Temperature (°C)	Tolerance (°C)	PV Reading (°C)	Difference (°C)	Measurement uncertainty (°C)
90.0	0:00	90.0	± 1	89.71	0.3	± 0.1
90.0	10:00	90.0	± 1	89.72	0.3	± 0.1
90.0	15:00	90.0	± 1	89.72	0.3	± 0.1
90.0	20:00	90.0	± 1	89.71	0.3	± 0.1
90.0	25:00	90.0	± 1	89.72	0.3	± 0.1
90.0	30:00	90.0	± 1	89.71	0.3	± 0.1



Technical Signatory
ZW de Wit
Report no SM32089

Page 3 of 4

Calibration Certificate

3.1.5 Temperature controller probe accuracy test @ 120.0 °C

Set Point (°C)	Approximate (Min:Sec)	Applied Actual Temperature (°C)	Tolerance (°C)	PV Reading (°C)	Difference (°C)	Measurement uncertainty (°C)
120.0	0:00	120.0	± 1	119.51	0.5	± 0.1
120.0	10:00	120.0	± 1	119.50	0.5	± 0.1
120.0	15:00	120.0	± 1	119.51	0.5	± 0.1
120.0	20:00	120.0	± 1	119.51	0.5	± 0.1
120.0	25:00	120.0	± 1	119.50	0.5	± 0.1
120.0	30:00	120.0	± 1	119.52	0.5	± 0.1

3.1.6 Temperature controller probe accuracy test @ 150.0 °C

Set Point (°C)	Approximate (Min:Sec)	Applied Actual Temperature (°C)	Tolerance (°C)	PV Reading (°C)	Difference (°C)	Measurement uncertainty (°C)
150.0	0:00	150.0	± 1	149.50	0.5	± 0.5
150.0	10:00	150.0	± 1	149.49	0.5	± 0.5
150.0	15:00	150.0	± 1	149.50	0.5	± 0.5
150.0	20:00	150.0	± 1	149.50	0.5	± 0.5
150.0	25:00	150.0	± 1	149.49	0.5	± 0.5
150.0	30:00	150.0	± 1	149.50	0.5	± 0.5

4. Comments

4.1 **Bold** - highlights indicate out of tolerance values.



Technical Signatory
ZW de Witt
Report no SM32089

Page 4 of 4



Certificate of Calibration

This certificate is issued without alteration, and in accordance with the conditions of accreditation granted by SANAS. It is a correct record of the measurements made at the time of calibration. Copyright of this certificate is owned by InterCal and may not be reproduced other than in full, except with the prior written approval of InterCal. The values given in this certificate were correct at the time of calibration. Subsequently the accuracy will depend on factors such as care exercised in handling the instrument and frequency of use. Recalibration should be performed after a period which has been chosen to ensure that, under normal circumstances, the instruments accuracy remains within the desired limits. The accuracies of all measurements were traceable to the national measuring standards as maintained in South Africa, unless otherwise noted.

The reported expanded uncertainties are based on a standard uncertainty multiplied by a coverage factor $k = 2$ providing a level of confidence of approximately 95%. The uncertainties of measurement have been estimated in accordance with the principles defined in the GUM, Guide to Uncertainty of Measurement, ISO, Geneva, 1993

Certificate No : 50453

Manufacturer : Agilent
Description : Digital Thermometer and 12 Probes
Model No : 34972A
Serial No : MY49009493 (probes: see results)
Plant No : None

Calibrated for : Separation Technology
Address : Department Process Engineering
 Stellenbosch University
 Banghoek Road
 Stellenbosch
 7600

Calibration Environment

Temperature : 23 °C (± 1°C)
Relative Humidity : 35 %rh (± 2%rh)

Date of calibration : 22 February 2013
Expiry Date : 22 August 2014

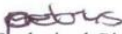
Print Date : 25 February 2013

Calibrated by : C.Pretorius

Checked by : 



The South African National Accreditation System (SANAS) is a member of the International Laboratory Accreditation Cooperation (ILAC) Mutual Recognition Arrangement (MRA). This Arrangement allows for the mutual recognition of technical test and calibration data by the member accreditation bodies worldwide. For more information in the Arrangement please consult www.ilac.org


 Technical Signatory
 C.Pretorius

Page 1 of 4

InterCal CC Reg: CK1992/28397/23
 InterCal Test and Measurement Center, 907 Richards Drive, Halfway House, Midrand
 PO Box 10907 Vorna Valley 1686
 Tel: (011) 315 4321 Fax: (011) 312 1322 e-mail: intercal@intercal.co.za www.intercal.co.za

Members: PS Haarhoff GC Snelling

Certificate of Calibration

Certificate No: 50453

1. Standards and equipment

Asset ID	Make	Model	Description	Serial Number	Due Date	Certificate No
3-138	Isotech	935-14-95-H	PT 100 Probe	32230/1	July 2013	THIRT-6473
1-82	Hewlett Packard	34401A	Multimeter Oil Bath	3146A37027	July 2013	I27772

The standards used in this calibration have themselves been calibrated traceable to the National Measuring Standards maintained by the NMISA.

2. Procedure

2.1 The UUT (unit under test) was calibrated by comparison to the laboratory standard at the listed temperatures in accordance with procedure 3/P/003.

3. Results

3.1 Temperature

Channel 101 - 104

Measured Temperature (°C)	UUT Value (1) EC-FR (°C)	UUT Value (2) EC-BR (°C)	UUT Value (3) EC-FL (°C)	UUT Value (4) EC-BL (°C)	Uncertainty of measurement (°C)
30.00	29.98	30.04	30.04	30.05	± 0.1
60.00	59.94	60.04	60.04	60.4	± 0.1
90.00	89.93	90.02	90.01	90.01	± 0.1
120.00	119.96	120.08	120.05	120.01	± 0.1
150.00	149.93	150.01	150.01	149.97	± 0.1


Technical Signatory

Page 2 of 4

Certificate of Calibration

Certificate No: 50453

3.2 Corrections
Channel 101 - 104

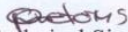
Measured Temperature (°C)	UUT Corrections (1) EC-FR (°C)	UUT Corrections (2) EC-BR (°C)	UUT Corrections (3) EC-FL (°C)	UUT Corrections (4) EC-BL (°C)	Uncertainty of measurement (°C)
30.00	+0.02	-0.04	-0.04	-0.05	±0.1
60.00	+0.06	-0.04	-0.04	-0.04	± 0.1
90.00	+0.07	-0.02	-0.01	-0.01	± 0.1
120.00	+0.04	-0.08	-0.05	-0.01	± 0.1
150.00	+0.07	-0.01	-0.01	+0.03	± 0.1

3.3 Temperature
Channel 105-108

Measured Temperature (°C)	UUT Value (5) HFI-FR (°C)	UUT Value (6) HFI-BR (°C)	UUT Value (7) HFI-FL (°C)	UUT Value (8) HFO-BL (°C)	Uncertainty of measurement (°C)
30.00	30.58	30.04	30.05	29.96	± 0.1
90.00	90.63	89.97	90.02	89.91	± 0.1
150.00	150.80	149.98	150.07	149.91	± 0.1

3.4 Corrections
Channel 105-108

Measured Temperature (°C)	UUT Corrections (5) HFI-FR (°C)	UUT Corrections (6) HFI-BR (°C)	UUT Corrections (7) HFI-FL (°C)	UUT Corrections (8) HFO-BL (°C)	Uncertainty of measurement (°C)
30.00	-0.58	-0.04	-0.05	+0.04	± 0.1
90.00	-0.63	+0.03	-0.02	-0.09	± 0.1
150.00	-0.80	+0.02	-0.07	+0.09	± 0.1


Technical Signatory

Page 3 of 4

Certificate of Calibration

Certificate No: 50453

3.5 Temperature
Channel 109, 110, 201, 202

Measured Temperature (°C)	UUT Value (9) OVN-FR (°C)	UUT Value (10) OVN-BR (°C)	UUT Value (11) OVN-FL (°C)	UUT Value (12) OVN-BL (°C)	Uncertainty of measurement (°C)
30.00	29.99	30.04	30.05	30.07	± 0.1
90.00	89.94	89.99	89.98	90.01	± 0.1
150.00	149.96	149.98	149.97	150.0	± 0.1

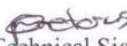
3.5 Corrections
Channel 109, 110, 201, 202

Measured Temperature (°C)	UUT Corrections (9) OVN-FR (°C)	UUT Corrections (10) OVN-BR (°C)	UUT Corrections (11) OVN-FL (°C)	UUT Corrections (12) OVN-BL (°C)	Uncertainty of measurement (°C)
30.00	+0.01	-0.04	-0.05	-0.07	± 0.1
90.00	+0.06	+0.01	+0.02	-0.01	± 0.1
150.00	+0.04	+0.02	+0.03	0.0	± 0.1

4. Comments

- 4.1 The UUT was only calibrated at the above temperatures in accordance with the customer's instruction.
- 4.2 Please note that channel or probe 110 has an intermittent problem; occasionally reading: "OVLD".

----- End of document -----


Technical Signatory

Page 4 of 4



Certificate of Calibration

This certificate is issued without alteration, and in accordance with the conditions of accreditation granted by SANAS. It is a correct record of the measurements made at the time of calibration. Copyright of this certificate is owned by InterCal and may not be reproduced other than in full, except with the prior written approval of InterCal. The values given in this certificate were correct at the time of calibration. Subsequently the accuracy will depend on factors such as care exercised in handling the instrument and frequency of use. Recalibration should be performed after a period which has been chosen to ensure that, under normal circumstances, the instruments accuracy remains within the desired limits. The accuracies of all measurements were traceable to the national measuring standards as maintained in South Africa, unless otherwise noted. The reported expanded uncertainties are based on a standard uncertainty multiplied by a coverage factor $k = 2$ providing a level of confidence of approximately 95%. The uncertainties of measurement have been estimated in accordance with the principles defined in the GUM, Guide to Uncertainty of Measurement, ISO, Geneva, 1993

Certificate No : 50454

Manufacturer : Julabo
Description : Waterbath Controller and Probe
Model No : Me-6
Serial No : 10163505
Plant No : (13) EC-DIAG

Calibrated for : Separation Technology
Address : Department Process Engineering
 Stellenbosch University
 Banghoek Road
 Stellenbosch
 7600

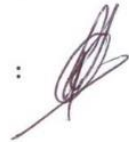
Calibration Environment

Temperature : 23 °C (± 1°C)
Relative Humidity : 40 %rh (± 2%rh)

Date of calibration : 25 February 2013
Expiry Date : 25 August 2014

Print Date : 26 February 2013

Calibrated by : C.Pretorius

Checked by : 



The South African National Accreditation System (SANAS) is a member of the International Laboratory Accreditation Cooperation (ILAC) Mutual Recognition Arrangement (MRA). This Arrangement allows for the mutual recognition of technical test and calibration data by the member accreditation bodies worldwide. For more information in the Arrangement please consult www.ilac.org


 Technical Signatory
 C.Pretorius

Page 1 of 2

InterCal CC Reg: CK1992/28397/23
 InterCal Test and Measurement Center, 907 Richards Drive, Halfway House, Midrand
 PO Box 10907 Vorna Valley 1686
 Tel: (011) 315 4321 Fax: (011) 312 1322 e-mail: intercal@intercal.co.za www.intercal.co.za

Members: PS Haarhoff GC Snelling

Certificate of Calibration

Certificate No: 50454

1. Standards and equipment

Asset ID	Make	Model	Description	Serial Number	Due Date	Certificate No
3-138	Isotech	935-14-95-H	PT 100 Probe	32230/1	July 2013	THRT-6473
1-82	Hewlett Packard	34401A	Multimeter Oil Bath	3146A37027	July 2013	I2772

The standards used in this calibration have themselves been calibrated traceable to the National Measuring Standards maintained by the NMISA.

2. Procedure

- 2.1 The UUT (unit under test) was calibrated by comparison to the laboratory standard at the listed temperatures in accordance with procedure 3/P/003.

3. Results

3.1 Temperature

Measured Temperature (°C)	UUT Value (°C)	UUT Correction (°C)	Uncertainty of measurement (°C)
30.00	29.47	+0.53	± 0.1
60.00	59.45	+0.55	± 0.1
90.00	90.42	+0.58	± 0.1
120.00	119.41	+0.59	± 0.1
150.00	149.40	+0.60	± 0.1

4. Comments

- 4.1 The UUT was only calibrated at the above temperatures in accordance with the customer's instruction.

----- End of document -----


Technical Signatory

Page 2 of 4



Certificate of Calibration

This certificate is issued without alteration, and in accordance with the conditions of accreditation granted by SANAS. It is a correct record of the measurements made at the time of calibration. Copyright of this certificate is owned by InterCal and may not be reproduced other than in full, except with the prior written approval of InterCal. The values given in this certificate were correct at the time of calibration. Subsequently the accuracy will depend on factors such as care exercised in handling the instrument and frequency of use. Recalibration should be performed after a period which has been chosen to ensure that, under normal circumstances, the instruments accuracy remains within the desired limits. The accuracies of all measurements were traceable to the national measuring standards as maintained in South Africa, unless otherwise noted. The reported expanded uncertainties are based on a standard uncertainty multiplied by a coverage factor $k = 2$ providing a level of confidence of approximately 95%. The uncertainties of measurement have been estimated in accordance with the principles defined in the GUM, Guide to Uncertainty of Measurement, ISO, Geneva, 1993

Certificate No : 50455

Manufacturer : Gefran
Description : 2 Temperature Controllers and 2 Probes
Model No : 600
Serial No : Process, Overtemp
Plant No : None

Calibrated for : Separation Technology
Address : Department Process Engineering
 Stellenbosch University
 Banghoek Road
 Stellenbosch
 7600

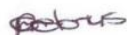
Calibration Environment
Temperature : 25 °C (± 1°C)
Relative Humidity : 30 %rh (± 2%rh)

Date of calibration : 23 February 2013 **Print Date** : 25 February 2013
Expiry Date : 23 August 2014

Calibrated by : C.Pretorius/ S.R Lamola **Checked by** : 



The South African National Accreditation System (SANAS) is a member of the International Laboratory Accreditation Cooperation (ILAC) Mutual Recognition Arrangement (MRA). This Arrangement allows for the mutual recognition of technical test and calibration data by the member accreditation bodies worldwide. For more information in the Arrangement please consult www.ilac.org


 Technical Signatory
 C.Pretorius

Page 1 of 2

InterCal CC Reg: CK1992/28397/23
 InterCal Test and Measurement Center, 907 Richards Drive, Halfway House, Midrand
 PO Box 10907 Vorna Valley 1686
 Tel: (011) 315 4321 Fax: (011) 312 1322 e-mail: intercal@intercal.co.za www.intercal.co.za
 Members: PS Haarhoff GC Snelling

Certificate of Calibration

Certificate No: 50455

1. Standards and equipment

Asset ID	Make	Model	Description	Serial Number	Due Date	Certificate No
3-139	Isotech	935-14-95-H	PT 100 Probe	32230/2	July 2013	THIRT-6474
1-82	Hewlett Packard	34401A	Multimeter	3146A37027	July 2013	I27772
			Oil Bath			

The standards used in this calibration have themselves been calibrated traceable to the National Measuring Standards maintained by the NMISA.

2. Procedure

2.1 The UUT (unit under test) was calibrated by comparison to the laboratory standard at the listed temperatures in accordance with procedure 3/P/003.

3. Results

3.1 Temperature Process

Measured Temperature (°C)	UUT Value (°C)	UUT Correction (°C)	Uncertainty of measurement (°C)
30.0	29.6	+0.4	± 0.1
90.0	89.4	+0.6	± 0.1
150.0	149.2	+0.8	± 0.1

3.2 Temperature Overtemp

Measured Temperature (°C)	UUT Value (°C)	UUT Correction (°C)	Uncertainty of measurement (°C)
30.0	29.9	+0.1	± 0.1
90.0	89.7	+0.3	± 0.1
150.0	149.5	+0.5	± 0.1

4. Comments

4.1 The UUT was only calibrated at the above temperatures in accordance with the customer's instruction.

----- End of document -----


Technical Signatory

Page 2 of 2



Calibration and Services
calibration • validation • training

Calibration certificate

CAL-UC-S-T-141203L05
certificate number



	INSTRUMENT	PROBE	
Type	Digital Multimeter	4-wire-Pt100 immersion	Channel 1
Manufacturer	Agilent	Wika	
Part Nr.	34972 A	SS 316	
Serial Nr.	MY 49009493	(1) EC-FR	

Calibration of hi-accuracy digital thermometer with 1/10 4-wire-Pt100 immersion probe

Location **Laboratory - Unitemp cc.**
47 Flamingo Crescent
Lansdowne
Cape Town



Customer Address **University of Stellenbosch**
Kamer 225
Chemiese Ingenieurs
Stellenbosch

Order Nr. **314653**
Date of calibration **4-Dec-2014**

Was adjustment of the instrument done?

yes

no

The reported expanded uncertainty is based on a standard uncertainty multiplied by a coverage factor $k = 2$ providing a level of confidence of approximately 95%. The uncertainty of measurement has been estimated in accordance with the principles defined in the GUM, guide to uncertainty of measurement, ISO, Geneva, 1995.

This calibration certificate may not be reproduced other than in full, and with the permission of SANAS & Unitemp Laboratory.

Calibration certificates without an authorized signature and seal are not valid.

Person Responsible: F.F. Rivera
F Fernandez-Rivera

Technical Signatory: a
Roy MacGregor

page 1 of 2



www.unitemp.com

sales@unitemp.com

Unitemp c.c. Reg. No. CK1986/008689/23
Members: H.A. Hitzeroth D.R. Butow U.H. Hitzeroth A. Sample

Unitemp Laboratory

Temperature Insertion Probe Calibration Protocol

Date:	3-12-14	Company Name:	UNIVERSITY OF STELLENBOSCH
I/O No	314653	Cert.no:	CAL-UGS-T-141203LOS
Person Responsible:	Francisco PZ		
Ambient Conditions:	22.7 °C	49.7	%RH
Instrument:	Digital Multichannel	Probe:	1/10 PE 100 - 4-wire immersion
PART NUMBER:	34972 A	PART NUMBER	wa 55316
SERIAL NUMBER:	MY49009493	SERIAL NUMBER:	(1) EC-FR
MANUFACTURER:	AGILENT	MANUFACTURER:	wa WLEA

Measuring Point (°C)	Reference value (°C)	Measured value (°C)	Info
30 °C	30.024	30.00	PE-100
0.01 Resolution	29.998	30.00	2385
Accuracy	30.022	30.03	4-wire
4 Reference	30.031	30.03	1/10
7 Bath	30.022	30.02	
	30.009	30.00	
60 °C	60.072	60.02	CHANNEL
0.01 Resolution	60.109	60.05	(1)
Accuracy	60.097	60.04	
4 Reference	60.111	60.06	
7 Bath	60.099	60.04	
	60.069	60.02	
90 °C	90.036	89.94	
0.01 Resolution	90.030	89.94	
Accuracy	90.056	89.95	
4 Reference	90.049	89.95	
7 Bath	90.067	89.96	
	90.079	89.98	
120 °C	120.055	119.90	
0.01 Resolution	120.060	119.90	
Accuracy	120.036	119.87	
4 Reference	120.039	119.90	
7 Bath	120.044	119.89	
	120.036	119.89	

Immersion depth (mm)	Temp. (°C)
55	30
70	60
70	90
70	120

φ 3mm

Prober came bent by client.





Calibration and Services

calibration • validation • training

Calibration certificate CAL-UC-S-T-141203L05
certificate number



363

Lab measurement equipment with certified traceability to international standards

Description	Cert. No.	Equipment. Number
Testo 400 with PT100 probe	T55698	Unitemp4
Testo 400 with PT100 probe	T57306	Unitemp3
Testo 735 with PT100 probe	THDG-6609	Unitemp41

Ambient conditions.

Temperature: 23 °C ± 5 °C

Measuring procedure (P0051)

The measurements read on this test item, in a thermostatic bath, were obtained while placed in very close proximity of a reference probe.

The result is calculated from an average of **6** readings @ **30** seconds intervals

Measurement results for hi-accuracy digital thermometer with 1/10 4-wire-Pt100 immersion probe

Indication from reference in °C	Indication from your measuring instrument in °C	Deviation in °C	Manufacture's allowed tolerance in °C	Expanded uncertainty of measurement in °C	Probe insertion depth in mm	Reference Equipment Used
30.034	30.01	-0.02	n/a	± 0.05	55	Unitemp4
60.105	60.04	-0.06	n/a	± 0.05	70	Unitemp4
90.060	89.95	-0.11	n/a	± 0.05	70	Unitemp4
120.054	119.89	-0.16	n/a	± 0.05	70	Unitemp4

Validity of Certificate

The measurement results recorded in this certificate relate only to the instrument & attachments specified, and were correct at the time. Only the above points have been checked & performance at other points is not certain. Subsequent accuracy will depend on factors such as care, handling and frequency of use. It is recommended that recalibration be undertaken at an interval that will ensure that the instrument remains within the desired limits.

page 2 of 2

END



www.unitemp.com

sales@unitemp.com

Unitemp c.c. Reg. No. CK1986/008689/23
Members: H.A. Hitzeroth D.R. Bütow U.H. Hitzeroth A. Semple



Calibration and Services
calibration • validation • training

Calibration certificate

CAL-UC-S-T-141203L05
ADDENDUM 1A certificate number



	INSTRUMENT	PROBE	
Type	Digital Multimeter	4-wire-Pt100 immersion	Channel 2
Manufacturer	Agilent	Wika	
Part Nr.	34972 A	SS 316	
Serial Nr.	MY 49009493	(2) EC-BR	

Calibration of hi-accuracy digital thermometer with 1/10 4-wire-Pt100 immersion probe

Location **Laboratory - Unitemp cc.**
 47 Flamingo Crescent
 Lansdowne
 Cape Town

Customer **University of Stellenbosch**
Address **Kamer 225**
 Chemiese Ingenieurs
 Stellenbosch

Order Nr. **314653**
Date of calibration **4-Dec-2014**

Was adjustment of the instrument done?

yes

no

The reported expanded uncertainty is based on a standard uncertainty multiplied by a coverage factor $k = 2$ providing a level of confidence of approximately 95%. The uncertainty of measurement has been estimated in accordance with the principles defined in the GUM - guide to uncertainty of measurement, ISO, Geneva, 1993

This calibration certificate may not be reproduced other than in full, and with the permission of SANAS & Unitemp Laboratory.

Calibration certificates without an authorized signature and seal are not valid.

Person Responsible: *F.F. Rivera*
F Fernandez-Rivera

Technical Signatory: *Roy MacGregor*
Roy MacGregor



www.unitemp.com

sales@unitemp.com

Unitemp c.c. Reg. No. CK1986/008689/23
Members: H.A. Hitzeroth D.R. Butow U.H. Hitzeroth A. Semple

Unitemp Laboratory

Temperature Insertion Probe Calibration Protocol

Date:	3-12-14	Company Name:	UNIVERSITY OF STELLENBOSCH
I/O No:	314 653	Cert.no:	CAL-ULG-ST-141203 L0 65
Person Responsible:	Francisco PZ		
Ambient Conditions:	22.7 °C	49.7 %RH	
Instrument:	Digital Multichannel	Probe:	1/10 PE100 - 4-wire immersion
PART NUMBER:	34972 A	PART NUMBER:	WFA SS 316
SERIAL NUMBER:	MY49009493	SERIAL NUMBER:	(2) EC- BR
MANUFACTURER:	AGILENT	MANUFACTURER:	WFA WIFA

Addendum
1A

102
3-12-14
102

Measuring Point (°C)	Reference value (°C)	Measured value (°C)	Info
30 °C	30.022	30.06	PE100
0.01 Resolution	30.034	30.06	+385
Accuracy	30.054	30.09	4-wire
4 Reference	30.052	30.09	1/10
7 Bath	30.045	30.08	
	30.036	30.06	
60 °C	60.083	60.09	CHANNEL
0.01 Resolution	60.073	60.07	(2)
Accuracy	60.038	60.05	
4 Reference	60.039	60.04	
7 Bath	60.041	60.04	
	60.053	60.08	
90 °C	90.027	89.99	
0.01 Resolution	90.054	90.03	
Accuracy	90.064	90.02	
4 Reference	90.033	90.00	
7 Bath	90.034	89.99	
	90.038	90.01	
120 °C	120.083	120.00	
0.01 Resolution	120.050	119.98	
Accuracy	120.051	119.98	
4 Reference	120.054	119.99	
7 Bath	120.073	120.00	
	120.062	119.99	

3-12-14

Immersion depth (mm)	Temp. (°C)
80	30
80	60
80	90
80	120

Ø 3mm

Probe came bent by client.





Calibration and Services

calibration • validation • training

Calibration certificate CAL-UC-S-T-141203L05
ADDENDUM 1A certificate number



363

Lab measurement equipment with certified traceability to international standards

Description	Cert. No.	Equipment Number
Testo 400 with PT100 probe	T55698	Unitemp4
Testo 400 with PT100 probe	T57306	Unitemp3
Testo 735 with PT100 probe	THDG-6609	Unitemp41

Ambient conditions.

Temperature: 23 °C ± 5 °C

Measuring procedure (P0051)

The measurements read on this test item, in a thermostatic bath, were obtained while placed in very close proximity of a reference probe.

The result is calculated from an average of **6** readings @ **30** seconds intervals

Measurement results for hi-accuracy digital thermometer with 1/10 4-wire-Pt100 immersion probe

Indication from reference in °C	Indication from your measuring instrument in °C	Deviation in °C	Manufacture's allowed tolerance in °C	Expanded uncertainty of measurement in °C	Probe insertion depth in mm	Reference Equipment Used
30.057	30.07	0.01	n/a	± 0.05	80	Unitemp4
60.067	60.06	-0.01	n/a	± 0.05	80	Unitemp4
90.049	90.01	-0.04	n/a	± 0.05	80	Unitemp4
120.073	119.99	-0.08	n/a	± 0.05	80	Unitemp4

Validity of Certificate

The measurement results recorded in this certificate relate only to the instrument & attachments specified, and were correct at the time. Only the above points have been checked & performance at other points is not certain. Subsequent accuracy will depend on factors such as care, handling and frequency of use. It is recommended that recalibration be undertaken at an interval that will ensure that the instrument remains within the desired limits.

page 2 of 2

END



www.unitemp.com

sales@unitemp.com

Unitemp c.c. Reg. No. CK1986/008689/23
Members: H.A. Hitzeroth D.R. Butow U.H. Hitzeroth A. Semple

Unitemp Laboratory

Temperature Insertion Probe Calibration Protocol

Date:	3-12-14	Company Name:	UNIVERSITY OF STELLENBOSCH
I/O No	314653	Cert.no:	CAL-UC-ST-141203L075
Person Responsible:	Francisco PZ		
Ambient Conditions:	22.7 °C	49.7 %RH	
Instrument:	Digital Multichannel	Probe:	1/10 PE 100 - 4-wire immersion
PART NUMBER:	34972 A	PART NUMBER	WTA S\$316
SERIAL NUMBER:	MY49009493	SERIAL NUMBER:	(3) EC-FL
MANUFACTURER:	AGILENT	MANUFACTURER:	WTA WILKA

PZ
4-12-14
Addendum
2A

1104

CHANNEL (3)

103

Measuring Point (°C)		Reference value (°C)	Measured value (°C)	Info
30	°C	30.035	30.05	PE100
0.01	Resolution	30.034	30.06	2385
	Accuracy	30.030	30.08	4-wire
4	Reference	30.036	30.05	110
7	Bath	30.040	30.07	
		30.054	30.08	
60	°C	60.037	60.04	CHANNEL
0.01	Resolution	60.031	60.03	(3)
	Accuracy	60.046	60.04	
4	Reference	60.049	60.06	
7	Bath	60.078	60.08	
		60.049	60.05	
90	°C	90.004	90.00	
0.01	Resolution	90.039	90.03	
	Accuracy	90.044	90.03	
4	Reference	90.022	90.01	
7	Bath	90.043	90.03	
		90.031	90.03	
120	°C	120.048	120.02	
0.01	Resolution	120.061	120.01	
	Accuracy	120.035	120.00	
4	Reference	120.056	120.01	
7	Bath	120.038	119.98	
		120.029	120.00	

Immersion depth (mm)	Temp. (°C)
60	30
60	60
60	90
60	120

Probes came bent by client.

φ 3 mm



Document: R0012
Laserfiche Version: 3
Date: 07 May 2012



Calibration and Services

calibration • validation • training

Calibration certificate

CAL-UC-S-T-141203L05
ADDENDUM 2A certificate number



363

Lab measurement equipment with certified traceability to international standards

Description	Cert. No.	Equipment. Number
Testo 400 with PT100 probe	T55698	Unitemp4
Testo 400 with PT100 probe	T57306	Unitemp3
Testo 735 with PT100 probe	THDG-6809	Unitemp41

Ambient conditions.

Temperature: 23 °C ± 5 °C

Measuring procedure (P0051)

The measurements read on this test item, in a thermostatic bath, were obtained while placed in very close proximity of a reference probe.

The result is calculated from an average of 6 readings @ 30 seconds intervals

Measurement results for hi-accuracy digital thermometer with 1/10 4-wire-PT100 immersion probe

Indication from reference in °C	Indication from your measuring instrument in °C	Deviation in °C	Manufacture's allowed tolerance in °C	Expanded uncertainty of measurement in °C	Probe insertion depth in mm	Reference Equipment Used
30.055	30.07	0.02	n/a	± 0.05	60	Unitemp4
60.060	60.05	-0.01	n/a	± 0.05	60	Unitemp4
90.038	90.02	-0.02	n/a	± 0.05	60	Unitemp4
120.054	120.00	-0.05	n/a	± 0.05	60	Unitemp4

Validity of Certificate

The measurement results recorded in this certificate relate only to the instrument & attachments specified, and were correct at the time. Only the above points have been checked & performance at other points is not certain. Subsequent accuracy will depend on factors such as care, handling and frequency of use. It is recommended that recalibration be undertaken at an interval that will ensure that the instrument remains within the desired limits.



page 2 of 2

END

www.unitemp.com

sales@unitemp.com

Unitemp c.c. Reg. No. CK1986/008689/23
Members: H.A. Hitzeroth D.R. Bütow U.H. Hitzeroth A. Sample



Calibration and Services
calibration • validation • training

Calibration certificate

CAL-UC-S-T-141203L05
ADDENDUM 3A certificate number



363

	INSTRUMENT	PROBE	
Type	Digital Multimeter	4-wire-Pt100 immersion	Channel 4
Manufacturer	Agilent	Wika	
Part Nr.	34972 A	SS 316	
Serial Nr.	MY 49009493	(4) EC-BL	

Calibration of hi-accuracy digital thermometer with 1/10 4-wire-Pt100 immersion probe

Location Laboratory - Unitemp cc.
47 Flamingo Crescent
Lansdowne
Cape Town

Customer University of Stellenbosch
Address Kamer 225
Chemiese Ingenieurs
Stellenbosch

Order Nr. 314653
Date of calibration 4-Dec-2014

Was adjustment of the instrument done?

yes

no

The reported expanded uncertainty is based on a standard uncertainty multiplied by a coverage factor $k = 2$ providing a level of confidence of approximately 95%, the uncertainty of measurement has been estimated in accordance with the principles defined in the GUM: guide to uncertainty of measurement, ISO, Geneva, 1993.

This calibration certificate may not be reproduced other than in full, and with the permission of SANAS & Unitemp Laboratory.

Calibration certificates without an authorized signature and seal are not valid.

Person Responsible:

F Fernandez-Rivera

Technical Signatory:

Roy MacGregor

page 1 of 2



www.unitemp.com

sales@unitemp.com

Unitemp c.c. Reg. No. CK1986/008689/23
Members: H.A. Hitzeroth D.R. Bütow U.H. Hitzeroth A. Semple

Unitemp Laboratory

Temperature Insertion Probe Calibration Protocol

Date:	3-12-14	Company Name:	UNIVERSITY OF STELLENBOSCH
I/O No	314653	Cert.no:	CAL-UCS-T-141203L085
Person Responsible:	Francis FZ		
Ambient Conditions:	22.7 °C	49.7 %RH	
Instrument:	Digital Multichannel	Probe:	110 PE 100 - 4-wire immersion
PART NUMBER:	34972 A	PART NUMBER	HTA 55316
SERIAL NUMBER:	MY49009493	SERIAL NUMBER:	(4) EC-BL
MANUFACTURER:	AGILENT	MANUFACTURER:	HTAWIKA

Addendum
3A

immersion

CHANNEL 4 104

Measuring Point (°C)	Reference value (°C)	Measured value (°C)	Info
30 °C	30.074	30.10	PE 100
0.01 Resolution	30.035	30.07	2385
Accuracy	30.039	30.07	4-wire
4 Reference	30.050	30.08	110
7 Bath	30.047	30.08	
	30.053	30.09	
60 °C	60.02857	60.0407	CHANNEL 4
0.01 Resolution	60.059	60.06	(4)
Accuracy	60.052	60.07	
4 Reference	60.054	60.08	
7 Bath	60.047	60.06	
	60.057	60.06	
90 °C	90.008	90.01	
0.01 Resolution	90.030	90.02	
Accuracy	90.039	90.02	
4 Reference	90.040	90.02	
7 Bath	90.013	90.01	
	90.018	90.00	
120 °C	120.066	119.99	
0.01 Resolution	120.071	120.00	
Accuracy	120.091	120.02	
4 Reference	120.058	119.97	
7 Bath	120.042	119.99	
	120.071	120.00	

FZ
3-12-14

Immersion depth (mm)	Temp. (°C)
85	30
85	60
85	90
85	120

Prober came bent by client.



Document: R0012
Laserfile Version: 3
Date: 07 May 2012



Calibration and Services

calibration • validation • training

Calibration certificate CAL-UC-S-T-141203L05
ADDENDUM 3A certificate number



363

Lab measurement equipment with certified traceability to international standards

Description	Cert. No.	Equipment. Number
Testo 400 with PT100 probe	T55698	Unitemp4
Testo 400 with PT100 probe	T57306	Unitemp3
Testo 735 with PT100 probe	THDG-6609	Unitemp41

Ambient conditions.

Temperature: 23 °C ± 5 °C

Measuring procedure (P0051)

The measurements read on this test item, in a thermostatic bath, were obtained while placed in very close proximity of a reference probe.

The result is calculated from an average of **6** readings @ **30** seconds intervals

Measurement results for hi-accuracy digital thermometer with 1/10 4-wire-Pt100 immersion probe

Indication from reference in °C	Indication from your measuring instrument in °C	Deviation in °C	Manufacture's allowed tolerance in °C	Expanded uncertainty of measurement in °C	Probe insertion depth in mm	Reference Equipment Used
30.066	30.08	0.01	n/a	± 0.05	85	Unitemp4
60.066	60.07	0.00	n/a	± 0.05	85	Unitemp4
90.032	90.01	-0.02	n/a	± 0.05	85	Unitemp4
120.076	120.00	-0.08	n/a	± 0.05	85	Unitemp4

Validity of Certificate

The measurement results recorded in this certificate relate only to the instrument & attachments specified, and were correct at the time. Only the above points have been checked & performance at other points is not certain. Subsequent accuracy will depend on factors such as care, handling and frequency of use. It is recommended that recalibration be undertaken at an interval that will ensure that the instrument remains within the desired limits.



page 2 of 2

END

www.unitemp.com

sales@unitemp.com

Unitemp c.c. Reg. No. CK1986/008689/23
Members: H.A. Hitzeroth D.R. Bütow U.H. Hitzeroth A. Semple

Unitemp Laboratory

Temperature Insertion Probe Calibration Protocol

Date:	3-12-14	Company Name:	UNIVERSITY OF STELLENBOSCH
I/O No	314653	Cert.no:	CAL-UC-ST-141203206
Person Responsible:	Francisco FC		
Ambient Conditions:	22.7 °C	49.2	%RH
Instrument:	Bath	Probe:	1/10 PE100 4 wire Immersion
PART NUMBER:	ME-6	PART NUMBER	55316
SERIAL NUMBER:	00296264	SERIAL NUMBER:	(13)EC-DIAG
MANUFACTURER:	SULABO	MANUFACTURER:	WIFA

P2
4-12-14
06

EXTERNAL CHANNEL

Measuring Point (°C)		Reference value (°C)	Measured value (°C)	Info
30	°C	30.014	29.45	PE100
0.01	Resolution	30.002	29.45	±385
	Accuracy	30.002	29.47	4-wire
4	Reference	30.027	29.48	1/10
7	Bath	30.036	29.48	
		30.027	29.47	
60	°C	60.073	59.28	EXTERNAL
0.01	Resolution	60.115	59.32	CHANNEL
	Accuracy	60.082	59.30	
4	Reference	60.064	59.29	
7	Bath	60.096	59.31	
		60.106	59.33	
90	°C	90.06029	89.11	
0.01	Resolution	90.047	89.13	
	Accuracy	90.017	89.11	
4	Reference	90.029	89.14	
7	Bath	90.026	89.13	
		90.022	89.14	
120	°C	120.051	119.23	
0.01	Resolution	120.059	119.24	
	Accuracy	120.033	119.22	
4	Reference	120.048	119.23	
7	Bath	120.061	119.25	
		120.060	119.25	

P2
3-12-14

P2
3-12-14

Immersion depth (mm)	Temp. (°C)
45	30
45	60
45	90
45	120

Probe bent by client.



Document: R0012
Laserfiche Version: 3
Date: 07 May 2012



Calibration and Services
calibration • validation • training

Calibration certificate CAL-UC-S-T-141203L06
certificate number



363

Lab measurement equipment with certified traceability to international standards

Description	Cert. No.	Equipment Number
Testo 400 with PT100 probe	T55698	Unitemp4
Testo 400 with PT100 probe	T57306	Unitemp3
Testo 735 with PT100 probe	THDG-6609	Unitemp41

Ambient conditions.

Temperature: 23 °C ± 5 °C

Measuring procedure (P0051)

The measurements read on this test item, in a thermostatic bath, were obtained while placed in very close proximity of a reference probe.

The result is calculated from an average of 6 readings @ 30 seconds intervals

Measurement results for hi-accuracy digital thermometer with 1/10 4-wire-Pt100 immersion probe

Indication from reference in °C	Indication from your measuring instrument in °C	Deviation in °C	Manufacture's allowed tolerance in °C	Expanded uncertainty of measurement in °C	Probe insertion depth in mm	Reference Equipment Used
30.035	29.47	-0.56	n/a	± 0.05	45	Unitemp4
60.101	59.31	-0.79	n/a	± 0.05	45	Unitemp4
90.036	89.13	-0.91	n/a	± 0.05	45	Unitemp4
120.061	119.24	-0.82	n/a	± 0.05	45	Unitemp4

Validity of Certificate

The measurement results recorded in this certificate relate only to the instrument & attachments specified, and were correct at the time. Only the above points have been checked & performance at other points is not certain. Subsequent accuracy will depend on factors such as care, handling and frequency of use. It is recommended that recalibration be undertaken at an interval that will ensure that the instrument remains within the desired limits.



page 2 of 2

END

www.unitemp.com

sales@unitemp.com

Unitemp c.c. Reg. No. CK1986/008689/23
Members: H.A. Hitzeroth D.R. Bötow U.H. Hitzeroth A. Semple



Calibration and Services
calibration • validation • training

Calibration certificate

CAL-UC-S-T-141204L06
certificate number



363

	INSTRUMENT	PROBE
Type	600	3-wire-Pt100
Manufacturer	Gefran	n/a
Part Nr.	F028415 B10	n/a
Serial Nr.	08450896	Process

Calibration of digital thermometer with 3-wire-Pt100 probe

Location Laboratory - Unitemp cc.
47 Flamingo Crescent
Lansdowne
Cape Town



Customer University of Stellenbosch
Address Kamer 225
Chemiese Ingenieurs
Stellenbosch

Order Nr. 314653
Date of calibration 4-Dec-2014

Was adjustment of the instrument done?

yes

no

The reported expanded uncertainty is based on a standard uncertainty multiplied by a coverage factor $k = 2$ providing a level of confidence of approximately 95%, the uncertainty of measurement has been estimated in accordance with the principles defined in the GUM, guide to uncertainty of measurement, ISO, Geneva, 1993

This calibration certificate may not be reproduced other than in full, and with the permission of SANAS & Unitemp Laboratory

Calibration certificates without an authorized signature and seal are not valid.

Person Responsible: *F.F. Rivera*
F Fernandez-Rivera

Technical Signatory: *R.M. MacGregor*
Roy MacGregor

page 1 of 2



www.unitemp.com

sales@unitemp.com

Unitemp c.c. Reg. No. CK1986/008689/23
Members: H.A. Hitzeroth D.R. Bütow U.H. Hitzeroth A. Semple

Unitemp Laboratory Air Probe Calibration Protocol

Date: 4-12-14		Company Name: UNIVERSITY OF STELLENBOSCH	
I/O No: 314 653		Cert.no: CAL-UC-S-T-141204L06	
Person Responsible:		Francisco PZ	
Ambient Conditions:		22.7 °C	58.7 %RH
Instrument: 600		Probe: PE100 3-wire	
PART NUMBER:	F028415 B10	PART NUMBER	n/a
SERIAL NUMBER:	084508 96	SERIAL NUMBER:	PROCESS
MANUFACTURER:	GEFRAV	MANUFACTURER:	n/a

Measuring Point (°C)		Reference value (°C)	Measured value (°C)	Info
30	°C	29.995	29.7	
0.1	Resolution	30.29.001	29.7	
	Accuracy	29.991	29.6	
4	Reference	29.988	29.6	
24DB	Bath	29.992	29.5	
		29.966	29.6	
75	°C	74.999	74.3	
0.1	Resolution	75.010	74.3	
	Accuracy	74.995	74.3	
4	Reference	75.74.011	74.3	
24DB	Bath	75.006	74.3	
		75.008	74.3	
120	°C	120.103	119.2	
0.1	Resolution	120.093	119.2	
	Accuracy	120.048	119.2	
4	Reference	120.059	119.2	
24DB	Bath	120.103	119.2	
		120.045	119.2	

PZ

5-12-14

Remarks: It is assumed all air probes are full immersion probes. Thus the immersion depth in sand or dry block should have a negligible effect if shaft length is long.

Immersion depth: = 130 mm
Shaft diameter: 6 mm



Document: R0036
 Laserfiche Version: 3
 Date: 07 May 2012



Calibration and Services

calibration • validation • training

Calibration certificate CAL-UC-S-T-141204L06
certificate number



363

Lab measurement equipment with certified traceability to international standards

Description	Cert. No.	Equipment Number
Testo 400 with PT100 probe	T55698	Unitemp4
Testo 400 with PT100 probe	T57306	Unitemp3
Testo 735 with PT100 probe	THDG-6609	Unitemp41

Ambient conditions.

Temperature: 23 °C ± 5 °C

Measuring procedure (P0001)

The measurements read on this test item were obtained while placed in the dry block and compared to a reference probe.

The result is calculated from an average of **6** readings @ **30** seconds intervals

Measurement results for a digital thermometer with 3-wire-Pt100 probe

Indication from reference in °C	Indication from your measuring instrument in °C	Deviation in °C	Manufacture's allowed tolerance in °C	Expanded uncertainty of measurement in °C	Probe insertion depth in mm	Reference Equipment Used
30.010	29.6	-0.4	n/a	± 0.5	130	Unitemp4
75.011	74.3	-0.7	n/a	± 0.5	130	Unitemp4
120.081	119.2	-0.9	n/a	± 0.5	130	Unitemp4

Validity of Certificate

The measurement results recorded in this certificate relate only to the instrument & attachments specified, and were correct at the time. Only the above points have been checked & performance at other points is not certain. Subsequent accuracy will depend on factors such as care, handling and frequency of use. It is recommended that recalibration be undertaken at an interval that will ensure that the instrument remains within the desired limits.



page 2 of 7

END

www.unitemp.com

sales@unitemp.com

Unitemp c.c. Reg. No. CK1986/006689/23
Members: H.A. Hitzeroth D.R. Bütow U.H. Hitzeroth A. Semple

FACULTY: ENGINEERING

Thermon South Africa (Pty) Ltd. - Cape Lab

Temperature Insertion Probe Calibration Protocol

Dept: Process Engineering

Date:	29-2-2016	Company Name:	University of Stellenbosch
I/O No:	TZAFS006458	Cert.no:	CAL-UC-S-T-160229X02
Person Responsible:	Francis FR		
Ambient Conditions:	24.4 °C	—	%RH
Instrument:	Digital Multimeter	Probe:	4-wire Pt100 immersion 1/10
PART NUMBER:	34972 A	PART NUMBER:	SS316
SERIAL NUMBER:	MY 49009493	SERIAL NUMBER:	(1) EC-FR
MANUFACTURER:	Agilent	MANUFACTURER:	Wika

CHANNEL 1

Measuring Point (°C)	Reference value (°C)	Measured value (°C)	Info
30 °C	29.971	29.972	Last
0.01 Resolution	29.965	29.967	digits
Accuracy	29.951	29.96	"jumps"
4 Reference	29.958	29.96	No possible
24LI Bath	29.956	29.96	to lead
	29.954	29.95	
60 °C	60.134	60.08	
0.01 Resolution	60.131	60.08	
Accuracy	60.126	60.08	
4 Reference	60.131	60.09	
24LI Bath	60.130	60.08	
	60.134	60.08	
90 °C	90.209	90.12	
0.01 Resolution	90.206	90.11	
Accuracy	90.198	90.11	
4 Reference	90.194	90.10	
24LI Bath	90.193	90.09	
	90.195	90.10	
120 °C	120.139	120.00	
0.01 Resolution	120.130	119.99	
Accuracy	120.134	120.00	
4 Reference	120.132	119.98	
24LI Bath	120.126	119.99	
	120.132	119.99	

Immersion depth (mm)	Temp. (°C)
50mm	30
50	60
50	90
50	120

Twisted probe
φ 3mm



Thermon
South Africa (Pty) Ltd.



Calibration certificate CAL-UC-S-T-160229X02
certificate number



1573, 373

Lab measurement equipment with certified traceability to international standards

Description	Cert. No.	Equipment. Number
Testo 400 with PT100 probe	THDG-6754	Unitemp4

Ambient conditions.

Temperature: 23 °C ± 5 °C

Measuring procedure (P0051)

The measurements read on this test item, in a thermostatic bath, were obtained while placed in very close proximity of a reference probe.

The result is calculated from an average of 6 readings @ 30 seconds intervals

Measurement results for hi-accuracy digital thermometer with 1/10 4-wire-Pt100 probe (Channel 1)

Indication from reference in °C	Indication from your measuring instrument in °C	Deviation in °C	Manufacture's allowed tolerance in °C	Expanded uncertainty of measurement in °C	Probe insertion depth in mm	Reference Equipment Used
29.982	29.96	-0.02	n/a	± 0.05	50	Unitemp4
60.153	60.08	-0.07	n/a	± 0.05	50	Unitemp4
90.221	90.11	-0.11	n/a	± 0.05	50	Unitemp4
120.153	119.99	-0.16	n/a	± 0.05	50	Unitemp4

Validity of Certificate

The measurement results recorded in this certificate relate only to the instrument & attachments specified, and were correct at the time. Only the above points have been checked & performance at other points is not certain. Subsequent accuracy will depend on factors such as care, handling and frequency of use. It is recommended that recalibration be undertaken at an interval that will ensure that the instrument remains within the desired limits.



page 2 of 2

END

Calibration • Validation • Training

Email: sales.za@thermon.com Web: www.thermon.co.za

Thermon South Africa (Pty) Ltd. Reg. No. 2015/020118/07, VAT No. 4750268387, Directors: G.P. Alexander, R.L. Bingham, J.C. Peterson



Thermon
South Africa (Pty) Ltd.



Calibration certificate

CAL-UC-S-T-160229X02
ADDENDUM 1A certificate number



	INSTRUMENT	PROBE
Type	Digital Multimeter	1/10 4-wire-Pt100
Manufacturer	Agilent	Wika
Part Nr.	34972 A	SS 316
Serial Nr.	MY 49009493	(2) EC-BR

Calibration of hi-accuracy digital thermometer with 1/10 4-wire-Pt100 probe (Channel 2)

Location **On Site at Customer**
Department of Process Engineering

Customer **University of Stellenbosch**
Address **Banhoek Road**
Stellenbosch, 7600
Western Cape

Order Nr. TZAFS006458
Date of calibration 29-Feb-2016

Was adjustment of the instrument done?

yes

no

The reported expanded uncertainty is based on a standard uncertainty multiplied by a coverage factor $k = 2$ providing a level of confidence of approximately 95%. the uncertainty of measurement has been estimated in accordance with the principles defined in the GUM, guide to uncertainty of measurement, ISO, Geneva, 1993

This calibration certificate may not be reproduced other than in full, and with the permission of SANAS & Thermon Laboratory.

Calibration certificates without an authorized signature and seal are not valid.

Person Responsible & Technical Signatory: F Fernandez-Rivera

page 1 of 2



Calibration • Validation • Training

Email: sales.za@thermon.com Web: www.thermon.co.za

Thermon South Africa (Pty) Ltd. Reg. No. 2015/020118/07, VAT No. 4750268387, Directors: G.P. Alexander, R.L. Bingham, J.C. Peterson

Thermon South Africa (Pty) Ltd. - Cape Lab Temperature Insertion Probe Calibration Protocol

Date:	29-2-2016	Company Name:	University of Stellenbosch	Addende 1A
I/O No:	TZAFS 006458	Cert.no:	CAL-UC-ST-160229 X 02	
Person Responsible:	Francisco FZ			1/10
Ambient Conditions:	24.5 °C	— %RH		
Instrument:	Digital Multimeter	Probe:	4-wire-Pt100 immersion	
PART NUMBER:	34972A	PART NUMBER:	SS316	
SERIAL NUMBER:	MY49009493	SERIAL NUMBER:	(2) EC-BR	
MANUFACTURER:	Agilent	MANUFACTURER:	wika	

CHANNEL 2

Measuring Point (°C)		Reference value (°C)	Measured value (°C)	Info
30	°C	30.035	30.07	1
0.01	Resolution	30.034	30.07	2
	Accuracy	30.032	30.07	3
4	Reference	30.027	30.07	
24LI	Bath	30.029	30.07	
		30.030	30.06	
60	°C	60.119	60.12	1
0.01	Resolution	60.126	60.12	2
	Accuracy	60.127	60.12	3
4	Reference	60.128	60.13	
24LI	Bath	60.127	60.12	
		60.122	60.12	
90	°C	90.164	90.14	1
0.01	Resolution	90.163	90.14	2
	Accuracy	90.162	90.14	3
4	Reference	90.166	90.15	
24LI	Bath	90.172	90.15	
		90.173	90.15	
120	°C	120.004	119.90	1
0.1	Resolution	120.008	119.90	2
	Accuracy	120.002	119.90	3
4	Reference	120.007	119.91	
24LI	Bath	120.010	119.91	
		120.008	119.91	

Immersion depth (mm)	Temp. (°C)
55	30
65	60
65	90
68	120

∅ 3 mm

Document: RC0012
 Laserfiche Version: 4
 Date: 29 June 2015

Path: UNITEMP\Testo App\Calibration Laboratory\Controlled Documents\Forms Templates\Work Templates\Protocol sheets\CT\Temperature\Insertion Probes

Next Review date: June 2018



Thermon
South Africa (Pty) Ltd.



Calibration certificate CAL-UC-S-T-160229X02
ADDENDUM 1A certificate number



1573, 373

Lab measurement equipment with certified traceability to international standards

Description	Cert. No.	Equipment. Number
Testo 400 with PT100 probe	THDG-6754	Unitemp4

Ambient conditions.

Temperature: 23 °C ± 5 °C

Measuring procedure (P0051)

The measurements read on this test item, in a thermostatic bath, were obtained while placed in very close proximity of a reference probe.

The result is calculated from an average of 6 readings @ 30 seconds intervals

Measurement results for hi-accuracy digital thermometer with 1/10 4-wire-Pt100 probe (Channel 2)

Indication from reference in °C	Indication from your measuring instrument in °C	Deviation in °C	Manufacture's allowed tolerance in °C	Expanded uncertainty of measurement in °C	Probe insertion depth in mm	Reference Equipment Used
30.054	30.07	0.02	n/a	± 0.05	65	Unitemp4
60.147	60.12	-0.03	n/a	± 0.05	65	Unitemp4
90.189	90.15	-0.04	n/a	± 0.05	65	Unitemp4
120.027	119.91	-0.12	n/a	± 0.05	68	Unitemp4

Validity of Certificate

The measurement results recorded in this certificate relate only to the instrument & attachments specified, and were correct at the time. Only the above points have been checked & performance at other points is not certain. Subsequent accuracy will depend on factors such as care, handling and frequency of use. It is recommended that recalibration be undertaken at an interval that will ensure that the instrument remains within the desired limits.

page 2 of 2

END



Calibration • Validation • Training

Email: sales.za@thermon.com Web: www.thermon.co.za

Thermon South Africa (Pty) Ltd. Reg. No. 2015/020118/07, VAT No. 4750268387, Directors: G.P. Alexander, R.L. Bingham, J.C. Peterson



Thermon
South Africa (Pty) Ltd.



Calibration certificate

CAL-UC-S-T-160229X02
ADDENDUM 2A certificate number



1573, 373

	INSTRUMENT	PROBE
Type	Digital Multimeter	1/10 4-wire-Pt100
Manufacturer	Agilent	Wika
Part Nr.	34972 A	SS 316
Serial Nr.	MY 49009493	(3) EC-FL

Calibration of hi-accuracy digital thermometer with 1/10 4-wire-Pt100 probe (Channel 3)

Location **On Site at Customer**
Department of Process Engineering

Customer **University of Stellenbosch**
Address **Banhoek Road**
Stellenbosch, 7600
Western Cape

Order Nr. TZAFS006458
Date of calibration 29-Feb-2016

Was adjustment of the instrument done?

yes

no

The reported expanded uncertainty is based on a standard uncertainty multiplied by a coverage factor k = 2 providing a level of confidence of approximately 95%, the uncertainty of measurement has been estimated in accordance with the principles defined in the GUM, guide to uncertainty of measurement, ISO, Geneva, 1993

This calibration certificate may not be reproduced other than in full, and with the permission of SANAS & Thermon Laboratory.

Calibration certificates without an authorized signature and seal are not valid.

Person Responsible & Technical Signatory: F Fernandez-Rivera

page 1 of 2



Calibration • Validation • Training

Email: sales.za@thermon.com Web: www.thermon.co.za

Thermon South Africa (Pty) Ltd. Reg. No. 2015/020118/07, VAT No. 4750268387, Directors: G.P. Alexander, R.L. Bingham, J.C. Peterson

Faculty: Engineering

Thermon South Africa (Pty) Ltd. - Cape Lab

Temperature Insertion Probe Calibration Protocol

Dept: Process Engineering

Date:	29-2-2016	Company Name:	University of Stellenbosch
I/O No:	TZAFS 006458	Cert.no:	CAL-UCS-T-160229X02
Person Responsible:	Francis FZ		
Ambient Conditions:	24.6 °C	%RH	—
Instrument:	Digital Multimeter	Probe:	4-wire-PE100 immersion
PART NUMBER:	34972A	PART NUMBER:	SS316
SERIAL NUMBER:	MY49009493	SERIAL NUMBER:	(3) EC-FL
MANUFACTURER:	Agilent	MANUFACTURER:	Wika

Addendum 2A
1/10

CHANNEL 3

Measuring Point (°C)	Reference value (°C)	Measured value (°C)	Info
30 °C	30.022	30.06	
0.01 Resolution	30.019	30.06	
Accuracy	30.015	30.05	
4 Reference	30.012	30.05	
24LI Bath	30.014	30.05	
	30.013	30.05	
60 °C	60.105	60.13	
0.01 Resolution	60.107	60.13	
Accuracy	60.109	60.13	
4 Reference	60.107	60.13	
24LI Bath	60.105	60.12	
	60.102	60.13	
90 °C	90.142	90.10	
0.01 Resolution	90.137	90.09	
Accuracy	90.138	90.10	
4 Reference	90.140	90.10	
24LI Bath	90.148	90.11	
	90.149	90.11	
120 °C	120.043	119.93	
0.01 Resolution	120.038	119.93	
Accuracy	120.035	119.91	
4 Reference	120.016	119.90	
24LI Bath	120.015	119.90	
	120.018	119.91	

Immersion depth (mm)	Temp. (°C)
40	30
40	60
40	90
40	120

∅ 3mm
Twisted probe

∅ 3mm

Document: RC0012
Laserfiche Version: 4
Date: 29 June 2015

Path: UNITEMP\Testo App\Calibration Laboratory\Controlled Documents\Forms Templates\Work Templates\Protocol sheets\CT\Temperature\Insertion Probes

Next Review date: June 2018



Thermon
South Africa (Pty) Ltd.



Calibration certificate CAL-UC-S-T-160229X02
ADDENDUM 2A certificate number



1573, 373

Lab measurement equipment with certified traceability to international standards

Description	Cert. No.	Equipment. Number
Testo 400 with PT100 probe	THDG-6754	Unitemp4

Ambient conditions.

Temperature: 23 °C ± 5 °C

Measuring procedure (P0051)

The measurements read on this test item, in a thermostatic bath, were obtained while placed in very close proximity of a reference probe.

The result is calculated from an average of 6 readings @ 30 seconds intervals

Measurement results for hi-accuracy digital thermometer with 1/10 4-wire-Pt100 probe (Channel 3)

Indication from reference in °C	Indication from your measuring instrument in °C	Deviation in °C	Manufacture's allowed tolerance in °C	Expanded uncertainty of measurement in °C	Probe insertion depth in mm	Reference Equipment Used
30.039	30.05	0.01	n/a	± 0.05	40	Unitemp4
60.128	60.13	0.00	n/a	± 0.05	40	Unitemp4
90.164	90.10	-0.06	n/a	± 0.05	40	Unitemp4
120.048	119.91	-0.14	n/a	± 0.05	40	Unitemp4

Validity of Certificate

The measurement results recorded in this certificate relate only to the instrument & attachments specified, and were correct at the time. Only the above points have been checked & performance at other points is not certain. Subsequent accuracy will depend on factors such as care, handling and frequency of use. It is recommended that recalibration be undertaken at an interval that will ensure that the instrument remains within the desired limits.

page 2 of 2

END



Calibration • Validation • Training

Email: sales.za@thermon.com Web: www.thermon.co.za

Thermon South Africa (Pty) Ltd. Reg. No. 2015/020118/07, VAT No. 4750268387, Directors: G.P. Alexander, R.L. Bingham, J.C. Peterson

Faculty: Engineering
Thermon South Africa (Pty) Ltd. - Cape Lab

Temperature Insertion Probe Calibration Protocol

Dept: Process Engineering

Date:	29-2-2016	Company Name:	University of Stellenbosch
I/O No:	TZAFS 006458	Cert.no:	CAL-UCS-T-160229X02
Person Responsible:	Francisco FE		
Ambient Conditions:	24.6 °C	— %RH	
Instrument:	Digital Multimeter	Probe:	4-wire-Pt100 immersion
PART NUMBER:	34972A	PART NUMBER:	SS 316
SERIAL NUMBER:	MY49009493	SERIAL NUMBER:	(4) EC-BL
MANUFACTURER:	Agilent	MANUFACTURER:	Wika

Addenda 3A
1/10
CHANNEL 4

Measuring Point (°C)	Reference value (°C)	Measured value (°C)	Info
30 °C	30.017	30.06	
0.01 Resolution	30.013	30.06	
Accuracy	30.012	30.06	
4 Reference	30.003	30.05	
24LI Bath	2930 - 999	30.05	
	30.005	30.06	
60 °C	60.078	60.12	
0.01 Resolution	60.079	60.13	
Accuracy	60.090	60.13	
4 Reference	60.091	60.13	
24LI Bath	60.083	60.13	
	60.086	60.13	
90 °C	90.067	90.11	
0.01 Resolution	90.063	90.11	
Accuracy	90.060	90.11	
4 Reference	90.058	90.10	
24LI Bath	90.056	90.11	
	90.056	90.11	
120 °C	120.018	119.95	
0.01 Resolution	120.023	119.96	
Accuracy	120.023	119.95	
4 Reference	120.028	119.96	
24LI Bath	120.034	119.96	
	120.034	119.97	

Immersion depth (mm)	Temp. (°C)
80	30
74	60
77	90
75	120

∅3 mm

Document: RC0012
 Laserfiche Version: 4
 Date: 29 June 2015

Path: UNITEMP\Testo App\Calibration Laboratory\Controlled Documents\Forms Templates\Work Templates\Protocol sheets\CT\Temperature\Insertion Probes

Next Review date: June 2018



Thermon
South Africa (Pty) Ltd.



Calibration certificate CAL-UC-S-T-160229X02
ADDENDUM 3A certificate number



1573, 373

Lab measurement equipment with certified traceability to international standards

Description	Cert. No.	Equipment. Number
Testo 400 with PT100 probe	THDG-6754	Unitemp4

Ambient conditions.

Temperature: 23 °C ± 5 °C

Measuring procedure (P0051)

The measurements read on this test item, in a thermostatic bath, were obtained while placed in very close proximity of a reference probe.

The result is calculated from an average of 6 readings @ 30 seconds intervals

Measurement results for hi-accuracy digital thermometer with 1/10 4-wire-Pt100 probe (Channel 4)

Indication from reference in °C	Indication from your measuring instrument in °C	Deviation in °C	Manufacture's allowed tolerance in °C	Expanded uncertainty of measurement in °C	Probe insertion depth in mm	Reference Equipment Used
30.031	30.06	0.03	n/a	± 0.05	80	Unitemp4
60.107	60.13	0.02	n/a	± 0.05	74	Unitemp4
90.082	90.11	0.03	n/a	± 0.05	77	Unitemp4
120.047	119.96	-0.09	n/a	± 0.05	75	Unitemp4

Validity of Certificate

The measurement results recorded in this certificate relate only to the instrument & attachments specified, and were correct at the time. Only the above points have been checked & performance at other points is not certain. Subsequent accuracy will depend on factors such as care, handling and frequency of use. It is recommended that recalibration be undertaken at an interval that will ensure that the instrument remains within the desired limits.

page 2 of 2

END



Calibration • Validation • Training

Email: sales.za@thermon.com Web: www.thermon.co.za

Thermon South Africa (Pty) Ltd. Reg. No. 2015/020118/07, VAT No. 4750268387, Directors: G.P. Alexander, R.L. Bingham, J.C. Peterson

Faculty = Engineering

Thermon South Africa (Pty) Ltd. - Cape Lab

Temperature Insertion Probe Calibration Protocol

Dept: Process Engineering

Date:	29-2-2016	Company Name:	University of Stellenbosch
I/O No:	TAFS006458	Cert.no:	CAL-UC-ST-160229 X03
Person Responsible:	Francisco FZ		
Ambient Conditions:	24.7 °C	— %RH	
Instrument:	Bath	Probe:	4-wire-Pt100 immersion 110
PART NUMBER:	ME-6	PART NUMBER	SS 316
SERIAL NUMBER:	00296264	SERIAL NUMBER:	(13) EC-DIAG
MANUFACTURER:	Sulabo	MANUFACTURER:	WIKA

EXTERNAL PROBE

Measuring Point (°C)	Reference value (°C)	Measured value (°C)	Info
30 °C	29.996	29.44	1
0.01 Resolution	29.993	29.44	2
Accuracy	29.991	29.43	3
4 Reference	29.990	29.43	
24LI Bath	29.991	29.43	
	29.991	29.43	
60 °C	60.137	59.27	1
0.01 Resolution	60.147	59.28	2
Accuracy	60.152	59.28	3
4 Reference	60.162	59.30	
24LI Bath	60.164	59.31	
	60.161	59.30	
90 °C	90.058	89.50	1
0.01 Resolution	90.052	89.52	2
Accuracy	90.070	89.53	3
4 Reference	90.051	89.52	
24LI Bath	90.046	89.52	
	90.056	89.52	
120 °C	119.989	119.41	1
0.01 Resolution	120.015	119.42	2
Accuracy	120.031	119.43	3
4 Reference	120.005	119.43	
24LI Bath	120.028	119.43	
	120.016	119.41	

Immersion depth (mm)	Temp. (°C)
45	30
45	60
45	90
45	120

Approx. immersion depth $\varnothing 3 \text{ mm}$

Document: RC0012
 Laserfiche Version: 4
 Date: 29 June 2015

Path: UNITEMP\Testo App\Calibration Laboratory\Controlled Documents\FORMS Templates\Work Templates\Protocol sheets\CT\Temperature\Insertion Probes

Next Review date: June 2018



Thermon
South Africa (Pty) Ltd.



Calibration certificate CAL-UC-S-T-160229X03
certificate number



1573, 373

Lab measurement equipment with certified traceability to international standards

Description	Cert. No.	Equipment. Number
Testo 400 with PT100 probe	THDG-6754	Unitemp4

Ambient conditions.

Temperature: 23 °C ± 5 °C

Measuring procedure (P0051)

The measurements read on this test item, in a thermostatic bath, were obtained while placed in very close proximity of a reference probe.

The result is calculated from an average of 6 readings @ 30 seconds intervals

Measurement results for hi-accuracy digital thermometer with 1/10 4-wire-Pt100 external probe

Indication from reference in °C	Indication from your measuring instrument in °C	Deviation in °C	Manufacture's allowed tolerance in °C	Expanded uncertainty of measurement in °C	Probe insertion depth in mm	Reference Equipment Used
30.015	29.43	-0.58	n/a	± 0.05	45	Unitemp4
60.176	59.29	-0.89	n/a	± 0.05	45	Unitemp4
90.078	89.52	-0.56	n/a	± 0.05	45	Unitemp4
120.035	119.42	-0.61	n/a	± 0.05	45	Unitemp4

Validity of Certificate

The measurement results recorded in this certificate relate only to the instrument & attachments specified, and were correct at the time. Only the above points have been checked & performance at other points is not certain. Subsequent accuracy will depend on factors such as care, handling and frequency of use. It is recommended that recalibration be undertaken at an interval that will ensure that the instrument remains within the desired limits.

page 2 of 2

END



Calibration • Validation • Training

Email: sales.za@thermon.com Web: www.thermon.co.za

Thermon South Africa (Pty) Ltd. Reg. No. 2015/020118/07, VAT No. 4750268387, Directors: G.P. Alexander, R.L. Bingham, J.C. Peterson



Thermon
South Africa (Pty) Ltd.



Calibration certificate

CAL-UC-S-T-160229X01
certificate number



	INSTRUMENT	PROBE
Type	600	3-wire-Pt 100
Manufacturer	Gefran	n/a
Part Nr.	F028415 B10	n/a
Serial Nr.	08450896	Process

Calibration of digital thermometer with 3-wire-Pt 100 air probe

Location **On Site at Customer**
Department of Process Engineering



Customer **University of Stellenbosch**
Address **Banhoek Road**
Stellenbosch, 7600
Western Cape

Order Nr. **TZAFS006458**
Date of calibration **29-Feb-2016**

Was adjustment of the instrument done?

yes

no

The reported expanded uncertainty is based on a standard uncertainty multiplied by a coverage factor $k = 2$ providing a level of confidence of approximately 95%, the uncertainty of measurement has been estimated in accordance with the principles defined in the GUM, guide to uncertainty of measurement, ISO, Geneva, 1993

This calibration certificate may not be reproduced other than in full, and with the permission of SANAS & Thermon Laboratory.

Calibration certificates without an authorized signature and seal are not valid.

Person Responsible & Technical Signatory: **F Fernandez-Rivera**

page 1 of 2



Calibration • Validation • Training

Email: sales.za@thermon.com Web: www.thermon.co.za

Thermon South Africa (Pty) Ltd. Reg. No. 2015/020118/07, VAT No. 4750268387. Directors: G.P. Alexander, R.L. Bingham, J.C. Peterson

FACULTY ENGINEERING

Thermon South Africa (Pty) Ltd. - Cape Lab

Temperature Insertion Probe Calibration Protocol

Dept: Process Engineering

Date:	29-2-2016	Company Name:	University of Stellenbosch
I/O No:	TZAF5006458	Cert.no:	CAL-UC-S-T-160229 X01
Person Responsible:	Francisco FRZ		
Ambient Conditions:	24.5 °C		%RH
Instrument:	600	Probe:	3-wire - Pt100 Air Probe
PART NUMBER:	F028415 B10	PART NUMBER:	n/a
SERIAL NUMBER:	08450896	SERIAL NUMBER:	Process
MANUFACTURER:	BEFRAN	MANUFACTURER:	n/a

Measuring Point (°C)		Reference value (°C)	Measured value (°C)	Info
30	°C	30.001	29.8	
0.1	Resolution	30.005	29.8	
	Accuracy	29.987	29.8	
4	Reference	29.953	29.8	
24DB	Bath	29.947	29.8	
75	°C	75.037	74.4	
0.1	Resolution	75.042	74.4	
	Accuracy	75.044	74.4	
4	Reference	75.004	74.4	
24DB	Bath	75.065	74.4	
120	°C	120.037	119.3	
0.1	Resolution	120.022	119.3	
	Accuracy	120.005	119.3	
4	Reference	119.988	119.3	
24DB	Bath	120.013	119.3	
	°C			
	Resolution			
	Accuracy			
	Reference			
	Bath			
Immersion depth (mm)	Temp. (°C)			
130	30			
130	75			
130	120			
130				

Document: RC0012
 Laserfiche Version: 4
 Date: 29 June 2015

Path: UNITEMP\Testo App\Calibration Laboratory\Controlled Documents\FORMS Templates\Work Templates\Protocol sheets\CT\Temperature\Insertion Probes

Next Review date: June 2018



Thermon
South Africa (Pty) Ltd.



Calibration certificate CAL-UC-S-T-160229X01
certificate number



1573, 373

Lab measurement equipment with certified traceability to international standards

Description	Cert. No.	Equipment. Number
Testo 400 with PT100 probe	TH/DG-6754	Unitemp4

Ambient conditions.

Temperature: 23 °C ± 5 °C

Measuring procedure (P0001)

The measurements read on this test item were obtained while placed in a thermostatic dry block and compared to a reference probe.

The result is calculated from an average of 5 readings @ 30 seconds intervals

Measurement results for a digital thermometer with 3-wire-Pt 100 air probe

Indication from reference in °C	Indication from your measuring instrument in °C	Deviation in °C	Manufacture's allowed tolerance in °C	Expanded uncertainty of measurement in °C	Probe insertion depth in mm	Reference Equipment Used
30.002	29.8	-0.2	n/a	± 0.3	130	Unitemp4
75.060	74.4	-0.7	n/a	± 0.3	130	Unitemp4
120.035	119.3	-0.7	n/a	± 0.3	130	Unitemp4

Validity of Certificate

The measurement results recorded in this certificate relate only to the instrument & attachments specified, and were correct at the time. Only the above points have been checked & performance at other points is not certain. Subsequent accuracy will depend on factors such as care, handling and frequency of use. It is recommended that recalibration be undertaken at an interval that will ensure that the instrument remains within the desired limits.



page 2 of 2

END

Calibration • Validation • Training

Email: sales.za@thermon.com Web: www.thermon.co.za

Thermon South Africa (Pty) Ltd. Reg. No. 2015/020118/07, VAT No. 4750268387, Directors: G.P. Alexander, R.L. Bingham, J.C. Peterson

Pressure calibration			1 November 2011	
T actual [°C]	T setpoint [°C]	T display [°C]	T ambient [°C]	
35.00	34.69	34.71	19	
P applied [bar]			P display [bar]	
0		-1.4		
5		3.6		
20		17.0		
35		21.6		
50		46.5		
65		61.5		
80		76.5		
95		91.6		
110		106.7		
125		121.9		
140		137.1		
155		152.2		
170		167.4		
185		182.5		
200		197.7		
215		212.8		
230		228.0		
245		243.0		
260		258.1		
275		273.2		
290		288.2		
295		293.2		
300		298.2		
304		302.2		

* Tussen 35°C en 43°C heb ik een meetfout van 1.4 bar. Tussen 35 en 43°C maak ik wel die fout los/op, en P is tot -1.7 bar. En onder die -1.4 bar.

Pressure calibration			1 November 2011	
T actual [°C]	T setpoint [°C]	T display [°C]	T ambient [°C]	
43.00	42.68	42.68	16°C	
P applied [bar]			P display [bar]	
0		-1.7		
5		2.6		
20		17.1		
35		31.8		
50		46.6		
65		61.6		
80		76.8		
95		92.0 91.8		
110		107.0		
125		122.2		
140		137.4		
155		152.5		
170		167.7		
185		182.9		
200		198.0		
215		213.1		
230		228.3		
245		243.4		
260		258.4		
275		273.6		
290		288.6		
295		293.6		
300		298.6		
304		302.6		

Pressure calibration			2 November 2011	
T actual [°C]	T setpoint [°C]	T display [°C]	T ambient [°C]	
45.00	44.68	44.67/68	16°C	
P applied [bar]			P display [bar]	
0		-1.8 bar		
5		2.9		
20		17.2 bar		
35		31.8 bar		
50		46.7		
65		61.7		
80		76.8		
95		92.0		
110		107.2		
125		122.4		
140		137.4		
155		152.6		
170		167.8		
185		182.9		
200		198.1		
215		213.2		
230		228.3		
245		243.4		
260		258.5		
275		273.6		
290		288.7		
295		293.7		
300		298.7		
304		302.7		

9-72

Pressure calibration				2 November 2011	
T _{actual} [°C]	T _{setpoint} [°C]	T _{display} [°C]	T _{ambient} [°C]	P _{applied} [bar]	P _{display} [bar]
55.00	54.66	54.45/66	16		
				0	-1.1 bar
				5	3.6
				20	17.7
				35	32.4
				50	47.3
				65	62.4
				80	77.3
				95	92.5
				110	107.6
				125	122.8
				140	138.0
				155	153.2
				170	168.3
				185	183.5
				200	198.6
				215	213.8
				230	228.9
				245	244.0
				260	259.2
				275	274.1
				290	289.2
				295	294.2
				300	299.2
				304	303.2

Pressure calibration				2 November 2011	
T _{actual} [°C]	T _{setpoint} [°C]	T _{display} [°C]	T _{ambient} [°C]	P _{applied} [bar]	P _{display} [bar]
60.00	59.66	59.66	16		
				0	-1.0
				5	4.4
				20	17.9
				35	32.6
				50	47.6
				65	62.6
				80	77.6
				95	92.8
				110	108.0
				125	123.0
				140	138.2
				155	153.4
				170	168.5
				185	183.7
				200	198.9
				215	214.0
				230	229.1
				245	244.2
				260	259.3
				275	274.4
				290	289.4
				295	294.4
				300	299.5
				304	303.5

Pressure calibration				2 November 2011	
T _{actual} [°C]	T _{setpoint} [°C]	T _{display} [°C]	T _{ambient} [°C]	P _{applied} [bar]	P _{display} [bar]
65.00	64.65	64.67/66	16		
				0	-0.6
				5	5.1
				20	18.2
				35	32.9
				50	47.8
				65	62.8
				80	77.9
				95	93.0
				110	108.2
				125	123.3
				140	138.5
				155	153.7
				170	168.8
				185	184.0
				200	199.2
				215	214.4
				230	229.4
				245	244.5
				260	259.6
				275	274.7
				290	289.7
				295	294.7
				300	299.7
				304	303.7

9-73

9-74

Pressure calibration		2 November 2011	
T _{actual} [°C]	T _{setpoint} [°C]	T _{display} [°C]	T _{ambient} [°C]
75.00	74.64	74.64/5	17
P _{applied}		P _{display}	
[bar]		[bar]	
0	0.0		
5	4.6		
20	19.2		
35	33.8		
50	48.8		
65	63.7		
80	78.7		
95	93.8		
110	109.0		
125	124.1		
140	139.3		
155	154.4		
170	169.6		
185	184.8		
200	200.0		
215	215.0		
230	230.2		
245	245.3		
260	260.3		
275	275.4		
290	290.4		
295	295.4		
300	300.4		
304	304.4		

Pressure calibration		2 November 2011	
T _{actual} [°C]	T _{setpoint} [°C]	T _{display} [°C]	T _{ambient} [°C]
80.00	79.64	79.67/66/65	17
P _{applied}		P _{display}	
[bar]		[bar]	
0	0.0		
5	4.6		
20	19.2		
35	33.9		
50	48.9		
65	63.8		
80	78.9		
95	94.0		
110	109.1		
125	124.3		
140	139.5		
155	154.6		
170	169.8		
185	185.0		
200	200.1		
215	215.2		
230	230.4		
245	245.5		
260	260.6		
275	275.6		
290	290.6		
295	295.7		
300	300.8		
304	304.8		

PRESSURE CALIBRATION				7 March 2013	
Calibration [°C]	35 °C	T _{ambient} [°C]	Julabo (13) EC-DIAG	T _{ambient} [°C]	24.5 °C
Gefran Process					
T _{sepoint-gr} [°C]	34.6 °C	T _{sepoint-113} [°C]	34.6 °C	T _{display-113} [°C]	34.65/6 °C
T _{display-gr} [°C]	34.7/6 °C	T _{display-113} [°C]	34.65/6 °C	T _{display-113} [°C]	34.65/6 °C
P _{applied} [bar]	P _{display} [bar]	P _{display} [m]	Time		
0	0.1 bar	4.01	18:06		
5	5.0	4.23	18:09		
20	19.0	4.88	18:10		
35	33.7	5.55	18:12		
50	48.5	6.23	18:13		
65	63.5	6.91	18:14		
80	78.5	7.60	18:15		
95	93.6	8.29	18:17		
110	108.8	8.98	18:18		
125	124.23.9	9.67	18:19		
140	139.0	10.36	18:21		
155	154.1/2	11.057	18:24		
170	169.3	11.75	18:26		
185	184.5	12.44	18:28		
200	199.6	13.13	18:31		
215	214.7	13.825/7	18:32		
230	229.8	14.52	18:34		
245	244.9	15.207	18:36		
260	260.0	15.893	18:37		
275	275.0	16.584	18:39 (?)		
290	290.0	17.271	18:40		
295	295.0	17.499	18:41		
300	300.0	17.730	18:43		
304	304.0	17.911	18:45		

PRESSURE CALIBRATION				7 March 2013	
Calibration [°C]	45 °C	T _{ambient} [°C]	Julabo (13) EC-DIAG	T _{ambient} [°C]	24.5 °C
Gefran Process					
T _{sepoint-gr} [°C]	44.6 °C	T _{sepoint-113} [°C]	44.6 °C	T _{display-113} [°C]	44.65/4 °C
T _{display-gr} [°C]	44.7/6 °C	T _{display-113} [°C]	44.65/4 °C	T _{display-113} [°C]	44.65/4 °C
P _{applied} [bar]	P _{display} [bar]	P _{display} [m]	Time		
0	1.6	4.083	22:08		
5	5.6	4.267	22:10		
20	19.7	4.912	22:12		
35	34.4	5.585	22:13		
50	49.3	6.263	22:15		
65	64.2	6.951	22:17		
80	79.3	7.635	22:18		
95	94.4	8.327	22:19		
110	109.6	9.017	22:21		
125	124.6	9.709	22:23		
140	139.8	10.402	22:24		
155	154.9	11.094	22:27		
170	170.1	11.785	22:29		
185	185.2	12.480	22:31		
200	200.4	13.172	22:32		
215	215.5	13.865	?		
230	230.6	14.556	22:35		
245	245.7	15.245	22:37		
260	260.8	15.935	22:39		
275	275.8	16.620	22:40		
290	290.8	17.309	22:41		
295	295.7	17.531	22:43		
300	300.8	17.764	22:44		
304	304.8	17.947	22:45		

PRESSURE CALIBRATION				8 March 2013	
Calibration [°C]	55 °C	T _{ambient} [°C]	Julabo (13) EC-DIAG	T _{ambient} [°C]	24 °C
Gefran Process					
T _{sepoint-gr} [°C]	54.5 °C	T _{sepoint-113} [°C]	54.5 °C	T _{display-113} [°C]	54.65/6 °C
T _{display-gr} [°C]	54.5/6 °C	T _{display-113} [°C]	54.65/6 °C	T _{display-113} [°C]	54.65/6 °C
P _{applied} [bar]	P _{display} [bar]	P _{display} [m]	Time		
0	1.6	4.082	16:38		
5	6.4	4.299	16:40		
20	20.8	4.961	16:42		
35	35.4	5.628	16:44		
50	50.2	6.310	16:45		
65	65.2	6.992	16:47		
80	80.2	7.679	16:48		
95	95.3	8.373	16:50		
110	110.4	9.061	16:51		
125	125.6	9.751	16:53		
140	140.8	10.442	16:54		
155	155.8	11.137	16:56		
170	171.0	11.828	16:57 (P)		
185	186.1	12.521	16:59		
200	201.2	13.210	17:00		
215	216.3	13.899	17:02		
230	231.4	14.591	17:05		
245	246.5	15.281	17:05		
260	261.6	15.969	17:06		
275	276.6	16.659	17:08		
290	291.7	17.347	17:10		
295	296.6	17.574	17:11		
300	301.6	17.804	17:14		
304	306.6	17.985	17:15		

PRESSURE CALIBRATION				9 March 2013	
Calibration [°C]	60 °C	T _{ambient} [°C]	23 °C		
Gefran Process			Julabo (13) EC-DIAG		
T _{setpoint-gp} [°C]	57.5 °C	T _{setpoint-13} [°C]	57.65 °C		
T _{display-gp} [°C]	57.6/7 °C	T _{display-13} [°C]	57.64/5 °C		
P _{applied} [bar]	Display [bar]	P _{display} [ma]	Time		
0	no load 1.7	4.088	10:17		
5	6.4	4.300	10:20		
20	20.7	4.969	10:22		
35	35.6	5.637	10:24		
50	50.4	6.319	10:25		
65	65.4	7.000	10:27		
80	80.4	7.688	10:28		
95	95.5	8.375	10:31		
110	110.6	9.066	10:32		
125	125.7	9.760	10:33		
140	140.9	10.450	10:35		
155	156.0	11.142	10:37		
170	171.2	11.834	10:38		
185	186.3	12.527	10:39		
200	201.4	13.217	10:41		
215	216.5	13.907	10:42		
230	231.6	14.600	10:44		
245	246.7	15.289	10:45		
260	261.7	15.978	10:47		
275	276.8	16.666	10:48		
290	291.8	17.353	10:49		
295	296.8	17.583	10:51		
300	301.8	17.811	10:52		
304	305.8	17.996	10:53		

PRESSURE CALIBRATION				9 March 2013	
Calibration [°C]	65 °C	T _{ambient} [°C]	23 °C		
Gefran Process			Julabo (13) EC-DIAG		
T _{setpoint-gp} [°C]	64.5 °C	T _{setpoint-13} [°C]	64.64 °C		
T _{display-gp} [°C]	64.6/7 °C	T _{display-13} [°C]	64.64/5/6 °C		
P _{applied} [bar]	Display [bar]	P _{display} [ma]	Time		
0	1.9	4.103	12:18		
5	6.9	4.312 4.287	12:23		
20	21.4	4.990	12:28		
35	36.1	5.664	12:30		
50	51.0	6.343	12:31		
65	65.9	7.025	12:32		
80	81.0	7.714	12:32		
95	96.0	8.402	12:36		
110	111.2	9.094	12:38		
125	126.3	9.783	12:39		
140	141.4	10.477	12:41		
155	156.6	11.171	12:43		
170	171.7	11.862	12:45		
185	186.9	12.555	12:46		
200	202.0	13.247	12:48		
215	217.1	13.939	12:50		
230	232.2	14.627	12:51		
245	247.3	15.317	12:53		
260	262.4	16.006	12: ?		
275	277.4	16.694	12:56		
290	292.4	17.382	12:57		
295	297.4	17.610	12:59		
300	302.4	17.838	13:01		
304	306.4	18.020	13:02		

PRESSURE CALIBRATION				9 March 2013	
Calibration [°C]	75 °C	T _{ambient} [°C]	24 °C		
Gefran Process			Julabo (13) EC-DIAG		
T _{setpoint-gp} [°C]	74.5 °C	T _{setpoint-13} [°C]	74.64 °C		
T _{display-gp} [°C]	74.6/7 °C	T _{display-13} [°C]	74.3/4 °C		
P _{applied} [bar]	Display [bar]	P _{display} [ma]	Time		
0	28.3 3.1	4.150/4	16:55		
5	8.0	4.380	16:57		
20	22.5	5.043	16:59		
35	37.2	5.715	17:01		
50	52.1	6.394	17:03		
65	67.0	7.079	17:06		
80	82.1	7.766	17:07		
95	97.1	8.454	17:08		
110	112.2	9.145	17:10		
125	127.3	9.837	17:11		
140	142.4	10.525	17:13		
155	157.6	11.216	17:15		
170	172.7	11.911	17:16		
185	187.8	12.599	17:18		
200	202.9	13.289	17:19		
215	217.9	13.979	17:21		
230	232.9	14.665	17:23		
245	248.0	15.352	17:25		
260	263.1	16.041	17:26		
275	278.1	16.734	17:28		
290	293.2	17.423	17:30		
295	298.2	17.650	17:31		
300	303.2	17.877	17:33		
304	307.2	18.061	17:34		

PRESSURE CALIBRATION		9 Maart 2013	
T _{calibration} [°C]	80 °C	T _{ambient} [°C]	23.5 °C
Gefran Process		Julabo (13) EC-DIAG	
T _{setpoint-GP} [°C]	77.4 °C	T _{setpoint-J13} [°C]	77.64 °C
T _{display-GP} [°C]	77.5/6/4 °C	T _{display-J13} [°C]	77.63/4 °C
P _{applied}	P _{display}	P _{display}	Time
[bar]	[bar]	[mA]	
0	3.3	4.164	20:07
5	8.4	4.398	20:10
20	22.9	5.057	20:12
35	37.6	5.729	20:13
50	52.4	6.411	20:15
65	67.4	7.091	20:16
80	82.4	7.781	20:18
95	97.5	8.468	20:19
110	112.5	9.156	20:22
125	127.7	9.847	20:24
140	142.8	10.541	20:25
155	157.9	11.231	20:27
170	173.0	11.923	20:28
185	188.1	12.614	20:30
200	203.2	13.305	20:32
215	218.4	13.996	20:33
230	233.4	14.684	20:35
245	248.4	15.372	20:36
260	263.5	16.061	20:38
275	278.5	16.750	20:40
290	293.6	17.436	20:41
295	298.5	17.662	20:43
300	303.5	17.893	20:44
304	307.5	18.075	20:45

PRESSURE CALIBRATION		9 Maart 2013	
T _{calibration} [°C]	85 °C	T _{ambient} [°C]	23 °C
Gefran Process		Julabo (13) EC-DIAG	
T _{setpoint-GP} [°C]	84.4 °C	T _{setpoint-J13} [°C]	84.63 °C
T _{display-GP} [°C]	84.5/4 °C	T _{display-J13} [°C]	84.62/3 °C
P _{applied}	P _{display}	P _{display}	Time
[bar]	[bar]	[mA]	
0	3.6	4.176	22:52
5	8.9	4.417	22:56
20	23.2	5.069	22:58
35	37.8	5.740	22:59
50	52.7	6.423	23:00
65	67.6	7.104	23:02
80	82.6	7.792	23:03
95	97.7	8.479	23:05
110	112.8	9.169	23:06
125	127.9	9.860	23:07
140	143.0	10.551	23:09
155	158.1	11.241	23:10
170	173.2	11.931	23:11
185	188.3	12.623	23:13
200	203.4	13.312	23:14
215	218.5	14.003	23:17
230	233.6	14.694	23:19
245	248.7	15.383	23:20
260	263.8	16.073	23:23
275	278.8	16.759	23:24
290	293.8	17.447	23:27
295	298.8	17.678	23:28
300	303.8	17.903	23:29
304	307.8	18.089	23:31

PRESSURE CALIBRATION				22 Sep. 2014	
Calibration [°C]	35 °C	Temp [°C]	22.17 °C	Julabo (13) EC-DIAG	
Gefran Process					
Temp:ref [°C]	34.6	Temp:113 [°C]	34.46		
Temp:ref [°C]	34.8/9/6/7	Temp:113 [°C]	34.46/7		
Applied [bar]	Display [bar]	Display [mA]	Time		
0	-2.1	3.887	10:43		
5	2.0	4.097	10:51		
20	16.8	4.779	10:53		
35	31.3	5.426	10:55		
50	46.1	6.115	10:57		
65	61.20	6.799	10:58:11:00		
80	76.1	7.483	11:02		
95	91.2	8.174	11:04		
110	106.4	8.868	11:05		
125	121.4	9.557	11:08		
140	136.6	10.250	11:11		
155	151.7	10.941	11:13		
170	166.9	11.634	11:15		
185	182.1	12.324	11:18		
200	197.2	13.016	11:20		
215	212.4	13.707	11:23		
230	227.4	14.398	11:25		
245	242.5	15.085	11:27		
260	257.6	15.777	11:29		
275	272.6	16.461	11:31		
290	287.6/7	17.150	11:34		
295	292.6	17.377	11:36		
300	297.6/7	17.608	11:39		
304	301.6/7	17.790	11:41		

PRESSURE CALIBRATION				22 Sep.	
Calibration [°C]	55 °C	Temp [°C]	22.4 °C	Julabo (13) EC-DIAG	
Gefran Process					
Temp:ref [°C]	54.5	Temp:113 [°C]	54.45		
Temp:ref [°C]	54.7/6	Temp:113 [°C]	54.45/4		
Applied [bar]	Display [bar]	Display [mA]	Time		
0	0.0	3.992	14:36		
5	4.4	4.211	14:39		
20	18.8	4.864	14:40		
35	33.3	5.536	14:43		
50	48.2	6.210	14:44		
65	63.2	6.895	14:46		
80	78.2	7.582	14:48		
95	93.3	8.274	?		
110	108.5/14	8.965	14:52		
125	123.6/7	9.657	14:54		
140	138.8	10.351	14:56		
155	154.0	11.042	14:58		
170	169.0	11.735	15:01		
185	184.2	12.429	15:03		
200	199.3	13.120	15:05		
215	214.4/5	13.811	15:07		
230	229.6	14.502	15:10		
245	244.6	15.189	15:12		
260	259.7	15.880	15:14		
275	274.8	16.567	15:16		
290	289.8/7	17.253	15:19		
295	294.8/9	17.480	15:21		
300	299.8/7	17.709	15:23		
304	303.8/7	17.893	15:26		

PRESSURE CALIBRATION				23 Sep. 2014	
Calibration [°C]	75 °C	Temp [°C]	22.9 °C	Julabo (13) EC-DIAG	
Gefran Process					
Temp:ref [°C]	74.5	Temp:113 [°C]	74.44		
Temp:ref [°C]	74.7	Temp:113 [°C]	74.44/5		
Applied [bar]	Display [bar]	Display [mA]	Time		
0	1.7	4.085	11:54		
5	6.5	4.310	11:56		
20	21.0	4.974	11:58		
35	35.7	5.645	12:00		
50	50.5	6.320	12:02		
65	65.6	7.006	12:05		
80	80.5	7.692	12:07		
95	95.6	8.378	12:09		
110	110.6	9.069	12:13		
125	125.7/8	9.760	12:15		
140	140.9	10.452	12:17		
155	156.0/1	11.141	12:20		
170	171.2/3	11.834	12:22		
185	186.3/4	12.522	12:28		
200	201.4	13.216	12:30		
215	216.5	13.907	12:32		
230	231.6	14.597	12:35		
245	246.6	15.282	12:37		
260	261.7/6	15.973	12:40		
275	276.8	16.659	12:42		
290	291.7/6	17.345	12:45		
295	296.6	17.570	12:46		
300	301.6/7	17.799	12:48		
304	305.6/7	17.983	12:51		

PRESSURE CALIBRATION					
Calibration [°C]	35 °C	Tambient [°C]	22. December 2014		
Gefran Process					
Tsetpoint-gr [°C]	34.5	Tsetpoint-ls [°C]	34.40		
Tdisplay-gr [°C]	34.5/6	Tdisplay-ls [°C]	34.39/40		
Applied [bar]	Passive [bar]	Passive [mA]	Time		
0	-1.8	3.906	19:39		
5	2.5	4.129	19:42		
20	17.0	4.790	19:44		
35	31.7	5.459	19:45		
50	46.5	6.138	19:47		
65	61.4	6.820	19:48		
80	76.5/4	7.506	19:51		
95	91.6	8.196	19:52		
110	106.6	8.886	19:55		
125	121.8	9.576	19:57		
140	136.9	10.268	20:01		
155	152.1	10.964	20:02		
170	167.2/3	11.655	20:04		
185	182.4	12.348	20:06		
200	197.6	13.038	20:08		
215	212.6	13.731	20:09		
230	227.7	14.420	20:11		
245	242.8/9	15.108	20:13		
260	257.8	15.797	20:15		
275	272.9	16.487	20:17		
290	288.0	17.172	20:19		
295	292.9	17.403	20:21		
300	298.0	17.632	20:22		
304	302.0/1	17.815	20:25		

PRESSURE CALIBRATION					
Calibration [°C]	55 °C	Tambient [°C]	23/12/2014		
Gefran Process					
Tsetpoint-gr [°C]	54.4	Tsetpoint-ls [°C]	54.29		
Tdisplay-gr [°C]	54.5/4/3	Tdisplay-ls [°C]	54.29/3/30		
Applied [bar]	Passive [bar]	Passive [mA]	Time		
0	0.0	4.002	08:31		
5	4.8	4.233	08:40		
20	19.0	4.884	08:41		
35	33.7	5.534	08:46		
50	48.6	6.237	08:48		
65	63.6	6.918	08:49		
80	78.6	7.605	08:51		
95	93.7	8.293	08:53		
110	108.8	8.985	08:55		
125	124.0	9.680	08:57		
140	139.0	10.367	08:59		
155	154.2	11.060	09:01		
170	169.3	11.750	09:02		
185	184.5	12.446	09:04		
200	199.6/7	13.134	09:06		
215	214.8	13.828	09:08		
230	229.7	14.514	09:10		
245	244.9/8	15.204	09:12		
260	260.0	15.895	09:14		
275	274.9/275.0	16.581	09:17		
290	290.0/1	17.268	09:19		
295	295.0	17.497	09:20		
300	300.0/1	17.730	09:22		
304	304.0/1	17.910	09:24		

PRESSURE CALIBRATION					
Calibration [°C]	75 °C	Tambient [°C]	23/12/2014		
Gefran Process					
Tsetpoint-gr [°C]	74.3	Tsetpoint-ls [°C]	74.15		
Tdisplay-gr [°C]	74.3/4	Tdisplay-ls [°C]	74.14/3/5		
Applied [bar]	Passive [bar]	Passive [mA]	Time		
0	1.8	4.095	13:02		
5	6.8	4.324	13:14		
20	21.2	4.982	13:17		
35	36.0	5.651	13:19		
50	50.8	6.332	13:21		
65	65.7	7.015	13:23		
80	80.8	7.702	13:25		
95	95.8	8.392	13:27		
110	110.9	9.082	13:28		
125	126.0/1	9.773	13:31		
140	141.2	10.463	13:33		
155	156.2	11.155	13:36		
170	171.4	11.848	13:38		
185	186.5	12.537	13:40		
200	201.7/6	13.233	13:42		
215	216.8	13.919	13:44		
230	231.8	14.610	13:46		
245	246.9	15.296	13:47		
260	262.0	15.987	13:49		
275	277.0	16.676	13:51		
290	292.0/1	17.362	13:53		
295	297.0	17.590	13:55		
300	302.0/1	17.820	13:56		
304	306.0/1	18.000	13:58		

WS output = 50.1/2 Hz at start of calibration.

PRESSURE CALIBRATION				15 July 2015	
Calibration [°C]	SS °C	Tambient [°C]	Julabo (13) EC-DIAG		
Gefran Process					
Ttemp-cp [°C]	54.4	Ttemp-t13 [°C]	54.29 °C		
Tdisplay-gr [°C]	54.4/16 °C	Tdisplay-t13 [°C]	54.276/16		
Papplied [bar]	Display	Display	Time		
0	1.2	4.058	11:31		
5	6.0	4.283	11:35		
20	20.4	4.933	11:38		
35	34.9	5.605	11:39		
50	48.8	6.282	11:41		
65	44.8	6.98	11:42		
80	77.7	7.649	11:43		
95	94.9	8.339	11:45		
110	110.0	9.026	11:46		
125	125.2	9.718	11:48		
140	140.2	10.411	11:49		
155	155.3	11.100	11:50		
170	170.5	11.792	11:52		
185	185.6	12.482	11:53		
200	200.8	13.172	11:55		
215	215.8	13.864	11:56		
230	230.9	14.552	11:57		
245	245.0	15.244	11:58		
260	261.0	15.927	12:00		
275	274.0/1	16.615	12:01		
290	291.0/1	17.303	12:02		
295	296.0/1	17.927	12:?		
300	301.1	17.759	12:05		
304	305.1	17.944	12:07		

V prior to starting display was 1.0 bar (as the case after zeroing last night) but a jump occurred after connecting the dead weight vessel.

PRESSURE CALIBRATION				15 July 2015	
Calibration [°C]	35 °C	Tambient [°C]	Julabo (13) EC-DIAG		
Gefran Process					
Ttemp-cp [°C]	34.5	Ttemp-t13 [°C]	34.40		
Tdisplay-gr [°C]	34.6	Tdisplay-t13 [°C]	34.41/0		
Papplied [bar]	Display	Display	Time		
0	-0.8	3.951	11:11		
5	3.8	4.185	11:20		
20	18.0	4.830	11:21		
35	32.6	5.477	11:23		
50	47.6	6.178	11:25		
65	62.5	6.852	11:27		
80	77.6	7.546	11:29		
95	92.6	8.237	11:31		
110	107.7/8	8.927	11:34		
125	122.9	9.618	11:36		
140	138.1	10.315	11:38		
155	153.2/3	11.004	11:40		
170	168.4/5	11.697	11:42		
185	183.6	12.386	11:43		
200	198.8	13.081	11:45		
215	213.8	13.772	11:47		
230	228.9	14.460	11:49		
245	244.0/1	15.151	11:51		
260	259.2	15.839	11:53		
275	274.1	16.528	11:55		
290	289.2	17.209	11:57		
295	294.2	17.443	11:59		
300	299.2	17.670	17:01		
304	303.2	17.851	17:02		

WS (bubbler) output at 50.1/2 Hz.
 of the time, T bar (cocked)
 at 29 °C.
 load shedding prior to reading at 295 bar, generator did not activate;

Pressure Transmitter Zero Adjustment 14 July 2015

$T_f = 54.29\text{ °C}$ $T_g = 54.5\text{ °C}$ $T_{amb} \approx 13.8\text{ °C}$

$P_{disp} = -1.2/3\text{ bar}$ \rightarrow $P_{disp} = +0.9/1.0\text{ bar}$

PRESSURE CALIBRATION				15 July 2015	
Calibration [°C]	75 °C	Tambient [°C]	Julabo (13) EC-DIAG		
Gefran Process					
Ttemp-cp [°C]	74.3	Ttemp-t13 [°C]	74.15		
Tdisplay-gr [°C]	74.4/3	Tdisplay-t13 [°C]	74.143/4/5		
Papplied [bar]	Display	Display	Time		
0	3.0	4.448	20:47		
5	8.0	4.373	20:55		
20	22.4	5.029	20:57		
35	36.9	5.697	20:58		
50	57.8	6.376	21:00		
65	66.8	7.056	21:02		
80	81.7	7.741	21:03		
95	96.8/9	8.428	21:05		
110	112.0	9.120	21:07		
125	127.0	9.811	21:08		
140	142.1	10.501	21:10		
155	157.3	11.193	21:12		
170	172.5	11.881	21:13		
185	187.6	12.572	21:15		
200	202.8	13.265	21:17		
215	217.8	13.952	21:19		
230	232.9	14.645	21:20		
245	248.0	15.335	21:22		
260	263.0	16.021	21:23		
275	278.1	16.707	21:25		

PRESSURE CALIBRATION 14 March 2018

Calibration [°C]	55 °C	Tambent [°C]	Julabo (13) EC-DIAG	23.8 °C
Gefran Process				
Tsetpoint-gp [°C]	54.6	Tsetpoint-j13 [°C]	54.42	
Tdisplay-gp [°C]	54.6/7	Tdisplay-j13 [°C]	54.42/1/3	
Applied [bar]	Display	Display	Time	
0	1.0	4.040065	15:53	
5.0	6.0	4.285145	15:59	
20.0	20.1	4.931346	16:01	
35.0	34.8	5.603518	16:02	
50.0	49.6/7	6.283225	16:05	
64.9	64.6	6.914502	16:07	
79.9	79.6/7	7.653051	16:08	
94.9	94.8	8.341386	16:09	
109.9	109.8	9.033200	16:11	
124.9	124.9	9.722359	16:13	
139.9	140.1	10.41373	16:14	
154.8	155.2	11.10609	16:16	
169.8	170. 170.2	11.79547	16:20	
184.8	185.4	12.48863	16:22	
199.8	200.5	13.18206	16:24	
214.8	215.6	13.87200	16:25	
229.8	230.7	14.55801/11	16:27	
244.7	245.7	15.24796	16:?	
259.7	260.8	15.93637	16:31	
274.7	275.8	16.62457	16:32	
289.7	290.9/8	17.31167	16:34	
294.7	295.8	17.54115	16:36	
299.7	300.8/9	17.76844	16:37	
303.7	304.9/8	17.95237	16:39	

PRESSURE CALIBRATION 14 March 2016

Calibration [°C]	75 °C	Tambent [°C]	Julabo (13) EC-DIAG	23.9 °C
Gefran Process				
Tsetpoint-gp [°C]	74.5	Tsetpoint-j13 [°C]	74.34	
Tdisplay-gp [°C]	74.7/6	Tdisplay-j13 [°C]	74.34/5	
Applied [bar]	Display	Display	Time	
0	2.9	4.168374	21:53	
5.0	7.8	4.370235	22:01	
20.0	22.0/1	5.020460	22:03	
35.0	34.8	5.689783	22:05	
50.0	51.6	6.369089	22:06	
64.9	66.5	7.050854	22:08	
79.9	81.6	7.738774	22:10	
94.9	96.5	8.424954	22:11	
109.9	111.7	9.117789	22:13	
124.9	124.8/9	9.808232	22:15	
139.9	142.0	10.49874	22:17	
154.8	157.0	11.19255	22:19	
169.8	172.1	11.88404	22:21	
184.8	187.3	12.57210	22:23	
199.8	202.4/5	13.26400	22:25	
214.8	217.4/5	13.95133	22:28	
229.8	232.5	14.64431	22:29	
244.7	247.6/7	15.33273	22:30	
259.7	262.6	16.02311	22:32	
274.7	277.7	16.70760	22:34	
289.7	292. 292.6	17.39557	22:40	
294.7	297.7	17.62330	22:38	
299.7	302.6	17.85060	22:42	
303.7	306.6	18.03474	22:44	

PRESSURE CALIBRATION 15 March 2016

Calibration [°C]	35 °C	Tambent [°C]	Julabo (13) EC-DIAG	21.8 °C
Gefran Process				
Tsetpoint-gp [°C]	34. 34.7	Tsetpoint-j13 [°C]	34.42	
Tdisplay-gp [°C]	34.8/9/35.0	Tdisplay-j13 [°C]	34.42/3/2	
Applied [bar]	Display	Display	Time	
0	-14	3.922577	08:52	
5.0	3.2	4.150702	09:01	
20.0	17.4	4.804407	09:03	
35.0	32.1	5.471610	09:05	
50.0	44.9	6.155320	09:06	
64.9	62.0	6.83934	09:08	
79.9	76.9	7.526136	09:10	
94.9	92.0/1	8.219820	09:12	
109.9	107.2	8.908914	09:14	
124.9	122.4	9.602315	09:16	
139.9	127.6	10.29469	09:18	
154.8	152.6	10.98726	09:22	
169.8	167.8	11.68075	09:24	
184.8	183.0	12.37640	09:26	
199.8	198.1	13.06635	09:27	
214.8	213.3/2	13.75781	09:29	
229.8	228.4	14.44906	09:31	
244.7	243.4	15.13878	09:33	
259.7	258.5	15.82632	09:36	
274.7	273.6	16.51256	09:38	
289.7	288.6	17.200359	09:40	
294.7	293.6/7	17.43415	09:44	
299.7	298.6	17.65882	09:44	
303.7	302.5	17.84101	09:46	



Unique Metrology

Ekim Research & Innovation Centre
Lower Gernsion Road • Rosherville
P O Box 145296 • Bracken Gardens • 1452
Tel: 011 626 3603 • Cell: 083 254 3635 • Fax: 086 910 4196
Web: www.unimel.co.za



SANAS ACCREDITED CALIBRATION LABORATORY No 205

PRESSURE METROLOGY

CERTIFICATE OF CALIBRATION

Date of issue : 25/02/2016

Certificate No : 1602P6223-1

Technical Signatory

M Mathieson.

Page 1 of 4 pages.

The results of all measurements are traceable to the national measuring standards.

The values in this certificate are correct at the time of calibration. Subsequently the accuracy will depend on such factors as the care executed in handling and use of the device, and the frequency of use. Recalibration should be performed after the period so chosen to ensure that the instrument's accuracy remains within the desired limits.

This certificate is issued in accordance with the conditions of the accreditation granted by the South African National Accreditation System (SANAS). It is a correct record of the measurements made. This certificate may not be reproduced other than in full except with prior written approval of the issuing laboratory. Legal liability shall be limited to the cost of recalibration and/or certification, but the applicant indemnifies Unique Metrology (Pty) Ltd against any consequential or other loss.

The South African National Accreditation System (SANAS) is a member of the International Laboratory Accreditation Cooperation (ILAC) Mutual Recognition Arrangement (MRA). This arrangement allows for the mutual recognition of technical test and calibration data by the member accreditation bodies worldwide. For more information on the Arrangement please contact www.ilac.org.



Unique Metrology

Esikom Research & Innovation Centre
 Lower Gamston Road - Rossmore
 P O Box 145296 - Bracken Gardens - 1452
 Tel: 011 626 3608 • Cell: 063 254 3635 • Fax: 086 610 4196
 Web: www.unimet.co.za



CERTIFICATE OF CALIBRATION

Page 2 of 4 pages.

Certificate Number	:	1602P6223-1		
Calibration of a	:	Pressure Balance		
Manufacturer & Type	:	Barnetts		
Serial Number	:	3892/74		
Calibrated for	:	Stellenbosch University, Stellenbosch.		
Procedure Number	:	53-131		
Date of Calibration	:	25/02/2016		
Date of Issue	:	25/02/2016		
Laboratory Environment	:	20.3 °C		
Reference Standards	:	205-S-06	Budenberg 280D	S/N 27702
	:	205-S-07	Budenberg Mass Set	S/N 205-S-07
	:	205-S-10	Mass Set	S/N 1406-01
	:	205-S-11	Mass Set	S/N 1406-02

1. Procedure

The values of the pressure balance ring weights and of the weight of the piston assembly were determined by comparison against calibrated standard mass pieces.

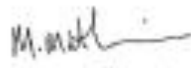
The piston-cylinder assembly was balanced against a calibrated standard piston-cylinder assembly at several pressures within the normal working range. The effective area was determined and corrected to 20 °C assuming an increase in area of 22 ppm/°C rise in temperature.

2. Results

2.1 Weights

See next page for weight values.

Calibrated by : A Mathieson


 Technical Signatory



Unique Metrology

Eskom Research & Innovation Centre
 Lower Germiston Road • Rosheville
 P O Box 145298 • Braamfontein Gardens • 1452
 Tel: 011 628 3556 • Cell: 083 254 3636 • Fax: 086 610 4195
 Web: www.unicmet.co.za



CERTIFICATE OF CALIBRATION

Certificate Number : 1602P6223-1
 Calibration of a : Pressure Balance
 Manufacturer & Type : Barnetts

Page 3 of 4 pages.

2.1 Weights (cont)

Component marked		Nominal Value (kg)	Value measured (kg)	Uncertainty of measurement (g)	Error %
150 kPa	1	1.23371	1.23389	0.07	0.015
150 kPa	2	1.23371	1.23391	0.07	0.016
150 kPa	3	1.23371	1.23394	0.07	0.019
150 kPa	4	1.23371	1.23388	0.07	0.014
150 kPa	5	1.23371	1.23386	0.07	0.012
150 kPa	6	1.23371	1.23393	0.07	0.018
150 kPa	7	1.23371	1.23383	0.07	0.010
150 kPa	8	1.23371	1.23392	0.07	0.017
150 kPa	9	1.23371	1.23385	0.07	0.011
150 kPa	10	1.23371	1.23392	0.07	0.017
150 kPa	11	1.23371	1.23389	0.07	0.015
150 kPa	12	1.23371	1.23395	0.07	0.019
150 kPa	13	1.23371	1.23392	0.07	0.017
150 kPa	14	1.23371	1.23301	0.07	0.016
150 kPa	15	1.23371	1.23368	0.07	0.014
150 kPa	16	1.23371	1.23384	0.07	0.010
150 kPa	17	1.23371	1.23386	0.07	0.014
150 kPa	18	1.23371	1.23388	0.07	0.014
150 kPa	19	1.23371	1.23386	0.07	0.012
50 kPa	1	0.411237	0.411342	0.024	0.026
50 kPa	2	0.411237	0.411383	0.024	0.036
10 kPa	1	0.082247	0.082282	0.006	0.042
10 kPa	2	0.082247	0.082286	0.006	0.047
10 kPa	3	0.082247	0.082275	0.006	0.034
10 kPa	4	0.082247	0.082278	0.006	0.037
Piston Assy		Unknown	0.411942	0.022	

Calibrated by : A Mathieson

Technical Signatory



Unique Metrology

Eskom Research & Innovation Centre
 Lower Germiston Road • Rosheville
 P.O. Box 145296 • Bracken Gardens • 1432
 Tel: 011 626 3908 • Cell: 083 254 3935 • Fax: 086 810 4198
 Web: www.unimet.co.za



CERTIFICATE OF CALIBRATION

Certificate Number : 1602P6223-1 Page 4 of 4 pages
 Calibration of a : Pressure Balance
 Manufacturer & Type : Bametts

2.2 Piston-cylinder assembly

The effective area of the high-pressure piston-cylinder assembly was found to be expressible as

where

$$A = A_0(1 + \beta P)$$

$$A_0 = 8.0641 \pm 0.0070 \text{ mm}^2$$

$$\beta = 3.92\text{E-}6 \pm 2.5\text{E-}6 \text{ /MPa}$$

P is the pressure in MPa.
 The nominal value is 8.0645 mm².

3. Accuracy of pressure measurement.

When the pressure balance is used with the weight set supplied and after making suitable corrections for gravity, temperature and air buoyancy the total error in pressure measurement (ie the deviation from the nominal value) does not exceed 0.04% above 2 MPa.

4. Notes

The reference level for the pressure measurements was taken to be the base of the piston's cylinder.
 The oil used for the calibration was a mineral oil of nominal density 870 kg/cm³.
 The buoyancy volume was found to be negligible.

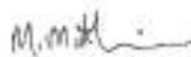
5. Uncertainty of Calibration

The reported uncertainty is based on a standard uncertainty multiplied by a coverage factor of k=2, which unless specifically stated otherwise, provides a confidence level of 95%, in accordance with the Guide to the expression of Uncertainty in Measurement, first edition, 1993.

6. Comments.

The weight set was marked with the serial number 3692/74.

Calibrated by : A Mathieson


 Technical Signatory

CMeTSA Pressure Metrology Course **FORMULAE AND REFERENCE VALUES**

MANOMETERS AND BAROMETERS

Principle: $P = h \cdot \rho \cdot g$
 Where P is pressure (Pa)
 h is column height (m)
 ρ is fluid density (kg m⁻³)
 and g is the acceleration due to gravity (m s⁻²).

THE PRESSURE BALANCE

The pressure is given from first principles by:

P = Force/Area
 or P = $\frac{mg}{A}$

Where m is the total mass (kg)
 g is the acceleration due to gravity (m s⁻²), and
 A is the area of the PCU

Principle:
$$P = \frac{m \left(1 - \frac{\rho_a}{\rho_m} \right) g}{A_{e,20} (1 + \beta P) (1 + \alpha (t - 20))}$$

General formula for pressure

$$P = \frac{\left\{ \sum \left[m \left(1 - \frac{\rho_a}{\rho_m} \right) - v \rho_f \right] g + (\sigma c) \right\}}{A_{e,20} (1 + \beta P) (1 + \alpha (t - 20))} + h \rho_f g$$

where the symbols have the usual meanings.

- where
- P is the applied pressure
 - m is the mass of the components of the load
 - ρ_a is the density of the air
 - ρ_m is the density of the mass m (which can be different for each component)
 - v is the buoyancy volume is the volume of the piston protruding into the oil below the reference level
 - ρ_f is the fluid density.
 - g is the value of local gravity
 - σ is the surface tension
 - c is the circumference of the piston.
 - h is the height difference
 - A_{e,20} is the effective area of the PC assembly at zero applied pressure and a temperature of 20 °C.
 - β is the pressure distortion coefficient.
 - α is the area coefficient of thermal expansion
 - t temperature of ambient air or piston.

SA Metrology
23 Platinum Business Park
Taurus Street
Brackenell
Tel 0834502615 / Fax (086) 540 2284



Certificate of Calibration

This certificate is issued in accordance with the ISO 17025:2005 International Standard and is traceable through the National Metrology Laboratory (NML) in Pretoria, SANAS recognised National or International Laboratories

Manufacturer : Afriso
Description : Pressure Transducer
Model No : 311148S
Serial No : 1307171
Asset No : Unknown
Calibrated for : CME Metrology
Cape Town
Temperature : 20 °C ± 3 °C
Relative humidity : 48 %RH ± 5 %RH
Date of calibration : 23 December 2010
Issue Date : 29 December 2010
Calibrated by : P Coetsee

This Report is issued without alteration. Copyright of this Report is owned by SAME and may not be reproduced other than in full, except with the prior written approval of SAMET. The values given in this Report were correct at the time of Test. Subsequently the accuracy will depend on factors such as care exercised in handling the instrument and frequency of use. Retest should be performed after a period, which has been chosen to ensure that, under normal circumstances, the instruments accuracy remains within the desired limits. The uncertainties of measurement were estimated for a coverage factor of k=2 which approximates a 95% confidence level.



Technical Signatory
ZW de Witt
Report no SM31504

Page 1 of 3

Calibration Certificate

1. Standards and equipment

Ref	Make	Model	Description	Serial no
50	Fluke	5500A	Calibrator	7270009
201	Fluke	716	Pressure calibrator	7047016
219	Fluke	8506A	DMM True RMS 7.5 Digit	6275404
19	Fluke	525A	Calibrator	9005276
220	Aquatech Inc	DBX1	Precision Digital Barograph	220
230	Fluke	700P01	Pressure Module:	79900103
236	Fluke	700P09	Pressure Module	1500 PSIG
238	Druck	DPI-701	Pressure Calibrator	701051 5805
221	Fluke	700P07	Pressure Module:	73950703
237	Druck	DPI-601	Digital Pressure Calibrator	601478906

2. Procedure

- 2.1 The UUT (Unit under test) was partially calibrated in terms of the manufacturers' accuracy specification, with reference to the typical manufacturers recommended procedure
- 2.2 The UUT was subjected to pressure using filtered air pressure in a direct comparison method against a Certified Digital Pressure transducer in a split system configuration supported by a Process Calibrator.
- 2.3 Calibration procedure no SM P2 001 was used

3. Results

3.1 Decreasing Pressure

Range	Applied Value	UUT Down Pressure	Correction	Tolerance	Measurement uncertainty
1 Bar To 0 Bar	1.0000 Bar	10.000 V	0.0000 Bar	± 0.35 %	± 0.1 %
	0.9980 Bar	9.980 V	0.0000 Bar	± 0.35 %	± 0.1 %
	0.9960 Bar	9.960 V	0.0000 Bar	± 0.35 %	± 0.1 %
	0.9940 Bar	9.940 V	0.0000 Bar	± 0.35 %	± 0.1 %
	0.9900 Bar	9.801 V	-0.0001 Bar	± 0.35 %	± 0.1 %
	0.8000 Bar	8.002 V	-0.0002 Bar	± 0.35 %	± 0.1 %


 Technical Signatory
 ZW de Witt
 Report no SM31504

Page 2 of 3

Calibration Certificate

3.1 Increasing Pressure

Range	Applied Value	UUT Up Pressure	Correction	Tolerance	Measurement uncertainty
1 Bar To 0 Bar	0.8000 Bar	8.003 V	-0.0003 Bar	± 0.35 %	± 0.1 %
	0.9800 Bar	9.802 V	-0.0002 Bar	± 0.35 %	± 0.1 %
	0.9940 Bar	9.941 V	-0.0001 Bar	± 0.35 %	± 0.1 %
	0.9980 Bar	9.980 V	0.0000 Bar	± 0.35 %	± 0.1 %
	0.9980 Bar	9.980 V	0.0000 Bar	± 0.35 %	± 0.1 %
	1.0000 Bar	10.000 V	0.0000 Bar	± 0.35 %	± 0.1 %

4. Comments

Bold - highlights indicate out of tolerance values


 Technical Signatory
 ZW de Witt
 Report no SM31504

Page 3 of 3

ALEXANDER WIEGAND

SE & Co. KG



zertifiziert nach DIN ISO 9001
certified by DIN ISO 9001
DQS Reg. Nr. 1833-01

UniTrans

Messwertprotokoll für Drucktransmitter

Test certificate for Pressure Transmitter

Gerätedaten: Instrument Data:	Kopf-Nr. Head No.	Messbereichsanfang Start of Range	Messbereichsende End of Range	Druckeinheit Unit of Pressure	Genauigkeit [%] Accuracy [%]
	5265	0	1,6	bar / abs.	0,1

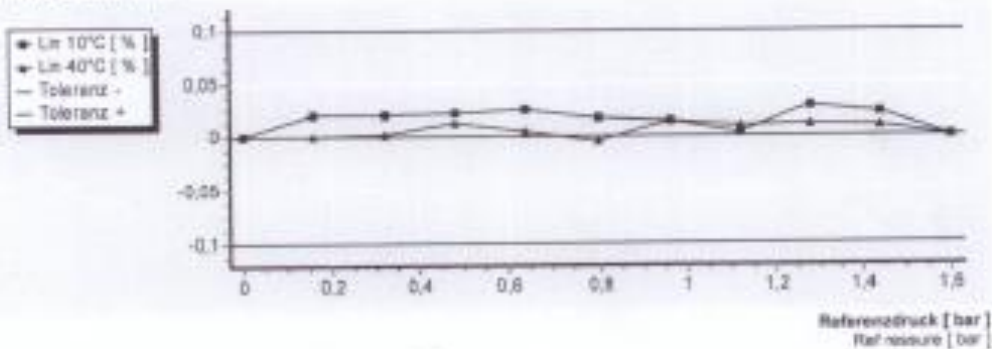
Ausgang bei 20°C:
Output at 20°C:

Nullpunkt Zero		Endwert Full Scale	
3,50	mA	20,00	mA

Kennlinienwerte:
Characteristics:

Referenzdruck Ref Pressure		Linearitätsabweichung [%] Deviation of linearity [%]	
[%]	[bar]	bei / at 10°C	bei / at 40°C
0	0,000	0,000	0,000
10	0,160	0,020	0,001
20	0,320	0,021	0,002
30	0,480	0,021	0,013
40	0,640	0,024	0,005
50	0,800	0,016	-0,005
60	0,960	0,014	0,014
70	1,120	0,003	0,009
80	1,280	0,028	0,010
90	1,440	0,022	0,009
100	1,600	0,000	0,000

Linearitätsabweichung [%]:
Deviation of linearity [%]



Datum: 10.09.2012
Date

geprüft von: 012
tested by

Die Produktionsabteilung für Druckmessgeräte wird unterstützt und überwacht von dem WIKAL DQD-Kalibrierlabor für Druck DQD-K-03701
The pressure department is supported and monitored by the WIKAL pressure DQD-Calibration-Laboratory DQD-K-03701

Druck + Temperatur

WIKAL Alexander Wiegand SE & Co. KG
Alexander-Wiegand-Strasse 38
69811 Klingenberg
Germany

Tel: +49 9072 132-0
Fax: +49 9072 132-406
E-Mail: info@wika.de
www.wika.de

Konzerngesellschaft, Sitz: Klingenberg
Anlagenstr. Aachaffenburg 148a 18119
Konzernzentrale: WIKAL Werksstraße SE & Co. KG -
33122 Klingenberg - Anlagenstr. Aachaffenburg 148a 4820

Konzernleiter:
WIKAL International SE - 812 Klingenberg -
Anlagenstr. Aachaffenburg 148b 18120
Vorstand: Alexander Wiegand
Vorstand: des Aufsichtsrats: Dr. Max Egel



METROLOGY



Lab no.1419

Po Box 99 Eppindust 7475, Benbow Avenue, Epping 1, Cape Town, 7460 Tel 021-535 1499 Fax 021-535 2191

Mass Laboratory Certificate of Calibration

Calibration performed using measuring equipment traceable to National Measurement Standards

Mass Laboratory Standards: Serial Number: CN001A

Calibration Procedure: ML11

Page No. 1 of 1

Certificate Number:

M3678/9

Customer Details:

Calibration for: Stellenbosch University
Department of Process Engineering
Address: Stellenbosch

Calibration Details:

Description: Balance
Make: Ohaus
Serial Number: M60737
Type of Unit: Electronic

Location/Department: Room 403
Condition on receipt: Satisfactory
Calibration performed at: Stellenbosch University
Department of Process Engineering

Measuring Range:
Minimum: 0g
Maximum: 120g
Resolution: 0.00001/0.0001g

Unit of Measure: g

Type of Calibration: Full

Date of Calibration: 22-06-2011

Date of Issue: 23-06-2011

Requested
recalibration date: June-12

Calibration Results

Nominal Test Position	Accuracy Test As Found	Accuracy Test	Repeatability	0.0001g
g	g	g	Mass Used	50g
10	9.9998	9.9998	Zero Error	0g
20	19.9999	19.9999	Off Centre Error	0.0004g
50	50.0000	49.9999	Mass Used	20g
70	69.9997	69.9998	Sensitivity	0g
100	200.0000	99.9997	Linearity	0.0003g
<i>Measurement Uncertainty @ 95% confidence level ±</i>				0.0005g

Remarks: None

Signatories:

Technical Signatory: F Arnold

Calibrated by: F Arnold

The reported uncertainties of measurement were calculated and expressed in accordance with EA-4/02. The calculations are based on a standard uncertainty multiplied by a coverage factor of K=2 which unless specifically stated otherwise provides a level of confidence of approximately 95%. This certificate is issued in accordance with ISO IEC 17025, the conditions approved by SANAS and the policies of CME METROLOGY. It is a correct record of measurements made and relate only to the items calibrated. This certificate may not be reproduced other than in full, except with prior written approval of the issuing laboratory. The values in this certificate are valid at the time calibration. Subsequently the accuracy shall depend on such factors as the care exercised in handling, use of the instrument and frequency of use. Re-calibration should be performed after a period which has been chosen to ensure that the instrument's accuracy remains within the desired limits. The applicant hereby indemnifies, holds harmless and absolves CME METROLOGY and the Mass-Pressure and Torque laboratories, from any damage whatsoever and any legal liability in the event of a mistake in the services performed for the applicant.

doc: ML 1 (rev12) March 2011

End of Certificate



METROLOGY



Lab no.1419

Po Box 99 Eppindust 7475, Cnr Riley & Brentford Streets, Beaconvale, Cape Town, Tel 021-931 1101 Fax 021-931 1126

Mass Laboratory
Certificate of Calibration

Calibration performed using measuring equipment traceable to National Measurement Standards

Mass Laboratory Standards: Serial Number: FA005

Calibration Procedure: ML11
Page No. 1 of 1

Certificate Number:
M9150/3

Customer Details:

Calibration for: Stellenbosch University
Address: Department of Process Engineering
Cnr Bosmans & Banghoek roads
Stellenbosch

Calibration Details:

Description: Balance
Make: Ohaus
Serial Number: M60737
Type of Unit: Electronic

Location/Department: Room403

Condition on receipt: Satisfactory
Calibration performed at: Stellenbosch University

Type of Calibration: Full

Measuring Range:

Minimum: 0g
Maximum: 100g
Resolution: 0,0001g

Unit of

Measure: g

Date of Calibration: 03/07/2015

Date of Issue: 14/07/2015

Requested

recalibration date: N/a

Calibration Results

Nominal Test Position	Accuracy Test As Found	Accuracy Test As Left	Repeatability	0,0002g
g	g	g	Mass Used	50g
0.2	0.2000	0.2000	Zero Error	0g
0.5	0.5000	0.4999	Off Centre Error	0,0025g
1	1.0000	0.9999	Mass Used	20g
2	1.9999	2.0002	Sensitivity	0g
5	4.9999	5.0002	Linearity	0,0005g
10	9.9998	10.0001		
20	19.9996	20.0002		
50	49.9994	50.0003		
100	99.9980	100.0004		
Measurement Uncertainty @ 95% confidence level ±				0,0018g

Remarks: Reset

Signatories:

Technical Signatory: F Arnold

Calibrated by: F Arnold

The reported uncertainties of measurement were calculated and expressed in accordance with the principles defined in the GUM, Guide to Uncertainty of Measurement, ISO, Geneva, 1993. The calculations are based on a standard uncertainty multiplied by a coverage factor of K=2 which unless specifically stated otherwise provides a level of confidence of approximately 95%.

This certificate is issued in accordance with ISO IEC 17025, the conditions approved by SANAS and the policies of CME METROLOGY. It is a correct record of measurements made and relate only to the items calibrated. This certificate may not be reproduced other than in full, accept with prior written approval of the issuing laboratory. The values in this certificate are valid at the time calibration. Subsequently the accuracy shall depend on such factors as the care exercised in handling, use of the instrument and frequency of use. Re-calibration should be performed after a period which has been chosen to ensure that the instrument's accuracy remains within the desired limits. The applicant hereby indemnifies, holds harmless and absolves CME METROLOGY and the Mass-Pressure and Torque laboratories, from any damage whatsoever and any legal liability in the event of a mistake in the services performed for the applicant.

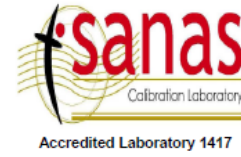
MLBC Rev4 April 2015
End of Certificate

ON-SITE CALIBRATION CERTIFICATE

Pc Lab Services CC

PO Box 12236
Aston Manor, 1630
Tel: (011) 396-2334
Fax: (011) 979-3410

**Calibration Certificate Number:
SJ0003491**



This certificate is issued under the authority and conditions granted by the South African National Accreditation System and may not be reproduced except in full and without prior written approval.

Issued to: University Of Stellenbosch
Address: Stellenbosch

Uut Make: PRECISA
Model: XT4200C
Serial No: 2805807
Capacity: 4200 (g)
Graduations: 0,01 (g)

Procedure: This instrument was calibrated with standard weights of known value, traceable to the National Standard, in accordance with our calibration procedure PROC1.

Condition of Calibration: AMBIENT

Traceability: Serial No: PCL4 PCL4 PCL6
Dated: 2009/10/06 2009/10/06 2009/11/02

Calibration Results:

Repeatability: (g)	Accuracy and Linearity:		
Load Applied:	Load Applied (g)	Before Adjustment (g)	After Adjustment (g)
2 000,00	4 000,00	3 996,38	4 000,05
Settling Time (Sec): 3	3 000,00	2 997,26	3 000,02
2 000,01	2 000,00	1 998,15	2 000,00
2 000,01	1 000,00	999,06	999,99
2 000,01	500,000	499,53	500,01
2 000,01	200,0000	199,81	200,01
2 000,02			
Standard Deviation: (g)			
0,0041			

Eccentric Error:	Comments										
Load Applied: 1 500,00 (g) Readings (g) <div style="display: flex; align-items: center;"> <table style="border-collapse: collapse;"> <tr><td>1:</td><td>1 500,01</td></tr> <tr><td>2:</td><td>1 500,05</td></tr> <tr><td>3:</td><td>1 500,05</td></tr> <tr><td>4:</td><td>1 499,97</td></tr> <tr><td>5:</td><td>1 499,97</td></tr> </table> </div>	1:	1 500,01	2:	1 500,05	3:	1 500,05	4:	1 499,97	5:	1 499,97	
1:	1 500,01										
2:	1 500,05										
3:	1 500,05										
4:	1 499,97										
5:	1 499,97										
Maximum Error: 0,04 (g)											

Uncertainty: The uncertainty of measurement is + or - **0.12 (g)** and was calculated and expressed in accordance with BIPM, IEC, ISO, IUPAP, OIML document entitled "Guide to the Expression of Uncertainty in Measurement" and is based on a standard uncertainty multiplied by a coverage factor k = 2 which, unless specifically stated otherwise, provides a level of confidence of approximately 95%.

Validity: The values in this certificate are correct at the time of calibration. Subsequently the accuracy will depend on such factors as the care exercised in handling and use of the instrument as well as the frequency of use. Re-calibration should be performed after such a period which is chosen to ensure that the instrument's accuracy remains within the desired limits.

Calibrated By: D CrowCour

Date Calibrated: 2010/10/13

Technical Signatory



Po Box 99 Eppindust 7475, Cnr Riley & Brentford Streets, Beaconvale, Cape Town, Tel 021-931 1101 Fax 021-931 1126

Mass Laboratory
Certificate of Calibration

Calibration performed using measuring equipment traceable to National Measurement Standards

Mass Laboratory Standards: Serial Number: FA005,FA001,CN001

Calibration Procedure: ML11

Page No. 1 of 1

Certificate Number:

M9786/1

Customer Details:

Calibration for: Stellenbosch University
Address: Department of Process Engineering
Cnr Bosmans & Banghoek roads
Stellenbosch

Calibration Details:

Description: Balance
Make: Precisa
Serial Number: 2805807
Type of Unit: Electronic

Measuring Range:

Minimum: 0g
Maximum: 4000g
Resolution: 0.01g

Unit of

Measure: g

Condition on receipt: Satisfactory
Calibration performed at: Department of Process Engineering
Location/Department: Room301
Temperature(°C): 18-25
Type of Calibration: Full

Date received: 13/11/2015

Date of Calibration: 04/12/2015

Date of Issue: 08/12/2015

Requested recalibration date: December-16

Calibration Results

Nominal Test Position	Accuracy Test As Found	Accuracy Test As Left	Repeatability	0.01g
g	g	g	Mass Used	2000g
20	20.00	20.00	Zero Error	0g
50	50.00	50.00	Off Centre Error	0.04g
100	100.00	100.00	Mass Used	1000g
200	200.00	200.00	Sensitivity	0g
300	300.00	300.00	Linearity	0.05g
500	500.00	500.00		
1000	999.99	999.99		
1500	1500.00	1500.00		
2000	1999.99	1999.99		
3000	3000.02	3000.02		
4000	4000.05	4000.05		
Measurement Uncertainty @ 95% confidence level ±				0.04g

Remarks: Off Centre error taken starting in lefthand corner at the back of pan.

Signatories:

Technical Signatory: F Arnold 

Calibrated by: F Arnold 

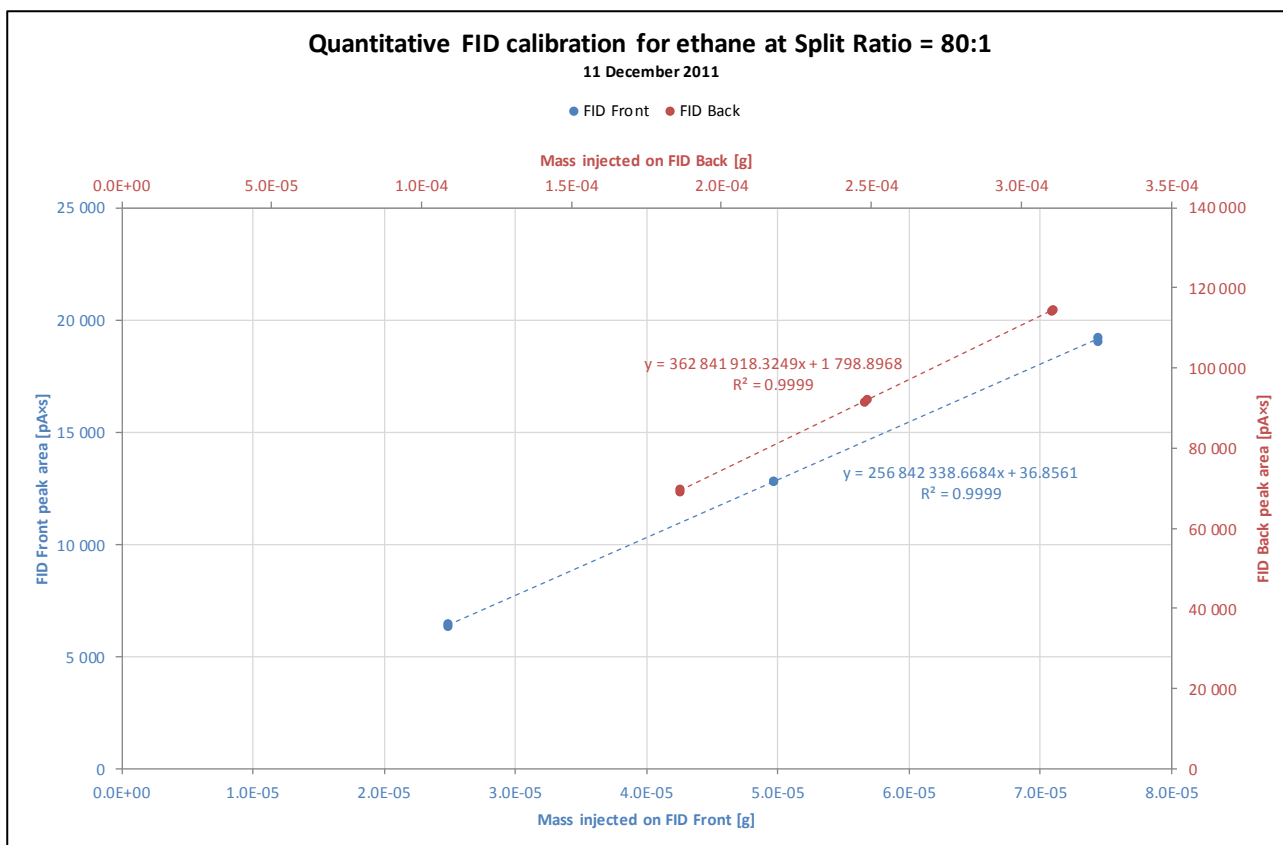
The reported uncertainties of measurement were calculated and expressed in accordance with the principles defined in the GUM, Guide to Uncertainty of Measurement, ISO, Geneva, 1993. The calculations are based on a standard uncertainty multiplied by a coverage factor of K=2 which unless specifically stated otherwise provides a level of confidence of approximately 95%.

This certificate is issued in accordance with ISO IEC 17025, the conditions approved by SANAS and the policies of CME METROLOGY. The accuracy of the equipment used during calibration is traceable to the National Measuring Standards as maintained in the Republic of South Africa or International Measuring Standards. It is a correct record of measurements made and relate only to the items calibrated. This certificate may not be reproduced other than in full, except with prior written approval of the issuing laboratory. The values in this certificate are valid at the time calibration. Subsequently the accuracy shall depend on such factors as the care exercised in handling, use of the instrument and frequency of use. Re-calibration should be performed after a period which has been chosen to ensure that the instrument's accuracy remains within the desired limits. The applicant hereby indemnifies, holds harmless and absolves CME METROLOGY and the Mass-Pressure and Torque laboratories, from any damage whatsoever and any legal liability in the event of a mistake in the services performed for the applicant.

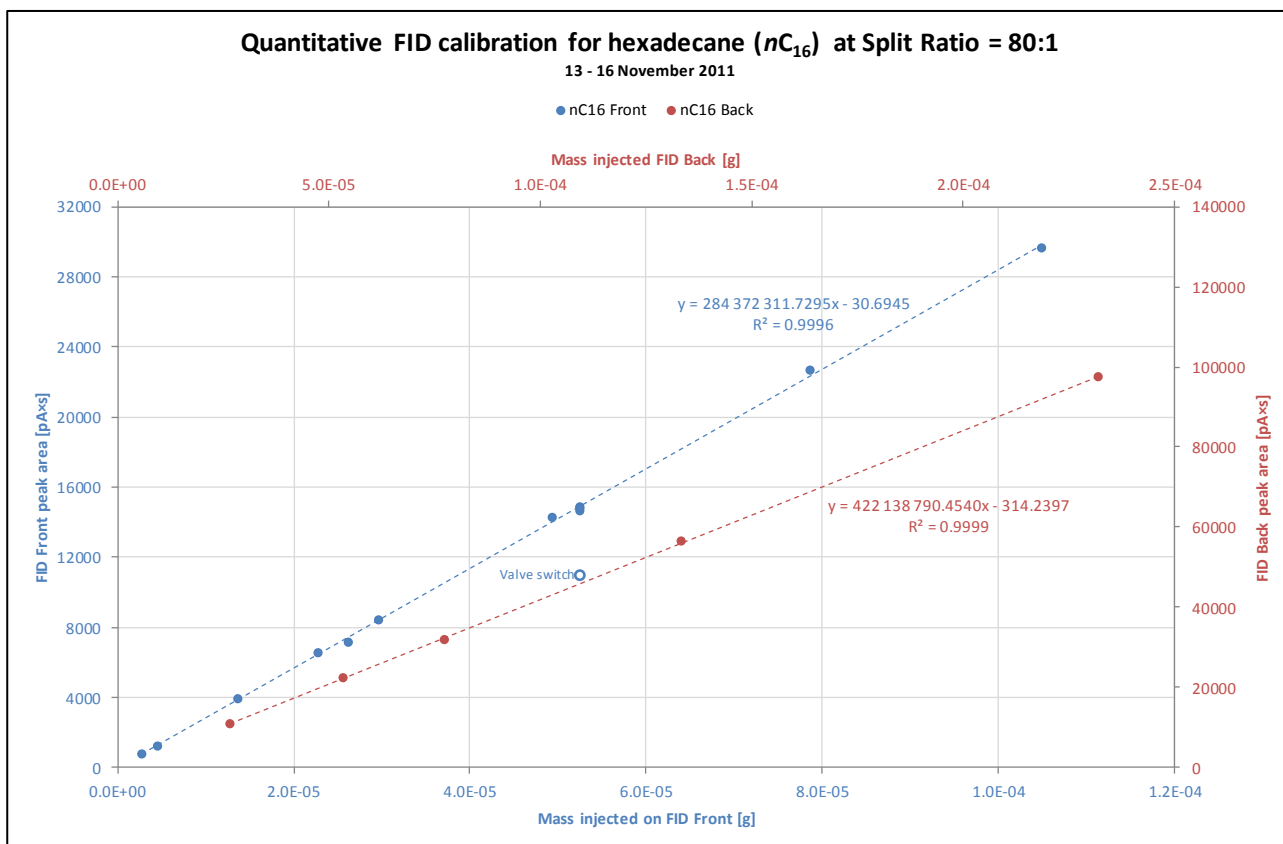
MLBC Rev5 September 2015
End of Certificate

Appendix E. GAS CHROMATOGRAPH CALIBRATION CURVES

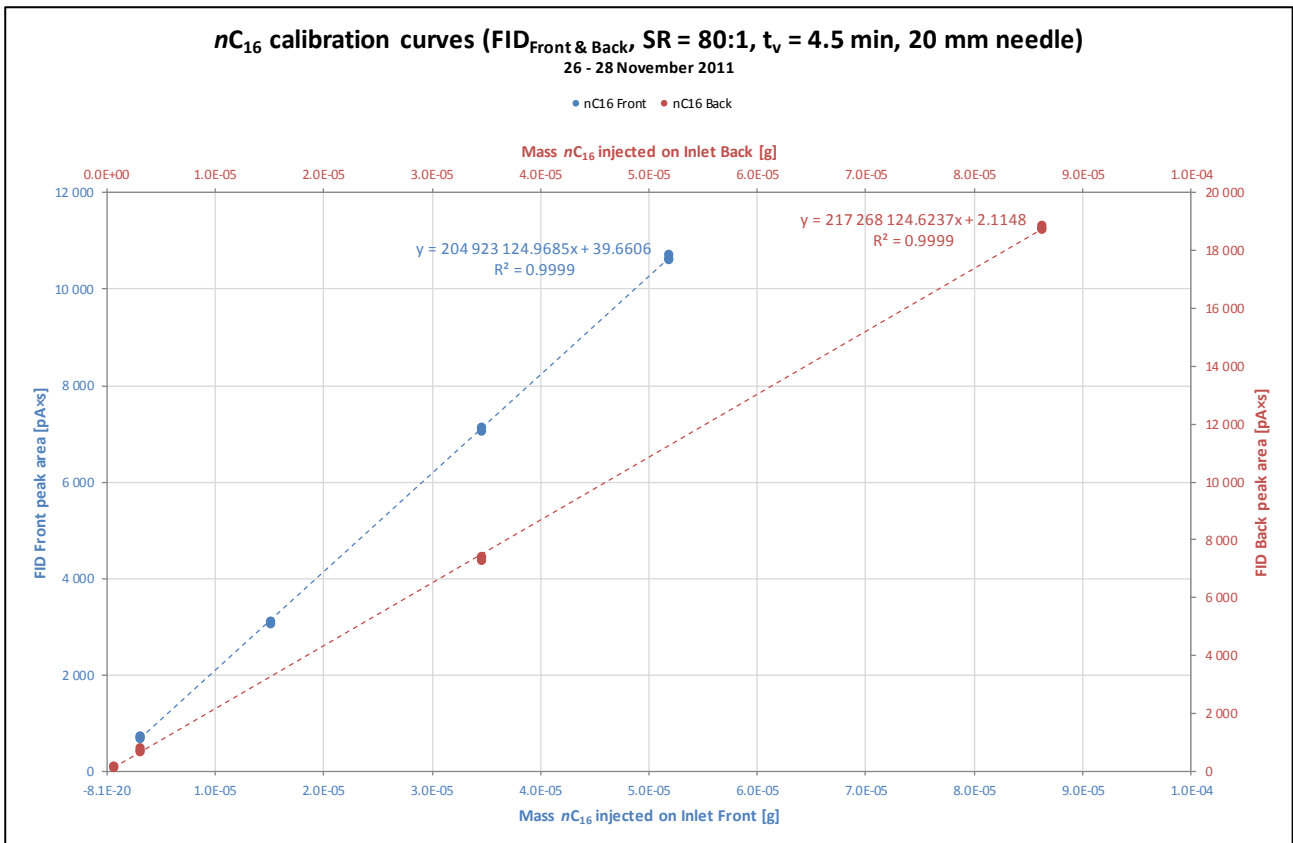
Appendix E-1	Ethane calibration curves	350
Appendix E-2	nC_{16} calibration curves (1)	350
Appendix E-3	nC_{16} calibration curves (2)	351
Appendix E-4	$C_{12}OH$ calibration curves (1)	351
Appendix E-5	$C_{12}OH$ calibration curves (2)	352
Appendix E-6	C_8OH calibration curves	352
Appendix E-7	CO_2 calibration curves (1)	353
Appendix E-8	CO_2 calibration curves (2)	353
Appendix E-9	CO_2 calibration curves (3)	354
Appendix E-10	CO_2 calibration curves (4)	354
Appendix E-11	CO_2 calibration curves (5)	355
Appendix E-12	CO_2 calibration curves (6)	355
Appendix E-13	nC_{12} calibration curves (1)	356
Appendix E-14	nC_{12} calibration curves (2)	356
Appendix E-15	nC_{12} calibration curves (3)	357
Appendix E-16	nC_{12} calibration curves (4)	357
Appendix E-17	nC_{12} calibration curves (5)	358
Appendix E-18	37DM1O calibration curves (1).....	358
Appendix E-19	37DM1O calibration curves (2).....	359
Appendix E-20	37DM1O calibration curves (3).....	359
Appendix E-21	37DM1O calibration curves (4).....	360
Appendix E-22	37DM1O calibration curves (5).....	360
Appendix E-23	$C_{10}OH$ calibration curves (1)	361
Appendix E-24	$C_{10}OH$ calibration curve (2)	361
Appendix E-25	$C_{10}OH$ calibration curves (3)	362
Appendix E-26	$C_{10}OH$ calibration curves (4)	362
Appendix E-27	$C_{10}OH$ calibration curves (5)	363



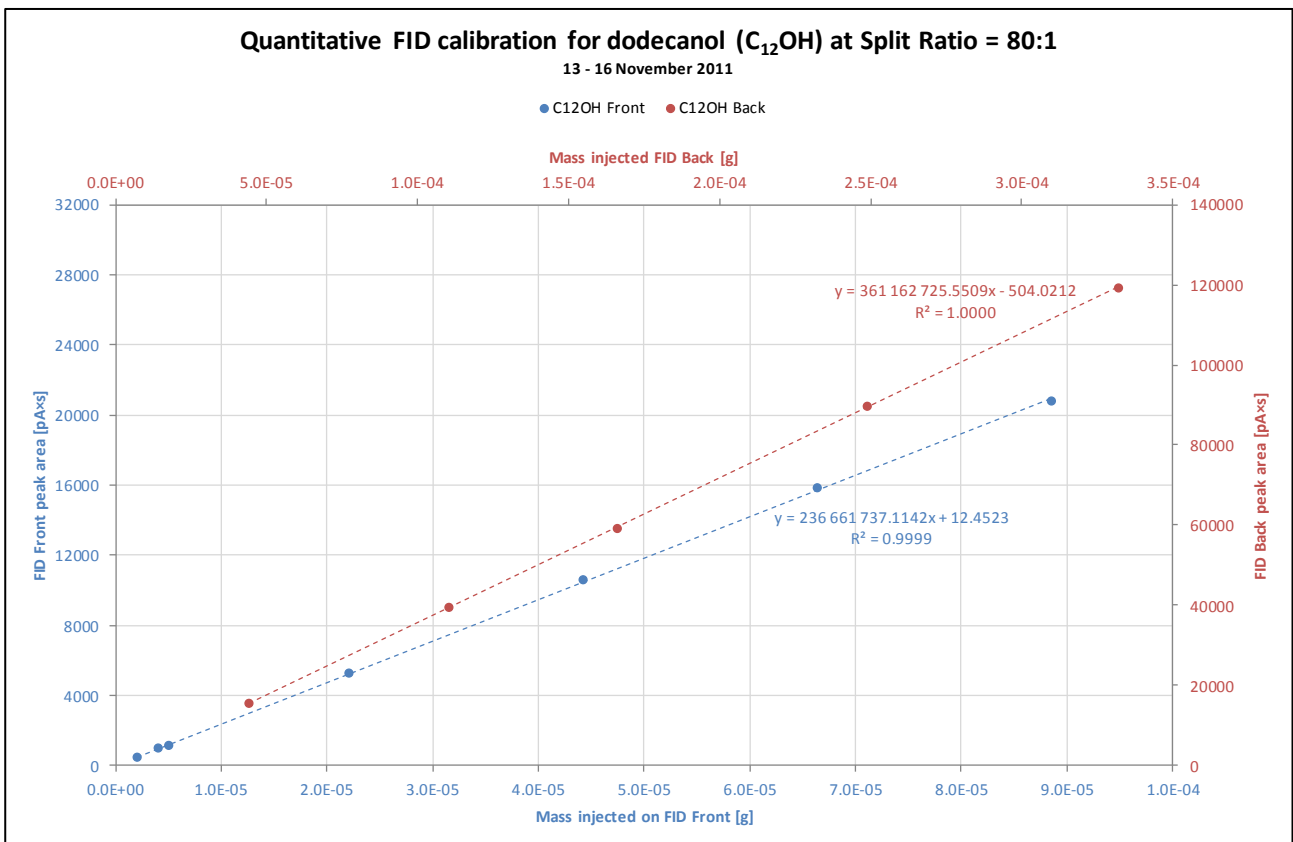
Appendix E-1 ETHANE CALIBRATION CURVES



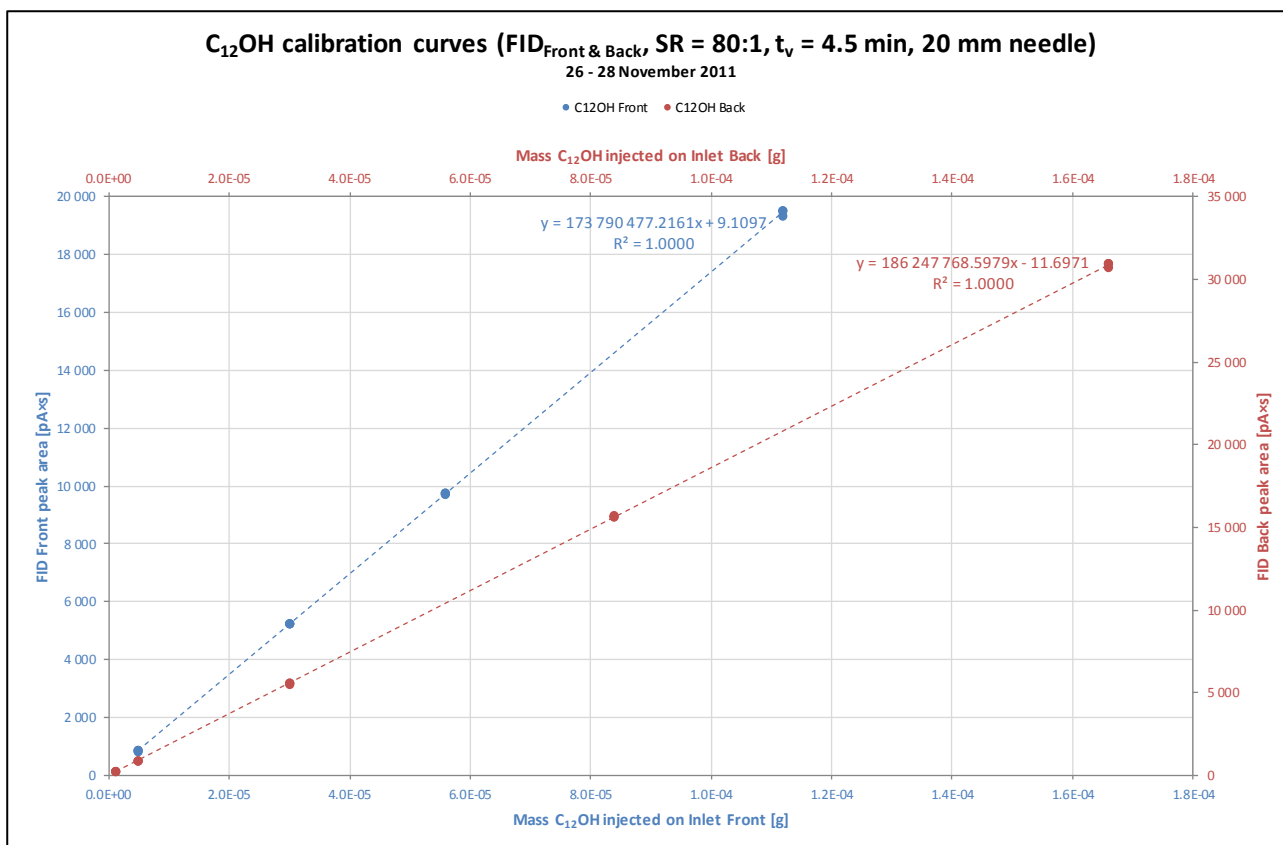
Appendix E-2 nC₁₆ CALIBRATION CURVES (1)



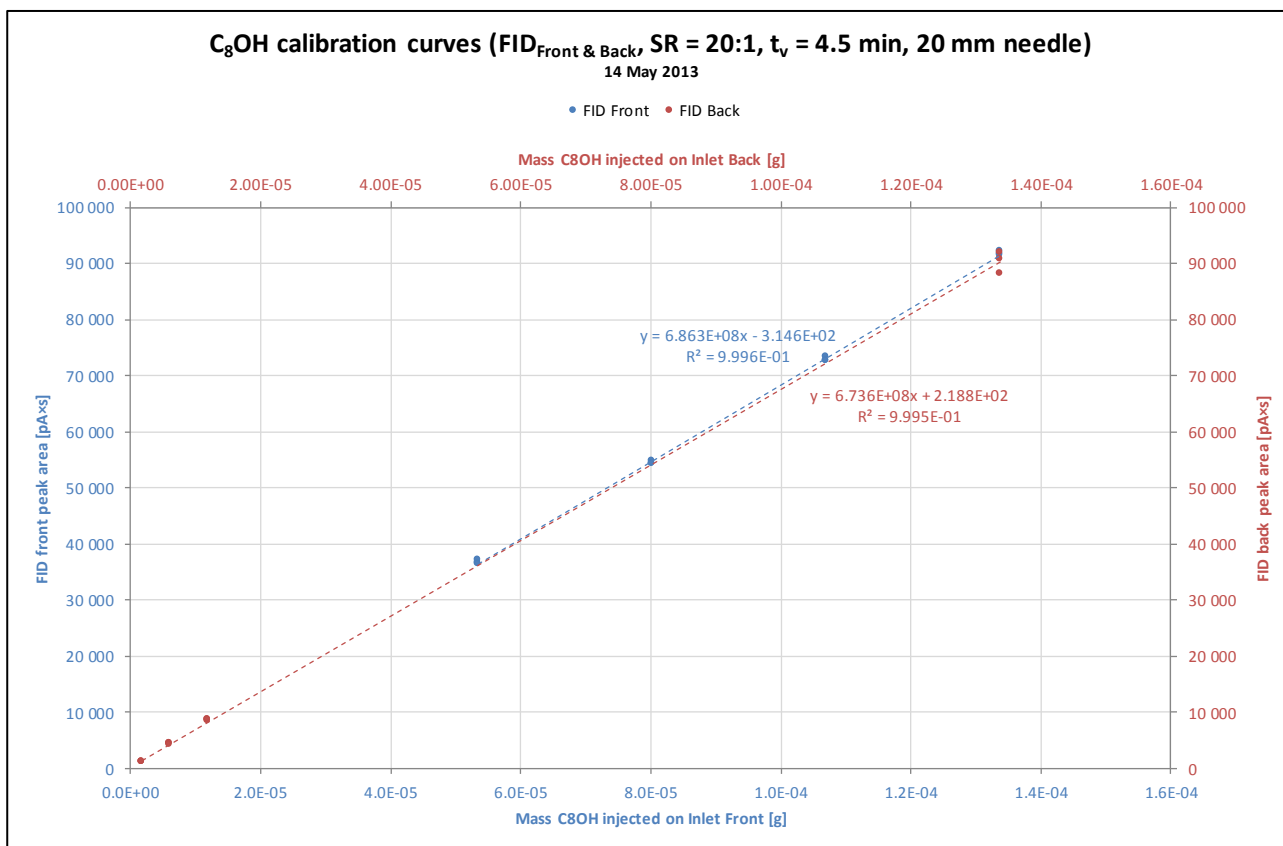
Appendix E-3 nC_{16} CALIBRATION CURVES (2)



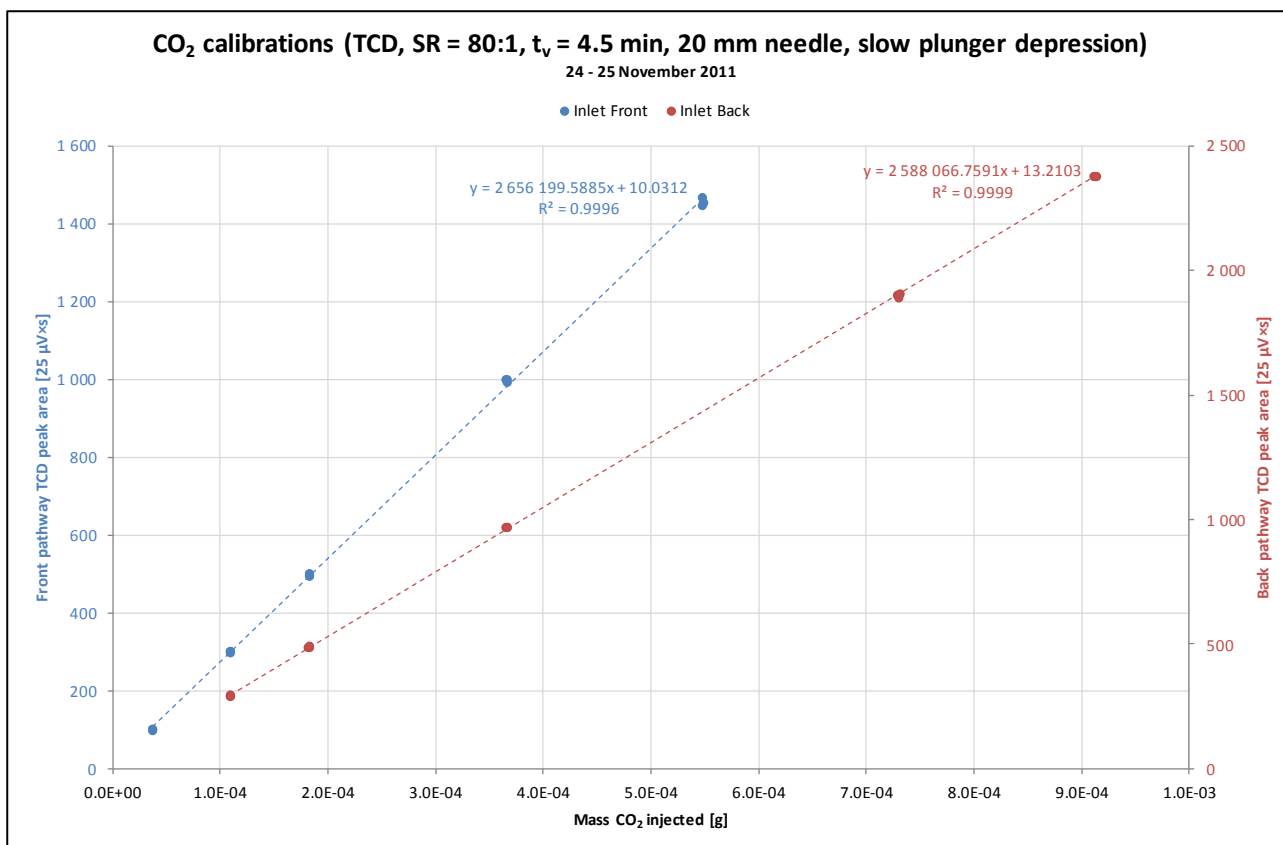
Appendix E-4 $C_{12}OH$ CALIBRATION CURVES (1)



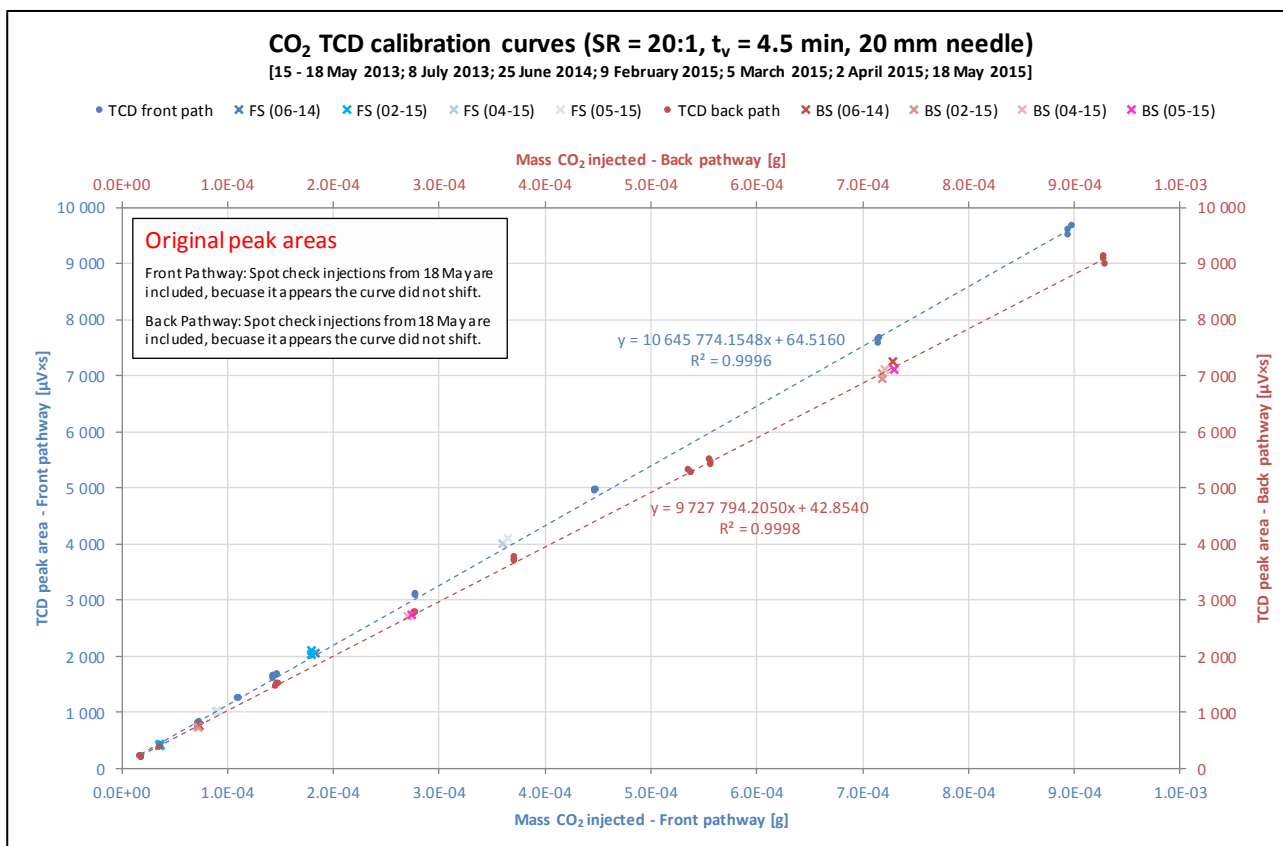
Appendix E-5 C₁₂OH CALIBRATION CURVES (2)



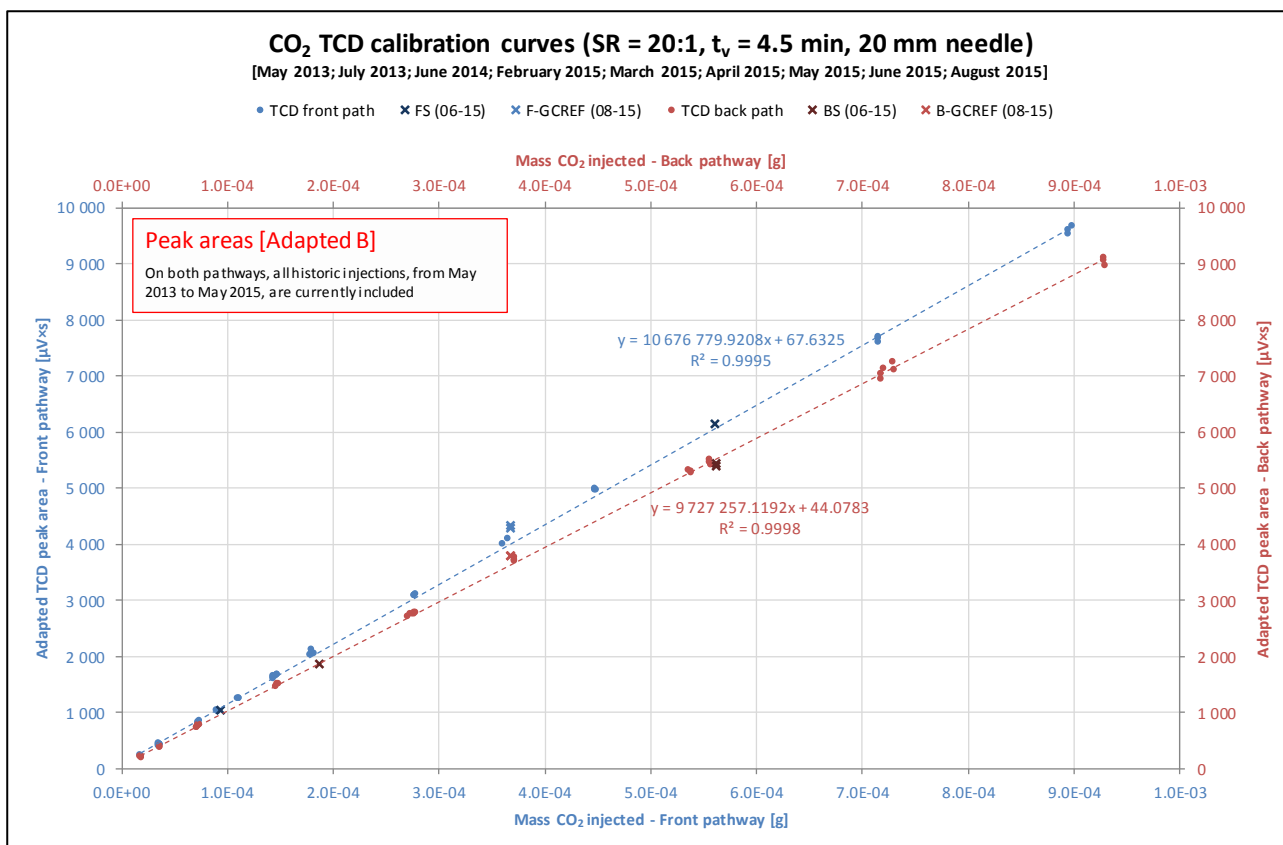
Appendix E-6 C₈OH CALIBRATION CURVES



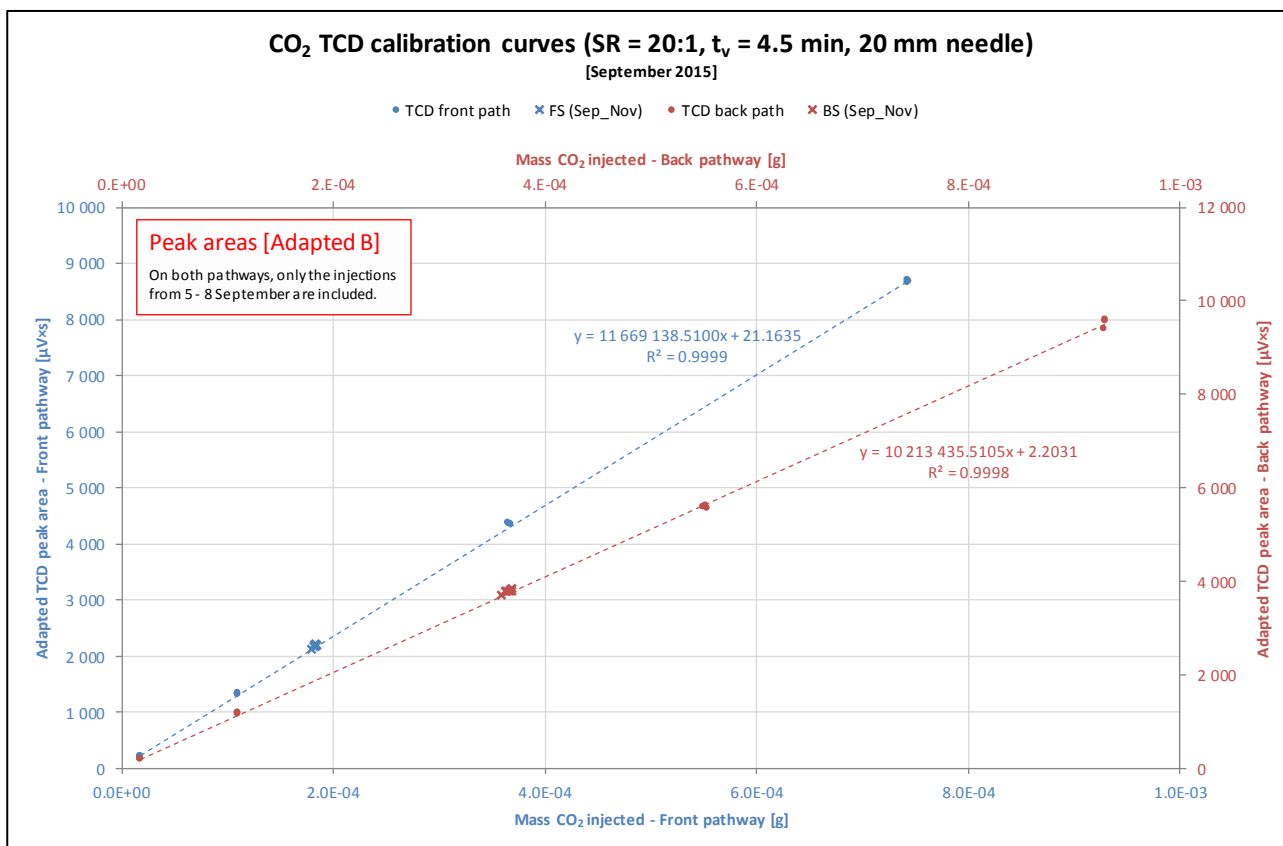
Appendix E-7 CO₂ CALIBRATION CURVES (1)



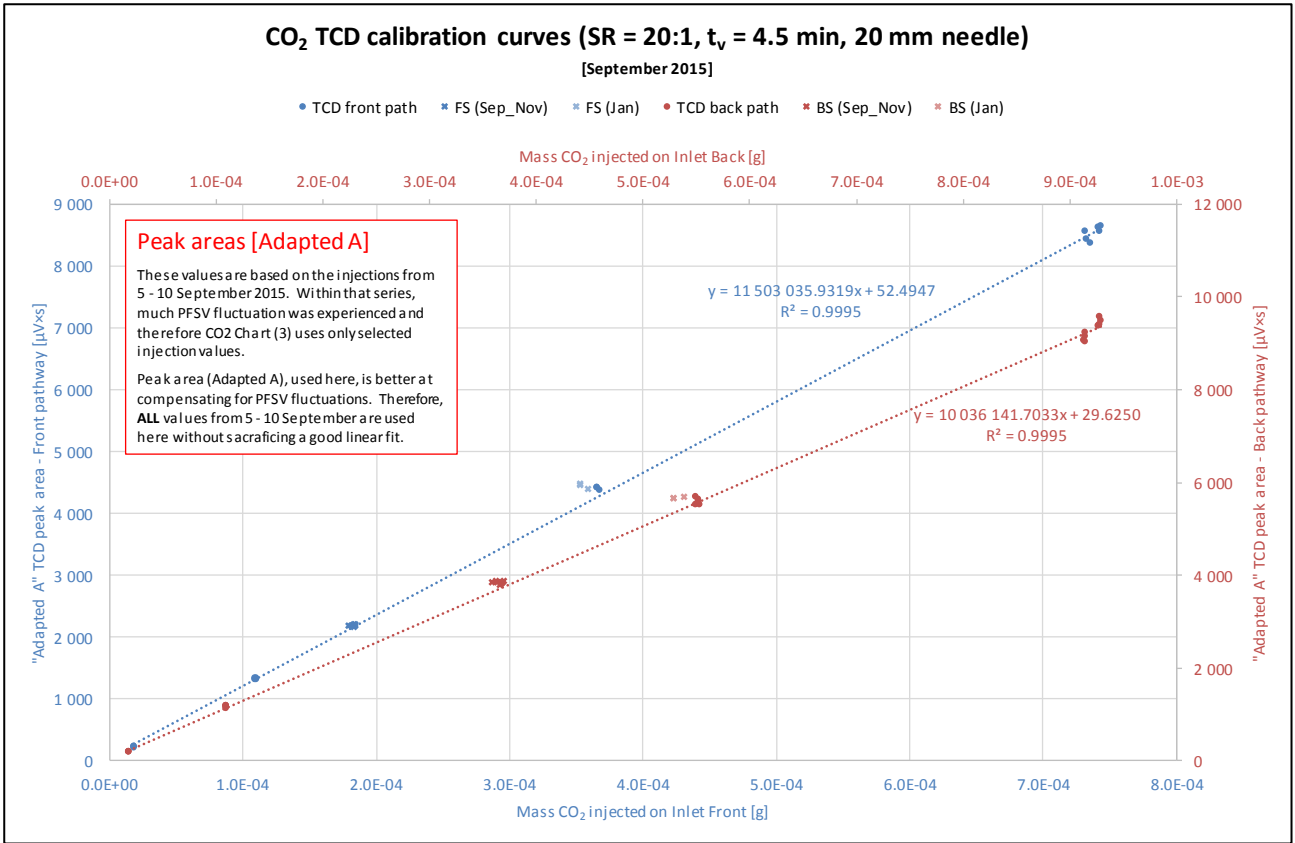
Appendix E-8 CO₂ CALIBRATION CURVES (2)



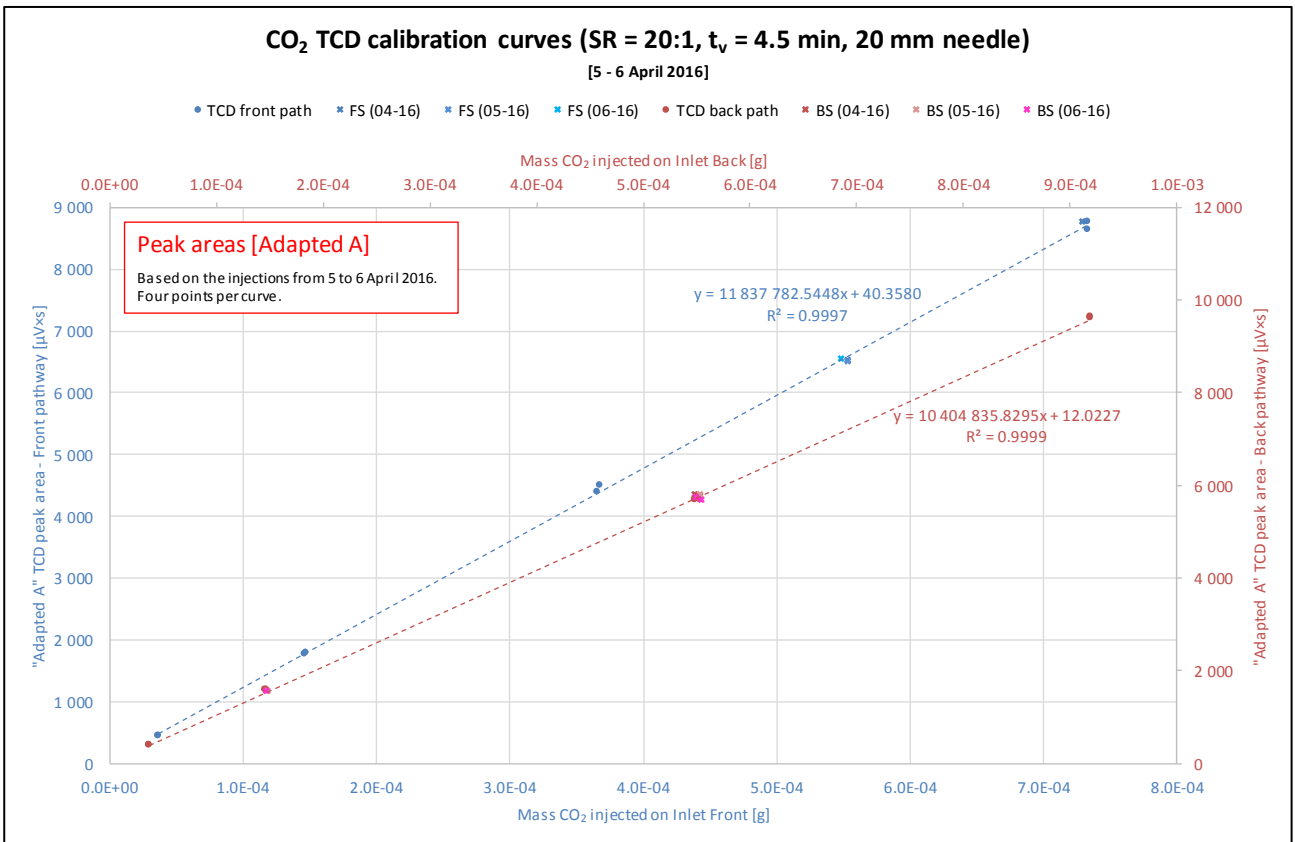
Appendix E-9 CO₂ CALIBRATION CURVES (3)



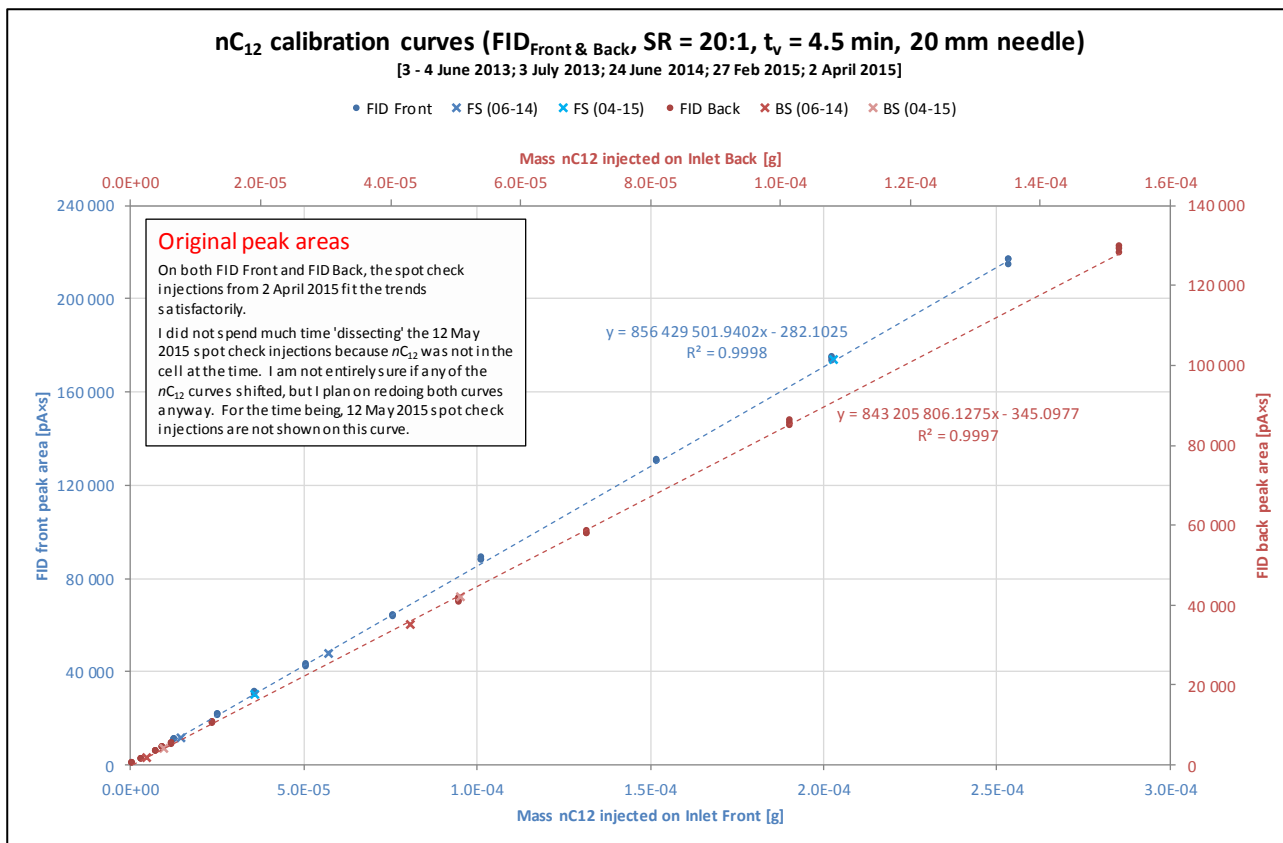
Appendix E-10 CO₂ CALIBRATION CURVES (4)



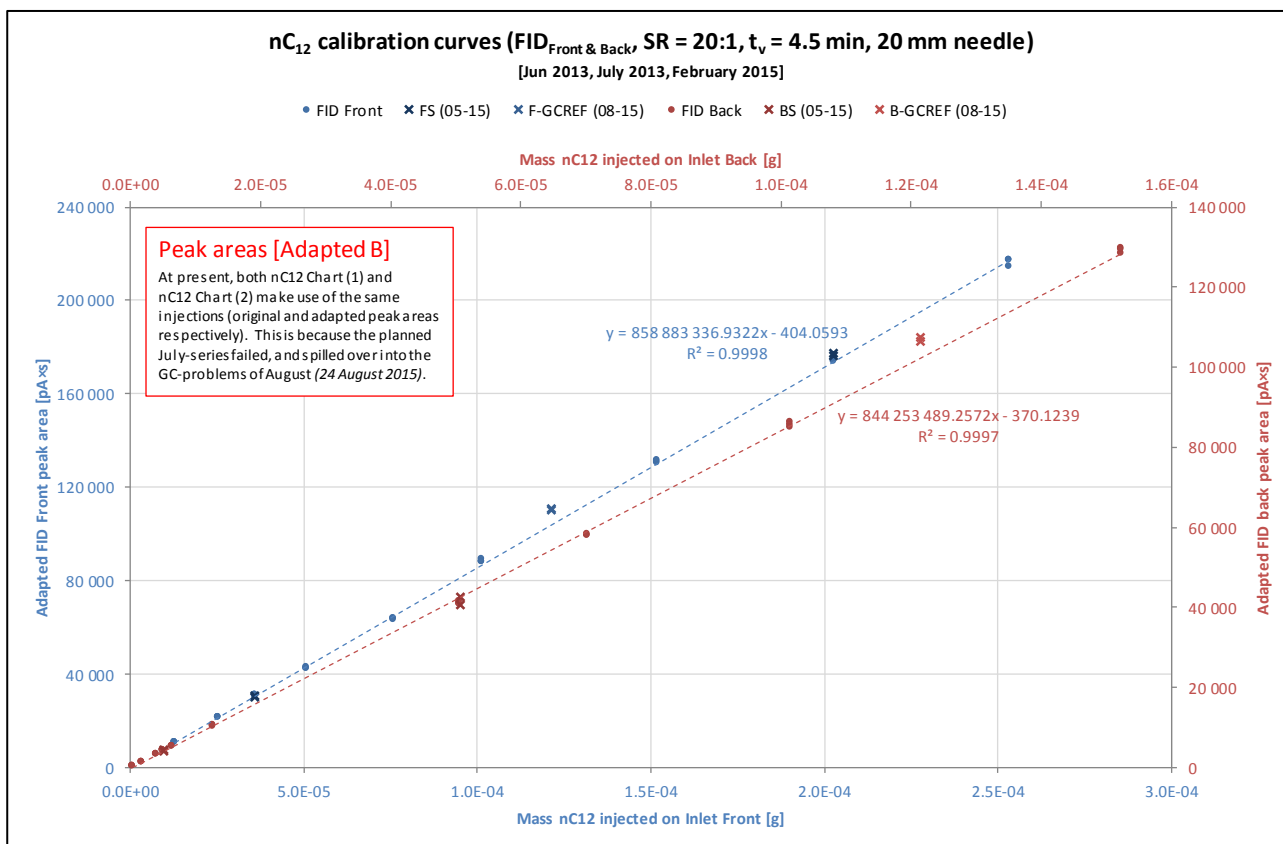
Appendix E-11 CO₂ CALIBRATION CURVES (5)



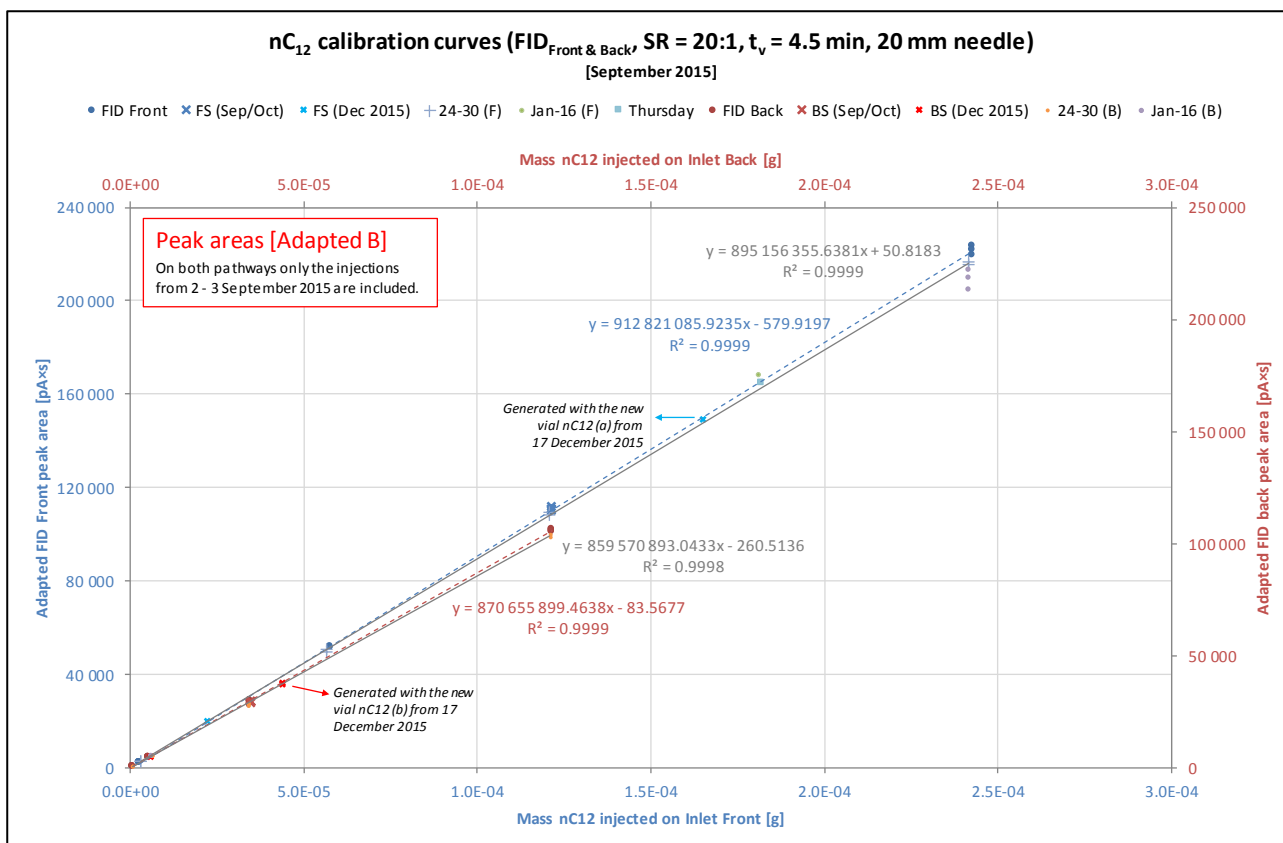
Appendix E-12 CO₂ CALIBRATION CURVES (6)



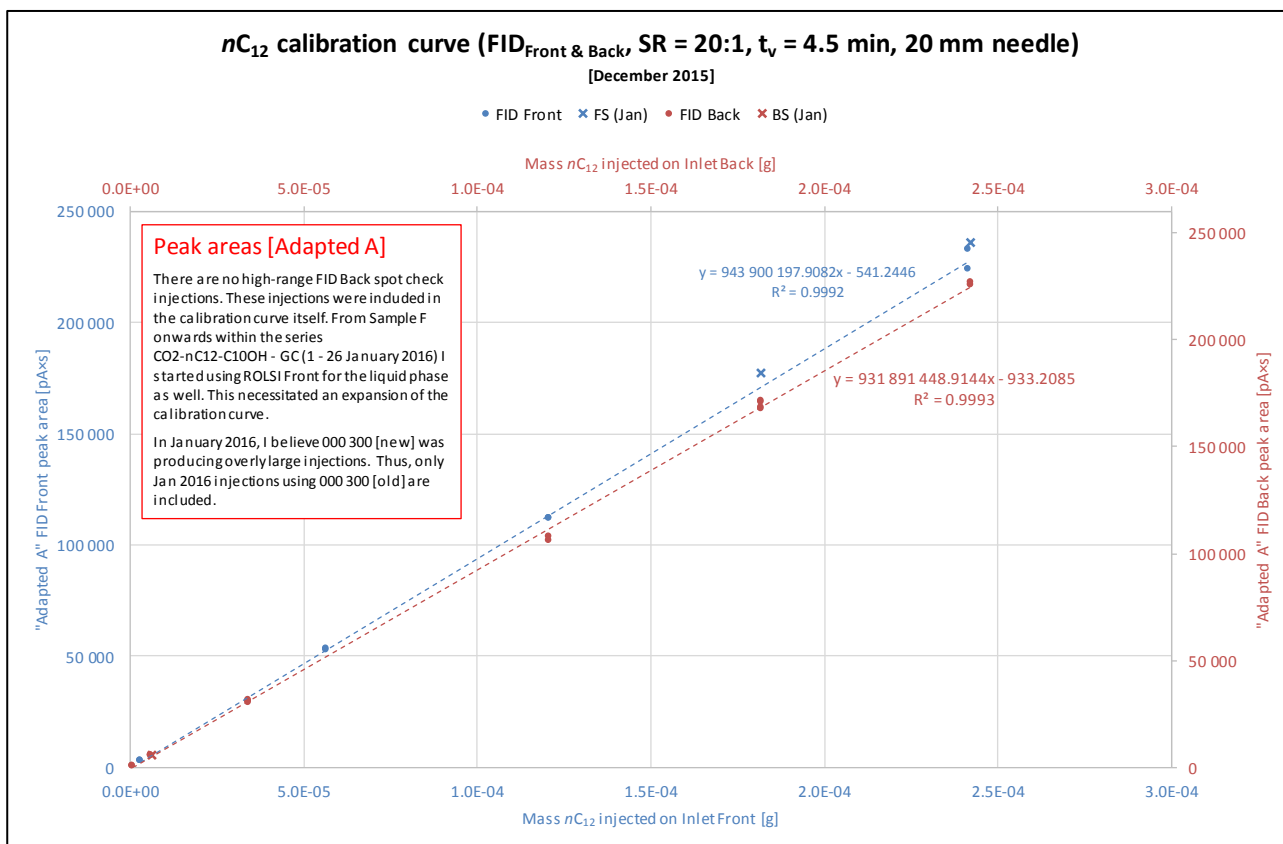
Appendix E-13 nC₁₂ CALIBRATION CURVES (1)



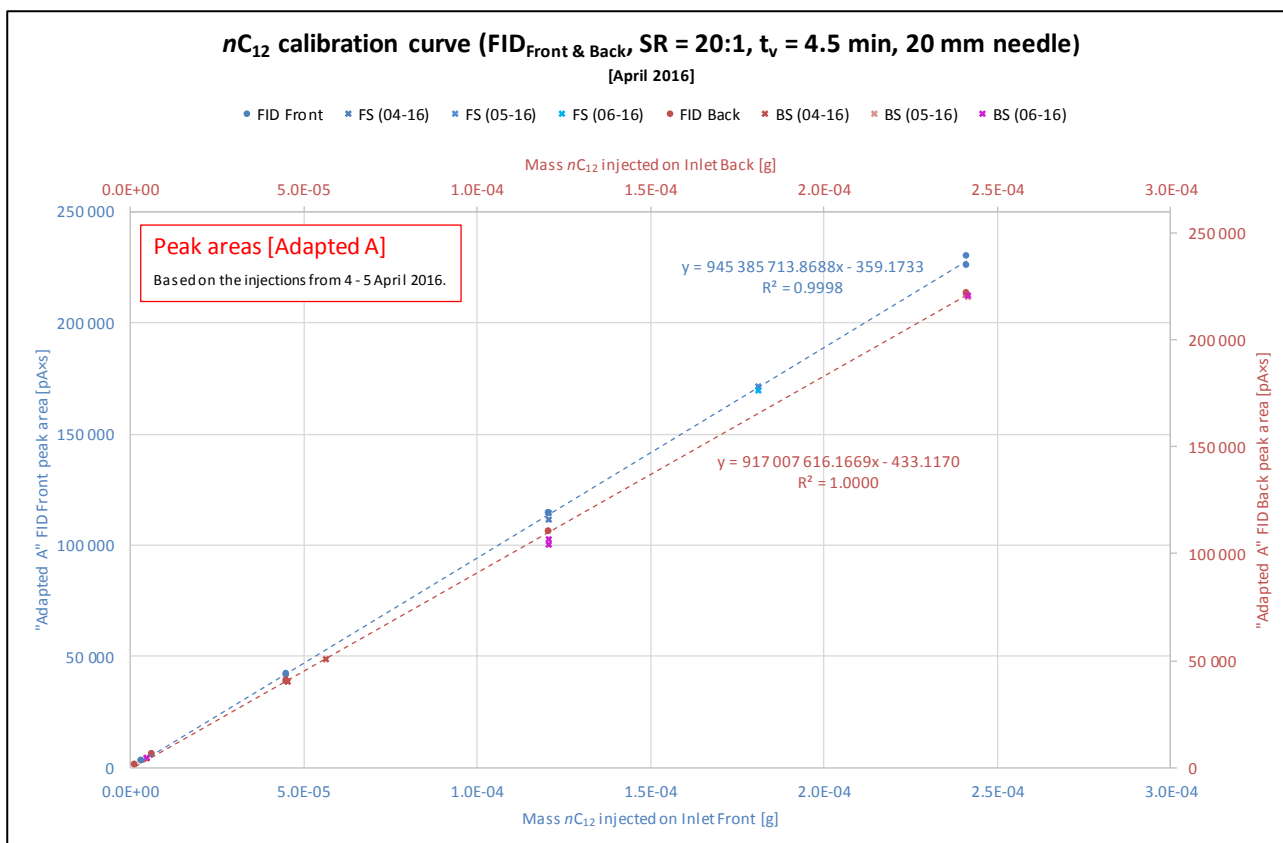
Appendix E-14 nC₁₂ CALIBRATION CURVES (2)



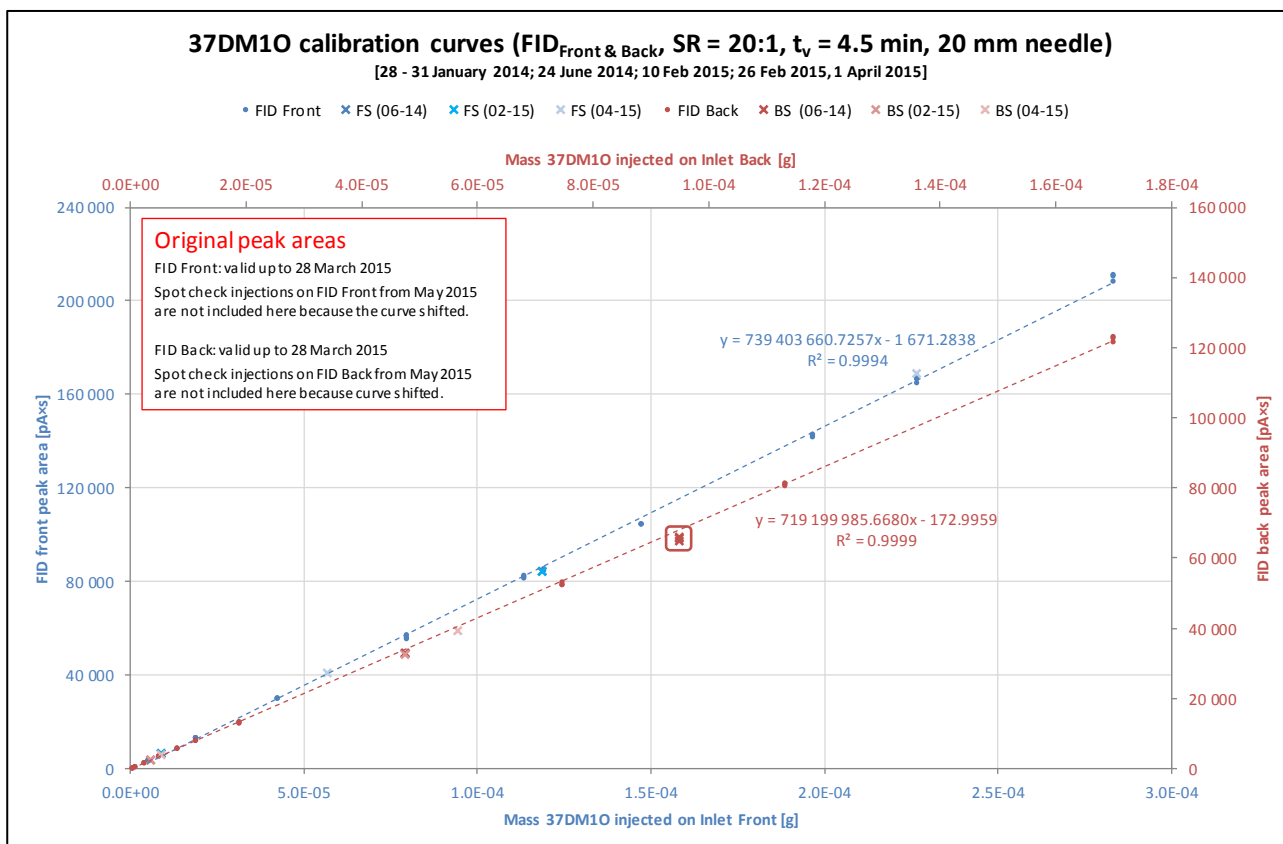
Appendix E-15 nC₁₂ CALIBRATION CURVES (3)



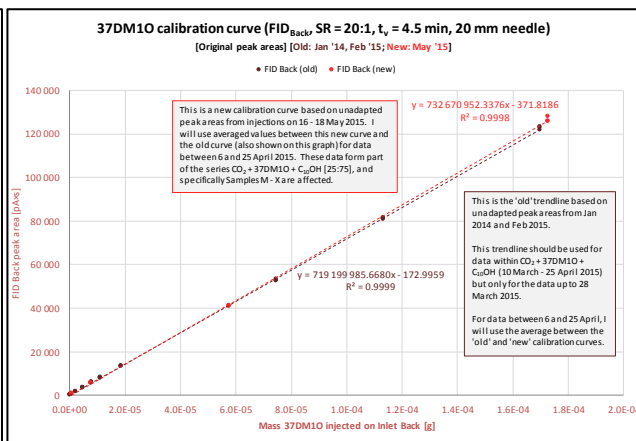
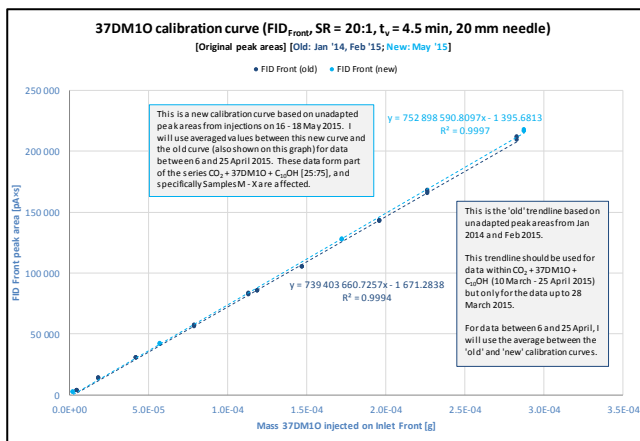
Appendix E-16 nC₁₂ CALIBRATION CURVES (4)



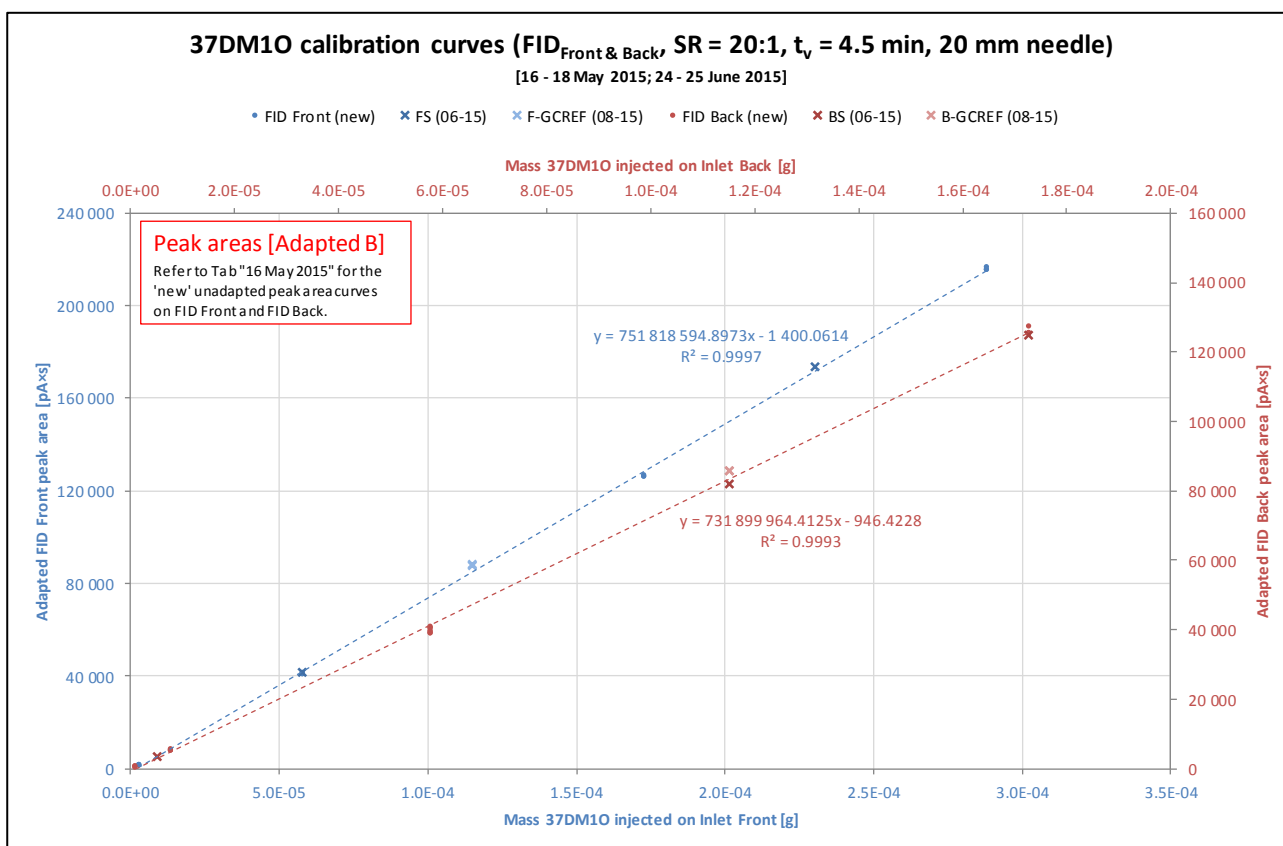
Appendix E-17 nC_{12} CALIBRATION CURVES (5)



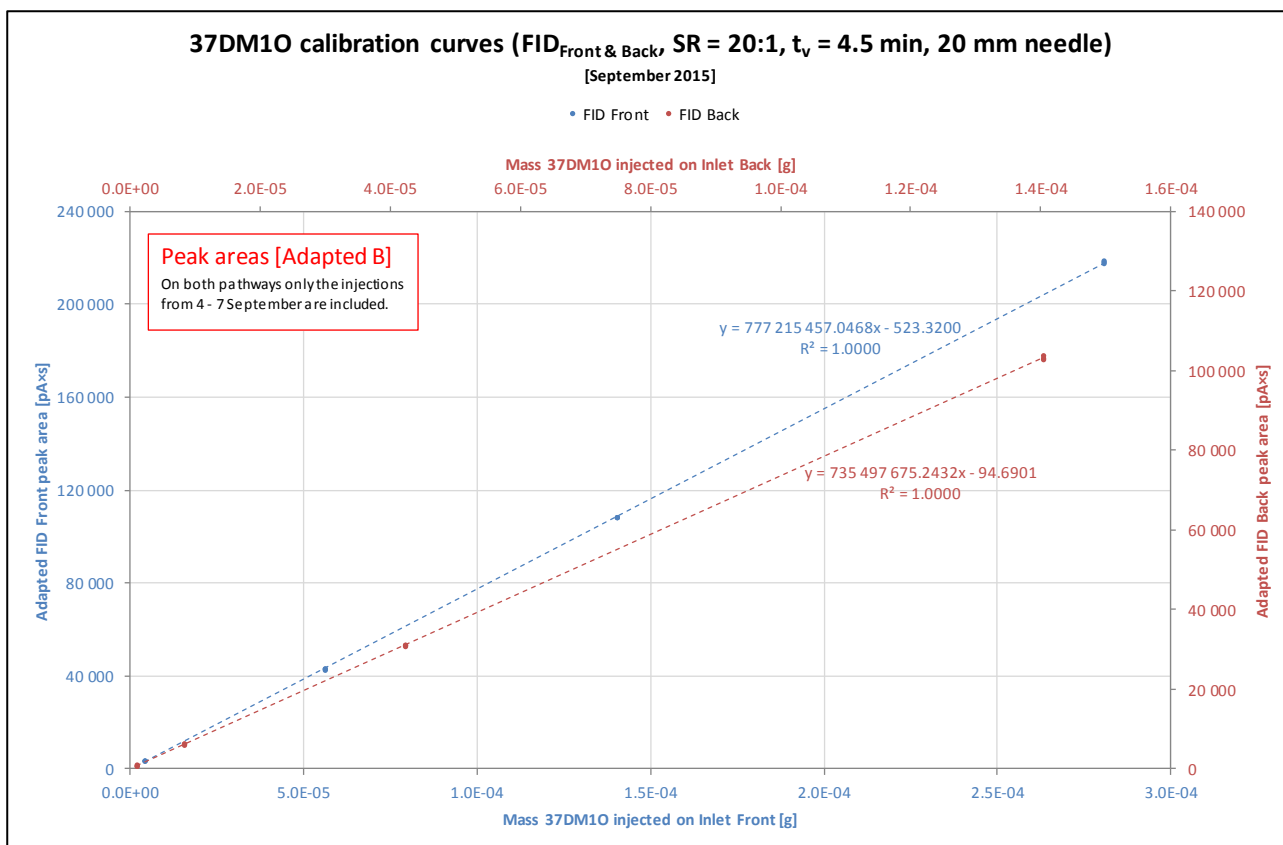
Appendix E-18 37DM10 CALIBRATION CURVES (1)



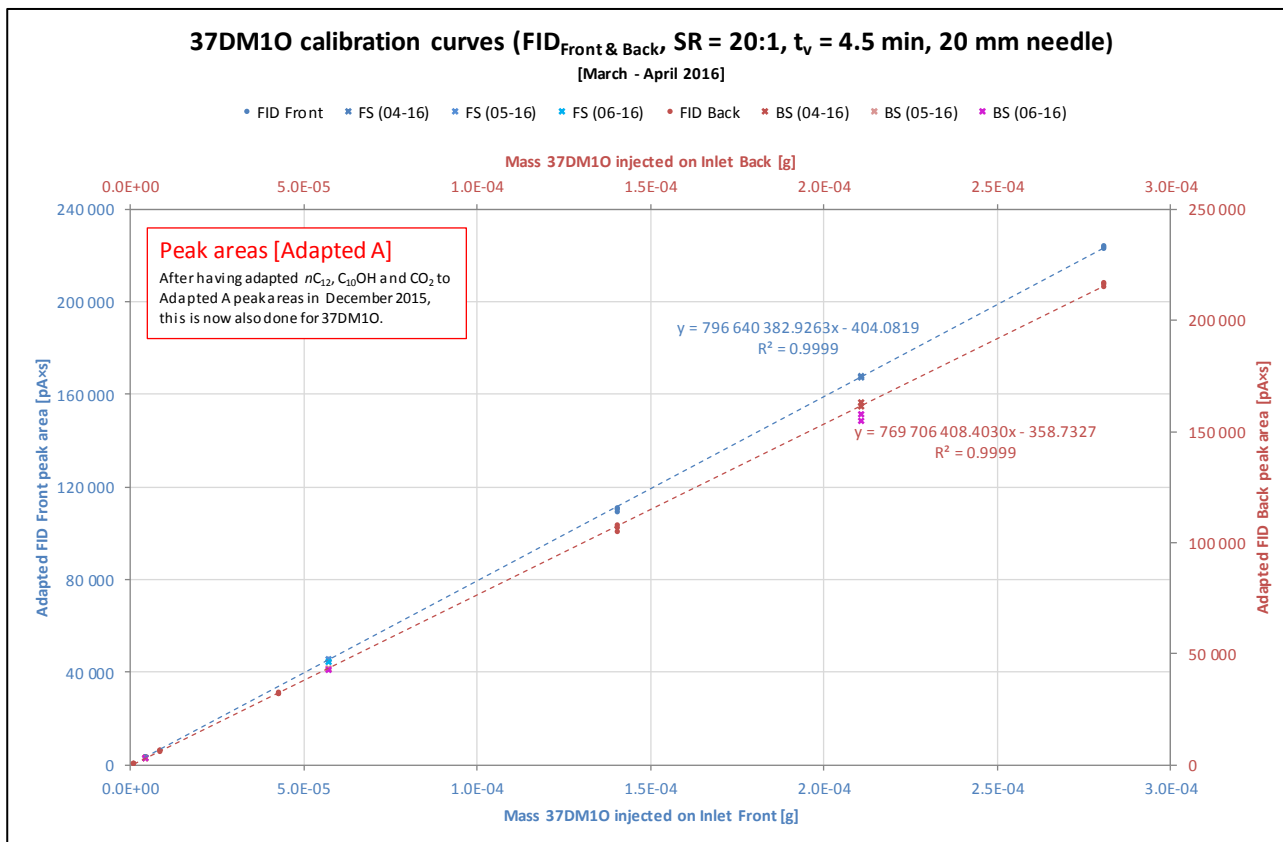
Appendix E-19 37DM10 CALIBRATION CURVES (2)



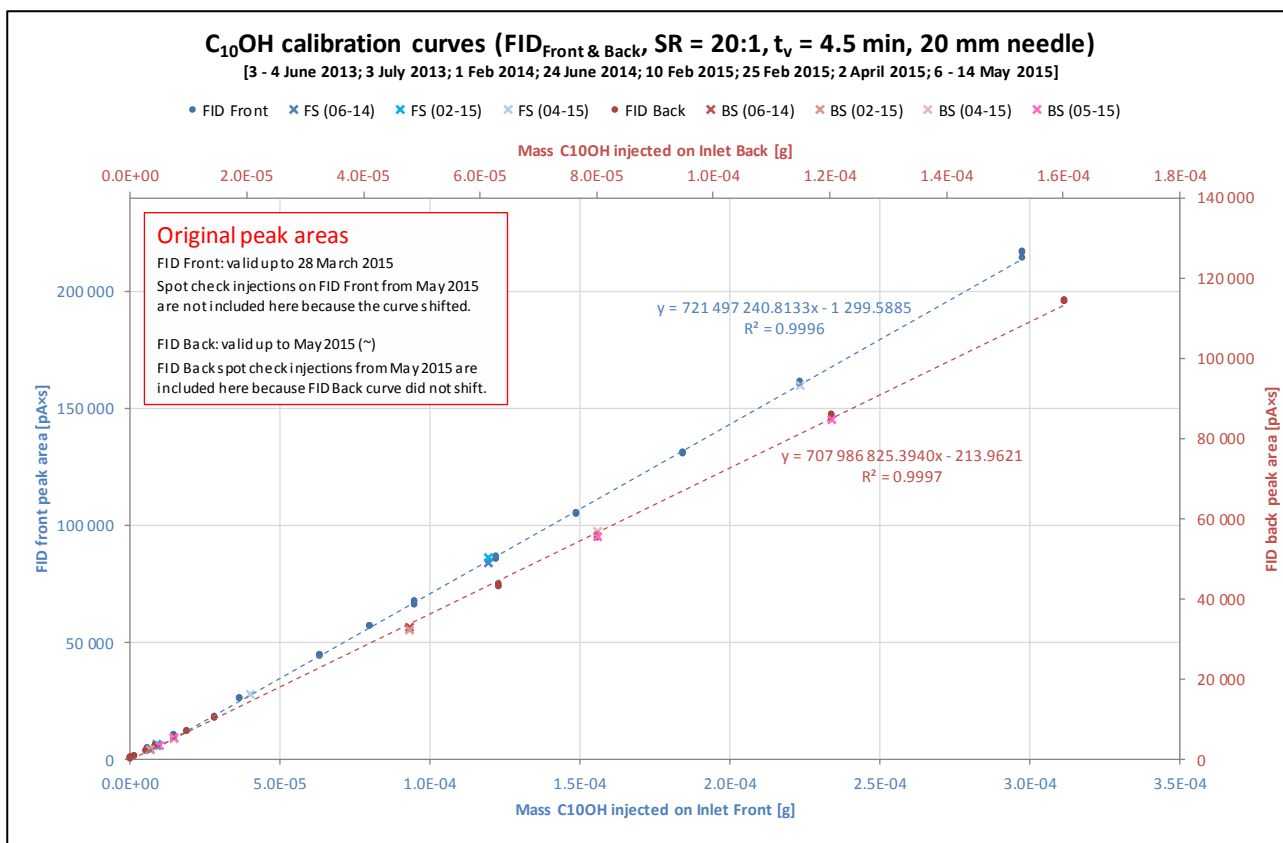
Appendix E-20 37DM10 CALIBRATION CURVES (3)



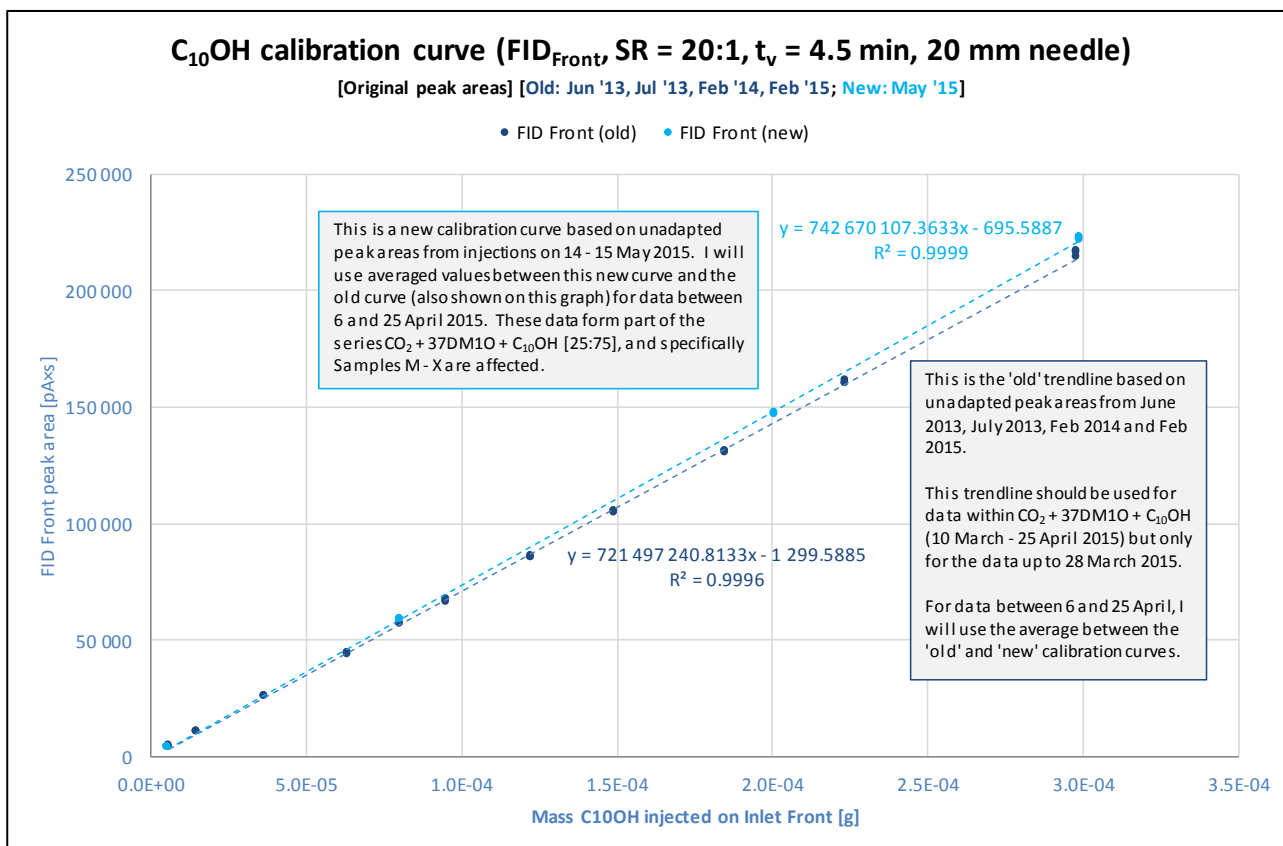
Appendix E-21 37DM10 CALIBRATION CURVES (4)



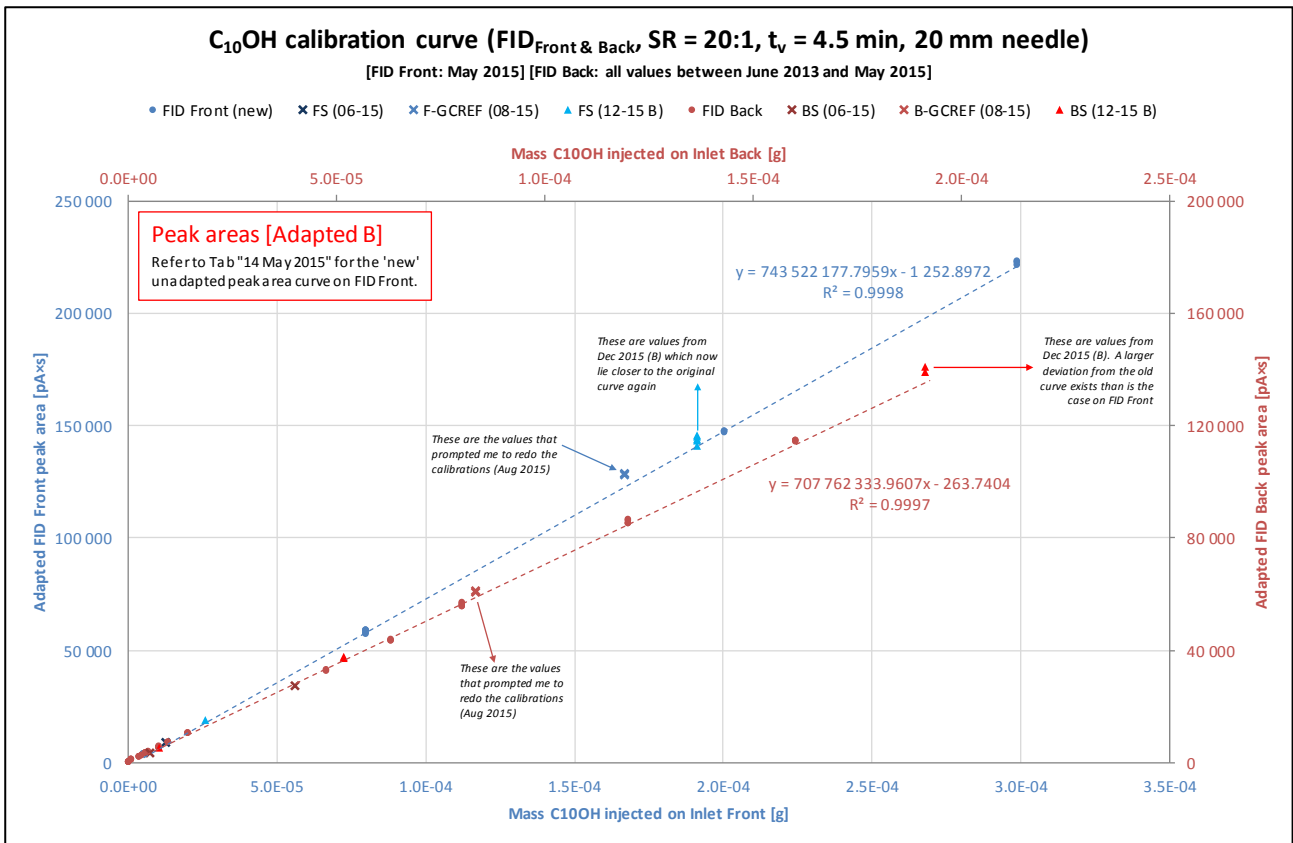
Appendix E-22 37DM10 CALIBRATION CURVES (5)



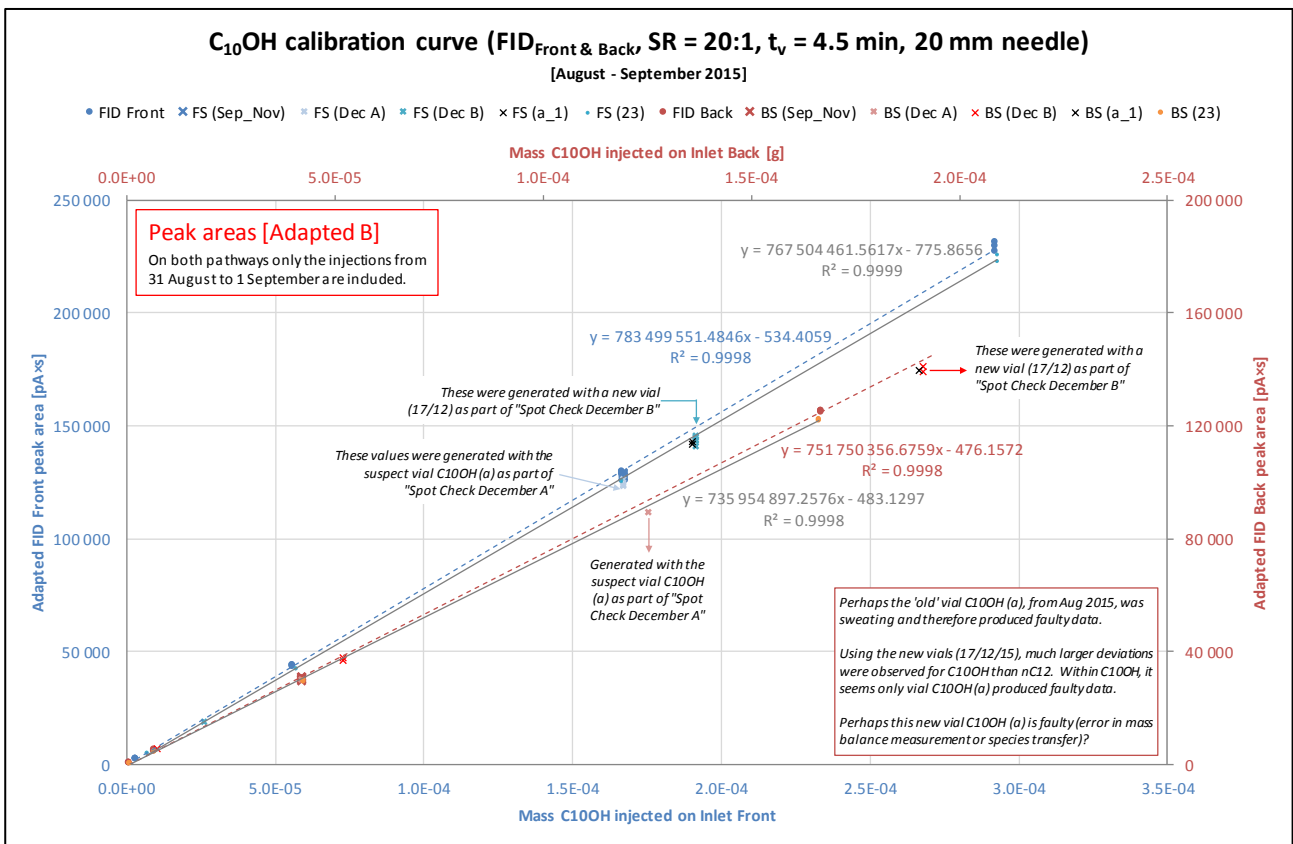
Appendix E-23 C₁₀OH CALIBRATION CURVES (1)



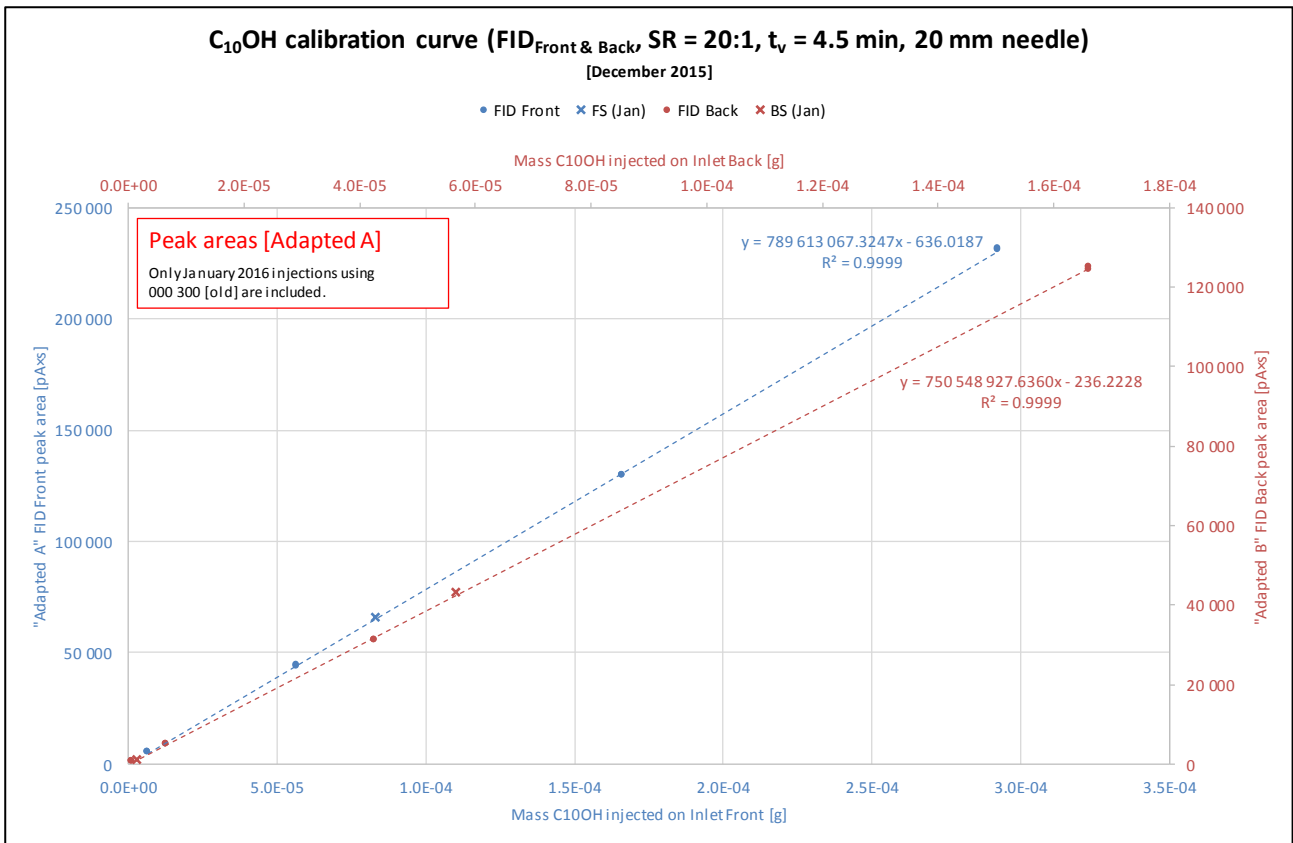
Appendix E-24 C₁₀OH CALIBRATION CURVE (2)



Appendix E-25 C₁₀OH CALIBRATION CURVES (3)



Appendix E-26 C₁₀OH CALIBRATION CURVES (4)



Appendix E-27 C₁₀OH CALIBRATION CURVES (5)